PORTOFOLIU DE LUCRĂRI ȘTIINȚIFICE
Șef lucr. dr. Cătălina Bogdan

OPIS

Nr.	Articol	Pagina
1	**Bogdan, Catalina**; Iurian, Sonia; Tomuta, Ioan; Moldovan, Mirela. Improvement of skin condition in striae distensae: development, characterization and clinical efficacy of a cosmetic product containing *Punica granatum* seed oil and *Croton lechleri* resin extract. DRUG DESIGN DEVELOPMENT AND THERAPY. 2017. 11;521:531. doi:10.2147/DDDT.S128470. WOS:000395329300001. (FI=2.935; Q2) https://www.webofscience.com/wos/woscc/full-record/WOS:000395329300001	3
2	**Bogdan, Catalina**; Pop, Anca; Iurian, Sonia M.; Benedec, Daniela; Moldovan, Mirela L. Research Advances in the Use of Bioactive Compounds from Vitis vinifera By-Products in Oral Care. ANTIOXIDANTS. 2020.9; 6; 502. 10.3390/antiox9060502. WOS:000551534100001 (IF=6.313, Q1) https://www.webofscience.com/wos/woscc/full-record/WOS:000551534100001	14
3	Pașcalău, Violeta; *__Bogdan, Cătălina__; Pall, Emoke; Matroș, Luminița; Pandrea, Stanca-Lucia; Suciu, Maria; Borodi, Gheorghe; Iuga, Cristina Adela; Știufiuc, Rareș; Topală, Tamara; Pavel, Codruța; Popa, Cătălin; Moldovan, Mirela Liliana. Development of BSA gel/pectin/chitosan polyelectrolyte complex microcapsules for berberine delivery and evaluation of their inhibitory effect on Cutibacterium acnes. REACTIVE & FUNCTIONAL POLYMERS. 2020. 147; 104457. 10.1016/j.reactfunctpolym.2019.104457. WOS:000512484100019 (IF= 3.975, Q2) https://www.webofscience.com/wos/woscc/full-record/WOS:000512484100019	47
4	Iurian, Sonia M.; Adespei, Diana-Roxana; Pop, Anca; Fizesan, Ionel; Carpa, Rahela; Moldovan, Mirela L.; Loghin, Felicia; Achim, Marcela; **Bogdan, Catalina**. Development of a Mouthwash Using Freeze-Drying Technique: An Optimization Study. APPLIED SCIENCES-BASEL. 2021. 11;20:-9609 doi:10.3390/app11209609. WOS:000714721100001. (FI=2.838; Q2) https://www.webofscience.com/wos/woscc/full-record/WOS:000714721100001	59
5	Safta, Diana Antonia; *__Bogdan, Cătălina__; Moldovan, Mirela Liliana. Vesicular nanocarriers for phytocompounds in wound care: Preparation and characterization. PHARMACEUTICS. 2022. 14; 5: 991. 10.3390/pharmaceutics14050991. WOS:000801509600001 (IF=5.4,Q1) https://www.webofscience.com/wos/woscc/full-record/WOS:000801509600001	75
6	***Bogdan, Catalina**; Hales, Dana; Cornila, Andreea; Casian, Tibor; Iovanov, Rares; Tomuta, Ioan; Iurian, Sonia. Texture analysis-A versatile tool for pharmaceutical evaluation of solid oral dosage forms. INTERNATIONAL JOURNAL OF PHARMACEUTICS. 2023. 638122916 1.0.1016/j.ijpharm.2023.122916. WOS:000981742000001. (FI=5.3; Q1) https://www.webofscience.com/wos/woscc/full-record/WOS:000981742000001	111
7	Savencu, Ioana; Iurian, Sonia; *__Bogdan, Catalina__; Spinu, Nicoleta; Suciu, Maria; Pop, Anca; Toc, Alexandru; Tomuta, Ioan. Design, optimization and pharmaceutical characterization of wound healing film dressings with chloramphenicol and ibuprofen.DRUG DEVELOPMENT AND INDUSTRIAL PHARMACY. 2024. 50; 5:446-459. 10.1080/03639045.2024.2339306. WOS:001202979200001.(IF=2.4,Q3) https://www.webofscience.com/wos/woscc/full-record/WOS:001202979200001	141
8	**Bogdan, Catalina**; Safta, Diana Antonia; Iurian, Sonia; Petrusca, Dyana Roxana; Moldovan, Mirela-Liliana. QbD Approach in Cosmetic Cleansers Research: The Development of a Moisturizing Cleansing Foam	

Nr.	Articol	Pagina
	Focusing on Thickener, Surfactants, and Polyols Content.GELS. 10;8:484. doi: 10.3390/gels10080484. WOS:001305505300001. (IF= 5,Q1) https://www.webofscience.com/wos/woscc/full-record/WOS:001305505300001	156
9	Safta, Diana Antonia; *__Bogdan, Cătălina__; Moldovan, Mirela-Liliana. SLNs and NLCs for skin applications: Enhancing the bioavailability of natural bioactives. PHARMACEUTICS. 2024. 16;10:1270. doi: 10.3390/pharmaceutics16101270. WOS:001342974800001. (FI=5.5, Q1) https://www.webofscience.com/wos/woscc/full-record/WOS:001342974800001	175
10	__Bogdan, Cătălina__; Molnar, Mara; Dima, Elena Ines; Olteanu, Andreea Alexandra; Safta, Diana Antonia; Moldovan, Mirela-Liliana. Marine Macroalgae in Topical Formulations: Bioactive Compounds, Variability, Analytical Challenges and Skin Benefits. PHARMACEUTICS. 2025.17; 9:1143. 10.3390/pharmaceutics17091143. WOS:001579891100001. (FI=5.5; 2025) https://www.webofscience.com/wos/woscc/full-record/WOS:00157989110000	206

*autor corespondent

Drug Design, Development and Therapy

Dovepress
open access to scientific and medical research

Open Access Full Text Article

ORIGINAL RESEARCH

Improvement of skin condition in striae distensae: development, characterization and clinical efficacy of a cosmetic product containing *Punica granatum* seed oil and *Croton lechleri* resin extract

Cătălina Bogdan[1]
Sonia Iurian[2]
Ioan Tomuta[2]
Mirela Moldovan[1]

[1]Department of Dermatopharmacy and Cosmetics, [2]Department of Pharmaceutical Technology and Biopharmacy, Faculty of Pharmacy, University of Medicine and Pharmacy Iuliu Haţieganu, Cluj-Napoca, Romania

Abstract: Striae distensae are a frequent skin condition associated with pregnancy, weight change or lack of skin elasticity. The aim of this research was to obtain a topical product containing herbal active ingredients with documented antioxidant and anti-inflammatory activity (*Punica granatum* seed oil and *Croton lechleri* resin extract) and demonstrate its positive effect on prevention and treatment of striae distensae. First, the cream base formulation was optimized through experimental design. Secondly, the cream containing the two active ingredients was investigated in an interventional nonrandomized clinical trial. The clinical outcome was assessed through biophysical parameters and ultrasonographic evaluation. The state of the skin was evaluated by biophysical measurements and ultrasonography at the beginning of the study and after 3 and 6 weeks. The experimental design was successfully used to set the best ranges for the technological and formulation factors to obtain a cosmetic formulation with optimal characteristics. The study of clinical efficacy on the optimal formulation revealed an increase in the dermis thickness, hydration and elasticity values in both groups after 6 weeks of cream application. The new oil-in-water cream containing *P. granatum* seed oil and *C. lechleri* resin extract can be helpful in the prevention or improving of skin changes associated with striae.

Keywords: stretch marks, ultrasonography, texture analysis, design of experiments, oil-in-water emulsion

Introduction

Striae distensae (SD) represent dermal lesions with multifactorial physiopathology, but their occurrence mechanisms have not been fully elucidated until now. Although rarely inducing major medical problems, striae represent an esthetic concern for those affected.[1] SD appear as linear bands with an erythematous to violaceus color (striae rubrae) and gradually become hypopigmented atrophic lines (striae albae). Striae albae represent the stabilized form of striae, characterized by the absence of erythema and the decrease of melanization.[2] Rarely, in people with darker skin, striae appear darker because of increased melanization as striae cerulae (blue) or striae nigrae (black).[1–4] The color of SD is linked to the stage of their evolution and to the influence of melanocyte mechanobiology.[5] Also, in case of striae nigrae and striae cerulae, the releasing of cytokines, such as the stem cell factor and hepatocyte growth factor, may induce epidermal hyperpigmentation.[2]

The anatomical appearance sites include abdomen and breasts areas in case of striae gravidarum, thighs and lumbosacral regions in adolescent males and abdomen,

Correspondence: Sonia Iurian
Department of Pharmaceutical Technology and Biopharmacy, Faculty of Pharmacy, University of Medicine and Pharmacy Iuliu Haţieganu, 41 V Babeş Street, 400012 Cluj-Napoca, Romania
Tel +40 745 629 083
Email iuriansonia@yahoo.com

submit your manuscript | www.dovepress.com
Dovepress
http://dx.doi.org/10.2147/DDDT.S128470

© 2017 Bogdan et al. This work is published and licensed by Dove Medical Press Limited. The full terms of this license are available at https://www.dovepress.com/terms.php and incorporate the Creative Commons Attribution – Non Commercial (unported, v3.0) License (http://creativecommons.org/licenses/by-nc/3.0/). By accessing the work you hereby accept the Terms. Non-commercial uses of the work are permitted without any further permission from Dove Medical Press Limited, provided the work is properly attributed. For permission for commercial use of this work, please see paragraphs 4.2 and 5 of our Terms (https://www.dovepress.com/terms.php).

breasts and thighs in adolescent females.[1,6,7] Numerous risk factors, such as topical or systemic use of corticosteroids, pregnancy, adolescence, weight variation and tissue expansion, Cushing, and Marfan syndrome, have been associated with the presence of striae.[3,8–10] The genetic predisposition, family history, race and skin type also represent etiological risk factors.[6] Among all forms of SD, striae gravidarum appear with a high prevalence, estimated at up to 90% of pregnant women. The most important factors involved in pathogenesis of striae gravidarum are the mechanical stress of the skin, hormonal variations and pre-existing dermal pathology.[3,8,11,12]

The physiopathogenetic mechanism of SD involves changes similar with scar formation process.[1,7,10] In an initial stage, inflammation and edema of the dermis develop, followed by the deposition of dermal collagen along the lines of mechanical stress and the flattering of rete pegs.[1,9] Another hypothesis suggests that the formation of SD is related to the reorganization and diminution of dermal elastic fibers network, rather than collagen transformation.[13] Excessive mechanical stretching of the skin determines the rupture of the elastic fibers while the fibroblasts are unable to repair the components of the extracellular matrix.[14] The quality of fibroblasts is also altered in striae, with a reduction in fibronectin, and type I and type III procollagen expression in fibroblasts from SD.[8] The atrophic aspect of SD is determined by the decrease of the amounts of fibrillin surrounding the dermo-epidermal junction and the elastin in the papillary dermis, together with the realignment of elastin and fibrillin fibers in deep dermis.[1,11]

In recent years, ultrasonography emerged as an efficient method to monitor the evolution of skin characteristics after topical products application. Ultrasonographic evaluation of SD reveals a heteroechoic hyperechoic area with the decrease of dermis thickness and an increased heterogeneity and density, showing a morphologic similarity with atrophic scars (Figure 1).

In order to improve SD aspect, multiple therapeutic options exist, but no standard treatment was yet found to cure striae albae with the pathology and associated symptoms.[4,11] For this purpose, numerous topical treatments including tretinoin, glycolic acid, trichloroacetic acids, silicone gel and cosmetic preparations were evaluated,[7,15–19] together with nonpharmacologic interventions, such as microdermabrasion, laser techniques and surgical methods.[20–23] Vitamin C and fruity acids showed positive effects on striae rubrae, together with highly moisturizing preparations. Among the herbal actives, creams with *Centella asiatica* extract, as trofolastin cream, were the most efficient supporting treatment, even in striae gravidarum.

Topical preparations used in the prevention and treatment of the early-stage SD are expected to induce the following processes: increase fibroblastic activity, collagen and fibronectin production, improve blood perfusion and anti-inflammatory properties, and stimulate cell proliferation.[4,19] At a global level, these effects correlate to the skin texture, meaning improved skin hydration and increased elasticity and dermis thickness.

Punica granatum seed oil represents a rich source of conjugated fatty acids (punicic acid), flavonoids and anthocyanidins (delphinidin, cyanidin and pelargonidin) with antioxidant and anti-inflammatory activity and conventionally used for the antiaging effect.[24] According to previous research of *P. granatum* seeds exhibits DPPH free radicals scavenging, the antioxidant activity being three times greater than green tea extract.[25,26] Also, on a human skin cells study, Aslam et al reported that *P. granatum* seed oil stimulates keratinocyte proliferation and induces a mild thickening of the epidermis without the loss of ordered differentiation.[27] In complementary medicine, the effect of *P. granatum* extract in diabetes mellitus and irritable bowel syndrome was investigated.[28,29]

Croton lechleri (Dragon's blood) presents antioxidant, anti-inflammatory and healing properties due mainly to the principal constituents of the resin: proanthocyanidins; taspin, an alkaloid; catechin; epigallocatechin; and epicatechin. Regarding the healing process, previous studies have showed that *C. lechleri* extract stimulates the proliferation and

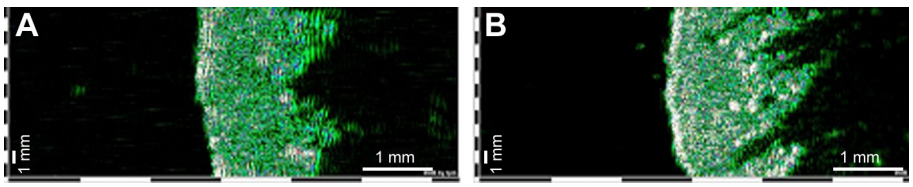


Figure 1 Ultrasonographic aspect of healthy skin (**A**) and skin with stretchmarks (**B**). 22 MHz transducer, B-scan; images from the same individual (Dub®cutis, Lüneburg, Germany). Striae distensae are delineated as low-echogenic bands inside the dermis surrounded by high-echogenic areas.

migration of fibroblasts and also the production of collagen and the epithelial regeneration. There are numerous studies concerning the multitude of medicinal properties of *C. lechleri* extract, such as wound healing, cicatrizing, antibacterial, antiviral, anti-inflammatory and antioxidant activity.[30]

The cosmetic cream represents a complex formulation, where the effect is not only due to the active ingredients but also to emollient ingredients which can improve SD. Emollient ingredients (*Mangifera indica* seed butter and Butyrospermum parkii butter) were incorporated in the formulation for the beneficial effect on improving skin elasticity. As shown in other previous histological studies, elastic fibers represent the primary target in the pathological process of SD. In the incipient phase, mast cell degranulation and macrophage activation lead to release of elastases, followed by alteration of collagen, elastin and fibrillin.[31]

So far, many cosmetic formulations containing herbal extracts were developed for antistretchmark effect, but the proofs supporting their clinical efficacy are limited.[19]

The aim of this research was to obtain a cosmetic cream containing herbal active ingredients with documented antioxidant and anti-inflammatory activity: *P. granatum* seed oil and *C. lechleri* resin extract. First, the cream base formulation was optimized according to a design of experiments (DoE) regarding its viscosity, texture and stability. In a second stage, the two active ingredients were added to the optimal cream base and the efficacy of the final product was investigated in an interventional nonrandomized study. The clinical outcome was assessed through biophysical parameters and ultrasonographic evaluation.

Materials and methods

Materials

Abil® EM 180 (cetyl PEG/PPG-10/1 dimethicone; Evonik Goldschmidt, Essen, Germany), glyceryl stearate (Elemental, Oradea, Romania) and Olliva (cetearyl olivate/sorbitan olivate; Elemental) were chosen as lipophilic surfactants, and Simulgel INS100 (hydroxyethyl acrylate/sodium acryloyldimethyl taurate copolymer and isohexadecane and Polysorbate 60; Seppic, Paris, France) was chosen as the co-surfactant. The cetylstearyl alcohol was supplied by Vitamar (Bucharest, Romania); *B. parkii* butter (shea butter), *M. indica* seed butter (mango butter), glycerin, and Olliva were supplied by Elemental. The other materials used were the following: *P. granatum* seed oil (Elemental), *C. lechleri* resin extract (Aroma-Zone, Paris, France), caprylic/capric triglycerides (Croda, Snaith, UK), Sepigel 305 (polyacrylamide and C13-14 isoparaffin and laureth-7; Seppic), Euxyl PE 9010® (phenoxyethanol and ethylhexylglycerin; Schülke & Mayr, Norderstedt, Germany), and Xiameter® PMX-0246 (cyclohexasiloxane and cyclopentasiloxane; Dow Corning, Midland, MI, USA).

Methods

Experimental design for base formulation

The experimental work was conducted by a D-Optimal DoE with six factors and three levels (Modde 11.0 software; Umetrics, Umea, Sweden). The studied factors were the type of emulsifier (X_1) with three variables: E1 (Abil EM 180), E2 (glyceryl stearate) or E3 (Olliva); the amount of oily phase (g; X_2); the stirring rate (X_3); the stirring time for the emulsification step (X_4); the ratio of surfactant (%; X_5); and the presence of 2% Simulgel INS100 as co-surfactant (X_6). The software generated 18 experimental trials and 3 center points, presented in Table 1.

The dependent variables were firmness (Y_1), consistency (Y_2), adhesive force (Y_3), adhesiveness (Y_4), stringiness (Y_5), stringiness length (Y_6), spreadability (Y_7), viscosity (Y_8), and the physical stability of the creams (Y_9).

Quality-of-fit assessment, coefficient calculation and statistic parameters evaluation were performed with Modde 11.0 software (Umetrics). The data fitting was done using partial least-squares method. To determine the influence of each factor on the properties of the emulsions, the results

Table 1 Experimental design matrix

Exp	X_1	X_2 (g)	X_3 (rpm)	X_4 (min)	X_5 (%)	X_6
N1	E1	19	500	5	1.50	Yes
N2	E1	28.5	1,000	10	2	Yes
N3	E1	38	1,500	15	3	Yes
N4	E2	19	500	10	2	Yes
N5	E2	28.5	1,000	15	2.50	Yes
N6	E2	38	1,500	5	1	Yes
N7	E3	19	1,000	5	3	Yes
N8	E3	28.5	1,500	10	2	Yes
N9	E3	38	500	15	2.5	Yes
N10	E1	19	1,500	15	2	No
N11	E1	28.5	500	5	2.5	No
N12	E1	38	1,000	10	1.5	No
N13	E2	19	1,000	5	1	No
N14	E2	28.5	1,500	5	1.5	No
N15	E2	38	500	10	2.5	No
N16	E3	19	1,500	10	3	No
N17	E3	28.5	500	15	2	No
N18	E3	38	1,000	10	2.5	No
N19	E1	28.5	1,000	10	2	Yes
N20	E1	28.5	1,000	10	2	Yes
N21	E1	28.5	1,000	10	2	Yes

Abbreviations: Exp, experiment; E1, surfactant Abil EM 180; E2, surfactant glyceryl stearate; E3, surfactant Olliva; X_1, emulsifier type; X_2, amount of oily phase; X_3, stirring rate; X_4, time of stirring; X_5, ratio of the surfactant; X_6, the use of a co-surfactant (yes/no).

were evaluated by means of statistical analysis using analysis of variance (ANOVA) test.

Based on the experimental design results, an optimal formulation was generated using the same software, by applying a set of constraints for each of the responses. The model validity was assessed by comparing the obtained results with the ones predicted by the program.

Cream preparation

The cream was prepared by heating separately the aqueous phase (Sepigel 305, Euxyl PE 9010, glycerol and distilled water) and the oily phase (cetylstearyl alcohol, *B. parkii* butter, *M. indica* seed butter, caprylic/capric triglycerides and Xiameter PMX-0246) containing the surfactants (E1, E2, or E3 in the proportions indicated in Table 1). The aqueous phase was added in the oily phase under continuous stirring (DLS Stirrer; Velp Scientifica, Usmate, Italy) at controlled temperature (50°C±2°C). The active ingredients were added in the oily and aqueous phase, depending on their solubility.

Characterization of creams

Viscosity (Y_8)

Viscosity measurements were performed at 50 rpm using a rotational rheometer DV-III Ultra (Brookfield Engineering Laboratories, Middleborough, MA, USA), equipped with cylindrical spindle 64. The measurements were carried out in triplicate at 22°C±2°C, and mean viscosities ± standard deviation were reported.

Texture analysis (Y_1–Y_7)

CT3 Texture Analyzer (Brookfield Engineering Laboratories) was used for texture profile determination, following the methods listed in Table 2 for each of the following parameters: firmness, consistency, adhesive force, adhesiveness, stringiness, stringiness length and spreadability. Compression test type was used with TA-BT-KIT fixture, having a specified distance as target (Table 2). Both the test speed and the post-test speed were 2 mm/s. The results were recorded using Texture ProCT Software 1.5 (Brookfield Engineering Laboratories). For each formulation, three measurements were carried out, and the mean ± standard deviation was reported.

Table 2 Texture analyzer settings and test methods used for the calculated parameters

Texture parameter	Probe	Target value (mm)	Trigger load (g)
Firmness (g)	TA-DEC	25	10
Consistency (mJ)	TA-DEC	25	10
Adhesive force (g)	TA-SF	15	2
Adhesiveness (mJ)	TA-SF	15	2
Spreadability (g)	TA-SF	15	2
Stringiness work done (mJ)	TA-10	25	10
Stringiness length (mm)	TA-10	25	10

Physical stability evaluation (Y_9)

The physical stability of the creams was evaluated after storage under standardized test conditions at 25°C±2°C for 60 days. The stability of the disperse system was assessed by visual observation using a 5-point scale where: 1 = stable homogeneous emulsion system and 5 = system where breakdown processes such as creaming or coalescence occurred.

In vivo cream efficacy evaluation

Study design

Subjects

An interventional, nonrandomized study, approved by the Research Ethics Committee of the Iuliu Haţieganu University of Medicine and Pharmacy (clinical trial registration number: 244; date of approval: June 9, 2016) was carried out on 20 healthy female volunteers aged between 21 and 48 years, divided into two subgroups: 10 volunteers with striae albae at the hip level and 10 volunteers with no stretchmarks on the test area. The in vivo study aimed to observe the clinical changes at the epidermis and dermis level both in case of already defined striae and in case of no striae on the area of interest.

Before enrolling in the study, every subject was informed about the purpose of the study and signed an informed consent. The cosmetic cream was applied once daily, on the hip area, for a period of 6 weeks. During the study, each volunteer used the same hygiene product and no other cosmetic cream was applied on the tested areas.

The instrumental measurements (skin hydration level, skin elasticity and thickness of the dermis) were performed at the beginning of the study (T_0), after 3 weeks (T_1) and at the end of the study – after 6 weeks (T_2). The volunteers were preconditioned in the test room for at least 15 minutes before the measurements.

Ultrasound scanning

The ultrasonographic evaluation was performed using Dub®cutis skinscanner system (Taberna pro medicum, Lüneburg, Germany), a high-resolution ultrasound scanner using a 22-MHz transducer that allows visualizing structures up to 6–7 mm in depth, including epidermis, dermis and partially subcutaneous fatty tissue.

Biophysical parameter measurements

Skin hydration values and elasticity measurements were recorded using Multi Probe Adapter (MPA Systems) (Courage + Khazaka Electronic GmbH, Köln, Germany) equipped with the probes Corneometer® CM 825 (stratum corneum hydration) and Cutometer® dual MPA 580 (viscoelasticity of the skin).

Results and discussion

Experimental design

Table 3 presents the matrix of the responses analyzed in the experimental plan. The validity of the experimental design was checked, and the results obtained after data fitting showed that the results fit the models. Partial least-squares method was applied to fit the experimental results to the model, and the statistical parameters R^2, Q^2 and model validity were calculated (Table 4).

ANOVA was performed to evaluate model significance (Table 4). All models were significant since *P*-value was <0.05 and lack of fit was not significant ($P>0.05$).

R^2 is a measure of how well the regression model fits the experimental data. The closer the correlation values are to 1, the better is the developed model and its prediction. Our results showed a good fit for each of the responses, with values over 0.6, which indicates high model significance. The validity parameter shows if the appropriate type of model was chosen; in our case, the validity was good for all responses. Reproducibility, which reflects experimental variability, attained high values, between 0.782 and 0.971.

Influence of independent variables on the texture analysis parameters

Texture analysis involves the compression of a sample using a certain probe, at a constant predetermined rate. The product resistance is recorded as load values versus distance or time. Each compression cycle results in a graphical representation of the load (g) as a function of time (s); all the texture describing parameters can be calculated directly from the texture profile plot, using appropriate mathematical equations.

The maximum force on the graph measures firmness (Y_1), whereas the area under the positive part of the graph indicates the consistency (Y_2) of the sample (Figure 2A). Spreadability of the samples was (Y_7) recorded while the cone probe was forced down into the conical sample holder filled with the cream. The firmness of the sample measured as the maximum force on the graph indicates the spreadability of the sample (Figure 2B). The negative part of the plot is generated while the probe returns to the starting point and the maximum negative force of the compression cycle is

Table 3 Matrix of responses

	Firmness (g) (Y_1)	Consistency (mJ) (Y_2)	Adhesive force (g) (Y_3)	Adhesiveness (mJ) (Y_4)	Stringiness work done (mJ) (Y_5)	Stringiness length (Y_6)	Spreadability (g) (Y_7)	Viscosity (cP) (Y_8)	Stability (Y_9)
N1	1,045.30±36.70	212.26±7.77	191.80±32.20	8.72±0.56	0.66±0.10	3.72±0.21	313.80±42.70	102,800±1,744	2.00
N2	1,361.00±23.50	281.97±9.20	207.70±65.30	9.30±0.86	2.17±0.22	9.88±2.08	355.30±89.20	133,200±6,548	3.00
N3	1,233.00±118.60	250.53±18.28	284.80±40.10	8.32±1.32	1.18±0.03	8.33±0.42	494.20±83.40	80,600±2,163	2.00
N4	1,941.20±157.40	367.57±24.01	179.00±25.90	9.91±1.45	4.54±0.24	18.03±2.02	331.50±39.50	68,933±3,172	1.00
N5	2,477.80±58.40	425.51±11.37	142.20±27.30	3.01±0.51	6.97±1.23	16.48±2.54	551.70±122.30	67,867±4,601	3.00
N6	2,468.50±27.50	476.99±35.68	138.70±7.80	2.98±0.40	6.76±1.29	13.31±3.30	498.50±47.30	47,867±6,839	4.00
N7	1,453.00±80.20	290.32±13.53	135.00±12.70	6.29±1.90	4.55±0.43	23.76±1.33	282.30±8.60	47,067±4,549	2.00
N8	2,093.30±83.00	433.09±14.95	112.80±27.20	2.62±0.34	8.23±1.50	20.37±2.71	411.80±68.40	57,333±1,155	3.00
N9	2,615.00±156.60	530.71±42.27	103.70±13.70	2.35±0.63	8.06±0.13	21.2±1.21	359.20±12.90	35,800±2,307	3.00
N10	1,033.50±30.04	170.71±12.73	229.00±42.50	6.65±0.81	0.55±0.08	3.04±0.51	334.50±61.70	10,7067±5,001	1.00
N11	993.50±42.30	200.06±14.08	212.80±60.30	7.62±0.11	1.57±0.37	7.22±0.85	334.80±86.50	74,533±2,626	2.00
N12	1,183.50±54.70	243.66±16.58	179.80±34.20	8.79±0.73	1.79±0.34	5.53±0.23	336.80±51.60	86,600±1,249	2.00
N13	2,230.70±205.30	419.03±46.58	160.50±12.80	9.80±0.74	1.76±0.29	6.59±0.75	241.80±21.50	125,333±7,943	1.00
N14	1,741.30±73.90	308.65±6.71	159.30±33.20	8.74±1.16	0.87±0.18	2.47±0.35	282.50±44.20	75,467±3,029	2.00
N15	2,128.70±135.40	404.51±28.40	168.80±64.80	5.31±2.91	4.56±0.63	10.04±1.17	377.80±27.50	35,200±6,437	3.00
N16	1,715.80±241.30	312.25±35.92	82.50±9.20	5.12±0.42	2.66±3.50	0.23±0.06	191.30±14.80	67,867±3,802	1.00
N17	2,362.50±117.70	477.92±27.15	95.00±9.70	5.31±0.54	4.49±0.28	17.8±2.76	247.50±22.30	79,933±8,556	1.00
N18	2,229.70±26.40	379.78±44.92	87.00±8.20	2.33±0.26	6.68±0.43	21.2±1.20	245.30±16.60	41,200±4,970	3.00
N19	1,025.00±58.70	203.00±11.04	242.70±38.50	7.30±0.72	0.75±0.06	8.1±1.14	391.50±54.40	105,333±3,802	2.50
N20	1,258.00±15.60	259.72±23.43	192.70±22.30	8.41±0.24	2.93±0.14	0.14±0.02	320.30±31.40	126,233±4,306	3.00
N21	1,408.00±17.05	301.00±14.72	244.70±37.30	9.05±1.11	1.68±0.09	8.87±0.37	409.00±58.80	119,267±2,386	3.50

Notes: Y_1, firmness; Y_2, consistency; Y_3, adhesive force; Y_4, adhesiveness; Y_5, stringiness; Y_6, stringiness length; Y_7, spreadability; Y_8, viscosity; Y_9, physical stability (mean ± SD).
Abbreviation: Exp, experiment.

Table 4 Statistical parameters – ANOVA test

Response	SS	*df*	MS (variance)	*F*	*P*-value	Lack of fit	R^2	Q^2	Model validity
Y_1	6.79E+07	21	3.23E+06	24.2954	0	0.298	0.859	0.756	0.697
Y_2	2.52E+06	21	119,854	17.2079	0	0.408	0.811	0.688	0.775
Y_3	663,238	21	31,582.7	19.6317	0	0.67	0.867	0.731	0.900
Y_4	1,033.86	21	49.2316	8.99197	0.001	0.178	0.613	0.404	0.569
Y_5	389.273	21	18.5368	16.441	0	0.287	0.804	0.673	0.687
Y_6	3,537.78	21	168.466	6.97795	0.001	0.523	0.699	0.352	0.838
Y_7	2.71E+06	21	129,028	9.21479	0	0.278	0.697	0.489	0.680
Y_8	1.54E+11	21	7.34E+009	8.71337	0	0.266	0.789	0.552	0.668
Y_9	126.5	21	6.02381	14.838	0	0.352	0.724	0.58	0.739

Abbreviations: ANOVA, analysis of variance; SS, sum of squares; *df*, degrees of freedom; MS, mean of square; *F*, Fischer's ratio; R^2, regression coefficient; Q^2, predictive power of the model.

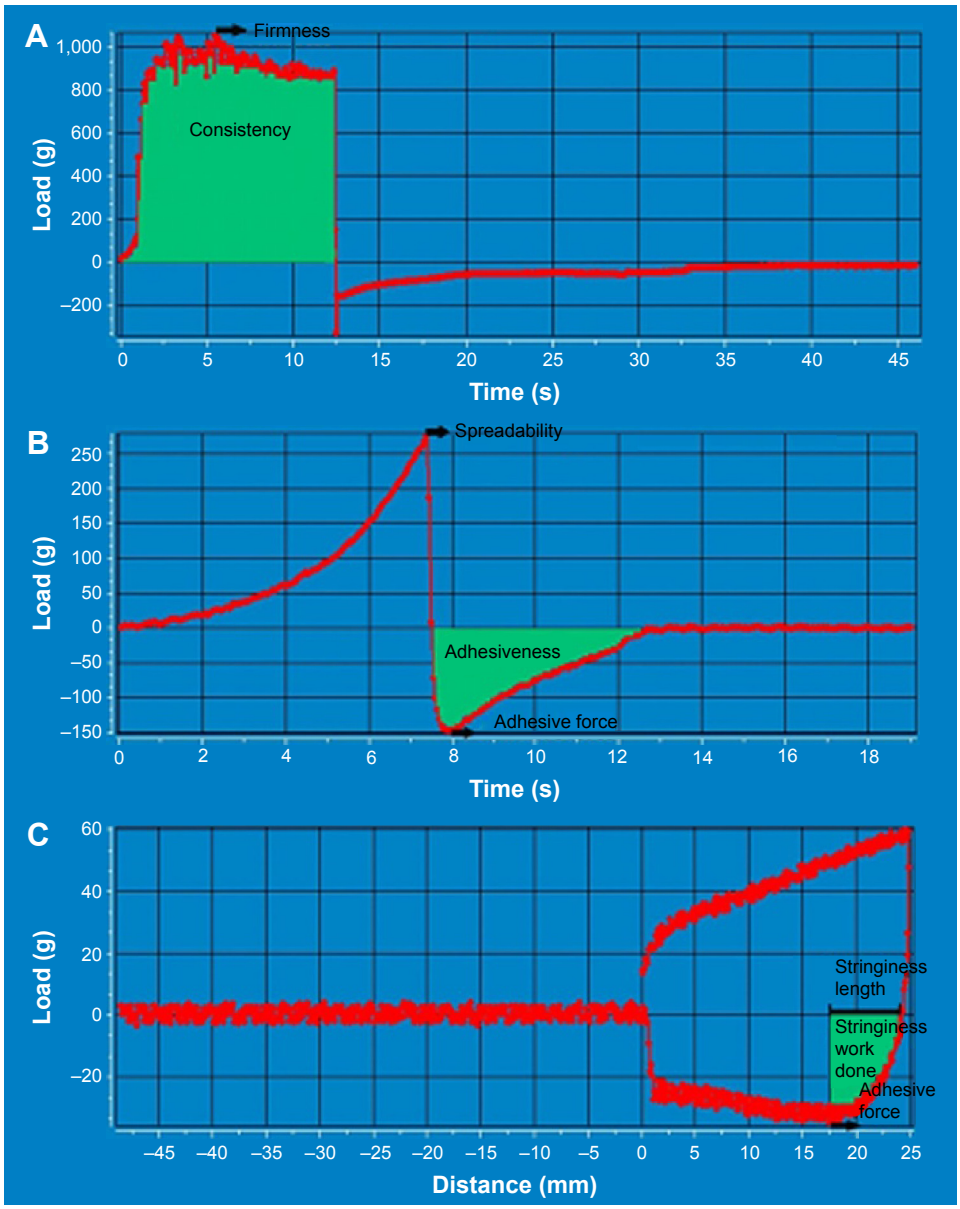


Figure 2 Texture analysis plot showing calculations for (**A**) firmness and consistency, (**B**) spreadability, adhesive force and adhesiveness and (**C**) stringiness and stringiness length.

considered as adhesive force (Y_3), while the area under the negative part leads to the adhesiveness value (Y_4). Stringiness (Y_5) of the sample is calculated as the area under the load versus distance curve, measured from where cycle one reaches zero load, to the adhesive force. Stringiness length (Y_6) represents the distance from the zero load to the adhesive force (Figure 2C).

Revised models (Table 5) were developed to evaluate the effects of independent variables for each response, based on the regression coefficient values and signs ("+" for positive influence and "–" for negative influence).

The firmness of the creams ranged between 993.50±42.30 and 2,615.00±156.60 g, whereas the consistency ranged between 170.71±12.73 and 530.71±42.27 mJ. Y_1 and Y_2 were mainly influenced by the type of emulsifying agent (X_1) and the oily phase amount (X_2). The use of E1, a liquid emulsifier, had a negative influence on the firmness and consistency values, whereas E2 and E3 (solid waxy emulsifiers) increased Y_1 and Y_2 values. The formulations with a high ratio of shea butter and mango butter in the oily phase also increased the load profile due to the solid emollients added.

Previous studies confirmed that between texture analysis and sensory characteristics exist direct correlations, and the sensory profile of a cosmetic product could be predicted through instrumental assessments.[32] Adhesive properties define the sensory attributes of the cosmetic cream and influence consumers' acceptance, while the spreadability also influences the efficacy of the cosmetic product. In our study, adhesive force (Y_3), adhesiveness (Y_4) and spreadability (Y_7) were significantly influenced by the type of emulsifying agent (E1 enhanced the adhesive properties, whereas E3 led to less sticky formulations). Spreadability was favored by a higher emulsifying agent content, especially E2 and also by adding of the co-surfactant.

Stringiness (Y_5 and Y_6) of the creams is correlated with filament-stretching properties and influences the easy pick-up of the cosmetic product from the container. In the current study, stringiness was influenced by E3, the co-surfactant and a high level of lipophilic phase. The viscosity (Y_8) varied between and was mainly influenced by emulsifying agent type and ratio. E1 determined higher viscosity values, whereas E3 determined lower ones.

A high percentage of lipophilic phases and the presence of the co-surfactant improved the stability (Y_9) of the emulsions, but apparently, long processing times led to less stable products. Stirring time usually increases emulsions stability, up to an optimal value that when exceeded can produce system creaming.

Cream optimization

The sensation produced after the topical application of a cosmetic product is an important factor for the consumer preference. Consumer acceptability and the efficacy of topical products involve optimal mechanical properties (firmness), appropriate adhesiveness and a good spreadability.[33]

To achieve an optimal formulation regarding the stability and the sensorial characteristics, an optimization process was carried out. The conditions selected were the following: the spreadability and the stability were maximized, the firmness and the adhesiveness were minimized and the consistency was maintained at a medium value. The experimental conditions and the qualitative and quantitative parameters for the optimal formulation are shown in Table 6.

For the optimal formulation, the experimental data revealed a good correlation between the predicted model

Table 5 The revised quantitative factor effects of the responses

Factor	Firmness (g) (Y_1)	Consistency (mJ) (Y_2)	Adhesive force (g) (Y_3)	Adhesiveness (mJ) (Y_4)	Stringiness work done (mJ) (Y_5)	Stringiness length (Y_6)	Spreadability (g) (Y_7)	Viscosity (cP) (Y_8)	Stability (Y_9)
Constant	1,804.71[a]	346.75[a]	159.69[a]	6.26[a]	3.72[a]	11.22[a]	339.53[a]	763.12[a]	2.22[a]
X_1 (E1)	–633.51[a]	–110.87[a]	58.64[a]	1.89[a]	–2.56[a]	–6.13[a]	8.87	276.47[a]	–
X_1 (E2)	359.99[a]	53.62[a]	–1.61	0.36	0.51	–0.07	41.09[a]	–62.01	–
X_1 (E3)	273.51[a]	57.25[a]	–57.03[a]	–2.25[a]	2.05	6.20[a]	–49.97[a]	–214.45[a]	–
X_2	203.24[a]	42.83[a]	–	–1.36[a]	1.19[a]	2.02	51.38[a]	–159.83[a]	0.75[a]
X_3	–	–	–	–	–	–2.52	–	32.49	–
X_4	–	–	7.55	–	–	–	–	89.72	–0.33[a]
X_5	–115.16	–31.64[a]	12.29	–	–	–	–	–105.61[a]	–
X_6 (yes)	–	–	6.95	–	0.95[a]	2.98[a]	51.50[a]	–	0.44[a]
X_6 (no)	–	–	–6.95	–	–0.95[a]	–2.98[a]	–51.50[a]	–	–0.44[a]

Note: [a]Statistically significant effects ($P<0.05$).

Abbreviations: E1, surfactant Abil EM 180; E2, surfactant glyceryl stearate; E3, surfactant Olliva; X_1, emulsifier type; X_2, amount of oily phase; X_3, stirring rate; X_4, time of stirring; X_5, ratio of the surfactant; X_6, the use of a co-surfactant.

Table 6 Experimental conditions for the optimal formulation

Factor	Optimal level
X_1	E3
X_2	–0.5190
X_3	0.9983
X_4	0.9880
X_5	–0.9974
X_6	No
Ingredients	**Amount (%)**
Cetylstearyl alcohol	2.48
Mangifera indica seed butter	6.20
Butyrospermum parkii butter	6.20
Caprylic/capric triglycerides	6.20
Xiameter® PMX-0246	2.48
Olliva	2.00
Sepigel 305	1.50
Euxyl PE 9010®	1.00
Glycerol	5.00
Distilled water	to 100

Abbreviations: E3, surfactant Olliva; X_1, emulsifier type; X_2, amount of oily phase; X_3, stirring rate; X_4, time of stirring; X_5, ratio of the surfactant; X_6, the use of a co-surfactant.

and the experimental values, thus indicating the validity of the proposed model (data not shown).

An oil-in-water cream containing Olliva (2%) as emulsifying agent and 23.56% oily phase was obtained using following process parameters: stirring rate – 1,500 rpm and stirring time –15 min. The active ingredients *P. granatum* seed oil (4%) and *C. lechleri* resin extract (3%) were incorporated in the optimal formulation, and the potential effect on preventing or improving SD was investigated.

In vivo efficacy study

In vivo efficacy study was carried out on 20 volunteers to observe the skin characteristics comparatively, before and after the treatment. Preclinical studies on animals were also considered, but there is no animal model for SD and this skin condition cannot be induced experimentally. Considering the mechanism of action of the ingredients from the cosmetic formulation, hydration and elasticity level of the skin and thickness of the dermis have been assessed to evaluate the clinical changes.

Figure 3 shows comparative ultrasonographic images of the skin at baseline (A), after 3 weeks (B) and after 6 weeks of cream application (C). Statistical analysis highlighted a significant increase in dermis thickness at the end of the study (Figure 4) in both subgroups. Ultrasound investigation of the skin revealed new echogenic areas instead of SD and also an improved acoustic homogeneity of the dermis.

Statistical analysis also demonstrated positive results on hydration and elasticity levels of the skin in both subgroups. Mean values and standard deviation are represented in Figures 5 and 6.

In vivo clinical study revealed significant skin changes of the dermis thickness, hydration and elasticity of stratum corneum. For the SD subgroup, the increase in dermis thickness was 14.85%, the hydration increased 30.32% and the elasticity increased 9.75% from baseline. The subjective self-assessment of the volunteers indicated that, after 6 weeks of cream application, striae become less defined and less depressed.

In case of the subgroup with no SD, the increase in dermis thickness was 15.86%, whereas hydration and elasticity increased from baseline, 38.40% and 5.86%, respectively. The volunteers also noticed an improved appearance of the skin. The results obtained in both subgroups suggest that it is possible to minimize or prevent the skin alterations which appear in SD.

Even if there are a large number of marketed topical products, no standard treatment exists for the management of SD. An increase in the elasticity of connective tissue represents one of the main goals of the antistriae formulations. Other topical formulations for SD present different mechanisms of action, which include the increasing collagen

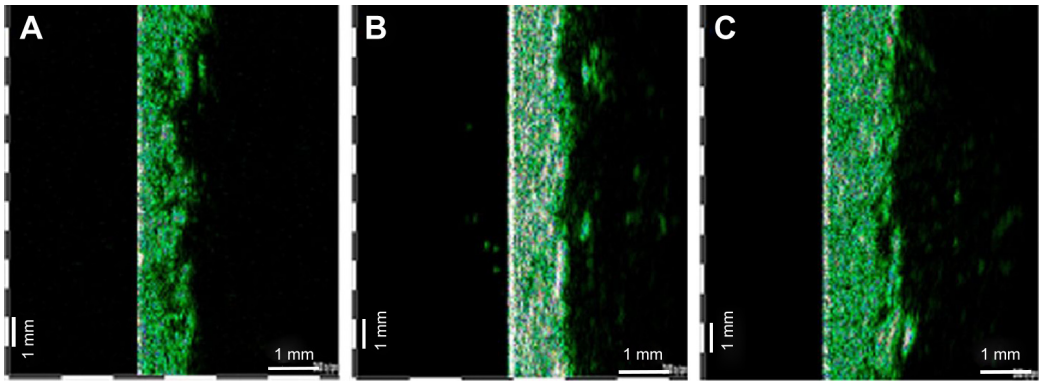


Figure 3 Ultrasonographic aspect of SD before (**A**), after 3 weeks (**B**) and after 6 weeks (**C**) of cream application- 22 MHz transducer, B-scan.
Abbreviation: SD, striae distensae.

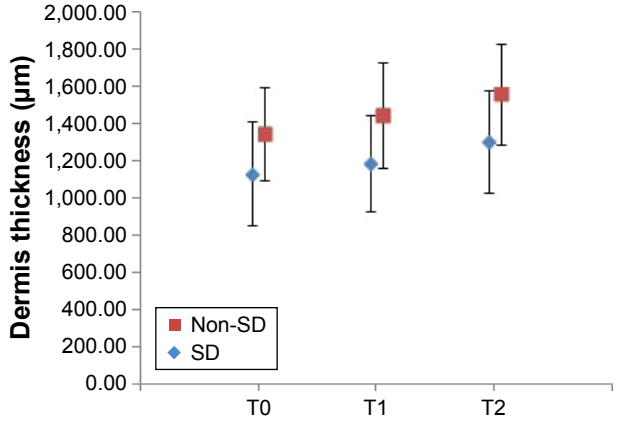


Figure 4 Relative changes in dermis thickness values during the study (mean ± standard deviation).
Notes: T0 – baseline determination, T1 – after 3 weeks, T2 – after 6 weeks of cream application; non-SD – subgroup without striae (N=10, *P*=0.0000486709), SD – subgroup with striae (N=10, *P*=0.00004455191).
Abbreviation: SD, striae distensae.

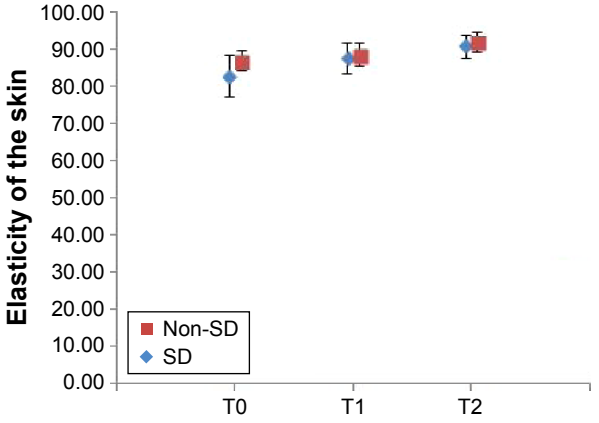


Figure 6 Relative changes in the elasticity of the skin during the study (mean ± standard deviation).
Notes: T0 – baseline determination, T1 – after 3 weeks, T2 – after 6 weeks of cream application; non-SD – subgroup without striae (N=10, *P*=0.0017748), SD – subgroup with striae (N=10, *P*=0.000067221).
Abbreviation: SD, striae distensae.

production, anti-inflammatory effects as well as rehydration of the skin.[4]

Although numerous studies showed multiple advantages of some topical products recommended for SD, there is limited evidence that topical therapy can thoroughly eradicate the lesions. Moreover, only a few studies are supported by high-quality controlled trials to demonstrate antistriae efficacy.[24] In one of those trials, a double-blind controlled study, Ud-Din et al reported an improving SD albae and SD rubrae after 6 weeks of topical application of a silicone gel. They evaluated the clinical efficacy with noninvasive devices, histologically, and the preliminary findings revealed a decrease in the vascularity, hemoglobin, pliability, collagen and an increase in the pigmentation.[7]

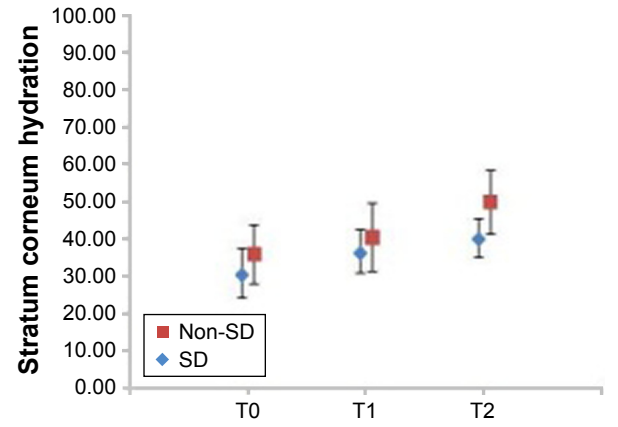


Figure 5 Relative changes of stratum corneum hydration level during the study (mean ± standard deviation).
Notes: T0 – baseline determination, T1 – after 3 weeks, T2 – after 6 weeks of cream application; non-SD – subgroup without striae (N=10, *P*=0.000109062), SD – subgroup with striae (N=10, *P*=0.0000332375).
Abbreviation: SD, striae distensae.

In another study, Bleve et al carried out a clinical trial to monitor SD maturation and to evaluate their changes after the topical treatment with a marketed commercial product. The evaluation of topical treatment efficacy was performed using ultrasound scanning and Primos system, and the results showed that after 2 months of treatment only striae rubra were treated successfully.[1]

In all those cases, the topical products were applied by local massage on SD and it is difficult to establish the influence of the massage on the improvement of striae. Timur Taşhan and Kafkasli evaluated the application of almond oil with or without massage therapy and demonstrated that almond oil applied through a 15-minute massage reduced the development of striae gravidarum, whereas the use of almond oil without massage had no effect.[34]

As well, various vegetal oils have been evaluated for their beneficial effect in SD, the most commonly investigated being olive oil. The results of the study noticed no significant difference in development or severity of SD between treatment and control groups.[35–37]

The results of the present study are in accordance with those presented in similar research.[35–37] Although the topical application of the tested cosmetic cream improved skin parameters (dermis thickness, hydration and elasticity), the repairing process is incomplete since the changes in SD are irreversible. Therefore, the most appropriate approach in SD management is prophylaxis.

To our knowledge, this is the first study reported in the literature which evaluates the antistriae effect of a formulation containing *P. granatum* seed oil and *C. lechleri* resin extract. The results are supported by an interventional

nonrandomized clinical study, where the changes were evaluated both in volunteers with SD or on healthy skin. In addition, the use of DoE provides a new approach to the cosmetic formulation which overcomes the deficiencies of traditional formulation methods to obtain a cosmetic product with desired characteristics using a minimal number of experimental runs.

Conclusion

An emollient oil-in-water cream containing *P. granatum* seed oil and *C. lechleri* resin extract was formulated. The experimental design was successfully used to set the best ranges for the technological and formulation factors to obtain a cosmetic formulation with optimal characteristics. The study of clinical efficacy on the optimal formulation revealed an increase in the dermis thickness, hydration and elasticity values, suggesting that it can be helpful in prevention or improving skin changes associated with *striae*.

Acknowledgments

The authors gratefully acknowledge Sanorama Company, Cluj-Napoca, Romania, for allowing the use of the ultrasound equipment and Farmec Company, Cluj-Napoca, Romania, for the substances supplied. This research was financially supported by the University of Medicine and Pharmacy, Cluj-Napoca, Romania, Grant 1495/7/28.01.2014.

Disclosure

The authors report no conflicts of interest in this work.

References

1. Bleve M, Capra P, Pavanetto F, Perugini P. Ultrasound and 3D skin imaging: methods to evaluate efficacy of striae distensae treatment. *Dermatol Res Prat*. 2012;2012:673706.
2. Hermanns JF, Piérard GE. High-resolution epiluminescence colorimetry of striae distensae. *J Eur Acad Dermatol Venereol*. 2006;20(3):282–287.
3. Cordeiro RC, Zecchin KG, de Moraes AM. Expression of estrogen, androgen, and glucocorticoid receptors in recent striae distensae. *Int J Dermatol*. 2010;49(1):30–32.
4. Brennan M, Young G, Devane D. Topical preparations for preventing stretch marks in pregnancy. *Cochrane Database Syst Rev*. 2012;11:CD000066.
5. Pierard-Franchimont C, Hermanns JF, Hermanns-Le T, Piérard GE. Striae distensae in darker skin types: the influence of melanocyte mechanobiology. *J Cosmet Dermatol*. 2005;4(3):174–178.
6. Al-Himdani, Ud-Din S, Gilmore S, Bayat A. Striae distensae: a comprehensive review and evidence-based evaluation of prophylaxis and treatment. *Br J Dermatol*. 2014;170(3):527–547.
7. Ud-Din S, McAnelly SL, Bowring A, et al. A double-blind controlled clinical trial assessing the effect of topical gels on striae distensae (stretch marks): a non-invasive imaging, morphological and immunohistochemical study. *Arch Dermatol Res*. 2013;305(7):603–617.
8. Gilmore SJ, Vaughan BL Jr, Madzvamuse A, Maini PK. A mechanochemical model of striae distensae. *Math Biosci*. 2012;240(2):141–147.
9. Hengge UR, Ruzicka T, Schwartz RA, Cork MJ. Adverse effects of topical glucocorticosteroids. *J Am Acad Dermatol*. 2006;54(1):1–15.
10. Yosipovitch G, DeVore A, Dawn A. Obesity and the skin: skin physiology and skin manifestations of obesity. *J Am Acad Dermatol*. 2007;56(6):901–916.
11. Nussbaum R, Bendetto AV. Cosmetic aspects of pregnancy. *Clin Dermatol*. 2006;25:133–141.
12. Kasielska-Trojan A, Sobczak M, Antoszewski B. Risk factors of striae gravidarum. *Int J Cosmet Sci*. 2015;37(2):236–240.
13. Watson RE, Parry EJ, Humphries JD, et al. Fibrillin microfibrils are reduced in skin exhibiting striae distensae. *Br J Dermatol*. 1998;138(6):931–937.
14. Mitts TF, Jimenez F, Hinek A. Skin biopsy analysis reveals predisposition to stretch mark formation. *Aesthet Surg J*. 2005;25(6):593–600.
15. Rangel O, Arias I, García E, Lopez-Padilla S. Topical tretinoin 0.1% for pregnancy-related abdominal striae: an open-label, multicenter, prospective study. *Adv Ther*. 2001;18(4):181–186.
16. Adatto MA, Deprez P. Striae treated by a novel combination treatment–sand abrasion and a patent mixture containing 15% trichloracetic acid followed by 6–24 hrs of a patent cream under plastic occlusion. *J Cosmet Dermatol*. 2003;2(2):61–67.
17. Mazzarello V, Farace F, Ena P, et al. A superficial texture analysis of 70% glycolic acid topical therapy and striae distensae. *Plast Reconstr Surg*. 2012;129(3):589e–590e.
18. Summers B, Lategan M. The effect of a topically-applied cosmetic oil formulation on striae distensae. *SA Fam Pract*. 2009;51:332–336.
19. Ud-Din S, McGeorge D, Bayat A. Topical management of striae distensae (stretch marks): prevention and therapy of striae rubrae and albae. *J Eur Acad Dermatol Venereol*. 2016;30(2):211–222.
20. Karimipour DJ, Kang S, Johnson TM, et al. Microdermabrasion: a molecular analysis following a single treatment. *J Am Acad Dermatol*. 2005;52(2):215–223.
21. Suh DH, Chang KY, Son HC, Ryu JH, Lee SJ, Song KY. Radiofrequency and 585-nm pulsed dye laser treatment of striae distensae: a report of 37 Asian patients. *Dermatol Surg*. 2007;33(1):29–34.
22. Trelles MA, Levy JL, Ghersetich I. Effects achieved on stretch marks by a nonfractional broadband infrared light system treatment. *Aesthetic Plast Surg*. 2008;32(3):523–530.
23. Al-Dhalimi MA, Abo Nasyria AA. A comparative study of the effectiveness of intense pulsed light wavelengths (650 nm vs 590 nm) in the treatment of striae distensae. *J Cosmet Laser Ther*. 2013;15(3):120–125.
24. Jadoon S, Karim S, Bin Asad MH, et al. Anti-aging potential of phytoextract loaded-pharmaceutical creams for human skin cell longetivity. *Oxid Med Cell Longev*. 2015;2015:709628.
25. Singh RP, Chidambara Murthy KN, Jayaprakasha GK. Studies on the antioxidant activity of pomegranate (*Punica granatum*) peel and seed extracts using in vitro models. *J Agric Food Chem*. 2002;50(1):81–86.
26. Rahimi HR, Arastoo M, Ostad SN. A comprehensive review of *Punica granatum* (Pomegranate) properties in toxicological, pharmacological, cellular and molecular biology researches. *Iran J Pharm Res*. 2012;11(2):385–400.
27. Aslam MN, Lansky EP, Varani J. Pomegranate as a cosmeceutical source: pomegranate fractions promote proliferation and procollagen synthesis and inhibit matrix metalloproteinase-1 production in human skin cells. *J Ethnopharmacol*. 2006;103(3):311–318.
28. Lauche R, Kumar S, Hallmann J, et al. Efficacy and safety of ayurvedic herbs in diarrhoea-predominant irritable bowel syndrome: a randomised controlled crossover trial. *Complement Ther Med*. 2016;26:171–177.
29. Ceylan S, Azal O, Taşlipinar A, Türker T, Açikel CH, Gulec M. Complementary and alternative medicine use among Turkish diabetes patients. *Complement Ther Med*. 2009;17(2):78.
30. Namjoyan F, Kiashi F, Moosavi ZB, Saffari F, Makhmalzadeh BS. Efficacy of Dragon's blood cream on wound healing: a randomized, double-blind, placebo-controlled clinical trial. *J Tradit Complement Med*. 2015;6(1):37–40.

31. Sheu HM, Yu HS, Chang CH. Mast cell degranulation and elastolysis in the early stage of striae distensae. *J Cutan Pathol*. 1991;18:410–416.
32. Gilbert L, Savary G, Grisel M, Picard C. Predicting sensory texture properties of cosmetic emulsions by physical measurements. *Chemometr Intell Lab Syst*. 2013;124:21–31.
33. Estanqueiro M, Amaral MH, Sousa Lobo JM. Comparison between sensory and instrumental characterization of topical formulations: impact of thickening agents. *Int J Cosmet Sci*. 2016;38(4):389–398.
34. Timur Taşhan S, Kafkasli A. The effect of bitter almond oil and massaging on striae gravidarum in primiparaous women. *J Clin Nurs*. 2012;21(11–12):1570–1576.
35. Soltanipour F, Delaram M, Taavoni S, Haghani H. The effect of olive oil and the Saj® cream in prevention of striae gravidarum: a randomized controlled clinical trial. *Complement Ther Med*. 2014;22(2):220–225.
36. Soltanipoor F, Delaram M, Taavoni S, Haghani H. The effect of olive oil on prevention of striae gravidarum: a randomized controlled clinical trial. *Complement Ther Med*. 2012;20(5):263–266.
37. Taavoni S, Soltanipour F, Haghani H, Ansarian H, Kheirkhah M. Effects of olive oil on striae gravidarum in the second trimester of pregnancy. *Complement Ther Clin Pract*. 2011;17(3):167–169.

Drug Design, Development and Therapy

Dovepress

Publish your work in this journal

Drug Design, Development and Therapy is an international, peer-reviewed open-access journal that spans the spectrum of drug design and development through to clinical applications. Clinical outcomes, patient safety, and programs for the development and effective, safe, and sustained use of medicines are the features of the journal, which has also been accepted for indexing on PubMed Central. The manuscript management system is completely online and includes a very quick and fair peer-review system, which is all easy to use. Visit http://www.dovepress.com/testimonials.php to read real quotes from published authors.

Submit your manuscript here: http://www.dovepress.com/drug-design-development-and-therapy-journal

antioxidants

MDPI

Review

Research Advances in the Use of Bioactive Compounds from *Vitis vinifera* By-Products in Oral Care

Cătălina Bogdan [1], Anca Pop [2,*], Sonia M. Iurian [3], Daniela Benedec [4] and Mirela L. Moldovan [1]

[1] Department of Dermopharmacy and Cosmetics, Faculty of Pharmacy, "Iuliu Haţieganu" University of Medicine and Pharmacy, 12 I. Creangă Street, 400010 Cluj-Napoca, Romania; catalina.bogdan@umfcluj.ro (C.B.); mmoldovan@umfcluj.ro (M.L.M.)

[2] Department of Toxicology, Faculty of Pharmacy, "Iuliu Haţieganu" University of Medicine and Pharmacy, 6 L. Pasteur Street, 400349 Cluj-Napoca, Romania

[3] Department of Pharmaceutical Technology and Biopharmacy, Faculty of Pharmacy, "Iuliu Haţieganu" University of Medicine and Pharmacy, 41 V. Babeş Street, 400012 Cluj-Napoca, Romania; sonia.iurian@umfcluj.ro

[4] Department of Pharmacognosy, Faculty of Pharmacy, "Iuliu Haţieganu" University of Medicine and Pharmacy, 12 I. Creangă Street, 400010 Cluj-Napoca, Romania; dbenedec@umfcluj.ro

* Correspondence: anca.pop@umfcluj.ro

Received: 17 May 2020; Accepted: 4 June 2020; Published: 8 June 2020

Abstract: Oral health is considered an important factor of general health and it contributes to the quality of life. Despite the raising awareness of preventive measures, the prevalence of oral health conditions continues to increase. In this context, a growing interest in investigating natural resources like *Vitis vinifera (V. vinifera)* phenolic compounds (PhCs) as oral health promoters has emerged. This paper aims to review the evidence about the bioactivities of *V. vinifera* by-products in oral health. Up to date, a high number of studies have thoroughly reported the antimicrobial and antiplaque activity of *V. vinifera* extracts against *S. mutans* or in multi-species biofilms. Moreover, the bioactive compounds from *V. vinifera* by-products have been shown to modulate the periodontal inflammatory response and the underlying oxidative stress imbalance induced by the pathogenic bacteria. Considering these beneficial effects, the utility of *V. vinifera* by-products in the maintaining of oral health and the necessary steps towards the development of oral care products were emphasized. In conclusion, the high potential of *V. vinifera* by-products could be valorized in the development of oral hygiene products with multi-target actions in the prevention and progression of several oral conditions.

Keywords: *Vitis vinifera*; by-products; oral health; antimicrobial; anti-inflammatory; antioxidant; mouthwash; toothpaste

1. Introduction

According to the World Health Organization, oral health is an important element of general health and is crucial for the quality of life. Dental caries, periodontal disease, edentulism, and oral cancer are oral diseases/conditions recognized worldwide as a public health issue. Poor mouth hygiene is a key risk factor for oral diseases. Oral diseases and widespread chronic diseases (e.g., diabetes mellitus, cardiovascular diseases, respiratory diseases) share many common risk factors (e.g., sugar rich diet, tobacco use, alcohol consumption) [1]. Moreover, oral infection/inflammation represents a risk factor for the development and/or severity of several systemic diseases [2,3].

In this context, dental hygiene products are deemed essential for oral health. Historically, the first dental cream, containing the powder of oxen hooves, ashes, eggshells, and pumice, was invented around 3000–5000 BC by the Egyptians. A few--thousand years later, the Romans and Greeks increased the abrasivity of the toothpaste by adding crushed bones and oyster shells and added the first flavoring agents. During the same period, the Chinese added ginseng and herbal mints to remove bad breath and also to improve palatability [4]. The development of oral hygiene products has continuously changed ever since, and the products became multi-functional due to the addition of various active ingredients and formulation excipients. As consumers become more and more concerned about the quality of life and the potential unwanted side-effects of some chemicals used in products, natural compound-based cosmetics have seen extensive growth. Nowadays, a high number of cosmetic products for oral care are currently available, while the formulations are continuously improved to achieve multiple benefits, better efficacy, and greater bioavailability of active ingredients or sustainable products.

In the last few years, naturally occurring antioxidants received increased attention not only in academic research, but also in industry field, as these compounds display a wide range of utility in the pharmaceutical and cosmetic industry due to their beneficial effects on general human health. *V. vinifera* by-products represent an easily available and valuable source of natural antioxidants. Grapes are among the largest fruit crops in the world with an annual production of more than 79 million tons in 2018 [5], from which about 80 percent is used in wine production [6]. These activities generate important waste, up to 30% of the total processed mass [7]. While industries focus on reducing the environmental impact of by-product disposal, consumers have become increasingly aware of the need for health products containing natural ingredients. The bioactive compounds found in winery residues represent important candidates for their cytoprotective, anti-inflammatory, and antioxidant effects [8,9]. In this regard, phenolic compounds (PhCs) are considered the most important active compounds, being responsible for most of the health benefits of vine extracts. Many papers reported the antibacterial, antifungal and antiviral activity of PhCs through their direct action against oral pathogens or by the inhibition of virulence factors [10,11]. In addition, *V. vinifera* extracts have been shown to modulate oxidative stress imbalance and the bacterial-induced inflammatory response in periodontal disease (PD) [12]. However, the PhC's role in preventing oral diseases is far from being completely understood [11]. Many aspects, including the mechanism of action of PhCs in the oral cavity and the complex interaction between PhCs and microbiota need yet to be considered. Moreover, even though the PhC's effects were thoroughly described both *in vitro* and *in vivo,* current evidence on the efficacy of *V. vinifera* extracts in oral care products is scarce. In this context, the purpose of this review is to summarize the bioactivities of *V. vinifera* by-products, emphasizing the role of phenolic compounds for the prevention of oral disease and the treatment of different oral health conditions. Furthermore, key elements of the development of oral hygiene products based on *V. vinifera* by-products, with multi-target actions in PD, were highlighted.

2. Active Compounds in *V. vinifera* By-Products

The phenolic compounds include many classes of substances existing in the plant kingdom, which can be divided into simple phenols and polyphenols. The simple phenols include two categories: the coumarins, commonly existing as glycosides, and the phenolic acids, with two subgroups: hydroxybenzoic acids and hydroxycinnamic acids. The polyphenols categories include the flavonoids, the most diverse class, of which the most important are flavones, isoflavones, flavonols, flavanols, flavanones, chalcones and anthocyanins; other phenolic compounds are stilbenes with a structure derived from trans-resveratrol; lignans composed of two phenylpropane units and tannins, which groups the esters of gallic acids, i.e., hydrolyzable tannins and condensed tannins or proanthocyanidins. In regards to *V. vinifera* extracts, phenolic compounds are present in significant amounts in grapes, being the third most abundant constituents [13], mainly distributed in grape skin and seeds [14], but they can also be found in leaves [15] or tendrils [16]. The phenolic content differs according to the variety, degree of maturity and part of the plant studied [17]. The

pretreatment of the samples, the extraction technique, as well as the solvent used may have a significant influence on the recovery of PhCs from natural matrices [18]. Even though a high number of studies show that acetone and methanol lead to the highest yield of individual extraction of polyphenols, hydroethanolic mixtures had shown a better recovery rate of total polyphenols [19]. Considering the solvent choice, ethanol is considered the best option for further incorporation of the extracts in oral care products due to its efficiency, low toxicity, and GRAS status. Moreover, ethanol has the advantage of being reusable and environmentally friendly solvent [19,20]. Table 1 presents the main PhCs identified in *V. vinifera* by-products along with the extraction parameters using suitable solvents for cosmetic and pharmaceutical applications.

The flavonoids were identified as the principal phenolic compounds from *V. vinifera* by-products [21]. The main categories of PhCs present in grapes are phenolic acids (most frequently benzoic and hydroxycinnamic acids), simple flavonoids (mainly catechins, anthocyanins, flavonols) as well as tannins and proanthocyanidins [6]. As regards the biological effects, antioxidant activity was attributed to phenolic acids, flavonoids, lignans and stilbenes compounds while the antimicrobial activity is related to both the flavonoid (flavanols and flavonols) and nonflavonoid (phenolic acids and stilbenes) content [22].

The main by-products resulting from the winemaking process include grape pomace (10–20% from the entire mass processed) and stems (2–8%). The pomace contains seeds, pulp and skins, stems, and leaves [23] which consists of 30% polysaccharides, 20% pectic acids, 15% proanthocyanidins, proteins and phenols [24]. For this reason, grape pomace was broadly studied, entirely or as individual constituents [7]. The highest concentration of PhCs was reported in stems, skins and seeds [25]. In the vinification process, the PhCs are poorly extracted, over 70% of PhCs remaining in grape pomace [14,25]. The most abundant phenolic compounds in pomace include hydroxybenzoic and hydroxycinnamic acids, anthocyanins, monomeric and oligomeric proanthocyanidins, flavanols, flavonols, and stilbenes [6,7,25–27].

The range of seeds varies from 38 to 52% in dry pomace [28]. The content of PhCs is about 7% of the total weight of seeds, of which proanthocyanidins are predominant [8]. Gallic acid and resveratrol are also found in significant amounts [22,29]. In red grape seeds, protocatechuic acid is the most abundant hydroxybenzoic acid, while in white grape seeds, gallic acid and protocatechuic acid were reported in similar amounts [7]. Grape seeds have been reported to have a higher antimicrobial effect than other grape by-products [8]. The antioxidant potential of grape seeds, mainly ascribed to flavonoid content, was extensively investigated by both *in vitro* and *in vivo* studies [7].

The polyphenolic profile of skins is influenced by both agricultural variables (cultivation practices and cultivar) and ecological variables (soil, climate, geographic origin and exposure to plant pathogens) [13]. Grape skins represent up to 65% of dry pomace [7] and contain mainly phenolic acids, proanthocyanidins, anthocyanins, flavonols, flavanols, and resveratrol [8]. The anthocyanin content from the skin is responsible for the color of red grape cultivars [30]. On the other hand, the antioxidant and anti-glycation effect of grape skins is related to anthocyanin and proanthocyanidin content [7].

Grape stems range between 1.4% and 7.0% of press residue, out of which phenolic content represents about 5.8% [7]. The phytochemical profile of polyphenols from grape stems has shown that the most abundant phenolic compounds are hydroxybenzoic (gallic acid) and hydroxycinnamic acids, flavonols (glycosylated derivatives of quercetin and kaempferol), flavones, stilbenes (*trans*-resveratrol and ε -viniferin) and anthocyanins [31–33]. Despite the significant variation of PhC groups determined in grape stems, they display comparable antimicrobial efficacy [31].

V. vinifera tendrils have been reported to have considerable amounts of valuable compounds, such as phenolic acids (gallic, protocatechuic, caffeic, ellagic and caftaric acids) and flavonols (rutin), [16,34,35]. Grape leaves are documented for a wide range of compounds of interest: phenolic acids, flavonols, procyanidins, anthocyanins, and tannins [34,36,37]. Flavonol glycosides were detected in higher amounts in leaves than in other by-products [7]. The valuable properties of grape leaves are

recognized by the inclusion in pharmacopoeia monographs. Marketed medicinal products containing leaf extracts are also available [36].

Extensive studies on the chemical composition of grape canes have shown that canes could be considered a valuable raw material for isolation of *trans*-resveratrol. Additionally, benzoic and hydroxycinnamic acids, (+)-catechin, (−)-epicatechin and proanthocyanidins are bioactive compounds identified in important amounts [38–41]. In terms of biological effects, Moreira et al. demonstrated high antioxidant activity of gallic acid, catechin, myricetin and kaempferol-3-*O*-rutinoside from grape canes [42].

Table 1. Overview of main bioactive compounds, extraction techniques and solvents of phenolic compounds (PhCs) from *V. vinifera* by-products.

By-Product Type	Extraction Techniques	Solvent	Analytical Methods	Main Compounds	Reference
Pomace 	SLE—conventional shaker, UAE, Sequential UAE + SLE	Water 100%, EtOH 100%, Water:EtOH (3:1, 1:1, 1:3)	HPLC-UV/Vis	Phenolic acids: gallic acid, protocatechuic acid, hydroxybenzoic and hydroxycinnamic acids Flavanols: (+)-catechin, (−)-epicatechin Anthocyanins Flavonol derivatives: quercetin, laricitrin and syringetin derivatives Stilbenes: *trans*-resveratrol, piceatannol	[6,7,18,41,43–52]
	EA, EtOH-based extraction	Ezymatic digestion, EtOH 95% (*v*/*v*)	HPLC-DAD		
	EA, *DoE*	Aqueous enzymatic digestion, pH, t °C	HPLC-DAD		
	PEF + SLE	Water: EtOH (1:1)	HPLC-UV/Vis		
	SLE	Water: EtOH (1:1), 120 min, 60 °C	HPLC-UV/Vis		
	EA, EtOH-based extraction	Enzymatic digestion or water, EtOH	HPLC-DAD		
	SAS of EtOH extract, *DoE*	EtOH	HPLC-DAD		
	MAE, *DoE*	EtOH 30–60%, 5–15 min	UHPLC-UV/Vis		
	SLE, reflux method *DoE*	EtOH 40–60%, 50–65–80 °C	LC-MS		
	HVED, US-SLE, PEF	Water	HPLC-UV/Vis		
Seeds 	SPE	Water	HPLC-DAD HPLC-MS	Proanthocyanidins Phenolic acids: gallic acid, protocatechuic acid, syringic acid Polyunsaturated fatty acids: linoleic acid, oleic acid, palmitic acid, stearic acid Tocopherols Stilbenes: *trans*-resveratrol	[7,24,26,53–57]
	SLE	70% EtOH, 60 °C, 5 h	HPLC-UV/Vis		
	SLE, maceration 2–10 days	EtOH 0–15% (*v*/*v*), water	HPLC-DAD		
	SLE	Water, 70% EtOH	HPLC-UV-MS		

Skins 	MAE, SLE, *DoE*	EtOH 40–80%, 50–70 °C	UV/Vis	Anthocyanins (red grapes): cyanidin, peonidin, petunidin, delphinidin, and malvidin Procyanidins Phenolic acids: hydroxycinnamic acids, gallic acid Catechins: catechin, epicatechin, epigallocatechin Flavonols: quercetin, quercetin derivatives kaempferol, kaempferol derivatives Stilbenes: *trans*-resveratrol, *trans*-polydatin	[20,25,53,58–64]
	SLE, UAE, MAE	EtOH 8–92%, solid:liquid ratio (1:3–1:17)	HPLC-DAD		
	PHWE	Water, 40–120 °C, 15 MPa, 3 × 5 min	HPLC-DAD		
	SLE, MAE, UAE	Deep eutectic solvents, SLE-12 h MAE 50–90 °C, 15–90 min UAE 30–90 °C, 15–90 min	HPLC-DAD		
	ASE, SLE, *DoE*	ASE EtOH 20–60%, 5–25 min, 40–80 °C SLE EtOH 49%, 5 h, 50°	HPLC-UV/Vis UHPLC-UV/Vis		
Stems 	PLE, *DoE*	0–100% EtOH, 40–120 °C, 1–11 min	RP-HPLC-DAD-MS; PLC-UV/Vis	Stilbenes: *trans*-resveratrol, piceatannol Flavanols: (+)-catechin Phenolic acids: gallic acid Procyanidins: procyanidin B3	[19,33,65]
	Superheated liquid EtOH, Supercritical EtOH extraction	EtOH, 60–300 °C, 1 h	Microplate reader (UV/Vis)		
Tendrils 	SLE, reflux method	50% EtOH, 60 °C, 30 min	LC-MS/MS	Phenolic acids: gallic acid, protocatechuic acid, caffeic acid, ellagic acid, caftaric acid Flavonols: rutin, quercetin-3-*O*-glucuronide Organic acids: fumaric acid, citric acid	[34,35]
	SLE, reflux method	70% EtOH, 60 °C, 20 h	HPLC-DAD		
Leaves 	SLE, reflux method	50% EtOH, 60 °C, 30 min	LC-MS/MS	Flavones: quercetin, kaempferol Anthocyans: anthocyanidins, procyanidins Flavonols: quercetol	[34,36,37,66,67]
	SLE, kinetic maceration	Water, 25 min	LC/MS-MS UV/Vis-LC-DAD		

	UAE	20–60% EtOH, 30–70 °C, 5–55 min solid:liquid ratio (1:10–1:30)	HPLC, UV/Vis	Glycoside flavonoids: hyperoside, isoquercitrin, quercitrin Flavanols: catechin, gallocatechin, epigallocatechin Stilbenes: *trans*-resveratrol	
	Thermomaceration (skins, seeds, leaves canes), *DoE*	Grape must, 20–60 °C, 0–24 h	HPLC–DAD LC-MS/MS		
Canes 	OH, conventional heating	45% EtOH, 80 °C, 20–90 min	UHPLC-UV/Vis	Flavanols: (+)-catechin, (−)-epicatechin Phenolic acids: caffeic acid, trans-*p*-coutaric acid, trans-caftaric acid, gallic acid, syringic acid Stilbenes: *trans*-resveratrol Minerals: K, Ca, Fe, Mg, P, Zn	[39–41,68]
	SLE	60% EtOH, 80 °C, 30 min	HPLC-DAD		
	SLE, SLDE, MAE, PLE	Water, SLE 100 °C, 15–60 min SLDE 25–27 °C, 8 bar, MAE 100 °C, 5–15 min, PLE 30–100 °C, 50–100 bar, 10–30 min	HPLC-DAD-MS HS-SBSE-GC-MS		

SLE—Conventional Solid−liquid extraction, UAE—Ultrasound solid−liquid extraction, EA—Enzyme assisted extraction, PEF—Pulse electric field, SAS—Supercritical antisolvent process, MAE—Microwave assisted technology, HVED—High voltage electric discharge, PEF—Pulsed electric field treatment, SPE—Solid phase extraction, PHWE—Pressurized hot water extraction, ASE—Accelerated solvent extraction, PLE—Pressurized Liquid Extraction, OH—Ohmic heating, SLDE—Solid−liquid dynamic extraction, *DoE*—Design of Experiments, EtOH—Ethanol, HPLC—High-performance liquid chromatography, DAD—Diode array detection, MS—Mass spectrometry, UV/Vis—UV/Vis detection, UHPLC—Ultra high-performance liquid chromatography, LC-MS—Liquid Chromatography tandem Mass Spectrometry, RP-HPLC Reversed-phase high-performance liquid chromatography, HS-SBSE Headspace stir bar sorptive extraction.

3. Bioactivity—Oral Cavity Conditions as Targets of Phenolic Compounds

Despite the increasing awareness of the preventive measures, including fluoride exposure, and improved access to oral health services, oral health conditions are still highly prevalent. In recent years, the World Health Organization has endorsed public health interventions aimed at improving oral health, mainly in low-income populations. At the same time, the strategy shifts the approach from invasive dental interventions to prevention or minimum invasive dental treatments. A great number of oral health diseases could be prevented or resolved in their early stages [1]. Preventive strategies aim to control dental plaque, usually through mechanical and antimicrobial approaches. In this context, a growing interest in investigating by-products as an economical source of natural compounds with antimicrobial properties has been noted. The multiple biological effects targeting the prevention and treatment of microbial-mediated oral pathology are further described.

3.1. Microbiota and Antimicrobial Activity of V. vinifera By-Products

Oral microbiota is the second most complex microbial environment of the human body after gut microbiota. About 700 types of microorganisms inhabit the oral cavity. Bacteria are the most prevalent, but fungi, viruses, protozoa and archaea are also present in the oral environment. The composition of the microbiota of healthy people from different communities is similar. Dysbiosis, the unbalance of the dynamic equilibrium between commensal microorganism and oral pathogens, may be related to oral or systemic pathologies [11,69].

Microbial-mediated oral pathologies are the result of homeostasis disruption due to the interaction between the host resident microbiome, the host susceptibility and the environmental changes [11]. Dental caries and periodontal diseases (i.e., gingivitis and periodontitis) are considered plaque-mediated diseases, probably occurring as the most prevalent infectious diseases affecting humans [70].

Dental plaque (oral biofilm, plaque biofilm) consists of highly organized microbial colonies attached to teeth surfaces [71]. Plaque biofilm is usually localized at the interface of tooth and gingiva and comprises about 50 bacterial species [3,72–74]. *Streptococcus mutans* (*S. mutans*), *Streptococcus sobrinus*, *Lactobacillus spp.*, *Streptococcus mitis* and *Streptococcus sanguis* are among the most prevalent bacteria in dental plaque [70]. The microorganisms are embedded in a matrix of excreted polymeric compounds adhering to solid surfaces, in both natural dentition and dental prostheses. Extracellular polymeric substances are mainly composed of exopolysaccharides and proteins, but also of nucleic acids and lipids. The bacteria embedded in the biofilm are able to circumvent the host immune system defense mechanisms [71]. The microbial composition differs between supragingival and subgingival (periodontopathogenic) dental plaque. Supragingival plaque or cariogenic plaque is colonized with facultative anaerobic bacteria, such as *Streptococcus spp* or *Actynomices spp* [75].

3.1.1. Dental Caries

Dental caries is defined as the progressive destruction of hard tissues of teeth (enamel and dentine) by acidic compounds converted from free sugars, together with an insufficient removal of dental plaque and inadequate exposure to fluoride [1,76]. Dental caries of permanent teeth is globally the most prevalent health condition. The destruction process is dynamic, being controlled by the pH value of dental biofilm and characterized by alternating periods of demineralization and remineralization [76]. The development of dental caries involves both acidogenic (acid-producing) and aciduric (acid-tolerating) bacterial species. On these conditions, the variety of microbiota is decreased because of the acidic pH. Dental caries, or tooth decay, is the result of complex poly-microbial activity at the tooth surface, inadequate oral hygiene, and a high frequency of free sugar intake. The decrease of the buffering capacity of saliva together with low pH conditions lead to an increase in the solubility of hydroxyapatite, the main chemical component of tooth enamel and thus, enamel dissolution and tooth decay occur. *S. mutans* and *Streptococcus sobrinus* are the main acidogenic pathogens in the early development of the carious disease. *Streptococcus mutans*, a

Gram-positive coccus, is present in over 90% of isolates from human caries [77]. The pathogenicity of *S. mutans* resides in its ability to induce low pH conditions and to modulate sugar metabolism pathways. In the next step, *S. mutans* co-adheres with other pathogens such as *Candida albicans* and spreads in the oral cavity leading to permanent colonization of hard surfaces and gingival areas. The association between *S. mutans* and *Candida albicans* is based on their biochemical characteristics. The significant role of *Candida albicans* in caries development and progression was previously described [78]. *S. mutans* possess a remarkable ability to transport and transform carbohydrates in organic acids and to grow in low pH stress conditions [79]. As the oral environment is changing, the cavitation progresses gradually, the dissolution of hydroxyapatite crystals in enamel and dentin increases and produces deeper cavitation into the tooth [78]. Subsequently, in advanced stages, *Lactobacillus spp*. promotes the progression of enamel destruction through the increased production of lactic acid. During the progression of the disease other bacteria genera are also abundant in caries microbiota: *Bifidobacterium, Selenomonas, Neisseria* or *Scardovia* [11,70]. Recent studies revealed that other bacteria, such as *Prevotella spp.*, *Dialister spp.*, and *Filifactor spp.*, are involved in the occurrence and progression of dental caries [69,80].

3.1.2. Antimicrobial Effects of *V. vinifera* Extracts in Dental Caries

A high number of in vitro studies have thoroughly reported the antimicrobial and antiplaque activity of *V. vinifera* extracts. The antimicrobial activity of wine and *V. vinifera* extracts is mainly due to several phenolic compounds, such as flavanols, gallic acid, hydroxycinnamic acid, *trans*-resveratrol, and epicatechin [81,82]. Concerning the precise mechanism of antimicrobial activity, several hypotheses have been proposed, underlying the role of phenolic acids [83], the inhibition of extracellular enzymes or the complexation of metal ions from bacterial media [84]. For this purpose, several studies were performed to isolate and identify antimicrobial compounds from *V. vinifera* extracts. The study conducted by Rivero-Cruz et al. aimed at the fractionation of hexane- and ethyl acetate-soluble partitions of *V. vinifera* extract and the isolation of antimicrobial compounds, followed by an evaluation of antimicrobial activity on *S. mutans*. Among all the compounds tested, oleanolic acid, oleanolic aldehyde, 5-(hydroxymethyl)-2-furfural (7), and rutin showed an inhibitory effect against *S. mutans* [85].

Of all the *V. vinifera* by-products, grape seed extracts (GSEs) have been extensively investigated. Most in vitro studies investigated the effect of GSEs on bacterial biofilms. As *S. mutans* is considered the key pathogen involved in caries development, most of the studies focus on the activity of *V. vinifera* extracts against *S. mutans* and *S. mutans* virulence factors. Thus, the use of *S. mutans* biofilm models to induce caries-like lesions has been widely used in experimental studies.

Zhao et al. found that the GSE at 4 mg/mL inhibited the growth of *S. mutans* and biofilm formation, leading to the suppression of acid production and enamel demineralization [86]. Comparable results in terms of antimicrobial activity were obtained for grape pomace extract at a concentration level of 2 mg/mL. Moreover, the grape pomace extract proved to be efficient in the reduction of *S. mutans* biofilms' adherence in in vitro experimental conditions [87]. Timothe et al. investigated the chemical composition of different varieties of grape extracts and pomace extracts. Despite the high variability of anthocyanins and flavan-3-ol in the samples studied, grape pomace extract proved to be at least as effective as fruit extracts against *S. mutans* virulence factors by reducing the activity of glucosyltransferases, enzymes involved in the synthesis of extracellular polysaccharides. The extracts also reduced bacterial acidogenicity [88].

Even though most studies were performed on a single type of bacteria, namely *S. mutans*, several studies investigated the antiplaque effect of GSE, grape pomace and red wine extract on *Streptococcus sobrinus, Lactobacillus rhamnosus, Actinomyces viscosus, Porphyromonas gingivalis (P. gingivalis)* and *Fusobacterium nucleatum (F. nucleatum)* [87,89,90]. The GSE effectiveness against biofilm formation was maximum at 2 mg/mL, the inhibitory effect increasing in a dose-dependent manner [89]. In a different study, the same authors assessed the antibiofilm activity of GSE alone or in combination with amine fluoride. The combination of 2 mg/mL GSE and 10.2 mg/mL amine

fluoride proved to be efficient in reducing the biofilm formation by suppressing bacterial adhesion to the teeth surface [90].

The experiments conducted by Muñoz-Gonzalez et al. investigated the antibacterial effect of red wine and different oenological extracts including GSE, on a different biofilm model of supragingival plaque consisting of *Actinomyces oris*, *F. nucleatum*, *Streptococcus oralis*, *S.mutans* and *Veillonella dispar* [91]. Among all of the extracts studied, red wine extract solutions spiked with GSE showed the highest antimicrobial activity. Compared to other wine extracts, the higher antimicrobial activity of GSE can be explained by the high concentration of flavonoids and their derivatives in GSE, which is mainly responsible for the antimicrobial activity [91].

The data obtained during in vitro studies are supported by studies on human volunteers that investigated the antimicrobial efficacy of grape-based oral care formulations. The study conducted by Singla et al. assessed the effect of a mouthwash containing 12.5% GSE on oral streptococci count, in children aged 8 to 10 years after using the product twice daily for seven days. The results showing a significant decrease in salivary streptococci count supported the effectiveness of GSE in preventing dental caries [17]. Another in vivo study concluded that oral rinse for 10 min with red wine led to a significant reduction of bacterial adherence to enamel [92].

Besides the activity on *S. mutans* of GSE, the potential effect of proanthocyanidins from GSEs on caries-affected dentin was also investigated. The organic matrix of dentine is mainly composed of fibrillar type I collagen (90%) and non-collagenous proteins, such as phosphoproteins proteoglycans that account for about 10% of the matrix. During the cariogenic process, the organic matrix is degraded by proteases secreted by cariogenic bacteria and host-derived enzymes, specifically matrix metalloproteinases (MMPs) from dentine or gingival crevicular fluid [93]. Proanthocyanidins are considered natural cross-linking agents in the collagen from the dentine matrix as they promote the hydrogen bond formation in type I collagen [94]. Firouzmandi et al. analyzed the remineralization of dentin after the treatment with GSE and GSE+ silver diamine fluoride. The results showed that both agents increased the hardness values, but not the elastic modulus of caries-affected dentin [95]. These findings are consistent with the previous studies showing that GSE can improve the mechanical properties of demineralized dentin by stimulating the inter- and intrafibrillar cross-links in the collagen matrix from dentin [96–102] and by improving resin-dentin bond strength [101,103]. Furthermore, proanthocyanidins from GSE exhibited a significant inhibition, higher than chlorhexidine, on dentine proteases (matrix metalloproteinases and cysteine cathepsins), responsible for progressive degradation of exposed collagen fibrils [94,104]. Thus, through the combined action of proanthocyanidins, the organic matrix of dentine could be preserved, and the remineralization process could be increased [93].

These studies support the complex role of *V. vinifera* extracts in processes from the oral cavity and the anticaries effect through different mechanisms, depending on the phytochemical composition of the extracts.

3.1.3. Periodontal Disease

PD represents a chronic medical condition that progresses from gingivitis to the gradual destruction of supporting structures of the teeth, the loss of the alveolar bone and the deepening periodontal pocket, swelling and/or suppuration leading finally to the loss of teeth [12].

Unlike supragingival plaque, periodontal diseases (gingivitis and periodontitis) are directly associated with the proliferation of Gram-negative anaerobic bacteria. The subgingival plaque developed between teeth and gingival crevice is difficult to remove. The gingival crevicular fluid is considered to be the main source of nutrients for the subgingival plaque [105]. It is an inflammatory exudate composed of serum and different tissue breakdown products, inflammatory mediators, serum transudate, subgingival microbial plaque, extracellular proteins [106,107].

The main causes identified are poor oral hygiene, tobacco use and diabetes [1,74]. Recent studies revealed the high prevalence of this disease worldwide, affecting up to 90% of the general population [75]. The milder form of the disease, gingivitis, consists of an inflammation of the gingiva, associated with erythema and bleeding [12]. The proliferation of bacteria in the pathogenic

oral biofilm is considered essential for the initiation and progression of the disease [75]. Due to the bacterial factors, pro-inflammatory cytokines are released and the inflammatory cascade is promoted, leading to periodontal tissue destruction [108].

Although bacterial proliferation is critical for the initiation of periodontal disease, chronic inflammation plays a decisive role in the progression of the disease through host-mediated destruction of the supporting structures of the teeth. Currently, the PD is rather perceived as the result of an imbalance between bacterial aggression and host response [72].

The etiological agents of periodontitis are *P. gingivalis*, *Prevotella intermedia*, *F. nucleatum*, *Tannerella forsythia*, *Treponema denticola* and *Aggregatibacter actinomycetemcomitans* [72,75]. The progression of PD is the cumulative result of the combined action of these microorganisms, the individual strains alone being less pathogenic. *Porphyromonas gingivalis* is considered the main etiological factor in the pathogenesis and progression of PD. A characteristic bacterial complex recognized as the "red complex" including *Porphyromonas gingivalis, Treponema denticola* and *Tannerella forsythia* has been detected in advanced periodontal lesions. The synergic action of the complex expresses numerous virulence factors, including enzymes, lipopolysaccharides (LPS) and proteins that could trigger periodontium destruction, bone resorption and initiates the host defense mechanism through cytokine production. Another bacterium, *Fusobacterium nucleatum*, is also a key component in the PD due to its capacity to aggregate to *P. gingivalis* [109]. In aggressive forms of PD *Aggregatibacter actinomycetemcomitans* was identified as the main specific pathogen [110].

3.1.4. Antimicrobial Effects of *V. vinifera* Extracts in Periodontal Disease

As regards the periodontal pathogens, the antimicrobial activity was investigated using single species or multi-species microbial biofilm. Thus, the antibacterial action of GSE against two of the anaerobic bacteria associated with the periodontal disease, *P. gingivalis* and *F. nucleatum* was reported by Furiga et al. [89] Another study investigated different compounds isolated from Thompson seedless raisins, out of which oleanolic acid, oleanolic aldehyde, and 5-(hydroxymethyl)-2-furfural were shown to suppress the growth of *P. gingivalis* [27]. Recently, the antibacterial activity against *P. gingivalis* and *S. mutans* was reported for tendrils and leaves extracts [34].

The effect of red wine PhCs (caffeic acid and *p*-coumaric acid) and oenological extracts against *P. gingivalis*, *F. nucleatum*, and *S. mutans* was investigated using an in vitro model of human gingival fibroblasts. The results showed the inhibition of bacterial adhesion to human fibroblasts, probably due to a steric impediment for bacterial attachment to cellular receptors. Moreover, the bacterial metabolization of phenolic compounds was found in the case of proanthocyanidins, catechins, and epicatechin and so was a degradation of 3,5-dihydroxybenzoic acid due to both cellular and bacterial activity. The study highlighted the complex action of bacterial combinations as compared to the individual species leading to different transformations depending on the oral environment [111]. The above-mentioned observations were in agreement with the findings of Sánchez et al. which demonstrated the antibacterial activity against *F. nucleatum* in case of GSE, but when tested on total biofilm bacteria, no significant effects were noted [72].

Table 2 summarizes the studies investigating the antimicrobial activity of *V. vinifera* extracts against microorganisms involved in dental caries and periodontal disease.

Table 2. Summary of antimicrobial activity of *Vitis vinifera* extracts against microorganisms involved in dental caries and periodontal disease.

By-Product Type	Microbial Strains	Concentration Tested	Reference
Pomace	*Staphylococcus aureus, Bacillus cereus, Escherichia coli, Pseudomonas aeruginosa, Candida albicans, Candida parapsilosis, Candida krusei*	3.9–2000 μg/mL	[82]
	Streptococcus mutans, Streptococcus sobrinus, Lactobacillus rhamnosus, Actinomyces viscosus,	2000–8000 μg/mL	[87]

	Fusobacterium nucleatum, Porphyromonas gingivalis		
	Streptococcus mutans	62.5–500 μg/mL	[88]
Black grape skin	*Staphylococcus aureus, Enterococcus faecalis, Enterobacter aerogenes, Salmonella typhimurium, Escherichia coli, Penicillium chrysogenum, Penicillium expansum, Aspergillus niger, Aspergillus versicolor*	260 mg, 540 mg, 1080 mg TAE (tannic acid equivalents)/mL	[84]
Thompson seedless raisins	*Streptococcus mutans, Porphyromonas gingivalis*	3.9–500 mg/mL	[85]
Seeds	*Streptococcus mutans, Streptococcus sobrinus, Lactobacillus rhamnosus, Actinomyces viscosus, Porphyromonas gingivalis, Fusobacterium nucleatum*	1000–8000 μg/mL	[89]
	Streptococcus mutans, Streptococcus sobrinus, Actinomyces viscosus, Lactobacillus rhamnosus, Porphyromonas gingivalis, Fusobacterium nucleatum	250–8000 μg/mL	[90]
	Streptococcus mutans	1–3 mg/mL	[86]
	Actinomyces oris, Fusobacterium nucleatum, Streptococcus oralis, Streptococcus mutans, Veillonella dispar	10 g/L	[91]
Red wine extract and seed extract	*Aggregatibacter actinomycetemcomitans, Fusobacterium nucleatum, Porphyromonas gingivalis, Streptococcus oralis, Veillonella parvula, Actinomyces naeslundii*	20 g/L	[72]

3.2. Periodontal Inflammation

In recent years, the link between oxidative stress and the inflammation observed in PD has gained more attention, as these processes are highly intertwined. The oral cavity is subjected to many pro-oxidative factors resulting from physiological metabolism or through exposure to xenobiotics (microorganism, air pollution, alcohol and tobacco), food, dental treatment or dental materials. Moreover, PD represents a major source of reactive oxygen species (ROS), an increased rate of free radicals and lower antioxidant capacity being detected in plasma, saliva or gingival crevicular fluid of patients with periodontal disease [111,112].

ROS, such as nitric oxide, hydroxyl radicals and superoxide anions, are generated in periodontal tissue by activated phagocytes as a defense mechanism to bacterial aggression. Moreover, the physiologically produced ROS can improve wound healing [113]. NADPH (nicotinamide adenine dinucleotide phosphate) oxidase and purine degradation pathways are responsible for the accelerated ROS production [114] that can exert direct or indirect effects in periodontal tissue. Under oxidative stress, the nuclear factor erythroid 2-related factor-2 (Nrf2) is translocated into the nucleus where it binds to the antioxidant response element of the DNA, regulating the expression of antioxidant enzymes encoding genes [115]. However, in the pathological situation like PD, this defensive mechanism is overwhelmed, and inflammation occurs. If not resolved, chronic inflammation leads to tissue damage that will further activate macrophages, neutrophils, and fibroblasts that further sustain the inflammatory process mediators.

In gingival cells, bacterial components such as LPS and bacterial DNA are detected by CD14 and Toll-like receptor TLR4, key proteins of pathogen recognition that induce the activation of activator protein 1 (AP-1) and nuclear factor-κB (NF-κB) intracellular signaling pathways [108,116]. The central role of NF-κB in many inflammatory diseases is well recognized, as the nuclear translocation of this transcription factor results in the expression of a plethora of pro-inflammatory mediators that underlie the pathophysiological mechanisms present in PD. Even though the activation of this pathway is meant to have a protective effect, the persistence of stimuli can induce a state of chronic inflammation in the gingival tissue. Following the NF-κB translocation, soluble and membrane-bound chemoattractants, such as IL-6, IL-8, ICAM-1 [117], and tissue remodeling enzymes such as MMP, are expressed [118]. Hard tissue remodeling following osteoclast activation and osteogenic differentiation due to Receptor Activator for NF-κB (RANKL) expression has been observed in PD [108,119]. Recruited immune cells, such as mononuclear phagocytes, antigen-presenting cells and specific lymphocytes T, migrate to the inflammation sites and release

locally pro-inflammatory cytokines [120]. Other inflammatory mediators, such as chemokines, prostaglandins, and proteolytic enzymes, are released, contributing to the inflammatory cascade. In each stage of the inflammatory process, pro-inflammatory mediators are produced, leading eventually to a chronic inflammatory response, increased osteoclastic activity and the alveolar bone resorption [121].

The pathogens involved in periodontal diseases, tissue destruction with ROS generation and inflammation with clastogenic and metalloproteinase increased activity are all interconnected, forming a vicious circle.

To prevent periodontitis from spreading, numerous non-surgical treatment strategies are being used. The first step of the treatment consists of a machine-driven or manual instrumentation aimed to reduce the intraoral bacterial load responsible for the increased reactive oxygen species production following the interaction with the polymorphonuclear neutrophils from the gingival tissue. Those interventions must be accompanied by local and systemic antibiotics and/or antimicrobials [122]. However, the bacterial resistance and the medication's adverse effects tend to limit this approach, highlighting the need for a co-treatment without long-term side effects that could inhibit the bacteria development and decrease the oral oxidative status [123]. Special attention was directed at the extracts from wine industry by-products that demonstrated—so far—various biological activities, including anti-adhesive and antioxidant effects, considered to increase the efficiency of periodontitis treatment.

3.2.1. Antioxidant and Anti-Inflammatory Effects of *V. vinifera* Extracts in Periodontal Disease

Bioactive compounds present in natural plant extracts have been shown to modulate the periodontal inflammatory response and the underlying oxidative stress imbalance induced by pathogenic bacteria [124]. The extensive research on green tea PhCs revealed beneficial effects in the management of PD, justifying the need to investigate other natural resources rich in bioactive compounds [125]. Several studies showing the beneficial effects of specific subclasses or individual PhCs in relation to periodontal inflammation have been published. Based on the current knowledge, PhCs proved to be powerful antioxidants in vitro, having the capacity to counter a wide range of free radicals and to inhibit the lipid autoxidation chain reactions. Moreover, they act as antioxidants in vitro by sequestrating Fe^{3+} and thus inhibiting the Fenton reaction. The antioxidant potential is strongly correlated with the structure of the molecule, in terms of hydroxyl groups and their position, making quercetin, 3-hydroxy group flavonol a compound with high antioxidant properties. It should be emphasized that during the ROS neutralization, antioxidant molecules become pro-oxidants when losing an electron, albeit a more stable one. Additionally, antioxidant molecules can become pro-oxidants in reaction with and transition metal ions, thus further nuancing the protective antioxidant effects of PhCs [126,127].

Besides the direct action on the neutralization free radicals, measured by the chemical DPPH, ORAC and FRAP assays [128], PhCs restore the redox homeostasis by enhancing the activities of the antioxidant enzymes superoxide dismutase (SOD), catalase (CAT) glutathione peroxidase (GPx) and glutathione reductase (GR) in cellular and animal studies [129,130]. These restorative properties are related to the Nrf-2 transcription factor that modulates the expression of antioxidant molecules and enzymes, subsequent to ROS insults. The Nrf-2 translocation can also be initiated following the interaction with the cytosolic aryl hydrocarbon receptor (AhR), with several flavonols and flavones including quercetin, luteolin and apigenin being confirmed as AhR agonists and inducers of the Nrf-2 pathway [115,131]. Moreover, by favoring the nuclear translocation of the Nrf-2 transcription factor, PhCs inhibit the nuclear translocation of NF-kB, thus inhibiting the pro-inflammatory and the associated pro-oxidative cellular responses [130].

Regarding the use of *V. vinifera* extracts in the management of PD, a large body of studies focused on the beneficial effects of resveratrol, as the consumption of moderate quantities of wine was associated with improved cardiovascular status [132]. In this sense, it was shown that resveratrol may reduce the production of pro-inflammatory cytokines in human periodontal ligament cells exposed to *P. gingivalis* [133], reduce alveolar bone loss in an animal model of

periodontitis and also decrease IL-1β, IL-6, IL-8 and TNF-α [134]. In a study on human volunteers, undertaken to evaluate the impact of resveratrol supplementation in diabetic patients, it was shown that resveratrol significantly improves the periodontal status [135].

For resveratrol extraction, the whole grape is used however, the winery industry is challenged with the disposal of a high quantity of by-products that can be further valued as they represent a rich source of bioactive compounds that could prove their utility in PD management and other inflammation-related diseases [132].

GSE represents one of the most studied *V. vinifera* by-products, phytochemical analysis indicating a high content of proanthocyanidins with broad pharmacological activities and therapeutic potential. In addition, other monomeric phenolic compounds such as (+)-catechins, (−)-epicatechin, (−)-epicatechin-3-*O*-gallate were quantified in GSE. Encouraging results for the use of this by-product as an agent in the prevention and/or management of the PD were obtained in non-cellular studies by Furiga et al., who demonstrated a protective activity of the extract against oxidative stress by measuring the scavenging activity of GSE in comparison with vitamin C and E [89,90]. The non-cellular data are confirmed by in vitro studies—the response of murine macrophages stimulated with LPS of periodontopathogens being reduced after GSE exposure. Exposure to GSE inhibited the generation of nitric oxide (NO) and ROS and modulated the expression of nitric oxide synthase [136]. In a comparative study, Anastasiadi et al. evaluated the phytochemical profile of berries, seeds, skins, pomace and stems of four cultivars of *V. vinifera*, and their antioxidant activities in smooth muscle cell culture and reported an improved antioxidant activity for the GSE [137]. Another in vitro study from Dang La et al. reported that macrophage treatment with GSE before the *A. actinomycetemcomitans* LPS stimulation clearly showed a reduction in the activation of NF-κB p65 and AP-1, this suppression being associated with the inhibition of MMP secretion [138]. An in vivo study using rats fed with a high-fat diet, expected to prompt an excess of reactive oxygen species, supplemented with grape seeds confirmed the protective effects against ROS observed in vitro. The authors reported an increase in the antioxidant system with a decrease in the concentrations of plasma and hepatic lipid peroxide [139]. The anti-inflammatory effect of proanthocyanidins from GSE was investigated by Li et al. [140] in an experimental animal model of inflammation. The dose-dependent anti-inflammatory activity observed was explained through different mechanisms: the suppression of inflammatory cytokine production, namely IL-1β and TNF-α, the inhibition of lipid peroxidation and production of Prostaglandin E 2 (PGE_2) and nitric oxide (NO). Similarly, in the study conducted by Özden [141], the interference of GSE in the inflammatory process from the periodontal tissues was investigated through histomorphometric and immunohistochemical analyses. The histomorphometric parameters showed a lower degree of inflammation as well as the improvement of connective tissue level and bone healing [141]. In line with the reports of the proanthocyanidins from *V. vinifera*, proanthocyanidins from cranberries have been shown to be effective in treating periodontitis by inhibition of: (1) the biofilm formation by *P. gingivalis* and *F. nucleatum*; (2) the adhesion of *P. gingivalis* to different proteins; (3) the growth of *P. gingivalis*, *Treponema denticola* and *Tannerella forsythia* in periodontal pockets; (4) the production of proinflammatory cytokines; (5) the production of MMPs [142].

Stem extract was also investigated for its free radical-scavenging capacity using the DPPH method, the results obtained indicated stems as an inexpensive, abundant and valuable source of natural antioxidant [33,65,143,144]. In addition, grape stem extracts displayed the capability to prevent the oxidation of LDL–lipoprotein at very low concentrations and to decrease the ROS concentration. [33]. An increase in the glutathione levels is responsible for the effect of stem extracts on endothelial and muscle cells, a reduction of lipid peroxidation and protein oxidation being observed following the extract treatment, significantly improving the cellular redox status [65].

Important effects that could contribute to the cell protection from oxidative insults were also described after the exposure of normal human keratinocytes to tendril aqueous extract when an increase in the reduced glutathione concentration in a time- and dose-dependent manner was observed [145]. In a comparative study between leaves and tendril extracts, Moldovan at al. reported that the tendril extract exhibited better antioxidant, anti-inflammatory and cytoprotective effects on

human gingival fibroblasts [34]. The authors hypothesized that the difference in the observed effects is due to the higher total phenolic content measured in tendrils extract [34].

The analysis of a *V. vinifera* root extract indicated a high content of dimeric and oligomeric stilbenoids, partially responsible for the free radical scavenging activity observed. Additionally, an antioxidant activity, characterized by Nrf2 activation with the subsequent initiation of antioxidant genes transcription, was observed after the incubation of Huh-7 cells with the extract. In the same study, the murine macrophages pre-treated with the root extract and further stimulated with LPS, displayed a significant decreased in the NF-κB target genes IL-1β and iNOS on the mRNA level [146].

Grapevine leaves contain more than 200 identified substances, including a high content of flavonoids such as quercetin glucuronide and kaempferol glucosides [36]. Due to their composition, the leaf extract can protect against the oxidation of emulsified linoleic acid and it displays a high free radical scavenging ability, high chelating activity on metal ions and high reducing power [147]. Recent research has shown the effect of grapevine leaves in NF-κB pathway inhibition through the reduction of nuclear factor-κB driven transcription and nuclear translocation in human gastric epithelial cells [148] and in human keratinocytes cell lines [149]. The anti-inflammatory activity of the *V. vinifera* leaves has also been tested in another in vitro study using human keratinocytes exposed to UV radiation. [150]. The possible utility of leaf extract in the management of the PD associated inflammation was recently reported by Moldovan et al. in an in vitro model using human gingival fibroblasts. Exposure to the leaves extract attenuated the pro-inflammatory response after LPS stimulation by decreasing the levels of IL-1β, IL-6 and IL-8. Moreover, the extract displayed a cytoprotective effect, by decreasing the nicotine-induced toxicity, nicotine being one of the most important factors in the development and the progression of PD [34]. The anti-inflammatory effect of grapevine leaf extract was also confirmed by in vivo studies [151].

Grape pomace is another *V. vinifera* by-product with important free radical scavenging activities, able to prevent lipid peroxidation [152]. In this context, a cytoprotective effect of grape pomace in H_2O_2 induced oxidative stress was investigated by Maluf et al., demonstrating a beneficial impact even at the lowest concentration tested [153]. These results are in line with the findings of Goutzourelas et al., who demonstrated that, following the exposure to grape pomace extract, the enzymatic activity of gamma-glutamylcysteine synthetase and glutathione S-transferase from endothelial and muscle cells increased [129]. In addition, a regenerative potential of PhCs from grape pomace extract was investigated on human mesenchymal stem cells, the authors describing a decrease of NF-κB ligand activator/osteoprotegerin ratio and an increase of expression of genes involved in osteoblast differentiation [154]. Grape pomace PhCs have been also shown to increase the mechanical properties of pericardium membrane, acting as natural collagen crosslinkers, with relevance to periodontal regeneration [155]. Chidambara et al. support the in vitro findings by revealing a protective effect of the extract in CCl_4 exposed rats. Co-administration of the extract was associated with a significant improvement of the CAT, SOD, and GPx activities and a decrease of lipid peroxidation to control values [152].

Table 3 summarizes both in vitro and in vivo studies investigating antioxidant and anti-inflammatory effects of *V. vinifera* extracts.

Table 3. Summary of in vitro and in vivo studies investigating antioxidant and anti-inflammatory effects of *V. vinifera* extracts.

By-Product Type		Type of Assay	Observed Effect	Concentration Tested	Reference
Leaves	in vitro	HGF cell line	↓ ROS production	10–300 μg/mL	[34]
			↓ IL-1 beta, IL-6, IL-8		
		AGS cell line	↓ IL-8, NF-κB Nuclear Translocation	1–100 μg/mL	[148]
		HaCaT cell line	↓ IL-8, NF-κB Nuclear Translocation, VEGF	1–100 μg/mL	[149]
	in vivo	Swiss albino mice	↓ Carrageenan-induced paw oedema	100–400 mg/kg	[151]
			↓ Acetic acid induced vascular permeability		
			↓ Yeast induced pyrexia		
Pomace	in vitro	C2C12 cell line	↑ GCS levels, GST activity	2.5 and 10 μg/mL	[129]
			↓ CAT levels + activity		
		EA.hy926 cell line	↑ GCS levels, GST activity	0.068 and 0.250 μg/mL	
		3T3 cell line	↓ ROS production	0.73–3.65 mg/mL	[153]
		hMSCs	↓ RANKL/OPG ratio	10 and 20 μg/mL	[154]
			↑ BMP2 and Runx2 expression		
	in vivo	Wistar rats treated with CCl4	↑ CAT, SOD, peroxidase activity	50 mg/kg	[152]
			↓ MDA levels		
Root	in vitro	Huh7 cell line	↑ Nrf2 transactivation	1–50 μg/mL	[145]
			↑ HO-1 and GCS		
		RAW264.7 cell line	↓ IL-1β and iNOS genes	20 μg/mL	
Tendrils	in vitro	HGF cell line	↓ ROS production	10–300 μg/mL	[34]
			↓ IL-1 beta, IL-6, IL-8		
		NCTC 2544 cell line	↑ GSH levels	12.5–62.5 mg/mL	[145]
Seeds	in vitro	RAW 264.7 cell line	↓ ROS production	0.5–100 μg/mL	[136]
			↓ NO production		
			↓ iNOS expression		
		HVTs-SM1 cell line	↓ ROS production	1–100 μg/mL	[137]

		Monocyte (U937)-Derived Macrophages	↓ MMP-1, -7, -8, -9, and -13 secretion ↓ activation of NF-kB p65 ↓ AP-1 activation ↓ MMP-1 and -9 activity	25–100 μg/mL	[138]
	in vivo	Sprague-Dawley rats	↓ lipid peroxide ↑ hepatic GST activity ↑ GSH/GSSG	diet with 5% grape seed	[139]
		Kunming mice	↓ Croton oil-induced ear oedema	10–40 mg/kg proanthocyanidins fraction	[140]
		Wistar rats	↓ Carrageenan-induced paw oedema ↓ MDA, NOS activity, NO, IL-1β, TNF-α, PGE_2		
		Sprague Dawley rats	↓ Inflammatory cell number ↑ Connective tissues attachment level ↓ Osteoclast density	200 mg/kg	[141]
Stem	in vitro	HVTs-SM1 cell line	↓ ROS production	1.1–100 μg/mL	[33]
		C2C12 cell line	↓ ROS production ↑ GSH levels ↓ lipid and protein peroxidation	0.95 μg/mL	[65]
		EA.hy926 cell line	↓ lipid and protein peroxidation ↑ GSH levels	0.20 μg/mL	

↓ - decrease, ↑- increase, ROS - reactive oxygen species, VEGF - Vascular endothelial growth factor, GCS - gamma-glutamylcysteine synthetase, GST - glutathione S-transferase, RANKL - Receptor Activator for NF-κB, CAT -catalase, OPG – osteoprotegerin, MDA- malondialdehyde, NO – nitric oxide, MMP – matrix metalloproteinase, GSH – glutathione, HO-1 – heme oxygenase-1, AP-1 – activator protein-1 .

3.3. Patent Review

The recovery of bioactives from winery waste products is a subject with important economic implications, thus, it is a domain open to technological innovations. Innovations of all kinds are summarized in patents—legal documents that ensure exclusive rights for an invention. They describe products or processes that offer new solutions to particular problems and contain vast amounts of technical information; therefore, patent analysis is a useful tool to summarize the progress made in a specific field [156]. As previously shown, scientific literature provides plenty of data regarding *V. vinifera* parts and the rich composition in polyphenols of winery by-products. Their effects were thoroughly studied both in vitro and in vivo, but there is little scientific information about their inclusion in cosmetic products and especially oral care products. Table 4 describes some examples of patents or patent applications filed for oral care products that include *V. vinifera* extracts.

In 2002, Procter and Gamble Co. filed the patent *Oral Care Compositions* for the development of the so-called portable oral care products that claimed to provide benefits comparable to frequent brushing. The described products are in the forms of dentifrices, mouthwashes and chewing gums. Their effect relies on the synergy between Citrus or Vitis seed or pulp extract with at least 15% polyphenol content, and other oral care actives, as anti-calculus agents, desensitizing agents, anti-plaque agents or oral malodor-controlling agents at ratios between 0.5% and 7%. The particular types of polyphenols responsible for the effects are flavonoids (flavanols, proanthocyanidins, flavanones and flavonols, anthocyanins, anthocyanidins, and anthocyanosides) obtained by solvent extraction using water, alcohols, glycerol, propylene glycol or their mixtures as the solvent. The authors claimed that if products contain less than 10% of water, they preserve their stability over time, without degradation or discoloring phenomena. The described mouthwash contained 10% ethanol, 8% glycerol and about 70% water and the extracts 0.5% were associated with 0.25% zinc chloride. The proposed toothpaste contained 2% extract together with 2% sodium lauryl sulphate, a surfactant with foaming properties, 20% precipitated silica as an abrasive agent and 2% hydrophilic polymers as thickening agents [157].

Table 4. Patents/patent applications for oral care products containing *V. vinifera* extracts.

Type of Oral Care Product	Type of Extract	Bioactive Compounds	Other Actives in the Product	Claimed Effects	Patent/Patent Application Number
Toothpaste Oral rinse	*V. vinifera* seed or pulp extracts	Polyphenols	Potassium nitrate Metal cations salts Polyphosphates, pyrophosphates, phosphonates Fluoride ion source Xylitol	Prevention or treatment of halitosis Antimicrobial effect	US 6,706,256 B2 [157]
Rinse, wet wipe towelettes or spray for dental appliances hygiene	*V. vinifera* seed or pulp extracts	Polyphenols	α- hydroxy- acid, hydrogen peroxide, denatured alcohol, or ethanol	Antimicrobial effect Anti-odor effect Stain remover	US 2012/0207806 A1 [158]
Oral hygiene composition	*V. vinifera* seed aqueous extract	Polyphenols, mainly oligo-proanthocyanidin	Inorganic fluorine salts	Anti-biofilm effect Reduced microbial colonization	US 2010/0129297 A1 [159]
Oral rinse	*V. vinifera* seed extract	Polyphenols	Essential oil Hydrogen peroxide Alcohol	Antimicrobial Anti-inflammatory	US 8,273,385 B1 [160]
Dentifrice	*V. vinifera* extract	Not mentioned	Calcium carbonate Red iron oxide	Astringent effect Antibacterial Anti-inflammatory	US 7,736,629 B2 [161]
Oral hygiene tablets and capsules	*V. vinifera* skin extract	Anthocyanins	Other herbal ingredients	Anti-inflammatory Soothing effect Protective effect on gums and mouth tissue	US 8,728,446 B2 [162]
Quick-dissolving cleansing agent	*V. vinifera* extract	Not mentioned	Sodium fluoride	Antioxidant Vasoconstriction Astringent effect	US 6,664,225 B2 [163]

Vezin applied for a patent in the U.S. in 2008 for the use of an aqueous grape seed extract combined with at least one fluorine salt to combat the formation and accumulation of dental biofilm and compositions comprising said combination. The extracts were obtained from white grape pomace, extracted with sulfurized water, a process that led to a total content of 33.0% oligo-proanthocyanidins and 13.32% epicatechin. The author claimed that the extract proved an anti-adhesion activity, inhibiting the attachment of bacteria cells to the buccal surfaces, without perturbing the equilibrium of the oral ecosystem. The effect of extracts was potentiated by sodium fluoride or fluorinol. The compositions, used as mouthwash, gel, toothpaste, gingival gel or chewing gum, would contain between 1 mg/mL and 3 mg/mL of aqueous grape extract and between 1000 ppm and 1500 ppm of fluorine [159].

LoPesio applied for a patent in 2011, entitled *Multi-purpose dental appliance cleaner*, a composition delivered as a rinse, wet wipe towelette or spray with antimicrobial properties as hygiene products for dental appliances like athletic mouth guards, night guards, orthodontic retainers and teeth whitening trays. The antimicrobial effects are due to plant-based extracts obtained from the seeds, pulp and/or fruit of *Citrus* or *Vitis* which contain quercetin, quercetin glycoside, halperidin, campherol glycoside, apigenin, and dihydrocampherol glycoside, converted to ammonium salts in the extract mixture to improve stability. The plant-based actives are associated with a "generally recognized as safe" cleaning agent. Such cleaning products include acetic acid, glycolic acid, lactic acid and citric acid, as well as hydrogen peroxide or denatured alcohol. The invented product comes as a solution available for use as a rinse, impregnated in towels or used as a spray, containing between 0.5% and 2.5% extract, 0.3–1% glacial acetic acid, 2–20% glycerin, a flavor, a stabilizing agent, a coloring agent and deionized water. The inventor emphasizes the absence of several compounds commonly found in oral care products, thus the reduced risk of adverse events. The bacteria count tests made on dental appliances cleaned with the invented product resulted in up to 99.9% microorganism reduction [158].

A patent on *Oral rinse composition and method* was filed by Shine in 2009 and assigned to Thres Flo, LLC, based on a mixture of active ingredients with claimed effects on various symptoms of periodontal disease. The solution contained one or more essential oils or volatile substances as 0.028–0.03% eucalyptol, 0.012–0.016% menthol, 0.018–0.022% methyl salicylate, 0.019–0.023% thymol or 0.031–0.035% tea tree oil for their antimicrobial and analgesic effects. Hydrogen peroxide as a 3% solution was added as a debriding agent from about 30% to about 35%. Alcohols such as ethanol, 1-propanol, 2-propanol, 1-butanol, 2-butanol, 2-methyl-2-propanol or propylene glycol, were necessary as solvents for the water-insoluble ingredients. Extracts were selected from the group consisting of antioxidants and anti-inflammatory and antimicrobials actives, thus containing phytochemicals such as polyphenols, flavanols, proanthocyanidins. The GSE content was between 0.032% and 0.041% w/v. Nonionic surfactants were recommended for complete dispersion of low water solubility active ingredients, such as poloxamer 407 from 0.03% to 0.18%. The tests performed on patients suffering from various dental conditions revealed important positive effects on bleeding, pain, odor and clean feel [160].

Kamath and Nair applied for a patent in 2006 for the Colgate-Palmolive Company based upon the preparation of a *Red herbal dentifrice*. A blend of botanical ingredients was used at ratios comprised between 1% and 10%, among which was basil oil, black pepper oleoresin, camphor, *Terminalia chebula*, clove oil, ginger oleoresin, neem oil and plant extracts like GSE. The herbal extracts were accounted for their pain-relieving, astringency, antibacterial and anti-inflammatory properties. They were associated with natural calcium carbonate as a mild abrasive, but also with red iron oxide as low abrasive agent. The declared proportion of the components is about 0.5 to 20 parts of herbal blend to 100 parts of calcium carbonate and red iron oxide. The formulations do not exclude other oral care actives like fluoride ion sources, antibacterial agents, enhancing agents, whitening agents, anticalculus agents, antioxidants, sialagogues, breath freshening agents, antiplaque agents, anti-inflammatory agents or desensitizing agents, in the corresponding ratios [161].

In 2003, Mumoli filed a patent for a *Single-dose quick dissolving cleansing agent with medicinal properties*. It contained about 10% to 30% of a surfactant, a mixture of disintegrants up to a total of 15% to 75% and between 3% and 20% phytotherapeutic extract. The product was obtained by compressing the mixture into compacts of 0.3–5 g. The high disintegrant content would promote fast disintegration in contact with water together with a cleansing effect due to surfactants. Upon hydration, the product could be used as toothpaste. The phytotherapeutic actives can be selected from the following list *Betula alba, Aloe ferox, Achillea millefollum, Arnica montana, Calendula officinalis, Fucus vesiculosus, Humulus lupulus, Melissa officinalis, Urtica dioica, Rosmarinus officinalis, Rosa aff. rubiginosa, Salvia officinalis, Sambucus nigra* or *V. vinifera* for their therapeutic or protective effects. *V. vinifera* extract was chosen for the high amount of antioxidants and its vasoconstrictor and astringent tonic effects [163].

An innovative oral care product was described in a patent filed by Markell Hurwitz in 2008, entitled *Oral hygiene tablets and capsules for direct oral delivery of active ingredients*. The tablets or capsules were supposed to be dissolved in the saliva and/or water delivering immediately the actives to the oral cavity. An inner cavity of the tablet/capsule protected by an outer shell would host the active ingredients consisting in mouthwash, toothpaste, mouth soothing and numbing agents or fluoride rinses. The tablet is composed of a mixture of sodium bicarbonate and citric acid to produce effervescence and fast dissolution, flavors, pigments, sweeteners, or binders. Each tablet/capsule would contain between 7 g and 15 g toothpaste or mouthwash, preferably of natural origin and lipophilic character like essential oils and extracts, to avoid the degradation of the outer shell. The grape extract was associated with menthol, and extracts of *Piper cubeba*, *Glycyrrhiza glabra*, *Acorus calamus*, *Alpinia galanga*, *Aloe vera* gel, *Hydrastis canadensis*, *Calendula officinalis* or *Sanguinaria canadensis* [162].

3.4. Key-Points of the Oral Care Formulations based on V. vinifera By-Products

3.4.1. Selection of Ingredients for Oral Care

Currently, there is a growing interest to develop formulations with clinically proven efficacy which could prevent and control dental plaque and gingivitis and, at the same time, have favorable organoleptic properties, suitable for mass market applications [164]. The high potential of *V. vinifera* by-products could be valorized in the development of oral hygiene products, as dentifrice and mouthwash with multi-target actions in the prevention and progression of several oral conditions.

In this context, certain features of natural active ingredients need yet to be considered. The efficacy of oral care products mainly depends on the concentration of actives, and their overall composition and stability when all ingredients are combined in the formulation. Despite the promising studies, further research is needed to explain the delivery of PhCs to the oral mucosa level. The interaction between polyphenols and the oral cavity is a complex process, which has not been fully clarified and has bidirectional implications: on one side, PhCs can modulate oral microbiota inducing quantitative and qualitative changes, and on the other side, the microbiota can cause a possible bacterial catabolism [11,165]. For example, in vitro studies on cell cultures showed that flavonol-3-*O*-glycosides can be metabolized by bacteria present in the oral cavity and/or by epithelial cells to corresponding aglycones. Moreover, the polyphenolic compounds are susceptible to degradation in the presence of human saliva in a structure-dependent manner [91,165]. Considering these points, and also the scarce information about in vivo efficacy of *V. vinifera* extracts in oral care, additional experiments should be carried out to elucidate the precise mechanism of PhC interaction with microbiota and the potential implications to be taken into account when developing cosmetic formulations.

As regards in vivo evidence of *V. vinifera* extracts in oral care, Singla et al. have clinically investigated aqueous grape extracts used as actives in alcohol-free mouthwashes. They showed a significant reduction in oral streptococci after 48 h and seven days use at lower ratios when compared to pomegranate and guava extracts [17]. However, clinical studies focus on the activity of concentrated individual extracts or bioactive principles, while cosmetic products are complex

formulations with many actives usually used in low concentrations and numerous inactive ingredients [166]. Besides the potential beneficial effects of *V. vinifera* extracts in oral care, in cosmetic development, it must also consider the appropriateness of the chosen excipients for PD. Thus, a prudent approach should consider whether the presence of some widely used ingredients, such as surfactants, abrasives and ethanol in toothpaste is advisable for patients with PD.

Sodium lauryl sulphate (SLS) is a commonly used surfactant in oral care products up to 2.5%. The use of SLS in these preparations may be associated with certain undesirable effects, such as inflammation and desquamation of the oral mucosa [167,168]. A causal link has also been shown between the use of this ingredient in products for oral cavity hygiene and the increased frequency of recurrent aphthous stomatitis in certain patients [169]. It has been observed that SLS may exacerbate oral conditions in case of disruption of the epithelial barrier [170]. Therefore, the use of mild surfactants with a lower irritant potential may be an alternative in the case of periodontal inflammation. Consistent with these observations, a clinical study assessed the effect of two kinds of toothpaste containing Steareth 30, a non-ionic polyethylene glycol ether of stearic acid, and SLS on oral epithelial integrity (desquamation). The results indicated a lower level of desquamation in oral mucosa following the use of the toothpaste containing Steareth 30 [170]. Other surfactants that are commonly mentioned in toothpaste composition are cocamidopropyl betaine, sodium methyl cocoyl taurate and less commonly, sodium C14–16 olefin sulfonate and sodium C14–17 secondary alkyl sulfonate. More recently, coco glucoside and decyl glucoside were mentioned in natural dentifrices as alternatives to SLS [4,171,172].

Abrasive agents are ingredients typically present in toothpastes that can increase the abrasive action of tooth brushing [173]. The abrasivity of dentifrices for adult use, quantified through the Relative dentin abrasivity scale, must have a value below 250 to be regarded as safe and efficient [168]. If not mechanically removed using "calculus control" or "tartar control" toothpaste, dental plaque could calcify. The abrasivity of toothpastes should be appropriate to remove dental plaque, but the effect of the abrasives on tooth structures should be considered because of the risk of dental abrasion or gingival lesions [174]. Concern is growing around patients with exposed root surfaces. Moreover, the abrasive tooth brushing is incriminated in the gingival recession and the loss of attached gingiva [173]. Each abrasive has a hardness value influenced by the particle size and morphology. Abrasives used in dentifrices must have hardness values up to three on the Mohs scale, about half of the enamel's hardness and equal or slightly bigger than dentine's. Abrasives with smooth surface particles smaller than 20 μm are usually preferred in toothpastes, avoiding rod and needle-shaped particles. Silica, silica hydrate and calcium carbonate are the most commonly used abrasives, at concentrations between 8 and 20%, sodium bicarbonate may be added in concentrations up to 50%; calcium phosphate dibasic and calcium phosphate dibasic dehydrate are also used usually in combination with other abrasives, at concentrations up to 50% [4,175].

The prevention and therapy of PD aim to remove or decrease the plaque biofilm around the periodontium. In this regard, the use of mouthwashes containing chemical inhibitors of plaque biofilm is necessary to control the microbial biofilm [173]. In mouthwashes, the ethanol is usually used in concentrations of 6–26.9% as the solvent, as well as antiseptic and preservative [167]. The presence of ethanol in the mouthwashes is associated with poor palatability of the cosmetic product, a possible irritating effect, mucosal pain and dryness and degradation of composite dental materials [176,177]. Alcohol-free mouthwashes are recommended in patients with xerostomia [178], smokers [176] or mucosal injuries [179]. In vitro studies have shown that ethanol can increase the penetration of carcinogenic substances through the oral mucosa present in tobacco smoke [177]. Although the studies that have been undertaken so far failed to find a statistically significant association between mouthwash use and risk of oral cancer [178,180,181], mouthwash use may act as an effect modifier of tobacco smoking [180]. This is a major concern since tobacco smoking is considered the external factor with the greatest impact on the development and the progression of PD, being associated with high loads of periodontal pathogens, but also to impaired immune host responses and slow clinical healing processes [182]. A dose-dependent relation was confirmed between the number of cigarettes smoked per day and the probability of periodontitis occurrence [182]. Out of the thousands of

substances identified in tobacco smoke, nicotine is the most pharmacologically active, reported for free radical production with consequences on gingival and periodontal ligament fibroblast functions [183]. The cytoprotective effect of PhCs was confirmed by in vitro studies on cells exposed to nicotine [34,182,184]. Given the possible implications of tobacco smoking with the concomitant use of mouthwashes containing ethanol in PD, the use of alcohol-free formulations containing PhCs may be considered due to the protective effect on gums.

3.4.2. Formulation Design of Oral Care Products

Although the in vitro results support the bioactivity of natural compounds applied in periodontal disease, their effect when incorporated into cosmetic products depends on many variables. The formulation of toothpastes includes numerous inactive ingredients, with different functions, as thickening agents (xanthan gum, carrageenan), humectants (glycerin), abrasive bases (calcium carbonate, silica, hydrated silica), foaming agents (lauryl glycoside, sodium lauroyl sarcosinate, and sodium lauryl sulphate), preservatives (sodium benzoate), sweeteners, flavors and water as the solvent. The mouthwashes also contain a plethora of inactive ingredients like solvents (water, ethanol, glycerin, propylene glycol, PEG 40), surfactants (PEG-40 hydrogenated castor oil), preservatives, sweeteners and flavors [166,185]. All these compounds in both kinds of toothpastes and mouthwashes can influence the release of actives and impact the quality of the product. A rational strategy is necessary when choosing the actives and their doses, as well as the associations of excipients, with a focus on the Quality Target Profile of the desired product, its addressability and expected effects.

The development of oral care products as part of the general category of cosmetics is usually performed in an empirical way, guided by formulation principles such as those previously described, clinical evidence and the formulator's expertise. However, Regulation EC N° 1223/2009 emphasizes the need for safe cosmetic products, constant quality assurance and compliance to Good Manufacturing Practices. Moreover, the Product Information File (PIF), mandatory documentation when a cosmetic product is placed on the market contains safety and quality issues whose assurance demands previous planning in the formulation and development phases [186]. Quality by Design (QbD) is a concept applied in several fields of industry, including the pharmaceutical industry, which aims to identify, analyze, and manage all sources that might impact the quality and safety of a product. In this context, the application of the QbD concept to oral care product development leads to an easy and cost-effective development and manufacturing process with consistent and quality products and robust processes. Thus, the development of oral care products should consider all the variables that contribute to the quality of the final product. The Design of Experiments (DoE), as a tool of QbD strategy, can be used to develop cosmetic formulations. DoE represents a systematic study based on statistical models that enables the best ranges for the formulation factors with a minimal number of experimental runs [187]. The optimal formulation resides in a Design Space, an area in the experimental domain where all the conditions requested by the Quality Target Product Profile are fulfilled [188,189]. A coherent control strategy, included in the key points of the process, grants the flexibility of the manufacturing and the constant quality of the cosmetic product. So far, the DoE methodology has proven its efficacy in cosmetic formulation, and also in finding the optimal conditions for PhC extraction from winery by-products [41,45,47,51,67]. Thereby, the formulation obtained attains physicochemical and organoleptic characteristics that could contribute to the in vivo performance of the product.

4. Conclusion and Perspectives

The novelty of this work not only consists of finding new exploitation directions of *V. vinifera* by-products based on recent progress made in this field, but also in defining the scientific framework for the development of oral care formulations based on *V. vinifera* by-products.

Despite the high number of studies showing that winery by-products are a widely available source of bioactive phytocompounds, especially natural antioxidants, these products are currently underexploited in the cosmetic field. Only a few applications in oral care have been found so far, and

additional research is needed to achieve full benefits. In our opinion, for the efficient exploitation of *V. vinifera* by-products, future research should focus on several points:

- The use of emerging techniques with a low environmental impact and sustainable production costs for extract preparation.
- The use of GRAS solvents to obtain low toxicity and biocompatible extracts suitable for oral care products.
- The use of a systematic approach in cosmetic manufacturing that allows for the time-effective and cost-effective development of oral care products.
- Further studies should be conducted to assess the complex interaction between PhCs and inactive ingredients, and also between polyphenols and oral mucosa.
- The development of formulations that fulfill organoleptic characteristics required by consumers.
- The development of highly effective and cost-effective formulations that justify the recycling process.

The rising awareness concerning the environmental impact of by-products has led to new research, aimed towards strategies to reduce waste disposal. In this sense, the sustainable reuse of grape by-products in pharmaceutical or cosmetic sectors could represent alternative approaches. *V. vinifera* is a rich source of bioactive compounds since over 70% of PhCs remain in grape pomace during the winemaking process. The current work reviewed the evidence about the bioactivities of *V. vinifera* by-products in oral health, emphasizing the applicability in oral hygiene products. Thus, several studies supporting the antimicrobial and antiplaque activity of *V. vinifera* extracts against *S. mutans* or in multi-species biofilms were presented. Moreover, the role of the bioactive compounds from *V. vinifera* by-products, concerning the periodontal inflammatory response and the underlying oxidative stress imbalance, was investigated. Considering the complex biological effects of PhCs in the prevention and treatment of microbial-mediated oral pathology, PhCs from *V. vinifera* by-products could be used to control periodontal diseases.

Author Contributions: Conceptualization, C.B., M.L.M.; writing—original draft preparation, C.B., A.P., S.I., D.B., M.L.M.; writing—review and editing, C.B., A.P., S.I., D.B., M.L.M.; project administration, M.L.M.; funding acquisition, M.L.M. All authors have read and agreed to the published version of the manuscript.

Funding: This works was supported by a grant of the Romanian Ministry of Research and Innovation, CCCDI-UEFISCDI, project number PN-III-P1-1.2-PCCDI-2017-0251/4PCCDI/2018, within PNCD III.

Conflicts of Interest: The authors declare no conflict of interest.

References

1. Oral Health. Available online: https://www.who.int/news-room/fact-sheets/detail/oral-health (accessed on 16 March 2020).
2. Oral Infection/Inflammation as a Risk Factor for Systemic Diseases | FDI World Dental Federation. Available online: https://www.fdiworlddental.org/resources/policy-statements-and-resolutions/oral-infectioninflammation-as-a-risk-factor-for-systemic (accessed on 16 March 2020).
3. Jin, L.J.; Lamster, I.B.; Greenspan, J.S.; Pitts, N.B.; Scully, C.; Warnakulasuriya, S. Global burden of oral diseases: emerging concepts, management and interplay with systemic health. *Oral Dis.* **2016**, *22*, 609–619.
4. Lippert, F. An introduction to toothpaste - its purpose, history and ingredients. *Monogr Oral Sci.* **2013**, *23*, 1–14.
5. FAOSTAT, Food and Agriculture Organization of the United Nations, 2018 Available online: http://www.fao.org/faostat/en/?#data/QC (accessed on 28 May 2020).
6. Fontana, A.R.; Antoniolli, A.; Bottini, R. Grape pomace as a sustainable source of bioactive compounds: Extraction, characterization, and biotechnological applications of phenolics. *J. Agric. Food Chem.* **2013**, *61*, 8987–9003.

7. Teixeira, A.; Baenas, N.; Dominguez-Perles, R.; Barros, A.; Rosa, E.; Moreno, D.A.; Garcia-Viguera, C. Natural bioactive compounds from winery by-products as health promoters: A review. *Int. J. Mol. Sci.* **2014**, *15*, 15638–15678.
8. Xia, E.Q.; Deng, G.F.; Guo, Y.J.; Li, H. Bin Biological activities of polyphenols from grapes. *Int. J. Mol. Sci.* **2010**, *11*, 622–646.
9. Zhang, H.; Tsao, R. Dietary polyphenols, oxidative stress and antioxidant and anti-inflammatory effects. *Curr. Opin. Food Sci.* **2016**, *8*, 33–42.
10. Daglia, M. Polyphenols as antimicrobial agents. *Curr. Opin. Biotechnol.* **2012**, *23*, 174–181.
11. Esteban-Fernández, A.; Zorraquín-Peña, I.; González de Llano, D.; Bartolomé, B.; Moreno-Arribas, M.V. The role of wine and food polyphenols in oral health. *Trends Food Sci. Technol.* **2017**, *69*, 118–130.
12. Pizzorno, J.E.; Murray, M.T.; Joiner-Bey, H.; Pizzorno, J.E.; Murray, M.T.; Joiner-Bey, H. Periodontal disease. In *The Clinician's Handbook of Natural Medicine*; Churchill Livingstone: London, UK, 2016; pp. 787–795.
13. Garrido, J.; Borges, F. Wine and grape polyphenols—A chemical perspective. *Food Res. Int.* **2013**, *54*, 1844–1858.
14. Soto, M.; Falqué, E.; Domínguez, H. Relevance of natural phenolics from grape and derivative products in the formulation of cosmetics. *Cosmetics* **2015**, *2*, 259–276.
15. Šuković; Knežević; Gašić, U.; Sredojević; Ćirić; Todic, S.; Mutic, J.; Tesic, Z. Phenolic profiles of leaves, grapes and wine of grapevine variety Vranac (*Vitis vinifera* L.) from Montenegro. *Foods* **2020**, *9*, 138.
16. Fraternale, D.; Ricci, D.; Verardo, G.; Gorassini, A.; Stocchia, V.; Sestili, P. Activity of *Vitis vinifera* tendrils extract against phytopathogenic fungi. *Nat. Prod. Commun.* **2015**, *10*, 1037–42.
17. Singla, S.; Malhotra, R.; Shashikiran, N.D.; Saxena, S. Antibacterial efficacy of mouthwash prepared from pomegranate, grape seed and guava extracts against oral streptococci: An in vivo study. *J. Clin. Pediatr. Dent.* **2018**, *42*, 109–113.
18. Ferri, M.; Bin, S.; Vallini, V.; Fava, F.; Michelini, E.; Roda, A.; Minnucci, G.; Bucchi, G.; Tassoni, A. Recovery of polyphenols from red grape pomace and assessment of their antioxidant and anti-cholesterol activities. *N. Biotechnol.* **2016**, *33*, 338–344.
19. Nieto, J.A.; Santoyo, S.; Prodanov, M.; Reglero, G.; Jaime, L. Valorisation of grape stems as a source of phenolic antioxidants by using a sustainable extraction methodology. *Foods* **2020**, *9*.
20. Li, J.; Zhang, S.; Zhang, M.; Sun, B. Novel approach for extraction of grape skin antioxidants by accelerated solvent extraction: Box–Behnken design optimization. *J. Food Sci. Technol.* **2019**, *56*, 4879–4890.
21. de Camargo, A.C.; Biasoto, A.C.T.; Schwember, A.R.; Granato, D.; Rasera, G.B.; Franchin, M.; Rosalen, P.L.; Alencar, S.M.; Shahidi, F. Should we ban total phenolics and antioxidant screening methods? The link between antioxidant potential and activation of NF-κB using phenolic compounds from grape by-products. *Food Chem.* **2019**, *290*, 229–238.
22. Friedman, M. Antibacterial, antiviral, and antifungal properties of wines and winery byproducts in relation to their flavonoid content. *J. Agric. Food Chem.* **2014**, *62*, 6025–6042.
23. González-Centeno, M.R.; Rosselló, C.; Simal, S.; Garau, M.C.; López, F.; Femenia, A. Physico-chemical properties of cell wall materials obtained from ten grape varieties and their byproducts: Grape pomaces and stems. *Food Sci. Technol.* **2010**, *43*, 1580–1586.
24. Lavelli, V.; Kerr, W.L.; García-Lomillo, J.; González-SanJosé, M.L. Applications of Recovered Bioactive Compounds in Food Products. In *Handbook of Grape Processing by-Products: Sustainable Solutions*; Galanakis, C.M., Ed.; Academic Press: Cambridge, MA, USA, 2017; pp. 230–267.
25. Nunes, M.A.; Rodrigues, F.; Oliveira, M.B.P.P. Grape Processing By-Products as Active Ingredients for Cosmetic Proposes. In *Handbook of Grape Processing By-Products: Sustainable Solutions*; Galanakis, C.M., Ed.; Academic Press: Cambridge, MA, USA, 2017; pp. 267–292.
26. Ky, I.; Lorrain, B.; Kolbas, N.; Crozier, A.; Teissedre, P.L. Wine by-Products: Phenolic characterization and antioxidant activity evaluation of grapes and grape pomaces from six different French grape varieties. *Molecules* **2014**, *19*, 482–506.
27. Moldovan, M.; Bogdan, C.; Iurian, S.; Roman, C.; Oniga, I.; Benedec, D. Phenolic content and antioxidant capacity of pomace and canes extracts of some *Vitis vinifera* varieties cultivated in Romania. *Farmacia* **2020**, *68*, 15–21.

28. Ghafoor, K.; Choi, Y.H.; Jeon, J.Y.; Jo, I.H. Optimization of ultrasound-assisted extraction of phenolic compounds, antioxidants, and anthocyanins from grape *(Vitis vinifera*) seeds. *J. Agric. Food Chem.* **2009**, *57*, 4988–4994.
29. Nassiri-Asl, M.; Hosseinzadeh, H. Review of the Pharmacological Effects of *Vitis vinifera* (Grape) and its Bioactive Constituents: An Update. *Phyther. Res.* **2016**, 1392–1403.
30. Farida, B.; Cadot, Y.; Djamai, R.; Djermoun, L. Determination of major anthocyanin pigments and flavonols in red grape skin of some table grape varieties (*Vitis vinifera* sp.) by high-performance liquid chromatography-photodiode array detection (HPLC-DAD). *OENO One* **2016**, *50*, 125–135.
31. Gouvinhas, I.; Santos, R.A.; Queiroz, M.; Leal, C.; Saavedra, M.J.; Domínguez-Perles, R.; Rodrigues, M.; Barros, A. Monitoring the antioxidant and antimicrobial power of grape (*Vitis vinifera* L.) stems phenolics over long-term storage. *Ind. Crops Prod.* **2018**, *126*, 83–91.
32. Leal, C.; Santos, R.A.; Pinto, R.; Queiroz, M.; Rodrigues, M.; José Saavedra, M.; Barros, A.; Gouvinhas, I. Recovery of bioactive compounds from white grape (*Vitis vinifera* L.) stems as potential antimicrobial agents for human health. *Saudi J. Biol. Sci.* **2020**, *27*, 1009–1015.
33. Anastasiadi, M.; Pratsinis, H.; Kletsas, D.; Skaltsounis, A.L.; Haroutounian, S.A. Grape stem extracts: Polyphenolic content and assessment of their in vitro antioxidant properties. *Food Sci. Technol.* **2012**, *48*, 316–322.
34. Moldovan, M.L.; Carpa, R.; Fizeșan, I.; Vlase, L.; Bogdan, C.; Iurian, S.M.; Benedec, D.; Pop, A. Phytochemical profile and biological activities of tendrils and leaves extracts from a variety of *Vitis vinifera L. Antioxidants 2020* **2020**, *9*, 373.
35. Fraternale, D.; Rudov, A.; Prattichizzo, F.; Olivieri, F.; Ricci, D.; Giacomini, E.; Carloni, S.; Azzolini, C.; Gordillo, B.; Jara-Palacios, M.J. Chemical composition and "*in vitro*" anti-inflammatory activity of *Vitis vinifera L.*(var. Sangiovese) tendrils extract. *J. Funct. Foods* **2016**, *20*, 291–302.
36. European Medicines Agency Assessment report on *Vitis vinifera L.*, folium - Final Available online: www.ema.europa.eu/contact (accessed on 27 April 2020).
37. Dresch, R.; Dresch, M.; Guerreiro, A.; Biegelmeyer, R.; Holzschuh, M.; Rambo, D.; Henriques, A. Phenolic compounds from the leaves of Vitis labrusca and *Vitis vinifera L.* as a source of waste byproducts: development and validation of LC Method and antichemotactic activity. *Food Anal. Methods* **2014**, *7*.
38. Montero, L.; Sáez, V.; von Baer, D.; Cifuentes, A.; Herrero, M. Profiling of *Vitis vinifera L.* canes (poly)phenolic compounds using comprehensive two-dimensional liquid chromatography. *J. Chromatogr. A* **2018**, *1536*, 205–215.
39. Çetin, E.S.; Altinöz, D.; Tarçan, E.; Göktürk Baydar, N. Chemical composition of grape canes. *Ind. Crops Prod.* **2011**, *34*, 994–998.
40. Sánchez-Gómez, R.; Zalacain, A.; Alonso, G.L.; Salinas, M.R. Vine-shoot waste aqueous extracts for re-use in agriculture obtained by different extraction techniques: Phenolic, volatile, and mineral compounds. *J. Agric. Food Chem.* **2014**, *62*, 10861–10872.
41. Moldovan, M.; Iurian, S.; Bischin Pușcaș, C.; Silaghi-Dumitrescu, R.; Hanganu, D.; Bogdan, C.; Vlase, L.; Oniga, I.; Benedec, D. A Design of Experiments strategy to enhance the recovery of polyphenolic compounds from *Vitis vinifera* by-products through heat reflux extraction. *Biomolecules* **2019**, *9*, 529.
42. Moreira, M.M.; Barroso, M.F.; Porto, J.V.; Ramalhosa, M.J.; Švarc-Gajić, J.; Estevinho, L.; Morais, S.; Delerue-Matos, C. Potential of Portuguese vine shoot wastes as natural resources of bioactive compounds. *Sci. Total Environ.* **2018**, *634*, 831–842.
43. Peixoto, C.M.; Dias, M.I.; Alves, M.J.; Calhelha, R.C.; Barros, L.; Pinho, S.P.; Ferreira, I.C.F.R. Grape pomace as a source of phenolic compounds and diverse bioactive properties. *Food Chem.* **2018**, *253*, 132–138.
44. Zhu, W.; Sun, S.; Yang, F.; Zhou, K. UHPLC/MS Identifying potent α-glucosidase inhibitors of grape pomace via Enzyme Immobilized Method. *J. Food Sci.* **2018**, *83*, 1131–1139.
45. Nayak, A.; Bhushan, B.; Rosales, A.; Turienzo, L.R.; Cortina, J.L. Valorisation potential of Cabernet grape pomace for the recovery of polyphenols: Process intensification, optimisation and study of kinetics. *Food Bioprod. Process.* **2018**, *109*, 74–85.
46. Ferri, M.; Rondini, G.; Calabretta, M.M.; Michelini, E.; Vallini, V.; Fava, F.; Roda, A.; Minnucci, G.; Tassoni, A. White grape pomace extracts, obtained by a sequential enzymatic plus ethanol-based extraction, exert antioxidant, anti-tyrosinase and anti-inflammatory activities. *N. Biotechnol.* **2017**, *39*, 51–58.

47. Meini, M.R.; Cabezudo, I.; Boschetti, C.E.; Romanini, D. Recovery of phenolic antioxidants from Syrah grape pomace through the optimization of an enzymatic extraction process. *Food Chem.* **2019**, *283*, 257–264.
48. Brianceau, S.; Turk, M.; Vitrac, X.; Vorobiev, E. Combined densification and pulsed electric field treatment for selective polyphenols recovery from fermented grape pomace. *Innov. Food Sci. Emerg. Technol.* **2015**, *29*, 2–8.
49. Antoniolli, A.; Fontana, A.R.; Piccoli, P.; Bottini, R. Characterization of polyphenols and evaluation of antioxidant capacity in grape pomace of the cv. Malbec. *Food Chem.* **2015**, *178*, 172–178.
50. Natolino, A.; Da Porto, C.; Rodríguez-Rojo, S.; Moreno, T.; Cocero, M.J. Supercritical antisolvent precipitation of polyphenols from grape marc extract. *J. Supercrit. Fluids* **2016**, *118*, 54–63.
51. Garrido, T.; Gizdavic-Nikolaidis, M.; Leceta, I.; Urdanpilleta, M.; Guerrero, P.; de la Caba, K.; Kilmartin, P.A. Optimizing the extraction process of natural antioxidants from chardonnay grape marc using microwave-assisted extraction. *Waste Manag.* **2019**, *88*, 110–117.
52. Barba, F.J.; Brianceau, S.; Turk, M.; Boussetta, N.; Vorobiev, E. Effect of alternative physical treatments (Ultrasounds, Pulsed Electric Fields, and High-Voltage Electrical Discharges) on selective recovery of bio-compounds from fermented grape pomace. *Food Bioprocess Technol.* **2015**, *8*, 1139–1148.
53. Rinaldi, A.; Iturmendi, N.; Jourdes, M.; Teissedre, P.L.; Moio, L. Transfer of tannin characteristics from grape skins or seeds to wine-like solutions and their impact on potential astringency. *Food Sci. Technol.* **2015**, *63*, 667–676.
54. Garcia-Jares, C.; Vazquez, A.; Lamas, J.P.; Pajaro, M.; Alvarez-Casas, M.; Lores, M.; Segura-Carretero, A.; Arrá Ez-Romá, D. Antioxidant white grape seed phenolics: pressurized liquid extracts from different varieties. *Antioxidants* **2015**, *4*, 737–749.
55. Chedea, V.S.; Echim, C.; Braicu, C.; Andjelkovic, M.; Verhe, R.; Socaciu, C. Composition in polyphenols and stability of aqueous grape seed extract from the Romanian variety 'Merlot Recas'. *J. Food Biochem.* **2011**, *35*, 92–108.
56. Mildner-Szkudlarz, S.; Zawirska-Wojtasiak, R.; Gośliński, M. Phenolic compounds from winemaking waste and its antioxidant activity towards oxidation of rapeseed oil. *Int. J. Food Sci. Technol.* **2010**, *45*, 2272–2280.
57. Hernández-Jiménez, A.; Kennedy, J.A.; Bautista-Ortín, A.B.; Gómez-Plaza, E. Effect of ethanol on grape seed proanthocyanidin extraction. *Am. J. Enol. Vitic.* **2012**, *63*, 57–61.
58. Yilmaz, Y.; Toledo, R.T. Major flavonoids in grape seeds and skins: antioxidant capacity of catechin, epicatechin, and gallic acid. *J. Agric. Food Chem.* **2004**, *52*, 255–260.
59. Deng, Q.; Penner, M.H.; Zhao, Y. Chemical composition of dietary fiber and polyphenols of five different varieties of wine grape pomace skins. *Food Res. Int.* **2011**, *44*, 2712–2720.
60. Kwiatkowski, M.; Kravchuk, O.; Skouroumounis, G.K.; Taylor, D.K. Response surface parallel optimization of extraction of total phenolics from separate white and red grape skin mixtures with microwave-assisted and conventional thermal methods. *J. Clean. Prod.* **2020**, *251*, 119563.
61. Caldas, T.W.; Mazza, K.E.L.; Teles, A.S.C.; Mattos, G.N.; Brígida, A.I.S.; Conte-Junior, C.A.; Borguini, R.G.; Godoy, R.L.O.; Cabral, L.M.C.; Tonon, R.V. Phenolic compounds recovery from grape skin using conventional and non-conventional extraction methods. *Ind. Crops Prod.* **2018**, *111*, 86–91.
62. Nogales-Bueno, J.; Baca-Bocanegra, B.; Jara-Palacios, M.J.; Hernández-Hierro, J.M.; Heredia, F.J. Evaluation of the influence of white grape seed extracts as copigment sources on the anthocyanin extraction from grape skins previously classified by near infrared hyperspectral tools. *Food Chem.* **2017**, *221*, 1685–1690.
63. Stavikova, L.; Polovka, M.; Hohnová, B.; Karásek, P.; Roth, M. Antioxidant activity of grape skin aqueous extracts from pressurized hot water extraction combined with electron paramagnetic resonance spectroscopy. *Talanta* **2011**, *85*, 2233–2240.
64. Cvjetko Bubalo, M.; Ćurko, N.; Tomašević, M.; Kovačević Ganić, K.; Radojcic Redovnikovic, I. Green extraction of grape skin phenolics by using deep eutectic solvents. *Food Chem.* **2016**, *200*, 159–166.
65. Goutzourelas, N.; Stagos, D.; Spanidis, Y.; Liosi, M.; Apostolou, A.; Priftis, A.; Haroutounian, S.; Spandidos, D.A.; Tsatsakis, A.M.; Kouretas, D. Polyphenolic composition of grape stem extracts affects antioxidant activity in endothelial and muscle cells. *Mol. Med. Rep.* **2015**, *12*, 5846–5856.
66. Sun, H.; Lin, Q.; Wei, W.; Qin, G. Ultrasound-assisted extraction of resveratrol from grape leaves and its purification on mesoporous carbon. *Food Sci. Biotechnol.* **2018**, *27*, 1353–1359.

67. Aguilar, T.; Loyola, C.; de Bruijn, J.; Bustamante, L.; Vergara, C.; von Baer, D.; Mardones, C.; Serra, I. Effect of thermomaceration and enzymatic maceration on phenolic compounds of grape must enriched by grape pomace, vine leaves and canes. *Eur. Food Res. Technol.* **2016**, *242*, 1149–1158.
68. Jesus, M.S.; Ballesteros, L.F.; Pereira, R.N.; Genisheva, Z.; Carvalho, A.C.; Pereira-Wilson, C.; Teixeira, J.A.; Domingues, L. Ohmic heating polyphenolic extracts from vine pruning residue with enhanced biological activity. *Food Chem.* **2020**, *316*, 126298.
69. Lu, M.; Xuan, S.; Wang, Z. Oral microbiota: A new view of body health. *Food Sci. Hum. Wellness* **2019**, *8*, 8–15.
70. Chinsembu, K.C. Plants and other natural products used in the management of oral infections and improvement of oral health. *Acta Trop.* **2016**, *154*, 6–18.
71. Digel, I.; Kern, I.; Geenen, E.M.; Akimbekov, N. Dental plaque removal by ultrasonic toothbrushes. *Dent. J.* **2020**, *8*, 28.
72. Sánchez, M.C.; Ribeiro-Vidal, H.; Esteban-Fernández, A.; Bartolomé, B.; Figuero, E.; Moreno-Arribas, M.V.; Sanz, M.; Herrera, D. Antimicrobial activity of red wine and oenological extracts against periodontal pathogens in a validated oral biofilm model. *BMC Complement. Altern. Med.* **2019**, *19*, 1–12.
73. Hakeem, K.R.; Abdul, W.M.; Hussain, M.M.; Razvi, S.S.I. Oral health and herbal medicine. In *SpringerBriefs in Public Health*; Springer International Publishing: New York, NY, 2019; pp. 1–46.
74. Levine, R.S. Advancing the scientific basis of oral health education. *Community Dent. Health* **2015**, *32*, 66–67.
75. Milovanova-Palmer, J.; Pendry, B. Is there a role for herbal medicine in the treatment and management of periodontal disease? *J. Herb. Med.* **2018**, *12*, 33–48.
76. Peres, M.A.; Macpherson, L.M.D.; Weyant, R.J.; Daly, B.; Venturelli, R.; Mathur, M.R.; Listl, S.; Celeste, R.K.; Guarnizo-Herreño, C.C.; Kearns, C.; et al. Oral diseases: a global public health challenge. *Lancet* **2019**, *394*, 249–260.
77. Wu, C.D. Grape Products and Oral Health. *J. Nutr.* **2009**, *139*, 1818S-1823S.
78. Metwalli, K.H.; Khan, S.A.; Krom, B.P.; Jabra-Rizk, M.A. *Streptococcus mutans*, *Candida albicans*, and the human mouth: a sticky situation. *PLoS Pathog.* **2013**, *9*, e1003616.
79. Lemos, J.A.; Palmer, S.R.; Zeng, L.; Wen, Z.T.; Kajfasz, J.K.; Freires, I.A.; Abranches, J.; Brady, L.J. The Biology of *Streptococcus mutans*. *Microbiol. Spectr.* **2019**, *7*.
80. Wang, Y.; Zhang, J.; Chen, X.; Jiang, W.; Wang, S.; Xu, L.; Tu, Y.; Zheng, P.; Wang, Y.; Lin, X.; et al. Profiling of oral microbiota in early childhood caries using single-molecule real-time sequencing. *Front. Microbiol.* **2017**, *8*, 2244.
81. Kouidhi, B.; Al Qurashi, Y.M.A.; Chaieb, K. Drug resistance of bacterial dental biofilm and the potential use of natural compounds as alternative for prevention and treatment. *Microb. Pathog.* **2015**, *80*, 39–49.
82. Oliveira, D.A.; Salvador, A.A.; Smânia, A.; Smânia, E.F.A.; Maraschin, M.; Ferreira, S.R.S. Antimicrobial activity and composition profile of grape (*Vitis vinifera*) pomace extracts obtained by supercritical fluids. *J. Biotechnol.* **2013**, *164*, 423–432.
83. Van Loveren, C.; Broukal, Z.; Oganessian, E. Functional foods/ingredients and dental caries. *Eur. J. Nutr.* **2012**, *51*, S15-S25.
84. Yadav, D.; Kumar, A.; Kumar, P.; Mishra, D. Antimicrobial properties of black grape (*Vitis vinifera L.*) peel extracts against antibiotic-resistant pathogenic bacteria and toxin producing molds. *Ind. J. Pharmacol.* **2015**, *47*, 663.
85. Rivero-Cruz, J.F.; Zhu, M.; Kinghorn, A.D.; Wu, C.D. Antimicrobial constituents of Thompson seedless raisins (*Vitis vinifera*) against selected oral pathogens. *Phytochem. Lett.* **2008**, *1*, 151–154.
86. Zhao, W.; Xie, Q.; Bedran-Russo, A.K.; Pan, S.; Ling, J.; Wu, C.D. The preventive effect of grape seed extract on artificial enamel caries progression in a microbial biofilm-induced caries model. *J. Dent.* **2014**, *42*, 1010–1018.
87. Furiga, A.; Lonvaud-Funel, A.; Dorignac, G.; Badet, C. *In vitro* anti-bacterial and anti-adherence effects of natural polyphenolic compounds on oral bacteria. *J. Appl. Microbiol.* **2008**, *105*, 1470–1476.
88. Thimothe, J.; Bonsi, I.A.; Padilla-Zakour, O.I.; Koo, H. Chemical characterization of red wine grape (*Vitis vinifera* and *Vitis* interspecific hybrids) and pomace phenolic extracts and their biological activity against *Streptococcus mutans*. *J. Agric. Food Chem.* **2007**, *55*, 10200–10207.
89. Furiga, A.; Lonvaud-Funel, A.; Badet, C. *In vitro* study of antioxidant capacity and antibacterial activity on oral anaerobes of a grape seed extract. *Food Chem.* **2009**, *113*, 1037–1040.

90. Furiga, A.; Roques, C.; Badet, C. Preventive effects of an original combination of grape seed polyphenols with amine fluoride on dental biofilm formation and oxidative damage by oral bacteria. *J. Appl. Microbiol.* **2014**, *116*, 761–771.
91. Muñoz-González, I.; Thurnheer, T.; Bartolomé, B.; Moreno-Arribas, M.V. Red wine and oenological extracts display antimicrobial effects in an oral bacteria biofilm model. *J. Agric. Food Chem.* **2014**, *62*, 4731–4737.
92. Hannig, C.; Sorg, J.; Spitzmüller, B.; Hannig, M.; Al-Ahmad, A. Polyphenolic beverages reduce initial bacterial adherence to enamel *in situ*. *J. Dent.* **2009**, *37*, 560–566.
93. Pavan, S.; Xie, Q.; Hara, A.T.; Bedran-Russo, A.K. Biomimetic approach for root caries prevention using a proanthocyanidin- rich agent. *Caries Res.* **2011**, *45*, 443–447.
94. Epasinghe, D.J.; Yiu, C.K.Y.; Burrow, M.F.; Hiraishi, N.; Tay, F.R. The inhibitory effect of proanthocyanidin on soluble and collagen-bound proteases. *J. Dent.* **2013**, *41*, 832–839.
95. Firouzmandi, M.; Shafiei, F.; Jowkar, Z.; Nazemi, F. Effect of silver diamine fluoride and proanthocyanidin on mechanical properties of caries-affected dentin. *Eur. J. Dent.* **2019**, *13*, 255–260.
96. Bedran-Russo, A.K.B.; Pereira, P.N.R.; Duarte, W.R.; Drummond, J.L.; Yamauchi, M. Application of crosslinkers to dentin collagen enhances the ultimate tensile strength. *J. Biomed. Mater. Res. Part B Appl. Biomater.* **2007**, *80B*, 268–272.
97. Bedran-Russo, A.K.B.; Pashley, D.H.; Agee, K.; Drummond, J.L.; Miescke, K.J. Changes in stiffness of demineralized dentin following application of collagen crosslinkers. *J. Biomed. Mater. Res. - Part B Appl. Biomater.* **2008**, *86*, 330–334.
98. MacEdo, G.V.; Yamauchi, M.; Bedran-Russo, A.K. Effects of chemical cross-linkers on caries-affected dentin bonding. *J. Dent. Res.* **2009**, *88*, 1096–1100.
99. He, L.; Mu, C.; Shi, J.; Zhang, Q.; Shi, B.; Lin, W. Modification of collagen with a natural cross-linker, procyanidin. *Int. J. Biol. Macromol.* **2011**, *48*, 354–359.
100. Liu, R.; Fang, M.; Xiao, Y.; Li, F.; Yu, L.; Zhao, S.; Shen, L.; Chen, J. The effect of transient proanthocyanidins preconditioning on the cross-linking and mechanical properties of demineralized dentin. *J. Mater. Sci. Mater. Med.* **2011**, *22*, 2403–2411.
101. Al-Ammar, A.; Drummond, J.L.; Bedran-Russo, A.K. The use of collagen cross-linking agents to enhance dentin bond strength. *J. Biomed. Mater. Res. Part B Appl. Biomater.* **2009**, *91B*, 419–424.
102. Castellan, C.S.; Pereira, P.N.; Grande, R.H.M.; Bedran-Russo, A.K. Mechanical characterization of proanthocyanidin-dentin matrix interaction. *Dent. Mater.* **2010**, *26*, 968–973.
103. Fang, M.; Liu, R.; Xiao, Y.; Li, F.; Wang, D.; Hou, R.; Chen, J. Biomodification to dentin by a natural crosslinker improved the resin-dentin bonds. *J. Dent.* **2012**, *40*, 458–466.
104. Green, B.; Yao, X.; Ganguly, A.; Xu, C.; Dusevich, V.; Walker, M.P.; Wang, Y. Grape seed proanthocyanidins increase collagen biodegradation resistance in the dentin/adhesive interface when included in an adhesive. *J. Dent.* **2010**, *38*, 908–915.
105. Berger, D.; Rakhamimova, A.; Pollack, A.; Loewy, Z. Oral Biofilms: development, control, and analysis. *High-Throughput* **2018**, *7*, E24.
106. Subbarao, K.; Nattuthurai, G.; Sundararajan, S.; Sujith, I.; Joseph, J.; Syedshah, Y. Gingival crevicular fluid: An overview. *J. Pharm. Bioallied Sci.* 2019, *11*, S135–S139.
107. Khurshid, Z.; Mali, M.; Naseem, M.; Najeeb, S.; Zafar, M. Human gingival crevicular fluids (GCF) proteomics: an overview. *Dent. J.* **2017**, *5*, E12.
108. Dahiya, P.; Kamal, R.; Gupta, R.; Bhardwaj, R.; Chaudhary, K.; Kaur, S. Reactive oxygen species in periodontitis. *J. Indian Soc. Periodontol.* **2013**, *17*, 411–416.
109. How, K.Y.; Song, K.P.; Chan, K.G. *Porphyromonas gingivalis*: an overview of periodontopathic pathogen below the gum line. *Front. Microbiol.* **2016**, *7*.
110. Kinane, D.F.; Stathopoulou, P.G.; Papapanou, P.N. Periodontal diseases. *Nat. Rev. Dis. Prim.* **2017**, *3*, 17038.
111. Esteban-Fernández, A.; Zorraquín-PenÌa, I.; Ferrer, M.D.; Mira, A.; Bartolomé, B.; González De Llano, D.; Victoria Moreno-Arribas, M. Inhibition of oral pathogens adhesion to human gingival fibroblasts by wine polyphenols alone and in combination with an oral probiotic. *J. Agric. Food Chem.* **2018**, *66*, 2071–2082.
112. Yoshihara-Hirata, C.; Yamashiro, K.; Yamamoto, T.; Aoyagi, H.; Ideguchi, H.; Kawamura, M.; Suzuki, R.; Ono, M.; Wake, H.; Nishibori, M.; et al. Anti-HMGB1 neutralizing antibody attenuates periodontal inflammation and bone resorption in a murine periodontitis model. *Infect. Immun.* **2018**, *86*.

113. Pham-Huy, L.A.; He, H.; Pham-Huy, C. Free radicals, antioxidants in disease and health. *Int. J. Biomed. Sci. IJBS* **2008**, *4*, 89.
114. Chen, S.; Meng, X.F.; Zhang, C. Role of NADPH oxidase-mediated reactive oxygen species in podocyte injury. *Biomed Res. Int.* **2013**, *2013*.
115. Rubiolo, J.A.; Mithieux, G.; Vega, F.V. Resveratrol protects primary rat hepatocytes against oxidative stress damage: Activation of the Nrf2 transcription factor and augmented activities of antioxidant enzymes. *Eur. J. Pharmacol.* **2008**, *591*, 66–72.
116. Pan, W.; Wang, Q.; Chen, Q. The cytokine network involved in the host immune response to periodontitis. *Int. J. Oral Sci.* **2019**, *11*, 1–13.
117. Nichols, T.C.; Fischer, T.H.; Deliargyris, E.N.; Baldwin, A.S. Role of nuclear factor-kappa B (NF-kappa B) in inflammation, periodontitis, and atherogenesis. *Ann. Periodontol.* **2001**, *6*, 20–29.
118. Bondm, C. Inhibition of transcription factor NF-kappaB reduces matrix metalloproteinase-1, -3 and -9 production by vascular smooth muscle cells. *Cardiovasc. Res* **2001**, *50*, 556.
119. Żukowski, P.; Maciejczyk, M.; Waszkiel, D. Sources of free radicals and oxidative stress in the oral cavity. *Arch. Oral Biol.* **2018**, *92*, 8–17.
120. Badisa, R.B.; Tzakou, O.; Couladis, M.; Pilarinou, E. Cytotoxic activities of Salvia plants of the Labiatae family. *Pharm. Biol.* **2004**, *42*, 640–645.
121. Yucel-Lindberg, T.; Båge, T. Inflammatory mediators in the pathogenesis of periodontitis. *Expert Rev. Mol. Med.* **2013**, *15*.
122. Krayer, J.W.; Leite, R.S.; Kirkwood, K.L. Non-surgical chemotherapeutic treatment strategies for the management of periodontal diseases. *Dent. Clin.* **2010**, *54*, 13–33.
123. Dabholkar, C.S.; Shah, M.; Kathariya, R.; Bajaj, M.; Doshi, Y. Comparative evaluation of antimicrobial activity of pomegranate-containing mouthwash against oral-biofilm forming organisms: an *in vitro* microbial study. *J. Clin. Diagn. Res.* **2016**, *10*, ZC65.
124. Palaska, I.; Papathanasiou, E.; Theoharides, T.C. Use of polyphenols in periodontal inflammation. *Eur. J. Pharmacol.* **2013**, *720*, 77–83.
125. Forester, S.C.; Lambert, J.D. The role of antioxidant versus pro-oxidant effects of green tea polyphenols in cancer prevention. *Mol. Nutr. Food Res.* **2011**, *55*, 844–854.
126. Tsao, R. Chemistry and biochemistry of dietary polyphenols. *Nutrients* **2010**, *2*, 1231–1246.
127. Bouayed, J.; Bohn, T. Exogenous antioxidants—double-edged swords in cellular redox state: health beneficial effects at physiologic doses versus deleterious effects at high doses. *Oxid. Med. Cell. Longev.* **2010**, *3*, 228–237.
128. Tsao, R.; Li, H. Antioxidant properties in vitro and in vivo: realistic assessments of efficacy of plant extracts. *Plant Sci. Rev.* **2012**, *7*, 11–13.
129. Goutzourelas, N.; Stagos, D.; Housmekeridou, A.; Karapouliou, C.; Kerasioti, E.; Aligiannis, N.; Skaltsounis, A.L.; Spandidos, D.A.; Tsatsakis, A.M.; Kouretas, D. Grape pomace extract exerts antioxidant effects through an increase in GCS levels and GST activity in muscle and endothelial cells. *Int. J. Mol. Med.* **2015**, *36*, 433–441.
130. Chuang, C.-C.; McIntosh, M.K. Potential mechanisms by which polyphenol-rich grapes prevent obesity-mediated inflammation and metabolic diseases. *Annu. Rev. Nutr.* **2011**, *31*, 155–176.
131. Köhle, C.; Bock, K.W. Activation of coupled Ah receptor and Nrf2 gene batteries by dietary phytochemicals in relation to chemoprevention. *Biochem. Pharmacol.* **2006**, *72*, 795–805.
132. Das, S.; Das, D.K. Anti-inflammatory responses of resveratrol. *Inflamm. Allergy Drug Targets* **2007**, *6*, 168–173.
133. Rizzo, A.; Bevilacqua, N.; Guida, L.; Annunziata, M.; Romano Carratelli, C.; Paolillo, R. Effect of resveratrol and modulation of cytokine production on human periodontal ligament cells. *Cytokine* **2012**, *60*, 197–204.
134. Corrêa, M.G.; Pires, P.R.; Ribeiro, F.V.; Pimentel, S.Z.; Casarin, R.C. V.; Cirano, F.R.; Tenenbaum, H.T.; Casati, M.Z. Systemic treatment with resveratrol and/or curcumin reduces the progression of experimental periodontitis in rats. *J. Periodontal Res.* **2017**, *52*, 201–209.
135. Zare Javid, A.; Hormoznejad, R.; Yousefimanesh, H. allah; Zakerkish, M.; Haghighi-zadeh, M.H.; Dehghan, P.; Ravanbakhsh, M. The impact of resveratrol supplementation on blood glucose, insulin, insulin resistance, triglyceride, and periodontal markers in type 2 diabetic patients with chronic periodontitis. *Phyther. Res.* **2017**, *31*, 108–114.

136. Houde, V.; Grenier, D.; Chandad, F. Protective effects of grape seed proanthocyanidins against oxidative stress induced by lipopolysaccharides of periodontopathogens. *J. Periodontol.* **2006**, *77*, 1371–1379.
137. Anastasiadi, M.; Pratsinis, H.; Kletsas, D.; Skaltsounis, A.-L.; Haroutounian, S.A. Bioactive non-coloured polyphenols content of grapes, wines and vinification by-products: Evaluation of the antioxidant activities of their extracts. *Food Res. Int.* **2010**, *43*, 805–813.
138. La, V.D.; Bergeron, C.; Gafner, S.; Grenier, D. Grape seed extract suppresses lipopolysaccharide-induced matrix metalloproteinase (MMP) secretion by macrophages and inhibits Human MMP-1 and− 9 activities. *J. Periodontol.* **2009**, *80*, 1875–1882.
139. Choi, S.K.; Zhang, X.H.; Seo, J.S. Suppression of oxidative stress by grape seed supplementation in rats. *Nutr. Res. Pract.* **2012**, *6*, 3–8.
140. Li, W.G.; Zhang, X.Y.; Wu, Y.J.; Tian, X. Anti-inflammatory effect and mechanism of proanthocyanidins from grape seeds. *Acta Pharmacol. Sin.* **2001**, *12*, 1117–1120.
141. Özden, F.O.; Sakallioğlu, E.E.; Sakallioğlu, U.; Ayas, B.; Erişgin, Z. Effects of grape seed extract on periodontal disease: An experimental study in rats. *J. Appl. Oral Sci.* **2017**, *25*, 121–129.
142. Bonifait, L.; Grenier, D. Cranberry polyphenols: Potential benefits for dental caries and periodontal disease. *J. Can. Dent. Assoc. (Tor).* **2010**, *76*, a130.
143. Llobera, A. Study on the antioxidant activity of grape stems (*Vitis vinifera*). A preliminary assessment of crude extracts. *Food Nutr. Sci.* **2012**, *3*, 500–504.
144. Apostolou, A.; Stagos, D.; Galitsiou, E.; Spyrou, A.; Haroutounian, S.; Portesis, N.; Trizoglou, I.; Hayes, A.W.; Tsatsakis, A.M.; Kouretas, D. Assessment of polyphenolic content, antioxidant activity, protection against ROS-induced DNA damage and anticancer activity of *Vitis vinifera* stem extracts. *Food Chem. Toxicol.* **2013**, *61*, 60–68.
145. Fraternale, D.; De Bellis, R.; Calcabrini, C.; Potenza, L.; Cucchiarini, L.; Mancini, U.; Dachà, M.; Ricci, D. Aqueous extract from *Vitis vinifera* tendrils is able to enrich keratinocyte antioxidant defences. *Nat. Prod. Commun.* **2011**, *6*, 1315–1319.
146. Esatbeyoglu, T.; Ewald, P.; Yasui, Y.; Yokokawa, H.; Wagner, A.E.; Matsugo, S.; Winterhalter, P.; Rimbach, G. Chemical characterization, free radical scavenging, and cellular antioxidant and anti-inflammatory properties of a stilbenoid-rich root extract of *Vitis vinifera*. *Oxid. Med. Cell. Longev.* **2016**, *2016*, 8591286.
147. Katalinić, V.; Generalić Mekinić, I.; Skroza, D.; Ljubenkov, I.; Teskera, A.; Konta, I.; Boban, M. Insight in the phenolic composition and antioxidative properties of *Vitis vinifera* leaves extracts. *Croat. J. Food Sci. Technol.* **2009**, *1*, 7–15.
148. Sangiovanni, E.; Di Lorenzo, C.; Colombo, E.; Colombo, F.; Fumagalli, M.; Frigerio, G.; Restani, P.; Dell'Agli, M. The effect of *in vitro* gastrointestinal digestion on the anti-inflammatory activity of *Vitis vinifera L.* leaves. *Food Funct.* **2015**, *6*, 2453–63.
149. Sangiovanni, E.; Di Lorenzo, C.; Piazza, S.; Manzoni, Y.; Brunelli, C.; Fumagalli, M.; Magnavacca, A.; Martinelli, G.; Colombo, F.; Casiraghi, A.; et al. Vitis vinifera L. Leaf extract inhibits *in vitro* mediators of inflammation and oxidative stress involved in inflammatory-based skin diseases. *Antioxidants* **2019**, *8*.
150. Marabini, L.; Melzi, G.; Lolli, F.; Dell'Agli, M.; Piazza, S.; Sangiovanni, E.; Marinovich, M. Effects of *Vitis vinifera L.* leaves extract on UV radiation damage in human keratinocytes (HaCaT). *J. Photochem. Photobiol. B Biol.* **2020**, *204*, 111810.
151. Aouey, B.; Samet, A.; Fetoui, H.; Simmonds, M.; Bouaziz, M. Anti-oxidant, anti-inflammatory, analgesic and antipyretic activities of grapevine leaf extract (*Vitis vinifera*) in mice and identification of its active constituents by LC–MS/MS analyses. *Biomed. Pharmacother.* **2016**, *84*, 1088–1098.
152. Chidambara Murthy, K.N.; Singh, R.P.; Jayaprakasha, G.K. Antioxidant activities of grape (*Vitis vinifera*) pomace extracts. *J. Agric. Food Chem.* **2002**, *50*, 5909–5914.
153. Maluf, D.F.; Gonçalves, M.M.; D'Angelo, R.W.O.; Girassol, A.B.; Tulio, A.P.; Pupo, Y.M.; Farago, P.V. Cytoprotection of antioxidant biocompounds from grape pomace: Further exfoliant phytoactive ingredients for cosmetic products. *Cosmetics* **2018**, *5*, 46.
154. Torre, E.; Iviglia, G.; Cassinelli, C.; Morra, M.; Russo, N. Polyphenols from grape pomace induce osteogenic differentiation in mesenchymal stem cells. *Int. J. Mol. Med.* **2020**, *45*, 1721.
155. Russo, N.; Cassinelli, C.; Torre, E.; Morra, M.; Iviglia, G. Improvement of the physical properties of guided bone regeneration membrane from porcine pericardium by polyphenols-rich pomace extract. *Materials (Basel).* **2019**, *12*.

156. Silveira, N.; Sandjo, L.P.; Biavatti, M.W. Spilanthol-containing products: A patent review (1996–2016). *Trends Food Sci. Technol.* **2018**, *74*, 107–111.
157. US6706256B2—Oral care compositions—Google Patents Available online: https://patents.google.com/patent/US6706256B2/en (accessed on 28 April 2020).
158. US20120207806A1—Multi-purpose dental appliance cleaner—Google Patents Available online: https://patents.google.com/patent/US20120207806A1/en?oq=US+2012%2F0207806A1+ (accessed on 28 April 2020).
159. US20100129297A1—Use of an aqueous grape seed extract combined with at least one fluorine salt to combat the formation or accumulation of dental biofilm and compositions comprising said combination—Google Patents Available online: https://patents.google.com/patent/US20100129297A1/en?oq=US+2010%2F0129297+A1 (accessed on 28 April 2020).
160. US8273385B1—Oral rinse composition and method - Google Patents Available online: https://patents.google.com/patent/US8273385B1/en?oq=US+8%2C273%2C385+B1 (accessed on 28 April 2020).
161. US7736629B2—Red herbal dentifrice—Google Patents Available online: https://patents.google.com/patent/US7736629B2/en?oq=US+Pat.+No.+7%2C736%2C629+B2 (accessed on 28 April 2020).
162. US8728446B2—Oral hygiene tablets and capsules for direct oral delivery of active ingredients - Google Patents Available online: https://patents.google.com/patent/US8728446B2/en?oq=US+Pat.+No.+8%2C728%2C446+B2 (accessed on 28 April 2020).
163. US6664225B2 - Single-dose quick-dissolving cleansing agent with medicinal properties - Google Patents Available online: https://patents.google.com/patent/US6664225B2/en?q=Single-dose+quick+dissolving+cleansing+agent&oq=Single-dose+quick+dissolving+cleansing+agent+ (accessed on 28 April 2020).
164. Mason, S. Dental Hygiene. In *Poucher's Perfumes, Cosmetics and Soaps*; Butler, H., Ed.; Springer: Heidelberg, Germany, 2000; pp. 217–253.
165. Requena, T.; Monagas, M.; Pozo-Bayón, M.A.; Martín-Álvarez, P.J.; Bartolomé, B.; del Campo, R.; Ávila, M.; Martínez-Cuesta, M.C.; Peláez, C.; Moreno-Arribas, M.V. Perspectives of the potential implications of wine polyphenols on human oral and gut microbiota. *Trends Food Sci. Technol.* **2010**, *21*, 332–344.
166. Braga, A.S.; Girotti, L.D.; de Melo Simas, L.L.; Pires, J.G.; Pelá, V.T.; Buzalaf, M.A.R.; Magalhães, A.C. Effect of commercial herbal toothpastes and mouth rinses on the prevention of enamel demineralization using a microcosm biofilm model. *Biofouling* **2019**, *35*, 796–804.
167. Iqbal, K.; Asmat, M.; Jawed, S.; Mushtaque, A.; Mohsin, F.; Hanif, S.; Sheikh, N. Role of different ingredients of tooth pastes and mouthwashes in oral health. *JPDA* **2011**, *20*, 163–170.
168. Toothpastes. Available online: https://www.ada.org/en/member-center/oral-health-topics/toothpastes (accessed on 21 April 2020).
169. Shim, Y.J.; Choi, J.H.; Ahn, H.J.; Kwon, J.S. Effect of sodium lauryl sulfate on recurrent aphthous stomatitis: A randomized controlled clinical trial. *Oral Dis.* **2012**, *18*, 655–660.
170. Green, A.; Crichard, S.; Ling-Mountford, N.; Milward, M.; Hubber, N.; Platten, S.; Gupta, A.K.; Chapple, I.L.C. A randomised clinical study comparing the effect of Steareth 30 and SLS containing toothpastes on oral epithelial integrity (desquamation). *J. Dent.* **2019**, *80*, S33–S39.
171. Patel, K. 'Natural' toothpastes. *Br. Dent. J.* **2019**, *226*, 912.
172. WO2014059678A1—Toothpaste composition—Google Patents Available online: https://patents.google.com/patent/WO2014059678A1/en (accessed on 14 May 2020).
173. Perry, D.A.; Takei, H.H.; Do, J.H. Plaque biofilm control for the periodontal patient. In *Newman and Carranza's Clinical Periodontology*; Elsevier—Health Sciences Division: PA, USA, 2019; pp. 510–520.
174. Nayudu, A.; Lam, T.; Ho, J.; Forghany, A.; Vu, T.; Ngo, W.; Ajdaharian, J.; Wilder-Smith, P. Plaque removal and gingival health after use of a novel dental gel: a clinical study. *Dentistry* **2016**, *6*, 1–6.
175. Vranić, E.; Lacević, A.; Mehmedagić, A.; Uzunović, A. Formulation ingredients for toothpastes and mouthwashes. *Bosn. J. Basic Med. Sci.* **2004**, *4*, 51–58.
176. Takenaka, S.; Ohsumi, T.; Noiri, Y. Evidence-based strategy for dental biofilms: Current evidence of mouthwashes on dental biofilm and gingivitis. *Jpn. Dent. Sci. Rev.* **2019**, *55*, 33–40.
177. Werner, C.W.D.A.; Seymour, R.A. Are alcohol containing mouthwashes safe? *Br. Dent. J.* **2009**, *207*, E19.
178. Mouthwash (Mouthrinse). Available online: https://www.ada.org/en/member-center/oral-health-topics/mouthrinse (accessed on 22 April 2020).

179. Marchetti, E.; Tecco, S.; Caterini, E.; Casalena, F.; Quinzi, V.; Mattei, A.; Marzo, G. Alcohol-free essential oils containing mouthrinse efficacy on three-day supragingival plaque regrowth: a randomized crossover clinical trial. *Trials* **2017**, *18*, 154.
180. Gandini, S.; Negri, E.; Boffetta, P.; La Vecchia, C.; Boyle, P. Mouthwash and oral cancer risk—Quantitative meta-analysis of epidemiologic studies. *Ann. Agric. Environ. Med.* **2012**, *19*, 173–180.
181. Aceves Argemí, R.; González Navarro, B.; Ochoa García-Seisdedos, P.; Estrugo Devesa, A.; López-López, J. Mouthwash with alcohol and oral oarcinogenesis: systematic review and meta-analysis. *J. Evid. Based Dent. Pract.* **2020**, 101407.
182. Desjardins, J.; Grenier, D. Neutralizing effect of green tea epigallocatechin-3-gallate on nicotine-induced toxicity and chemokine (C-C motif) ligand 5 secretion in human oral epithelial cells and fibroblasts. *J. Investig. Clin. Dent.* **2012**, *3*, 189–197.
183. Chang, Y.C.; Huang, F.M.; Tai, K.W.; Yang, L.C.; Chou, M.Y. Mechanisms of cytotoxicity of nicotine in human periodontal ligament fibroblast cultures *in vitro*. *J. Periodontal Res.* **2002**, *37*, 279–285.
184. Warnakulasuriya, S.N.; Rupasinghe, H.P.V. Novel long chain fatty acid derivatives of quercetin-3-*O*-glucoside reduce cytotoxicity induced by cigarette smoke toxicants in human fetal lung fibroblasts. *Eur. J. Pharmacol.* **2016**, *781*, 128–138.
185. Rowe, R.C.; Sheskey, P.; Quinn, M. *Handbook of Pharmaceutical Excipients*; Pharmaceutical Press: London, UK, 2009;
186. Kovács, A.; Erős, I.; Csóka, I. Optimization and development of stable w/o/w cosmetic multiple emulsions by means of the Quality by Design approach. *Int. J. Cosmet. Sci.* **2016**, *38*, 128–138.
187. Peres, D.D.; Ariede, M.B.; Candido, T.M.; de Almeida, T.S.; Lourenço, F.R.; Consiglieri, V.O.; Kaneko, T.M.; Velasco, M.V.R.; Baby, A.R. Quality by design (QbD), Process Analytical Technology (PAT), and design of experiment applied to the development of multifunctional sunscreens. *Drug Dev. Ind. Pharm.* **2017**, *43*, 246–256.
188. International Conference On Harmonisation Of Technical Requirements For Registration Of Pharmaceuticals For Human Use Pharmaceutical Development Q8(R2). Available online: https://database.ich.org/sites/default/files/Q8_R2_Guideline.pdf (accessed on 28 April 2020).
189. Bogdan, C.; Iurian, S.; Tomuta, I.; Moldovan, M. Improvement of skin condition in *striae distensae:* Development, characterization and clinical efficacy of a cosmetic product containing *Punica granatum* seed oil and *Croton lechleri* resin extract. *Drug Des. Devel. Ther.* **2017**, *11*.



© 2020 by the authors. Licensee MDPI, Basel, Switzerland. This article is an open access article distributed under the terms and conditions of the Creative Commons Attribution (CC BY) license (http://creativecommons.org/licenses/by/4.0/).

Reactive and Functional Polymers 147 (2020) 104457

Contents lists available at ScienceDirect

Reactive and Functional Polymers

journal homepage: www.elsevier.com/locate/react

Development of BSA gel/Pectin/Chitosan polyelectrolyte complex microcapsules for Berberine delivery and evaluation of their inhibitory effect on *Cutibacterium acnes*

Violeta Paşcalău[a], Cătălina Bogdan[b,*], Emoke Pall[c], Luminiţa Matroş[b], Stanca-Lucia Pandrea[b,d], Maria Suciu[e,f], Gheorghe Borodi[e], Cristina Adela Iuga[b,g], Rareş Ştiufiuc[b,g], Tamara Topală[b], Codruţa Pavel[a], Cătălin Popa[a], Mirela Liliana Moldovan[b]

[a] Technical University of Cluj-Napoca, 28 Memorandumului Street, 400000 Cluj-Napoca, Romania
[b] "Iuliu Haţieganu" University of Medicine and Pharmacy, 8 Victor Babes Street, 400012 Cluj-Napoca, Romania
[c] University of Agricultural Science and Veterinary Medicine, 3-5 Calea Manastur Street, 400372 Cluj-Napoca, Romania
[d] Regional Institute of Gastroenterology and Hepatology "Prof. Dr. O. Fodor", 19-21 Croitorilor Street, 400162 Cluj-Napoca, Romania
[e] National Institute for Research and Development of Isotopic and Molecular Technologies, 67-103 Donath Street, 400293 Cluj-Napoca, Romania
[f] Babes-Bolyai University, 5-7 Clinicilor Street, 400084 Cluj-Napoca, Romania
[g] MedFuture Research Center for Advanced Medicine, "Iuliu Haţieganu" University of Medicine and Pharmacy Cluj-Napoca, 4 Louis Pasteur Street, 400349 Cluj-Napoca, Romania

ARTICLE INFO

Keywords:
Core-shell microcapsules
Berberine
Acne
BSA
Pectin
Chitosan

ABSTRACT

The aim of this work was to develop a novel fully natural drug delivery system for the treatment of acne, based on core-shell microcapsules that contain Berberine (Brb). The two main objectives of the work were: a) the synthesis and the characterization of complex microcapsules (ms), ms encapsulating Berberine (ms-Brb), and b) *in vitro* evaluation of the release of Brb, of the cytotoxicity on normal skin cells and of the antimicrobial effect on *Cutibacterium acnes* (formerly *Propionibacterium acnes*) (*C. acnes*). For a), bovine serum albumin (BSA) gel-core microcapsules with alternating multilayer shells of calcium cross-linked Pectin (P) hydrogel and the polyelectrolyte complex formed by P and Chitosan (Chi) (BSA gel/P/Chi/P) were synthesized. The BSA gel-core microcapsules were obtained using a sacrificial $CaCO_3$ template method, while the multilayer shell was formed through a technique consisting in the layer-by-layer (Lbl) deposition of polyelectrolyte complex formed by P and Chi. Brb was encapsulated into the resulting microcapsules, by a process of diffusion from solution. The structure characterization of ms/ms-Brb was performed by FTIR and UV–Vis spectroscopy, X-ray diffraction, confocal laser scanning microscopy, and scanning electron microscopy. The *in vitro* assessment of ms/ms-Brb cytotoxicity on skin cells was performed using keratinocyte (HaCaT) cell line. Results of physicochemical analyses confirm the successful encapsulation of Brb in ms, and the *in vitro* biological study recommends ms-Brb as a candidate for future *in vivo* research targeting anti-acne treatment.

1. Introduction

Acne vulgaris is the most common disorder of the pilosebaceous unit, being caused by the specific changes in the microenvironment of sebaceous follicles. It is a multifactorial disease with complex pathogenesis. Four main factors are considered to play a major role in the development of acne lesions: an increased sebum production due to the stimulation of androgen hormones, the obstruction of the pilosebaceous unit by abnormal keratinization which prompts the formation of comedo, the proliferation of *C. acnes* in the duct of the sebaceous follicle, prompting the inflammation mediated by both chemotactic factors and various enzymes [1], as well as the development of specific lesions. The latest findings support the hypothesis that acne is primarily an inflammatory disease [2]. The current anti-acne therapy includes topical and systemic retinoids, antimicrobial agents, and systemic hormonal drugs. Emerging bacterial resistance following the antibacterial treatment for acne vulgaris has been a permanent concern. Recently, new retinoids with additional anti-inflammatory action are being co-administered with antibiotics in order to reduce the risk of bacterial resistance. Therefore, an agent that is able to inhibit *C. acnes* growth and

* Corresponding author.
E-mail address: catalina.bogdan@umfcluj.ro (C. Bogdan).

https://doi.org/10.1016/j.reactfunctpolym.2019.104457
Received 1 August 2019; Received in revised form 31 October 2019; Accepted 21 December 2019
Available online 24 December 2019
1381-5148/ © 2019 Elsevier B.V. All rights reserved.

to suppress the inflammatory response will provide promising benefits to patients with acne vulgaris. Due to its numerous pharmacological properties, Brb, an isoquinoline alkaloid, has been extensively studied over the past years. Brb has a broad spectrum of pharmacological effects, such as anti-cancer, anti-microbial, and anti-inflammatory effects [3]. Nevertheless, the precise mechanism of action has not been fully explained. Previous studies reported the beneficial roles of Brb in different skin conditions such as psoriasis [4], melanoma [3], squamous cell carcinoma [5]. There has been reported an antibacterial activity of Brb against *C. acnes* [6], which is more effective than some antibiotics, such as minocycline or erythromycin [7]. In addition, the use of this natural compound may prevent antibiotic resistance. Furthermore, Brb inhibits the pro-inflammatory activity induced by tumor necrosis factor-alpha (TNF-α) [8] in a dose-dependent manner. Recent studies have shown that Brb has androgen-inhibiting properties, decreasing the sebum production by over 60% in animal models and suppressing the progression of comedogenesis [9].

There are many reported attempts to develop carriers for berberine encapsulation and delivery for multiple applications, including gels based on polymers blending, lyposomal products, microparticulate systems loaded with the self-assembled berberine-phospholipid complex-based phytosomes, dendrimers encapsulating conjugated berberine and nano strategies using pure berberine or different complexes and derivatives. The systems proposed for berberine delivery are addressed to a wide range of applications of berberine, due to its multiple pharmacological effects. The preparation of nano/microparticles may be performed by the same methods. Understanding skin physiology and the interactions of the different delivery systems with the skin, is essential for a correct selection of the most suitable delivery system, as well as its materials and preparation method. Nanoparticles have a greater tendency to aggregate and can lead to a faster release by diffusion. The potential application in acne treatment requires larger particles (3–10 μm) in order to remain at follicular level without penetrating into *stratum corneum* and without penetration into viable epidermis. Our approach is represented by development of all natural novel architecture system based on BSA gel network offering multiple sites to fix Brb via electrostatic interactions and a multilayer shell formed by the polyelectrolite complex P/Chi, two polysaccharides with high mucoadhesive potential suitable in topical application for acne treatment. This interaction extends the residence time at the site of the drug and favors drug absorption to enhance the bioavailability. The use of natural polymers in microcapsules building is a warranty of less cytotoxicity and biodegradability [10]. On the other hand, encapsulation of pure Brb avoid the Brb complex formation which has the disadvantage to include chemical synthesis steps requiring repeated purification steps leading to drawbacks such as undesirable chemical reagents traces. In contrast to the lipid microparticle delivery systems our developed core-shell microcapsules are very stable even in different pH media during storage, they could be degraded only in biological environment containing enzymes. In order to enhance topical or transdermal delivery of active pharmaceutical ingredients, many drug delivery systems, have been extensively studied [11]. In this regard, the aim of the present paper has been to develop a novel fully natural drug delivery system for the treatment of acne, based on core-shell microcapsules made of BSA gel-core and a polyelectrolyte complex P/Chi/P multilayer shell, entrapping the natural product, Brb.

The experimental approach is based on microencapsulation technology for drug loading, administration and release, using Brb and core-shell microcapsules that are exclusively based on natural components. With BSA in the core and P/Chi/P polyelectrolyte complex in the shell, ms-Brb could use the additional electrostatic interactions between the ionized functional groups of BSA, P and Brb charges, in a pH dependent manner. Moreover, the possible formation of new bonds facilitates the loading and prolonged delivery of Brb. BSA has been chosen as a naturally abundant protein candidate for drug delivery due to its intrinsic biodegradability, biocompatibility, and lack of toxicity and immunogenicity [12]. This protein has been intensively investigated as protein model for the transport of different hydrophobic macro- or small drug molecules to the target sites [13], looking for a possible synergistic therapeutic effect. The BSA gel-core of ms is a network structure stabilized by hydrophobic interactions, disulfide bonds, and hydrogen bonds [14]. BSA, is an ampholyte, with pH dependent charge, providing reversible sites to bind and release drugs, which makes it an ideal candidate for loading and releasing drugs [15]. Both natural and synthetic polymers can be assembled in microcapsules for controlled drug delivery, but those made of natural polymers show the advantage of biocompatibility and biodegradability [16]. The multilayer shell structure is based on the property of anionic polysaccharides, such as P, to be cross-linked with metallic cations (Ca^{2+}) and turned into hydrogels as well as of the polysaccharides with opposite charges to form polyelectrolyte complexes through electrostatic interactions [17]. As natural polyelectrolytes, P and Chi are good candidates for the preparation of the multilayer shell, using a Lbl deposition technique of the polyelectrolyte complex formed between them [18]. Many polysaccharides have been used in hydrogel preparations for pharmaceutical applications. Among them, Chi is the one of the cationic polysaccharides due to its glucosamine groups. Chi is a nontoxic, biodegradable, and biocompatible [19] linear copolymer of β-(1–4) linked 2-acetamido-2-deoxy-β-D-glucopyranose and 2-amino-2-deoxy-β-D-glucopyranose, obtained by the deacetylation of chitin, a polysaccharide component of crustacean shells, insect cuticles, and fungi [20]. Chi is poorly soluble but in diluted acidic solutions it becomes a soluble polycation, which can form complexes through electrostatic interactions with a wide variety of anionic species as a result of protonating amino groups of the D-glucosamine residues.

Chi is one of many mucoadhesive polymers, whose mucoadhesivity is due to the interactions between positively charged amino groups with the negatively charged sialic acid of the mucous layer at the mucosal surfaces [21]. P is an edible and water soluble polysaccharide of d-galactouronic acid units in which carboxyl groups (–COOH) are partially methoxylated. The different degree of metoxylation is source dependent [22]. Some species of P such as Tamarind P have been reported to act as a binding agent, emulsifier, suspending agent, as hydrogel, and as a mucoadhesive agent sustaining drug release for rectal and nasal drug delivery [23]. P is one of the most widely investigated polysaccharides in colon-specific drug delivery due to its selective digestion by the microflora (*Bacteroids ovatus*) present in the colon and its resistance to proteases and amylases of the upper gastrointestinal tract [24], but also for skin delivery, P being able to act as penetration enhancer [25]. The ability of Chi and P to form a polyelectrolyte complex by electrostatic interactions was largely exploited in processing nano−/microcarriers for colon-specific drug delivery [26]. Considering the mucoadhesive properties of both P and Chi, as well as their ability to form the polyelectrolytic complex involved in building the multilayer architecture of the microcapsule shell, the purpose of the work was to obtain microcapsules with increased adhesiveness, which could lead to a prolonged release of Brb at the application site. Moreover, this paper proposes a vehicle for Brb, all based on natural biocompatible compounds used in medical studies, in order to obtain a targeted and sustained release of Brb and to support its applicability in the treatment of some dermatoses.

Generally, there are three steps for producing microcapsules with polymeric multilayer shell [27]. Firstly, the protein is co-precipitated in sacrificial porous microtemplates [28]. Secondly, these microtemplates are coated through the Lbl technique using electrostatic interactions or hydrogen bonding as the driving force for multilayer build-up [29]. Thirdly, the sacrificial dissolved microtemplates are removed through the semipermeable polyelectrolyte shell, the protein remaining in the core of the capsules [30]. We used the $CaCO_3$ template to synthesize non-toxic $CaCO_3$/BSA particles as microtemplates. The shell was assembled through a LbL deposition technique of calcium cross-linked P hydrogel alternating with the polyelectrolytes complex hydrogel

formed via electrostatic interactions between P and Chi. After the removal of $CaCO_3$, the BSA core was turned into a BSA gel by thermal treatment. The BSA gel microcapsules have been then loaded with Brb, through a process of diffusion from solution.

Since Brb has a poor solubility in both water and other solvents, its encapsulation has been studied in both organic solvents (data not shown) and different pH buffer solutions. Brb release from ms-Brb was also evaluated in different pH media in order to determine the best conditions of administration in the above-mentioned medical applications. The *in vitro* assessment of ms/ms-Brb cytotoxicity on skin cells using keratinocyte (HaCaT) cell line and the antibacterial activity against *C. acnes* was performed. As well, the biodegradability of ms and ms-Brb in fresh human saliva was studied.

The results of physicochemical tests confirmed the successful encapsulation of Brb in ms-Brb, and the *in vitro* biological study indicates ms-Brb as a candidate for future *in vivo* research in the anti-acne treatment. To our knowledge, this is the first report to propose this approach.

2. Materials and methods

2.1. Materials

BSA, albumin fraction V for biochemistry, Calcium chloride, anhydrous Sodium carbonate and Ethylenediaminetetraacetic acid (EDTA) were purchased from Merck; Pectin 85% deacetylated (UNIPECTINE™ MRS 150 CITRUS) was obtained from Cargill; Chitosan from shrimp shell (75% deacetylated) and Berberine chloride form were purchased from Sigma Aldrich; Sigma Dubelcco's phosphate buffered saline (PBS) sterile filtered – endotoxin tested – for research or further manufacturing uses only, and all the reagents used in biological studies from SIGMA Life Science.

2.2. Methods

2.2.1. Obtaining of $CaCO_3$/BSA microparticles

The sacrificial $CaCO_3$/BSA microtemplate was build up by co-precipitating $CaCO_3$ with BSA. In a 0.33 M $CaCl_2$ solution containing 0.75% BSA, the same volume of 0.33 M Na_2CO_3 solution was added under vigorous mechanical stirring (500 rpm) at room temperature for a short time (30 s). After keeping the mixture for 15 min without stirring, the white particles formed were centrifuged for 5 min at 4000 rpm and repeatedly washed with distilled water to remove traces of Ca^{2+} and carbonate CO_3^{2-}, in order to avoid the growth of the co-precipitate particles.

2.2.2. Preparing the multilayer shell of $CaCO_3$/BSA/P/Chi/P microparticles

The multilayer shell of microparticles was built by a Lbl deposition technique of calcium cross-linked P hydrogel, alternating with the polyelectrolyte complex hydrogel formed by P and Chi. A 1% P aqueous solution was made under continuous stirring, being heated up to 90 °C until complete dissolution; then a solution containing 1% Chi dissolved in 1% acetic acid solution was prepared by stirring it at room temperature. The deposition process was conducted in a polysaccharide solution at 40 °C under slow magnetic stirring (500 rpm) for 15 min for each layer, followed by centrifugation (4000 rpm, 3 min) and washing three times, after each layer deposition. First, the particles were introduced in the P solution at a ratio of 1:6 (*v*/v). The second alternating layer was formed by Chi, under the same conditions. Five double layers followed by washing and centrifugation after each layer deposition were formed.

2.2.3. Obtaining the BSA gel/P/Chi/P microcapsules

The multilayered shell microparticles based on $CaCO_3$/BSA/P/Chi/P, ms, were thoroughly treated four times using a double volume of 0.2 M EDTA solution pH 7.5, and then were carefully washed with deionized water. In order to completely remove $CaCO_3$ from the particles, they were treated for a short period of time with an adequate volume of 0.1 M HCl solution until the observed effervescence stopped. The hence synthesized capsules with the BSA solution in the core were washed to achieve a neutral pH, heated for 30 min at 80 °C under stirring (250 rpm) to turn the BSA solution into a gel, cooled at room temperature and then centrifuged. The sediment consisting of ms was a colorless gel mass containing 3.5×10^8 ms/mL. The 1:10 dilution of concentrated ms with pure water resulted in a suspension that contained approximately 3.5×10^7 ms/mL (measured using a Hemocytometer with a Bürker camera), which was stored at 4 °C until used.

2.2.4. Berberine encapsulation

Brb encapsulation was achieved by diffusion, using the preexisting ms suspension and Brb solutions in three different pH buffers. Three buffer solutions, i.e. pH 5.6 acetate, pH 6 acetate and pH 6.8 phosphate buffer solutions, were used to prepare the 1.6 mg/mL Brb solutions with an Ultrasonic bath (Elmasonic Elma S10H). The pH of the solutions was adjusted using a Hanna HI 208 pH meter. Homogenization was achieved using a Velp Scientific vortex mixer at 800 rpm for 30 s. For each of the different pH solutions the ms:Brb solution (volumes) ratio used was 1:40. The incubation of ms with the Brb solution was performed for 24 h, in the dark at 37 °C using a Thermo-shaker (Biosan) at 250 rpm. The Brb encapsulation studies were performed in triplicate. The ms-Brb was separated from the Brb feeding solution by centrifugation for 20 min at 14000 rpm and stored at 4 °C. The hence obtained ms-Brb were used for further *in vitro* studies.

2.2.5. Encapsulation and loading efficiency of Brb into ms

In order to calculate the Encapsulation efficiency (E_{ef}), an UV–Vis spectrophotometry quantitative method (spectrophotometer Specord 200 Plus (Analytic Jena) and WinAspect Plus software v. 4.2.0.0, Analytic Jena) was used to determine the Brb concentration at $\lambda = 344$ nm. After the incubation of the ms with Brb solution for 24 h, the samples were centrifuged at 14000 rpm for 5 min. The volume of the removed supernatant was measured. The sedimented ms-Brb were washed using small amounts of buffer solution. The amount of Brb was quantified by UV–Vis spectrometry at $\lambda = 344$ nm, based on calibration curves, separately registered, using five diluted solutions of Brb in each buffer solution, with concentrations between 0.001 mg/mL and 0.02 mg/mL. The Brb calibration curve was used to determine the concentration of Brb in the solution remaining from the Brb loading (free Brb). The E_{ef} for Brb was estimated according to Eq. (1) [31]:

$$\text{Eef}\,(\%) = (\text{Total feeding Brb} - \text{Free Brb}) \times 100/\text{Total feeding Brb} \quad (1)$$

where Total feeding Brb (mg) is calculated according to Eq. (2):

$$\text{Total feeding Brb (mg)} = \text{Vol of feeding Brb solution} \times \text{Brb concentration (mg/mL)} \quad (2)$$

and Free Brb (mg) using Eq. (3):

$$\text{Free Brb (mg)} = \text{Vol of feeding Brb solution} \times \text{Free Brb concentration (mg/mL)} \quad (3)$$

The Brb loading efficiency in ms-Brb (Brb load ef) (%) was calculated according to Eq. (4):

$$\text{Brb load ef}\,(\%) = \text{Total loaded Brb} \times 100/\text{Total ms} \quad (4)$$

where Total loaded Brb = Total feeding Brb – Free Brb.

2.2.6. FTIR spectroscopy

The functional groups of the ms and ms-Brb were identified by FT-IR spectra recorded using a TR FT-IR spectrometer (Jasco FT-IR 4100) equipped with a ZnSe ATR crystal. The spectra were collected using the

attenuated total reflection technique in the 4000–500 cm^{-1} spectral range with a resolution of 4 cm^{-1} and averaged over 32 scans, and interpreted using a Jasco Manager 2 software.

2.2.7. X-ray diffraction

The X-ray diffraction patterns were recorded using a D8 Advance Diffractometer and a sealed Cu tube equipped with an incident beam Ge 111 monochromator, and wavelength λ = 1.54056 Å. The diffraction data were recorded in the range of 3–70° with 0.02° 2Θ step size.

2.2.8. Confocal laser scanning microscopy

Confocal microscopy analysis was performed for a proper assessment of microcapsules morphology and in order to prove the presence of Brb by means of fluorescence microscopy. Freshly prepared ms dispersions were poured onto glass slides and then imaged. Fluorescence and differential interference contrast (DIC) images were captured on an Olympus FV1200 Confocal Laser Microscope using an UPLSAPO40X2 objective (NAL0.95). Zoomed images were acquired with digital magnification so as to comply with the Nyquist criterion on the X and Y axes. Emission for Brb was established by performing k-scans with an excitation laser of 340 nm. The resulting images were processed using ImageJ software as follows: DIC Images were filtered with a horizontal bandpass filter with brightness and contrast set to automatic, whereas fluorescence images were set to automatic and were displayed with an arbitrary LUT. A single 2.0 pixel median filter was applied to the images before the acquisition of the surface and line profile plots. Scale calibration was performed with pixel sizes obtained from the metadata.

2.2.9. Scanning electron microscopy

Scanning electron microscopy micrographs were used to highlight the changes of surface morphology of ms after Brb loading and also at different times after Brb release. In this respect, samples of both ms and ms-Brb suspensions were deposited onto a cover glass and dried at room temperature. The dried samples were mounted on carbon sticky tabs and then covered with a 10 nm Au layer. The samples were analyzed using a Hitachi SU8230 scanning electron microscope at 30 kV, 10 uA, and 8 mm working distance.

2.2.10. In vitro release study

The *in vitro* Brb release study was performed at 34 °C, slow vortex (250 rpm) in the dark using a Thermoshaker (Biosan) during 48 h in three different pH media: pH 4 acetate buffer solution, pH 4.4 acetate buffer solution, and pH 6 acetate buffer solution, respectively. The release studies were performed in triplicate using the ms-Brb loaded in pH 6 acetate buffer solution. In each sealed tube that contained 5 mL of release medium, a certain amount (m) of ms-Brb was introduced. At different time intervals, the three samples were centrifuged for 2 min at 7000 rpm, an aliquot of 0.1 mL of the supernatant was removed and replaced with the same volume of the corresponding release medium. The extracted volume of supernatant was diluted to 5 mL using the adequate buffer solution and kept in the dark until the quantification of Brb was performed at λ = 344 nm, using the previously registered calibration curve. A control sample was prepared with pure water as release medium and analyzed on the same experimental conditions. The amount of Brb released in the buffer solution was determined by the UV/VIS quant mode, based on the calibration curve of Brb registered at λ = 344 nm. The Brb cumulative % was calculated based on the Brb amount released at a specific time n (n = 5 min, 10 min, 20 min, 30 min, 45 min, 1 h, 2 h, 3 h, and 4 h) relative to the total Brb contained in ms-Brb. The Brb concentration at any specified time (n) (Cn) was determined. The Cumulative Brb release % (Cumm Brb rel %) was calculated according to Eq. (5):

$$\text{Cumm Brb rel (\%)} = \text{Quantum of Brb at specific time n} \times 100/\text{Total feeding Brb} \quad (5)$$

where:

Quantum of Brb at a specific time n, (m_n) was calculated according to Eq. (6):

$$m_n = C_nV_0 + C_{n-1}V \quad (6)$$

and the cumulative Brb released quantum ($m_{n\ cumulative}$) was calculated according to Eq. (7):

$$m_{n\ cumulative} = V_0c_n + V(c_1 + c_2 + ...c_n) \quad (7)$$

where V_0 is the total volume of the release medium and V is the removed and replaced volume. The Total Brb before releasing was calculated by Eq. (8):

$$\text{The Total Brb before releasing} = \text{Brb load ef (\%)} \times m/100 \quad (8)$$

The Cumulative release (%) of Brb against the release time was further plotted.

2.3. Biological experiments

2.3.1. Cytotoxicity assay of ms and ms-Brb

The cell line used for the cytotoxicity assay of ms and ms-Brb performed at pH 6.8 was the normal human keratinocyte line (HaCaT). The potential cytotoxicity of the four samples (ms suspension, ms-Brb suspension 86 mg/mL and 43 mg/mL, respectively and pure Brb water solution 0.01 mg/mL was evaluated by 3-(4,5-dimethylthiazol-2-yl)-2,5-diphenyltetrazolium bromide (MTT) assay. MTT is a tetrazolium salt that is converted by cell mitochondrial reductases of viable cells into a dark blue compound-formazan. The cells were cultivated on standard conditions. In order to obtain cell suspensions, the cells were treated with 0.25% trypsin-EDTA, and after centrifugation (1000 rpm for 5 min), 1×10^4 cells/well were seeded on 96 wells plates in 200 µL complete culture medium and incubated at 37 °C overnight. After 24 h of culture, five different volumes (1 µL, 2.5 µL, 5 µL, 8 µL, and 10 µL, respectively) of each of the four samples were added on HaCaT cells. The control samples were untreated cells. All treatments and controls were performed in triplicate. After 24 h, the medium was removed and 100 µL of 1 mg/mL MTT solution was added. The plates were further incubated for 3 h at 37 °C in the dark and, subsequently, the supernatants were removed and 150 µL DMSO solutions were added to each well. Absorbance was read on a multiplate reader (Bio-Rad PR4100). The optical density of the chromogenic reaction was evaluated at 450 nm using BioTek Synergy 2 microplate reader. Optical density is proportional to the number of viable cells.

2.3.2. Antimicrobial activity on Cutibacterium acnes

The ms-Brb were tested for their *in vitro* antimicrobial activity on *C. acnes* reference strain ATCC 11827 (KWIK-STIK™ Plus, Microbiologics) using the Kirby-Bauer method. The reference strain *C. acnes* was isolated on Brucella Blood Agar (BioMérieux, France), under anaerobic conditions (GENbag, anaer generator sachet, BioMérieux, France) at 37 °C for 48 h. A standardized microbial inoculum of 0.5 McFarland was spread on Brucella Blood Agar and further, two test methods were performed.

2.3.2.1. Well diffusion method. Six wells of 6 mm diameter have been punched into the agar medium, and filled with 50 µL of test sample in the following order: ms-Brb (3.5×10^7 microcapsules/mL), ms-Brb water suspension 86 mg/mL, ms-Brb water suspension 43 mg/mL, ms (3.5×10^7 microcapsules/mL) (negative control), pure Brb water solution 0.1 mg/mL and pure Brb water solution 1 mg/mL.

2.3.2.2. Disc diffusion method. The blank discs (Oxoid, UK) with a diameter of 6 mm. were placed on the agar surface and were impregnated with 50 µl of test sample, following the same order as in the previous method.

In both cases, the plates were incubated at 37 °C, under anaerobic

conditions for 48 h. Antimicrobial activity was evaluated by measuring the diameter of growth inhibition zone.

Antimicrobial susceptibility testing has been also performed on clindamycin, antibiotic commonly used in acne vulgaris therapy, in order to compare the effect of Brb. The test was performed using the Kirby-Bauer method on Brucella Blood Agar, with clindamycin (2 μg/disc). Incubation was performed for 48 h at 37 °C under anaerobic conditions. The diameters of the inhibition zones were measured, and the interpretation was made using the standard of Comité de l'antibiogramme de la Société Française de Microbiologie Recommandations [32]. In order to confirm the reproducibility of the results, the tests were performed in triplicate.

2.3.3. Biodegradation of the microcapsules

It was reported that polysaccharides from hydrogels and polyelectrolyte complex can be degraded by enzymes which are present in saliva and plasma (hyaluronidase, lysozyme and amylase) [33]. The polyelectrolyte complex P/Chi constructing the multilayer shell of ms, was subjected to a degradation process using fresh human saliva collected according to the protocol approved by the Research Ethics Committee of the Iuliu Haţieganu University of Medicine and Pharmacy (date of approval: 447/22 October 2019). The fresh collected saliva has been centrifuged for 5 min at 4000 rpm. The supernatant was separated and used in the following study. Briefly, 100 μL ms, and ms-Brb suspension, respectively, were incubated with 200 μL saliva in Eppendorf tubes using a Biosan Thermo-shaker TS-100 setup at 37 °C, 500 rpm, for 6 h. After 0.5 h, 1 h, 2 h, 3 h, 4 h, 5 h and 6 h, respectively, the samples were centrifuged and washed with deionized water. Samples of ms from the each sediment were deposited on cover glass and dried at room temperature. Optical microscopy images were captured using Olympus GX 51 microscope. Each sample was made in triplicate. For ms-Brb samples, CLSM images were acquired according to the above described procedure.

3. Results and discussion

3.1. Encapsulation and loading efficiency of Brb into the microcapsules

The influence of the pH Brb feeding solution on E_{ef} (%) and $Load_{ef}$ (%) of Brb into the ms-Brb was studied. Experiments were performed starting from the same concentration of Brb feeding solution (1.6 mg/mL) and ms volume/Brb feeding solution. The encapsulation process was carried out in two acetate buffer solutions at pH 5.6 and pH 6 and also using phosphate buffer solution at pH 6.8, all of them being over the isoelectric point of BSA (pH 4.8). The results are listed in Table 1.

In the literature there are reported many values for Brb E_{ef} (%) whose are dependent of the specific delivery system, such as from 6.25% for Brb incorporated in the carboxymethyl chitosan/low MW hyaluronic acid gels [34], 10.4% and 14% for liposomal Brb [35,36], 29.9% for Brb encapsulation efficiency in dendrimers (e.g. PAMAM) [37] and 22%–45% for the E_{ef} determined for different variants of Brb-loaded Chi nanoparticles by using ELISA reader at 420 nm wavelength, a more precise and more expensive analytical technique. Higher values for Brb E_{ef} (%) were only obtained in the case of complexes formated between Brb and delivery system, such as 54.4% for the Brb/heparin/Chi nanoparticles when ionized Brb and heparin form polyelectrolyte complexes by electrostatic interactions between the positively charged Brb and the negatively charged heparin, 85% in the phytosomes loaded with berberine-phospholipid complex [38], 86% for gold nanoparticles with functional groups as linkers to attach berberine hydrochloride [39] and up to 94.3% in a study using A23187-mediated ZnSO4 gradient method to prepare berberine hydrochloride long-circulating liposomes, A23187 beeing a mobile ion-carrier that forms stable complex with divalent cations [40].

Table 1
The mean values of Encapsulation efficiency (%) and Loading efficiency (%) of Brb encapsulation processes carried out in pH 5.6, 6 and 6.8 buffer solutions.

pH of feeding solutions	pH 5.6	pH 6	pH 6.8
Encapsulation efficiency (%) ± SD	21.04 ± 2.18	23.47 ± 2.57	25.11 ± 4.04
Loading efficiency (%) ± SD	1.85 ± 0.25	2.68 ± 0.31	4.02 ± 0.17

In our developed delivery system, based on microcapsules with polyelectrolite complex multilayer shell of P/Chi focus has been both on the Brb encapsulation efficiency and the mucoadhesiveness provided to the system by the intrinsic property of P and Chi, suitable for topical application. Although the encapsulation efficiency of Brb into ms was moderate, but comparable to similar studies, the antimicrobial effect on *C. acnes* of ms-Brb was significant. The aim of the paper was to overcome some limitations of Brb in its clinical applications, the most important of which is its poor aqueous solubility and poor absorption in the gastrointestinal tract (about 5%), due to high binding of plasma proteins to Brb, remaining a low unbound fraction of Brb to reach and penetrate into target tissues [39]. The poor aqueous solubility of Brb is one of the possible causes of low encapsulation efficiency.

Based on E_{ef} (%) values, the best encapsulation can be achieved at pH 6.8, as expected, due to the ionic interactions between BSA gel-Brb. Both ms and ms-Brb are prepared and stored in aqueous suspension. The ms core consists of BSA gel, and the P/Chi polyelectrolyte complex multilayer shell, both in the hydrated form. As a result, both the core and the shell are swelled networks, with enlarged pores. This state facilitates the diffusion of small Brb molecules, controlled by the concentration gradient, first through the porous shell and then into the ms core. The penetration of Brb molecules in the BSA gel network is favored by the multiple interactions that stabilize the gel network, such as hydrophobic interactions, disulfide bonds, and hydrogen bonds, providing potential space for drug loading. Finally, the Brb molecules are embedded in the pores and meshes of the two networks. BSA is an ampholite and its charge is pH dependent. The isoelectric point of BSA is 4.8. On the other hand, the spontaneous deposition effect, driven by electrostatic interaction between BSA and Brb molecules, is expected to be pH controlled. In a pH solution below pH 4.8 the BSA positive charges are prevalent, leading to a repulsion of the positively charged Brb molecules. In a pH solution over pH 4.8 the negative charges of BSA are attracted by the positively charged Brb molecules dissolved in acetate buffer solution at pH 5.6 and phosphate buffer solution at pH 6.8. Therefore, ms-Brb loaded at pH 6.8 were chosen for use in the further *in vitro* studies.

3.2. FTIR spectroscopy

Fig. 1a shows the FTIR spectra of raw materials, BSA, P and Chi of the final product, ms. The spectra of P and Chi have both common bands of polysaccharides (band due to vibrations of the cyclic etheric bond at 1035–1150 cm^{-1}, the vibrations bands of C-H bond from, -CH_2 and -CH_3 groups, the band corresponding to the vibration of O-H bond of the hydroxyl groups at around 3300 cm^{-1}) and characteristic bands, such as the band of -NH_2 and acetyl amino NH–C=O from P at 1615 cm^{-1} and 1730 cm^{-1}, respectively and the bands associated to the specific bands of Chi at 1384 cm^{-1}, and 881 cm^{-1}, and 1590 cm^{-1}, due to the stretching vibrations of C-N and the out-of-plane bend and scissors vibration bands of the NH_2 group, respectively. The BSA IR spectrum contains characteristic bands of amino acids constituting albumin, the two amide bands, I and II, at 1542 $cm^{-1}$and 1663 cm^{-1}, carboxylic band from 1,400 cm^{-1}, as well as the methyl and methylene bands between 2800 and 2950 cm^{-1}. As illustrated in the figure, the spectrum of ms shows bands derived from polysaccharides (1033 cm^{-1}, 1241 cm^{-1} and 1615 cm^{-1}) overlapped with the bands belonging the functional groups of BSA. The absence of $CaCO_3$ bands in the microcapsules spectrum is an argument supporting the microcapsules

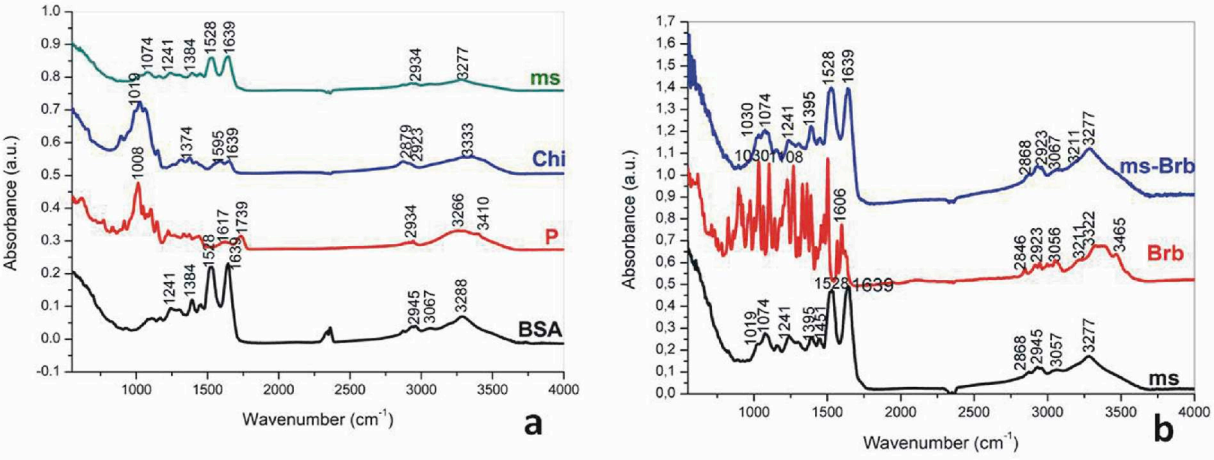


Fig. 1. Overlapped FTIR spectra of: a) BSA, P, Chi and ms; b) ms, Brb and ms-Brb.

formation by the complete removal of $CaCO_3$ from the particles. Most Brb bands overlap the P and Chi bands, excepting for the vibration band at 1030 cm^{-1} of the cycloether group (-O-C-O-) and a C-O-C asymmetric stretching vibration at 1108 cm^{-1}, as low intensity bands appearing in the ms-Brb spectrum (Fig. 1b).

3.3. X-ray diffraction

The overlapped XRD patterns of ms, Brb and ms-Brb (Fig. 2) highlight the presence of Brb diffraction lines in the ms-Brb XRD pattern, but at a smaller intensity, confirming the successful encapsulation of Brb into ms.

3.4. Confocal laser scanning microscopy

CLSM images of ms-Brb loaded at pH 6.8 are presented in Fig. 3. As illustrated in Fig. 3(a), the microcapsules have a regular morphology, with well-defined edges and a uniform distribution of Brb fluorescence. Fig. 3 (b) confirms ms-Brb average size of 7–8 μm. Fig. 3(c) is a 2.5D reconstruction showing the fluorescence intensity profiles of the microcapsules from image 3a. CLSM images reconstructed from multiple depths in the sample, revealed the fluorescence profile due to the encapsulated Brb. This aspect supports the achievement of Brb encapsulation instead of the physical adsorption on the surface of the microcapsules only.

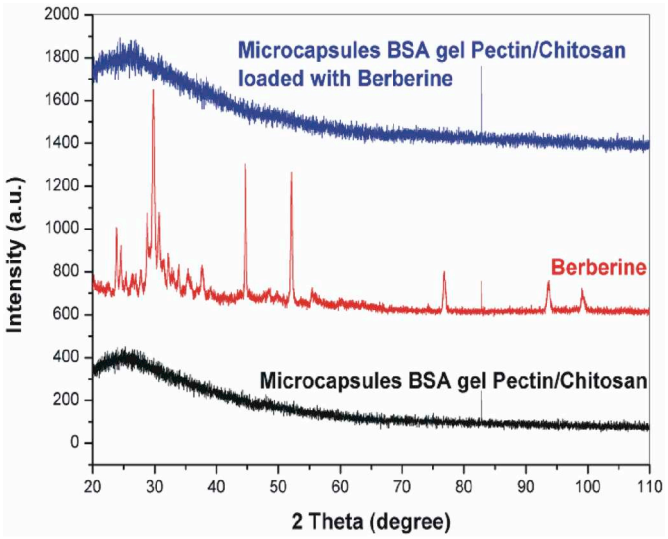


Fig. 2. XRD patterns of ms, Brb and ms-Brb.

3.5. Scanning electron microscopy

The SEM micrographs (Fig. 4) of ms (a-c); ms-Brb loaded in pH 5.6 acetate buffer solution (d-f); ms-Brb loaded in acetate buffer solution of pH 6 (g–i), and ms-Brb loaded in phosphate buffer solution of pH 6.8 (j-l) show the appearance and size of the microcapsules derived from different pH loading media, in particular their surface appearance. They also allow us to distinguish between the unloaded ms and ms-Brb. The ms-Brb derived from the loading process in phosphate buffer solution at pH 6.8 had a smoother surface than the other ms-Brb loaded at pH 5.6 and pH 6, respectively. Since above the isoelectric point BSA becomes negatively charged, and attracts the positive ions of Brb, as the pH value increases, it is expected that these interactions also increase. This hypothesis is confirmed by the change noted in the appearance of ms-Brb surface (Fig. 4 (j-1)) and by the highest value of $Load_{ef}$. Since both the core and the ms shell are porous, it might be expected for the encapsulation of Brb molecules not to cause any significant changes in the ms-Brb size. The BSA gel matrix and the swollen hydrogels of the P/Chi polyelectrolyte complex provide an appropriate microstructure for Brb loading. The particular appearance of ms-Brb samples subjected to the release step in different pH media and recovered after the same period, is revealed in Fig. 5. The different dynamics of Brb release from ms-Brb, which is dependent on the pH of the release medium, could be explained by the different appearance of ms-Brb recovered after the same amount of time spent in the corresponding medium as a result of the specific pH-dependent electrostatic interactions.

3.6. In vitro release study

The percentage of cumulative released Brb was calculated using Eq. (4) and plotted against time (Fig. 6). The data related to the concentration of released Brb (mg/mL) at time n (Cn), have been collected by quantitative UV–Vis spectroscopy determinations. Similar to other release studies with a low amount of ms in small volumes of release medium [41], it was necessary to apply some corrections on the determined Brb concentration when computing the cumulative released Brb, using Eq. (6), so as to take into account the amount of Brb, that was previously removed for analysis, which had to be added back to the released Brb calculation. The release profile of Brb shows a faster release at pH 4, followed by the release at pH 4.4, and a slower release at pH 6.8. This could be explained by a better hydration of the shell at a lower pH. On the contrary, in case of higher pH solutions (PBS pH 6.8), the number of charged species increases, delaying hence the access of water molecules around the hydrophilic functional group, and reducing

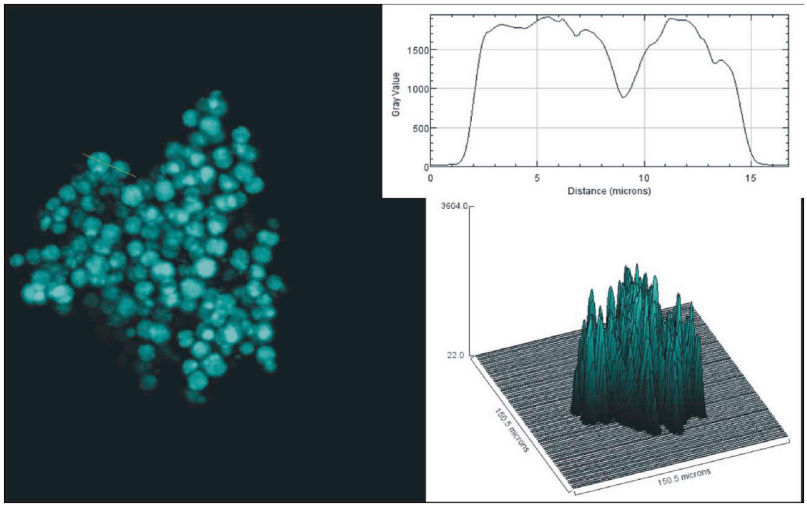


Fig. 3. Confocal images of the three-dimensional reconstructed ms-Brb (a, b); the fluorescence intensity profile of the highlighted ms-Brb (c).

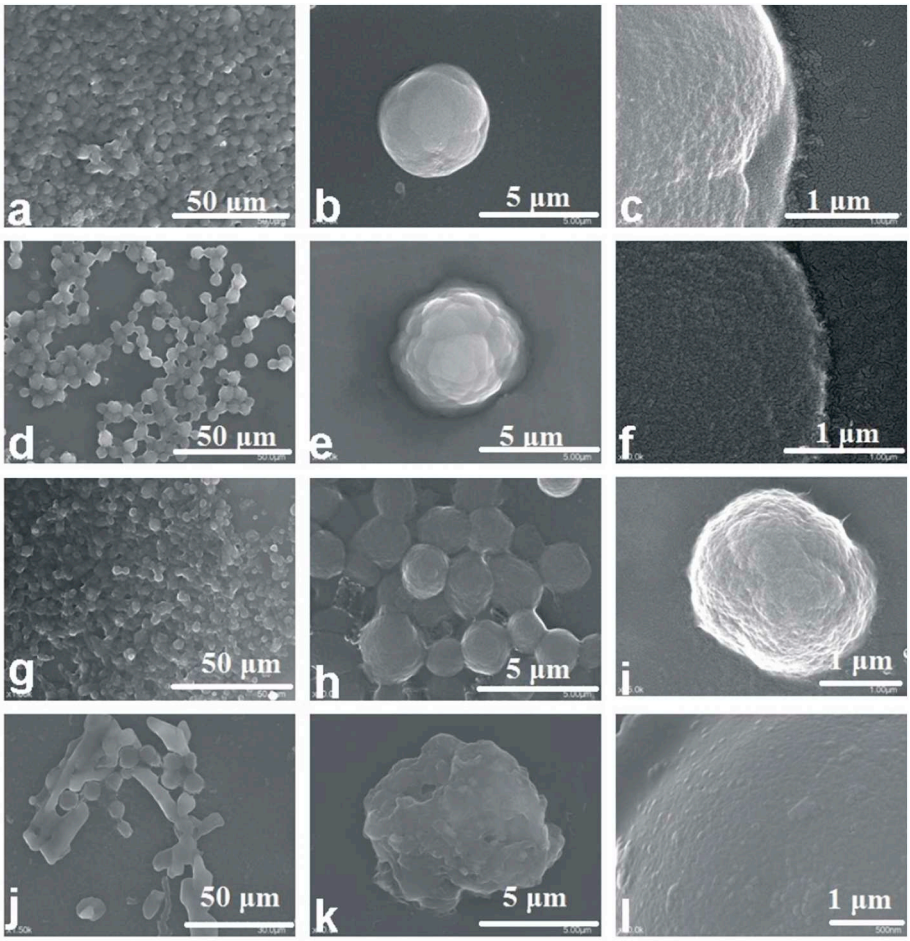


Fig. 4. SEM images of ms (a-c) and ms-Brb loaded in pH 5.6 acetate buffer solution (d–f); ms-Brb loaded in acetate buffer solution of pH 6 (g–i), and ms-Brb loaded in pH 6.8 phosphate buffer solution (j–l).

thereby the hydration process and the permeability of ms shell.

3.7. Cytotoxicity assay on ms and ms-Brb

The results of the cytotoxicity assay on the four samples studied, including ms, ms-Brb and pure Brb in two different concentrations, are illustrated in Fig. 7. The results of MTT assay reveal that neither the pure Brb nor ms-Brb exhibits any cytotoxicity on HaCat cells. Moreover, the Brb encapsulation process preserves the non-toxic properties. Brb favors the proliferation of HaCaT cells at concentrations higher than 0.25 g Brb/1 × 10^4 cells (5 µL Brb water solution 0.01 mg/mL/well). In most of the tested samples an increase in the proliferation rate was recorded as compared to the control wells, the variations depending on the composition of the sample. A different behavior was observed in the

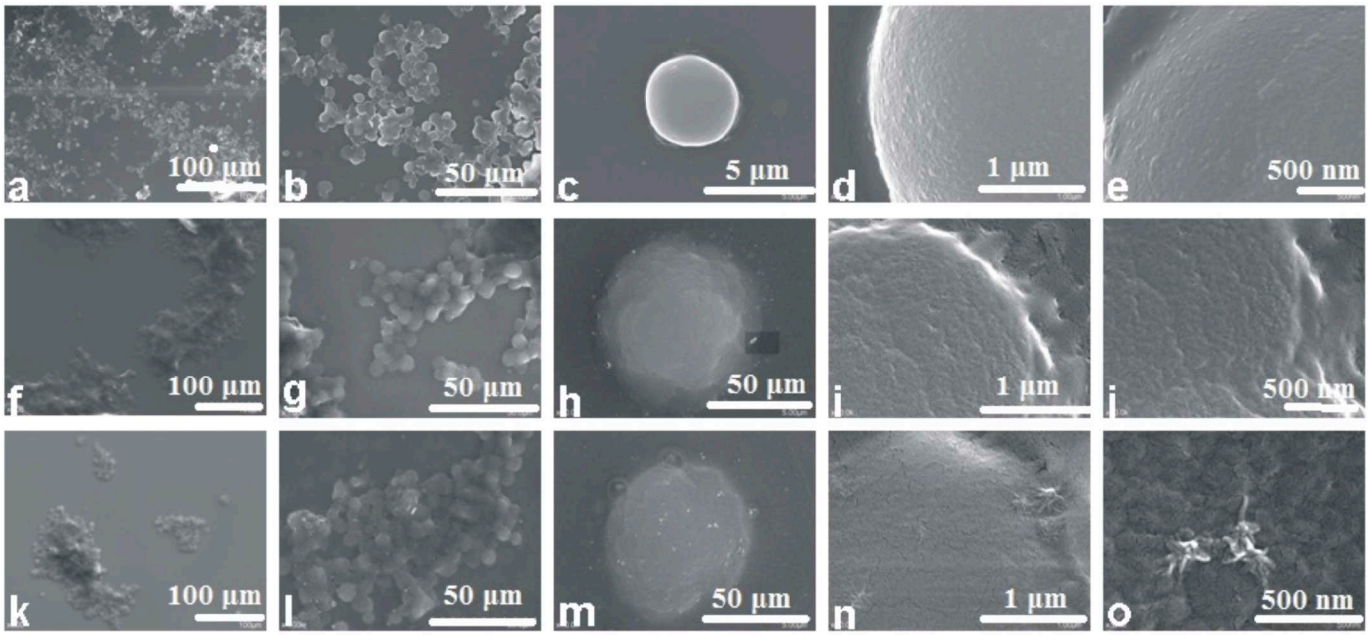


Fig. 5. SEM images of ms-Brb samples isolated from the release medium at pH 4 (a-e); pH 4.4 (f-j) and pH 6, respectively (k-o).

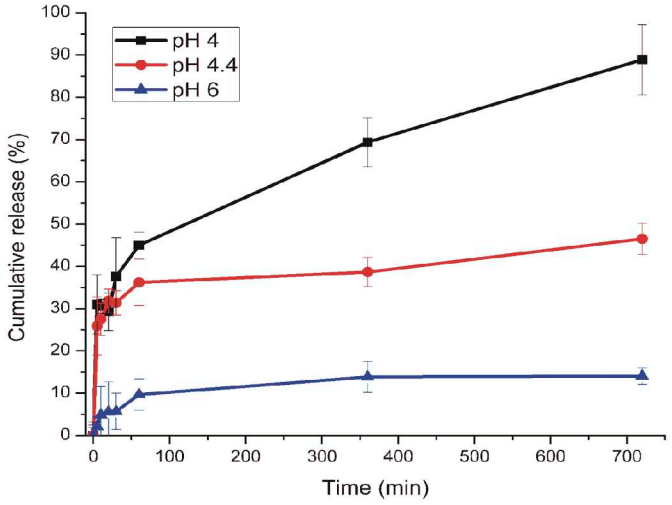


Fig. 6. *In vitro* release profile of ms-Brb in different pH conditions: pH 4, pH 4.4, and pH 6.

case of the wells with ms, where the proliferation rate was lower compared to the control wells. The overall outcome of the MTT assay shows that the use of an adequate concentration of ms-Brb (86 mg/mL suspension increases cell viability and proliferation, probably as a result of the prolonged release of Brb from ms-Brb and also due to the cells bioadhesiveness of ms-Brb. Thereby, the amount of Brb delivered is enhanced.

3.8. Antimicrobial activity against Cutibacterium acnes

Table 2 summarizes the results on the antimicrobial activity of Brb solution, ms and ms-Brb, where inhibition is expressed as diameter of the inhibition zone in mm. The results indicate that ms-Brb showed an antimicrobial activity against *C. acnes*, which was stronger than that of the pure Brb water solution. Ms-Brb revealed an increased antimicrobial effect against *C. acnes*, as compared to that of clindamycin, an antibiotic that is currently used in acne therapy.

The ms-Brb testing revealed higher values of inhibition zones diameter (55 ± 1.52 mm) than those of ms-Brb diluted suspensions (20 ± 0.57 mm and 13 ± 1.15 mm, respectively) as well as those of pure Brb solutions (0.1 mg/mL and 1 mg/mL, respectively). As expected, the antimicrobial effect correlates with the amount of Brb released from ms-Brb and also with the loading efficiency of Brb. The diameters of the inhibition zone corresponding to the ms-Brb also indicate a higher amount of the released Brb than the pure Brb from Brb solution (both 0.1 mg/mL and 1 mg/mL). The tests performed revealed that *C. acnes* was susceptible to clindamycin. Moreover, other authors, such as Lee et al. (2018) demonstrated an anti-inflammatory effect of Brb in *C. acnes*-stimulated HaCaT keratinocytic cells [42], which could be also helpful in acne therapy.

The hyperproliferation of *C. acnes* in the pilosebaceous unit leading to a disruptive effect on skin microbiota is considered one of the driving factors in acne physiopathology. Therefore, an ideal anti-acne product should demonstrate an efficient specific antibacterial activity against *C. acnes* while preserving the local microbiota. The loss of the microbial diversity, mainly due to the use of antibiotics, along with the activation of the innate immunity, may lead to chronic inflammatory diseases [43]. The developed ms-Brb system as microcarriers for Brb has the advantage of an efficient antibacterial activity against *C. acnes*, less toxicity, biocompatibility and biodegradability, making them suitable as delivery systems in anti-acne applications. Our results on the activity of Brb against *C. acnes* are consistent with *in vitro* studies reported by other authors [44].

Previous studies have proposed the microencapsulation of Brb in different types of carriers using *Saccharomyces cerevisiae* yeast cells [45], formaldehyde-free agar/gelatin microcapsules [46] or alginate microspheres [47]. To the best of our knowledge, this is the first time when this natural carrier based on core-shell microcapsules for Brb delivery is described in the literature.

The ms-Brb will be further tested *in vivo* in order to support the current results and to investigate the follicular penetration of Brb from the core-shell microcapsules. The sebaceous gland and infundibulum of the pilosebaceous follicle serve as a potential therapeutic target site for several skin conditions, including acne. The effectiveness of acne treatment may be improved by specifically targeting these sites where pathological changes occur. Due to the architectural structure of the hair follicle, follicular penetration is a complex process divided at least

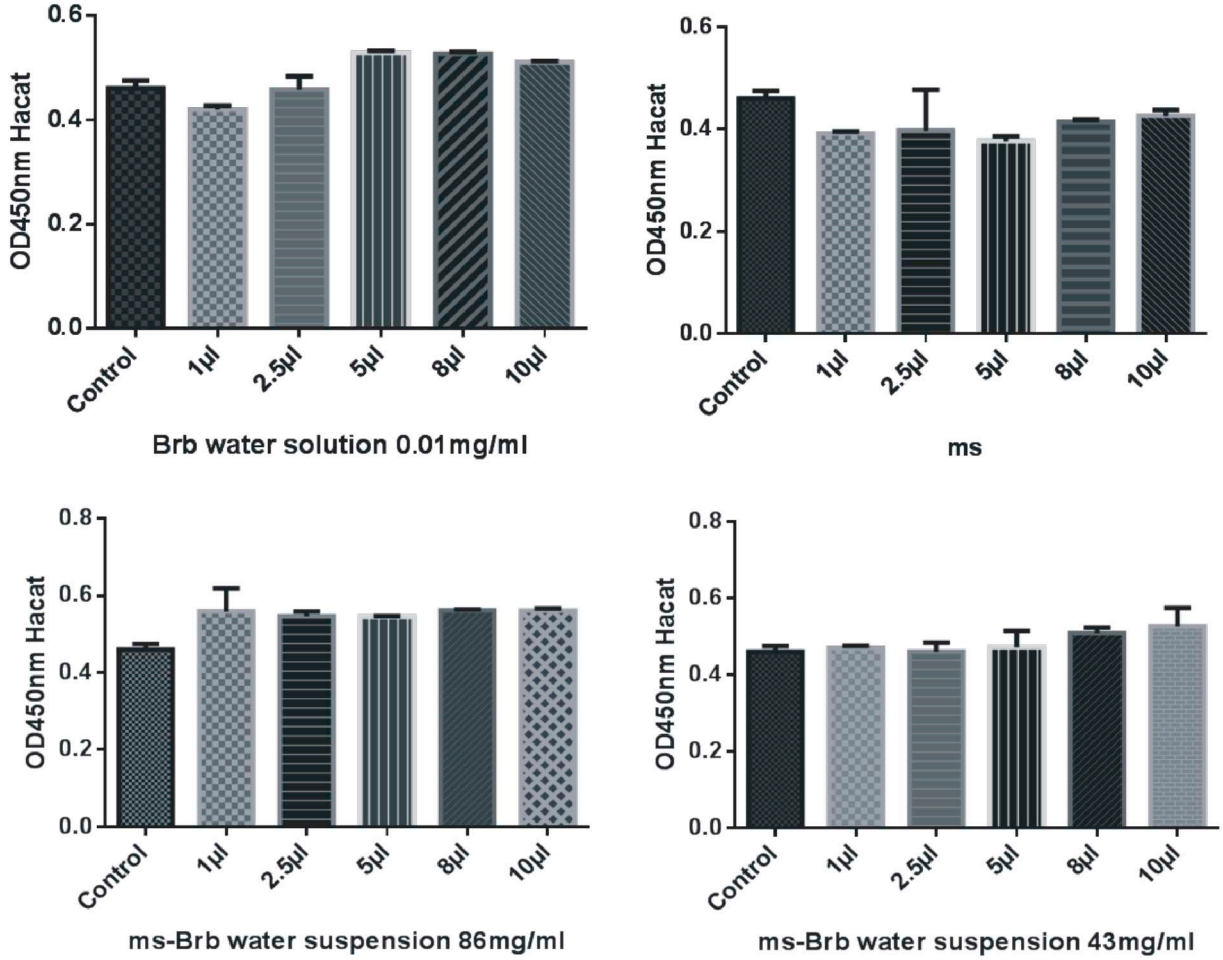


Fig. 7. MTT assay graphical presentation of optical density values after 24 h of incubation of HaCaT cells with ms, ms-Brb water suspensions and pure Brb water solution (0.01 mg/mL).

into two steps, i.e. the penetration into the hair follicle and the transfollicular penetration into the living tissue surrounding the hair follicle. Efficient drug delivery and the pharmacological effect of the applied compound presumably depend on the interactions between the drug and sebum as well as on the physicochemical properties of the vehicle. The physico-chemical properties of a topically administered substance determine its follicular penetration depth [48] and whether or not the substance is able to penetrate transfollicularly. Follicular targeting of the microspheres is possible by choosing the right size. Thus, microspheres of 3–10 µm remain at follicular level without penetrating into stratum corneum and without penetration into viable epidermis [49,50]. Based on the recent findings on follicular penetration, we can assume that our proposed carrier system could be suitable to deliver active substances into the hair follicle. The ms-Brb will be further tested *in vivo* in order to support the current results and to investigate the follicular penetration of Brb released from the core-shell microcapsules.

3.9. Biodegradation of the microcapsules

The optical microscopy images of ms and CLSM images of ms- Brb samples after saliva incubation are presented in Figs. 8 and 9, respectively. The change in the ms aspect can be observed even after 0.5 h. The spherical shape of ms gradually disappears, beginning in the first 30 min, being replaced by much smaller particles with an irregular shape. As the incubation period increases, more and more needle shaped crystals begin to appear, visibles mostly in the Fig. 8 (c-h), which can be attributed to the BSA released from the ms core. The process of ms/ms-Brb degradation begins in the first 30 min and

Table 2
Antimicrobial activity of Brb solution, ms and ms-Brb against *C. acnes*.

Tested samples	Agar well diffusion method Mean diameter of the inhibition zone (mm) ± SD	Agar disc diffusion method Mean diameter of the inhibition zone (mm) ± SD
ms-Brb	55 ± 1.52	38.5 ± 0.57
ms-Brb water suspension (86 mg/mL)	20 ± 0.57	6
ms-Brb water suspension (43 mg/mL)	13 ± 1.15	6
ms (negative control)	6	6
Pure Brb water solution (0.1 mg/mL)	6	6
Pure Brb water solution (1 mg/mL)	47 ± 1	30 ± 0.57
Clindamycin (2 µg/disc)	–	40 ± 1.15

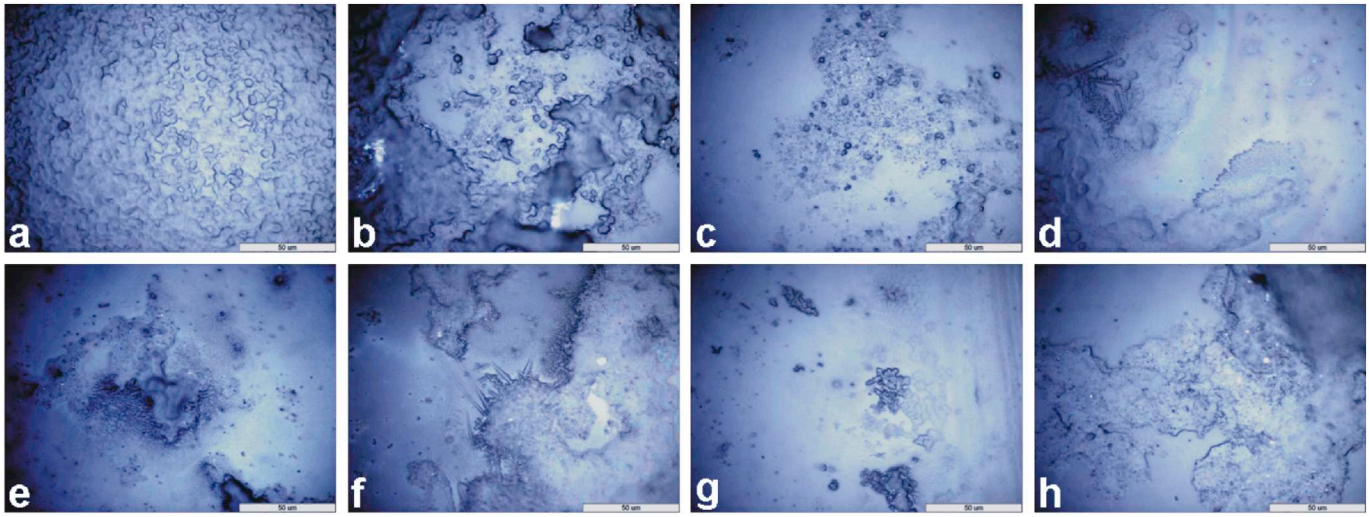


Fig. 8. Optical microscopy images (magnification x1000) of ms samples before (a) and after undergoing the degradation process for 30 min (b); 1 h (c); 2 h (d); 3 h (e); 4 h (f); 5 h (g); and 6 h (h).

continues for at least 6 h. The CLSM images show broken ms-Brb together with the intact ones, their ratio depending on the period of the biodegradation, as well as the release of Brb.

4. Conclusions

In this work novel natural microcarriers, based on natural polysaccharides, calcium cross-linked P hydrogel and polyelectrolyte complex P/Chi deposited onto the $CaCO_3$/BSA microtemplate, finally resulting in BSA gel/P/Chi/P microcapsules suitable for Berberine encapsulation. The structure of the synthesized microcapsules was proven by physical-chemical analyses (FTIR, XRD, CLSM, SEM). CLSM and SEM images confirmed the achievement of capsules with a uniform micron size distribution. A low encapsulation efficiency (25.11%) is specific to hydrophobic active agents. The profile of Brb release from ms-Brb studied on different pH conditions (pH 4, pH 4.4 and pH 6) revealed a pH dependent prolonged release of Brb, which is useful in the pharmaceutical development of sustained release dosage forms. Due to the lack of cytotoxicity, ms-Brb may be used in topical treatment of skin disorders. In addition, the antimicrobial effect against *C. acnes* is a promising premise of Brb application through ms-Brb carrier in the specific anti-acne therapy. It is relevant that degradation is connected with drug release and the specific time is important for each application.

The obtained results allow us to conclude that the core-shell microcapsules made of BSA gel-core and a polyelectrolyte complex P/Chi/P multilayer shell are a promising carrier for targeted and prolonged delivery of Brb. Further research will be focused on the development of an adequate topical delivery system containing ms-Brb and also, on specific *in vivo* studies aiming to evaluate the cutaneous absorption, mainly the follicular penetration.

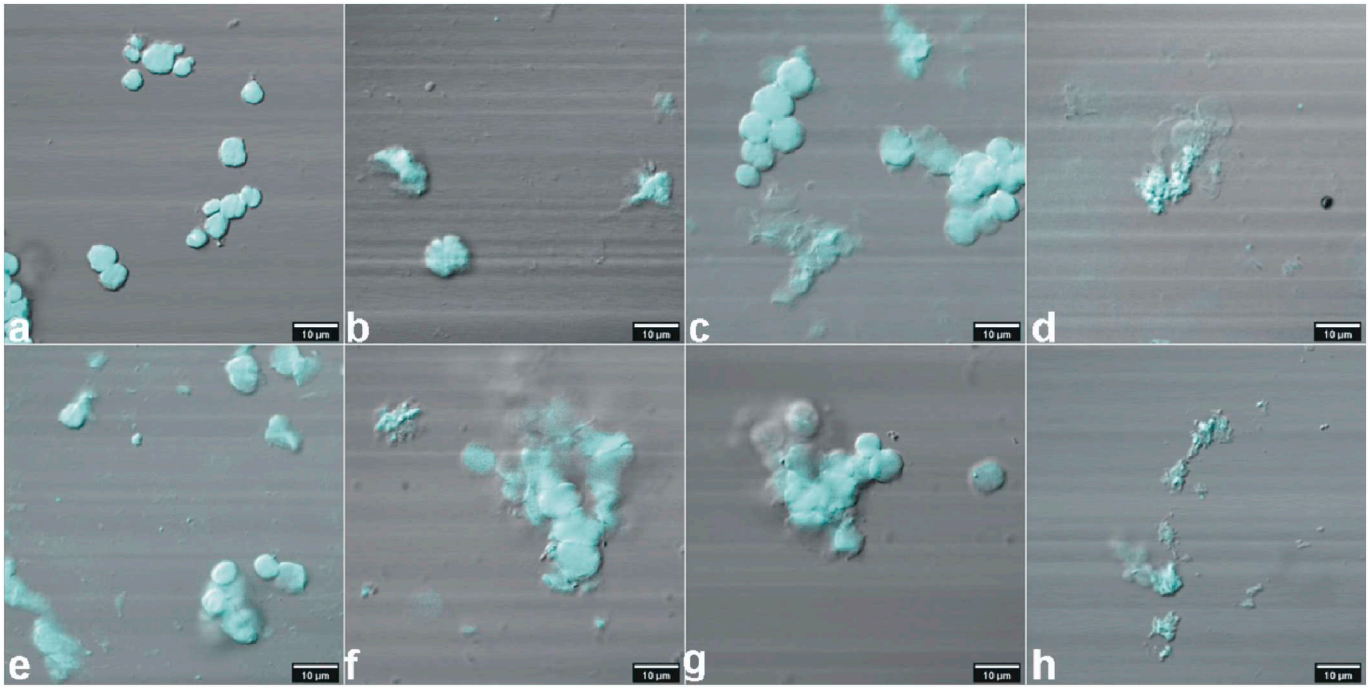


Fig. 9. CLSM images of ms-Brb samples before (a) and after undergoing the degradation process for 30 min (b); 1 h (c); 2 h (d); 3 h (e); 4 h (f); 5 h (g); and 6 h (h).

Data availability

The raw/processed data required to reproduce these findings cannot be shared at this time due to technical or time limitations.

Declaration of Competing Interest

None

Acknowledgement

This work was supported by a grant of the Romanian Ministry of Research and Innovation, CCCDI – UEFISCDI, project number PNIII-P1-1.2-PCCDI-2017-0221/59PCCDI/2018 (IMPROVE), within PNCDI III. This work was partially supported through POS CCE 2.2.1 632/11.03.2014 CETATEA. This work was supported by a grant of the Romanian Ministry of Research and Innovation, CCCDI-UEFISCDI, project number PN-III-P1-1.2-PCCDI-2017-0251/4PCCDI/2018, within PNCD III.

References

[1] J. McLaughlin, S. Watterson, A.M. Layton, A.J. Bjourson, E. Barnard, A. McDowell, Propionibacterium acnes and Acne Vulgaris: new insights from the integration of population genetic, multi-omic, biochemical and host-microbe studies, Microorganisms. 7 (2019), https://doi.org/10.3390/microorganisms7050128.

[2] E.A. Tanghetti, The role of inflammation in the pathology of acne, J. Clin. Aesthet. Dermatol. 6 (2013) 27–35.

[3] Y. Kou, L. Li, H. Li, Y. Tan, B. Li, K. Wang, B. Du, Berberine suppressed epithelial mesenchymal transition through cross-talk regulation of PI3K/AKT and RARα/RARβ in melanoma cells, Biochem. Biophys. Res. Commun. 479 (2016) 290–296, https://doi.org/10.1016/j.bbrc.2016.09.061.

[4] W.P. Gulliver, H.J. Donsky, A report on three recent clinical trials using Mahonia aquifolium 10% topical cream and a review of the worldwide clinical experience with Mahonia aquifolium for the treatment of plaque psoriasis, Am. J. Ther. 12 (2005) 398–406.

[5] D.X. Li, J. Zhang, Y. Zhan, P.W. Zhao, L.M. Yang, Inhibitory effect of berberine on human skin squamous cell carcinoma A431 cells, Genet. Mol. Res. 14 (2015) 10553–10568, https://doi.org/10.4238/2015.

[6] C. Nam, S. Kim, Y. Sim, I. Chang, Antiacne effects of Oriental herb extracts: a novel screening method to select antiacne agents, Skin. Pharmacol. Appl. Skin. Physiol. 16 (2003) 84–90, https://doi.org/10.1159/000069030.

[7] S. Higaki, M. Nakamura, M. Morohashi, Y. Hasegawa, T. Yamagishi, Activity of eleven kampo formulations and eight kampo crude drugs against Cutibacterium acnes isolated from acne patients: retrospective evaluation in 1990 and 1995, J. Dermatol. 23 (1996) 871–875, https://doi.org/10.1111/j.1346-8138.1996.tb02717.x.

[8] Q. Wang, J. Qi, R. Hu, Y. Chen, A. Kijlstra, P. Yang, Effect of berberine on proinflammatory cytokine production by ARPE-19 cells following stimulation with tumor necrosis factor-a, Invest. Ophthalmol. Vis. Sci. 53 (2012) 2395–2402, https://doi.org/10.1167/iovs.11-8982.

[9] S.D. Patel, S. Shah, N. Shah, A review on herbal drugs acting against acne vulgaris, J. Pharm. Sci. Bio-sci. Res. 5 (2015) 165–171.

[10] P.L. Lam, R. Gambari, Advanced progress of microencapsulation technologies: In vivo and in vitro models for studying oral and transdermal drug deliveries, Journal of Controlled Release 178 (2014) 25–45, https://doi.org/10.1016/j.jconrel.2013.12.028.

[11] E. Głowka, H. Wosicka-Frackowiak, K. Hyla, J. Justyna Stefanowska, K. Jastrzębska, Ł. Klapiszewski, T. Jesionowski, K. Cal, Polymeric nanoparticles-embedded organogel for roxithromycin delivery to hair follicles, Eur. J. Pharm. Biopharm. 88 (2014) 75–84, https://doi.org/10.1016/j.ejpb.2014.06.019.

[12] F. Kratz, Albumin as a drug carrier: design of prodrugs, drug conjugates and nanoparticles, J. Control. Release. 132 (2008) 171–183, https://doi.org/10.1016/j.jconrel.2008.05.010.

[13] O. Grinberg, M. Hayun, B. Sredni, A. Gedanken, Characterization and activity of sonochemically-prepared BSA microspheres containing taxol – an anticancer drug, Ultrason. Sonochem. 14 (2007) 661–666, https://doi.org/10.1016/j.ultsonch.2006.11.004.

[14] H.J. Shen, H. Shi, K. Ma, M. Xie, L.L. Tang, S. Shen, B. Li, X.S. Wang, Y. Jin, Polyelectrolyte capsules packaging BSA gels for pH-controlled drug loading and release and their antitumor activity, Acta Biomater. 9 (2013) 6123–6133, https://doi.org/10.1016/j.actbio.2012.12.024.

[15] M. Achim, I. Tomuta, L. Vlase, C. Iuga, M. Moldovan, S.E. Leucuta, Paclitaxel-loaded poly(lactic-co-glycolic acid) microspheres: preparation and in vitro evaluation, J. Drug. Deliv. Sci. Technol. 18 (2008) 410–416, https://doi.org/10.1016/S1773-2247(08)50080-3.

[16] R. Cassano, S. Trombino, T. Ferrarelli, A.R. Bilia, M.C. Bergonzi, A. Russo, F. Amicis, N. Picci, Preparation, characterization and in vitro activities evaluation of curcumin based microspheres for azathioprine oral delivery, React. Funct. Polym. 72 (2012) 446–450, https://doi.org/10.1016/j.reactfunctpolym.2012.04.003.

[17] W.E. Hennink, C.F. van Nostrum, Novel crosslinking methods to design hydrogels, Adv. Drug Deliver. Rev. 64 (2012) 223–236, https://doi.org/10.1016/j.addr.2012.09.009.

[18] T. Kean, M. Thanou, Chitin and chitosan—sources, production and medical applications, in: P.A. Williams, R. Arshady (Eds.), Desk Reference of Natural Polymers, Their Sources, Chemistry and Applications, Kentus Books, London, 2009, pp. 327–361.

[19] M. Thanou, J.C. Verhoe, H.E. Junginger, Oral drug absorption enhancement by chitosan and its derivatives, Adv. Drug Deliver. Rev. 52 (2001) 117–126, https://doi.org/10.1016/S0169-409X(01)00231-9.

[20] M. Dash, F. Chiellini, R.M. Ottenbrite, E. Chiellini, Chitosan—a versatile semi-synthetic polymer in biomedical applications, Prog. Polym. Sci. 36 (2011) 981–1014, https://doi.org/10.1016/j.progpolymsci.2011.02.001.

[21] A. Kumar, A. Vimal, A. Kumar, Why chitosan? From properties to perspective of mucosal drug delivery, Int. J. Biol. Macromol. 91 (2016) 615–622, https://doi.org/10.1016/j.ijbiomac.2016.05.054.

[22] R. Khurana, K. Singh, B. Sapra, A.K. Tiwary, V. Rana, Tamarindus indica pectin blend film composition for coating tablets with enhanced adhesive force strength, Carbohyd. Polym. 102 (2014) 55–65, https://doi.org/10.1016/j.carbpol.2013.11.005.

[23] V.D. Prajapati, G.K. Jani, N.G. Moradiya, N.P. Randeria, Pharmaceutical applications of various natural gums, mucilages and their modified forms, Carbohyd. Polym. 92 (2013) 1685–1699, https://doi.org/10.1016/j.carbpol.2012.11.021.

[24] W. He, Q. Du, D. Cao, B. Xiang, L. Fan, Study on colon-specific pectin/ethylcellulose film-coated 5-fluorouracil pellets in rats, Int. J. Pharm. 348 (2008) 35–45, https://doi.org/10.1016/j.ijpharm.2007.07.005.

[25] V.K. Thakur, M.K. Thakur, Handbook of Sustainable Polymers. Processing and Applications, CRC Press, 2016, pp. 458–465.

[26] F. Bigucci, B. Luppi, T. Cerchiara, M. Sorrenti, G. Bettinetti, L. Rodriguez, V. Zecchi, Chitosan/Pectin polyelectrolyte complexes: selection of suitable preparative conditions for colon-specific delivery of vancomycin, Eur. J. Pharm. Sci. 35 (2008) 435–441, https://doi.org/10.1016/j.ejps.2008.09.004.

[27] E. Donath, G.B. Sukhorukov, F. Caruso, F. Davis, H. Möhwald, Novel hollow polymer shells by colloid-templated assembly of polyelectrolytes, Angew. Chem. Int. Edit. 37 (1998) 2202–2205, https://doi.org/10.1002/(SICI)1521-3773(19980904)37:16<2201::AID-ANIE2201>3.0.CO;2-E.

[28] D.V. Volodkin, N.I. Larionova, G.B. Sukhorukov, Protein Encapsulation via porous CaCO3 microparticles templating, Biomacromolecules. 5 (2004) 1962–1972.

[29] G.B. Sukhorukov, E. Donath, H. Lichtenfeld, E. Knippel, M. Knippel, A. Budde, H. Möhwald, Layer-by-layer self assembly of polyelectrolytes on colloidal particles, Colloid Surface A. 137 (1998) 253–266, https://doi.org/10.1016/S0927-7757(98)00213-1.

[30] P. Rivera-Gil, S. De Koker, B.G. De Geest, W.J. Parak, Intracellular processing of proteins mediated by biodegradable polyelectrolyte capsules, Nano. Lett. 9 (2009) 4398–4402, https://doi.org/10.1021/nl902697j.

[31] A. Anitha, S. Maya, N. Deepa, K.P. Chennazhi, S.V. Nair, H. Tamura, R. Jayakumar, Efficient water soluble O-carboxymethyl chitosan nanocarrier for the delivery of curcumin to cancer cells, Carbohydr. Polym. 83 (2011) 452–461, https://doi.org/10.1016/j.carbpol.2010.08.008.

[32] R. Bonnet, J.P. Bru, F. Caron, V. Cattoir, P. Courvalin, L. Dubreuil, et al., Comité de l'antibiogramme de la Société Française de Microbiologie, https://www.sfm-microbiologie.org/.2019 (accessed 17 May 2019).

[33] C. Picart, Polyelectrolyte multilayer films: from physico-chemical properties to the control of cellular processes, Curr Med Chem 15 (2008) 685–697, https://doi.org/10.2174/092986708783885219.

[34] K.-Y. Lu, Y.-C. Lin, H.-T. Lu, Y.-C. Ho, S.-C. Weng, M.-L. Tsai, F.-L. Mi, A novel injectable in situ forming gel based on carboxymethyl hexanoyl chitosan/hyaluronic acid polymer blending for sustained release of berberine, Carbohyd. Polym. 206 (2019) 664–673, https://doi.org/10.1016/j.carbpol.2018.11.050.

[35] Iris E. Allijn, B.M.S. Czarny, X. Wang, S.Y. Chong, M. Weiler, A.E. da Silva, J.M. Metselaar, C.S.P. Lamg, G. Pastorin, D.P.V. de Kleijn, G. Storm, J.-W. Wang, R.M. Schiffelers, Liposome encapsulated berberine treatment attenuates cardiac dysfunction after myocardial infarction, J Control Release 247 (2017) 127–133.

[36] Y.-C. Lin, J.-Y. Kuo, C.-C. Hsu, W.-C. Tsai, W.-C. Li, M.-C. Yu, H.-W. Wen, Optimizing manufacture of liposomal berberine with evaluation of its antihepatoma effects in a murine xenograft model, Int. J. Pharm. 441 (2013) 381–388, https://doi.org/10.1016/j.ijpharm.2012.11.017.

[37] L. Gupta, A. Kumar Sharma, A. Gothwal, M.S. Khan, M.P. Khinchi, A. Qayum, S.K. Singh, U. Gupta, Dendrimer encapsulated and conjugated delivery of berberine: a novel approach mitigating toxicity and improving in vivo pharmacokinetics, Int. J. Pharm. 528 (2017) 88–99, https://doi.org/10.1016/j.ijpharm.2017.04.073.

[38] F. Yu, Y. Li, Q. Chen, Y. He, H. Wang, L. Yang, S. Guo, Z. Meng, J. Cui, M. Xue, X.D. Chen, Monodisperse microparticles loaded with the self-assembled berberine-phospholipid complex-based phytosomes for improving oral bioavailability and enhancing hypoglycemic efficiency, European Eur J Pharm Biopharm. 103 (2016) 136–148, https://doi.org/10.1016/j.ejpb.2016.03.019.

[39] E. Mirhadi, M. Rezaeeb, B. Malaekeh-Nikoueia, Nano strategies for berberine delivery, a natural alkaloid of Berberis, Biomed Pharmacother. 104 (2018) 465–473, https://doi.org/10.1016/j.biopha.2018.05.067.

[40] X. Luo, J. Li, L. Guo, X. Cheng, T. Zhang, Y. Deng, Preparation of berberine hydrochloride long-circulating liposomes by ionophore A23187-mediated ZnSO4 gradient method, Asian J. Pharm. 8 (4) (2013) 261–266, https://doi.org/10.1016/j.ajps.2013.09.009.

[41] V. Paşcalău, G. Dindelegan, N. Dirzu, A.M. Salantiu, C. Pavel, M.C. Dudescu, F. Popa, G. Borodi, F. Tabaran, C.A. Iuga, C. Popa, Bioactive Ti-base biomaterial

with sustained anti-bacterial response for endosseous applications, React. Funct. Polym. 125 (2018) 37–46, https://doi.org/10.1016/j.reactfunctpolym.2018.02.007.
[42] B. Dréno, S. Pécastaings, S. Corvec, S. Veraldi, A. Khammari, C. Roques, Cutibacterium acnes (Propionibacterium acnes) and acne vulgaris: a brief look at the latest updates, JEADV 32 (2018) 5–14, https://doi.org/10.1111/jdv.15043.
[43] J.W. Lee, Y.J. Kang, H.K. Choi, Y.G. Yoon, Fractionated Coptis chinensis extract and its bioactive component suppress Propionibacterium acnes-stimulated inflammation in human keratinocytes, J. Microbiol. Biotechnol. 28 (2018) 839–848, https://doi.org/10.4014/jmb.1712.12051.
[44] L. Slobodníková, D. Kosťálová, D. Labudová, D. Kotulová, V. Kettmann, Antimicrobial activity of Mahonia aquifolium crude extract and its major isolated alkaloids, Phytother. Res. 18 (2004) 674–676, https://doi.org/10.1002/ptr.1517.
[45] R. Salari, O. Rajabi, Z. Khashyarmanesh, M.F. Najafi, B. Sedigheh, F. Bazzaza, Characterization of encapsulated berberine in yeast cells of Saccharomyces cerevisiae. Iran, J. Pharm. Res. 14 (2015) 1247–1256.
[46] P.L. Lam, K.K.H. Lee, S.H.L. Kok, G.Y.M. Cheng, X.M. Tao, D.K.P. Hau, M.C.W. Yuen, K.H. Lam, R. Gambari, C.H. Chui, R.S.M. Wong, Development of formaldehyde-free agar/gelatin microcapsules containing berberine HCl and gallic acid and their topical and oral applications, Soft. Matter. 8 (2012) 5027–5037, https://doi.org/10.1039/c2sm07236j.
[47] A.M. Zhu, J.H. Chen, Q.L. Liu, Y.L. Jiang, Controlled release of berberine hydrochloride from alginate microspheres embedded within carboxymethyl chitosan hydrogels, J. Appl. Polym. Sci. 120 (2011) 2374–2380, https://doi.org/10.1002/app.33433.
[48] A. Patzelt, H. Richter, F. Knorr, U. Schäfer, C.M. Lehr, L. Dähne, W. Sterry, J. Lademann, Selective follicular targeting by modification of the particle sizes, J. Control. Release. 150 (2011) 45–48, https://doi.org/10.1016/j.jconrel.2010.11.015.
[49] H. Wosicka, K. Cal, Targeting to the hair follicles: Current status and potential, J Dermatol Sci. 57 (2010) 83–89, https://doi.org/10.1016/j.jdermsci.2009.12.005.
[50] A. Patzelt, J. Lademann, The increasing importance of the hair follicle route in dermal and transdermal drug delivery, in: N. Dragicevic-Curic, H.I. Maibach (Eds.), Percutaneous Penetration Enhancers Chemical Methods in Penetration enhancement – Drug Manipulation Strategies and Vehicle Effects, Springer-Verlag, Berlin Heidelberg, 2015, pp. 43–53, , https://doi.org/10.1007/978-3-662-45013-0_5.

applied sciences

MDPI

Article

Development of a Mouthwash Using Freeze-Drying Technique: An Optimization Study

Sonia M. Iurian [1,†], Diana-Roxana Adespei [2,†], Anca Pop [3,*], Ionel Fizeșan [3], Rahela Carpa [4], Mirela L. Moldovan [2], Felicia Loghin [3], Marcela Achim [1] and Cătălina Bogdan [2]

[1] Department of Pharmaceutical Technology and Biopharmacy, Faculty of Pharmacy, "Iuliu Haţieganu" University of Medicine and Pharmacy, 41 V. Babes Street, 400012 Cluj-Napoca, Romania; sonia.iurian@umfcluj.ro (S.M.I.); machim@umfcluj.ro (M.A.)
[2] Department of Dermopharmacy and Cosmetics, Faculty of Pharmacy, "Iuliu Haţieganu" University of Medicine and Pharmacy, 12 I. Creanga Street, 400010 Cluj-Napoca, Romania; diana.adespei@gmail.com (D.-R.A.); mmoldovan@umfcluj.ro (M.L.M.); catalina.bogdan@umfcluj.ro (C.B.)
[3] Department of Toxicology, Faculty of Pharmacy, "Iuliu Haţieganu" University of Medicine and Pharmacy, L. Pasteur Street, 400349 Cluj-Napoca, Romania; ionel.fizesan@umfcluj.ro (I.F.); floghin@umfcluj.ro (F.L.)
[4] Department of Molecular Biology and Biotechnology, Faculty of Biology and Geology, "Babes-Bolyai" University, 1 M. Kogalniceanu Street, 400084 Cluj-Napoca, Romania; rahela.carpa@ubbcluj.ro
* Correspondence: anca.pop@umfcluj.ro
† These authors contributed equally to this work.

Citation: Iurian, S.M.; Adespei, D.-R.; Pop, A.; Fizeșan, I.; Carpa, R.; Moldovan, M.L.; Loghin, F.; Achim, M.; Bogdan, C. Development of a Mouthwash Using Freeze-Drying Technique: An Optimization Study. *Appl. Sci.* **2021**, *11*, 9609. https://doi.org/10.3390/app11209609

Academic Editor: Alessandra Durazzo

Received: 10 September 2021
Accepted: 12 October 2021
Published: 15 October 2021

Publisher's Note: MDPI stays neutral with regard to jurisdictional claims in published maps and institutional affiliations.

Copyright: © 2021 by the authors. Licensee MDPI, Basel, Switzerland. This article is an open access article distributed under the terms and conditions of the Creative Commons Attribution (CC BY) license (http://creativecommons.org/licenses/by/4.0/).

Abstract: In recent years, the development of solid cosmetics, as part of sustainable cosmetics strategy, is generating increasing interest. In addition, novel approaches such as Quality by Design concept allowed the development of high-quality products together with a decrease in waste generation. The present study aimed the development of freeze-dried mouthwashes containing *Cetraria islandica* extract using the Quality by Design approach. Based on the results of preliminary experiments, a factorial design with three factors that varied on two levels was developed. As factors, the filler type (sorbitol or mannitol) was chosen as the qualitative factor and the two quantitative factors were: the filler ratio set from 3 to 5% and polymer (methylcellulose) ratio from 0 to 0.5%. After the preparation and the complete characterization of the formulations generated through the experimental design, the effect of the formulation variables on the lyophilized mouthwashes and the interactions between formulation factors were investigated. Finally, an optimal formulation with appropriate mechanical properties that ensure easy manipulation and no material loss when extracted from the package and fast reconstitution was generated.

Keywords: sustainable cosmetics; freeze-drying; natural extracts; mouthwash; design of experiments

1. Introduction

There is a growing need for performant, safe, and sustainable cosmetic products with a low environmental footprint. In recent years, relevant stakeholders have been working towards developing regulations and strategies to reduce the use of plastic material by the cosmetic industry. As part of the European Strategy for Plastics, the Directive 2019/904 and Implementing Regulation 2020/2151 set out the specifications for marking the products containing plastics. To reduce the quantity of waste generated, Member States of EU should encourage the use of products for multiple uses or provide suitable and more sustainable alternatives for single-use plastic products [1]. In this regard, solid cosmetics have gained importance in the last years due to their multiple advantages, mainly the reduced environmental impact. Solid cosmetics can be more appealing to consumers due to their different appearance and innovative concepts. This novel

approach gives rise to new challenges in the design of safe products that will preserve their properties during storage, handling, and transport [2] and in finding alternative approaches to standard manufacturing.

Out of the preparation methods, freeze-drying is employed to preserve the properties of pharmaceutical and cosmetic products [3]. Freeze-drying, also called "lyophilization" or "cryodesiccation" represents a drying technique that involves the removal of the solvent (usually water) by freezing and further evaporation by sublimation upon heating. During the lyophilization process, more than 90% of the containing water is lost. When reaching room temperature, the freeze-dried product remains dry and must be rehydrated before being used. Thus, the water removal prevents bacterial growth and stability issues, but also the need of adding preservatives [4]. The freeze-drying technique allows the development of lyophilized cosmetic compositions that are more stable than traditional products [5] and ensures the long-term stability of the bioactive compounds [3].

The medicinal use of the dried thallus of *Cetraria islandica* (L.) Acharius s.l. from the *Parmeliaceae* family, also known as Island moss or *Lichen islandicus* has been documented thoroughly. The principal phytoconstituents are polysaccharides, 25–50% (lichenan, isolichenan), lichen acids (depsidones fumaroprotocetraric acid, protolichesterinic acid and usnic acid), and minerals [6]. Several in vitro studies indicate the antimicrobial, immunomodulating, anti-inflammatory, antiviral, and antioxidative activity of the *Cetraria islandica* aqueous and ethanolic extracts [6]. The data obtained during in vitro studies are supported by in vivo studies investigating the activation of the reticuloendothelial system, anti-inflammatory, anti-proliferative, and antioxidative effects. Moreover, available clinical data support the efficacy of *Cetraria islandica* extract for the treatment of inflammations of oral mucosa and dryness of the oral cavity [6].

Developed initially by the pharmaceutical industry, the Quality by Design (QbD) concept was adopted lately by the cosmetic industry as a systematic approach for obtaining high-quality products with the desired product performance. The main goals of the QbD paradigm include the design of robust formulations and manufacturing processes to reliably provide the required product quality [7]. Application of QbD principles relies on the use of Design of Experiments (DoE), a basic concept in formulation and optimization which significantly reduces the number of tests, time, and costs [8]. In this work, the application of DoE in the development of freeze-dried mouthwashes has been investigated to select the most appropriate conditions to obtain fast-dissolving structures with appropriate mechanical properties. Preliminary studies were undertaken to investigate the biocompatibility of *Cetraria islandica* extract and the impact of the excipients on the lyophilized structures' properties; further, a two-level full factorial design with three factors was carried out and the obtained results were analyzed to establish the Design Space as the multidimensional combination of inputs that deliver the product to meet the desired attributes. Together, novel strategies such as the freeze-drying technique and QbD have shown their efficiency in the development and optimization of modern cosmetics by generating less waste and allowing greater flexibility.

2. Materials and Methods

2.1. Materials

The hydroalcoholic *Cetraria islandica* extract was obtained through a reflux extraction for 30 min at 60 °C in a 70% (*v*/*v*) aqueous ethanol solution at a solid: solvent ratio of 1:10 (*w*/*v*). After cooling, the sample was filtered, and the supernatant was recovered. Further, the extract was concentrated through rotary evaporation (Hei-VAP Advantage Rotary evaporator HL/G1 (Heidolph, Schwabach, Germany) under reduced pressure at 50 °C and 80 rpm until 40% of the initial mass. The substances used were the following: LMW (low molecular weight) hyaluronic acid and allantoin which were purchased from Elemental (Oradea, Romania), Poloxamer 407 and mannitol from Sigma-Aldrich (Darmstadt,

Germany), sorbitol from Fagron (St. Paul, MN, USA) and methylcellulose, Methocel MC 4000 cP (Fluka AG, Buchs, Switzerland).

2.2. Methods

2.2.1. In Vitro Evaluation of the *Cetraria islandica* Extract

Cell Culture

The normal human foreskin fibroblasts (BJ) were cultivated in DMEM (Dulbecco's modified Eagle's medium, Gibco, Paisley, UK) supplemented with 10% FBS (fetal bovine serum, Sigma Aldrich, Steinheim, Germany) and maintained in a humidified incubator with a 5% CO_2 atmosphere at 37 °C. Every 2–3 days the medium was replaced and the cells were subcultured at around 70–80% confluency.

Preparation of Extract Solutions

Working solutions with concentrations ranging from 2.5–100 mg/mL were prepared in DMSO (Riedel-de Haën, Seelze, Germany). These solutions were further diluted in cell culture medium to obtain the tested concentrations ranging from 10 to 400 μg/mL.
Cytotoxicity AssayTrypsinized cells were seeded in 96-well plates and left to attach for 24 h. PBS was used to wash the dead and unattached cells, while the viable cells were incubated with the *Cetraria islandica* extract. After 24 h the cells were washed with PBS and viability was assessed by Alamar Blue assay (Thermo Fisher Scientific, Waltham, MA, USA) a test that measures the cellular ability to convert a non-fluorescent compound such as resazurin to resorufin, a fluorescent compound. The fluorescence intensity was measured at λexcitation = 530/25, λemission = 590/35 following a 4 h exposure to a 200 μM resazurin solution, using a Synergy 2 multi-mode microplate reader (BioTek Instruments Inc., Winooski, VT, USA). DMSO (0.4% in cell culture medium) was used as the negative control.

Antibacterial Activity

The tested microorganisms were: *Enterococcus faecalis* ATCC 29212, *Escherichia coli* ATCC 25922 and *Staphylococcus aureus* ATCC 25923 (ATCC-American Type Culture Collection, Manassas, VA, USA). Out of each bacterial strain grown for 24 h on Nutrient Agar medium [9] a dilution of 0.5 McFarland in sterile saline solution was made.

For the agar-well diffusion method, Petri dishes with Mueller Hinton agar media (Oxoid, Hampshire, UK) were inoculated with each bacterial strain suspension and maintained at 37 °C for 20 min to infiltrate. Then, 5 mm diameter wells were carved in the agar using a sterile cut pipette tip. The wells were then filled with sterile cotton beads and each bead was loaded with 80 μL of *Cetraria islandica* extract. The plate also contained a control well loaded with the solvent used, prepared as an aqueous ethanol solution 70% (*v*/*v*) and then evaporated at 40% of the initial mass. After 24 h incubation at 37 °C, the hallow formed around the wells was measured, the larger the diameter of the inhibition zone, the higher the sensibility of bacteria to that plant extract [10]. Each experiment was conducted in duplicate, and the mean was calculated.

2.2.2. Preparation of Mouthwash Samples

All samples were prepared similarly: for each mouthwash, two separate 10 mL solutions were prepared and mixed at the end. The hydroalcoholic extract was gravitationally filtered and then transferred to a mortar where a surfactant solution (Poloxamer in 10 mL distilled water) was added dropwise and stirred continuously with a pestle until complete homogenization and defoaming. The second solution was prepared in a Berzelius beaker, by adding all the other ingredients (mannitol/sorbitol, methylcellulose, allantoin, hyaluronic acid, and flavoring agent) in 10 mL of distilled water and stirring until complete dissolution. The two solutions were mixed in a Berzelius

beaker and stirred using the VELP Scientifica Mechanic Stirrer (Usmate Velate, Italy) for 10 min at 500 rpm. Further, they were transferred to 2 mL blister pockets.

2.2.3. Freeze-Drying of Mouthwash Samples

The samples were freeze-dried using VirTis Advantage Plus Freeze Dryer (SP Scientific, Gardiner, MT, USA). They were first cooled to −55 °C for 12 h, then subjected to primary drying at −25 °C, 0.2 mbar for 24 h, followed by secondary drying at 20 °C for 12 h. The final freeze-dried products were kept in a desiccator until they were processed further, to prevent hydration and loss of proprieties.

2.2.4. Characterization of Mouthwash Samples

All samples were analyzed at an ambient temperature of 22 ± 5 °C.

Texture Analysis

The texture analysis was performed with the Brookfield CT3 Texture Analyzer (Brookfield Engineering, Middleboro, MA, USA) through compression tests on one freeze-dried tablet at a time. The sample was placed horizontally on the analysis surface and was subjected to a constant force applied by a TA10 probe with a speed of 0.1 mm/s and a load of 10 g until a target distance of 5 mm. For each test, three measurements were performed and the rigidity at two different distances, fracturability, load at target, mechanical work at the first fracture, deformation at the first fracture, mean load were determined using the TexturePro CT Software V 1.9 (Brookfield Engineering, Middleboro, MA, USA). For each parameter, the mean and standard deviation were calculated.

Reconstitution Time

Reconstitution times for each sample were measured by placing a lyophilizate in 10 mL of distilled water followed by manual stirring. The time required for the complete dissolution of the lyophilized tablet was measured with a digital stopwatch. For each test, three experiments were performed, and the mean and standard deviation were determined.

Weight Loss Percentage

To quantify the integrity of the lyophilizates, weight loss for each sample was measured after removing it from the blister pocket. Firstly, the lyophilizate was weighed into the alveolae, then it was removed and weighed separately, and finally after weighing the empty alveolae, we determined the weight difference. For each test, three experiments were performed, and the mean and standard deviation were determined.

Viscosity Measurement of the Reconstituted Mouthwashes

For the reconstituted mouthwashes, the rheological measurements were made using the Brookfield DV-III Ultra (Brookfield Engineering, Middleboro, MA, USA) equipped with LV-1 spindle, at a rotational speed of 200 rpm. For each test, three experiments were performed, and the mean and standard deviation were determined.

Experimental Design

To investigate the effects of the formulation variables on the lyophilized mouthwashes, a DoE was developed, with the possibility to highlight the interactions between factors, using the Modde 12 software (Umetrics, Umeå, Sweden). A full factorial design with three factors that varies on two levels, thus a total of eight runs and three center points, was generated. As factors, a qualitative one was chosen, the filler type (X1) that varied between mannitol or sorbitol, and two quantitative ones: the filler ratio (X2) set from 3 to 5% and methylcellulose (MC) ratio (X3) from 0 to 0.5%. The composition of the formulations is detailed in Table 1. The studied responses derived from the previously

described characterization methods: rigidity at 2 (Y1) and 4 mm (Y2), load at target (Y3), fracturability (Y4), first fracture work (Y5), first fracture deformation (Y6), mean load (Y7), the weight loss percent (Y8), reconstitution time (Y9), and viscosity (Y10). For optimizing the final formula, some constraints were applied: weight loss, reconstitution time were minimized and fracturability (measured as hardness values of initial fractures) and viscosity were maximized.

Table 1. The quantitative and qualitative composition of formulations F1–F11.

	Quantity *w*/*v*%										
Ingredient	**F1**	**F2**	**F3**	**F4**	**F5**	**F6**	**F7**	**F8**	**F9**	**F10**	**F11**
Mannitol	3.00	-	7.00	-	3.00	-	7.00	-	5.00	5.00	5.00
Sorbitol	-	3.00	-	7.00	-	3.00	-	7.00	-	-	-
Poloxamer	5.00	5.00	5.00	5.00	5.00	5.00	5.00	5.00	5.00	5.00	5.00
Methylcellulose	-	-	-	-	0.50	0.50	0.50	0.50	0.25	0.25	0.25
Allantoin	5.00	5.00	5.00	5.00	5.00	5.00	5.00	5.00	5.00	5.00	5.00
Hyaluronic acid	0.125	0.125	0.125	0.125	0.125	0.125	0.125	0.125	0.125	0.125	0.125
Cetraria islandica extract	5.00	5.00	5.00	5.00	5.00	5.00	5.00	5.00	5.00	5.00	5.00
Flavoring agent	0.50	0.50	0.50	0.50	0.50	0.50	0.50	0.50	0.50	0.50	0.50

2.2.5. Optimal Mouthwash Formulation

The optimal formula generated was prepared using the same method previously used for the 11 samples (Section 2.2.2). After preparation, the optimal formulation was subjected to freeze-drying process (as described in Section 2.2.3) and then characterized, using the same tests and the same procedures as for the initial 11 samples presented in Section 2.2.4:

- Texture analysis,
- Reconstitution time,
- The weight loss percent,
- Viscosity measurement of the reconstituted mouthwash.

Finally, the theoretical results obtained from the experimental design were interpreted and compared with the practical ones. The residual values were calculated as the difference between the experimental value and the one predicted by the model.

3. Results and Discussion

3.1. Evaluation of the Cetraria islandica Extract

3.1.1. In Vitro Testing

The *Cetraria islandica* extract was evaluated for a potential cytotoxic effect using a normal cell model, human foreskin fibroblasts following a 24 h exposure. No cytotoxic effects were observed instead, an increase in viability for the concentrations ranging from 75–400 μg/mL was detected (Figure 1). In the case of the higher concentrations tested (300 and 400 μg/mL) the increase in viability was 22–30%, while exposure to 200–150 μg/mL resulted in a 6–9% increase in viability. In the case of intermediary doses (75, 100 μg/mL) an approximately 3% increase was noticed. Our results are in agreement with a study published by Ögmundsdóttir et al. where a small, but consistent increase in viability was observed in fibroblast cultures exposed to protolichesterinic acid, a low-molecular-weight lichen metabolite [11]. The lack of in vitro toxicity encouraged the further preparation of the mouthwash formulations.

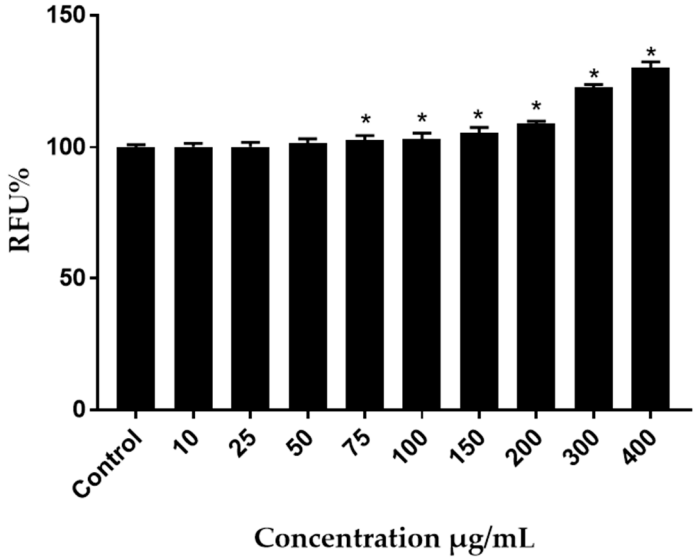


Figure 1. Effects of the *Cetraria islandica* extract on normal human foreskin fibroblasts cells' viability after 24 h exposure. The results are presented as relative mean values ± standard deviations, where the negative control (Control) is 100%. Significant differences in comparison with the negative control (ANOVA + Dunn's; $p < 0.05$) are marked with *. RFU, relative florescence units.

3.1.2. Antibacterial Activity

In this study, the antibacterial activity of *Cetraria islandica* extract against three bacterial strains: *Escherichia coli*, *Staphylococcus aureus* and *Enterococcus faecalis* (Table 2) was investigated. Even these microorganisms are considered less common in the oral microbiota, recent studied suggest their presence in the oral cavity more often than expected [12,13]. The antibacterial activity was investigated by direct contact between the plant extract and the culture medium. After the end of the incubation period, at 37 °C, the inhibition zones (mm) were determined for the tested bacterial strains. It was observed that the results from the tested samples varied in the size of the diameter of the inhibition zone, depending on the microbial strain tested.

Table 2. The diameter of inhibition zones (mm) for the tested plant extract.

Sample	*Escherichia coli*	*Staphylococcus aureus*	*Enterococcus faecalis*
	(mm)		
Cetraria islandica extract	0	7 ± 0.00	8.5 ± 0.70
Control	0	0	0

Following the antimicrobial test, it was noticed that *Cetraria islandica* extract had the best activity on *Enterococcus faecalis* strain, a slight lower activity on the Gram (+) strain (*Staphylococcus aureus*), while on *Escherichia coli* strains the extract did not exhibit bacterial inhibition. These results are in line with previously published studies where *Cetraria islandica* extract exhibited antibacterial activity against Gram (+) strains, but did not show antibacterial activity against Gram (−) strains tested in the study, including *Escherichia coli* [14].

3.2. Development and Evaluation of the Cetraria islandica Extract Mouthwash

Following a literature study on existing mouthwashes, active ingredients and natural extracts, some initial formulations were proposed. A complex composition was chosen for the mouthwash samples, which comprised both active ingredients and functional compounds that ensure product stability, acceptability and facilitate its use. *Cetraria*

isladica extract was chosen for its antioxidant, antimicrobial, anti-inflammatory activity [15–17]. Poloxamer 407 was chosen as it is a mild, nonionic surfactant, suitable for use in oral care products, that does not irritate the mucosa and membranes [18]. Sorbitol and mannitol were also added as cryoprotectants and structure agents for the freeze-dried product [19] and methylcellulose as matrix-forming agent [20]. Allantoin was previously used in oral care products for its healing, anti-irritant and repairing properties [21], while hyaluronic acid, a key element in the soft periodontal tissues, gingiva, and periodontal ligament can have an anti-inflammatory and tissue healing effect [22]. The flavoring agent was chosen to give a pleasant sensation to the consumer, during and after using the mouthwash and increase product acceptability.

The characterization follows the critical quality attributes of the products. The lyophilizates had to be easily extracted from the blister pockets, without material loss and had to withstand manipulation when reconstituted in water. Moreover, the obtained mouthwash should display appropriate rheology for a palatable product. Therefore, the characterization had to address every step of product use. As it is well known that products obtained by freeze-drying process are porous, with low crushing strength and highly brittle, texture analysis was selected as an adequate method to characterize the mechanical profile of the structures. The weight loss percent of the product was evaluated when extracted from the blister pocket and further, the reconstitution time was measured. Finally, the end product was tested for viscosity.

3.2.1. Experimental Design

In the complex composition of cosmetics, all the ingredients can exert an important impact on the characteristics of the final products. In this study, DoE was used as a strategy to assess the effects of the key ingredients on the quality attributes of the products. DoE allows knowledge and understanding not only of individual effects but can also show how the interaction between the compounds influences their characteristics. In the case of the freeze-dried mouthwashes, the filler needed to reinforce the structures could have an important influence on the mechanical profile, on the dissolution speed and the taste. Therefore, the type of filler (X1) was evaluated, with two options, mannitol and sorbitol. The first quantitative variable, the filler ratio (X2), varied between 3 and 7%. As a hydrophilic polymer is needed to ensure the three-dimensional structure and integrity of a freeze-dried product, methylcellulose ratio (X3) was chosen as a quantitative variable and varied between 0 and 0.5%. After the preparation and the complete characterization of the 11 formulations generated through DoE, the data analysis aimed at regression equations (model equations) for each of the responses as functions of the input variables X1, X2 and X3.

Several steps were taken to study the impact of variables on the results. The Modde software was used to perform data processing, then fitting the model, refining the coefficients of the results, and finally optimizing the input variables to reach an ideal formulation. Ten responses (Y1–Y10) were analyzed; the results of all the tests performed on the 11 formulations, that were used in the DoE analysis, are presented in Table 3.

Table 3. Values for DoE responses from the experimental analysis of the samples.

	Y1	Y2	Y3	Y4	Y5	Y6	Y7	Y8	Y9	Y10
	Rigidity at 2 mm (g)	Rigidity at 4 mm (g)	Load at target (g)	Fracturability (g)	1st Fracture work done (mJ)	1st Fracture deformation (mm)	Mean load (g)	Weight loss %	Reconstitution time	Viscosity (cP)
F1	703.50 ± 140.71	758.67 ± 118.31	1042.50 ± 207.03	738.83 ± 163.25	4.95 ± 2.02	1.44 ± 0.45	487.23 ± 86.40	5.78 ±1.35	46.00 ± 4.58	6.61 ± 0.11
F2	36.30 ± 22.60	262.50 ± 62.60	524.50 ± 190.00	151.17 ± 173.96	1.31 ± 1.81	1.79 ± 1.72	31.73 ± 11.47	39.58 ± 12.76	39.00 ± 5	6.31 ± 0.15
F3	1244.00 ± 49.39	1736.00 ± 35.77	2147.67 ± 167.61	1232.67 ± 109.58	9.63 ± 4.71	1.53 ± 0.37	868.57 ± 26.46	4.93 ± 0.35	51.00 ± 5	6.97 ± 0.09
F4	885.17 ± 161.82	1470.00 ± 223.34	2289.50 ± 389.54	716.00 ± 78.56	2.41 ± 0.65	0.76 ± 0.11	661.10 ± 118.05	48.73±9.50	31.00 ± 2.64	8.28 ± 0.03
F5	860.83 ± 208.11	1844.50 ± 196.44	3020.83 ± 443.61	2322.67 ± 1652.61	41.68 ± 35.45	3.57 ± 2.46	629.13 ± 146.88	3.61±1.27	95.00 ± 6.24	10.30 ± 0.10
F6	625.00 ± 28.70	1046.83 ± 94.40	1555.00 ± 202.21	1555.00 ± 202.21	34.99 ± 2.62	4.99 ± 0.01	409.77 ± 22.61	4.93±0.02	91.00 ± 3	11.53 ± 0.15
F7	997.50 ± 79.38	1831.33 ± 88.97	3634.00 ± 348.84	1839.50 ± 1567.23	26.47 ± 32.20	2.69 ± 2.02	710.83 ± 77.03	2.47±0.27	60.33 ± 8.62	10.33 ± 0.05
F8	1297.17 ± 253.33	1836.83 ± 333.32	3123.83 ± 852.02	1419.33 ± 238.16	8.50 ± 2.64	1.47 ± 0.29	868.73 ± 239.34	7.73±4.67	90.00 ± 4.58	8.57 ± 0.06
F9	1098.17 ± 229.28	1682.67 ± 282.89	2383.50 ± 483.05	1082.50 ± 295.28	8.91 ± 5.48	1.49 ± 0.42	770.27 ± 125.43	3.53±0.24	114.00 ± 3.60	8.94 ± 0.03
F10	1401.30 ± 198.56	2206.83 ± 121.00	3566.33 ± 201.66	1390.33 ± 166.97	13.79 ± 2.41	1.78 ± 0.14	963.90 ± 172.15	1.54±0.82	111.67 ± 3.51	10.47 ± 0.15
F11	1508.50 ± 87.72	2171.67 ± 147.07	3460.67 ± 407.48	1503.83 ± 183.35	12.00 ± 5.55	1.47 ± 0.44	1116.27 ± 97.59	3.48±0.58	103.00 ± 6.24	8.99 ± 0.01

Each of the responses (Y1–Y10) corresponding to a certain quality attribute was expressed mathematically as an equation that reveals its correlation to the formulation factors (X1–X3):

$$Y = b_0 + b_1X1 + b_2X2 + b_3X3 + + b_4X1^2 + b_5X2^2 + b_6X3^2 + b_7X1X2 + b_8X2X3 + b_9X1X3 + b_{10}X1X2X3 \quad (1)$$

where Y is the response, b0 is the mean response of the 11 formulations and b_i are the regression coefficients. X1–X3 represent the individual effects, X12–X32 are quadratic effects that indicate a non-linear correlation to the response, while X1X2, X3X2, X1X3, and X1X2X3 are interaction effects which show the variations of the responses when two or more factors are changed simultaneously [23].

3.2.2. Evaluation of the Quality of Fit

To check whether the regression equations fit the experimental results, several parameters were calculated (Table 4): R^2, the regression coefficient shows the fraction of the response variance explained by the model equation. The regression parameter R^2 had values over 0.9 for first fracture work, second fracture work, reconstitution time and over 0.8 for rigidity at 2 and 4 mm, fracturability, viscosity which shows a good fit of the data to the created model. For the load at target, mean load and the weight loss percentage, the R^2 values ranged between 0.6-0.8. Q^2 shows the quality of the prediction and had values between 0.5 and 0.7 for almost all responses, validating the predictive power of the model.

The ANOVA test completed the analysis to show if the variation of responses was determined by the input variables or it occurred by chance. A model is considered significant at a confidence level of 95%, therefore if $p < 0.05$. As shown in Table 3, the p-value was below 0.05 for all responses and indicated highly significant models and a non-significant lack of fit. The data analysis and fitting showed that all the selected independent variables (filler type and ratio and the MC ratio) had a significant influence on the responses.

Table 4. Statistical parameters for ANOVA test and quality of fit.

Parameter	Response	R^2	Q^2	*p*-Value	Lack of Fit	F-Value	Model Validity	Reproducibility
Rigidity 2mm	Y1	0.87	0.56	0.029	0.529	6.65	0.84	0.74
Rigidity 4mm	Y2	0.80	0.62	0.028	0.411	5.94	0.78	0.77
Load at target	Y3	0.79	0.65	0.009	0.677	8.62	0.90	0.61
Fracturability	Y4	0.94	0.72	0.001	0.721	24.43	0.92	0.86
1st fracture work	Y5	0.94	0.64	0.001	0.258	22.28	0.66	0.96
1st fracture deformation	Y6	0.90	0.69	0.004	0.171	13.77	0.56	0.96
Mean load	Y7	0.60	0.31	0.026	0.427	5.96	0.79	0.66
Weight loss percentage	Y8	0.92	0.79	0.002	0.730	13.64	0.92	0.80
Reconstitution time	Y9	0.94	0.73	0.005	0.167	15.06	0.55	0.96
Viscosity	Y10	0.80	0.49	0.027	0.360	6.03	0.74	0.80

R^2—Percent of the variation of the response explained by the model; Q^2—Percent of the variation of the response predicted by the model, F-value—The ratio of the group means and the mean within group variances; Model validity—Validity of the model; Reproducibility—Variation of the response under the identical conditions, compared to the total variation of the response.

The interpretation of the results relies on the coefficients of the regression equations displayed below as histograms. The way in which the studied factors influence the responses is shown by the + sign for positive influence and a-sign for a negative effect.

3.2.3. The Effect of the Formulation Factors on the Mechanical Profile of the Freeze-Dried Mouthwashes

Mechanical properties of freeze-dried products significantly impact their behavior during processing, packaging, transport, and use [24]. Texture analysis was chosen for mechanical characterization as a sensitive method that provides accurate results even for porous fragile structures [23]. During sample testing, the equipment records load vs. distance profiles out of which certain parameters can be determined (Figure 2).

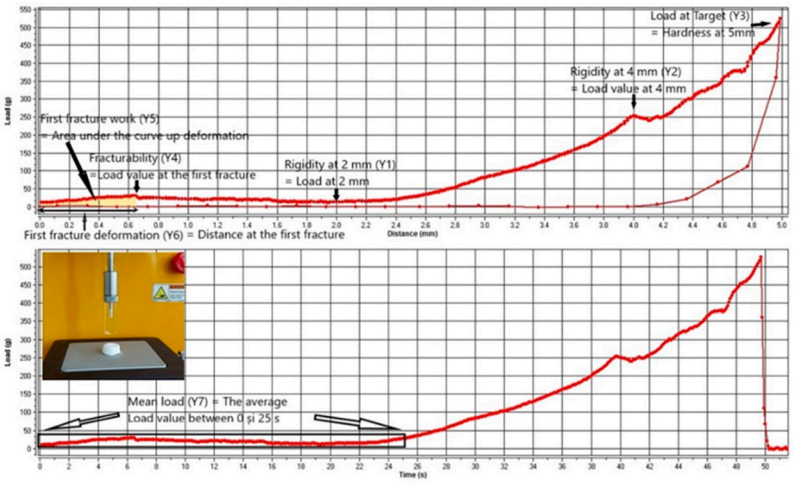


Figure 2. The determination of mechanical characterization responses out of the load vs. distance and load vs. time profiles generated by the texture analysis.

Rigidity values were measured at two distances, first at 2 mm (Y1) which ranged between 36.33–1508 g and second at 4 mm (Y2) with visibly higher results for each sample and values from 262.50 to 2171.67 g. These measurements indicate that the F2 sample with sorbitol and no polymer has the smallest rigidity, 36.33 g at 2 mm and 262.50 g at 4 mm, while some formulas with mannitol and MC display significantly higher values, such as F5 and F7-F11. These results are also supported by the regression coefficients histograms (Figure 3a,b) which show that the filler ratio is the most influential factor both on the rigidity at 2 mm and 4 mm; however, when measured at 4 mm, mannitol has a significant positive influence. In other words, the outer layer of the freeze-dried structure can be reinforced by increasing the amount of filler and for a rigid profound structure, the filler of choice should be mannitol.

Mannitol, a compound with the structure-forming ability [23] and sweetening properties, was selected as a bulking agent since it favors efficient freeze-drying and the attainment of elegant matrices [25]. It gave freeze-dried compacts with appropriate strength even without matrix-forming polymers and it showed superior mechanical properties when compared to trehalose, and lower when compared to maltodextrin [26].

Load at target (Y3) values were the lowest for F2 (524.50 g), F1 (1042.50 g), and F6 (1555.00 g), while the other formulations had values over 2000 g, with the highest for F7 sample (3634.00 g). The load at target corresponds to the hardness of the sample and corresponds to the resistance of all cumulated layers of product crushed under the texture probe. As expected, it was positively influenced by mannitol in high ratios and by high loads of MC (Figure 3c). Fracturability is an indirect measure of the brittleness of a product. It is recorded as the first load drop on the texture profile. For the fracturability measurements (Y4), the lowest value was obtained for F2 sample, 151.17 g, the most brittle product, compared to the highest one recorded of 2322.67 for F5. The increasing of the MC ratio (X3) conducted to increased resistance to fractures (Y4) (Figure 3d). As previous studies showed, the MC three-dimensional network constitutes the structure of the product that sustains the attached fillers. The presence of high amounts of polymers

reinforces the matrices and increases their elasticity [23], which explains the lower brittleness and the high fracturability values.

The other mechanical resistance parameters measured were the mechanical work needed for first fracture (Y5), which showed values within a high range from 1.31 mJ (F2) to 41.68 mJ (F5); the first fracture deformation (Y6), with F5 and F6 having the highest values of 3.57 mm and 4.99 mm; the mean load (Y7) with values of 31.73-1116.27 g, the lowest corresponding to F2 and the highest to F11.

As all the texture parameters, F2 was the weakest formulation, the most fragile, porous, and hard to handle, while F5 and F7 were just the opposite.

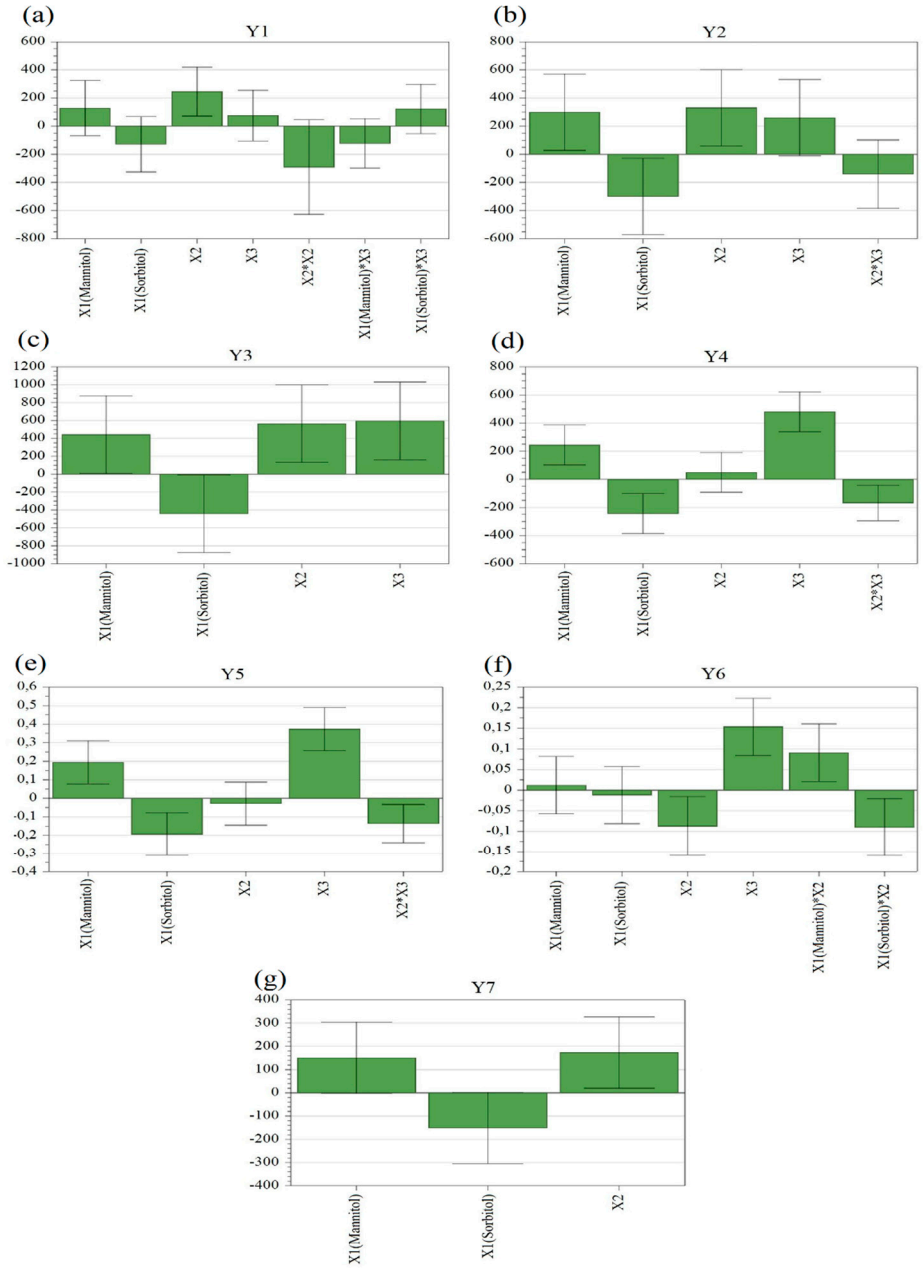


Figure 3. The influences of formulation factors (X1, X2, X3) on the mechanical characteristics of freeze-dried products: (**a**), rigidity at 2 mm (Y1); (**b**), rigidity at 4 mm (Y2), (**c**), load at target (Y3), (**d**), fracturability (Y4), (**e**), 1st fracture work (Y5), (**f**), 1st fracture deformation (Y6), (**g**), mean load (Y7).

3.2.4. The Effect of the Formulation Factors on the Weight loss Percentage (Y8) of the Freeze-Dried Mouthwashes

The weight loss percentage was calculated to evaluate the consequences of fragile structures on the manipulation and extraction from the blister pockets. It was meant to check if the entire product could be easily removed or a part of it remains stuck into the alveolae. The weight loss percentage (Y8) was strongly correlated to the mechanical profiles: the highest value was obtained for F2 and F4, formulations with small mechanical resistance, highly fragile samples, not appropriate for packaging and transporting. This behavior is upheld by the small fracturability values of the same formulas. In addition, the weight loss percentages for F7 and F10 were the lowest, in agreement with the fracturability values, which were the highest for these two samples. The filler type (X1) had considerable influence on Y8: the presence of sorbitol determined the embrittlement of the structures and loss of the integrity of the sample (Figure 4a). On the contrary, mannitol had a beneficial impact in maintaining the integrity of the matrices. As expected, the presence of MC in the formulations had a negative effect on the weight loss percentage (Y8), which could be due to the adhesive properties of hydrophilic polymers can contribute to preserving the porous structure and avoid material loss when manipulated.

3.2.5. The Effect of the Formulation Factors on the Reconstitution Time (Y9) of the Freeze-Dried Mouthwashes

Freeze-drying is considered an advantageous method to obtain porous structures which disintegrate rapidly [27]. As shown in Figure 5b, the most important effect on the reconstitution time came from X3, the hydrophilic polymer ratio.

Increasing the amount of MC (X3) led to the formation of dense structures with a slower penetration of the water into the lyophilizate network. It had a growing path along with increasing the filler and MC concentrations, with the highest values of 130.00-114.00 s for F9–F11, which were formulated with 5% filler and 0.25% MC, with one exception, the F7 that showed a small reconstitution time of only 60 s, even if it contains the highest concentrations chosen: 7% filler and 0.5% MC. The nonlinear effect with high magnitude shown on the histogram (Figure 4b) is more evident in the response surfaces of the reconstitution time displayed in Figure 5. The reconstitution time reaches a maximum inflection point at intermediate filler levels and high ratios of MC, while it decreases when large amounts of filler are associated with high ratios of MC. This effect was observed by other research groups and was explained by the presence of the easily soluble filler that promotes water absorption even in a structure with high loads of hydrophilic polymer [28].

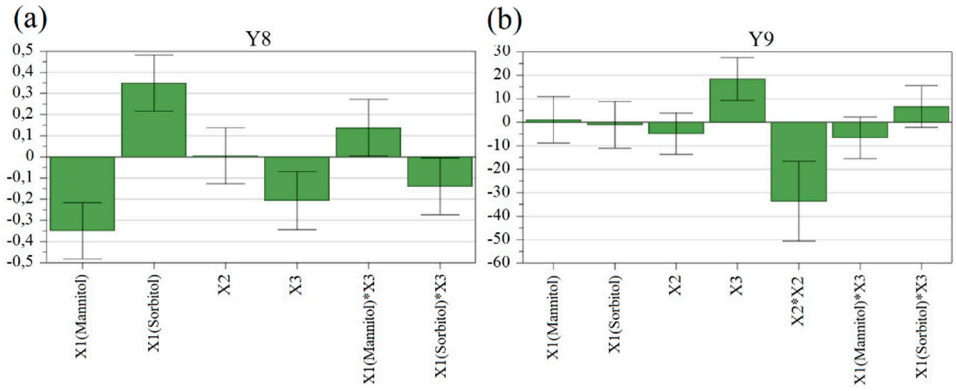


Figure 4. The influences of formulation factors (X1, X2, X3) on (**a**), weight loss percentage (Y8) and (**b**), reconstitution time (Y9).

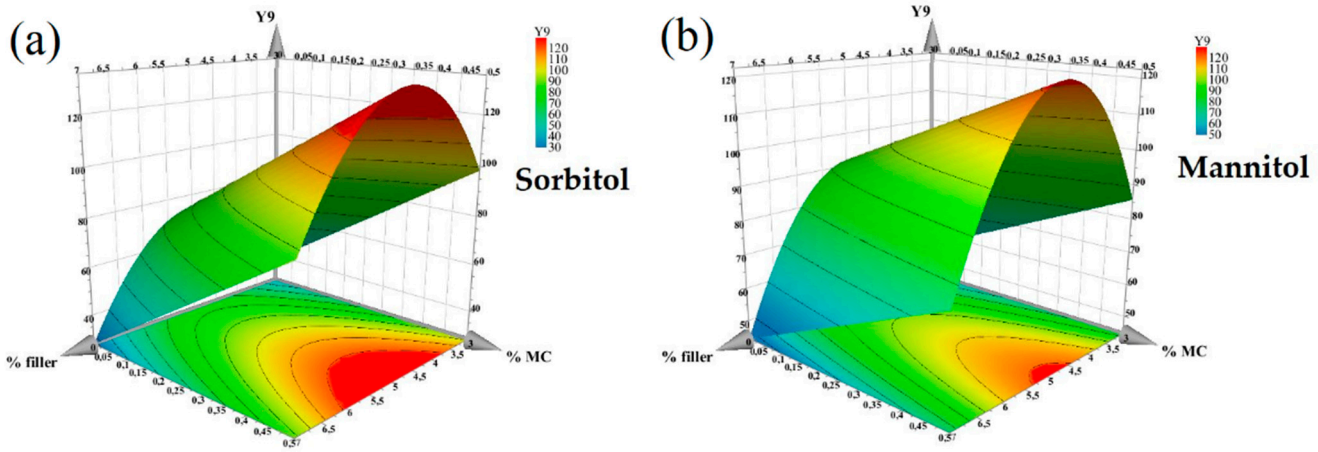


Figure 5. The influences of formulation factors (X1, X2, X3) on the reconstitution time when the filler is (**a**), sorbitol and (**b**), mannitol.

3.2.6. The Effect of the Formulation Factors on the Viscosity (Y10) of the Reconstituted Mouthwashes

For the viscosity of the reconstituted samples (Y10) the range of variation was not very wide. The MC ratio (X3), the viscosity modifying agent, was the only factor with a significant influence on the viscosity values (Y10) (Figure 6). The higher the MC ratio, the higher the viscosity. The lowest values (6.31–8.28 cP) corresponded to the first four formulations with no MC added (F1–F4).

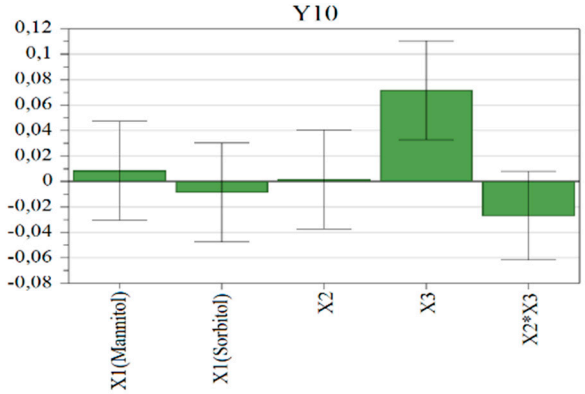


Figure 6. The influences of formulation factors (X1, X2, X3) on the viscosity of the reconstituted mouthwash (Y10).

3.2.7. Optimization of the *Cetraria islandica* Mouthwash Formulation

To obtain an optimal formula in terms of the desired lyophilized characteristics, an optimization process was performed. For that, a set of constraints was applied to the developed models of certain responses and only the formulations that fulfill those conditions with a certain degree of probability were considered. The conditions envisaged the maximization of fracturability, minimization of weight loss percentage, minimization of reconstitution time and maximization of viscosity. Such a formulation would ensure easy manipulation, with no material loss when extracted from the package, fast reconstitution, and a pleasant mouthfeel with good adherence to the oral cavity surface. The composition of the optimal formula generated by the software is presented in Table 5.

Table 5. The quantitative and qualitative composition of the optimal mouthwash formulation.

Factor	Value	Ingredient	Quantity (*w*/*v*%)
Filler Type (X1)	Mannitol	**Mannitol**	**7.00**
% filler (X2)	7	Poloxamer 407	5.00
% MC (X3)	0.5	**Methylcellulose**	**0.50**
	⇨	Allantoin	5.00
		Hyaluronic acid	0.125
		Cetraria islandica extract	5.00
		Flavoring agent	0.50

The bold data underlines the factors from the DoE.

For the next step, we prepared the sample according to the generated formula, freeze-dried it, and then analyzed it as the other samples before. The experimental values were collected using Modde software and, in the end, the predicted values were compared to the experimental ones, as residual values. As shown in Table 6, the values obtained experimentally were close to the values predicted by the software. Therefore, the experimental design showed high reliability and may be used in further studies regarding freeze-dried mouthwashes. This is an innovative product, with no correspondents on the market to be compared with. However, among pharmaceutical products, the oral lyophilizates are quite similar in terms of the production process, product characteristics and use. Literature reports give a hardness minimum limit of 4N for oral lyophilizates and a disintegration time of maximum 180 s, which are both in accordance with the developed freeze-dried mouthwash.

Table 6. Predictions for the optimal formula and experimental results.

Response	Predicted Value (Mean ± σ)	Experimental Value (Mean ± σ)	Residual
Fracturability (g)	1826.85	1951 ± 123	+124.15
Weight loss (%)	2.59	2.39 ± 0.91	−0.20
Reconstitution time (s)	74.71	80 ± 6.56	+5.29
Viscosity (cP)	9.84	8.42 ± 0.28	−1.42

σ = standard deviation.

Up to this point, the study demonstrated that freeze-dried mouthwashes with appropriate characteristics in both solid state and as reconstituted solutions are feasible and that the DoE strategy enabled the optimization of products. *Cetraria islandica* extract was successfully incorporated for its mentioned applications such as mouth and throat anti-irritant, antimicrobial, or moisturizing and soothing effects [29]. Besides the previously described roles of *Cetraria islandica* extracts, recent studies reported the ability of its polysaccharides to induce keratinocyte differentiation with important implications in wound healing [30]. Our results revealed the lack of toxicity of extracts and an antibacterial activity on *S. aureus* and *E. faecalis* which supported the hypothesis of oral care product preparation. As freeze-drying is a state-of-the-art method to dry or concentrate extracts without altering their biological properties, and its use was reported for lichen species, we assumed that the lyophilized mouthwash formulations would preserve the effects of extracts [16]. Future studies envisage the biological evaluation of freeze-dried formulations and in vivo studies in healthy volunteers.

4. Conclusions

The current work describes the application of the QbD approach in the development of freeze-dried mouthwashes. To obtain an optimal formulation of freeze-dried mouthwash, both qualitative and quantitative factors that may impact the main characteristics of the final product were investigated. A full factorial design with three factors and two levels was conceived and eleven mouthwash samples were prepared and

analyzed. The results revealed the positive influence of mannitol and methylcellulose to reinforce the structure of matrices and the positive effect of methylcellulose in preserving the integrity of the samples and avoiding material loss when manipulated. Finally, an optimal formula was generated and characterized showing the good predictive capacity of the statistical model. Although the freeze-dried mouthwash formulations with *Cetraria islandica* extract were not yet tested for their in vitro or in vivo efficacy, data regarding freeze-drying process leads to optimistic assumptions. This study offers the methodology for the preparation and optimization of solid mouthwashes loaded with herbal extracts, which could contribute to the development of a whole new area of the oral care industry that addresses the needs of consumers looking for stable, eco-friendly, light weight, easily transportable products.

Author Contributions: Conceptualization, C.B., S.M.I. and A.P.; methodology, C.B., S.M.I., D.-R.A., A.P., I.F. and R.C.; software, C.B., S.M.I., D.-R.A., A.P. and I.F.; validation, C.B., S.M.I., A.P., I.F. and M.A.; formal analysis, C.B., S.M.I., D.-R.A., A.P. and I.F.; writing—original, D.-R.A., S.M.I., C.B., A.P. and R.C.; writing—review and editing, D.-R.A., S.M.I., C.B., A.P., I.F., M.L.M., F.L. and M.A. All authors have read and agreed to the published version of the manuscript.

Funding: This research received no external funding.

Data Availability Statement: The data presented in this study are available on request from the corresponding author.

Conflicts of Interest: The author Diana Adespei is an employee of MDPI, however, she does not work for the journal Applied Sciences at the time of submission and publication.

References

1. Commission Implementing Regulation (EU). Directive 2019/904 and Implementing Regulation 2020/2151. Available online: https://eur-lex.europa.eu/eli/reg_impl/2020/2151 (accessed on 8 September 2021).
2. Gubitosa, J.; Rizzi, V.; Fini, P.; Cosma, P. Hair Care Cosmetics: From Traditional Shampoo to Solid Clay and Herbal Shampoo, A Review. *Cosmetics* **2019**, *6*, 13, doi:10.3390/cosmetics6010013.
3. Verri, W.A.; Vicentini, F.T.; Baracat, M.M.; Georgetti, S.R.; Cardoso, R.D.; Cunha, T.M.; Ferreira, S.H.; Cunha, F.Q.; Fonseca, M.J.; Casagrande, R. *Flavonoids as Anti-Inflammatory and Analgesic Drugs: Mechanisms of Action and Perspectives in the Development of Pharmaceutical Forms*; Elsevier: Amsterdam, The Netherlands, 2012; Volume 36, pp. 297–330; doi:10.1016/B978-0-444-53836-9.00026-8.
4. Luque García, J.L.; Luque de Castro, M.D. *Acceleration and Automation of Solid Sample Treatment*, 1st ed.; Elsevier: Amsterdam, The Netherlands, 2002.
5. Allemand, J.-L. G.; Masso, S.J.J.; Simonnet, A.M.C.; Vidal, S.C. Freeze-Dried Makeup Product, Corresponding Compositions and Method for Making Same. U.S. Patent Application No 11/910,368, 10 December 2009.
6. Committee on Herbal Medicinal Products (HMPC), Assessment Report on *Cetraria islandica* (L.) Acharius s.l., thallus. Available online: https://www.ema.europa.eu/en/documents/herbal-report/final-assessment-report-cetraria-islandica-l-acharius-sl-thallus-first-version_en.pdf (accessed on 8 September 2021).
7. Mittal, B. *How to Integrate Quality by Efficient Design (QbED) in Product Development*, 1st ed.; Academic Press: Cambridge, MA, USA, 2019.
8. Beg, S.; Rahman, M.; Iman, S.S.; Alruwaili, N.K.; Al Robaian, M.; Panda, S.K. *Pharmaceutical Drug Product Development and Process Optimization Effective Use of Quality by Design*; Apple Academic Press: Palm Bay, FL, USA, 2020.
9. Atlas, R.M. *Handbook of Microbiological Media*; CRC Press: Washington, DC, USA, 2010.
10. Carpa, R.; Dragan-Bularda, M.; Muntean, V. *Microbiologie Generala-Lucrari Practice*; Presa Universitara Clujeana: Cluj-Napoca, Romania, 2014; pp. 56–82.
11. Ögmundsdóttir, H.M.; Zoëga, G.M.; Gissurarson, S.R.; Ingolfsdottir, K. Anti-proliferative Effects of Lichen-derived Inhibitors of 5-Lipoxygenase on Malignant Cell-lines and Mitogen-stimulated Lymphocytes. *J. Pharm. Pharmacol.* **2011**, *50*, 107–115, doi:10.1111/j.2042-7158.1998.tb03312.x.
12. Garbacz, K.; Jarzembowski, T.; Kwapisz, E.; Daca, A.; Witkowski, J. Do the oral Staphylococcus aureus strains from denture wearers have a greater pathogenicity potential? *J. Oral Microbiol*. **2018**, *11*, 1536193, doi:10.1080/20002297.2018.1536193).
13. Komiyama, E.Y.; Lepesqueur, L.S.; Yassuda, C.G.; Samaranayake, L.P.; Parahitiyawa, N.B.; Balducci, I. Koga-Ito CY. Enterococcus Species in the Oral Cavity: Prevalence, Virulence Factors and Antimicrobial Susceptibility. *PLoS ONE* **2016**, *11*, e0163001, doi:10.1371/journal.pone.0163001.
14. Dülger, B.; Gücin, F.; Aslan, A. Antimicrobial Activity of the Lichen *Cetraria islandica* (L.) Ach. *Turk. J. Biol.* **1998**, *22*, 111–118.
15. Patriche, S.; Ghinea, I.O.; Adam, G.; Gurau, G.; Furdui, B.; Dinica, R.M.; Rebegea, L.-F.; Lupoae, M. Characterization of Bioactive Compounds from Romanian *Cetraria islandica* (L) Ach. *Rev. Chim.* **2019**, *70*, 2186–2191, doi:10.37358/rc.19.6.7302.

16. Freysdottir, J.; Omarsdottir, S.; Ingolfsdottir, K.; Vikingsson, A.; Olafsdottir, E. In vitro and in vivo immunomodulating effects of traditionally prepared extract and purified compounds from *Cetraria islandica*. *Int. Immunopharmacol.* **2008**, *8*, 423–430, doi:10.1016/j.intimp.2007.11.007.
17. Grujičić, D.; Stošić, I.; Kosanic, M.; Stanojkovic, T.; Ranković, B.; Milošević-Djordjević, O. Evaluation of in vitro antioxidant, antimicrobial, genotoxic and anticancer activities of lichen *Cetraria islandica*. *Cytotechnology* **2014**, *66*, 803–813, doi:10.1007/s10616-013-9629-4.
18. Dumortier, G.; Grossiord, J.L.; Agnely, F.; Chaumeil, J.C. A Review of Poloxamer 407 Pharmaceutical and Pharmacological Characteristics. *Pharm. Res.* **2006**, *23*, 2709–2728, doi:10.1007/s11095-006-9104-4.
19. Lee, M.K.; Kim, M.Y.; Kim, S.; Lee, J. Cryoprotectants for freeze drying of drug nano-suspensions: Effect of freezing rate. *J. Pharm. Sci.* **2009**, *98*, 4808–4817, doi:10.1002/jps.21786.
20. Kanlayavattanakul, M.; Lourith, N. *Biopolysaccharides for Skin Hydrating Cosmetics*; Springer: New York, NY, USA, 2015; pp. 1867–1892.
21. *International Cosmetic Ingredient Dictionary and Handbook*, 12th ed.; The Personal Care Products Council: Washington, DC, USA, 2008.
22. Dahiya, P.; Kamal, R. Hyaluronic acid: A boon in periodontal therapy. *N. Am. J. Med Sci.* **2013**, *5*, 309–315, doi:10.4103/1947-2714.112473.
23. Iurian, S.; Tomuta, I.; Bogdan, C.; Rus, L.; Tokes, T.; Barbu-Tudoran, L.; Achim, M.; Moldovan, M.L.; Leucuta, S. Defining the design space for freeze-dried orodispersible tablets with meloxicam. *Drug Dev. Ind. Pharm.* **2016**, *42*, 1977–1989, doi:10.1080/03639045.2016.1188108.
24. Thapa, P.; Jeong, S.H. Effects of Formulation and Process Variables on Gastroretentive Floating Tablets with A High-Dose Soluble Drug and Experimental Design Approach. *Pharmaceutics* **2018**, *10*, 161, doi:10.3390/pharmaceutics10030161.
25. Kumar, K.N.; Mallik, S.; Sarkar, K. Role of freeze-drying in the presence of mannitol on the echogenicity of echogenic liposomes. *J. Acoust. Soc. Am.* **2017**, *142*, 3670–3676, doi:10.1121/1.5017607.
26. Suciu, Ș.; Iurian, S.; Bogdan, C.; Rus, L.; Porav, A.S.; Borodi, G.; Tomuță, I. Design of experiments approach to assess the impact of API particle size on freeze-dried bulking agents. *Farmacia* **2021**, *69*, 279–289, doi:10.31925/farmacia.2021.2.13.
27. Jones, R.J.; Rajabi-Siahboomi, A.; Levina, M.; Perrie, Y.; Mohammed, A.R. The Influence of Formulation and Manufacturing Process Parameters on the Characteristics of Lyophilized Orally Disintegrating Tablets. *Pharmaceutics* **2011**, *3*, 440–457, doi:10.3390/pharmaceutics3030440.
28. Casian, T.; Iurian, S.; Bogdan, C.; Rus, L.; Moldovan, M.L.; Tomuta, I. QbD for pediatric oral lyophilisates development: Risk assessment followed by screening and optimization. *Drug Dev. Ind. Pharm.* **2017**, *43*, 1932–1944, doi:10.1080/03639045.2017.1350702.
29. Zhao, Y.; Wang, M.; Xu, B. A comprehensive review on secondary metabolites and health-promoting effects of edible lichen. *J. Funct. Foods* **2021**, *80*, 104283.
30. Zacharski, D.M.; Esch, S.; Konig, S.; Mormann, M.; Brandt, S.; Ulrich-Merzenich, G.; Hensel, A. B-1.3/1.4-Glucan lichenan from *Cetraria islandica* (L.)) ACH. Induces cellular differentiation of human keratinocytes. *Fitoterapia* **2018**, *129*, 226–236.

pharmaceutics

MDPI

Review

Vesicular Nanocarriers for Phytocompounds in Wound Care: Preparation and Characterization

Diana Antonia Safta, Cătălina Bogdan * and Mirela Liliana Moldovan

Department of Dermopharmacy and Cosmetics, Faculty of Pharmacy, "Iuliu Haţieganu" University of Medicine and Pharmacy, 12 I. Creanga Street, 400010 Cluj-Napoca, Romania; diana.an.safta@elearn.umfcluj.ro (D.A.S.); mmoldovan@umfcluj.ro (M.L.M.)

* Correspondence: catalina.bogdan@umfcluj.ro

Abstract: The need to develop wound healing preparations is a pressing challenge given the limitations of the current treatment and the rising prevalence of impaired healing wounds. Although herbal extracts have been used for many years to treat skin disorders, due to their wound healing, anti-inflammatory, antimicrobial, and antioxidant effects, their efficacy can be questionable because of their poor bioavailability and stability issues. Nanotechnology offers an opportunity to revolutionize wound healing therapies by including herbal compounds in nanosystems. Particularly, vesicular nanosystems exhibit beneficial properties, such as biocompatibility, targeted and sustained delivery capacity, and increased phytocompounds' bioavailability and protection, conferring them a great potential for future applications in wound care. This review summarizes the beneficial effects of phytocompounds in wound healing and emphasizes the advantages of their entrapment in vesicular nanosystems. Different types of lipid nanocarriers are presented (liposomes, niosomes, transferosomes, ethosomes, cubosomes, and their derivates' systems), highlighting their applications as carriers for phytocompounds in wound care, with the presentation of the state-of-art in this field. The methods of preparation, characterization, and evaluation are also described, underlining the properties that ensure good in vitro and in vivo performance. Finally, future directions of topical systems in which vesicle-bearing herbal extracts or phytocompounds can be incorporated are pointed out, as their development is emerging as a promising strategy.

Keywords: herbal extracts; phytocompounds; lipid vesicles; vesicular nanosystems; nanotechnology; wound healing; vesicles' preparation; vesicles' characterization

Citation: Safta, D.A.; Bogdan, C.; Moldovan, M.L. Vesicular Nanocarriers for Phytocompounds in Wound Care: Preparation and Characterization. *Pharmaceutics* **2022**, *14*, 991. https://doi.org/10.3390/pharmaceutics14050991

Academic Editors: Lenuţa Maria Şuta and Claudia Geanina Watz

Received: 7 April 2022
Accepted: 1 May 2022
Published: 5 May 2022

Publisher's Note: MDPI stays neutral with regard to jurisdictional claims in published maps and institutional affiliations.

Copyright: © 2022 by the authors. Licensee MDPI, Basel, Switzerland. This article is an open access article distributed under the terms and conditions of the Creative Commons Attribution (CC BY) license (https://creativecommons.org/licenses/by/4.0/).

1. Introduction

Wound healing is a complex process with great importance as healthy skin is a key to the maintenance of body homeostasis. The increasing prevalence of acute, surgical, and chronic wounds is expected to raise the global costs of wound care, up to USD 18.7 billion by 2027, and an increasing percentage of the health sector budget is assigned to chronic wound care. Expensive treatments, wound chronicity, and poor healing leading to long-term hospitalization represent the substantial challenges of actual wound-care products. There is a growing need for wound management products to control complex wounds, in the context of the increase of the aging population and the growing prevalence of diseases and conditions affecting the wound healing process, such as diabetes and obesity. Additionally, wound infection represents a major obstacle in the healing process, and the widespread bacterial resistance may contribute to increasing the rate of acute and chronic wounds. It is considered that 25% of diabetic patients will develop foot ulcers during their lifetime and about 60% of these patients will develop infections and subsequent complications [1,2]. Scleroderma skin ulcers, a consequence of systemic sclerosis, represent another category of skin lesions for which local therapy, such as chronic wound care, is critical [3,4].

The conventional strategies do not fully cover the large variety of wounds and the growing need for healing products. The significant costs for healthcare systems and the insufficient control of complex wounds underline the limited effectiveness of the current approaches. Although remarkable progress in wound healing research was recorded in the last one hundred years, gaps in wound research still exist [5]. Therefore, the development of new topical systems for the treatment of wounds and healing without scars or other complications is an intensely studied field nowadays.

Currently, research in wound healing is focusing on the development of vesicular systems with enhanced delivery performances [6]. Particularly, in the past years, special efforts have been made in the development of new, safe, green, scalable, and affordable delivery systems capable of transforming traditional herbal medicines into effective health-promoting products [7].

Herbal extracts (HEs) and phytocompounds (PCs) are the subject of considerable interest for their complex beneficial effects on skin health, such as regenerative, anti-inflammatory, antioxidant, and antimicrobial effects. During the last decade, among other versatile agents studied for wound healing, the plant-derived ingredients, also called phytodrugs, have attracted great attention because they are safe, easily available, and affordable [8–11]. Despite their beneficial effects in wound healing, their bioavailability is reduced because of poor membrane permeability and instability issues. Therefore, novel drug-delivery strategies including the incorporation of these PCs into delivery systems such as vesicular nanosystems (VNs) have been developed to overcome these limitations [12]. To date, a considerable number of studies have been conducted to develop different types of vesicles, such as liposomes, niosomes, ethosomes, transferosomes, cubosomes, and their derivates, but also to optimize the characteristics of these lipid vesicles.

In the context of the increasing rate of acute and chronic wounds, this topic is more relevant than ever. The development of novel delivery platforms based on PCs requires a deep knowledge of the current evidence. Thus, the current review article intends to support the scientists to find updated information by gathering recent relevant research undertaken so far in this field and contributes to a thorough understanding of the materials' selection and preparation method. The advances in the field are discussed, emphasizing the advantages of the entrapment of HEs and PCs in different types of lipid nanovesicles for the treatment of wounds, together with their methods of preparation and characterization. The main features concerning the use of PCs in wound care, but also the challenges associated with the incorporation of vesicular carriers into wound dressings, are discussed.

2. Presentation of the Cellular and Molecular Mechanisms of Wound Healing

The skin is the largest organ of the body and fulfills essential roles such as protection, thermoregulation, aesthetics, and sensory perception. Therefore, the integrity and functionality of the skin are critical. If the tissue suffers a lesion of various etiologies, the dynamic and complex physiological healing process is triggered [13]. It involves four successive and partially overlapping stages: hemostasis, the inflammatory phase, the proliferative phase, or granulation and maturation, also called remodeling. During these stages, numerous changes and interactions take place between the cells and the mediators at the wound site, leading to the healing of the tissue, with the restoration of the integrity and functions of the skin [5,14,15].

The first stage of healing, hemostasis, aims to stop the bleeding caused by tissue damage, with vasoconstriction, platelet aggregation, and fibrin clot formation, which lead to cessation of bleeding by coagulation cascade. Further, blood vessels dilate to allow essential cells to reach the site of the injury. Platelets activate and degranulate, releasing platelet-derived growth factor (PDGF), transforming growth factor beta (TGF-β), transforming growth factor alpha (TGF-α), basic fibroblast growth factor (bFGF), insulin-like growth factor-1 (IGF-1), and vascular endothelial growth factor (VEGF). Following the cytokines' release, neutrophils and monocytes-macrophages are recruited to initiate the

inflammatory response. They prevent the infection, cleanse the wound of debris, and release soluble mediators such as proinflammatory cytokines (interleukins: IL-1, IL-6, IL-8, and tumor necrosis factor alpha: TNF-α) and growth factors (such as PDGF, TGF-β, TGF-α, IGF-1, and FGF) that are involved in the recruitment and activation of fibroblasts and epithelial cells, making the transition to the next phase in healing. The proliferative phase consists of the granulation tissue formation, epithelialization by means of epidermal growth factor (EGF), keratinocyte growth factor (KGF), and TGF-α, followed by fibroblast migration and extracellular matrix production by synthesis of collagen, elastin, proteoglycans in fibroblasts (employing PDGF and TGF-β), angiogenesis (formation of new blood vessels by VEGF), and contraction, ending with wound closure. Maturation or remodeling of the lesion is the last stage of the healing process, during which structural reorganizations occur. Thus, type III collagen, initially synthesized at high levels, is replaced by type I collagen, the dominant fibrillar collagen in the skin. Maturation also implies the reduction in the number of capillaries, increase in tensile strength, and decrease in cell density and metabolic activity in the granulation tissue [5,14–17]. A summarization of the wound-healing process is presented in Figure 1.

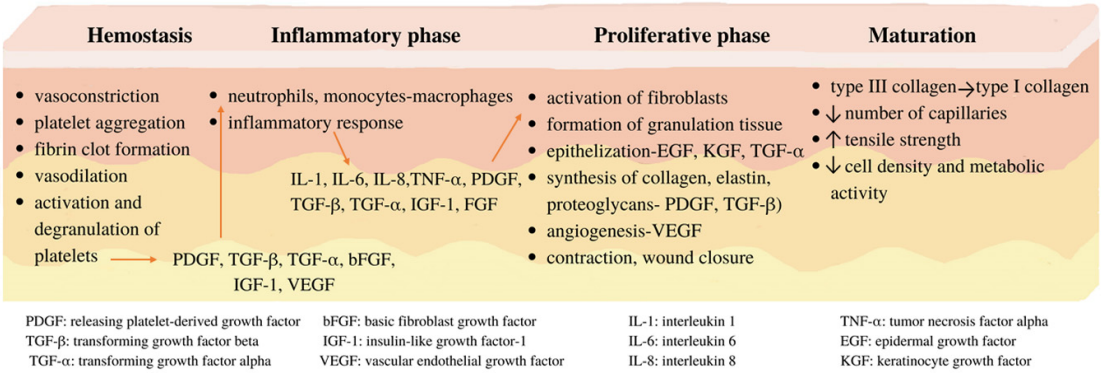


Figure 1. The main stages of the wound-healing process.

Often, the physiological healing process is not effective and fast enough, and therefore specific topical systems help patients to achieve optimal healing, by preventing infections and complications, and ensuring skin regeneration with minimal scarring [18]. The use of healing products is important, especially for chronic wounds, with poor healing, such as varicose veins, pressure ulcers or diabetic foot ulcers, bedsores, but also for healing acute wounds caused by abrasions, lacerations, cuts, surgery, or burns, which affect the patient's quality of life. They also predispose to complications, such as defective scarring, infections, and their extensions, which can even lead to bone infections, necrosis, amputations, etc. In addition, the high incidence of these diseases leads to increased costs in the medical system and the imperious need for efficient and economically advantageous products for the treatment of wounds [9]. Therefore, numerous studies related to the healing process are currently underway, with many of them aiming to understand the targets by which scarring agents can act. Elucidating the complex mechanisms of wound healing supports the development of products that improve this process, leading to rapid and effective wound healing.

3. The Role of the Phytocompounds in Wound Care

The importance of natural PCs in all health disorders is well-known. Some of the PCs stand out for their effectiveness in the treatment of wounds because they stimulate the growth factors involved in the process of healing, regulate collagen synthesis, and promote its deposition and the closure of the wound. Briefly, they can be wound-healing agents. Among them, *Aloe vera* [19] was intensely studied for its wound-healing

properties. The whole extract, rich in acemannan and β-sitosterol, can stimulate the expression of VEGF and potentiates the synthesis of nitric oxide (NO) by regulating NO synthase (NOS) activity [19]. Acemannan from *Aloe vera* is a polysaccharide able to increase fibroblast proliferation, the release of KGF-1 and VEGF, and the synthesis of type I collagen, being an important agent for tissue re-epithelization and angiogenesis [20]. Another well-known plant with wound healing properties is *Hypericum perforatum* [21,22], which enhances the migration of fibroblasts, collagen deposition, and by the action of hyperforin, PC, that is also antibacterial, increases the re-epithelization [21,22].

Plant-derived antioxidants may counteract the damaging effects of oxidative species in human tissues and can also accelerate the healing of wounds by regulating the redox environment [7,23]. It is well-known that skin lesions are usually associated with an important level of oxidative species [7]. Firstly, the reactive oxygen species (ROS) have a key role as mediators of intracellular signaling involved in the defense against the acquired pathogens in dermal injuries. On the other hand, excessive amounts of ROS are harmful because of the generation of free radicals and the oxidation of cellular components. Insufficient scavenging of the excessive amounts of ROS can affect the wound-healing process, resulting in delayed healing, an impaired or chronic wound, and even neoplastic transformation [23,24]. The topical application of compounds with free-radical scavenging and anti-inflammatory properties, such as quercetin, curcumin, and other polyphenols, has shown a significant improvement in wound healing and protection from oxidative damage [25]. Polyphenolic compounds can scavenge the ROS released during the inflammatory process, thus attenuating inflammation, and also having antioxidant and anti-inflammatory properties [26,27].

An important biological property of HEs, which is relevant in wound care, is represented by the anti-inflammatory effect. In this sense, terpenoids have strong antioxidant and anti-inflammatory as well as antimicrobial properties. However, the pharmaceutical applications of terpenoids remain challenging due to their poor water solubility and high volatility [28]. The aqueous extract of *Moringa oleifera* [29] was also found to reduce the levels of inflammatory markers in macrophages, including induced nitric oxide synthase (iNOS), TNF-α, and IL-1β [29]. Another PC with an anti-inflammatory effect is glycyrrhizin, from *Glycyrrhiza glabra* [30] extract, which inhibits inflammatory events, such as edema, apoptosis, iNOS expression, and NF-kB [30]. A less-studied PC with beneficial effects in wound healing, as an anti-inflammatory and antibacterial agent, is usnic acid, extracted from different lichens species [31]. According to a study conducted by Zhang et al., application of the sodium salt of usnic acid triggered the complete re-epithelialization, formation of well-organized bands of collagen, and epidermal keratinization. These effects are due to its capacity to decrease the inflammatory cells and to increase fibroblast proliferation, granulation tissue, and vascular regeneration by increasing VEGF levels [32].

Another important property of HEs or PCs used in the treatment of wounds is represented by the antibacterial activity. They should be active on the bacteria most commonly found in wound infections, such as aerobic bacteria—*Staphylococcus aureus* and resistant strains (e.g., MRSA: methicillin-resistant *Staphylococcus aureus*), some species of *Enterococcus* (the most abundant in diabetic wounds, in immune-compromised patients and abdominal surgeries), facultatively anaerobic bacteria, such as *Escherichia coli* and *Proteus mirabilis* frequently met in chronic wounds, as well as anaerobes, such as *Pseudomonas aeruginosa* (commonly isolated from wounds following surgeries and burns) [33]. Another risk factor for poor wound healing may be the infection with fungal species, of which *Candida* spp. can most often colonize burn wounds [34,35]. In this regard, essential oils from *Thymus* sp., *Citrus* sp., or terpenes isolated from oils are known for their antibacterial activity on strains involved in skin infection [36,37].

Recent studies are reported to elucidate the wound healing mechanisms of PCs. Although they have been used empirically for centuries in the treatment of various affections, including skin disorders, lately, relevant research has been undertaken to validate their

biological activity. Furthermore, their entrapment into topical systems to ensure the best effect is challenging [8,9,38,39]. The main beneficial effects of HEs in wound healing are presented in Figure 2.

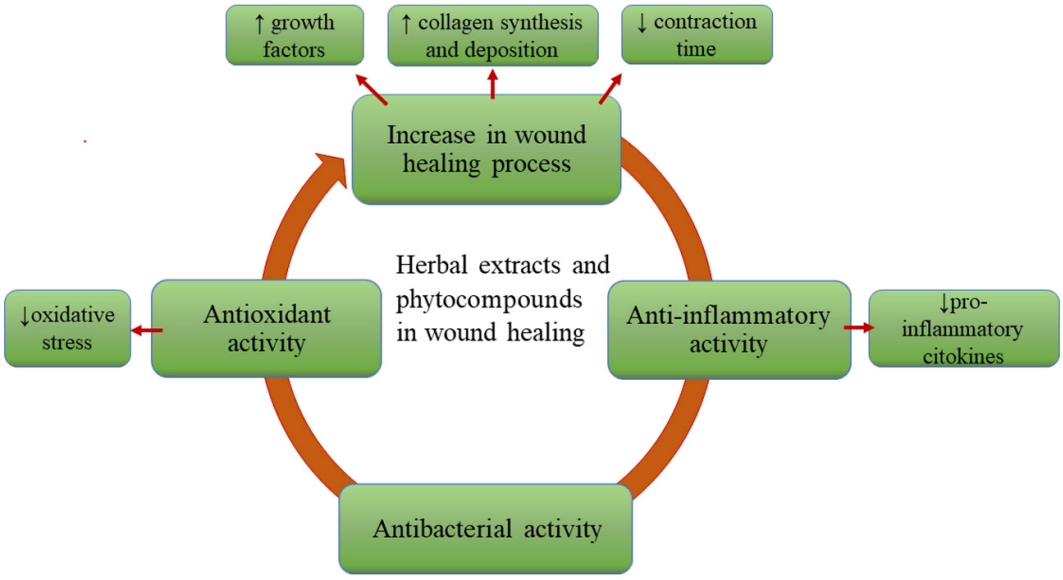


Figure 2. The main beneficial effects of herbal extracts and phytocompounds in wound care.

4. The Entrapment of Herbal Extracts into Vesicular Nanosystems—Challenges in the Formulation

A modern approach for improving the efficacy of phytocompounds at the skin level is represented by their incorporation into nanocarriers [40]. Among the high number of nanocarriers, phospholipid vesicles represent one of the most valuable and versatile systems, especially for skin delivery, owing to their structure, biocompatibility, and similarity to skin components [7,41]. Moreover, VNs have multiple advantages of enhancing the stability of loaded substances, preventing physical and chemical degradation induced by light, air, acid, and alkali, increasing the bioavailability of PCs, and improving their penetration across the skin. These advantages are ascribed to their size, elasticity, and lipid content, which facilitate the interaction with the skin layers. Moreover, phospholipid vesicles are biocompatible and non-toxic nanosystems, being able to incorporate and deliver PC molecules at the desired site of action [42–44]. The improvement of the effectiveness of molecules entrapped into phospholipid vesicles and accumulation into deep skin layers when applied topically is demonstrated by many studies. So far, the results provided by the experimental research revealed that each HE or PC requires a specific ad hoc tailored phospholipid vesicle formulation to maximize its efficacy [45,46].

To be effective in wound healing, the PCs must penetrate the skin to a significant extent. The absorption into the skin of topically applied molecules, including PCs, is governed by their partition coefficient, a function of their lipophilicity. Among the routes of skin penetration, the transepidermal route is important in this case. Hydrophilic molecules can pass through the transcellular route as an aqueous hydrophilic pathway, through the cytoplasm of keratinocytes and phospholipidic membranes. Although this is the shortest route, it encounters significant permeation resistance because the molecules must pass via the lipophilic membrane of each cell, being subjected to multiple partitioning and diffusion steps. Active molecules can also pass through the continuous lipid matrix and the small spaces between cells, via the intercellular pathway. Large molecules, such as PCs, are physically bound within the lipids for passing through the skin via an intercellular route, being known as the suitable absorption route for most penetrants [47].

The transfollicular route has also recently been identified as a significant penetration pathway. Nanoparticles, in particular, have a higher intrafollicular penetration rate and can be used to target specific cell populations within the hair follicle [48]. Liposomes penetrate as an intracellular delivery system and deposit the entrapped substances in the stratum corneum, having low drug penetration into the dermis. To release the medication into the dermis, transferosomes squeeze through the intercellular sections of the corneous layer or penetrate through the transfollicular pathway. Ethosomes use fluidization to permeate lipids in the stratum corneum, then release the actives into the dermis through transfollicular or intercellular routes [16]. Moreover, a few studies have assessed absorption through damaged human skin in vitro, showing a modest but clear increase in absorption compared to intact skin, more favorable for hydrophilic molecules [49].

A major impediment in percutaneous absorption is represented by the polar chemical groups from the structure of actives of herbal origin, such as hydroxyl substitutes and glycosides. Besides this, the natural compounds have large molecular weight and poor membrane permeability [44]. Most of the biologically active PCs, mainly the flavonoids, phenolics, and glycosidic aglycones, have limited bioavailability in the cellular media [50]. To solve this problem, the encapsulation in VNs seems to bring benefits, because in this way, the drug penetration into cell membranes is facilitated, increasing the permeability of active substances and topical therapeutic effectiveness [21,29]. The choice of the topical system has a decisive role concerning the penetration into the epidermis and maintenance of the therapeutic concentration in the skin tissue for a determined period [44,48]. It has been reported that liposomal formulations provide sufficient penetration of these molecules to the target tissue while minimizing systemic side effects and prolonging local therapeutic action. Additionally, the VNs are considered promising delivery systems due to the ability of the phospholipidic structure to mimic the structural component of the mammalian cell membrane. Thus, the active compounds can passively penetrate the lipophilic membrane without causing cell damage [21,29].

Another major obstacle in the utilization of phenolic antioxidant compounds is represented by their poor stability. Therefore, they are prone to degradation by the influence of various factors, such as high oxygen levels or alkaline pH. These compounds can be entrapped into a carrier system to protect them against degradation and oxidation, to increase the stability of these molecules during storage, and to maintain their antioxidant activity, important for the healing of the wound. Due to the presence of phospholipidic vesicle membranes, the reaction between oxygen and polyphenols is limited. Additionally, due to the slow release from the carrier system of the entrapped polyphenols, their degradation is less important in comparison to free polyphenols [51].

Essential oils, which are known for their antibacterial activity, can be effective in infected wound healing, but they have low stability due to their volatility [36]. Likewise, the essential oils' encapsulation in nanosystems can reduce their volatility and chemical instability, without changing their chemical ingredients, and can increase their safety. By encapsulation, the antimicrobial activity could be improved, while preserving or even increasing their clinical effectiveness. This is mainly due to the subcellular size of the VNs, which could strengthen the passive absorption mechanism and reduce the transport resistance of the substances [52,53].

Among the lipid-based entrapment technologies, liposomes have been the most successfully applied systems due to their numerous advantages, including the use of natural raw materials, the ability to entrap PCs with different solubilities, and the prevention of ingredient oxidation by free radicals, metal ions, and enzymes [51]. The property of liposomes to improve the cutaneous delivery of molecules with various molecular sizes is well-known. Recently, they have been successfully proposed for the skin delivery of PCs due to the increased loading efficiency and carrier abilities, as well as the affinity for different skin layers [36]. Therefore, phyto-phospholipidic complex formulations are exhaustively explored [21,29]. Figure 3 summarizes the main advantages of the entrapment

of PCs in VNs and highlights the overcoming of the bioavailability issues through the encapsulation in phospholipid vesicles.

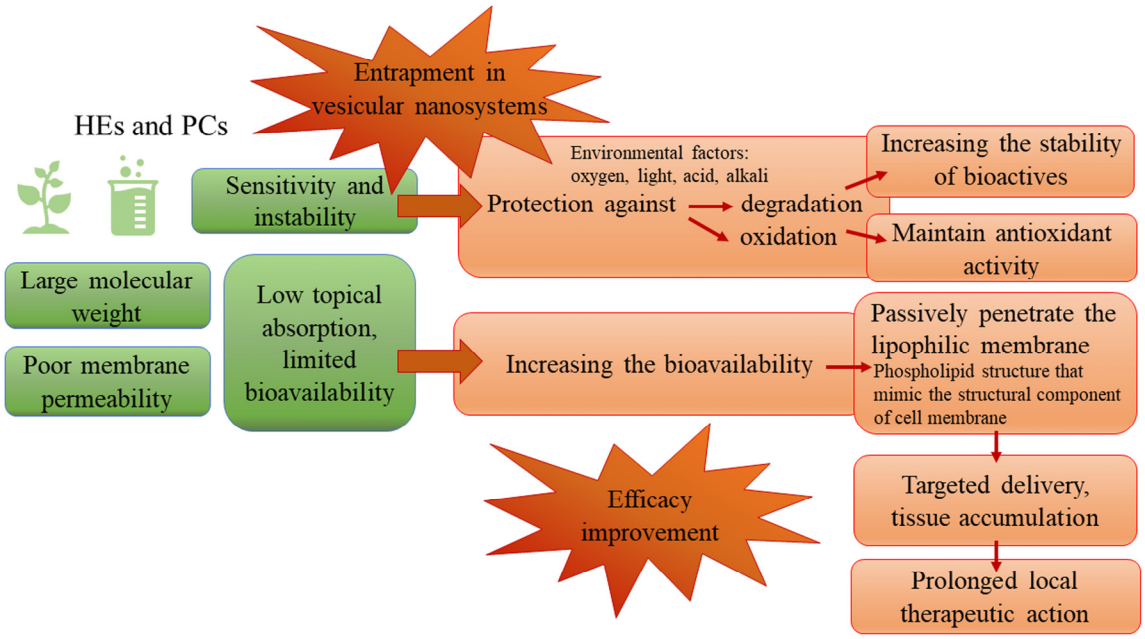


Figure 3. Advantages of herbal extracts' entrapment into vesicular nanosystems.

Besides the advantages of using vesicular nanosystems for wound care, the evaluation of safety for human health and the environment is very important in the development of nanomaterials. Thus, when evaluating novel topical herbal nanoformulations, a thorough assessment of safety is essential, taking into account issues such as toxicity, which can be attributed to either the nanosystem components or the herbal drug itself [54]. To this aim, a suitable characterization of the nanosystems should be performed [55]. Taking into consideration that in general the components of vesicular nanocarriers of HEs and PCs are biocompatible, environmental safety should not be a concern. Even after topical application, besides poor dermal penetration which limits their potential toxic effects, there is a probability of nanoparticles attaining systemic circulation, where they may interact unexpectedly with immune system cells or produce free radicals [54,55]. Thus, toxicity testing of products is necessary to ensure their safety [56].

5. Types of Vesicular Nanosystems

5.1. Liposomes

Liposomes are considered one of the most versatile nanocarrier systems [36], represented by colloidal systems, usually consisting of a central aqueous compartment (or more) surrounded by one or more concentric phospholipid bilayers, produced by self-assembly [51,57]. Hydrophilic substances can be encapsulated in the interior aqueous compartment, lipophilic drugs within lipid bilayers, and amphiphilic molecules can also be included in vesicles at the lipid/water interface. Liposomes are intensively studied and well-recognized as pharmaceutical carriers for the reduction of toxicity of encapsulated substances and efficacy enhancement, being able to provide and enhance the passage of active compounds in the skin due to the similarity to cell membrane structure [57,58]. They are biocompatible, biodegradable, non-immunogenic, and non-toxic systems widely studied for topical applications [57,58], recognized as the safest and most suitable nanosystems for application in human patients with high compatibility due to the membrane composition, phospholipids, and cholesterol, identical to cells' components [59].

Studies have shown that the antioxidant and immunomodulatory properties of lecithin liposomes might be effective in the improvement of wound healing as well as dermal drug-delivery systems. A study conducted by Nasab et al. compared the antioxidative and wound-healing effects of egg lecithin and soy lecithin liposomes, highlighting the increasing rate of radical scavenging activity of the liposomal lecithins. Wound-healing assessments showed a significant effect in the treatment with topical lecithin liposomes and better outcomes in the excision wound model of egg-lecithin in comparison to phenytoin 1% cream [23]. However, the incorporation of poorly water-soluble drugs in lipid bilayers is often limited, and the hydrophobic molecules can be rapidly released from the lipid bilayers. This may limit the potential application of liposome carriers in the case of hydrophobic molecules [57]. In addition, traditional liposomes have a limited penetration ability, since they cannot penetrate the stratum corneum and can only deliver drugs to the surface of the skin, without achieving the effect of deep penetration [60,61]. Another disadvantage of traditional liposomes is the peculiar rigidity of the lipid bilayer, which limits their application as topical drugs. On the contrary, ethosomes, and transferosomes, newer liposomal systems, are characterized by adequate deformability, which allows the interaction with skin structures and passage through the stratum corneum [62]. A comparative study between curcumin liposomes and nanoplexes, a novel drug nanoparticle complex with the oppositely charged polyelectrolyte, showed that curcumin liposomes were more efficient for scar treatment and exhibited faster in vivo wound healing than nanoplexes [59].

Though the structural membrane components, lipids, are biocompatible, their long-term stability is limited [21]. Taking this into consideration, novel carriers, namely polymersomes or hybrid lipid/polymer vesicles, have been developed. In this way, the inherent advantages of their components, such as the biocompatibility of lipids and the mechanical stability, were combined with the chemical versatility of copolymers [63,64]. These vesicles are composed of amphiphilic block copolymers, including polydimethylsiloxane, polybutadiene, and polyisobutylene, which are extensively investigated [65]. In comparison to liposomes, polymersomes exhibit superior stability, but insufficient permeability, which may hamper the release of the encapsulated substances. To solve this problem, many methods, such as the design of stimuli-responsive polymersomes, the introduction of channel proteins within bilayers, and the post-modification of bilayer membranes, have been proposed to regulate their permeability [63,64]. Stimulus-controlled drug delivery from polymersomes has been demonstrated as well, using triggers such as pH or temperature changes [65]. The interest of the scientific community in these polymeric vesicles has risen, but the research on this topic is still in its early stages. Regarding the topical systems for wound healing, only a few studies describe the development of polymersomes, such as antibacterial polymersome-based wound dressing spray with cysteine [66], polymersomes with nitric oxide for corneal wound healing [64], and polymersomes with trophic factors [65].

Invasomes are liposomes composed of unsaturated phospholipids, such as phosphatidylcholine, small amounts of ethanol, one or more different terpenes, and water. In addition to biological activity due to the antimicrobial, anti-inflammatory, and strong antioxidant properties, terpenoids can also serve as permeation enhancers for transdermal delivery and bioavailability enhancers [28]. Recent research shows that terpenes may enhance skin permeation through disruption of the stratum corneum lipids, interacting with intracellular proteins, and improving the distribution of the drug into the stratum corneum. Ethanol also improves the ability of the vesicles to penetrate the stratum corneum and provides a net negative surface charge, preventing vesicle aggregation due to electrostatic repulsion. Thus, it is underlined that invasomes enhance percutaneous penetration compared to conventional liposomes, due to a synergistic effect between terpenes and ethanol, showing promising results in increasing the bioavailability of terpenoid-based drugs, that can be further applied for treating severe bacterial infections [28].

An example of the skin application of invasomes is the entrapment of dapsone intended for the treatment of acne [67].

The study conducted by Castangia et al. described the development of new liposome-derived vesicles called santosomes**,** formulated using *Santolina insularis* essential oil [60], phosphatidylcholine, and propylene glycol. Santosomes were loaded with phycocyanin, a natural phycobiliprotein of blue-green algae with wound-healing properties. The essential oil of *Santolina insularis* played a double role in modifying the bilayer structure and, on the other hand, in improving the delivery of the loaded drug due to a synergistic effect of the terpenes and phospholipids [60].

Phytosomes or herbosomes are vesicular systems obtained through the interaction between hydrophilic parts of the phospholipids and the phyto-active components, resulting in the formation of hydrogen bonds between them [19,29,68]. Phytosomes are considered a type of liposomal formulation, also called phyto-phospholipid complexes. The structural difference between phytosomes and liposomes is that phytosomes entrap the vegetal active ingredient as a part of the phospholipidic membrane itself, bound in their structure, while liposomes have their active ingredient inside the hydrophilic cavity or within the layers of membranes. More specifically, the synthesis of phytosomes is based on the stoichiometric reaction between phosphatidylcholine (polar heads of phospholipids, e.g., positive ammonium and negative phosphate groups) and polyphenolic constituents or standardized extracts (flavonoids, tannins, terpenoids, xanthones) in an aprotic solvent. Of all the phytocompounds, only those having an active hydrogen atom (e.g., -COOH, -OH, -NH_2, -NH), such as polyphenols, can be integrated into a phytosome structure by forming hydrogen bonds between the herbal derivatives and the hydrophilic parts of amphiphilic molecules [69].

The main beneficial properties of phytosomes include high carrier loading capacity of substances, stability, ease of storage in a solid ready-to-reconstruct state, small size, and biocompatibility, making them suitable carriers for highly water-soluble drugs [19]. Other advantages are represented by the increase of the absorption rate of lipid insoluble phytomaterials, leading to more stable formulations within the formation of chemical bonds but also to an improved therapeutic benefit while decreasing the required dose for attaining the effect [70]. Alongside this, achieving a nano-sized phytosomal formulation or nanophytosome can further improve the bioavailability and distribution [19]. Since phytosomes exhibit a chemical bonding between phospholipid molecules and PCs, they are known for their improved stability [71].

A phytosomal formulation with *Aloe vera* and L-carnosine extract intended for type II diabetes mellitus-associated microvascular complications with an impaired angiogenesis background was developed by Darvishi et al., revealing a wound-healing effect of the formulation [19]. AuNP (gold nanoparticle) phytosomes with *Calendula officinalis* [70] extract have been prepared and characterized by Demir et al., with antioxidant and wound-healing effects of the product being reported [70]. Another phytosomal formulation with wound-healing effects was developed by Lim et al., by entrapment of *Moringa oleifera* extract [29].

Glycerosomes represent a novel type of modified liposomes containing glycerol, as a penetration enhancer. These vesicles are exploited to deliver PCs, such as extracts or oils, leading to an enhanced skin bioavailability of the encapsulated PCs , in comparison to the classical liposomes [37,45]. It is emphasized that glycerosomes can promote the accumulation of PC molecules in the different skin layers, mainly because of the moisturizing effect of glycerol, which may modify the ordered structure of the stratum corneum and favor the passage of the active substances [45]. Glycerosomes can be prepared by replacing a certain amount of water included in the composition of liposomes with glycerol [26].

There are several studies in which HEs or the phytocomponents were included in glycerosomes or derivate vesicles for the treatment of wounds. In a study undertaken by Allaw et al., glycerosomes including *Hypericum scruglii* [45] extract were modified through the addition of maltodextrin (glucidex) and a polymer (gelatin or hyaluronan) to obtain

gluglycerosomes and gel-gluglycerosomes. The study aimed to improve the performance of the vesicles by increasing the stability and the viscosity of the dispersions and by enhancing their ability to deliver the payloads to the wound site [45]. In another study conducted by Manconi et al., gly-hyalurosomes with *Citrus limon* var. *pompia* [26] extract have been developed by adding sodium hyaluronate to liposomes and glycerosomes, to prevent the oxidative damage and death of both keratinocytes and fibroblasts and to promote their viability [26]. Similarly, glycerosomes were used to entrap *Thymus capitatus* [37] oil, targeting the treatment of oral cavity diseases and *Rosmarinus officinalis* [51] extract to enhance the stability of the antioxidant polyphenols.

Penetration enhancer-containing vesicles (PEVs) were developed using polyethylene glycol, for the enhancement of skin penetration of *Thymus* essential oil in oral cavity wounds [37]. The incorporation of activators such as ethanol and propylene glycol into the liposomes, as safe and nontoxic agents, is acceptable in pharmaceutical and drug formulations [72].

Glycethosomes are a subtype of liposomes (even a subtype of glycerosomes) developed by hydrating phospholipids with a mixture of water, glycerol, and ethanol. Glycerol is added due to its moisturizing and cosolvent properties and ethanol as a penetration enhancer, both helping the active substance pass through the skin. In a recent study, mangiferin glycethosomes have been developed for the adjuvant treatment of psoriasis. The results underlined their superior ability to promote the healing of an experimental wound induced by 12-O-tetradecanoylphorbol-13-acetate, confirming their potential application for the treatment of psoriasis or other skin disorders [46].

Hyalurosomes have shown a higher mechanical resistance than liposomes due to the sodium hyaluronate network, which stiffens the phospholipid vesicles. This ensures an increased residence time of the formulation at the site of action, avoiding drug leakage [73]. As regards the application in wound healing, previous studies reported the successful entrapment of *Glycyrrhiza glabra* [73] extract and *Citrus limon* var. *pompia* [26] extract in hyalurosomes and the development of curcumin gel-core hyalurosomes [74].

Marinosomes, or marine lipid-based liposomes, contain a high ratio of polyunsaturated fatty acids, omega-6, or omega-3. Among their main advantages, they influence membrane fluidity and have the ability to reduce oxidative stress, inflammation, and abnormal cell proliferation [75].

Sphingosomes, also called sphingomyelin liposomes, represent another VN composed of sphingolipids [76]. The natural sources of sphingolipids, mainly sphingomyelin, are mammal milk, egg yolk, and the brain. Sphingomyelin molecules are the most abundant sphingolipids also found in biological membranes, where they have structural functions and preferentially interact with cholesterol to form ordered domains called lipid rafts [77]. Sphingomyelin, a primary component of biomembranes, hydrolyzes and generates ceramides, effective in skin moisturization. Thus, sphingomyelin-based liposomes proved to increase the ceramide II level in a three-dimensional cultured human skin model [78].

The main characteristics of these liposome-derived vesicles are summarized in Figure 4.

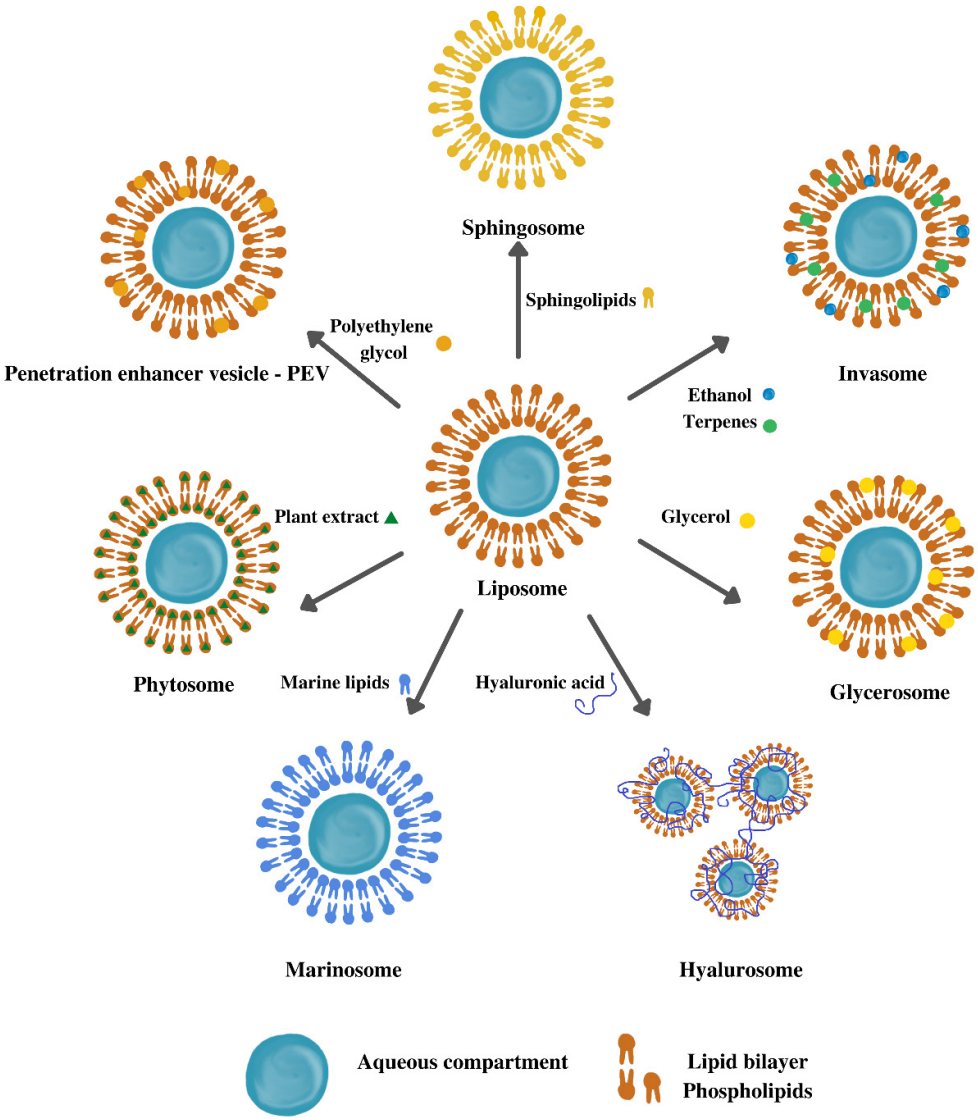


Figure 4. The main liposome derivates carriers.

To the best of our knowledge, several VNs, such as invasomes, marinosomes, and sphingosomes, bearing HEs or PCs have not been reported yet for wound-care applications. However, they have great potential to be studied in this regard.

5.2. Ethosomes

Ethosomes are vesicular multilamellar nanosystems, representing the third generation of elastic lipid carriers, that have a good ability to encapsulate drugs or HEs with different solubilities. These vesicles are composed of lipids, usually phosphatidylcholine, high concentrations of short-chain alcohols, in general between 20% and 50% ethanol, isopropyl alcohol, or propylene glycol up to 15%, cholesterol, and water. Ethanol, well-known as a permeation enhancer, confers softness, malleability, and ultra-deformability to the vesicle. Ethosomes have a smaller particle size as ethanol confers a negatively charged surface to the ethosomal vesicular system, good entrapment efficiency, and higher stability than traditional liposomes. Ethosomes are suitable for drug solubilization and improve skin delivery. The "ethanol effect" consists of its interspersion in the intercellular lipids, and changes within the dense alignment of the cell lipid layer, enhancing

the lipid fluidity and decreasing the structural density of the lipid multilayer. Afterward, the "ethosomes effect" occurs, by the opening of new pathways due to the malleability and fusion of these nanovesicles with skin lipids, enhancing the inter-lipid penetration and permeation. Thus, the result consists of the deposition and release of PCs into the deep layers of intact or damaged skin, revealing the potential of ethosomes in wound-healing applications [11,12,42,61,79–82].

In wound-healing applications, ethosomes encapsulating *Fraxinus angustifolia* [27] extract, PCs such as curcumin [80], or drugs such as piroxicam [79] have been previously reported. Currently, ethosomes are primarily used for efficient topical delivery into deep layers of the skin or across the skin for both local and systemic delivery [11,12,42,61,79–82].

By the addition of surfactants in ethosomes, a novel type of carriers has been obtained, the transethosomes, which are considered the second generation of ethosomes or a subtype of transferosomes. They have been developed by combining ethanol and a surfactant, employed as an edge activator to improve the deformability of vesicles. The characteristics of transethosomes are the increased flexibility and the major transdermal potential [41,82,83] even though some authors reported negative effects on human skin, such as inflammation induced by these surfactant-based nanocarriers [59].

5.3. Niosomes

Niosomes are novel drug-delivery systems, also called non-ionic surfactant vesicles, that might entrap lipophilic drugs into vesicular bilayer membranes and hydrophilic drugs in the aqueous compartments. Therefore, the niosomes can encapsulate both lipophilic and hydrophilic PCs [21,39,84]. Niosomal carriers protect the therapeutic agent and improve its stability since the encapsulated drug is stored in a semi-biological environment with a longer shelf-life [39]. Niosomes are composed of non-ionic surfactants, such as Span™ 60, instead of phospholipids, being obtained by self-assembling non-ionic surfactants and cholesterol [50,85]. Thus, they allow the controlled delivery of active compounds and better penetration than other preparations commonly used nowadays, such as transdermal drug-delivery systems [21]. In comparison with liposomes, niosomes are known as cost-effective preparations with superior chemical and storage stability [50]. The experiments conducted by Priprem et al. evaluated a topical niosomal gel with anthocyanin complex extract, showing the enhancement of the topical delivery of the PCs. This formulation exhibited an anti-inflammatory effect and promoted oral wound closure in rats [85]. Niosomes encapsulating HEs (*Hypericum perforatum* [19], *Calendula officinalis* [47]) or propolis extract have been reported with promising results in wound-healing applications [21,39,50].

5.4. Transferosomes

Transferosomes are ultra-deformable phospholipid vesicles, being more elastic and deformable than conventional liposomes, due to the presence of an edge activator, usually a surfactant or another molecule capable of modifying the assembly of the bilayer. Thus, they can be prepared by adding Tween 80 to phospholipid vesicles, leading to the increase of the bilayer fluidity and the ability of the vesicle to squeeze through the inter-corneocyte matrix, and finally increasing the active substance deposition into deeper skin layers. In a recent study, *Myrciaria jaboticaba* [30] extract was successfully entrapped into transferosomes designed for the treatment of skin wounds and oxidative stress-related skin disorders [30].

5.5. Cubosomes

Cubosomes, or cubic-phase nanoparticles, have great potential as an alternative to the conventional lipid vesicles, liposomes. These hydrophilic surfactant systems could self-assemble as a bi-continuous cubic liquid crystalline phase [86,87]. Liquid crystalline

nanoparticles are dispersions of liquid crystalline phases into a solvent, usually water, used in excess. Thus, cubosomes are liquid crystalline nanoparticles with the same unique properties of the bulk cubic phase but with a lower viscosity of the cubosome dispersion. The most investigated cubosomes are composed of binary systems of water and glyceryl monooleate. Since glyceryl monooleate is prone to lipolysis, the cubic phase is biodegradable [87–89].

Cubosomal systems are biocompatible, bio-adhesive, and biodegradable three-dimensional nanostructures with hydrophilic and hydrophobic domains, distinguished by their viscous nature, large surface area, and high ability to incorporate hydrophilic, lipophilic, and amphiphilic drugs. Concerning the applications of these vesicular systems, Thakkar et al. developed a silver sulfadiazine-entrapped cubosomal hydrogel with *Aloe vera* for topical treatment of infected burns, showing a superior healing rate compared to the cubogel with silver sulfadiazine alone [88]. Encouraging results for burn wound care were obtained by Morsi et al., who described the entrapment of silver sulfadiazine in cubosomes. The experimental data have shown better patient compliance and excellent healing results, with fewer side effects, than a commercially available product [87]. The main types of vesicular nanosystems with potential applications in wound healing are presented in Figure 5.

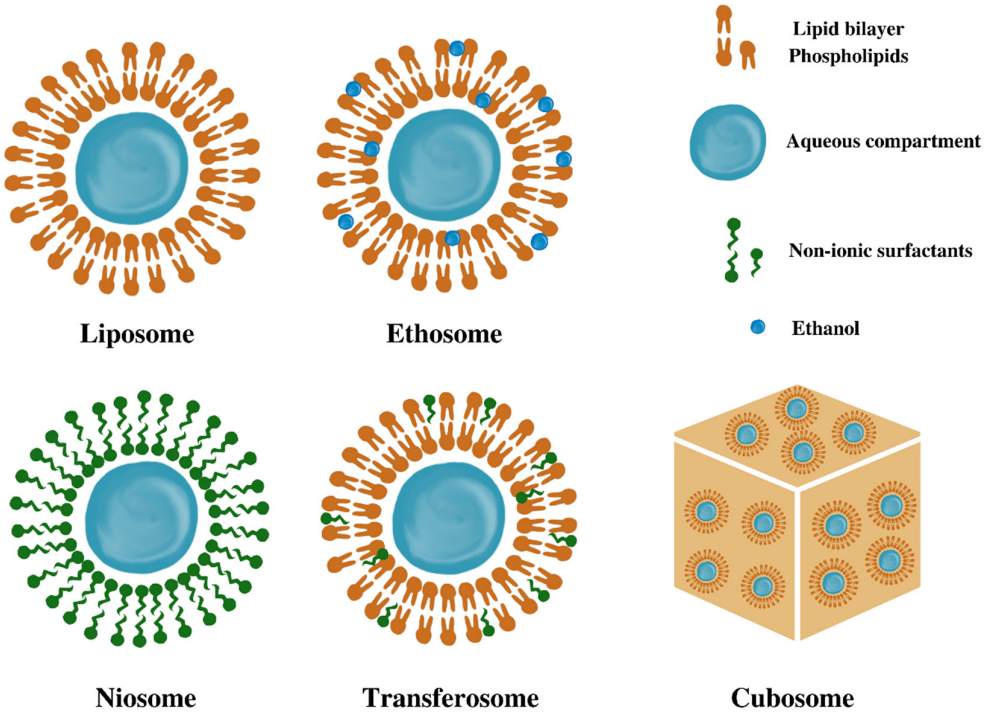


Figure 5. The main types of vesicular nanosystems with potential applications in wound healing.

Tables 1–4 summarize the studies investigating the development of VNs bearing HEs and PCs for wound healing.

Table 1. Vesicular nanosystems as carriers of herbal extracts with wound-healing effects.

Entrapped HEs	Method of Extraction	Active Compounds	Components of VNs	VNs' Preparation	Ref.
		Liposomes			
Carpobrotus edulis powder extract	Fresh leaves homogenized in distilled water, frozen, and lyophilized	Flavonoids	Hydrogenated phosphatidylcholine, cholesterol	Dry thin-film method	[90]
Pistacia lentiscus oil	Marketed product	Fatty acids, phenolic compounds [a]	Soy lecithin	Hydration, sonication	[40]
Aloe vera leaf gel extract	Fresh gel homogenized, frozen, defrosted, centrifugated	Glycoproteins, aloesin	Soy lecithin	Bangham method, mechanochemical method	[91]
Angelica sinensis and *Astragali radix* ratio 1:5	Decoction	Ferulic acid coupled with astragaloside IV	Soy phosphatidylcholine, cholesterol	Thin-film dispersion, ultrasonic method	[92]
Salvia aramiensis aerial part extract	Methanol, ethanol extraction in shaking bath, water extraction-infusion	n.a.	Dipalmitoylphosphatidylcholine, cholesterol	Dry thin-film hydration	[58]
		Liposomes and hyalurosomes			
Azadirachta indica oil (Neem oil)	Marketed product	Glycerides, fatty acids, sulfur-containing compounds, flavonoids [b]	Soy lecithin, argan oil, sodium hyaluronate	Direct sonication	[93]
Glycyrrhiza glabra root extract	Percolation in ethanol	Glycyrrhizin-triterpenoid saponin glycoside, polyphenols	Soy phosphatidylcholine, Phospholipon 90G, Sodium hyaluronate LMW	Hydration, sonication	[73]
		Niosomes			
Calendula officinalis flowers and leaves extract	Methanol extraction	Steroids, terpenoids, triterpenoids, phenolic acids, flavonoids, carotenes	Tween 60, cholesterol	Dry film hydration, sonication	[50]
Hypericum perforatum flowering tops	Ethanol extract, DIG–MAZ multifunctional extraction system	Hyperforin, hypericins, flavonoids	Span 20, 60, 80, cholesterol	Modified reverse phase evaporation	[21]
		Transferosomes			
Myrciaria jaboticaba fruits peel	Pressurized hot water extraction	Flavonoids, anthocyanins, ellagitannins	Lipoid S75, Tween 80, hydroxyethylcellulose, Sodium hyaluronate	Hydration, sonication	[30]
		Phytosomes			
Moringa oleifera leaves extract	Maceration, ultrasound-assisted extraction	Quercetin, kaempferol, chlorogenic acid, rosmarinic acid	L-α-lecithin, cholesterol, polysorbate 80	Thin-film hydration, sonication	[29]
		AuNP–phytosomes and liposomes			
Calendula officinalis flowers extract	Methanol for 6 h, at room temperature	Chlorogenic acid, quercetin	Egg phosphatidylcholine, cholesterol	Thin-film hydration, extrusion	[70]
		Ethosomes and PEVs			
Fraxinus angustifolia leaves and bark	Extraction in ethanol (1:4 *w*/*v*) under continuous stirring at room temperature, for 24 h.	Polyphenolic compounds [c]	Phospholipon50, Transcutol P, ethylene glycol triglycerides, fatty acids	Hydration, sonication	[27]

extract					
Glycerosomes, liposomes, gluglycerosomes, gel-gluglycerosomes, hyal-glulycerosomes					
Hypericum scruglii aerial parts extract	Marketed product	Naphthodianthrones [d], phloroglucinols [e], phenolic acids, flavonoids [f], xanthones, terpenes	Phospholipid S75, glycerol, dextrin, gelatin, hyaluronan	Hydration, sonication	[45]

Legend: [a] tocopherols, carotenoids, and anthocyanins; [b] quercetin, kaempferol, muricetine; [c] quercetin, catechin, rutin, tannic acid; [d] hypericin, pseudohypericin; [e] hyperforin, adhyperforin; [f] hyperoside, rutin, quercitrin. LMW—low molecular weight; n.a.—data not available; PEVs—penetration enhancer-containing vesicles; HE—herbal extract; PC—phytocompound.

Table 2. Vesicular nanosystems as carriers for phytocompounds with wound-healing effects.

Entrapped PC	Source of PCs	Components of VNs	VNs' Preparation	Ref.
Liposomes				
Bromelain extract	*Ananas comosus*	Egg phosphatidylcholine, cholesterol	Thin-film hydration	[94]
Madecassoside	*Centella asiatica*	Egg yolk lecithin, cholesterol	Thin-film hydration	[44]
Curcumin	*Curcuma longa*	Lecithin, cholesterol, propylene glycol	Hydration, sonication	[72]
Quercetin	Various species	Phosphatidylcholine, cholesterol	Thin-film hydration, sonication	[95]
Curcumin	*Curcuma longa*	Phospholipon 90G, oligochitosan (used for coating liposomes)	Thin-film hydration, sonication	[59]
Usnic acid	Lichens-*Cladonia substellata*	Phosphatidylcholine (Lipoid GMBH 75%)	Thin-film hydration	[31]
Nano-liposol				
Astaxanthin	Yeast, algae, and other aquatic species	L-α-phosphatidylcholine from soybean	Modified emulsion evaporation method	[96]
Liposomal locked-in dendrimers				
Shikonin	Species of genera *Alkanna*, *Lithospermum*, *Echium*, *Onosma*, *Anchusa*	Egg phosphatidylcholine	Thin-film hydration	[97]
Santosomes				
Phycocianin	Blue-green algae	*Santolina insularis* essential oil, hydrogenated phosphatidylcholine, propylene glycol	Hydration, sonication	[60]
Liposomes and PEVs				
Quercetin	Fruits, vegetables [a]	Lipoid S75, PEG 400	Hydration, sonication	[98]
Quercetin and curcumin	Various species	Lipoid S75, octyl-decyl polyglucoside, PEG 400	Hydration, sonication	[25]
PEVs				
Oryzanol and alpha-bisabolol	Oryzanol-rice bran oil and alpha bisabolol-Chamomile essential oil	Phospholipid (Epikuron 200), penetration enhancers (labrasol, transcutol)	Thin-film hydration	[99]

Phytosomes				
Sinigrin	Brassicaceae family	L-α-phosphatidylcholine hydrogenated (soybean)	Thin-film hydration	[71]
Ethosomes				
Curcumin	*Curcuma longa*	Egg lechitin, cholesterol	Ethanol injection, sonication	[80]
Hyalurosomes				
Curcumin	*Curcuma longa*	Enriched soy phosphatidylcholine (Phospholipon 90G)	Hydration, sonication	[100]
Gel-core hyaluosomes				
Curcumin	*Curcuma longa*	Lipoid S100, Hyaluronic acid, Tween 80, Poloxamer 407	Thin film evaporation, extrusion	[74]
ULs				
Asiaticoside	*Centella asiatica*	Fully saturated pure lecithin, saturated/unsaturated lecithins (Phospholipon 100G), sodium cholate	Thin-film hydration	[101]
Transferosomes, glycoltransferosomes				
Mangiferin	Various plants: mango leaves, fruits, by-products (e.g., peel, kernel seed)	Soy lecithin, glycerol, propylene glycol, Tween 80, mucin	Mangiferin dispersed in hydrating blend [b] sonicated, added in phospholipid and Tween 80, sonicated	[41]
Collagen-enriched transferosomes, glycerosomes, and glytransferosomes				
Oleuropein	Olive oil	Lipoid S75, collagen, Tween 80	Direct sonication	[7]

Legend: [a] apples, berries, onions; [b] water, glycerol, propylene glycol. PEVs—penetration enhancer-containing vesicles; ULs—ultra-deformable liposomes; HE—herbal extract; PC—phytocompound.

Table 3. Vesicular nanosystems including herbal extracts with potential benefits in the treatment of wounds.

Entrapped HEs	Active Compounds	Effect of HEs	Method of Extraction	Components of VNs	VNs' Preparation	Ref.
Liposomes						
Salvia triloba and *Rosmarinus officinalis* essential oils	Eucalyptol and camphor	Antioxidant, anti-inflammatory, antibacterial	Marketed product	Phospholipon 90G, cholesterol	Dry thin-film hydration	[102]
Citrus limon var. *pompia* essential oil or raw citral	Terpenes-citral	Antibacterial activity	Citral/ essential oil-steam distillation	Lipoid S75	Hydration, sonication	[36]
Cinnamon oil	Essential oil	Antimicrobial effect	Marketed product	Soy lecithin and cholesterol	Thin-film hydration	[52]
Glycerosomes						

Rosmarinus officinalis leaves extract	Polyphenolic compounds [a]	Antioxidant, antimicrobial	24 h stirring at room temperature with 70% ethanol	Phosphatidylcholine, glycerol	Hydration of phospholipids -Mozafari method	[51]
Liposomes, glycerosomes, PEVs						
Thymus capitatus essential oil	Carvacrol	Antimicrobial effect	Extraction with circulatory Clevenger-type apparatus	Soy lecithin, water/glycerol, water/propylene glycol	Hydration, sonication, dialysis	[37]
Glycerosomes, hyalurosomes, gly-hyalurosomes						
Citrus limon var. *pompia* fruits	Flavones [b]	Anti-inflammatory, antioxidant	Sonication, hydroethanolic extract	Lipoid S75, sodium hyaluronate	Hydration, sonication, dialysis	[26]
Ethosomes						
Achillea millefolium antenna parts	Flavonoids, caffeic acid derivatives	Antibacterial, antioxidant, wound healing	Maceration with 70% ethanol	Phospholipid, ethanol, propylene glycol	Cold method, sonication	[103]
Phytosomes						
Aloe vera dry extract [c]	Acemannan, β-sitosterol, glycosides (aloins), anthraquinone (aloe emodin)	Anti-inflammatory, antioxidant, cytoprotective, ↑ VEGF expression, ↑ NO synthesis	Marketed product	Soy lecithin	Antisolvent precipitation technique	[19]

Legend: [a] rosmarinic acid, carnosic acid, carnosol; [b] naringin, neoeriocitrin, neohesperidin; [c] co-encapsulation of L-carnosine/*Aloe vera* extract. VEGF—vascular endothelial growth factor, NO—nitric oxide; HE—herbal extract; PC—phytocompound.

Table 4. Vesicular nanosystems including phytocompounds with potential benefits in the treatment of wounds.

Entrapped PC	Effect of PCs	Source of PCs	Components of VNs	VNs' Preparation	Ref.
Invasomes					
Terpenoids [a]	Antibacterial, anti-inflammatory	Oil fraction of various plants	Soybean lecithin	Mixing the terpenoid with ethanol and phospholipids, extrusion	[28]
Liposomes and niosomes					
Resveratrol	Antioxidant	Grapes, nuts, berries	Soy phosphatidylcholine (Phospholipon 90G), glycerol monooleate, polyglyceryl-3 dioleate	Direct sonication	[104]
ULs					
Ammonium glycyrrhizate	Anti-inflammatory	*Glycyrrhiza glabra*	Soy phosphatidylcholine (Phospholipon 90G)	Thin-film hydration	[105]

Legend: [a] thymol, menthol, camphor, and 1,8-cineol. ULs—ultra-deformable liposomes; HE—herbal extract; PC—phytocompound.

6. Preparation Methods of Vesicular Nanosystems

All the methods of preparation of phospholipid vesicles are based on the phospholipidic property to form aggregated complexes when they are placed in an aqueous environment, because of their amphiphilic structures. In this way, hydrophobic parts avoid contact with the water molecules, while hydrophilic head groups remain in contact with the aqueous phase and are assembled in vesicular form. The underlying mechanism for the formation of the lipid vesicles is the hydrophilic–hydrophobic interactions and van der Waals forces between phospholipids and water molecules [106]. During the preparation of the VNs, the HEs and the PCs can be included in different steps of preparation, according to their solubility.

6.1. Hydration of Dry Thin Lipid Film: Bangham Method, Film Dispersion, or Thin-Layer Evaporation Method

In the first step, the phospholipids are dissolved in an organic solvent (chloroform, ethanol, methanol, etc.) in a round-bottom flask. In the second step, the organic solvent is completely evaporated under vacuum in a rotary evaporator, obtaining a thin film over the wall of the round-bottom flask. Afterward, the dried lipid film is hydrated with distilled water or isotonic PBS to form large multilamellar vesicles (MLVs). This process can be accelerated by using an ultrasound bath. The resulting large MLVs are subjected to sonication, finally obtaining small unilamellar vesicles (SUVs) [94,97].

The lipophilic PCs intended to be entrapped in vesicles can be dissolved in organic solvents together with phospholipids: *Myrciaria jaboticaba* [30] peel extract, *Narcissus tazetta* [84] extract, *Salvia triloba*, and *Rosmarinus officinalis* [102] essential oils, *Calendula officinalis* [70] extract, cinnamon oil [52], *Citrus limon* var. *pompia* [36] essential oil, or citral, ammonium glycyrrhizate [105], quercetin [95], curcumin [59], oryzanol [99], or asiaticoside [101], or with the surfactant for development of niosomes with *Calendula officinalis* [50] extract. Curcumin can also be dissolved in acetone and then mixed with phospholipid previously dissolved in the organic solvent [74]. Similarly, the shikonin solution was mixed with dendrimers solution, and then the phospholipids in organic solvents were added to obtain chimeric advanced drug-delivery nanosystems for shikonin, combining dendritic and liposomal technology [97].

Depending on their solubility, the PCs can also be added to the solutions used for film hydration. Thus, the thin film can be hydrated with the PBS HEs or PCs solution, such as *Carpobrotus edulis* [90] powder extract, anthocyanin complex [85], madecassoside [44], essential oil derivative alpha-bisabolol [99], with the ethanolic solution of the PC [74], with the aqueous solution of HEs (*Narcissus tazetta* extract [84]), or with the HE itself (Danggui Buxue extract [92], *Salvia aramiensis* extract [58], or *Aloe vera* leaf gel extract [91]). In some other cases, the extract can be added at the end and stirred with the vesicles dispersion (*Moringa oleifera* extract [29] and bromelain extract [94]).

6.2. Emulsion Evaporation

In this method, the lipids are dissolved in an organic solvent under mixing, and then slowly added to distilled water with gentle stirring and homogenized. The organic solvent is then removed by vacuum drying and the remaining solution is subjected to ultrasonication. Finally, the nanosystems' dispersion is purified by centrifugation. This method was used to obtain astaxanthin-loaded nano-liposol [96].

6.3. Direct Sonication

VNs can be prepared by simple dispersion of the components (phospholipid and HE or PCs) in water or other solvents, or in the HEs itself for a few hours, then sonicated until a homogenous system with a small particle size is obtained [28]. Using this method, *Hypericum scruglii* extract [45], *Thymus capitatus* essential oil [37], *Fraxinus angustifolia* extract [27], *Azadirachta indica* [93] (neem) oil, curcumin [72], *Glycyrrhiza glabra* extract, or raw

glycyrrhizin [73], resveratrol [104], oleuropein [7], phycocyanin [60], quercetin [25,98], and curcumin [25,100] were successfully incorporated.

The direct sonication of the dispersion containing phospholipids, HE, and water represents a green and fast preparation method since the use of organic solvents and dissipative processes are completely avoided [45,72]. Thus, a green method for the preparation of liposomes, without using an organic solvent, consisted of mixing the phospholipids and the lentisk oil with water, followed by a sonication step and purification through dialysis [40].

The HEs can also be dispersed in water or mixtures consisting of water/glycerol or water/sodium hyaluronate or water/glycerol/sodium hyaluronate to produce liposomes, glycerosomes, hyalurosomes, and gly-hyalurosomes, respectively, employed for hydration of the phospholipids, overnight, at room temperature; then, they are sonicated and purified by dialysis. In this way, *Citrus limon* var. *pompia* extract-loaded phospholipid vesicles were obtained [26]. Similarly, the phospholipids can be hydrated with the aqueous dispersion of HE [73].

In another study, a cold method was used to obtain *Achillea millefolium* extract-loaded ethosomes. Phospholipids were dissolved in ethanol and propylene glycol and HE was introduced with a syringe, followed by sonication [103].

6.4. Reverse Phase Evaporation Technique

In this technique, the lipids are dissolved in an organic solvent under mixing, and separately, the HE is dispersed in distilled water. Then, the HE is added to the solvent and homogenized. Finally, the suspension is heated in the water bath to evaporate the organic solvents and separated by centrifugation. In this way, *Hypericum perforatum* [19] extract-loaded niosomes were obtained [19].

6.5. Antisolvent Precipitation Technique

In this method of preparation, the lipids are dissolved in an organic solvent such as chloroform, and the aqueous solution containing the HE is slowly added to the lipophilic solution under vigorous stirring. The precipitate is separated by filtration or centrifugation and dried into a desiccator until complete solvent evaporation. By using this technique, *Aloe vera* whole extract and L-carnosine phytosomes were obtained [19].

6.6. Single-Step Injection Technique

Another preparation method consists of dissolving the active substance and the phospholipid in ethanol and propylene glycol under stirring. After this, the distilled water is directly injected into the previously obtained solution by using a microinjection pump or syringe. If a HE is used, after dissolving the phospholipids in ethanol and propylene glycol, the extract is injected slowly as a fine stream with a syringe in the solution and then the final volume is adjusted with distilled water. The resulting mixture is stirred and then sonicated to decrease the particle size [81,103].

After the preparation of the vesicle dispersion, it is subjected to purification by dialysis [7,25,100] or centrifugation [101]. The decrease in the particle size can be achieved by sonication, in most cases, or by extrusion in other cases [28,65,70,101,105]. In a study conducted by Paolino et al., another particular method was used, by applying alternative cycles of freezing and thawing and then extrusion to obtain unilamellar vesicles [101].

7. Characterization Methods of Vesicular Nanosystems

To ensure their in vitro and in vivo performance, VNs must be comprehensively characterized after their preparation, by evaluating their physicochemical properties [107]. Their attributes can affect the bulk properties, product performance, processability, stability, and appearance of the final product [106]. For an efficient active delivery at the wound site, the desirable properties of VNs are: small particle size, homogeneous

(monodisperse) systems, good stability of the dispersion, high encapsulation efficacy, and optimal release profile of the actives [106,107].

7.1. Particle Size

Particle size and size distribution of lipidic nanocarriers are critical quality attributes for VNs, as well as essential components of stability. The particle size, expressed as average size or average diameter, is usually measured by laser Doppler electrophoresis [53] or dynamic light scattering [19,51,105]. The size of the vesicle mainly depends on the different concentrations of lipid and ethanol included in the formulation [103]. Extrusion, sonication, homogenization, and/or freeze–thawing techniques are used to control the size and the size distribution of different nanocarriers [106].

The smaller the particle size, the larger the surface-to-volume ratio is. The small size of vesicles is important for enhancing the cellular uptake or internalization, with particle size and polydispersity index (PDI) being the main physiochemical attributes that influence the endocytosis-dependent cellular uptake [106]. It is generally accepted that the particle size should be smaller than 300 nm to ensure efficient skin penetration and delivery of the payload into the deeper layers of the skin [103,106]. Nanovesicles with a diameter of 70 nm or below have shown maximum deposition of actives in both viable dermal and epidermal layers. Generally, lipid vesicles have diameters ranging from 40 to 800 nm, allowing them to attach to the lipid matrix of the stratum corneum and enhance the amount of active substances that penetrate the deeper layers of the skin [16].

7.2. Polydispersity Index

To measure the broadness of the size distribution and the degree of heterogeneity of particles, a dimensionless parameter is used: the polydispersity index, which has values between 0 and 1 [11,30]. According to the value of this index, the systems can be classified as monodisperse or polydisperse. The average diameter and polydispersity index of the vesicles can be determined by dynamic light scattering [37] or by photon correlation spectroscopy [26,36]. An acceptable dispersion is obtained when PDI has values lower than 0.3, indicating a homogenous liposomal population [39,103,106]. The PDI can be reduced by extrusion or sonication processes to obtain more uniform vesicles [11].

The physicochemical properties of lipidic nanocarriers, particularly PDI, influence their ability to accumulate in the target tissue. As a result, the creation of homogeneous (monodisperse) populations of nanocarriers of a specific size is required for the formulation of safe, stable, and efficient nanocarriers. Thus, controlling the particle size distribution should take into account the composition of the nanocarriers as well as the type of solvents and co-solvents used in their preparation [106].

7.3. Particle Shape

The morphology of the VNs can be analyzed by scanning electron microscope (SEM), transmission electron microscopy (TEM), and cryogenic TEM [41,45]. These microscopic methods can confirm the formation of lamellar vesicles, and suggest the impact of the addition of different ingredients to the composition of vesicles, showing the morphology, shape, and dimensions of the vesicles [41,53]. TEM involves the removal of the native environment of vesicles for preparation and may induce alterations in liposomal shape (shrinkage, swelling, and artifacts' formation in the created image). The use of Cryo-TEM can overcome these limitations, keeping the vesicles close to their native state, and minimizing the shape distortion on shrinkage [107]. Moreover, information about the particle size and bilayer thickness can be obtained using Cryo-TEM images with the aid of the Fiji tool [28].

7.4. Zeta ζ-Potential (Surface Charge)

Zeta ζ-potential measurements are obtained through laser Doppler electrophoresis (measuring the electrophoretic mobility of particles) or dynamic light scattering [105]. The samples are suitably diluted beforehand to be optically clear and to avoid the reduction of scattered light that can be detected by the Zetasizer [30]. The zeta potential is caused by the net charge of the lipid structure in the formulation [6]. This is the main factor that indicates the general charge of a particle, and the repulsion or attraction forces between the particles. Thus, it provides a secondary parameter by which the stability of liposome dispersions is evaluated, by controlling the electrostatic interactions between the particles in suspension [21,51,107]. The negative charge of ethanol in the system prevents the aggregation of vesicles by electrostatic repulsion and resistance force. Moreover, negative zeta potential is responsible for higher percutaneous permeation of the drugs [11]. Differences in particle size provide information about aggregation and fusion phenomena. If the zeta potential of particles rises above –25 and +25 mV, it indicates an increase in stability, because they present repulsive forces that prevent the natural tendency to aggregate. The closer the potential value approaches to zero (uncharged particles), the faster the vesicles decompose by flocculation [21,107].

7.5. The Lipid Content of the Vesicle Dispersions

The lipid content of the vesicular dispersions could be assessed by the Stewart assay. An aliquot of vesicle suspension was added to a biphasic mixture of aqueous ammonium ferric thiocyanate solution (0.1 N) and chloroform. The concentration of the phospholipids can be obtained by measuring the absorbance of the organic phase. The aggregation efficiency (AE%) can be calculated as the effective amount of aggregated phospholipids, expressed as the percentage of the amount initially used [98].

7.6. Phase Behavior

Differential scanning calorimetry (DSC) may be used to confirm the formation of the vesicles, but also to investigate the presence of potential interaction or conformation between components of the vesicular systems. On the DSC thermograph, endothermic or exothermic peaks appear, which show the ingredients' degradation, and the differences between the thermographs of individual components and the mixture of them provides information about interactions or complex formation [19,71,95].

DSC also determines the transition temperature of the lipid bilayer, an important parameter that influences the fluidity of the liposomal lipid bilayer and may affect liposomal properties such as aggregation, fusion, and stability. Transition temperature may also be investigated by Fourier transform-infrared spectroscopy (FTIR) or X-ray diffraction studies (XRD) [107].

7.7. Entrapment Efficiency

Loading the right amount of active substance in VNs is crucial to achieving therapeutic efficacy [107]. The entrapment efficiency or encapsulation efficiency (EE%) is represented by the delivery potential of the VN that is directly associated with its drug-carrying capacity [11]. Briefly, EE% represents the amount of drug entrapped in the VN, and may be calculated by using the following equation [108]:

$$EE\% = \text{Entrapped drug concentration/Total drug concentration} \times 100 \quad (1)$$

The vesicular dispersion is placed into a dialysis cassette and further dialyzed, centrifuged, and then the supernatant is analyzed [44,53]. The quantification of the PCs is performed by specific methods, such as gas chromatography in the case of volatile oils, high-performance liquid chromatography with diode array detection (HPLC-DAD), or UV-Vis spectroscopy for other actives [39,40,53,92].

The EE% of the PC in the vesicles can be correlated with the antioxidant activity, reported as a percentage ratio between the antioxidant activity of the samples before and after the purification process (dialysis), measured by the DPPH colorimetric test and calculated according to the following equation [7,30]:

$$\text{Antioxidant activity\%} = [ABS_{DPPH} - ABS_{sample})/ABS_{DPPH}] \times 100 \quad (2)$$

The vesicle composition, the method of preparation, as well as the rigidity of the bilayer membrane, can have a crucial impact on the EE of a certain drug [107]. In the case of ethosomes, it is mentioned that the quantity of ethanol and phospholipids influences the encapsulation of PCs in a positive manner. Taking this into consideration, the ethanol concentration is usually up to 40%, as its fluidization effect at higher concentrations may cause leaking of HE from the lipid bilayer, subsequently with a decrease of EE% [11].

7.8. In Vitro Drug Release of the Active Substance

An appropriate release of PCs entrapped in VNs is mandatory for the efficacy of the product in wound healing. The aim is to achieve a sustained release of the active substances at the site of the injury and prolongation of their effect to speed up the wound-healing process [16].

In the development of liposomes for the controlled release of actives, the results obtained from the in vitro release studies are extensively accepted as an extrapolation to in vivo performance of liposomes [107].

The release of PCs from VNs can be analyzed by the dialysis method or Franz diffusion cells by using various release media. Samples are withdrawn from the release compartment at specific time intervals, with the volume being replaced with fresh release medium to maintain sink conditions. The amount of PC released can usually be determined by using UV-Vis spectrophotometry [72,97], HPLC methods [58,95,102], or measuring the antioxidant activity with the DPPH colorimetric test [7,45] or total phenolic content [73]. The percentage of released phytocompounds is calculated from the cumulative drug amount released at different time intervals, using the following equation [74,102]:

$$\text{Release\%} = [(\text{total amount of drug} - \text{detected amount of drug}) \times 100/\text{total amount of drug}] \quad (3)$$

The release of phytocompounds from the topical formulation containing the vesicle dispersion can also be determined. Moreover, supplementary information about the kinetics of active release can be obtained [21].

7.9. Physical Stability

The liposomal colloidal dispersion systems are thermodynamically unstable, being prone to aggregation, flocculation, and fusion, or the entrapped substance may precipitate during storage [44]. The verification of particular characteristics, such as chemical and physical stability, the size and structural conservation, the maintenance of encapsulated drugs, and the impact of biological fluids on liposomal properties, are all part of the evaluation of liposomal stability [107].

Mainly, the physical stability of liposomes is influenced by the temperature. This can be studied by monitoring the aggregation or fusion of liposomes and the leakage of the active substance. The turbidity assay is a practical approach to determine the relative size of liposomes and reflects the stability of the liposomes. This parameter is determined spectrophotometrically, with the increase of the absorbance values being correlated with the particle size increase [44]. The physical stability of the vesicles in the dispersion is evaluated by monitoring the average size, the polydispersity index, and the zeta potential for 1 month [53,102], 2 months [37,45], 3 months [30,40], 4 months [7], or 6 months [41] of storage at room temperature.

7.10. Leakage Rate

The leakage rate evaluates the performance of liposomes during their storage and represents the ratio of encapsulation efficiency during the storage period (W_i) to initial encapsulation efficiency (W_0). The leakage rate can be measured four weeks after preparation [44,92]. This parameter can be calculated using the following equation [44]:

$$Lr\% = (1 - W_i/W_0) \times 100 \quad (4)$$

7.11. Chemical Stability

Chemical stability refers to liposomes' capacity to maintain EE% levels when changes in the medium occur, such as pH alterations, electrolyte composition, oxidizing agents, and the presence of surface-active chemicals. As the lipids are prone to suffer oxidative reactions, their chemical degradation may induce permeability changes within the lipid membrane. Furthermore, the interactions between the entrapped drugs and phospholipids can also interfere with vesicles' chemical stability [107].

7.12. Other Characterization Methods

Fourier transform-infrared spectroscopy is performed for the analysis of functional groups of HE-loaded vesicles [103]. The analysis is performed for each main component and their physical mixture by using an FT-IR spectrometer [19].

X-ray diffraction studies are performed to record X-ray diffractograms for each main component and their physical mixture [19,98]. Small or wide-angle X-ray scattering analysis allows for obtaining relevant structural parameters on bilayer-based structures, e.g., vesicles and lamellar phases [25,100]. The vesicular dispersions are loaded into glass capillaries and the diffraction patterns are recorded, usually at 25 °C, followed by a calculation of the electron distance distribution and the bilayer electronic density profile. Through this method, relevant structural parameters are obtained, as well as the distribution of electron density in the polar and a-polar regions of membranes [98].

8. Methods of Evaluation of Vesicular Nanosystems for Wound Healing

8.1. In Vitro Skin Delivery of the Active Compounds

The analysis of the permeation of PCs is performed by using Franz diffusion cells. The receptor compartment is usually filled with saline or PBS and the samples of PC- or HE-loaded nanosystem suspension are applied onto the membrane surface. An exact amount of the receiving medium is withdrawn at different time intervals and the content in PCs is assessed by specific quantification methods (e.g., HPLC or UV-Vis spectroscopy). The extracted amount is replaced with fresh medium to maintain a constant volume in the receptor compartment [25,100,103,105].

The skin retention of PCs may also be analyzed using Franz diffusion cells, in ex vivo studies. Skin samples are collected and placed between receptor and donor compartments of Franz diffusion cells. The tested product is placed onto the skin, in the donor compartment. The quantity of PCs accumulating in different skin layers, expressed as an amount in $\mu g/cm^2$ and as a percentage of the total PC amount applied on the skin, may be determined in the stratum corneum by tape stripping and in the epidermis and dermis after their separation [99].

8.2. Cellular Uptake by Vesicles

After skin application of the vesicular systems, particularly when the skin is damaged, an increased local bioavailability and PCs' residence time in the injured tissue is obtained due to its internalization in the cells. Therefore, an increase in the activity of the PC is observed. A membrane marker is used to label the vesicles and a fluorescent molecule to identify the aqueous cell compartment. The cellular uptake of the active compounds is then studied by confocal microscopy after the incubation of different skin cells

with PC-loaded vesicles. The distribution of the fluorescent-labeled vesicles into the cells is checked [27,61,99].

8.3. Cell Viability Studies

The viability of cells is analyzed to indicate the biocompatibility of the formulation [30]. Cytotoxicity can be analyzed using MTT (3-[4, 5-dimethylthiazol-2-yl]-2, 5 diphenyl tetrazolium bromide) by a colorimetric assay. Results are shown as percent of cell viability in comparison with non-treated control cells (100% viability) [27,29].

8.4. Scratch Assay—In Vitro WoundHealing Effect, Cell Migration Assay

The in vitro scratch assay is performed using a monolayer of cells to analyze the ability of the HE in aqueous dispersion or incorporated into vesicles to stimulate the cell's proliferation and migration. The cells are seeded in plates and a mechanical scratch wound is produced in the confluent cell monolayer. The percentage of wound closure (wound healing %) is calculated by measuring the lesion areas or according to cell migration in the scratch area by using a computer program [30,70]. The percentage of migration can be calculated by using the following equation:

$$\text{Percentage of migration} = (A_0 - A_n)/A_0 \times 100\% \quad (5)$$

where A_0 is the initial area of the scratch site, and A_n is the area of the scratch site after the nth hour [29].

8.5. In Vivo Wound Healing Effect on Animal Model

The wound healing process after the topical application of the dosage forms may be measured at different time intervals. Usually, the in vivo efficacy test is evaluated on an experimental animal model after performing surgical procedures to create identical skin defects. The wounds are photographed at preset intervals of time (days), and then the wound area is measured using specific software. The percentage of wound reduction area is calculated with the following equation [80]:

$$\text{Wound reduction area\%} = [(\text{Wound area day 0} - \text{Wound area relative day})/\text{Wound area day 0}] \times 100 \quad (6)$$

The histopathological examination of the skin tissue samples may be assessed using a scoring system. For example, Abramov's method uses a score of 0–3 for each section for inflammatory cells, collagen deposition, angiogenesis, granulation tissue formation, and epithelialization [80].

Methods of characterization and other analyses undertaken on VNs bearing HEs or PCs are presented in Table 5, together with the results of each study.

Table 5. In vitro and in vivo studies undertaken for vesicular nanosystems loaded with herbal extract or phytocompounds.

Entrapped HE or PC	In Vitro Release Study/In Vitro Skin Permeation Study	Cell Culture Studies	In Vivo Studies	Main Results	Ref.
Liposomes					
Carpobrotus edulis powder extract	No/No	No	Male Wistar-albino rats	Positive effects on the healing process in both incisional and excisional wound tissues	[90]
Pistacia lentiscus oil	No/Franz cells, pig skin	HaCaT, primary mouse embryonic fibroblasts (3T3)	No	Stability of the system in dispersion, ↑ the PCs in the skin, ↑ the ability to counteract damages induced by oxidative processes, beneficial effect on lesion regeneration and healing	[40]
Aloe vera leaf gel extract	No/No	NB1RGB cells, NHEK(F) cells	No	↑ the cell proliferation and collagen synthesis, ↑ bioavailability of the HE, ↑ skin properties	[91]
Angelica sinensis and *Astragali radix* ratio 1:5	No/No	No	Adult male Sprague-Dawley rats	↑ therapeutic efficacy, ↑ wound closure; histological improvements, ↑ hydroxyproline levels; ↑ CD34, KI67, COL1α1, COL3α1 expression levels in wound granulation tissues compared to control groups in vivo, ↑ VEGF/PI3K/AKT and TGF-β/SMADS signaling pathways, which might contribute to the ability to ↑ full-thickness excisional wound healing in rats	[92]
Salvia aramiensis aerial part extract	Franz cells, dialysis membrane/No	L929 cell line (mouse fibroblast)	No	Strong antioxidant effect and potential wound-healing activity	[58]
Bromelain extract	No/No	No	Male Wistar rats	Absence of edema on the 14th day in animals treated with bromelain entrapped in nanocarriers	[94]
Curcumin	Dialysis, dialysis membranes/No	HDF	Male Wistar rats, New Zealand rabbits	Monodispersity and no vesicle aggregation even in long-term storage, considerable wound-healing properties in the early stage, antibacterial activity on burn wounds similar to SSD cream application	[72]
Quercetin	Diffusion cells system /No	No	No	Acceptable stability, biphasic pattern of drug release behavior	[95]
Curcumin	No/No	3T3 cells (mouse fibroblasts)	Mice *Mus musculus* var. albino.	↑ healing rates, ↑ scar treatment effects by incorporation in liposomes, compared to native curcumin, ↑ wound healing, ↑ scar treatment effect of curcumin liposomes compared to curcumin nanoplexes	[59]
Usnic acid	No/No	No	Male *Rattus norvegicus albinus*, Wistar lineage	↑ burn healing, probably related to the modulation of the inflammatory response, epithelialization, and collagen formation	[31]
Salvia triloba and *Rosmarinus officinalis* E.O.s	Dialysis, permeable bag membrane/No	No	No	Preservation of antioxidant properties of E.O. constituents, ↓ anti-inflammatory activity of the pure E.O. ↑ activities for the liposome-encapsulating E.O.	[102]
Citrus limon var. pompia E.O. or raw citral	No/No	HaCaT	No	Citral-loaded liposomes more effective than pompia E.O. liposomes in counteracting the growth of bacteria (*E. coli* and *S. aureus*) and fungi (*C. albicans*)	[36]
Cinnamon oil	No/No	No	No	↑ E.O. stability by liposome encapsulation	[52]

				↑ antibacterial activity on MRSA and MRSA biofilms, ↑ antibiofilm activities and active time of liposome-encapsulating E.O. compared to free E.O.	
Nano-liposol					
Astaxanthin	No/No	NIH 3T3 fibroblast cells	No	%EE ↑ of astaxanthin, good stability ↓ ROS, ↑ wound healing of fibroblasts without cytotoxicity	[96]
Liposomal locked-in dendrimers					
Shikonin	Dialysis, dialysis sacks/No	No	No	Adequate drug encapsulation, advantageous release profiles, satisfactory stability of liposomal formulations	[97]
Liposomes and hyalurosomes					
Glycyrrhiza glabra root extract	Dialysis, tubing Spectra/Por® membranes/No	Primary mouse embryonic fibroblasts (3T3)	Female CD-1 mice	↑ effect of licorice extract, especially when delivered from hyalurosomes, ability to retain the extract components over time, ↑ in vitro and in vivo biological activity	[73]
Liposomes and hyalurosomes					
Neem oil (*Azadirachta indica* oil)	No/No	HaCaT and fibroblasts (3T3)	No	↑ biocompatibility, effective protection of the skin cells from oxidative stress, ↑ efficacy of the oil; argan-hyalurosomes → more viscous, more suitable for skin application	[93]
Liposomes and PEVs					
Quercetin and curcumin	No/ Franz cells, pigskin	No	Female Hsd:ICR(CD-1) mice	↑ Anti-inflammatory activity → inhibition the onset of skin wounds during TPA treatment; protective effect, more relevant in curcumin PEG-PEV formulation, ↑ drug bioavailability in the target tissue	[25]
Quercetin	No/No	3T3 mouse fibroblasts, cellular uptake	Female cd-1 mice	In vitro studies—massive uptake and diffusion of PEVs in dermal fibroblasts; in vivo studies—amelioration of the tissue damage in TPA-inflamed skin, attenuation of edema and leukocyte infiltration, especially using 5% PEG-PEVs	[98]
PEVs					
Oryzanol and alpha-bisabolol	No/Franz cells, dorsal rat skin- ex vivo deposition/permeation	No	Male Wistar rats	Favorable properties in terms of size, charge, stability, skin deposition for studied PEVs; faster onset, superior wound healing for oryzanol and alpha-bisabolol-loaded PEVs compared to a marketed product; early signs of neo-angiogenesis and collagen production compared to groups treated with PEVs loaded with oryzanol only or the marketed product	[99]
ULs					
Asiaticoside	No/Franz cells, adult human skin	Primary human dermal fibroblasts	Rats—Male Sprague-Dawley	↑ asiaticoside permeation through human SCE, ↑ intracellular drug delivery into primary human fibroblasts, significant ↑ collagen biosynthesis both in vitro and in vivo compared to the simple aqueous drug solution.	[101]
Ammonium glycyrrhizate	Franz cells, human SCE/ synthetic membrane	No	Human volunteers	Biocompatible, deformable, allowed passage of ULs, delivery of A.G. in specific skin layers, pseudo-zero-order release kinetic, 50% of the entrapped drug is released in 24 h—potential depot effect of ULs in the skin; ↑ anti-inflammatory activity of drug of 15- and 30-fold compared to equivalent topical application of A.G. solution on healthy volunteers, time-dependent effect	[105]
Transferosomes					
Myrciaria	No/No	HaCaT	No	↓ H_2O_2 damage induced in cells, ↑ wound healing in HaCaT	[30]

jaboticaba fruits peel					
Transferosomes, glycoltransferosomes					
Mangiferin	No/No	Mouse embryonic fibroblasts (3T3)	Female CD-1 mice	Optimal performances of mangiferin delivery, ↑ wound-healing properties; cytocompatibility, protection of fibroblasts from oxidative stress, ↑ proliferation, migration, wound closure in vitro; protection of mouse skin from chemically induced injury in vivo, ↓ inflammatory infiltration; glycoltransferosomes and mucin-glycoltransferosomes, ↑ deposition of mangiferin in epidermis and dermis; ↑ ability to pass across the biological membranes	[41]
Collagen-enriched transferosomes, glycerosomes, and glytransferosomes					
Oleuropein	Dissolution tester/No	Mouse embryonic fibroblasts, keratinocytes	No	↑ woundhealing efficacy, ↓ production of NO along with the damage induced by ROS, especially when cells were treated with collagen-enriched vesicles	[7]
Hyalurosomes					
Curcumin	No/ Franz cells, pigskin	HaCaT	No	↑ physicochemical properties, ↑ biological performances by using sodium hyaluronate dispersion as a hydrating medium of phospholipids; immobilization of vesicles by hyaluronan → ↑ EE%, stability, rheological properties, local drug availability, therapeutic activity, in vivo fast healing process	[100]
Gel-core hyaluosome					
Curcumin	Dialysis/No	No	Female Sprague-Dawley rats	↑ curcumin skin penetration, dermal localization, protection against degradation, ↑ healing, ↑ histological progress, ↓ scar formation	[74]
Glycerosomes, hyalurosomes, gly-hyalurosomes					
Citrus limon var. *pompia* fruits	No/No	Primary mouse embryonic fibroblasts (3T3), HaCaT	No	Prevention of oxidative damage; ↑ viability; ↑ biological activity by incorporation of the extract in vesicles, especially gly-hyalurosomes	[26]
Glycerosomes, liposomes, gluglycerosomes, gel-gluglycerosomes, hyal-glulycerosomes					
Hypericum scruglii aerial parts extract	Polycarbonate dialysis tubes/No	HaCaT	No	↑ antioxidant activity, ↑cell uptake and wound-healing effects	[45]
Glycerosomes					
Rosmarinus officinalis leaves extract	No/No	No	No	↑ antioxidant activity by liposomal entrapment, better stability of the extract during storage in comparison to free extract	[51]
Niosomes					
Hypericum perforatum flowering tops	USP dissolution test apparatus/No	No	Adult Mongrel dogs	↓ inflammatory phase, ↑ early beginning of proliferative phase of wound healing, significant ↓ wound size compared to control and Panthenol® 2% cream	[21]
Calendula officinalis flowers and leaves extract	No/No	Vero cell line	No	↑ wound-healing and protective effect against oxidative stress of *Calendula officinalis* methanolic extract after entrapment into Tween 60 niosomes	[50]
Santosomes					
Phycocianin	No/No	HaCaT, endothelial cells, cell uptake	Female CD-1 mice	Easy internalization of phycocyanin from santosomes by keratinocytes and endothelial cells, protective effect against H_2O_2 stress; in vivo studies—wound-healing activity	[60]
Phytosomes					

Moringa oleifera leaves extract	No/No	NHDF	No	Cytocompatibility; ↑ dose-dependent effect in wound closure of filtered *Moringa oleifera* compared to unfiltered samples and controls	[29]
Sinigrin	No/No	HaCaT	No	At the highest tested concentration, 0.14 mg/mL (42 h), the sinigrin–phytosome complex completely cured the wound, whereas the sinigrin alone displayed only 71% wound healing	[71]
Aloe vera dry extract	Dialysis/No	HUVECs	No	↑ protective effects in suppressing MGO-induced endothelial cell cytotoxicity, anti-angiogenic effects, ↓ ROS overproduction and induction of oxidative stress; restorative effect on NO production; ↑ expression of several proangiogenic genes: VEGF-A, bFGF, KDR, Ang II, ↓ expression of anti-angiogenic such as Notch I, TGF-β	[19]
AuNP-phytosomes and liposomes					
Calendula officinalis flowers extract	No/No	NHDF, Vero cell line	No	↑ Antioxidant and wound-healing activity, ↑ stability compared to free forms of each encapsulated material, plain liposome, phytosome form	[70]
Ethosomes					
Curcumin	No/No	No	Male Wistar rats	↑ early stages of wound healing, antibacterial activity similar to SSD cream	[80]
Achillea millefolium antenna parts	No/Franz cells, rat skin	No	No	↑ skin penetration compared to conventional gel	[103]
Ethosomes and PEVs					
Fraxinus angustifolia leaves and bark extract	No/No	HaCaT, cell uptake fluorescent vesicles	Male CD-1 mice	↑ local bioavailability of the leaf phytocomplex, ↑ intracellular antioxidant activity in HaCaT, ↑ wound healing in TPA-mouse model for the simple extract ethanolic solution	[27]
Invasomes					
Terpenoids [a]	No/No	No	No	↑ bioavailability of terpenoid-based drugs, strong selective activity against Gram-positive bacteria.	[28]

Legend: [a] thymol, menthol, camphor, and 1,8-cineol. SCE—stratum corneum and epidermis, NB1RGB—normal human neonatal skin fibroblasts, NHEK(F)—normal human epidermal keratinocytes, HaCaT—human keratinocytes, HDF—human dermal fibroblast, HGF—human gingival fibroblast, HUVECs—human umbilical vein endothelial cells, SSD—silver sulfadiazine, A.G.—ammonium glycyrrhizate, ULs—ultra-deformable liposomes, MGO- methylglyoxal, E.O.—essential oil, HE—herbal extract, PC—phytocompound.

9. Topical Delivery Systems Containing Herbal Extracts

Current treatment options for wounds include more than 3000 wound dressings. Various options from traditional dressings such as gauze to film, hydrogel, hydrocolloid, foam, hydrofiber, alginate, biological, and composite dressings, are available. Lately, modern approaches such as 3D-printed dosage forms and drug-delivery devices were developed. The main challenges of conventional wound care are microbial infection, inflammation, and inadequate blood supply. In the past decades, advanced approaches such as oxygen therapy, negative-pressure wound therapy, or gene therapy were developed, but their clinical applications are limited by the high cost or the need for special technologies. Given the high diversity of wound care products, several classifications based on different criteria, such as clinical performance, physical form, or the source of the material, have been proposed. According to the FDA classification, wound-care products are classified as drugs, medical devices, biological products, or combination products. Conventional wound healing pharmaceutical formulations include liquid (solutions, suspensions, or emulsions) and semisolid (creams or ointments) products. Wound care devices may be Class I, II, III, or unclassified [109–111].

Lipid nanovesicles can be included in different topical systems, such as powders, gels, solutions, creams, ointments, and dressings, to facilitate the application to the wound. Targeted action of the formulation along with the sustained release of the active substances are considered the principal requirements in chronic wound healing. These criteria can be successfully fulfilled by using the lipid vesicles included in the appropriate formulations [112].

Many studies describe the assessment of the vesicular system after its incorporation into a gel vehicle, for a suitable topical application of formulation [21,80,85,92,103]. Hydrogels or hydrated polymer dressings are the most often employed gels for cutaneous application. They contain a high amount of water in a gel base, help to regulate the fluid exchange from the wound site, and confer to them a soft consistency, similar to the natural tissue. They also provide moisture to the wound, important to promote granulation, epithelialization, and autolytic debridement. The high water content of hydrogel dressings can cool the wound, producing pain relief that can last up to 6 h, and contribute to their biocompatibility and rehydrating capacity. Dressing-change discomfort is also reduced because hydrogels do not adhere to the wound surface due to low interfacial tension between the hydrogel surface and the body fluid. Additionally, the elastic nature of hydrated hydrogels minimizes irritation to the surrounding tissues. Hydrogels facilitate autolytic debridement, fill in the dead space from the surface of the wound, and can be used even when the infection is present [87,88].

An actual interest is the development of modern dressings (films, hydrogels, hydrocolloids, wafers, membranes, sponges, foams, etc.). These dressings cover the wound and ensure a moist environment, which is necessary for rapid and efficient healing, with reduced scar complications. Moreover, these dressings ensure non-adhesion to the injured area and do not cause trauma when removed. For chronic wounds and those with impaired healing, such as bedsores, venous ulcers, or diabetic foot ulcers, it has been found that wound dressings' application has significantly reduced the cost of the treatment. Modern dressings can incorporate and deliver active substances, such as antimicrobial, anti-inflammatory, or analgesic agents, at the wound site [94,113,114]. Including VNs in modern dressings can be an interesting field of research, because this may provide targeted and sustained delivery of constant concentrations of the drug on the wound site together with the improved penetration of the drug, swelling in the presence of wound exudates, better protection of active ingredients, and thereby favor the wound healing [112]. Recent studies highlighted that modern dressings with natural active compounds or HEs can be an ideal delivery system in wound healing [115,116]. In addition, other studies describing the incorporation of lipid vesicles in modern dressings for wound healing have shown promising results [117–120]. Although, a thorough search of the relevant

literature yielded only a limited number of studies in which VNs with PCs were included in polymeric dressings for wound healing [31,94]. Table 6 presents VNs bearing HEs or PCs incorporated in topical systems.

Table 6. Vesicular nanosystems bearing herbal extracts or phytocompounds incorporated in topical systems for wound healing.

VN	Topical Delivery System	Entrapped HE or PC	Ref.
Niosomes	Gel-sodium carboxymethyl cellulose and hydroxyethylcellulose	*Hypericum perforatum* flowering tops	[21]
Liposomes	Thermosensitive gel	*Angelica sinensis* and *Astragali radix* ratio 1:5	[92]
Liposomes	Membranes—CMC, acetylated arrowroot starch	Bromelain extract	[94]
Ethosomes	Carbopol gel	Curcumin	[80]
Liposomes	Collagen-based films	Usnic acid	[31]
Ethosomes	Gel-carbopol 940, hydroxyethylcellulose	*Achillea millefolium* antenna parts	[103]
Niosomes *	Sodium polyacrylate and carbomer mucoadhesive gel	*Zea mays* cobs and *Clitoria ternatea* petals	[85]

Legend: * for healing of oral cavity wounds; VN—vesicular nanosystem; CMC—carboxymethyl cellulose; HE—herbal extract; PC—phytocompound.

10. Conclusions

As a response to the increasing prevalence of acute and chronic wounds, currently, a high number of studies focus on formulating innovative and effective healing products. This paper highlighted the preparation and characterization of lipid vesicle nanocarriers bearing HEs or PCs for wound healing, by emphasizing the main types of phospholipid nanovesicles, together with the challenges of the entrapment of the PCs or HEs in those nanosystems. The main outcomes of recent studies investigating VNs loaded with HEs or PCs are presented, as a basis that might help researchers in future studies. In the future, the development of novel wound dressings containing vesicular nanocarriers with PCs is expected to gain importance due to their multiple advantages over traditional topical products.

Author Contributions: Conceptualization D.A.S., C.B. and M.L.M.; writing—original draft preparation D.A.S.; writing—review and editing, D.A.S., C.B. and M.L.M. All authors have read and agreed to the published version of the manuscript.

Funding: This research received no external funding.

Institutional Review Board Statement: Not applicable.

Informed Consent Statement: Not applicable.

Data Availability Statement: Not applicable.

Conflicts of Interest: The authors declare no conflict of interest.

References

1. Falanga, V. Mechanisms of Cutaneous Wound Repair. In *Fitzpatrick's Dermatology in General Medicine*; McGraw Hill Medical: New York, NY, USA, 2003; pp. 278–291.
2. Sen, C.K. Human Wound and Its Burden: Updated 2020 Compendium of Estimates. In *Advances in Wound Care*; Mary Ann Liebert Inc.: New York, NY, USA, 2021; Volume 10, pp. 281–292.
3. Suliman, Y.A.; Bruni, C.; Johnson, S.R.; Praino, E.; Alemam, M.; Borazan, N.; Cometi, L.; Myers, B.; Khanna, D.; Allanore, Y.; et al. Defining Skin Ulcers in Systemic Sclerosis: Systematic Literature Review and Proposed World Scleroderma Foundation (WSF) Definition. *J. Scleroderma Relat. Disord.* **2017**, *2*, 115–120. https://doi.org/10.5301/jsrd.5000236.
4. Giuggioli, D.; Manfredi, A.; Lumetti, F.; Colaci, M.; Ferri, C. Scleroderma Skin Ulcers Definition, Classification and Treatment Strategies Our Experience and Review of the Literature. *Autoimmun. Rev.* **2018**, *17*, 155–164. https://doi.org/10.1016/j.autrev.2017.11.020.
5. Wang, W.; Lu, K.J.; Yu, C.H.; Huang, Q.L.; Du, Y.Z. Nano-Drug Delivery Systems in Wound Treatment and Skin Regeneration. *J. Nanobiotechnol.* **2019**, *17*, 1–15. https://doi.org/10.1186/S12951-019-0514-Y.

6. Bhatia, S. Nanoparticles Types, Classification, Characterization, Fabrication Methods and Drug Delivery Applications. In *Natural Polymer Drug Delivery Systems*; Springer International Publishing: New York, NY, USA, 2016; pp. 33–93.
7. Allaw, M.; Manca, M.L.; Gómez-Fernández, J.C.; Pedraz, J.L.; Terencio, M.C.; Sales, O.D.; Nacher, A.; Manconi, M. Oleuropein Multicompartment Nanovesicles Enriched with Collagen as a Natural Strategy for the Treatment of Skin Wounds Connected with Oxidative Stress. *Nanomedicine* **2021**, *16*, 2363–2376. https://doi.org/10.2217/nnm-2021-0197.
8. Caddeo, C.; Manca, M.L.; Peris, J.E.; Usach, I.; Diez-Sales, O.; Matos, M.; Fernàndez-Busquets, X.; Fadda, A.M.; Manconi, M. Tocopherol-Loaded Transfersomes: In Vitro Antioxidant Activity and Efficacy in Skin Regeneration. *Int. J. Pharm.* **2018**, *551*, 34–41. https://doi.org/10.1016/j.ijpharm.2018.09.009.
9. Ghiulai, R.; Roşca, O.J.; Antal, D.S.; Mioc, M.; Mioc, A.; Racoviceanu, R.; Macaşoi, I.; Olariu, T.; Dehelean, C.; Creţu, O.M.; et al. Tetracyclic and Pentacyclic Triterpenes with High Therapeutic Efficiency in Wound Healing Approaches. *Molecules* **2020**, *25*, 5557. https://doi.org/10.3390/molecules25235557.
10. Barakat, H.; Aljabeili, H.S.; Rahman, H.A.A. Synergistic Effect of Thymus Vulgaris Essential Oil Oral Administration on Topically Treated Wound with Chitosan, Thyme Essential Oil and Their Combination in Rats. *J. Nutr. Food Sci.* **2018**, *8*, 1–6. https://doi.org/10.4172/2155-9600.1000695.
11. Javed, N.; Ijaz, S.; Akhtar, N.; Khan, H.M.S. Nanostructured Ethosomal Gel Loaded with Arctostaphylosuva-Ursi Extract; In-Vitro/In-Vivo Evaluation as a Cosmeceutical Product for Skin Rejuvenation. *Curr. Drug Deliv.* **2022**, *19*, 720–734. https://doi.org/10.2174/1567201818666210729111026.
12. Sasindran, S.; Easwaran, M.; Shyamala, G.; Karuppaiah, A.; Siram, K.; Veintramuthu, S. Phytochemical Screening and Cytotoxicity Evaluation of Crude Extracts: Toxicity Comparison of Crude Extracts and Its Ethosomal Formulations. *J. Cosmet. Dermatol.* **2020**, *19*, 1794–1803. https://doi.org/10.1111/jocd.13234.
13. Gupta, B.S.; Edwards, J.V. Textile Materials and Structures for Topical Management of Wounds. In *Advanced Textiles for Wound Care*; Elsevier Ltd.: London, UK, 2019; pp. 55–104.
14. Matter, M.T.; Probst, S.; Läuchli, S.; Herrmann, I.K. Uniting Drug and Delivery: Metal Oxide Hybrid Nanotherapeutics for Skin Wound Care. *Pharmaceutics* **2020**, *12*, 780. https://doi.org/10.3390/pharmaceutics12080780.
15. Falanga, V.; Iwamoto, S. Chapter 248: Mechanisms of Wound Repair, Wound Healing, and Wound Dressing. In *Fitzpatrick's Dermatology in General Medicine*; McGraw Hill: New York, NY, USA, 2022; pp. 1–28.
16. Matei, A.M.; Caruntu, C.; Tampa, M.; Georgescu, S.R.; Matei, C.; Constantin, M.M.; Constantin, T.V.; Calina, D.; Ciubotaru, D.A.; Badarau, I.A.; et al. Applications of Nanosized-Lipid-Based Drug Delivery Systems in Wound Care. *Appl. Sci.* **2021**, *11*, 4915. https://doi.org/10.3390/app11114915.
17. Schultz, G.S.; Chin, G.A.; Moldawer, L.; Diegelmann., R.F. Principles of Wound Healing. In *Mechanisms of Vascular Disease: A Reference Book for Vascular Specialists*; Fitridge, R., Thompson, M., Eds.; University of Adelaide Press: Adelaide, Australia, 2011; pp. 423–435.
18. Ilomuanya, M.O.; Cardoso-Daodu, I.M.; Ubani-Ukoma, U.N.; Adebona, A.C. Polymeric Biomaterials for Wound Healing Incorporating Plant Extracts and Extracellular Matrix Components. In *Recent Advances in Wound Healing*; Aghaei, S., Ed.; IntechOpen: London, UK, 2021; pp. 1–15.
19. Darvishi, B.; Dinarvand, R.; Mohammadpour, H.; Kamarul, T.; Sharifi, A.M. Dual l-Carnosine/Aloe Vera Nanophytosomes with Synergistically Enhanced Protective Effects against Methylglyoxal-Induced Angiogenesis Impairment. *Mol. Pharm.* **2021**, *18*, 3302–3325. https://doi.org/10.1021/acs.molpharmaceut.1c00248.
20. Koga, A.Y.; Pereira, A. V.; Lipinski, L.C.; Oliveira, M.R.P. Evaluation of Wound Healing Effect of Alginate Films Containing Aloe Vera (*Aloe barbadensis* Miller) Gel. *J. Biomater. Appl.* **2018**, *32*, 1212–1221. https://doi.org/10.1177/0885328218754615.
21. Ali, M.; Motaal, A.A.; Ahmed, M.A.; Alsayari, A.; El-Gazayerly, O.N. An in Vivo Study of Hypericum Perforatum in a Niosomal Topical Drug Delivery System. *Drug Deliv.* **2018**, *25*, 417–425. https://doi.org/10.1080/10717544.2018.1431977.
22. Güneş, S.; Tıhmınlıoğlu, F. Hypericum Perforatum Incorporated Chitosan Films as Potential Bioactive Wound Dressing Material. *Int. J. Biol. Macromol.* **2017**, *102*, 933–943. https://doi.org/10.1016/j.ijbiomac.2017.04.080.
23. Nasab, M.E.; Takzaree, N.; Saffaria, P.M. In Vitro Antioxidant Activity and in Vivo Wound-Healing Effect of Lecithin Liposomes: A Comparative Study. *J. Comp. Eff. Res.* **2019**, *8*, 633–643. https://doi.org/10.2217/cer-2018-0128.
24. Pandey, V.K.; Ajmal, G.; Upadhyay, S.N.; Mishra, P.K. Nano-Fibrous Scaffold with Curcumin for Anti-Scar Wound Healing. *Int. J. Pharm.* **2020**, *589*, 1–10. https://doi.org/10.1016/j.ijpharm.2020.119858.
25. Castangia, I.; Nácher, A.; Caddeo, C.; Valenti, D.; Fadda, A.M.; Díez-Sales, O.; Ruiz-Saurí, A.; Manconi, M. Fabrication of Quercetin and Curcumin Bionanovesicles for the Prevention and Rapid Regeneration of Full-Thickness Skin Defects on Mice. *Acta Biomater.* **2014**, *10*, 1292–1300. https://doi.org/10.1016/j.actbio.2013.11.005.
26. Manconi, M.; Manca, M.L.; Marongiu, F.; Caddeo, C.; Castangia, I.; Petretto, G.L.; Pintore, G.; Sarais, G.; D'Hallewin, G.; Zaru, M.; et al. Chemical Characterization of Citrus Limon Var. Pompia and Incorporation in Phospholipid Vesicles for Skin Delivery. *Int. J. Pharm.* **2016**, *506*, 449–457. https://doi.org/10.1016/j.ijpharm.2016.04.014.
27. Moulaoui, K.; Caddeo, C.; Manca, M.L.; Castangia, I.; Valenti, D.; Escribano, E.; Atmani, D.; Fadda, A.M.; Manconi, M. Identification and Nanoentrapment of Polyphenolic Phytocomplex from Fraxinus Angustifolia: In Vitro and in Vivo Wound Healing Potential. *Eur. J. Med. Chem.* **2015**, *89*, 179–188. https://doi.org/10.1016/j.ejmech.2014.10.047.
28. Kaltschmidt, B.P.; Ennen, I.; Greiner, J.F.W.; Dietsch, R.; Patel, A.; Kaltschmidt, B.; Kaltschmidt, C.; Hütten, A. Preparation of Terpenoid-Invasomes with Selective Activity against S. Aureus and Characterization by Cryo Transmission Electron Microscopy. *Biomedicines* **2020**, *8*, 105. https://doi.org/10.3390/BIOMEDICINES8050105.

29. Lim, A.W.; Ng, P.Y.; Chieng, N.; Ng, S.F. Moringa Oleifera Leaf Extract–Loaded Phytophospholipid Complex for Potential Application as Wound Dressing. *J. Drug Deliv. Sci. Technol.* **2019**, *54*, 101329. https://doi.org/10.1016/j.jddst.2019.101329.
30. Castangia, I.; Manca, M.L.; Allaw, M.; Hellström, J.; Granato, D.; Manconi, M. Jabuticaba (*Myrciaria jaboticaba*) Peel as a Sustainable Source of Anthocyanins and Ellagitannins Delivered by Phospholipid Vesicles for Alleviating Oxidative Stress in Human Keratinocytes. *Molecules* **2021**, *26*, 6697. https://doi.org/10.3390/molecules26216697.
31. Arajo, A.A.S.; Nunes, P.S.; Albuquerque-Jnior, R.L.C.; Cavalcante, D.R.R.; Dantas, M.D.M.; Cardoso, J.C.; Bezerra, M.S.; Souza, J.C.C.; Serafini, M.R.; Quitans, L.J., Jr.; et al. Collagen-Based Films Containing Liposome-Loaded Usnic Acid as Dressing for Dermal Burn Healing. *J. Biomed. Biotechnol.* **2011**, *2011*, 1–9. https://doi.org/10.1155/2011/761593.
32. Zhang, Z.; Zheng, Y.; Li, Y.; Bai, H.; Ma, T.; Song, X.; Zhao, J.; Gao, L. The Effects of Sodium Usnic Acid by Topical Application on Skin Wound Healing in Rats. *Biomed. Pharmacother.* **2018**, *97*, 587–593. https://doi.org/10.1016/J.BIOPHA.2017.10.093.
33. Kassam, N.A.; Damian, D.J.; Kajeguka, D.; Nyombi, B.; Kibiki, G.S. Spectrum and Antibiogram of Bacteria Isolated from Patients Presenting with Infected Wounds in a Tertiary Hospital, Northern Tanzania. *BMC Res. Notes* **2017**, *10*, 19–21. https://doi.org/10.1186/s13104-017-3092-9.
34. Capoor, M.R.; Sarabahi, S.; Tiwari, V.K.; Narayanan, R.P. Fungal Infections in Burns: Diagnosis and Management. *Indian J. Plast. Surg.* **2010**, *43*, S37–S42. https://doi.org/10.1055/S-0039-1699460.
35. Soliman, S.; Alnajdy, D.; El-Keblawy, A.A.; Mosa, K.A.; Khoder, G.; Noreddin, A.M. Plants' Natural Products as Alternative Promising Anti-Candida Drugs. *Pharmacogn. Rev.* **2017**, *11*, 104–122. https://doi.org/10.4103/PHREV.PHREV_8_17.
36. Usach, I.; Margarucci, E.; Manca, M.L.; Caddeo, C.; Aroffu, M.; Petretto, G.L.; Manconi, M.; Peris, J.E. Comparison between Citral and Pompia Essential Oil Loaded in Phospholipid Vesicles for the Treatment of Skin and Mucosal Infections. *Nanomaterials* **2020**, *10*, 286. https://doi.org/10.3390/nano10020286.
37. Manconi, M.; Petretto, G.; D'hallewin, G.; Escribano, E.; Milia, E.; Pinna, R.; Palmieri, A.; Firoznezhad, M.; Peris, J.E.; Usach, I.; et al. Thymus Essential Oil Extraction, Characterization and Incorporation in Phospholipid Vesicles for the Antioxidant/Antibacterial Treatment of Oral Cavity Diseases. *Colloids Surfaces B Biointerfaces* **2018**, *171*, 115–122. https://doi.org/10.1016/j.colsurfb.2018.07.021.
38. Rahman, H.S.; Othman, H.H.; Hammadi, N.I.; Yeap, S.K.; Amin, K.M.; Samad, N.A.; Alitheen, N.B. Novel Drug Delivery Systems for Loading of Natural Plant Extracts and Their Biomedical Applications. *Int. J. Nanomed.* **2020**, *15*, 2439–2483. https://doi.org/10.2147/IJN.S227805.
39. Behyari, M.; Imani, R.; Keshvari, H. Evaluation of Silk Fibroin Nanofibrous Dressing Incorporating Niosomal Propolis, for Potential Use in Wound Healing. *Fibers Polym.* **2021**, *22*, 2090–2101. https://doi.org/10.1007/s12221-021-0973-2.
40. Allaw, M.; Manconi, M.; Caboni, P.; Bacchetta, G.; Escribano-Ferrer, E.; Peris, J.E.; Nacher, A.; Diez-Sales, O.; Manca, M.L. Formulation of Liposomes Loading Lentisk Oil to Ameliorate Topical Delivery, Attenuate Oxidative Stress Damage and Improve Cell Migration in Scratch Assay. *Biomed. Pharmacother.* **2021**, *144*, 112351. https://doi.org/10.1016/j.biopha.2021.112351.
41. Allaw, M.; Pleguezuelos-Villa, M.; Manca, M.L.; Caddeo, C.; Aroffu, M.; Nacher, A.; Diez-Sales, O.; Saurí, A.R.; Ferrer, E.E.; Fadda, A.M.; et al. Innovative Strategies to Treat Skin Wounds with Mangiferin: Fabrication of Transfersomes Modified with Glycols and Mucin. *Nanomedicine* **2020**, *15*, 1671–1685. https://doi.org/10.2217/nnm-2020-0116.
42. Mota, A.H.; Prazeres, I.; Mestre, H.; Bento-Silva, A.; Rodrigues, M.J.; Duarte, N.; Serra, A.T.; Bronze, M.R.; Rijo, P.; Gaspar, M.M.; et al. A Newfangled Collagenase Inhibitor Topical Formulation Based on Ethosomes with Sambucus Nigra l. Extract. *Pharmaceuticals* **2021**, *14*, 467. https://doi.org/10.3390/ph14050467.
43. Manconi, M.; Marongiu, F.; Castangia, I.; Manca, M.L.; Caddeo, C.; Tuberoso, C.I.G.; D'hallewin, G.; Bacchetta, G.; Fadda, A.M. Polymer-Associated Liposomes for the Oral Delivery of Grape Pomace Extract. *Colloids Surfaces B Biointerfaces* **2016**, *146*, 910–917. https://doi.org/10.1016/j.colsurfb.2016.07.043.
44. Wang, H.; Liu, M.; Du, S. Optimization of Madecassoside Liposomes Using Response Surface Methodology and Evaluation of Its Stability. *Int. J. Pharm.* **2014**, *473*, 280–285. https://doi.org/10.1016/j.ijpharm.2014.07.010.
45. Allaw, M.; Manconi, M.; Aroffu, M.; Marongiu, F.; Porceddu, M.; Bacchetta, G.; Usach, I.; Rached, R.A.; Rajha, H.N.; Maroun, R.G.; et al. Extraction, Characterization and Incorporation of Hypericum Scruglii Extract in Ad Hoc Formulated Phospholipid Vesicles Designed for the Treatment of Skin Diseases Connected with Oxidative Stress. *Pharmaceutics* **2020**, *12*, 1010. https://doi.org/10.3390/pharmaceutics12111010.
46. Pleguezuelos-Villa, M.; Diez-Sales, O.; Manca, M.L.; Manconi, M.; Sauri, A.R.; Escribano-Ferrer, E.; Nácher, A. Mangiferin Glycethosomes as a New Potential Adjuvant for the Treatment of Psoriasis. *Int. J. Pharm.* **2020**, *573*, 118844. https://doi.org/10.1016/j.ijpharm.2019.118844.
47. Nafisi, S.; Maibach, H.I. Nanotechnology in Cosmetics. In *Cosmetic Science and Technology: Theoretical Principles and Applications*; Elsevier Inc.: Amsterdam, The Netherlands, 2017; pp. 337–365.
48. Patzelt, A.; Lademann, J. Recent Advances in Follicular Drug Delivery of Nanoparticles. *Expert Opin. Drug Deliv.* **2020**, *17*, 49–60. https://doi.org/10.1080/17425247.2020.1700226.
49. Gattu, S.; Maibach, H.I. Enhanced Absorption through Damaged Skin: An Overview of the in Vitro Human Model. *Skin Pharmacol. Physiol.* **2010**, *23*, 171–176. https://doi.org/10.1159/000288163.
50. Un, R.N.; Barlas, F.B.; Yavuz, M.; Ag Seleci, D.; Seleci, M.; Gumus, Z.P.; Guler, E.; Demir, B.; Can, M.; Coskunol, H.; et al. Phyto-Niosomes: In Vitro Assessment of the Novel Nanovesicles Containing Marigold Extract. *Int. J. Polym. Mater. Polym. Biomater.* **2015**, *64*, 927–937. https://doi.org/10.1080/00914037.2015.1030663.

51. Jahanfar, S.; Gahavami, M.; Khosravi-Darani, K.; Jahadi, M.; Mozafari, M.R. Entrapment of Rosemary Extract by Liposomes Formulated by Mozafari Method: Physicochemical Characterization and Optimization. *Heliyon* **2021**, *7*, e08632. https://doi.org/10.1016/j.heliyon.2021.e08632.
52. Cui, H.; Li, W.; Li, C.; Vittayapadung, S.; Lin, L. Liposome Containing Cinnamon Oil with Antibacterial Activity against Methicillin-Resistant Staphylococcus Aureus Biofilm. *Biofouling* **2016**, *32*, 215–225. https://doi.org/10.1080/08927014.2015.1134516.
53. Risaliti, L.; Pini, G.; Ascrizzi, R.; Donato, R.; Sacco, C.; Bergonzi, M.C.; Salvatici, M.C.; Bilia, A.R. *Artemisia annua* Essential Oil Extraction, Characterization, and Incorporation in Nanoliposomes, Smart Drug Delivery Systems against Candida Species. *J. Drug Deliv. Sci. Technol.* **2020**, *59*, 101849. https://doi.org/10.1016/j.jddst.2020.101849.
54. Khogta, S.; Patel, J.; Barve, K.; Londhe, V. Herbal Nano-Formulations for Topical Delivery. *J. Herb. Med.* **2020**, *20*, 100300. https://doi.org/10.1016/j.hermed.2019.100300.
55. Ferraris, C.; Rimicci, C.; Garelli, S.; Ugazio, E.; Battaglia, L. Nanosystems in Cosmetic Products: A Brief Overview of Functional, Market, Regulatory and Safety Concerns. *Pharmaceutics* **2021**, *13*, 1408. https://doi.org/10.3390/pharmaceutics13091408.
56. Kashyap, N.; Kumari, A.; Raina, N.; Zakir, F.; Gupta, M. Prospects of Essential Oil Loaded Nanosystems for Skincare. *Phytomed. Plus* **2022**, *2*, 100198. https://doi.org/10.1016/j.phyplu.2021.100198.
57. Sebaaly, C.; Charcosset, C.; Stainmesse, S.; Fessi, H.; Greige-Gerges, H. Clove Essential Oil-in-Cyclodextrin-in-Liposomes in the Aqueous and Lyophilized States: From Laboratory to Large Scale Using a Membrane Contactor. *Carbohydr. Polym.* **2016**, *138*, 75–85. https://doi.org/10.1016/j.carbpol.2015.11.053.
58. Karatoprak, G.Ş.; Yücel, Ç.; Göger, F.; Sobarzo-Sánchez, E.; Küpeli Akkol, E. Potential Antioxidant and Enzyme Inhibitory Effects of Nanoliposomal Formulation Prepared from Salvia Aramiensis Rech. f. Extract. *Antioxidants* **2020**, *9*, 293. https://doi.org/10.3390/antiox9040293.
59. Nguyen, M.H.; Vu, N.B.D.; Nguyen, T.H.N.; Le, H.S.; Le, H.T.; Tran, T.T.; Le, X.-C.; Le, V.-T.; Nguyen, T.-T.; Bui, C.-B.; et al. In Vivo Comparison of Wound Healing and Scar Treatment Effect between Curcumin-Oligochitosan Nanoparticle Complex and Oligochitosan-Coated Curcumin-Loaded-Liposome. *J. Microencapsul.* **2019**, *36*, 158–168. https://doi.org/10.1080/02652048.2019.1612476.
60. Castangia, I.; Manca, M.L.; Caddeo, C.; Bacchetta, G.; Pons, R.; Demurtas, D.; Diez-Sales, O.; Fadda, A.M.; Manconi, M. Santosomes as Natural and Efficient Carriers for the Improvement of Phycocyanin Reepithelising Ability in Vitro and in Vivo. *Eur. J. Pharm. Biopharm.* **2016**, *103*, 149–158. https://doi.org/10.1016/j.ejpb.2016.03.033.
61. Fu, X.; Shi, Y.; Wang, H.; Zhao, X.; Sun, Q.; Huang, Y.; Qi, T.; Lin, G. Ethosomal Gel for Improving Transdermal Delivery of Thymosin β-4. *Int. J. Nanomed.* **2019**, *14*, 9275–9284. https://doi.org/10.2147/IJN.S228863.
62. Cristiano, M.C.; Mancuso, A.; Fresta, M.; Torella, D.; De Gaetano, F.; Ventura, C.A.; Paolino, D. Topical Unsaturated Fatty Acid Vesicles Improve Antioxidant Activity of Ammonium Glycyrrhizinate. *Pharmaceutics* **2021**, *13*, 548. https://doi.org/10.3390/pharmaceutics13040548.
63. Magnani, C.; Montis, C.; Mangiapia, G.; Mingotaud, A.F.; Mingotaud, C.; Roux, C.; Joseph, P.; Berti, D.; Lonetti, B. Hybrid Vesicles from Lipids and Block Copolymers: Phase Behavior from the Micro-to the Nano-Scale. *Colloids Surfaces B Biointerfaces* **2018**, *168*, 18–28. https://doi.org/10.1016/j.colsurfb.2018.01.042.
64. Duan, Y.; Wang, Y.; Li, X.; Zhang, G.; Zhang, G.; Hu, J. Light-Triggered Nitric Oxide (NO) Release from Photoresponsive Polymersomes for Corneal Wound Healing. *Chem. Sci.* **2020**, *11*, 186. https://doi.org/10.1039/C9SC04039K.
65. Moquin, A.; Ji, J.; Neibert, K.; Winnik, F.M.; Maysinger, D. Encapsulation and Delivery of Neutrophic Proteins and Hydrophobic Agents Using PMOXA-PDMS-PMOXA Triblock Polymersomes. *ACS Omega* **2018**, *3*, 13882–13893. https://doi.org/10.1021/acsomega.8b02311.
66. Liu, D.; Liao, Y.; Cornel, E.J.; Lv, M.; Wu, T.; Zhang, X.; Fan, L.; Sun, M.; Zhu, Y.; Fan, Z.; et al. Polymersome Wound Dressing Spray Capable of Bacterial Inhibition and H2S Generation for Complete Diabetic Wound Healing. *Chem. Mater.* **2021**, *33*, 7972–7985. https://doi.org/10.1021/acs.chemmater.1c01872.
67. El-Nabarawi, M.A.; Shamma, R.N.; Farouk, F.; Nasralla, S.M. Dapsone-Loaded Invasomes as a Potential Treatment of Acne: Preparation, Characterization, and In Vivo Skin Deposition Assay. *AAPS PharmSciTech* **2018**, *19*, 2174–2184. https://doi.org/10.1208/s12249-018-1025-0.
68. Hoque, M.; Agarwal, S.; Gupta, S.; Garg, S.; Syed, I.; Rupesh, A.; Mohapatra, N.; Bose, S.; Sarkar, P. Lipid Nanostructures in Food Applications. In *Innovative Food Processing Technologies: A Comprehensive Review*; Knoerzer, K., Ed.; Elsevier Inc.: Amsterdam, The Netherlands, 2021; pp. 565–579.
69. Barani, M.; Sangiovanni, E.; Angarano, M.; Rajizadeh, M.A.; Mehrabani, M.; Piazza, S.; Gangadharappa, H.V.; Pardakhty, A.; Mehrbani, M.; Dell'agli, M.; et al. Phytosomes as Innovative Delivery Systems for Phytochemicals: A Comprehensive Review of Literature. *Int. J. Nanomed.* **2021**, *16*, 6983–7022. https://doi.org/10.2147/IJN.S318416.
70. Demir, B.; Barlas, F.B.; Guler, E.; Gumus, P.Z.; Can, M.; Yavuz, M.; Coskunol, H.; Timur, S. Gold Nanoparticle Loaded Phytosomal Systems: Synthesis, Characterization and in Vitro Investigations. *RSC Adv.* **2014**, *4*, 34687–34695. https://doi.org/10.1039/c4ra05108d.
71. Mazumder, A.; Dwivedi, A.; Du Preez, J.L.; Du Plessis, J. In Vitro Wound Healing and Cytotoxic Effects of Sinigrin-Phytosome Complex. *Int. J. Pharm.* **2016**, *498*, 283–293. https://doi.org/10.1016/j.ijpharm.2015.12.027.

72. Kianvash, N.; Bahador, A.; Pourhajibagher, M.; Ghafari, H.; Nikoui, V.; Rezayat, S.M.; Dehpour, A.R.; Partoazar, A. Evaluation of Propylene Glycol Nanoliposomes Containing Curcumin on Burn Wound Model in Rat: Biocompatibility, Wound Healing, and Anti-Bacterial Effects. *Drug Deliv. Transl. Res.* **2017**, *7*, 654–663. https://doi.org/10.1007/s13346-017-0405-4.
73. Castangia, I.; Caddeo, C.; Manca, M.L.; Casu, L.; Latorre, A.C.; Díez-Sales, O.; Ruiz-Saurí, A.; Bacchetta, G.; Fadda, A.M.; Manconi, M. Delivery of Liquorice Extract by Liposomes and Hyalurosomes to Protect the Skin against Oxidative Stress Injuries. *Carbohydr. Polym.* **2015**, *134*, 657–663. https://doi.org/10.1016/j.carbpol.2015.08.037.
74. El-Refaie, W.M.; Elnaggar, Y.S.R.; El-Massik, M.A.; Abdallah, O.Y. Novel Curcumin-Loaded Gel-Core Hyaluosomes with Promising Burn-Wound Healing Potential: Development, in-Vitro Appraisal and in-Vivo Studies. *Int. J. Pharm.* **2015**, *486*, 88–98. https://doi.org/10.1016/j.ijpharm.2015.03.052.
75. Ibrahim, S.; Tagami, T.; Kishi, T.; Ozeki, T. Curcumin Marinosomes as Promising Nano-Drug Delivery System for Lung Cancer. *Int. J. Pharm.* **2018**, *540*, 40–49. https://doi.org/10.1016/j.ijpharm.2018.01.051.
76. Thomas, D.A.; Sarris, A.H.; Cortes, J.; Faderl, S.; O'Brien, S.; Giles, F.J.; Garcia-Manero, G.; Rodriguez, M.A.; Cabanillas, F.; Kantarjian, H. Phase II Study of Sphingosomal Vincristine in Patients with Recurrent or Refractory Adult Acute Lymphocytic Leukemia. *Cancer* **2006**, *106*, 120–127. https://doi.org/10.1002/cncr.21595.
77. Lopez, C.; Mériadec, C.; David-Briand, E.; Dupont, A.; Bizien, T.; Artzner, F.; Riaublanc, A.; Anton, M. Loading of Lutein in Egg-Sphingomyelin Vesicles as Lipid Carriers: Thermotropic Phase Behaviour, Structure of Sphingosome Membranes and Lutein Crystals. *Food Res. Int.* **2020**, *138*, 109770. https://doi.org/10.1016/j.foodres.2020.109770.
78. Tokudome, Y.; Uchida, R.; Yokote, T.; Todo, H.; Hada, N.; Kon, T.; Yasuda, J.; Hayashi, H.; Hashimoto, F.; Sugibayashi, K. Effect of Topically Applied Sphingomyelin-Based Liposomes on the Ceramide Level in the Three Dimensional Cultured Human Skin Model. *J. Liposome Res.* **2010**, *20*, 49–54. https://doi.org/10.3109/08982100903062597.
79. Kazemi, M.; Mombeiny, R.; Tavakol, S.; Keyhanvar, P.; Mousavizadeh, K. A Combination Therapy of Nanoethosomal Piroxicam Formulation along with Iontophoresis as an Anti-Inflammatory Transdermal Delivery System for Wound Healing. *Int. Wound J.* **2019**, *16*, 1144–1152. https://doi.org/10.1111/iwj.13171.
80. Partoazar, A.; Kianvash, N.; Darvishi, M.H.; Nasoohi, S.; Rezayat, S.M.; Bahador, A. Ethosomal Curcumin Promoted Wound Healing and Reduced Bacterial Flora in Second Degree Burn in Rat. *Drug Res.* **2016**, *66*, 660–665. https://doi.org/10.1055/s-0042-114034.
81. Lin, H.; Lin, L.; Choi, Y.; Michniak-Kohn, B. Development and In-Vitro Evaluation of Co-Loaded Berberine Chloride and Evodiamine Ethosomes for Treatment of Melanoma. *Int. J. Pharm.* **2020**, *581*, 119278. https://doi.org/10.1016/j.ijpharm.2020.119278.
82. Sguizzato, M.; Ferrara, F.; Mariani, P.; Pepe, A.; Cortesi, R.; Huang, N.; Simelière, F.; Boldrini, P.; Baldisserotto, A.; Valacchi, G.; et al. "Plurethosome" as Vesicular System for Cutaneous Administration of Mangiferin: Formulative Study and 3D Skin Tissue Evaluation. *Pharmaceutics* **2021**, *13*, 1124. https://doi.org/10.3390/pharmaceutics13081124.
83. Touitou, E.; Natsheh, H. Topical Administration of Drugs Incorporated in Carriers Containing Phospholipid Soft Vesicles for the Treatment of Skin Medical Conditions. *Pharmaceutics* **2021**, *13*, 2129. https://doi.org/10.3390/pharmaceutics13122129.
84. Rameshk, M.; Sharififar, F.; Mehrabani, M.; Pardakhty, A.; Farsinejad, A.; Mehrabani, M. Proliferation and In Vitro Wound Healing Effects of the Microniosomes Containing Narcissus Tazetta L. Bulb Extract on Primary Human Fibroblasts (HDFs). *DARU J. Pharm. Sci.* **2018**, *26*, 31–42. https://doi.org/10.1007/s40199-018-0211-7.
85. Priprem, A.; Damrongrungruang, T.; Limsitthichaikoon, S.; Khampaenjiraroch, B.; Nukulkit, C.; Thapphasaraphong, S.; Limphirat, W. Topical Niosome Gel Containing an Anthocyanin Complex: A Potential Oral Wound Healing in Rats. *AAPS PharmSciTech* **2018**, *19*, 1681–1692. https://doi.org/10.1208/s12249-018-0966-7.
86. Ou, N.; Sun, Y.; Zhou, S.; Gu, P.; Liu, Z.; Bo, R.; Hu, Y.; Liu, J.; Wang, D. Evaluation of Optimum Conditions for Achyranthes Bidentata Polysaccharides Encapsulated in Cubosomes and Immunological Activity in Vitro. *Int. J. Biol. Macromol.* **2018**, *109*, 748–760. https://doi.org/10.1016/j.ijbiomac.2017.11.064.
87. Morsi, N.M.; Abdelbary, G.A.; Ahmed, M.A. Silver Sulfadiazine Based Cubosome Hydrogels for Topical Treatment of Burns: Development and in Vitro/in Vivo Characterization. *Eur. J. Pharm. Biopharm.* **2014**, *86*, 178–189. https://doi.org/10.1016/j.ejpb.2013.04.018.
88. Thakkar, V.; Korat, V.; Baldaniya, L.; Gohel, M.; Gandhi, T.; Patel, N. Development and Characterization of Novel Hydrogel Containing Antimicrobial Drug for Treatment of Burns. *Int. J. Pharm. Investig.* **2016**, *6*, 158. https://doi.org/10.4103/2230-973X.187343.
89. Farag, D.B.E.; Yousry, C.; Al-Mahallawi, A.M.; El-Askary, H.I.; Meselhy, M.R.; AbuBakr, N. The Efficacy of Origanum Majorana Nanocubosomal Systems in Ameliorating Submandibular Salivary Gland Alterations in Streptozotocin-Induced Diabetic Rats. *Drug Deliv.* **2022**, *29*, 62–74. https://doi.org/10.1080/10717544.2021.2018522.
90. Gunal, M.; Ayla, S.; Caglayan, B.; Beker, M.; Bedri, N.; Aslan, I.; Ozdemir, E.; Kilic, E.Y. Can Carpobrotus Edulis, Heal Incisional and Excisional Wounds on the Skin? *Bratisl. Med. J.* **2021**, *112*, 912–917. https://doi.org/10.4149/BLL_2021_147.
91. Takahashi, M.; Kitamoto, D.; Asikin, Y.; Takara, K.; Wada, K. Liposomes Encapsulating Aloe Vera Leaf Gel Extract Significantly Enhance Proliferation and Collagen Synthesis in Human Skin Cell Lines. *J. Oleo Sci.* **2009**, *58*, 643–650. https://doi.org/10.5650/jos.58.643.
92. Di Cui, M.; Pan, Z.H.; Pan, L.Q. Danggui Buxue Extract-Loaded Liposomes in Thermosensitive Gel Enhance in Vivo Dermal Wound Healing via Activation of the VEGF/PI3K/Akt and TGF-β/Smads Signaling Pathway. *Evid.-Based Complement. Altern. Med.* **2017**, *2017*, 8407249. https://doi.org/10.1155/2017/8407249.

93. Manca, M.L.; Manconi, M.; Meloni, M.C.; Marongiu, F.; Allaw, M.; Usach, I.; Peris, J.E.; Escribano-Ferrer, E.; Tuberoso, C.I.G.; Gutierrez, G.; et al. Nanotechnology for Natural Medicine: Formulation of Neem Oil Loaded Phospholipid Vesicles Modified with Argan Oil as a Strategy to Protect the Skin from Oxidative Stress and Promote Wound Healing. *Antioxidants* **2021**, *10*, 670. https://doi.org/10.3390/antiox10050670.
94. Miranda, Í.K.S.P.B.; Santana, F.R.; Camilloto, G.P.; Detoni, C.B.; Souza, F.V.D.; de Cabral-Albuquerque, E.C.M.; Alves, S.L.; Neco, G.L.; de Lima, F.O.; de Assis, S.A. Development of Membranes Based on Carboxymethyl Cellulose/Acetylated Arrowroot Starch Containing Bromelain Extract Carried on Nanoparticles and Liposomes. *J. Pharm. Sci.* **2021**, *110*, 2372–2378. https://doi.org/10.1016/j.xphs.2021.02.031.
95. Jangde, R.; Singh, D. Preparation and Optimization of Quercetin-Loaded Liposomes for Wound Healing, Using Response Surface Methodology. *Artif. Cells Nanomed. Biotechnol.* **2016**, *44*, 635–641. https://doi.org/10.3109/21691401.2014.975238.
96. Oh, H.; Lee, J.S.; Sung, D.; Lim, J.M.; Choi, W. Il Potential Antioxidant and Wound Healing Effect of Nano-Liposol with High Loading Amount of Astaxanthin. *Int. J. Nanomed.* **2020**, *15*, 9231–9240. https://doi.org/10.2147/IJN.S272650.
97. Kontogiannopoulos, K.N.; Assimopoulou, A.N.; Hatziantoniou, S.; Karatasos, K.; Demetzos, C.; Papageorgiou, V.P. Chimeric Advanced Drug Delivery Nano Systems (Chi-ADDnSs) for Shikonin Combining Dendritic and Liposomal Technology. *Int. J. Pharm.* **2012**, *422*, 381–389. https://doi.org/10.1016/j.ijpharm.2011.09.031.
98. Caddeo, C.; Díez-Sales, O.; Pons, R.; Fernàndez-Busquets, X.; Fadda, A.M.; Manconi, M. Topical Anti-Inflammatory Potential of Quercetin in Lipid-Based Nanosystems: In Vivo and in Vitro Evaluation. *Pharm. Res.* **2014**, *31*, 959–968. https://doi.org/10.1007/s11095-013-1215-0.
99. Aldalaen, S.; Nasr, M.; El-Gogary, R.I. Angiogenesis and Collagen Promoting Nutraceutical-Loaded Nanovesicles for Wound Healing. *J. Drug Deliv. Sci. Technol.* **2020**, *56*, 101548. https://doi.org/10.1016/j.jddst.2020.101548.
100. Manca, M.L.; Castangia, I.; Zaru, M.; Nácher, A.; Valenti, D.; Fernàndez-Busquets, X.; Fadda, A.M.; Manconi, M. Development of Curcumin Loaded Sodium Hyaluronate Immobilized Vesicles (Hyalurosomes) and Their Potential on Skin Inflammation and Wound Restoring. *Biomaterials* **2015**, *71*, 100–109. https://doi.org/10.1016/j.biomaterials.2015.08.034.
101. Paolino, D.; Cosco, D.; Cilurzo, F.; Trapasso, E.; Morittu, V.M.; Celia, C.; Fresta, M. Improved in Vitro and in Vivo Collagen Biosynthesis by Asiaticoside-Loaded Ultradeformable Vesicles. *J. Control. Release* **2012**, *162*, 143–151. https://doi.org/10.1016/j.jconrel.2012.05.050.
102. Risaliti, L.; Kehagia, A.; Daoultzi, E.; Lazari, D.; Bergonzi, M.C.; Vergkizi-Nikolakaki, S.; Hadjipavlou-Litina, D.; Bilia, A.R. Liposomes Loaded with Salvia Triloba and Rosmarinus Officinalis Essential Oils: In Vitro Assessment of Antioxidant, Antiinflammatory and Antibacterial Activities. *J. Drug Deliv. Sci. Technol.* **2019**, *51*, 493–498. https://doi.org/10.1016/j.jddst.2019.03.034.
103. Andleeb, M.; Shoaib Khan, H.M.; Daniyal, M. Development, Characterization and Stability Evaluation of Topical Gel Loaded With Ethosomes Containing *Achillea millefolium* L. Extract. *Front. Pharmacol.* **2021**, *12*, 603227. https://doi.org/10.3389/fphar.2021.603227.
104. Pando, D.; Caddeo, C.; Manconi, M.; Fadda, A.M.; Pazos, C. Nanodesign of Olein Vesicles for the Topical Delivery of the Antioxidant Resveratrol. *J. Pharm. Pharmacol.* **2013**, *65*, 1158–1167. https://doi.org/10.1111/jphp.12093.
105. Barone, A.; Cristiano, M.C.; Cilurzo, F.; Locatelli, M.; Iannotta, D.; Di Marzio, L.; Celia, C.; Paolino, D. Ammonium Glycyrrhizate Skin Delivery from Ultradeformable Liposomes: A Novel Use as an Anti-Inflammatory Agent in Topical Drug Delivery. *Colloids Surfaces B Biointerfaces* **2020**, *193*, 111152. https://doi.org/10.1016/j.colsurfb.2020.111152.
106. Danaei, M.; Dehghankhold, M.; Ataei, S.; Hasanzadeh Davarani, F.; Javanmard, R.; Dokhani, A.; Khorasani, S.; Mozafari, M.R. Impact of Particle Size and Polydispersity Index on the Clinical Applications of Lipidic Nanocarrier Systems. *Pharmaceutics* **2018**, *10*, 57. https://doi.org/10.3390/pharmaceutics10020057.
107. Guimarães, D.; Cavaco-Paulo, A.; Nogueira, E. Design of Liposomes as Drug Delivery System for Therapeutic Applications. *Int. J. Pharm.* **2021**, *601*, 120571. https://doi.org/10.1016/j.ijpharm.2021.120571.
108. Tefas, L.R.; Sylvester, B.; Tomuta, I.; Sesarman, A.; Licarete, E.; Banciu, M.; Porfire, A. Development of Antiproliferative Long-Circulating Liposomes Co-Encapsulating Doxorubicin and Curcumin, through the Use of a Quality-by-Design Approach. *Drug Des. Devel. Ther.* **2017**, *11*, 1605–1621. https://doi.org/10.2147/DDDT.S129008.
109. Chang, C.J.; Kazemzadeh-Narbat, M. Innovation in Wound Care Products: A FDA Regulatory Perspective. *J. Wound Care* **2021**, *30*, S3–S4. https://doi.org/10.12968/JOWC.2021.30.SUP2.S3.
110. Boateng, J.S.; Matthews, K.H.; Stevens, H.N.E.; Eccleston, G.M. Wound Healing Dressings and Drug Delivery Systems: A Review. *J. Pharm. Sci.* **2008**, *97*, 2892–2923. https://doi.org/10.1002/JPS.21210.
111. Han, S.K. *Innovations and Advances in Wound Healing*; Springer: Berlin/Heidelberg, Germany, 2015; pp. 1–287.
112. Avachat, A.M.; Takudage, P.J. Design and Characterization of Multifaceted Lyophilized Liposomal Wafers with Promising Wound Healing Potential. *J. Liposome Res.* **2018**, *28*, 193–208. https://doi.org/10.1080/08982104.2017.1335319.
113. Rajendran, S. *Advanced Textiles for Wound Care*, 2nd ed.; Elsevier Ltd.: Amsterdam, The Netherlands, 2019; pp. 1–591.
114. Dunne, C.P.; Gouveia, I.C.; Isabel, C. Gouveia Designing New Antibacterial Wound Dressings: Development of a Dual Layer Cotton Material Coated with Polyvinyl Alcohol and Chitosan Nanofibers Incorporating *Agrimonia eupatoria* L. Extract. *Molecules* **2021**, *26*, 83.
115. Patel, S.; Srivastava, S.; Singh, M.R.; Singh, D. Preparation and Optimization of Chitosan-Gelatin Films for Sustained Delivery of Lupeol for Wound Healing. *Int. J. Biol. Macromol.* **2017**, *107*, 1888–1897. https://doi.org/10.1016/j.ijbiomac.2017.10.056.

116. Colobatiu, L.; Gavan, A.; Mocan, A.; Bogdan, C.; Mirel, S.; Tomuta, I. Development of Bioactive Compounds-Loaded Chitosan Films by Using a QbD Approach—A Novel and Potential Wound Dressing Material. *React. Funct. Polym.* **2019**, *138*, 46–54. https://doi.org/10.1016/j.reactfunctpolym.2019.02.013.
117. Sağıroğlu, A.A.; Çelik, B.; Güler, E.M.; Koçyiğit, A.; Özer, Ö. Evaluation of Wound Healing Potential of New Composite Liposomal Films Containing Coenzyme Q10 and D-Panthenyl Triacetate as Combinational Treatment. *Pharm. Dev. Technol.* **2021**, *26*, 444–454. https://doi.org/10.1080/10837450.2021.1887892.
118. Umar, A.K.; Sriwidodo, S.; Maksum, I.P.; Wathoni, N. Film-Forming Spray of Water-Soluble Chitosan Containing Liposome-Coated Human Epidermal Growth Factor for Wound Healing. *Molecules* **2021**, *26*, 5326. https://doi.org/10.3390/MOLECULES26175326.
119. Vedovatto, S.; Facchini, J.C.; Batista, R.K.; Paim, T.C.; Lionzo, M.I.Z.; Wink, M.R. Development of Chitosan, Gelatin and Liposome Film and Analysis of Its Biocompatibility in Vitro. *Int. J. Biol. Macromol.* **2020**, *160*, 750–757. https://doi.org/10.1016/j.ijbiomac.2020.05.229.
120. Eid, H.M.; Ali, A.A.; Ali, A.M.A.; Eissa, E.M.; Hassan, R.M.; El-Ela, F.I.A.; Hassan, A.H. Potential Use of Tailored Citicoline Chitosan-Coated Liposomes for Effective Wound Healing in Diabetic Rat Model. *Int. J. Nanomed.* **2022**, *17*, 555–575. https://doi.org/10.2147/IJN.S342504.

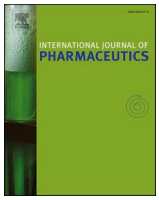
International Journal of Pharmaceutics 638 (2023) 122916



Contents lists available at ScienceDirect

International Journal of Pharmaceutics

journal homepage: www.elsevier.com/locate/ijpharm



Review



Texture analysis – A versatile tool for pharmaceutical evaluation of solid oral dosage forms

Cătălina Bogdan [a], Dana Hales [b,*], Andreea Cornilă [b], Tibor Casian [b], Rareș Iovanov [b], Ioan Tomuță [b], Sonia Iurian [b]

[a] Department of Dermopharmacy and Cosmetics, Faculty of Pharmacy, "Iuliu Haţieganu" University of Medicine and Pharmacy, 12 I. Creangă Street, 400010 Cluj-Napoca, Romania
[b] Department of Pharmaceutical Technology and Biopharmacy, Faculty of Pharmacy, "Iuliu Haţieganu" University of Medicine and Pharmacy, 41 V. Babes Street, 400012 Cluj-Napoca, Romania

ARTICLE INFO

Keywords:
Texture analysis
Solid oral dosage forms
Mechanical characterization
Mucoadhesion characterization
Disintegration time
In vitro – in vivo correlation

ABSTRACT

In the past few decades, texture analysis (TA) has gained importance as a valuable method for the characterization of solid oral dosage forms. As a result, an increasing number of scientific publications describe the textural methods that evaluate the extremely diverse category of solid pharmaceutical products. Within the current work, the use of texture analysis in the characterization of solid oral dosage forms is summarised with a focus on the evaluation of intermediate and finished oral pharmaceutical products. Several texture methods are reviewed regarding the applications in mechanical characterization, and mucoadhesion testing, but also in estimating the disintegration time and *in vivo* specific features of oral dosage forms. As there are no pharmacopoeial standards for pharmaceutical products tested through texture analysis, and there are important differences between reported results due to different experimental conditions, the choice of testing protocol and parameters is challenging. Thereby, this work aims to guide the research scientists and quality assurance professionals involved in different stages of drug development into the selection of optimal texture methodologies depending on the product characteristics and quality control needs.

1. Introduction

The oral route is by far the most frequently used in pharmacotherapy, due to the easy administration and varied release profiles that can be achieved (Awad et al., 2021). In recent years, the number of solid pharmaceutical forms for oral use has increased significantly as a response to some newly recognized therapy problems: the need for personalized treatment, doses, or drug release profiles, for specific combinations of active substances, or the need for easier administration to special groups of patients (Khan et al., 2022; Tidau and Finke, 2022; Wening and Breitkreutz, 2010). Several new dosage forms have emerged, such as orodispersible tablets (ODTs), oral lyophilisates, thin films, buccal tablets, 3D printlets with different disintegration or dissolution characteristics, minitablets, orodispersible minitablets (ODMTs), multiple layer tablets or compression coated tablets.

The texture is an important component of the sensory evaluation of any orally administered product. ISO 2008 defines it as "the combination of rheological and structure (geometrical and surface) attributes of a food product perceptible by means of mechanical, tactile, and where appropriate, visual and auditory receptors" ("ISO - ISO 5492:2008 - Sensory analysis — Vocabulary," n.d.; Schreuders et al., 2021). Particularly, since the appearance of dosage forms that maintain prolonged

Abbreviations: CQA, critical quality attribute; ISO, International Organization for Standardization; TPA, Texture Profile Analysis; TBI, Tablet Brittleness Index; IT, indentation test; PT, puncture test; TT, tensile test; FT, flexural test; CPs, composite particles; TA, texture analysis; HPMC, hydroxypropylmethylcellulose; OL, oral lyophilizate; API, active pharmaceutical ingredient; PVP, polyvinylpyrrolidone; ASTM, American Society for Testing and Materials; AUC, area under the curve; PEG, polyethylene glycol; HME, hot melt extrusion; PVA, polyvinyl alcohol; PLA, polylactic acid; PETG, polyethylene terephthalate glycol-modified; ABS, acrylonitrile butadiene styrene; CDI, Chewing Difficulty Index; CT, compression test; UTS, universal testing system; CM, creep meter; PEO, poly(ethylene oxide); HEC, hydroxyethylcellulose; 3PBT, three-point bend test; ODT, orodispersible tablet; MCC, microcrystalline celluose; MAP, mucoadhesion properties; IVIVC, *in vivo/in vitro* correlation; BT, buckling test; PLS, partial least squares.

* Corresponding author.
E-mail address: dudas.dana@umfcluj.ro (D. Hales).

https://doi.org/10.1016/j.ijpharm.2023.122916
Received 14 February 2023; Received in revised form 25 March 2023; Accepted 29 March 2023
Available online 4 April 2023
0378-5173/© 2023 Elsevier B.V. All rights reserved.

contact with the oral mucosa, texture has become a defining quality parameter in pharmaceutical development.

Quality control is essential for pharmaceutical product development to enable the marketing of products that meet the required quality, efficacy, and safety standards. Derived from the Quality Target Product Profile, each pharmaceutical product has a set of critical quality attributes (CQAs) of finite dosage forms or intermediate products whose assessment relies on corresponding characterization methods. The testing of CQAs requires the use of accurate and reproducible methods. Many of the characterization methods are found in the European Pharmacopiea in the chapter"2.9. Pharmaceutical technical procedures" and include procedures for physical characterization of finite dosage forms such as disintegration, dissolution, friability, resistance to crushing, consistency, etc, or intermediate products such as powder flow, particle surface area, particle size, particle size distribution, porosity and pore-size distribution, bulk and tapped density of powders, wettability etc (2.9. Pharmaceutical technical, n.d.). But many other characterization methods are currently used, reported in the literature, but not included in the Pharmacopiea. In this regard, TA is a simple methodology that enables the evaluation of mechanical features such as hardness, fracturability, elongation, flexibility, but also mucoadhesion properties of various solid orally administered dosage forms and their intermediate products. Thus far, a high number of experimental setups and procedures were reported in the literature to discriminate small variations in composition that impact the features of a particular material or dosage form.

Over the past years, there has been a considerable increase in the number of original articles that include methods for testing oral solid forms through TA. Thus, a brief literature search on the Web of Science database showed an approximately two-fold increase every past decade since the nineties, in the number of original research studies using this method (Fig. 1). Although TA has been used for many years to test newly developed products, to the best of the authors' knowledge, there is currently no review that summarizes the applications of TA in the evaluation of solid oral dosage forms.

The current paper focuses on the most important applications of TA in the evaluation of intermediate and finished oral pharmaceutical products. The in-depth analysis of the texture methods allows a thorough selection of parameters and perfecting TA methods to grant the optimal features of the product under development but also to reduce the development time. In consequence, the addressability of this review paper envisages research scientists, academia, and quality assurance professionals involved in different stages from early formulation design to research and development activities, and routine quality control in the pharmaceutical industry. The first part provides a short summary of the principles of TA with a focus on the technical parameters of different texture analyzers. Further, the tests and the parameters for the assessment of mechanical and mucoadhesion properties are discussed together with several applications of TA in the characterization of oral dosage forms. Emerging applications of TA in estimating the disintegration time and *in vivo* specific features of oral dosage forms are also discussed.

2. General principles of TA

TA was first used in the food industry for quality assessment and comparison of food products, in a reproducible manner, following a standardized procedure and often replacing sensory evaluation on human volunteers (Chen and Opara, 2013; Foegeding and Drake, 2007). This was made possible by the large number of accessories developed specifically for the particularities of food products, intending to simulate the handling of the product by the end user.

The determination of textural features is a physical test mainly based on bulk destruction and shear deformation (Prakash et al., 2013). TA is a mechanical method that relies on compressing, shearing or pulling the sample. Most frequently used, compression tests involve the uniaxial penetration of the probe into a product, up to a stipulated force, distance or deformation. Single-cycle or double-cycle compression tests are available, the latter known as Texture Profile Analysis (TPA), which were designed to mimic the mastication movement in the oral cavity.

Texture analyzers are composed of a sample holder or fixture located on a base plate and a mobile arm that allows vertical movement at a controlled speed or load (Fig. 2). The mobile arm can accommodate various types of probes depending on the sample features and the required measurements, whereas the samples can be either placed on the fixture plane, in special sample holders or even attached to the probe. The arm is connected to a load cell that measures the force opposed by the sample to the descent or ascent of the probe. Alternatively, the load cell can be set to maintain a specific load and record the probe position changes. Through deformation or even complete failure, TA methods are usually destructive, which can be regarded as their major limitation (Schreuders et al., 2021). As a result, data is gathered into texture profiles, representing load/force as a function of the time or the distance travelled by the probe into the sample. Texture profiles can be analysed and compared as such, or various parameters can be calculated for the sample characterization.

The parameters that describe the characteristics of the equipment and their variation limits are summarized in Table 1, based on the data published by two of the most important equipment manufacturers. The parameters are often connected to each other, for example high load cell equipment usually display low load resolution, while small load cells are more sensitive and able to apply high resolution loads. The maximum test speed also varies for different load cell capacities (CT3 Texture Analyzer, Ametek Brookfield," n.d.; TA.XTplus , n.d.).

Texture analyzers can be operated in many different ways depending on the chosen test parameters. As texture applications evolve, accurate and detailed descriptions of the methodology become increasingly important, because different conditions lead to variable results. Table 1 includes the most important testing variables along with their

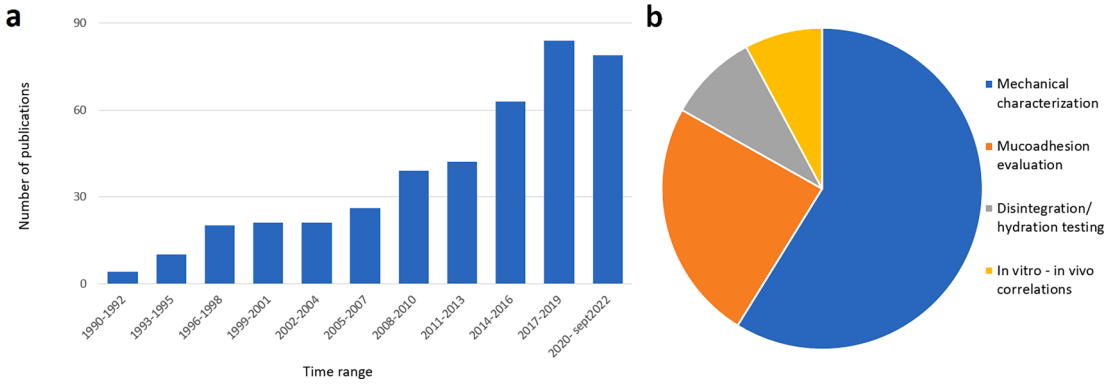


Fig. 1. Literature search results displayed as: a, number of publications per three years time range and b, TA applications.

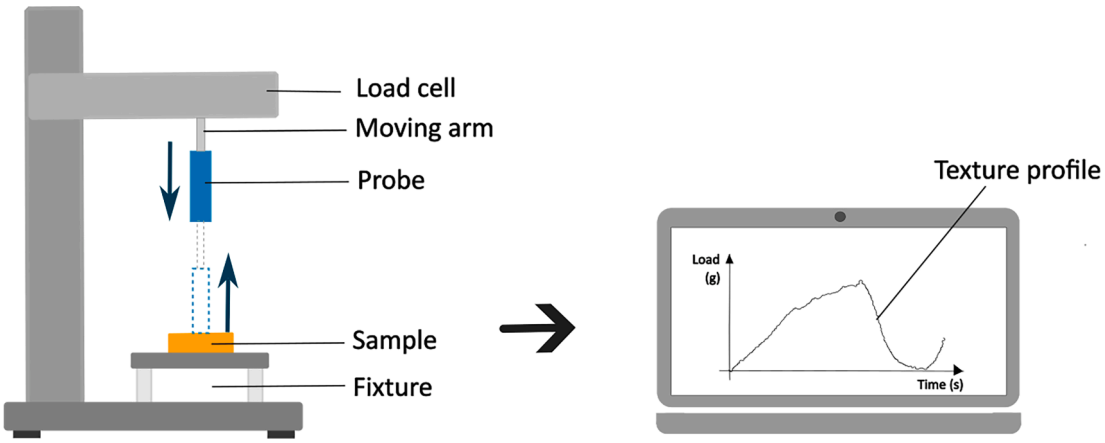


Fig. 2. Basic principle of texture analysis.

Table 1
Technical features of texture analyzers.

Equipment characteristics		Ref
Load cell capacity (kg.f)	0.1 – 750	("CT3 Texture Analyzer, Ametek Brookfield," n.d.; TA.XTplus , n.d.
Speed range (mm/s)	0.01 – 40	
Distance resolution (mm)	0.0005 – 0.001	
Data rate (pps)	500 – 2000	(TA.XTplus , n.d.)
Testing parameters		
The type of test	Compression/ Puncture/ Tensile/ Adhesion/ Fracture/ TPA	
The probe and fixture		
Test speed (mm/s)	The speed of the probe during the test	
Trigger load (g)	The load at which the test starts, meaning the instrument starts applying the set load or test speed and records the results	
Hold time (s)	Time length of contact between the probe and the sample	
Target load (g)	The load at which the test stops, and the probe returns to base	
Temperature (°C)	The temperature of the liquid media or the substrate that encounters the sample during the test	

definitions. When initiating a test, researchers must choose the test type and the accessories. The probes and fixtures that compose the experimental setups are actively developing in row with the numerous dosage forms and their needs. Further, the choice of testing parameters is not always straightforward, and strongly depends on the sample structure and on the desired outcome. For example, the test speed may not impact the results of a measurement that only targets the breaking force of a product but could be vital for a measurement on a hydrating or a disintegrating product. High values of the trigger load are acceptable for dense, hard structures, however, could lead to information loss when used with fragile, porous structures (Hackl and Ermolina, 2016). While most of the tests are performed at room temperature, when the tests aim *in vitro - in vivo* correlations, physiological temperature could be more appropriate.

3. TA in mechanical characterization

3.1. Tests and mechanical parameters

Mechanical characterization can be conducted through different types of tests such as compression, indentation, puncture, flexural or tensile tests, as described below. The mechanical parameters derived from the tests are listed in Table 2.

3.1.1. Compression tests (CT)

CT are the most common among those performed on pharmaceutical products and can be applied on a wide range of samples, from soft (Chachlioutaki et al., 2022) to hard (Oladeji et al., 2022) and from porous (Farias and Boateng, 2020) to dense materials (Fell and Newton, 1970). Flat cylindrical probes of different diameters compress the sample down to a certain distance, deformation or to complete structure failure (Fig. 3a).

For example, mechanical characterization of tablets frequently involves diametral CT, and their tensile strength is determined as described by Fell and Newton (Fell and Newton, 1970) or by using adapted formulas depending on the characteristics of the sample, as shown in Table 2. Variants of the diametral CT include the flattened Brazilian disc test (Mazel et al., 2016) and the diametral CT performed on tablets with perforated centers (Croquelois et al., 2017, 2020), which operate with certain adaptations of the aforementioned formula.

Out of the force/displacement curve certain parameters can be extrapolated, including the Tablet Brittleness Index (TBI) (Paul et al., 2021) used to determine the tabletability of an excipient mixture in tablet formulation development (de Backere et al., 2022; Dun et al., 2020; Gong and Sun, 2015; Paul and Sun, 2018).

Diametral CT also allow the determination of Young's modulus, calculated as the slope of the ascending portion of the stress/strain curve, and the elongation at the breakpoint, equal to the strain suffered by the material at the highest stress point (rupture stress) (Partheniadis et al., 2022). If the Poisson's ratio of the material is known, the Young's modulus can be extracted from the elastic deformation part of the curve (Flügel et al., 2020). Parameters such as the total load or hardness can easily be computed, as well as the total work and fracturability calculations that rely on the assessment of sudden load drops.

3.1.2. Indentation tests (IT)

IT assess the hardness of materials to deformation, by indenting the samples until an impression is formed at their contact area with the probe (Fig. 3b). They allow the determination of indentation hardness as well as of Young's modulus (Oliver and Pharr, 2004). Axial CT may complete the mechanical characterization as the force is applied on the surface of the tablets either with flat or with spherical indentation probes such as in the case of the Brinell Hardness test (Basim et al., 2019; Patel and Sun, 2016). IT can be used in the mechanical characterization of several dosage forms that are prone to deformation, however, they are rather specific to specimens in which the probe can reach a certain depth without passing through the sample.

3.1.3. Puncture tests (PT)

For thinner materials such as polymeric films, the PT has been developed as an adaptation of both mechanical and TT, aiming to

Table 2
Parameters derived from mechanical testing using TA.

	Equation	Parameter explanation	Observations	Reference
Diametral CT				
Tensile strength (σ)	$\sigma = \frac{2 \bullet P}{\pi \bullet D \bullet t}$	P – load applied to the tablet before it breaks D – diameter T – thickness	Described by Fell and Newton	(Fell and Newton, 1970)
	$\sigma = \frac{F_C \bullet D}{2 \bullet V_{eq}}$	Fc – diametrical breaking force Veq – the equivalent volume of the powder compact, calculated as a function of the tablet diameter and total thickness and the diameter and the volume of the cup in which the powder compact has been formed	For solid monolithic dosage forms without flat surfaces	(Mitra et al., 2015)
	$\sigma_{convex} = \frac{10 \bullet F}{\pi \bullet D^2}\left(\frac{2.84 \bullet H}{D} - \frac{0.126 \bullet H}{W} + \frac{3.15W}{D}\right)^{-1}$	D – diameter H – thickness of the entire tablet W – thickness of the flat-faced central segment	Convex-faced tablets with a specific width to diameter ratio	(Pitt et al., 1989)
Tablet Brittleness Index (TBI)	$TBI = \frac{1}{MES} = \frac{D}{MED}$	D – diameter MES – maximum elastic strain MED – maximum elastic deformation	Maximum elastic strain and deformation can be extrapolated from the force vs. displacement curve	(de Backere et al., 2022; Gong and Sun, 2015)
Young's modulus	$F_{el} = \frac{\pi hsE}{8(1-\nu^2)}$	F_{el} – force applied during the elastic deformation of the product h – specimen height s – displacement of the die during the elastic deformation process E – Young's modulus of the material ν – Poisson's ratio of the material	For materials with known Poisson's ratio	(Antonyuk et al., 2011; Flügel et al., 2020)
Indentation Tests (IT)				
Indentation hardness	$H = \frac{Pmax}{A}$	H – indentation hardness Pmax – maximum load A – projected contact area	Uses a wedge indenter	(Flügel et al., 2020; Oliver and Pharr, 2004)
Young's modulus	$S = \beta \bullet \frac{2}{\sqrt{\pi}} \bullet E_{eff} \bullet \sqrt{A}$	S – stiffness of the material β – dimensionless parameter specific to the type of indenter A – projected contact area E_{eff} – effective Young's modulus ν – Poisson's ratio of the sample E – Young's modulus of the sample νi – Poisson's ratio of the indenter Ei – Young's modulus of the indenter	Stiffness represents the slope of the initial segment of the unloading curve, β accounts for stiffness inconsistencies	(Flügel et al., 2020; Oliver and Pharr, 2004)
Tensile strength (σ)	$\sigma = \frac{F}{\pi r^2}$	F – maximum load applied to the tablet r – radius of the tablet	Axial CT	(Chang and Sun, 2019)
Hardness	$H = \frac{F}{A}$	F – the force applied to the surface of the tablet A – the projected area of the indent made into the tablet	Brinell hardness test Uses a spherical indentation probe	(Basim et al., 2019; Patel and Sun, 2016)
Puncture tests (PT)				
Puncture strength (PS)	$PS = \frac{F}{A_c} A_c = 2rh$	F – force needed to puncture the film sample A_c – cross-sectional area of the edge of the film located in the path of the cylindrical opening of the film holder r – radius of the hole h – mean thickness of the film	For film samples	(Kajthunyakarn et al., 2019; Peerapattana et al., 2015; Rongthong et al., 2013; Szabó et al., 2013)
Breaking factor (BF)	$BF = \frac{F_{max}}{h}$	F_{max} – puncture force h – film thickness		(Alaei et al., 2021)
Elongation at puncture (EAP, %)	$EAP\% = \frac{\sqrt{r^2 + D_T^2} - r}{r} \bullet 100$	D_T - displacement of the probe from the point of contact to the point of puncture r – radius of the hole		(Alaei et al., 2021; Kajthunyakarn et al., 2019; Peerapattana et al., 2015)
Energy to puncture (EP)	$EP = \frac{AUC}{SV}$	AUC – the area under the stress/strain or the force vs. displacement curve SV – sample volume		(Alaei et al., 2021; Preis et al., 2014b)
Young's modulus/ Elastic modulus (E)	$E = \frac{SL}{h \bullet CS}$	SL – slope of stress–strain curve in linear region h – thickness of the film CS – cross-head speed	Indicates the stiffness of a sample	(Alaei et al., 2021)
	$E = \frac{PS}{EAP\%}$	PS – puncture strength EAP – elongation at puncture		(Ciper and Bodmeier, 2005; Limmatvapirat et al., 2008; Peerapattana et al., 2015)
	$E = \frac{L_0}{A} \bullet S$	E – Young's modulus S – slope of force–deformation curve		(Baranauskaite et al., 2022)
Tensile tests (TT)				
Tensile strength (TS)	$TS = \frac{Fmax}{A}$	Fmax – maximum force A – cross-sectional area	The cross-sectional area is calculated from the characteristics of the filament or film	(Baranauskaite et al., 2022)

(*continued on next page*)

Table 2 (*continued*)

	Equation	Parameter explanation	Observations	Reference
Elongation at break (EAB, %)	$EAB\% = \frac{Lmax}{L_0} \bullet 100$	L_{max} – maximum length before breaking L_0 – initial length		(Baranauskaite et al., 2022)
Energy to break (EP)	$EP = \frac{AUC}{SV}$	AUC – the area under the force vs. displacement curve SV – sample volume		(Alaei et al., 2021; Preis et al., 2014b)
Flexural tests (FT)				
Flexural stress (σ_f)	$\sigma_f = \frac{F \bullet L}{\pi \bullet R^3}$	F – force needed to break the sample L – the size of the gap between the bending points R – radius of the analyzed specimen	Data from the 3PBT of filaments or other cylindrical samples	(Prasad et al., 2019; Samaro et al., 2021)
Flexural strain (ε_f)	$\varepsilon_f = \frac{600 \bullet s \bullet h}{L^2}$	s – deflection h – thickness of the analyzed specimen L – the size of the gap between the bending points		(Prasad et al., 2019; Samaro et al., 2021)
Flexural stress (σ_f)	$\sigma_f = \frac{3 \bullet F_f \bullet L}{2 \bullet D \bullet H}$	F_f – the force needed to break the tablet L – size of the gap between the bending points D – diameter of the tablet h – height of the tablet	Data from the 3PBT for tablets	(Rodríguez-Pombo et al., 2022)
	$\sigma_f = \frac{3 \bullet F_f \bullet L}{2 \bullet W \bullet H^2}$	F_f – the force needed to break the sample L – size of the gap between the bending points W – width of the specimen H – height of the specimen	Data from the 3PBT for rectangular specimens	(Chachlioutaki et al., 2022; Shumeyko et al., 2019)
Stiffness	$Stiffness = \frac{F}{\delta}$	F – applied force δ – deformation	Variant of the 3PBT	(Hu et al., 2022)

determine the force required to pierce the sample, thus its definitive and irreversible deformation. The setup for this test involves the use of a narrow cylindrical probe with a pointed or rounded contact area, along with a system that neatly fixes the specimen in horizontal position, while also allowing the needle probe to pass entirely through it (Fig. 3c) (Alaei et al., 2021; Kajthunyakarn et al., 2019; Peerapattana et al., 2015; Rongthong et al., 2013). Force-displacement profiles reveal parameters such as the maximum force used to calculate puncture strength. Further, elongation at puncture and energy to puncture can be determined, as well as the elastic modulus from the linear part of the stress–strain curve.

3.1.4. Tensile tests (TT)

TT measure the resistance of a product against a pulling force. The sample is usually placed vertically and attached on both sides with clamps or glued to the fixture and the probe (Fig. 3d). Such tests are frequently applied for products presenting certain flexibility, such as films or 3D printing filaments. Like PT, parameters such as tensile strength and elongation can be determined from the force–displacement or stress–strain curves, as well as the elastic modulus from the angular coefficient of the linear part of the profile. Although PT and TT lead to equivalent calculated parameters, some authors suggested that both should be applied as they complement each other in highlighting differences in the sample deformation mechanism (Radebaugh et al., 1988; Walicová et al., 2016).

3.1.5. Flexural tests (FT)

FT are meant for samples that display a certain flexibility, usually shaped as strips, bars or sticks. The 3-point bending test (3PBT) is a common method used in mechanics that involves a force applied perpendicularly to the middle of the sample placed horizontally on a fixture with two excentric arms (Fig. 3e). It became part of a battery of tests referred as Repka-Zhang methods for hot melt extruded (HME) filament characterization that included a first 3PBT in specified conditions, to determine flexibility. The buckling test (BT), also denoted as the resistance test (Xu et al., 2020) assumed the application of a force on the sample placed vertically into a cylindrical perforated sample holder (Fig. 3f). Most of the researchers reported parameters such as flexural strength, breaking distance or maximum stress, revealed by the texture profiles (Table 2). However, others defined parameters that better express the characteristics of the samples, such as brittleness, resistance, and toughness, calculated from the areas under the curves of the stress–strain profiles (Xu et al., 2020).

3.1.6. Texture profile analysis (TPA)

As TA was first designed to characterize foodstuff, the TPA is the most commonly used as a two-cycle CT. It is aimed to simulate mastication movements and forces (Chatzitaki et al., 2022) and is frequently used to evaluate chewable dosage forms. Samples are placed on a plane holder and compressed twice with a flat cylindrical probe whose diameter usually exceeds the size of the sample. Results are expressed as force–time profiles, out of which several parameters can be extracted, such as hardness which is linked to the force needed for the first bite. Cohesiveness, a measurement of how the material withstands the second compression cycle, considering the deformation already made in the first cycle, is related to a product's ability to withstand deformation when being chewed. Springiness is the ability of the material to go back to its original height between the two compression cycles and was reported to correlate to the elasticity of semi-solids, while adhesiveness (a measure of stickiness) and gumminess were accounted for the effort required for disintegration and breakage in the mouth (Chatzitaki et al., 2022). Chewiness is a parameter that could be associated with the difficulty to chew according to its mathematical definition, high values are obtained for hard, cohesive, and elastic materials (Texture Profile Analysis, n.d.).

3.2. Applications of TA in mechanical characterization

3.2.1. Raw materials

TA is known to be useful in the mechanical characterization of finished pharmaceutical products, but it was also reported in preformulation studies aimed at a better understanding of the properties of raw or processed material. For example, Flugel et al. aimed to study the effects of aging and structural relaxation on the mechanical properties of amorphous solid dispersions with a possible impact on compression behaviour. They applied both diametrical CT and IT to calculate and compare Young's modulus. The structural relaxation of amorphous material with ageing determined the increase of indentation hardness and Young's modulus derived from both tests, which translated into higher stiffness and resistance against elastic and plastic deformation. The results had a practical relevance as the tabletting performance

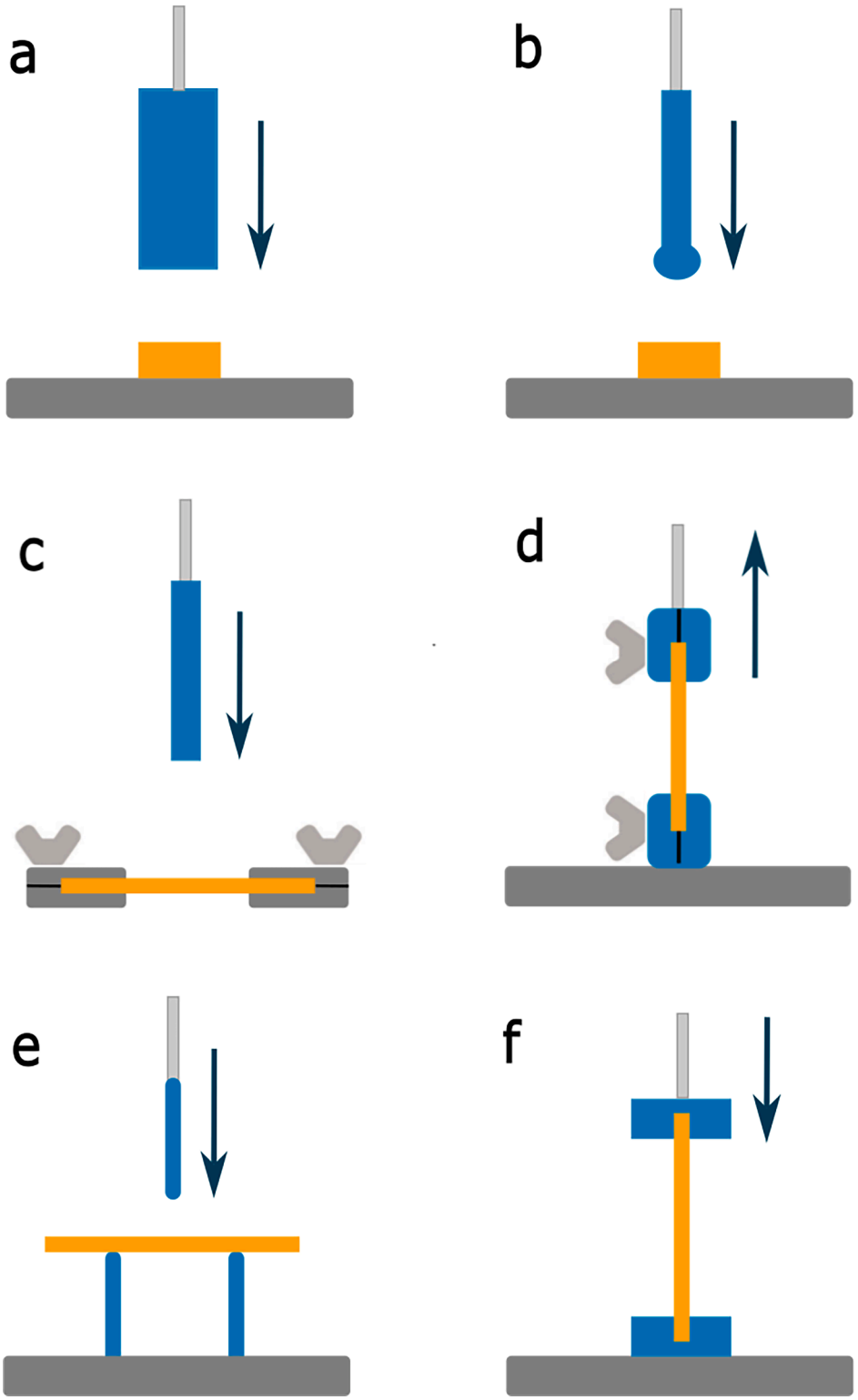


Fig. 3. Mechanical tests for different pharmaceutical products: principles and fixtures (a, compression test (CT); b, indentation test (IT); c, puncture test (PT); d, tensile tests (TT); e, 3-point bending test (3PBT); f, buckling test (BT); the sample is represented in orange). (For interpretation of the references to colour in this figure legend, the reader is referred to the web version of this article.)

of the materials worsened with time (Flügel et al., 2020). Zhou studied the impact of cocrystals of resveratrol with 4-aminobenzamide and isoniazid on the tabletability compared to their physical mixtures and to that of pure substances (Zhou et al., 2016).

In the attempt to optimize granulation, as it is known that both formulation and process parameters impact granules properties, Liu et al. measured granule‘s hardness on 30 granules per formulation for statistical reliability (Liu et al., 2022). Other researchers investigated the TPA characteristics of composite particles (CPs) of a natural extract and the stress–strain profiles of the resulting tablets and correlated them to the compactibility results to understand the functional properties of the CPs (Zhang et al., 2021). Electrospun nanofiber mats were tested for

Young's modulus, elongation at rupture and rupture stress, parameters which were further correlated to compaction measurements by means of Principal Component Analysis, and revealed good ability of TA to compare and distinguish between products (Partheniadis et al., 2022). Therefore, the particle behaviour studied through TA facilitated a better understanding of their subsequent processability aimed at obtaining solid dosage forms.

3.2.2. Tablets

One of the critical quality attributes of solid dosage forms is tensile strength. The diametrical force required for breaking is a standard test necessary as routine analysis for the determination of tensile strength of tablets, mini-tablets, and micro-tablets and can be measured using a texture analyzer equipped with a high-load cell (Basim et al., 2019; Bhatt et al., 2020; Chen et al., 2022, 2019; Croquelois et al., 2017; Dun et al., 2018; Hagen et al., 2016; Lura et al., 2021; Mazel et al., 2018; Meruva et al., 2021; Rai et al., 2012; Vreeman and Sun, 2022a). The test

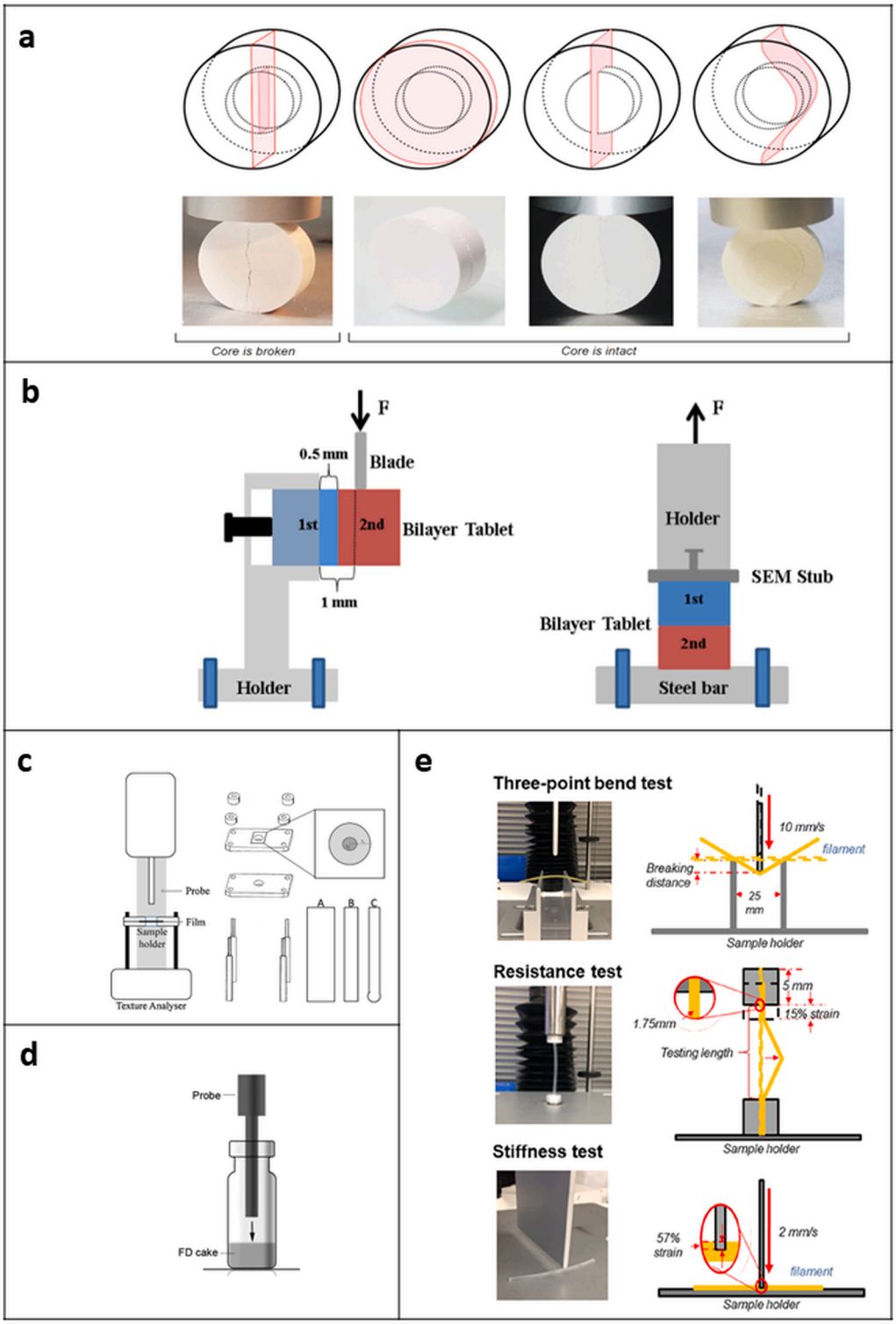


Fig. 4. Examples of experimental setups using texture analysers for the evaluation of: a, tablets through diametral compression tests (Reprinted with permission from Picart et al. (2022)); b, interfacial bonding strength of bilayer tablets (Reprinted with permission from Chang et al. (2017)); c, orodispersible films through puncture tests (Reprinted with permission from Preis et al. (2014b)); d, freeze-dried cakes in vials (Reprinted with permission from Hackl et al. (2016)); e, hot-melt extruded filaments through three different tests (Reprinted with permission from Xu et al. (2020)).

provides insight on the tablet behaviour through manufacturing stages, handling, packaging and transport, and tensile strength values comprised between 1.7 and 2 MPa are generally considered acceptable (Pitt and Heasley, 2013; Sabri et al., 2018). Many researchers plotted tensile strength versus compaction pressure to get insight on tabletability which contributes to preformulation knowledge and scale transfer (Lura et al., 2021, 2020; Perumalla and Sun, 2014; Vreeman and Sun, 2022a).

A more comprehensive material analysis can include plotting the force–displacement curve resulting from the diametrical fracture test that yields the maximum elastic deformation of a tablet with the further determination of TBI as friability indicator (de Backere et al., 2022; Gong and Sun, 2015; Paul and Sun, 2018). Gong and Sun applied two TA methods, a strain-based approach that led to the breakage of the tablet and an energy-based approach that avoided tablet breakage and allowed recovery measurements and came up with a total of 18 means to calculate TBI. Out of them, the best TBI as friability predictor was the reciprocal form of the elastic strain, which is convenient as it does not need additional experiments besides the diametrical breaking test (Gong and Sun, 2015). Further, Zhao et al. proposed an alternative parameter based on the previously demonstrated association between friability and diametrical deformation, as the ratio between the maximum strain and the maximum stress, called Strain/Stress Max (Zhao et al., 2022).

The gradient of the force–displacement curve can be assessed for the determination of Young's modulus, while the area under the curve can be associated to the tablet toughness defined as "the property of a tablet to absorb energy in the plastic region" (Sabri et al., 2018).

To investigate breakage phenomena in biconvex tablets and press-coated tablets, diametral CT were applied using systems equipped with cameras that captured the exact moment of tablet failure and contributed to the categorizing of the types of failures, as shown in Fig. 4a (Mazel et al., 2018; Picart et al., 2022).

Air entrapment during compression is one of the main reasons for tablet failure through lamination. To investigate the effect of deaeration through pre-compression on tablet quality, Vreeman et al. performed diametral crushing tests by TA, and measured the breaking forces instead of tensile strength for tablets that laminated with no diametrical breakage (Vreeman and Sun, 2022b).

Basim et al. used a spherical indentation probe to apply a 40 N force normal to the tablet plane and calculated the Brinell hardness, a material deformation-dependent parameter used to estimate tablet capping (Basim et al., 2019).

As solid material behavior under compression is a continuous concern of tablet formulation teams, Bonacucina et al. demonstrated that TA can be used to complement the information revealed by dynamic compression analysis fitted to Heckel equation. They performed two additional tests, for creep and stress vs. strain under static porosity conditions which enabled the determination of viscosity and elastic moduli and provided an optimal understanding of the material (Bonacucina et al., 2007). Zhang et al. performed TA on nano-silica modified plant extract powders as well as indentation and diametral CT on the resulting tablets and revealed that powder texture parameters are good indicators of tablet texture (Zhang et al., 2022c; Zhang et al., 2021).

As hardness testers only yield the force required for breakage, authors that needed more information on tablet failure performed TA to be able to distinguish between the compression and fragmentation phases. For instance, Rahman et al. compared force-distance curves of abuse deterrent Polyox tablet formulations to highlight the effects of polymer content and curing on the crushing resistance that could impact further manipulation (Rahman et al., 2017).

For mini-tablets, TA with diametrical CT seems to be the method of choice for the tensile strength evaluation, as the small sizes 1 – 3 mm hinder the use of conventional hardness testers (Hagen et al., 2016; Kottke et al., 2021; Kuck and Breitkreutz, 2022; Lura et al., 2021; Lura and Breitkreutz, 2022).

In what the mechanical characteristics of bilayer tablets are concerned, the achievement of sufficient interfacial bonding strength conditions their industrial production. In the attempt to develop standardized tests for the interfacial bonding strength evaluation, researchers tried to simulate the forces to which the tablets are subjected during handling and transport (Chang et al., 2017; Chang and Sun, 2019). Using a texture analyzer, a shear force parallel to the bilayer interface was applied for the shear method, on the tablet fixed vertically in a sample holder. The same authors applied a tensile method which involved a tensile force applied perpendicularly to the bilayer interface when tablets were placed horizontally on the fixture and glued on both sides to the fixture and the probe. Both setups are displayed in Fig. 4b. They showed that shear method results depend on tablet orientation and on the exact alignment of the sample holder at the interface, while the tensile method though time-consuming, does not depend on tablet orientation (Chang et al., 2017). Further, the developed tensile method allowed the understanding of the influence of particle size on the interfacial bonding strength in view of improving the mechanical characteristics of bilayer tablets (Chang and Sun, 2019).

Chewable gel tablets are usually evaluated applying TPA tests that are better correlated to mastication-related phenomena compared to other tests (Chatzitaki et al., 2022; Matulyte et al., 2021a, 2021b). Matulyte et al. determined the firmness, springiness, hardness, and stickiness of the products to assess the way formulation factors affect their quality after preparation and to investigate the changes occurred in one month (Matulyte et al., 2021a, 2021b).

3.2.3. Capsules

For capsules, equipment producers offer a special accessory to perform a TT and measure the force necessary to break a capsule. Machado et al. investigated the effects of lipid-based formulations with varying amounts of water on the integrity and mechanical properties of both gelatin and HPMC capsules to guide formulators in the development of robust liquid-filled capsules (Machado et al., 2016).

3.2.4. Oral lyophilisates (OLs)

TA is usually preferred for the evaluation of freeze-dried wafers because their porous structure and frailty makes conventional hardness testers use impractical (Vanbillemont et al., 2020) due to the high plastic deformation with no radial cracking. For OL mechanical testing, CT are usually applied to OLs down to a certain depth or deformation. Most of the authors chose to measure hardness and/or fracturability (Farias and Boateng, 2020) as they correlate them to the ease of handling and product integrity, or to simply compare load vs. distance profiles (Iurian et al., 2017a, 2017b). Hardness values between 3 and 6 N were considered appropriate (Boateng et al., 2010).

Additionally, other authors highlighted the importance of the relaxation phenomena that occur after removing the compressive force, depending on the penetration depth and quantified them as a compaction index (Boateng et al., 2010; Iftimi et al., 2019). Vanbillemont et al. applied an IT to determine the indentation hardness parameter that proved good discriminatory capacity between the commercial OLs. In addition to that, elastic recovery was also calculated and regarded as an indicator of behaviour upon unblistering (Vanbillemont et al., 2020). The same tests were further used in a study that aimed the development of OLs based on polyvinyl alcohol (PVA) loaded with a low-dose API (hydrochlorothiazide) and a high-dose active pharmaceutical ingredient (API) (paracetamol) through DoE methodology (Vanbillemont and de Beer, 2020).

To shorten the initial stages of OL development, Hackl et al. proposed a TA approach of testing freeze-dried cakes in vials for the quick determination of mechanical features as quality indicators for the final dosage forms or for lyophilization process performance (Hackl and Ermolina, 2016). They applied a CT with hold time to assess both stress and stress relaxation, using a setup shown in Fig. 4d. Results showed that TA profiles strongly depend on critical testing parameters. For instance, the recommended distance parameter should be below 55 – 60% of the

product's thickness to avoid structure densification. Furthermore, low testing speeds (0.01 – 0.05 mm/s) are preferable with porous and fragile matrices, for the high sensitivity to small load changes and the ability to differentiate brittle from soft materials out the appearance of the profile. As the proposed method caught the variability caused by material changes, preparation process and environmental factors, the authors further confirmed it with the development of polyvinyl pyrrolidone (PVP) and amino acids OLs (Hackl and Ermolina, 2019).

Besides CT that are appropriate for porous structures, Iftimi et al. also performed TT on several formulations of hydroxypropyl methylcellulose (HPMC)-based freeze-dried wafers (solid foams) intended for drug loading through inject printing. Comparing Young's modulus for flexibility, the ultimate tensile strength for overall substrate resistance, and the elongation at break for the capacity to deform without immediate failure, the authors were able to choose the optimal solid foam for injekt printing (Iftimi et al., 2019).

3.2.5. Films

The mechanical properties of films, either mucoadhesive, soluble or orodispersible are of paramount importance for the smooth running of the technological flow, packaging and handling by the patient when administered. They can be impacted by formulation factors, process parameters or storage conditions so they must be controlled throughout the development up to market release (Preis et al., 2014b). TA methods were described to characterize films obtained by solvent casting method (Speer et al., 2019), HME (Prodduturi et al., 2005, 2004) or electrostatic powder deposition (Prasad et al., 2015). Most researchers perform mechanical characterization by applying either TT (El-Malah and Nazzal, 2013; Owusu-Ware et al., 2019, 2016; Prodduturi et al., 2004), PT (Kajthunyakarn et al., 2019; Peerapattana et al., 2015) or sometimes both (Brniak et al., 2015). Strength and elongation at break are regularly considered to describe mechanical traits of films, either on dry (Alaei et al., 2021; Pongjanyakul and Khuathan, 2016; Preis et al., 2014b) or on wetted samples (Kajthunyakarn et al., 2019; Karrout et al., 2010; Khuathan and Pongjanyakul, 2014; Pongjanyakul and Khuathan, 2016).

For the evaluation of orodispersible films (ODFs), a strategy for the development of a PT (PT) was described, and revealed the selection of an appropriate probe that best distinguished between reference materials, and a sample holder that can accommodate small samples, usually down to 2 × 8 mm, as shown in Fig. 4c. A cylindrical flat surface probe was chosen, with a diameter of 4.8 mm. Besides strength and elongation, authors calculated the energy to puncture as the area under the force–displacement curve divided by the sample volume, which enabled the comparison of different thickness specimens (Preis et al., 2014b). The same parameter from PT was used to compare three-layer films of carrageenan: polyelectrolyte complex: chitosan with their single-layer correspondents (Volod'ko et al., 2021). However, Alaei, who evaluated films through PT, reported that out of all calculated parameters, the breaking factor was the only one that discriminated between commercial samples (Alaei et al., 2021).

Parameters derived from TA can be studied as responses in Design of Experiments (Kraisit et al., 2017; Peerapattana et al., 2015), as El-Malah et al. did with tensile strength and elastic modulus to estimate the effects of formulation factors (pullulan, HPMC, and PVP) on the strength and flexibility of films (El-Malah and Nazzal, 2013).

Brniak et al. investigated the effects of microparticles loaded into the films through TT and PT and showed the negative effect of microparticle inclusion on strength and flexibility. Also, they obtained high variability among Young's modulus results for films containing microparticles (Brniak et al., 2015). The mechanical properties of films can also be explained by the molecular mobility of polymers, as studies of Thermally Simulated Current demonstrated on hydroxyethyl cellulose (HEC) and plasticized hypromellose films (Owusu-Ware et al., 2016, 2019). Other authors highlighted the effects of moisture on hot-melt extruded films loaded with clotrimazole through TT performed on samples stored in different humidity conditions (Prodduturi et al., 2005, 2004). Tests were continued until film breakage, but results were considered valid only if films failed between the clamps and not at contact (Prodduturi et al., 2005, 2004).

On the other hand, films intended for microparticulate coating can be firstly solvent cast and evaluated for their mechanical properties (Khuathan and Pongjanyakul, 2014; Salawi et al., 2021). In this respect, Karrout et al. assessed the energy needed to break the films in their dry and wetted states to understand the way coatings could face mechanical stresses encountered in the gastrointestinal tract (Karrout et al., 2010).

Out of the applied tests, the puncture method was reported as less prone to set-up errors, less restrictive in terms of sample shape, and allows safe handling of fragile structures (Prasad et al., 2015).

The standard test method for tensile properties, ASTM D638 Type V requires dog bone shape samples which are not always appropriate for drug-containing films or for testing marketed formulations (Preis et al., 2014b).

3.2.6. Filaments

To assess filament mechanical properties and their printability most researchers apply FT such as the 3PBT (Alzahrani et al., 2022; Hu et al., 2022; Viidik et al., 2021; Zhang et al., 2017), BT (Xu et al., 2020) and stiffness tests (Crișan et al., 2022). Out of the mechanical parameters derived from this test, stiffness is the most frequently referred as a good printability indicator (Hu et al., 2022). Many authors reported the breaking forces, but when filaments with different diameters had to be compared Alzahrani et al. chose the breaking stress instead of the breaking force. Through a 3PBT, Alzahrani et al. fitted stress strain curves to Hooke's law to calculate k, the stiffness constant and demonstrated that high k values show better printability (Alzahrani et al., 2022).

Zhang et al. defined specific conditions to evaluate filaments for 3D printing through the so called Repka-Zhang methods. They include a first test to determine flexibility and brittleness/ toughness by means of a three-point bending test (3PBT) in specified conditions, and a second test that estimates filament stiffness by applying a force perpendicularly to the sample placed on a flat surface, which yields the peak stress as a stiffness indicator (Zhang et al., 2019). Flexibility was defined as "the tolerance of a filament to bending without breaking" and was measured by the breaking distance. The toughness or brittleness were described as "the breaking of a filament without significant plastic deformation" and stands for the breaking stress. Stiffness was equivaled to breaking stress in the second test, described as the load required to reach a certain deformation (Zhang et al., 2019). However, in other studies, the breaking distance was referred to as a measure of brittleness (Zhang et al., 2017, 2020).

The Repka-Zhang methods were taken over and sometimes adapted by other authors who aimed to optimize the mechanical properties of the filaments (Crișan et al., 2022; Than and Titapiwatanakun, 2021; Vo et al., 2020). An adapted version of the 3PBT with the edges of the filament fixed between clamps was used by Crișan et al. to estimate brittleness and flexibility of diclofenac sodium loaded filaments. The fracturability was obtained from the load value at break and was considered an indirect indicator of brittleness (Crișan et al., 2022).

In addition to the two tests described by Zhang, Xu added a third one, the resistance test, a BT to assess the softness of filaments, for which the testing parameters (sample length, speed and strain) were optimized through an experimental design to yield minimum result variability. The methodology of the three tests applied by Xu is briefly described in Fig. 4e. Comparing the results obtained with the three tests, the authors proposed stiffness test as the most appropriate for its accuracy, reliable results, ease of operation and low material investment. The toughness parameter calculated from the AUC of stress–strain profile of the stiffness test provided a comprehensive way to characterize filaments and predict printability (Xu et al., 2020). Samaro et al. reached the same conclusions regarding the relevance of toughness in printability prediction, however determined form a TT (Samaro et al., 2020).

Other authors also applied BT, referred to as dry spaghetti tests performed in food industry, and revealed filament flexibility as the breaking distance of the product (Gültekin et al., 2019, 2021).

TT were also reported for filaments although sometimes the fracture points do not show at the middle of the sample, in the measuring area, but at the contact with the grip which indicates a failure caused by the grip pressure rather than the applied tension. Zhang et al., who developed indomethacin/ Eudragit RL filaments reported an improvement after the addition of plasticizers in the mixture (Zhang et al., 2022a). Mirdamadian applied TT to check the effect of different loads of oxaliplatin alginate nanoparticles on the mechanical properties of Eudragit L100-55 filaments plasticized with PEG6000 and triethyl citrate (Mirdamadian et al., 2022). Tabriz et al. ranked a high number of polymers according to the results of TT (maximum tensile strength, Young's modulus and elongation at break) and matched the results with the actual printability through Principal Component Analysis. They revealed the importance of tensile stress in the accurate prediction of printability (Tabriz et al., 2021).

Applying three different mechanical testing methods (TT, 3PBT and BT), Samaro et al (2021) showed that printing with holt melt extrusion filaments could pose filament loading and printability issues that could be avoided with direct extrusion additive manufacturing technology (Samaro et al., 2021).

As shown above, most of the mechanical tests performed on filaments through TA aimed and achieved printability prediction. Still, the printing quality could not be accurately evaluated by such methods, so a 3D printed object retention rate was proposed for that (Zhang et al., 2022b). Regarding the acceptable values that some authors declare for certain filament formulations, these should not be considered as absolute values, but indicative and strictly correlated with the formulation in question and the test parameters. Even within the same group of authors, there were variations regarding the values of the mechanical parameters considered acceptable for printing (breaking distance $>$ 1 mm (Zhang et al., 2017), breaking distance $>$ 0.61 mm (Zhang et al., 2019)), which shows that printability is highly formulation dependent, and one parameter cannot be a sufficient descriptor of printing capacity. As there are no official regulations regarding the acceptable values for mechanical parameters of filaments, polyvinyl alcohol, polylactic acid (PLA) or acrylonitrile butadiene styrene (ABS) filaments are often used as a reference material in terms of mechanical properties (Samaro et al., 2020; Xu et al., 2020; Zhang et al., 2022b).

In the attempt to develop a new analytical tool to guide the selection of printing parameters, Gottschalk et al. used an experimental setup that included a texture analyzer to measure the feed forces needed to load a filament to a heated nozzle to print at a required speed. PLA, PVA and polyethylene terephthalate glycol-modified were used as testing materials, as well as a filament with PVA loaded with ketoconazole. Feed force limit assessment led to the prediction of printing parameters and the successful transfer to an actual printing process with final products within the 5% variation limit (Gottschalk et al., 2022).

3.2.7. 3D printlets

3D printed dosage forms are usually subjected to single or double CT under cylindrical probes (Cheng et al., 2020). Round-shaped chewable semi-solid dosage forms for paediatric use were 3D printed and subjected to a TPA test to simulate mastication. As there are no standard acceptability criteria, the calculated parameters such as hardness, cohesiveness, gumminess, chewiness, and adhesiveness were compared to the respective values obtained for well-accepted semi-solid foods such as peanut butter or banana (Chatzitaki et al., 2022). Other authors have considered printing and moulding different sizes and shapes of their products to get a better mechanical characterization through both CT and 3PBT. They linked their results obtained on chocolate samples to the sensory evaluation through the Chewing Difficulty Index (CDI), calculated using the breaking force value measured in the 3PBT (Chachlioutaki et al., 2022).

As shown in Table 3, many researchers combine texture characterization methods, using different fixtures, different test parameters or sample sizes to get an image as complete as possible on the mechanical profile of their samples. As different research groups describe different experimental setups, accessories and working conditions, their reported results are hardly comparable to one another. Sometimes results present high variability, therefore some authors chose to perform 10 (Mazel et al., 2016; Xu et al., 2020) or even 15 repetitions (Zhang et al., 2017, 2019).

4. TA in mucoadhesion

Mucoadhesion or bioadhesion represents one of the critical quality attributes of the mucoadhesive drug delivery systems which may influence the bioavailablity of the product. Briefly, the bioadhesion mechanism can be summarized in the following steps: 1) a good contact between the sample and the substrate that can be facilitated by the hydration of the bioadhesive surface; 2) the hydration favors the interpenetration of the polymer chain with the mucus to form semi-permanent bonds (Alaei and Omidian, 2021; Duchene et al., 2008).

The ability of a dosage form to adhere to a mucosa can be determined through TA by the measurement of the force and/or work needed to detach the dosage form from a mucosa or mucosa-like substrate (Hagesaether et al., 2009). During the CT, the force vs. time or force vs. distance curve can be plotted and the following parameters can be calculated: the detachment force (also reported as bioadhesion force or the force to detach the sample from the substrate) and the work of adhesion (also reported as adhesiveness or the work required to counteract the forces of attraction between the sample surface and the substrate when the probe withdraws), as depicted in Fig. 5. When the stress–strain plot is recorded, the value of maximum stress necessary to overcome the bond between the sample and substrate is a parameter of interest, as well as the adhesion energy which can be calculated as the area under the curve (Gennari et al., 2019). The adhesion energy value can be also calculated from the force of detachment and displacement at maximum load (Mizrahi et al., 2004). In addition, the post-peak area under the curve and the elongation at adhesive failure can be used to obtain information about the stringiness and the cohesiveness of the samples (Repka et al., 2006). In other studies, the cohesiveness was determined as the distance the samples moved before detaching from the substrate (Farias and Boateng, 2018).

Most of the TA studies report comparable experimental setups and procedures for the measurement of the adhesion; usually, the equipment used is a universal testing system or a texture analyzer (Carvalho et al., 2010). In most cases, the sample attached to the probe is lowered at a programmed speed until contact with the substrate, then a constant force is applied to the substrate for a defined time interval. After the hold time, the probe returns to the initial position (Fig. 6a) ("CT3 TEXTURE ANALYZER Operating Instructions," n.d.). In a second experimental setup, the substrate is fastened on the upper metal probe and the sample is fixed on the lower support of the device. The upper probe is moved downward until the contact with the sample and maintained for a predefined time, whereupon the probe returns to the starting position (Fig. 6b) (Nep and Conway, 2011; Tamburic and Craig, 1997).

In several research studies, the adhesion properties of the films were assessed by performing a mucin-interaction test where the 3 % mucin was evenly spread on two layers and, further attached to both the upper and the stationary part of the analyzer. The sample was placed in between, and the probe was lowered; a 200 g force was applied for 100 s and the probe was withdrawn while the displacement and force of detachment were recorded (Fig. 6c) (Alopaeus et al., 2020; Hagesaether et al., 2009).

Depending on the experimental setup, the technique can be optimized regarding the test parameters (test speed, contact time, or contact force) but also the pretreatment of the substrates (type and volume of the conditioning media, time to hydrate the substrate) to better

Table 3
Details on the methodology of mechanical tests using TA.

Experimental setup	Testing parameters	Sample details size	Parameters of interest (±acceptable values)	Reference
Tablets				
4 mm diameter cylindrical probe	TA (TA.XT2i), CT S: 1 mm/s	C: ibuprofen or acetaminophen, MCC at different ratios, magnesium stearate 1% Φ: 10 mm	Tensile strength	(Basim et al., 2019)
Flat surface probe	TA (TA.XT2i), CT S: 0.01 mm/s	C: acetaminophen and Copovidone solid dispersions Φ: 8 mm	Tensile strength	(Patel and Sun, 2016)
Flat surface probe	TA (TA.HDPlus), CT S: 0.1 mm/s	C: anhydrous calcium phosphate, magnesium stearate 2% Φ: 12 mm	Photographs of the failure modes	(Mazel et al., 2018)
	TA (TA.XT2i), CT S: 0.02 mm/s	C: MCC, HPC, povidone, lactose monohydrate, dibasic calcium phosphate, binary mixtures of diluents, magnesium stearate 0.5% Φ: 8 mm	TBI ($\langle 1\,5\,0 \rangle$)	(Gong and Sun, 2015)
	TA CT	C: lactose monohydrate, MCC at different ratios, magnesium stearate, sodium stearyl fumarate, stearic acid Φ: 9.5 mm	Tensile strength, TBI	(Paul et al., 2021)
Cylindrical probe 36 mm diameter	TA (TA.XTPlus), CT S: 0.1 mm/s D: 15%	C: MCC/ pre-gelatinized starch/ spray-dried monohydrate lactose/ dicalcium phosphate anhydrate, mannitol	Work of fracture, maximum stress, maximum strain, strain/stress max (<1 MPa^{-1} for friability $\ll$ 1%)	(Zhao et al., 2022)
	TA(TA.XTPlus), CT S: 1 mm/s	C: sotalol, Polyox™ 301 ± HPMC K100M or K4M/ monohydrate or anhydrous lactose/ MCC, magnesium stearate, butylated hydroxytoluene Φ: 8 mm	Hardness as force to fracture, fracture strain, gradient to fracture, work of fracture	(Rahman et al., 2017)
3.175 mm diameter indentation probe	TA (TA.XT2i) IT S: 0.05 mm/s F: 40 N	C: lactose monohydrate, MCC at different ratios, magnesium stearate, sodium stearyl fumarate, stearic acid Φ: 9.5 mm	Indentation hardness	(Paul et al., 2022)
3.18 mm diameter indentation probe	TA (TA.XT2i), IT S: 0.1 mm/s F: 40 N	C: ibuprofen or acetaminophen, MCC at different ratios, magnesium stearate 1% Φ: 10 mm	Brinell hardness	(Basim et al., 2019)
Mini-tablets				
4 mm diameter flat-faced probe	TA (TA.XTPlus), CT S: 0.1 mm/s	C: sodium salicylate and granulated or spray-dried mannitol Φ: 2 mm	Radial tensile strength	(Hagen et al., 2016)
5 mm punch	TA (TA.XTPlus), CT S: 0.1 mm/s	C: desmopressin acetate, povidone, and α-lactose monohydrate Φ: 2 mm	Tensile strength	(Kottke et al., 2021)
5 mm punch	TA (TA.XTPlus), CT S: 0.1 mm/s	C: Ludiflash®, Parteck® ODT, Prosolv® ODT, GalenIQ™ 721 or SuperTab® 50 ODT with different ratios of lubricants Φ: 2 mm	Tensile strength	(Kuck and Breitkreutz, 2022)
5 mm flat punch	TA (TA.XTPlus), CT S: 0.1 mm/s	C: Ludiflash®, GalenIQ™ 721, sodium stearyl fumarate Φ: 2 mm	Tensile strength (1 – 2 MPa), tabletability	(Lura et al., 2021)
Bilayer tablets				
Lateral sample holder	TA (TA.XT2i), CT S: 0.01 mm/s	C: binary mixtures of lactose and MCC of different grades Φ: 8 mm	Shear strength as interfacial bonding strength	(Chang and Sun, 2019)
Tablets attached on both sides to cylindrical probe	TA (TA.XT2i), TT S: 0.01 mm/s	C: binary mixtures of lactose and MCC of different grades Φ: 8 mm	Tensile strength as interfacial bonding strength	(Chang and Sun, 2019)
Chewable gel tablets				
–	TA (TA.XTPlus), TPA S: 1 mm/s D: 50% H: 60 s	C: gelatin, glycerol, water, Thyme syrup, preservatives Gummy bears	Firmness and springiness	(Matulyte et al., 2021b)
20 mm height probe	TA (TA.XTPlus), CT S: 2 mm/s D: 5 mm	C: gelatin, glycerol, water, Thyme syrup, Thyme extract, citric acid, nutmeg essential oil/ microcapsules Cylindrical tablets	Hardness, stickiness (adhesiveness)	(Matulyte et al., 2021a)
Capsules				
Capsule tensile rig	TA (TA.XT2i), 50 kg load cell TT S: 0.5 mm/s	C: gelatin and hypromellose capsules immersed in lipid-based formulations containing different amounts of water Capsules size 0	Elastic stiffness and elongation at break	(Machado et al., 2016)

(*continued on next page*)

Table 3 (*continued*)

Experimental setup	Testing parameters	Sample details size	Parameters of interest (±acceptable values)	Reference
Freeze-dried wafers				
Cylindrical probe 5 mm	TA (QTS- 25), CT S: 6 mm/min D: 2 mm	C: gelatin ± mannitol/sorbitol/sucrose ± Carbopol 974P-NF/Pluronic F217 Φ: 13.3 mm	Hardness at 1 mm depth (28 ± 3.3 N)	(Chandrasekhar et al., 2009)
Penetration probe	TA (QTS- 25), CT S: 6 mm/min D: 4 mm	C: gelatin ± mannitol/sorbitol/sucrose ± Carbopol 974P-NF/Pluronic F217 Φ: 13.3 mm	Fracturability at 3 mm depth	(Chandrasekhar et al., 2009)
Spherical indentation probe 1.5 mm diameter	TA (TA.XTPlus), 5 kg load cell IT S: 0.1 mm/s D: 0.65 mm	C: commercial OLs Samples of different diameters	Indentation hardness (12.45 – 322.74 kPa), elastic recovery (from dividing the area under the curve of the unloading plot with that of the loading plot)	(Vanbillemont et al., 2020)
Cylindrical probe 2 mm	TA (TA.HDPlus), 5 kg load cell CT	C: acetylsalicylic acid, Metolose®, kappa carrageenan/chitosan, and aspartame/sucralose Φ: 15.5 mm	Hardness	(Farias and Boateng, 2020)
Cylindrical probe with torsion area 20.27 mm^2	TA (TA.XTPlus), CT S: 0.01 mm/s D: 3 mm	C: povidone and mannitol and amino: acid L-alanine/ L-serine/ L-glycine/ L-proline 2 ml samples in 10 ml vials	Stress, stress relaxation, number of positive peaks, linear distance	(Hackl and Ermolina, 2019)
Conical penetration probe	TA (TA.XT2), CT S: 0.01 mm/s D: 1 mm	C: dextrin, β-limit dextrin or pre-gelatinised starch 18 mm diameter × 40 mm thickness	Force-distance profiles, strength	(Qi et al., 2012)
Cylindrical probe 5 mm, setup of two blank plates and a 1 cm diameter cylinder hole on the top plate	TA (TA.XT2), 5 kg load cell, CT S: 1 mm/s D: 2 mm TF: 5 g	C: sumatriptan succinate, gelatin, xanthan gum, disodium EDTA, magnesium stearate, ± Plasdone K90D, ± mannitol/ glycine/ sorbitol, ± camphor/ menthol, ± sucralose	Hardness (1.509 ± 0.131 kg)	(Gugulothu et al., 2015)
Tensile grips	TA (TA.XTPlus), 50 N load cell TT S: 5 mm/s D: 20 mm	C: hypromellose ± PEG 4000:Tween® 20: Glycerol (1:1:1) ± Poloxamer 188 20 × 70 mm samples	Young's modulus (12.2 mN/mm^2), ultimate tensile strength (218.9 mN/mm^2), elongation at break (23.5%)	(Iftimi et al., 2019)
Films				
Film fixture, semi-spherical probe head	TA (CT3-1000), PT S: 0.5 mm/s	Commercial oral film formulations of different sizes	Breaking factor (above 34.5 N/mm), elongation (below 5.55%)	(Alaei et al., 2021)
Film fixture	TA (TA.XT2), PT	C: casein sodium, glycerol ± halloysite 2 × 2 cm samples	Puncture strength and elongation on dry and wet films	(Kajthunyakarn et al., 2019)
Film fixture, 6 mm spherical probe	TA (TA.XT2), 50 kg load cell PT S: 0.1 mm/s	C: quaternary polymethacrylate ± sodium alginate 2 × 2 cm samples	Puncture strength and elongation on dry and wet films	(Khuathan and Pongjanyakul, 2014)
Film holder with mounting plates	TA (TA.XTPlus), 5 kg load cell PT S: 0.1 mm/s	C: hypromellose ± polycarbophil 3.5 × 0.6 cm samples	Puncture strength and elongation	(Kraisit et al., 2017)
Clamps fixture	TA (TA.XTPlus), 500 N load cell TT S: 0.5 mm/s	C: terbinafine HCl, povidone K30, Hypromellose and glycerol 3 × 1 cm samples	Tensile strength (>0.042 N/cm^2) and elongation at break (>36.15%)	(Arpa et al., 2021)
Clamps fixture	TA (Shimadzu EZ-SX) TT S: 10 mm/min	C: microparticles, hypromellose and glycerol/PEG 200 2 × 15 cm solvent cast film	Tensile strength (6.48 ± 0.37 MPa), Young's modulus (706.33 ± 96.89 MPa), % elongation (14.33 ± 1.8 %)	(Brniak et al., 2015)
Film fixture, 8 mm diameter spherical probe	TA (Shimadzu EZ-SX) PT S: 10 mm/min	C: microparticles, hypromellose and glycerol/PEG 200 2 × 15 cm samples	Maximum force (4.8 ± 1.6 N), displacement (1.16 ± 0.44 mm)	(Brniak et al., 2015)
Tensile grips setup	TA (TA.XTPlus), TT S: 5 mm/min	C: diclofenac sodium, pullulan, povidone, Hypromellose, glycerol, Tween 80 L: 40 mm solvent cast film	Tensile strength (11.21 MPa), elastic modulus (6.78 MPa%)	(El-Malah and Nazzal, 2013)
Tensile grips setup	TA (TA.Plus), TT S: 0.2 mm/s D: 300 mm	C: HEC films Dumb-bell shaped solvent cast samples	Tensile strength (10 ± 3 N/mm^2), elastic modulus (1150 ± 10 MPa), elongation at break (9%)	(Owusu-Ware et al., 2016)
Film fixture, 4.8 mm diameter flat probe	PT S: 5 mm/s	C: aripiprazole, HPC/povidone, citric acid, sucralose 22 × 22 × 0.1 mm 3D printed film	Puncture strength (>0.08 N/mm^2)	(Lee et al., 2022)
Film fixture, 4.8 mm diameter flat probe	TA (TA.XTPlus), 5 kg load cell PT S: 5 mm/s	C: commercial and newly developed ODFs with different compositions 20 × 30 mm solvent cast films	Puncture strength (>0.06 N/mm^2), elongation, energy to puncture	(Preis et al., 2014b)
TA, Tensile grips setup, grip distance 30 mm	TA (TA.XT2i), 5 kg load cell TT S: 2 mm/s	C: clotrimazole 10%, HPC of different grades 50 × 10 × 0.48 mm HME films	Tensile strength, elastic modulus, elongation at break	(Prodduturi et al., 2004)

(*continued on next page*)

Table 3 (*continued*)

Experimental setup	Testing parameters	Sample details size	Parameters of interest (±acceptable values)	Reference
Film fixture, cylindrical probe	TA (TA.XTPlus), PT S: 0.1 mm/s	C: metronidazole, polycaprolactone, HPMC, glyceryl monostearate 20 × 20 mm hot melt films	Puncture strength (11.58 ± 0.51 N/mm^2), elongation (33.51 ± 3.61%), Young's modulus (0.347 ± 0.021 N/mm^2)	(Peerapattana et al., 2015)
5 mm spherical puncture probe	TA (TA.XT2), load cell 500 N TT S: 0.1 mm/s	C: magnesium aluminium silicate, quaternary polymethacrylate 2 × 2 cm film	Puncture strength, elongation at break	(Rongthong et al., 2013)
Clamps fixture	TA (TA.XT2), load cell 500 N TT S: 15 mm/min	C: magnesium aluminium silicate, quaternary polymethacrylate 2 × 7 cm film	Tackiness	(Rongthong et al., 2013)
HME filaments				
3PBT rig 25 mm gap	TA (TA.XT2i), CT S: 10 mm/s D:15 mm	C: acetaminophen 30% ± different grades of polymers/ binary mixtures/ binary mixture + disintegrant 50 mm sample	Breaking stress (>2941 g/mm^2), breaking distance (>1 mm)	(Zhang et al., 2017)
3PBT rig 25 mm gap	TA (TA.XT2), CT S: 10 mm/s D:15 mm	C: acetaminophen 30% ± different grades of cellulose based polymers (HPC, HPMC, EC) 50 mm sample	Flexibility (breaking distance > 0.61 mm), toughness (breaking stress > 635.5 g/mm^2), stiffness (20758.3 g/mm^2)	(Zhang et al., 2019)
3PBT rig 20 mm gap	TA (TA.XT2), CT S: 5 mm/s D:15 mm	C: ibuprofen 20%, HPMCAS ± plasticizers 30 mm sample	Breaking force, breaking distance, gradient of the deflection curve	(Zhang et al., 2020)
3PBT rig 3 mm thick 25 mm gap	TA (TA.XTplus) CT S: 10 mm/s D:10 mm	C: different polymers ± ibuprofen 30% ± plasticizers 60 mm sample	The maximum force, fracture distance, the maximum stress and AUC of the stress–strain curve as brittleness	(Xu et al., 2020)
Cylinder rig with two sample holders for vertical placement of the sample	TA (TA.XTplus) CT S: 1 mm/s D: 5%	C: different polymers ± ibuprofen 30% ± plasticizers 40 mm sample	The maximum force, fracture distance, the maximum stress and AUC of the stress–strain curve as resistance	(Xu et al., 2020)
3PBT rig 3 mm thick (just the upper part) sample on a platform	TA (TA.XTplus) CT S: 2 mm/s D: 1 mm (57%)	C: different polymers ± ibuprofen 30% ± plasticizers 60 mm sample	The maximum force, fracture distance, the maximum stress and AUC of the stress–strain curve as toughness	(Xu et al., 2020)
3PBT rig	TA (TA.XT2i), CT S: 2 mm/s	C: ketoprofen 30%, HPMC K4M, HPMCAS HG ± HPC LF 50 mm sample	Breaking stress, breaking distance, stiffness (>63.46 ± 11.23 g/mm)	(Hu et al., 2022)
3PBT rig 25 mm gap	TA (TA.XT2), CT S: 10 mm/s D:1.5 mm	C: amlodipine besylate, polyvinyl alcohol, sorbitol; atorvastatin calcium, Kollidon® VA64 50 mm samples	Breaking stress (>330.6 ± 11.4 g/mm^2)	(Alzahrani et al., 2022)
Grip fixture	TT S: 20 mm/min	C: oxaliplatin nanoparticles loaded to filaments of Eudragit® L100-55, PEG6000, triethyl citrate 50 mm samples	Tensile strength (2.57 N/mm^2), Young's modulus (4.88 N/mm^2), elongation at break, stress–strain curves	(Mirdamadian et al., 2022)
Grip fixture	TA (TA.XT2), TT S: 5 mm/min	C: indomethacin, Eudragit RL, plasticizer	Yield strength (20.86 ± 1.31 Pa), fracture strength (27.96 ± 1.81 Pa)	(Zhang et al., 2022b)
TA, self-tightening roller grip system	TA (TA.XTPlus), load cell 50 kg TT S: 3 mm/s D: 140 mm	C: anhydrous theophylline (20% or 40%), Klucel™ HPC EF and LF/ Soluplus®/ Kollicoat® IR/ Affinisol™ 15cP and 4 M, Parteck® MXP/ Aquazol® 200 70 mm samples	Young's modulus, ultimate tensile strength, strain at breakage, toughness	(Samaro et al., 2020)
TA, self-tightening roller grip system	TA (TA. HDPlusC), load cell 30 kg TT S: 3 mm/s D: 140 mm	C: metoprolol tartrate 50%, different ethylene–vinyl acetate grades 70 mm samples	Elastic modulus calculated from the linear interpolation of 1% and 5% strain	(Samaro et al., 2021)
Mini 3 PB rig 8 mm gap	TA (TA. HDPlusC), load cell 30 kg CT S: 0.02 mm/s D: 20 mm	C: metoprolol tartrate 50%, different ethylene–vinyl acetate grades 20 mm samples	Flexural stress, flexural strain, flexural elastic modulus calculated from the linear interpolation of 1.5% and 5% strain	(Samaro et al., 2021)
BT gripper, cylinder rig with two sample holders for vertical placement of the sample	TA (TA. HDPlusC), load cell 30 kg CT S: 2 mm/s D: 15 mm	C: metoprolol tartrate 50%, different ethylene–vinyl acetate grades 60 mm samples	Buckling stress as the average maximum stress for each formulation	(Samaro et al., 2021)
Blade probe, plane fixture	TA (CT3-4500), CT S: 0.1 mm/s D: 5%	C: diclofenac sodium, polyvinyl alcohol, Kolliphor® TPGS, Aerosil® 200 5 mm sample	Peak stress (26.19 N/mm^2)	(Crișan et al., 2022)
Spaghetti flexure rig for vertical placement of the sample	TA (TA.XTPlus), TPA	C: Pramipexole monohydrate dihydrochloride, Polyox® N80 ± Eudragit® RSPO/RLPO ± Eudragit® RL100/RS100 50 mm sample	Flexibility	(Gültekin et al., 2021)

(*continued on next page*)

Table 3 (*continued*)

Experimental setup	Testing parameters	Sample details size	Parameters of interest (±acceptable values)	Reference
Spaghetti flexure rig for vertical placement of the sample	TA (TA.XTPlus), TPA	C: Pramipexole monohydrate dihydrochloride, Eudragit® EPO, Polyox™ WSRN10/WSRN80 50 mm sample	Flexibility	(Gültekin et al., 2019)
3D Printlets				
Cone penetrometer probe (30°)	TA (TA.XTPlus), CT S: 2 mm/s D: 10%	C: acetaminophen, Mycusini® 3D Choco Dark 15 × 15 × 10 mm sample	Hardness, fracturability	(Chachlioutaki et al., 2022)
3PBT set	TA (TA.XTPlus), CT S: 2 mm/s D: 20%	C: acetaminophen, Mycusini® 3D Choco Dark 60 × 15 × 10 mm sample	Flexural strength, CDI	(Chachlioutaki et al., 2022)
Cylindrical probe 50 mm	TA (TA.XTPlus), TPA S: 1 mm/s D: 40%	C: isoniazid, cornstarch 11.3 mm diameter × 6.5 mm height cylinders	Hardness, adhesiveness, cohesiveness, springiness, gumminess	(Chatzitaki et al., 2022)
Cylindrical probe 35 mm	TA (TA. XTPlusC), TPA S: 1 mm/s D: 50%	C: theophylline, HPMC K4M/E4M 20.37 × 8.35 × 6.6 mm samples	Hardness, adhesiveness, cohesiveness, springiness	(Cheng et al., 2020)

*Abbreviations: TA, texture analyzer; CT, compression test; TT, tensile test; 3PBT, 3-point bending test; TPA, TPA; S, probe speed; D, deformation; F, force; H, hydration time; C, composition; MCC, microcrystalline cellulose; HEC, hydroxyethylcellulose; HPC, hydroxypropylcellulose; HPMC, hydroxypropyl methylcellulose; EC, ethylcellulose; PEG, polyethylene glycol; TBI, Tablet Brittleness Index; CDI, Chewing Difficulty Index.
** Device model (Maximum load / Force resolution): CT3-1000 (1 kg/0.10 g), CT3-4500 (4.5 kg/0.50 g), TA.XTplus (50 kg/0.1 g), TA.HDplus (750 kg/0.10 g), TA. XTPlusC (50 kg/0.1 g), TA.HDplusC (30 kg/ 0.1 g), QTS- 2505 (5 kg/0.2 g), QTS- 2525 (25 kg/1 g), Shimadzu EZ-SX (500 N/2.5 N).

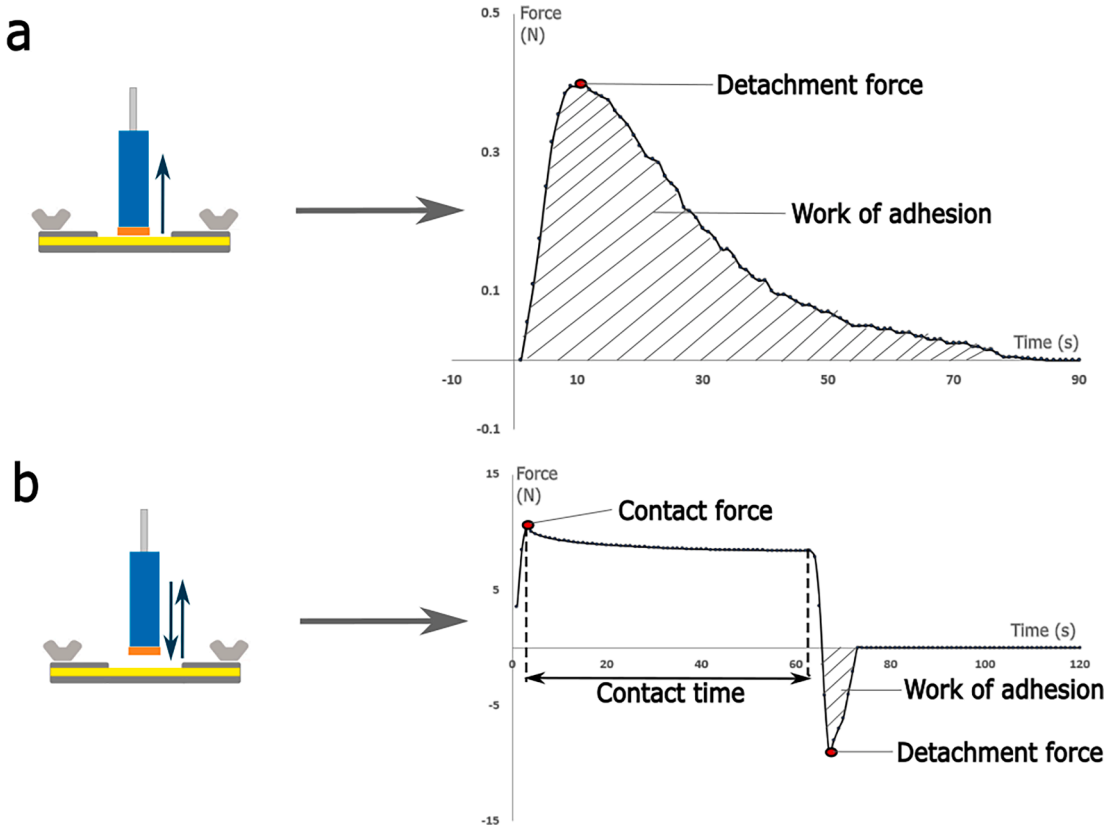


Fig. 5. Mucoadhesion parameters determined through TA when: a, recording starts after the contact between sample (orange) and substrate (yellow), and b, recording starts at the probe descent, before the contact between sample (orange) and substrate (yellow). (For interpretation of the references to colour in this figure legend, the reader is referred to the web version of this article.)

reproduce the *in vivo* conditions but also to discriminate small variations of mucoadhesive properties (Alaei et al., 2021; Shakweh et al., 2007).

According to the diffusion theory of mucoadhesion, the interpenetration of polymer chains with mucus chains creates semipermanent adhesive bonds, and the adhesive forces increase with the contact time (Chickering and Mathiowitz, 1999). The contact time or holding time is defined as the duration the sample is in contact with the surface of the tissue (Singh and Rana, 2014). For the evaluation of the mucoadhesive tablets, Mizrahi et al. investigated the influence of contact time on adherence to mucosal tissue. The experimental result revealed that the

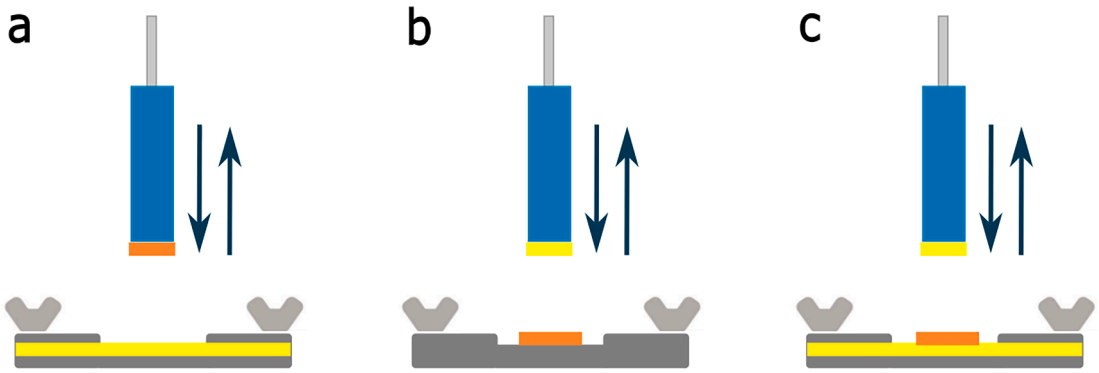


Fig. 6. Experimental setups for mucoadhesion testing with: a, the sample (orange) attached to the probe and substrate (yellow) on the fixture; b, the substrate (yellow) attached to the probe and the sample (orange) placed on the fixture; c, the substrate (yellow) placed on both the probe and the fixture and the sample (orange) between the two substrates. (For interpretation of the references to colour in this figure legend, the reader is referred to the web version of this article.)

detachment force and adhesion energy increased when the contact time varied between 10 and 600 s. In addition, patients' responses during the subsequent clinical trial confirmed that the mucoadhesive tablets exhibiting good mucoadhesion properties to the gums during the first minute of application ensure adequate mucoadhesion for the rest of the treatment (Mizrahi et al., 2004). Similar findings were reported for other types of mucoadhesive matrices (Singh and Rana, 2014; Thirawong et al., 2007). When extended-release tablets are characterized, the screening of bioadhesive behavior after a longer contact time is needed. Owens et al recorded the adhesion force and work of adhesion when the contact time varied between 30 s and 4 h. The optimal contact time to perform the experiments within an experimental design was selected as 300 s with a contact force of 20 g (Owens et al., 2005). In general, for most studies, a contact time between 60 and 300 s was considered a satisfactory value that helps to differentiate between small variations of adhesive features of the mucoadhesive tablets but also ensures the reproducibility of the test method (Table 4). In the case of conventional tablets, a shorter contact time is recommended. The study conducted by Shakwek et al. showed that a contact time higher than 2 min led to the disintegration of some formulations (Shakweh et al., 2007).

The adhesion bonds are efficient if the penetration and the entanglement of the polymer chains go up to 0.2–0.5 μm depth into the mucosal substrate; mucoadhesive strength is improved when the similarity of the sample and the mucosal tissue is higher (Chickering and Mathiowitz, 1999). Along with contact time, the contact force is another key factor in the bioadhesion mechanism. This parameter is defined as the adherence strength of the sample to the tissue's surface (Singh and Rana, 2014). Most *in vitro - ex vivo* methodologies report values for the contact force ranging from 0.05 to 5 N, most often values between 0.5 and 1 N which grants close contact of the dosage form with the substrate but also differentiates adhesive features of the samples. Singh et al. reported an optimal value of 1 N to be applied without the risk of destroying the tissue (Singh and Rana, 2014), while for gelatin-based substrates a lower value, of 0.1 N was found adequate (Göbel et al., 2021).

Other parameters related to the device settings that may impact the obtained results are the lowering speed and the return speed of the probe. These parameters can influence the sample-substrate interaction process and the formation of semi-permanent bonds between the polymer chains and the mucus glycoproteins. Intermediate values for contact force, contact speed, test speed, and return distance are recommended to obtain optimal values of mucoadhesion parameters (Singh and Rana, 2014). As regards the acceptable values, in the case of mucoadhesive tablets, a value of the detachment force above 100 g denotes good mucoadhesive properties of the product (Alam et al., 2015).

The tests measuring mucoadhesive strength are applied to investigate the mucoadhesion of dosage forms for different purposes, such as pharmaceutical development or quality control in the pharmaceutical industry (Alaei and Omidian, 2021). In most cases, TA is employed to evaluate the mucoadhesive properties of the developed products or commercial formulations, as a desired feature of the product. In other cases, mucoadhesivenes was evaluated as an undesirable characteristic of the product. Hence, the esophageal bioadhesive behavior of eight commercial formulations containing alendronate was determined to compare the risk of drug-esophageal bioadhesion, as a precondition of "pill-induced esophagitis". The differences in the bioadhesive behavior pointed out possible differences in the esophageal tolerance between the commercial formulations (Shakweh et al., 2007).

The methods of evaluating the mucoadhesiveness can be classified as *in vitro*, *ex vivo*, and *in vivo* depending on the substrates used to assess the mucoadhesion (Alaei and Omidian, 2021). Different *in vitro* substrates such as mucin, gelatin, agar, gellan gum, 2-hydroxyethyl methacrylate/N-acryloyl-D-glucosamine hydrogel were reported in the literature (Abdel-Haq et al., 2021; Alaei et al., 2021; Alopaeus et al., 2020; Chaud et al., 2013; Farias and Boateng, 2018; Gennari et al., 2019; Göbel et al., 2021; Hagesaether et al., 2009; Kawano et al., 2016; Kilicarslan et al., 2018; Kiniwa et al., 2019; Nep and Conway, 2011; Qi et al., 2012; Schmidt et al., 2022; Szekalska et al., 2015; Tamburic and Craig, 1997). The main advantages of artificial substrates are the reproducibility of the measurements and the ease of their purchasing. These are considered safer than *ex vivo* substrates since do not pose contamination issues. An adequate artificial substrate should have appropriate properties in terms of moisture content, flexibility, and permeability (Alaei et al., 2021).

Animal mucosal tissues are typically preferred as substrates for the evaluation of mucoadhesive properties. Depending on the animal model, the mucosal tissues have different characteristics as regards the composition, thickness, or mucus secretion (Alaei and Omidian, 2021; Woertz et al., 2013). The determinations using mucosal tissue may lead to a higher variability of the results (Woertz et al., 2013). According to the literature, the animal tissues employed in *ex vivo* studies on oral solid dosage forms include bovine mucosa (sublingual, gingival, esophageal, duodenal) (Accili et al., 2004; Mizrahi et al., 2004; Owens et al., 2005; Şenel et al., 1998), goat gastric mucosa (Alam et al., 2015; Karemore and Bali, 2021; Sankar and Jain, 2013), porcine mucosa (gastric, buccal, esophageal, intestinal) (do Couto et al., 2017; Eleftheriadis et al., 2020; Farias and Boateng, 2020; Göbel et al., 2021; Gurpreetarora et al., 2012; Hagesaether et al., 2009; Kraisit et al., 2017; LaFountaine et al., 2017; Pekoz et al., 2015; Pund et al., 2011; Sakloetsakun et al., 2016; Shakweh et al., 2007; Singh and Rana, 2014; Thirawong et al., 2007), rat gastric mucosa (Sharma et al., 2015), rabbit intestinal mucosa (Prodduturi et al., 2005; Repka et al., 2006) or chicken skin (Bodini et al., 2019). In the research conducted by La Fountaine et al, the quantitative *ex vivo* results were confirmed by the qualitative *in vivo* studies (LaFountaine et al., 2017).

To simulate the *in vivo* conditions, different wetting media

Table 4
Mucoadhesive properties assessment of solid oral dosage forms.

Experimental setup and testing parameters	Determined parameters	Substrate type	Sample details and recorded results regarding the mucoadhesive properties	Ref
Mucoadhesive tablets - *Setup in* Fig. 6a				
UTS (Instron 5543) F_{con} = 10 N, T_{con} = 5 min S_{det} = 5 mm/s	F_{det} W_{adh}	Sublingual, esophageal, duodenal bovine mucosa	Carbopol 974P tablets and Pharmacoat 606 tablets MAP depends on the type of mucosa and polymer type: Carbopol > Pharmacoat - sublingual mucosa, Carbopol ≈ Pharmacoat - oesophageal mucosa, Carbopol < Pharmacoat duodenal mucosa	(Accili et al., 2004)
UTS (Instron5965), load cell 50 N F_{con} = 1.3 N, T_{con} = 360 s S_{det} = 0.1 mm/s, T_{wet} = 5 min	σ_{max} W_{adh}	Mucin compacts (130 mg)	Mucoadhesive tablets for prolonged release of lysozyme obtained through freeze-drying The optimal ratio Na alginate/ HPMC E5 = 3/7 to obtain appropriate MAP W_{adh} = 4–5.7 mJ, σ_{max} = 35–58 kPa	(Gennari et al., 2019)
UTS (Instron 4301) F_{con} = 0.5 N, T_{con} = 10 min S_{det} = 5 mm/min	F_{det}	Bovine sublingual mucosa	Buccal bioadhesive tablets containing sodium glycodeoxycholate as penetration enhancer Addition of glycodeoxycholate → not significant impact on the MAP F_{det} = 9.52 ± 1.99 N	(Şenel et al., 1998)
UTS (Instron 4502) F_{con} = 0.5 N, S_{det} = 0.1 mm/s T_{con} = 10, 30, 120, 300, 600 s	F_{det} D_{max} E_{adh}	Bovine gingival tissue	Mucoadhesive tablet with hydroxypropyl cellulose, carbopol 934, citrus essential oil and magnesium salts ↗T_{con} →↗E_{adh} F_{det} = 0.3–2.07 N; D_{max} = 0.4–3.4 mm, E_{adh} = 1.5–6.2 mJ	(Mizrahi et al., 2004)
TA (TAX-TEE 32) S_{test} = 0.5 mm/s, F_{con} = 10 g T_{con} = 300 s	F_{det}	Goat gastric mucosa	Mucoadhesive osmotic pump tablets containing trimetazidine hydrochloride Linear increasing of AP with the increase of polymer amount; ↗ MAP when a combination of two polymers (ethyl cellulose and HPMC) was used F_{det} > 100 g	(Alam et al., 2015)
TA (TA.XT2i) F_{con} = 10–60 g, T_{con} = 30 s – 4 h	F_{det} W_{adh}	Bovine gingiva	Sodium fluoride bioadhesive tablets Various texture setups → selected conditions: F_{con} = 20 g, T_{con} = 300 s Positive effect of the F_{con} and T_{con} on the MAP F_{det} = 17.8–73.9 g; W_{adh} = 39 – 183.4 gs	(Owens et al., 2005)
TA (TA.XTPlus) Φ_{probe} = 6 mm S_{det} = 0.5 mm/s, F_{con} = 2 N, T_{con} = 60 s	W_{adh}	Porcine gastric mucosa	Mucoadhesive rifampicin tablets The optimal amount of Carbopol 71 G and MCC that maximizes the MAP and release properties - determined within DoE W_{ad} = 327.8–344 gs for the optimal formulation	(Pund et al., 2011)
TA (TA. XT Plus), S_{det} = 0.5 mm/s, F_{con} = 10 g T_{con} = 300 s, T_{wet} = 30 s	F_{det}	Goat gastric mucosa (2X2 cm)	Gastroretentive stained-release tablets containing acyclovir F_{det} ↘ when ↗ the ratio of polyethylene oxide An efficient water uptake of the sample → sufficient hydration of the polymer network, important in the mucoadhesion process F_{det} = 9.3 ± 4.7 g for the optimal formulation	(Sankar and Jain, 2013)
TA (QTS- 25), 5 kg load cell, S_{det} = 30 mm/s, D_{target} = 3 mm, T_{con} = 120 s	F_{det}	Rat stomach tissue	Gastroretentive tablets containing allopurinol The effect of the polymers on MAP was studied within a DoE: the polymers (CMCNa, polyoxyethylene oxide WSR 303) exhibited similar influence toward F_{det}; F_{det} ↗increased when the % of polymers ↗ F_{det} = 715.4–1097.6 mN	(Sharma et al., 2015)
TA (TA. XT Plus), Φ_{probe} = 10 mm S_{test} = 0.1, 0.3, 0.5, 1 mm/s F_{con} = 0.1, 0.2, 0.5, 1, 2 N T_{con} = 30, 60, 180, 300 s D_{return} = 10,15,20, 40 mm	F_{det} W_{adh}	Porcine stomach tissue	Polymeric tablets containing Eudragit-iron oxides conjugates Optimal value F_{con} = 1 N; optimal combination T_{con}↗ and ↘ S_{test} MAP ↗ F_{con} = 0.1 N −1N, MAP ↘ when F_{con} = 2.5 N MAP ↗ when T_{con}↗ F_{det} = 7.78–36.42 g	(Singh and Rana, 2014)
TA (TA. XT Plus), Φ_{probe} = 10 mm S_{test} = 0.5 mm/s, $F_{contact}$ = 1 N $T_{contact}$ = 60 s, D_{return} = 15 mm	F_{det}	Porcine stomach tissue	Mucoadhesive tablets containing 75 mg cinnarizine, Eudragit RLPO and iron oxide The effect of iron oxides on F_{det} studied within a DoE; Electrostatic interactions Eudragit RLPO-iron oxide polymer ↔ sialic acid → ↗MAP F_{det} = 5.7–42.8 g	(Singh and Rana, 2013)
TA (TA. XT Plus), 50 N load cell Φ_{probe} = 10 mm S_{det} = 0.1, 0.3, 0.5, 1.0 mm/s F_{con} = 0.05, 0.1, 0.2, 0.5 N T_{con} = 10, 30, 60, 180, 600 s T_{wet} = 0.5, 2, 5, 10, 20 min	F_{det} W_{adh}	Porcine buccal, stomach, small intestinal, large intestinal tissues (20x20 mm)	Pectin discs Selected optimal conditions: F_{con} = 0.05 N, T_{con} = 60 s The molecular weight and degree of esterification of pectin impact the MAP in the following rank order: CU201 > CU501 > CU020 > CU701 F_{det} = 55–85 mN	(Thirawong et al., 2007)
TA (CT3), Φ_{probe} = 12.7 mm S_{det} = 0.5 mm/s, F_{con} = 50 g, T_{con} = 5 min	F_{det}	Goat gastric mucosa 20 × 20 mm	Gastroretentive tablets containing cilnidipine DoE; F_{det} - Gellan gum > HPMC K4M F_{det} = 32.11–68.41 g	(Karemore and Bali, 2021)
Mucoadhesive tablets - *Setup in* Fig. 6b				
TA (TA. XTPlus), 5 kg load cell Φ_{probe} = 20 mm, T_{wet} = 1 min, F_{con} = 0.5 N, S_{det} = 10 mm/s, T_{con} = 60 s	F_{det} W_{adh}	30% mucin gel	Polymer compacts: Grewia polysaccharide gum, Carbopol 971P, HPMC, CMC and guar gum Comparable MAP of grewia polysaccharide gum to Carbopol 971P and HPMC W_{adh} = 1.23 ± 0.26 N.mm	(Nep and Conway, 2011)

(*continued on next page*)

Table 4 (*continued*)

Experimental setup and testing parameters	Determined parameters	Substrate type	Sample details and recorded results regarding the mucoadhesive properties	Ref
TA (TA. XT), 5 kg load cell F_{con} = 0.5 N, T_{con} = 60 s, S_{det} = 0.1 mm/s, T_{wet} = 1, 3, 5, 10, 20 min	F_{det}	30% mucin gel	Carbopol 974P, Carbopol 971P and Naveon AA-1 compacts MAP ↘ in the rank order: Carbopol 974P, Naveon AA-1, Carbopol 971P	(Tamburic and Craig, 1997)
Conventional tablets				
TA (TAXTT2), 50 N load cell T_{con} = 1, 2 min	F_{det} W_{adh}	Porcine esophageal mucosa	Eight commercial formulations containing alendronate Different mucoadhesive behaviors attributed to different excipients (HPC or sodium croscarmellose); T_{con} > 2 min → disintegration of some formulations F_{det} = 0.048–0.148 N; W_{adh} = 36.7–3461.5 x10^{-3} J	(Shakweh et al., 2007)
Minitablets				
TA (TA.XTPlus) Φ_{probe} = 7 mm, F_{con} = 0.1 N, T_{con} = 30 s	F_{det} W_{adh}	Porcine intestinal mucosa	Minitablets containing binary amorphous dispersion of itraconazole and Carbopol 71G *In vitro* MAP confirmed by *in vivo* results F_{det} = 100–200 mN; W_{adh} = 3.7–14 kPa s	(LaFountaine et al., 2017)
TA (TA.XTPlus), 5 kg load cell, Φ_{probe} = 10 mm, S_{test} = 1 mm/s, F_{con} = 500 g, T_{con} = 10 s, S_{det} = 0.5 mm/s	F_{det} W_{adh}	Porcine small intestine tissue	Chitosan–gum arabic polyelectrolyte complex films 600 kDA Chitosan: Arabic gum (1:0.75), 150 kDA Chitosan: Arabic gum (1:1) →↗MAP; Chitosan excess →↗MAP W_{adh} = 400–850 mJ	(Sakloetsakun et al., 2016)
TA (TA.XTPlus) F_{con} = 290 mN, T_{con} = 180 s, S_{det} = 0.1 mm/s	W_{adh}	Mucin disks	3D printed films containing triamcinolone acetonide in SBA-15 mesoporous silica ↗MAP of loaded films by comparison to unloaded films W_{adh} = 0.147–420 mN.mm	(Schmidt et al., 2022)
Mucoadhesive orally disintegrating tablets				
UTS (Force Tester MCT-2150) T_{con} = 20 s	W_{adh}	10% Mucin layer	Orally disintegrating tea tablets containing arabic gum, carrageenan, guar gum, tamarind gum and pectin The highest MAP for the samples prepared with tamarind gum	(Kiniwa et al., 2019)
TA (TA-XT2), Φ_{probe} = 37 mm, S_{test} = 0.1 mm/s, F_{con} = 0.25 N, T_{con} = 60 s, S_{det} = 1 mm/s	F_{det}	0.5% porcine mucin applied on nutrient agar	Wafers containing β-limit dextrin or pre-gelatinized starch β-limit dextrin wafers exhibited superior MAP F_{det} = 1.9–53.7 N	(Qi et al., 2012)
Freeze-dried wafers				
TA (HDPlus), 5 kg load cell F_{con} = 1 N, T_{con} = 60 s	F_{det} W_{adh} D_{cohes}	6.67 % gelatin gel	Composite wafers with acetylsalicylic acid Differences in the MAP when using pH 6.8 PBS and pH 6.8 simulated saliva → simulated saliva reproduces better the *in vivo* conditions F_{det} = 0.04–0.51 N; W_{adh} = 0.02–0.31 mPa; D_{cohes} = 0.73–1.37 mm	(Farias and Boateng, 2018)
TA (HDPlus), 5 kg load cell S_{test} = 0.5 mm/s, T_{con} = 60 s, S_{det} = 1 mm/s	F_{det} W_{adh} D_{cohes}	6.67 % gelatin gel, porcine buccal tissue	Wafers containing acetylsalicylic acid and taste-masking sweeteners MAP > when the porcine tissue was used *In vitro*: F_{det} = 0.03–0.21 N; W_{adh} = 0.01–0.12 mJ; D_{cohes} = 0.81–1.18 mm *Ex vivo:* F_{det} = 0.15–0.37 N; W_{adh} = 0.42–0.93 mJ; D_{cohes} = 5.14–11.53 mm	(Farias and Boateng, 2020)
Raw materials				
TA (TA.XTPlus), 5 kg load cell S_{test} = 0.1 mm/s, F_{con} = 1 N, T_{con} = 180 s, S_{det} = 0.1 mm/s	F_{det} W_{adh}	Gelatin, mucin, porcine stomach mucosa	Alginate microspheres containing ranitidine MAP - inversely correlated with the amount of the ranitidine F_{det} = 0.16–0.91 kg m s^{-2}; W_{adh} = 340.6–989.2 mJ	(Szekalska et al., 2015)
TA (TA.XTPlus), S_{test} = 0.5 mm/s, F_{con} = 2 mN, T_{con} = 10 min	F_{det} W_{adh}	Mucin disks	Solid dispersions with praziquantel and sodium starch glycolate The solid dispersion ↘ MAP of the glycolate F_{det} = 0.852 N; W_{adh} = 1058 μJ	(Chaud et al., 2013)
Mucoadhesive thin films - *Setup in* Fig. 6a				
TA (CT3-1000), 1 kg load cell Φ_{probe} = 12.7 mm, S_{det} = 0.01–0.5 mm/s, F_{con} = 0,49–1,96 N, T_{con} = 5–60 s	F_{det}	Agar, gellan gum, gelatine	Commercial films: Vitamin B12 Fast Dissolving strips, B12 Fast Dissolving Strips Listerine Breath Strips, Ziminta Mouth Freshener Films Different volumes of artificial saliva, different CT by varying target load, target speed and hold time → Unsatisfactory results for gelatine and agar substrates S_{det} = 0.1 mm/s, F_{con} = 0.98 N, T_{con} = 15 s, 4% w/v gellan gum and 2% w/v glycerine and 200 μl of artificial saliva → to discriminate the MAP F_{det} = 1.26–2.54 N	(Alaei et al., 2021)
TA (TA.XT Plus), 5 kg load cell S_{test} = 1 mm/s, F_{con} = 1 N, T_{con} = 30 s	W_{adh}	Porcine buccal mucosa	Dimenhydrinate buccal films prepared with xanthan gum or HEC Xanthan gum-based films exhibited better MAP W_{adh} = 1.994–3.055 mJ/cm^2	(Pekoz et al., 2015)
TA (TA.XT2i) F_{con} = 0.1 N, T_{con} = 60 s, S_{det} = 0.05 mm/s	F_{det} W_{adh}	Porcine cheeks esophagus, gelatin, HEMA/AGA hydrogel	Buccal films Among tested substrates 2-hydroxyethyl methacrylate (HEMA)/ N-acryloyl-D-glucosamine (AGA) hydrogel → similar results to tissue samples, variability ↘ than animal tissues	(Göbel et al., 2021)
TA (TA XTPlus) F_{con} = 0.5 N, T_{con} = 5 min, S_{det} = 1 mm/s	F_{det} W_{adh}	Porcine esophageal mucosa	Mucoadhesive films with prilocaine hydrochloride and lidocaine hydrochloride F_{det} and W_{adh} work were not significantly impacted when ↗ drug content F_{det} = 0.38–0.84 N, W_{adh} = 0.35–0.85 N/mm	(do Couto et al., 2017)

(*continued on next page*)

Table 4 (*continued*)

Experimental setup and testing parameters	Determined parameters	Substrate type	Sample details and recorded results regarding the mucoadhesive properties	Ref
TA (TA-XT), Φ_{probe} = 5 mm, S_{test} = 0.5 mm/s, F_{con} = 0.5 N, T_{con} = 120 s, S_{det} = 1 mm/s	F_{det} W_{adh}	Porcine buccal mucosa	3D printed mucoadhesive buccal films → films with chitosan ↗MAP Buccal films containing ketoprofen, lidocaine hydrochloride and l-menthol prepared through by combining fused deposition modeling and inkjet printing → ↗ adhesion values of the inkjet-printed films F_{det} = 8.1–9 N; W_{adh} = 14.2–18.3 N × m for the inkjet-printed films	(Eleftheriadis et al., 2019) (Eleftheriadis et al., 2020)
TA (TA.XTPlus), Φ_{probe} = 12 mm, S_{test} = 0.5 mm/s, D_{target} = 10 mm, T_{con} = 60 s, S_{det} = 0.5 mm/s	F_{det} W_{adh}	1 % mucin	Chitosan/alginate polyelectrolyte complex films containing clindamycin phosphate ↗ MAP when ↗ alginate ratio F_{det} = 0.080–2.601 N; W_{adh} = 0.007 – 0.187 N.mm	(Kilicarslan et al., 2018)
TA (TA.XTPlus), Φ_{probe} = 10 mm, S_{test} = 1 mm/s, F_{con} = 0.05 N, T_{con} = 60 s, S_{det} = 0.5 mm/s	F_{det} W_{adh}	Porcine buccal mucosa	HPMC/polycarbophil mucoadhesive films DoE to study the influence of the polymer on MAP F_{det} = 0.0191–0.0347 N; W_{adh} = 0.029–0.058 N.mm	(Kraisit et al., 2017)
TA (TA-XT2 *i*), Φ_{probe} = 7 mm, S_{test} = 0.1 mm/s, F_{con} = 3.5 N, T_{con} = 10, 20, 60 or 120 s, S_{det} = 0.5 mm/s	F_{det} W_{adh} D_{elong}	Rabbit intestinal mucosa	Hydroxypropylcellulose polymer matrices containing Δ^9-tetrahydrocannabidiol The addition of API in the matrix system ↘ W_{adh} W_{adh} ↗ when T_{con} ↗	(Repka et al., 2006)
TA (TA.XTPlus), S_{test} = 0.5 mm/s, F_{con} = 1 N, T_{con} = 60 s, S_{det} = 0.5 mm/s	F_{det}	Porcine gastric mucosa	Mucoadhesive matrix tablets of domperidone DoE to study the influence of HPMC K 15 M ratio on MAP F_{det} = 10.789–50.924 N	(Gurpreetarora et al., 2012)
Customized test-rig (Tribometer), dynamic adhesion measurements F_{con} = 1 N, T_{con} = 60 s	F_{det}	agar/mucin substrate	Poly(lactic-co-glycolic acid) films loaded with clotrimazole Adhesion ↗ when ↗ clotrimazole ratio	(Abdel-Haq et al., 2021)
CM (RHEONER II), F_{con} = 2 N, T_{con} = 30 s, S_{det} = 5 cm/min	F_{det}	10% mucin	Films containing xyloglucan and loperamide Adhesiveness of Xyloglucan films increased by adding HPMC	(Kawano et al., 2016)
Mucoadhesive thin films - *Setup in* Fig. 6b				
TA (TA.XT2i), 5 kg load cell Φ_{probe} = 7 mm, S_{det} = 0.5 mm/s, F_{con} = 3.5 N, T_{con} = 30 s, T_{wet} = 30 s	F_{det} W_{adh}	Rabbit intestinal mucosa	PEO films containing clotrimazole PEO N-750 had higher bioadhesion than PEO N-80 films due to the higher molecular weight of the polymer ↔ the long-chain molecules can form a stronger interpenetrating network with the mucus	(Prodduturi et al., 2005)
TA (TA.XT.Plus), Φ_{probe} = 20 mm S_{det} = 1 mm/s, F_{con} = 0.1 N, T_{con} = 30 s, T_{wet} = 20 s	F_{det}	Chicken skin	Orally disintegrating films based on HPMC and pre-gelatinized starch ↗ ratio of HPMC led to the ↘ MAP F_{det} = 0.4–1.9 N	(Bodini et al., 2019)
Mucoadhesive thin films - *Setup in* Fig. 6c				
TA (TA-XT2i) S_{det} = 0.01 mm/s, F_{con} = 200 g, T_{con} = 100 s	F_{det} W_{adh}	3 % porcine mucin	Mucoadhesive buccal films containing Soluplus, HPMC or Lycoat The films containing Soluplus and HPMC revealed favorable MAP	(Alopaeus et al., 2020)
TA (TA-XT2i) S_{det} = 0.01 mm/s, F_{con} = 200 g, T_{con} = 100 s	F_{det} W_{adh}	3 % porcine mucin	Pectin/chitosan films The peak force from *ex vivo* experiments was correlated to *in vitro* determinations; the friction test reproduces better the *in vivo* conditions	(Hagesaether et al., 2009)
Shear test: a 2x2 cm block on which the intestine was attached was displaced horizontally, S_{test} = 0.5 mm/s	F_{det} W_{adh}	Porcine small intestine	F_{det} = 6.8 = 27.5 g	

*Abbreviations: TA- texture analyzer; UTS- Universal Testing System; CM- Creep meter; Tcon- contact time; Twet- time of wetting the substrate or the sample; Sdet- detachment speed (speed of raising the upper probe); Stest- test speed of lowering the probe with the attached sample; Fcon- contact force; Dtarget- target distance; Dreturn- return distance; σmax - maximum stress necessary for detachment; Fdet - detachment force; Wadh - work of adhesion; Eadh - adhesion energy; Delong - elongation at adhesive failure; Dcohes – cohesiveness (the distance the samples moved before detaching from the substrate); Dmax displacement at maximal load; MAP- mucoadhesive properties; CMCNa, sodium carboxymethyl cellulose; HEC, hydroxyethylcellulose, HPMC, hydroxypropyl methylcellulose; PEO, Poly(Ethylene oxide); MCC, microcrystalline cellulose.

** Device model (Maximum load / Force resolution): CT3-1000 (1 kg/0.10 g), CT3-4500 (4.5 kg/0.50 g), TA.XTplus (50 kg/0.1 g), TA.HDplus (750 kg/0.10 g), QTS-2505 (5 kg/0.2 g), QTS-2525 (25 kg/1 g).

(phosphate buffer, artificial saliva, distilled water, etc.) were applied either to the substrate or to the sample, with a defined time interval before the determination. Farias et al. showed differences in the mucoadhesion profile when using different media such as phosphate buffer pH 6.8 or simulated saliva pH 6.8. More favorable results were obtained in the case of simulated saliva, which was considered to better mimic the *in vivo* conditions (Farias and Boateng, 2018). The research conducted by Alaei et al. analyzed the effect of artificial saliva volume on the measured adhesive properties of oral thin films. Different volumes between 50 and 300 μl were tested to hydrate but not to dissolve the films; finally, a volume of 200 μl was considered appropriate to differentiate the adhesive properties of the samples (Alaei et al., 2021).

A particular observation about the TA of the films regards the size of the samples analyzed and the type and size of the test probes. These features are reported only in a few studies even though the use of different dimensions probes and samples impact the obtained results. Thus, selected probes to perform the adhesion studies include 5-, 10-, 12.7-, and 20-mm cylindrical probes. (Alaei et al., 2021; Bodini et al., 2019; Eleftheriadis et al., 2020; Kraisit et al., 2017).

One of the current challenges of TA is represented by the difficulty of defining a set of standard parameters applicable to samples with substantially different characteristics. The adhesive behavior and implicitly the texture profile changes depend on factors such as the composition of the sample (type and ratio of polymer) (Accili et al., 2004; Alam et al.,

2015; Gennari et al., 2019; Karemore and Bali, 2021; Pekoz et al., 2015; Prodduturi et al., 2005; Sankar and Jain, 2013; Sharma et al., 2015; Tamburic and Craig, 1997; Thirawong et al., 2007) preparation method (Ikeuchi-Takahashi et al., 2013), type and ratio of API (Abdel-Haq et al., 2021; Repka et al., 2006; Schmidt et al., 2022; Szekalska et al., 2015). For an in-depth assessment of these influences, parameters derived from TA (adhesion force and work of adhesion) have been integrated as responses in Design of Experiments (Gurpreetarora et al., 2012; Karemore and Bali, 2021; Kraisit et al., 2017; Owens et al., 2005; Pund et al., 2011; Sharma et al., 2015; Singh and Rana, 2013). In the study conducted by Kraisit et al., the mucoadhesive properties of the films (work of adhesion and detachment force) were included as responses in a mixture design, and the effect of polymers and their interaction were analyzed to develop HPMC/polycarbophil films with higher mucoadhesion. (Kraisit et al., 2017). Different experimental design approaches were employed to obtain mucoadhesive tablets containing gum ghatti and HPMC K 15 M (Gurpreetarora et al., 2012), microcrystalline cellulose (MCC) and Carbopol 71G (Pund et al., 2011), sodium carboxymethyl cellulose (CMCNa) and polyoxyethylene oxide WSR 303 (Sharma et al., 2015), Eudragit RLPO and iron oxide (Singh and Rana, 2013) or gellan gum and HPMC K4M (Karemore and Bali, 2021) with optimal adhesive properties.

Based on the high number of published reports on this topic, it can be concluded that TA is a reliable method for the assessment of mucoadhesive properties; a rigorous choice of experimental setups, accessories, and testing conditions will guide the formulators in obtaining solid dosage forms with satisfactory mucoadhesive characteristics.

5. Disintegration and polymer hydration phenomena

Since the appearance of orodispersible dosage forms, new evaluation methods were proposed to resolve the drawbacks of compendial tests that usually fail to discriminate between their properties. First, Dor and Fix proposed a new disintegration method that involved the immersion with a constant force of a tablet attached to the probe in a small volume of media. The distance-time curves were regarded as disintegration profiles, as they allowed the detection of the onset and endpoint of disintegration (Dor and Fix, 2000). Further studies proposed maintaining the applied force for a predetermined time and placing the disintegration media, water, or simulated saliva, in a thermostated bath (Abdelbary et al., 2005; El-Arini and Clas, 2002). When investigating the media volume effect, it appeared that a volume increase from 1 to 3 ml determined faster disintegration onset and higher disintegration rate, but beyond 2 ml, no significant influence of the volume was shown. The applied force during testing did not impact disintegration-related parameters but could affect the measurement of dimensional changes produced by effervescence or burst effect, so a load of 50 g was considered appropriate (El-Arini and Clas, 2002). Abdelbary et al. implemented some changes to the previously reported operating structure to better mimic the oral conditions. Initially, they placed the tablet on a perforated grid, above the media layer, then a flat probe pushed the tablet into the media and maintained a constant load during disintegration. In contrast to prior methods, this allowed full contact between the tablet and the media and the continuous drainage of disintegrated particles during the process, just as it happens *in vivo*. As a result, disintegration times obtained with the instrumental method were close to those reported by volunteers and it was assumed that some parameters (such as penetration distance) could even be correlated to mouthfeel or residue (Abdelbary et al., 2005). Further, Szakonyi et al. modified the testing conditions by attaching the tablet to the probe and descending to a sieve covered with a thin layer of disintegration media. They showed the relevance of the pre-test speed, post-test speed and that of the disintegration media to the accuracy of results and optimized all these testing parameters through two experimental designs. Whereas previous papers reported time-distance curves as disintegration profiles, Szakonyi et al. used the load vs. distance curves and the area under the curve to estimate disintegration times (Szakonyi and Zelkó, 2013).

In a study that aimed at the development of paediatric dispersible tablets, Buck et al. compared the experimental setups reported by Dor and Fix (2000) and by Szakonyi (2013) to one where the tablet was attached vertically to the probe to improve the contact with the disintegration media on the flat sides of the tablet. The newly tested conditions provided the closest results to the disintegration in the beaker, which was used as a reference method, however, showed high variability for formulations with slow disintegration and high levels of viscosity enhancers (Buck et al., 2016). Fig. 7 depicts the most common ways results are recorded during TA disintegration tests of ODTs, depending on the established testing parameters.

Considering that TA techniques do not require visual observation of the beginning or the end point of disintegration, it was assumed that the evaluation of the behavior of ODTs in an opaque environment such as human milk would be feasible. Unlike previous methods, the tablets were placed vertically on the probe to increase the contact surface, then load and distance data were recorded versus time when the sample reached the sieve. This application could be used in the development of orodispersible forms intended to disintegrate in milk during administration, such as those given to newborns through nipple shields (Scheuerle et al., 2015).

While most of the developed methods evaluated disintegration during CT, Tomas et al. proposed a new method to investigate the early stages of tablet disintegration, based on the assessment of local stress relaxation that occurs in the product at the contact with the disintegration media. This involves applying an initial load on the tablet, allowing stress relaxation in the dry state under a particular hold time, then adding the disintegration media and recording the load changes. The proposed method can be exploited in the formulation development phases to better understand interparticulate bonding or in formulation troubleshooting (Tomas et al., 2018). Further, in the attempt to gain a better understanding of disintegration kinetics, TA was doubled by magnetic resonance imaging and particle size measurement of the disintegrating fragments which explained the way force relaxation curves can be used to measure disintegration rate (Dvořák et al., 2020).

Disintegration tests by TA became routine evaluation methods for researchers that aimed for the quick development of certain products to meet the compendial requirements and release on the market, and were also interested in the way certain process parameters such as compression force can impact disintegration (Wang et al., 2017a, 2017b).

Vanbillemont et al. investigated the different disintegration tests could be applied for commercial OLs. They compared the Pharmacopoeial tests with two TA-adapted tests reported in the literature and revealed that the texture approach was more appropriate for OL testing. First, they applied the El-Arini and Clas test developed for ODTs (El-Arini and Clas, 2002), which was unable to accurately evaluate the quick disintegration of OLs, and afterwards the Abdelbary test (Abdelbary et al., 2005), which was found suitable for OL testing and led to high result reproducibility (Vanbillemont et al., 2020).

Some authors prefer to complete the compendial disintegration tests by TA determinations, especially for less traditional dosage forms such as ODMTs, where the compendial methodology and acceptability limits do not necessarily apply (Hejduk et al., 2021).

For buccal film disintegration, a petri dish method was described in the literature as well as a method that records the time needed for a drop of water to penetrate through the film surface (Preis et al., 2014a). Still, as these methods do not subject the films to any mechanical force, TA methods were developed. Alopaeus et al. fixed the samples in a film holder and applied a force with a cylindrical punch onto the samples previously wetted with distilled water (Alopaeus et al., 2020). Due to the greater resistance of the unwetted film, the probe begins applying a larger force. The disintegration endpoint has been set as the moment when the probe returned to a force of 0.03 N, which was previously mentioned as the minimal force applied by tongue movement (Preis et al., 2014a). However, these conditions were unable to assess films

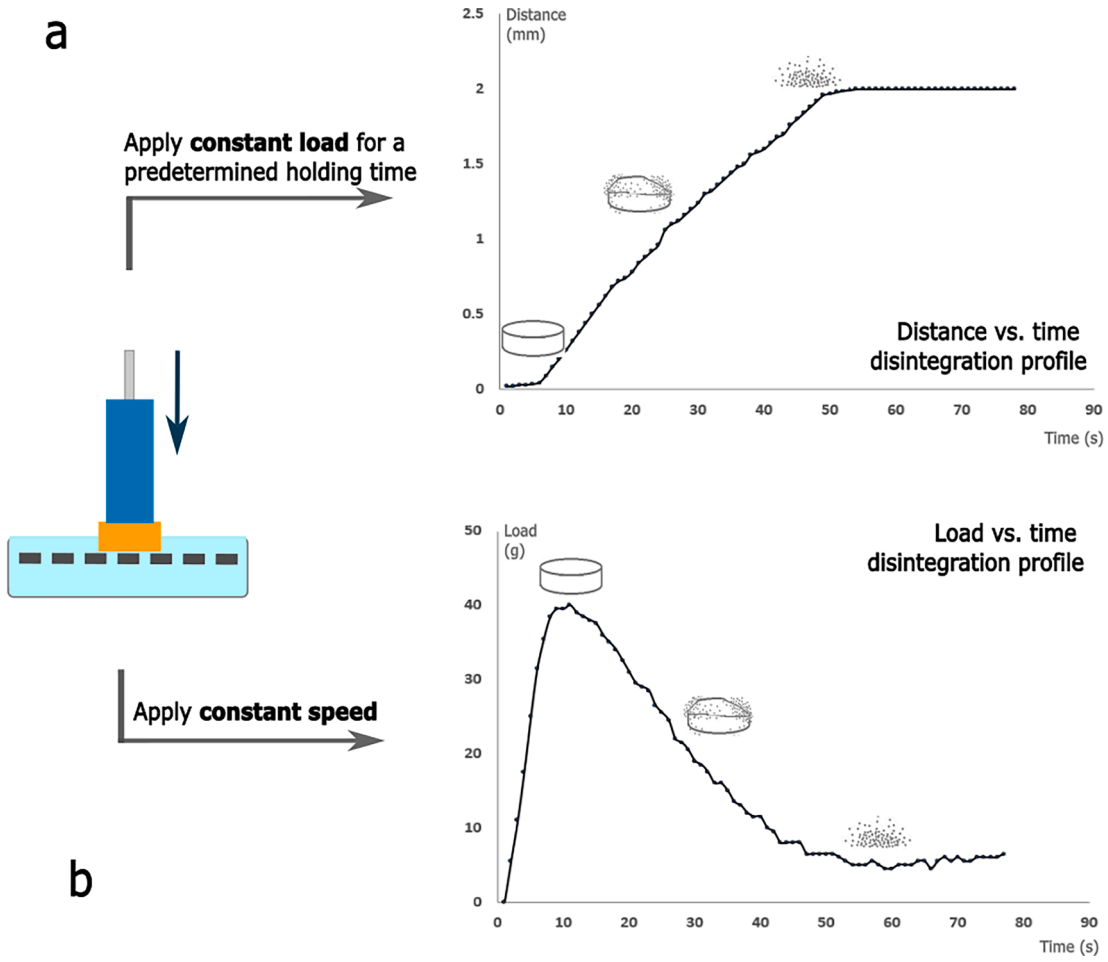


Fig. 7. Disintegration profiles for ODT disintegration testing when: a, a constant load is applied and distance vs. time profile is recorded, and b, when a constant speed is applied and the load vs. time profile is recorded (Fig. 7 b modified with permission from Szakonyi et al. (2013)).

with ultra fast disintegration or soft hydrogel formation (Alopaeus et al., 2020). More details regarding the experimental setups used in disintegration testing of different dosage forms are included in Table 5.

Modified-release dosage forms based on hydrophilic matrices also benefit from TA, not only from the point of view of their strength and hardness, but also from the results obtained in their hydrated states (Kulinowski et al., 2015). Hydrophilic matrix tablets can be evaluated for water content by interpreting force–displacement diagrams (Caccavo et al., 2015; Cascone et al., 2014; Li et al., 2014). When used as an alternative technique to the compendial dissolution tests to assess modified release matrix tablets, TA was able to detect differences in the internal structure properties of the products. While the compendial dissolution techniques revealed similar profiles for a developed formulation and the commercial reference, TA showed good discrimination capacity, which was further confirmed by biorelevant dissolution testing. In other words, TA (coupled with MRI or microCT techniques) included in matrix tablet R&D strategies could avoid bioequivalence pitfalls caused by the design based solely on compendial dissolution test results (Kulinowski et al., 2015).

Nazzal et al. developed a non-destructive TA probe that allows real-time measurements of swelling and erosion rates, as well as the size of the glassy core of tablets (Nazzal et al., 2007). The same experimental setup was later used to predict polymer (PVP, HPMC, Polyox) impact on drug dissolution for a compression coated pulsatile delivery system (El-Malah and Nazzal, 2010). As there is an established relationship between drug release and polymer hydration, TA was used to measure gel strength for dual-release bilayer tablets. The resulting profiles could be divided into three parts: erosion, gel, and dry core. The gel strength was estimated as the area under the curve of the gel region and contributed to the understanding of gelation mechanism as well as to the optimization of the two layers (Han et al., 2022). Li et al. applied TA to understand the swelling behavior of chitosan – anionic polymer drug delivery systems after a 12-hour dissolution study through load vs. time profiles comparison and the determination of the total work of penetration (Li et al., 2014).

6. *In vitro* – *In vivo* correlations derived from TA

There is a trend and a need for the use of characteristics determined *in vitro* to predict the *in vivo* behaviour and characteristics of dosage forms. The trend comes from the desire to simplify at most the characterization process during pharmaceutical drug development and therefore to reduce the costs involved. The need comes from the emergence of some situations in which it is difficult or impossible to test a certain pharmaceutical form on volunteers, for example in the case of the development of paediatric pharmaceutical forms. *In vitro - in vivo* correlations (IVIVC) have been reported to represent a powerful tool for predicting *in vivo* characteristics of oral dosage forms based on the *in vitro* assessments. As previously mentioned, among the benefits arising from IVIVC, the decrease of product development time and costs are of great importance (Patel et al., 2012).

TA is one of the *in vitro* methods used for estimating *in vivo* specific features of oral dosage forms, such as *in vivo* disintegration time, palatability, mouthfeel, transit time, ease of swallowing etc. (Asiri et al., 2021; Stokes et al., 2013). Mouthfeel, also referred to as oral sensory perception, and texture are mainly associated with foods and beverages,

Table 5
TA experimental setups reported for disintegration testing.

Experimental setup	Testing parameters	Sample composition, placement, size	Parameters of interest	Reference
ODTs				
0.5 in cylindrical acrylic flat-ended probe, 100 – 2000 μl water on a flat fixture	TA (TA-XT2i) CT PS: 5 mm/s S: 0.1 mm/s	C: Mannitol, maltose, 0.5 – 1% binder, 0.5 – 1% lubricant; samples attached to the probe Φ: NA	Extrapolation from the time-distance profile -identification of the start and the endpoint of disintegration Comparison with *in-vivo* data	(Dor and Fix, 2000)
Cylindrical stainless-steel flat-ended probe 1 cm^2, 1 – 6 ml water or simulated saliva in a thermostated bath	TA (TA-XT2i) CT L: 50 – 250 g HT: 60 s	C: commercial products representing the main ODT preparation technologies; samples attached to the probe Φ × h: 9.7 × 4 mm – 16 × 6.1 mm	Time-distance profile: disintegration onset, extrapolated disintegration time, total disintegration time, penetration distance	(El-Arini and Clas, 2002)
Cylindrical stainless-steel flat-ended probe 12 mm diameter; Perforated grid on top of a movable platform, immersed in a recipient with disintegration medium	TA (TA-XT2i) CT L: 50 – 250 g HT: 60 s	C: commercial products representing 3 of the main ODT preparation technologies, 2 wet granulated / emulsion granulated newly developed formulations; samples placed on the perforated grid Φ × h: 7.5 × 3.1 mm – 15.7 × 6.1 mm	Time-distance profile: disintegration onset, extrapolated disintegration time, total disintegration time, penetration distance Comparison with *in-vivo* data	(Abdelbary et al., 2005)
Acrylic cylindrical flat-ended probe 25.4 mm diameter; Stainless steel test sieve 38 mm diameter placed on an extruded polystyrene plate with 5.4 ml media	TA (CT3-4500) CT PS: 0.3 – 0.5 mm/s S: 0.04 – 0.05 mm/s	C: placebo ODT products composed of a directly compressible filler, superdisintegrant, sodium stearyl fumarate; samples attached to the probe Φ: 8 mm	Load-displacement curves	(Szakonyi and Zelkó, 2013)
14.23 mm diameter flat probe; Perforated horizontal platform immersed in 31 ml human/bovine milk	TA (TA.XTplus) CT L: 50 g HT: 60 s	C: commercial grade and in-house manufactured ODTs; samples attached vertically to the probe Φ: ~8 mm	Load vs. time and position vs. time profiles	(Scheuerle et al., 2015)
Needle probe 1 mm diameter; Crystallization dish where 80 ml disintegration medium was added to cover the tablet, after the hold time	TA (CT3) CT S: 0.1 mm/s F: 0.5; 1; 5; 10 N HT: 100 s	C: ibuprofen, lactose monohydrate, croscarmellose sodium; samples placed in the crystallization dish Φ: 8 mm	Wet relaxation expressed as the relative load (normalized by maximum force) vs. time Percentual structural change and wet relaxation rate were determined	(Tomas et al., 2018)
Spherical stainless-steel indenter 3.2 mm; 18.2 mm container; 2 ml simulated saliva added after the hold time with a syringe	TA (TA-XT2i) CT F: 3 N S: 0.1 mm/s HT: 30 s	C: metformin acesulfame salt, MCC, croscarmellose sodium, fumed silica, magnesium stearate; samples placed in the container then covered in 2 ml media Φ NA	Time-distance profile: disintegration time as the difference between the two plateau regions of the curve	(Wang et al., 2017a)
Spherical stainless-steel indenter 3.2 mm; 18.2 mm container; 2 ml simulated saliva added after the hold time with a syringe	TA (TA-XT2i) CT F: 3 N S: 0.01 mm/s HT: 30 s	C: diphenhydramine acesulfame salt, mannitol, croscarmellose sodium, fumed silica, magnesium stearate; samples placed in the container then covered in 2 ml media Φ NA	Time-distance profile: disintegration time as the difference between the two plateau regions of the curve	(Wang et al., 2017b)
Buccal films				
Flat-faced cylindrical probe of 7.03 mm diameter, fixture: plates with cylindrical hole of 38.82 mm^2 area; 200 μl of simulated saliva pipetted on the sample	TA (TA-XT2i) CT TD: 5 mm	C: furosemide, ± Soluplus®, ± HPMC and ± Lycoat®, glycerol; samples fixed between plates of the fixture 2 × 2 cm	Force vs. time profiles: disintegration endpoint was defined when the probe returned to a force of 0.03 N	(Alopaeus et al., 2020)

*Abreviation: S, test speed; PS, pretest speed; CT, compression test; HT, hold time; L, load; F, force; TD, target distance; C, composition; Φ, diameter; ODT, orodispersible tablet, MCC, microcrystalline cellulose.
* Device model (Maximum load / Force resolution): CT3-4500 (4.5 kg/0.50 g), TA.XTplus (50 kg/0.1 g).

in particular with their preference and acceptance (Guinard and Mazzucchelli, 1996). Lately, texture and mouthfeel were associated with pharmaceutical dosage forms, due to the need of assessing the acceptability of medicines (Asiri et al., 2021). Another discipline that contributes to the comprehension of texture and mouthfeel is tribology, which studies friction and lubrication between interacting surfaces in the mouth during the consumption of different products (Stokes et al., 2013). Tribological measurements are thus appreciated as one of the most adequate methods of evaluating oral textural phenomena associated with solid oral dosage forms and can be correlated with *in vivo* data (Hofmanová et al., 2021).

Although the value of IVIVC studies is indisputable and there are research groups that have studied the influence of the parameters obtained from TA with the data obtained *in vivo*, there is still a limited number of documents that can be found in this field. The articles included in this review meet the following criteria: they include TA; they correlate the parameters obtained from the TA with the data obtained *in vivo* and the tested product is a solid pharmaceutical form for oral administration (Table 6). There are many other publications that study IVIVC, but either they do not use TA as an *in vitro* characterization method, or the tested product belongs to another category of pharmaceutical forms, other than solid oral pharmaceutical forms (Baus et al., 2019; de Spiegeleer et al., 2001; Saab and Mehanna, 2019). Also, there are publications that predict the *in vivo* properties of dosage forms, without performing an *in vivo* study (Desai et al., 2022). As importantly, another category is the one in which the studies include TA and an *in vivo*

Table 6
In vitro - in vivo correlations for solid oral dosage forms.

Parameters of interest	*In vitro* experimental setup and testing parameters	*In vivo* experimental details	*In vitro - in vivo* correlations	Ref
ODTs				
In vitro: DT. Onset and end point of disintegration calculated by using the time-distance profiles obtained by the TA *In vivo*: oral DT	TA (TA-XT2i), CT, 2 kg load cell flat-ended acrylic cylindrical probe (Φ_{probe} = 0.5 in., H = 35 mm), $S_{pretest}$ = 5 mm/s, S_{test} = 0.1 mm/s	Recording the elapsed time between placing the tablet on the tongue and the moment of complete disintegration of the tablet	Force-displacement profiles generated by the TA software enabled accurate extrapolation of the start and end disintegration time by using a linear regression analysis between two variables An excellent correlation between the *in vivo* and *in vitro* disintegration times was found	(Dor and Fix, 2000)
In vitro: DT. Onset and end point of disintegration calculated by using the time-distance profiles obtained by the TA *In vivo*: oral DT	TA (TA-XT2i), CT,flat-bottomed cylindrical stainless steel probe (P/25, Φ_{probe} = 12 mm, H = 25 mm), perforated grid placed on the movable platform, F_{con} = 50 g, T_{con} = 60 s	Recording the elapsed time between placing the tablet on the tongue and the moment of complete disintegration of the tablet	An excellent correlation was observed for all tested tabletsThe new operating structure (the perforated grid on which the tablet is placed) appeared to be responsible for a better simulation of the *in vivo* conditions	(Abdelbary et al., 2005)
In vitro: DT *In vivo*: oral DT	TA (TA-XDPlus), CT, 5 kg load cell,flat-bottomed cylindrical stainless steel probe (P/25, Φprobe = 12 mm, H = 25 mm), F_{con} = 50 g, T_{con} = 60 s	Recording the elapsed time between placing the tablet on the tongue and the moment of complete disintegration of the tablet	There were no significant differences between texture analyzer and *in vivo* disintegration times. The TA method is an effective instrument for a precise and reproducible measurement of oral disintegration	(Gryczke et al., 2011)
In vitro: DT. Onset and end point of disintegration calculated by using the load–displacement profiles obtained by the TA. *In vivo*: oral DT	TA (CT3-4500), CT, 4.5 kg load cell,TA11/1000 (acrylic cylindrical) probe (Φ_{probe} = 25.4 mm),bottom: miniature stainless steel test sieve (Φ = 38 mm, aperture = 1.25 mm) placed on an extruded polystyrene plate	Recording the elapsed time between placing the tablet on the tongue and the moment of complete disintegration of the tablet	Sum of squared residuals function (SSR) used to compare *in vitro* and *in vivo* disintegration times. There was a good correlation between the *in vitro* results and the *in vivo* disintegration time Method optimization by mathematically predicting the method's efficiency using a theoretical patient group characterized by mild xerostomia Even if there were differences as against the original disintegration times, the method was able to predict the new *in vitro* values in this theoretical case	(Szakonyi and Zelkó, 2013)
In vitro: disintegration profile recorded as load vs. time curve. *In vivo*: oral DT, taste, volume of residue, roughness, palatability	TA (CT3-4500), CT, 4.5 kg load cell, TA10 probe, S_{test} = 0.01 mm/s	Recording the elapsed time between placing the tablet on the tongue and the moment of complete disintegration of the tabletTaste evaluation (sweet, salty, sour, bitter) using five scores VAS scales Volume of residue estimation using a five scores VAS scale. Roughness assessment using a five scores VAS scale.Palatability evaluation using a two scores scale (0 – rejected, 1 – accepted)	PLS was used in order to predict *in vivo* properties. Overall, the study managed to develop a model able to predict *in vivo* characteristics using instrumental analysis good prediction for *in vivo* disintegration time, volume of residue and total palatability Coupling of TA with multivariate data analysis enables the prediction of *in vivo* characteristics	(Casian et al., 2018)
Coated tablets				
In vitro: surface tribology *In vivo*: ease of swallowing, sensory attributes (roughness, adhesiveness, slipperiness)	Rheometer (DHR-2) with a tribo-rheology cell, top geometry: rotating, three tablets mounted on the flat top plate of the probe,bottom geometry: stationary, Transpore™ surgical tape (3 M™) attached to a clean steel cup (model for tongue asperity), F_{con} = 2 N, S_{test} = 0.001–1 rad/s	Ease of swallowing evaluation – swallowing tablet samples and assessing ease of swallowing on a 100 mm VASSensory attributes (roughness, adhesiveness, slipperiness) evaluation – maintaining the tablet in the mouth for minimum 10 s, then spit/swallow, then assess with 100 mm VAS	Pearson's correlation coefficient (r) and Spearman's correlation coefficient (rS) were used to assess the strength and direction of correlation between *in vitro* and *in vivo* variables Good IVIVC were obtained for ease of swallowing, slipperiness and stickiness Pearson's correlation coefficient was artificially increased when all tablet samples were included When only coated tablets were included, two significant linear correlations were obtained: high friction region at t = 30 s (COF_{30}) with slipperiness, and slip region at t = 10 s (COF_{10}) with stickiness The study demonstrated a relationship between tribological data and the oral sensory perception	(Hofmanová et al., 2021)
Buccal bioadhesive tablets				
In vitro: F_{det}, W_{adh}. *In vivo*: T_{adh}, AUC, C_{max}, T_{max}	TTing machine (L1000R), 20 N load cell	Measurement of the time after which the bioadhesive tablet was no longer visible under the lip by control at 30 min interval, following attachment to	The correlation studies showed an unclear correlation between the *in vitro* bioadhesive parameters (for which a difference was noticed between formulations) and *in vivo* adhesion time and biopharmaceutical	(Bouckaert et al., 1993)

(*continued on next page*)

Table 6 (*continued*)

Parameters of interest	*In vitro* experimental setup and testing parameters	*In vivo* experimental details	*In vitro - in vivo* correlations	Ref
		the gingiva Calculating the AUC, C_{max} and T_{max}	parameters (for which the difference between formulations was not significant) Therefore, differences observed *in vitro* are not necessarily transposed *in vivo*	
Soft chewable dosage forms				
In vitro: hardness, stickiness, water content, softening behaviour *In vivo*: chewing rate, number of chewing cycles to swallowing	TA (TA-XT2), CT, 5 kg load cell, cylindrical aluminum probe (Φ_{probe} = 5 mm), $S_{pretest}$ = 3.00 mm/s, S_{test} = 1.0 mm/s, $S_{posttest}$ = 1.00 mm/s	Counting the number of chewing cycles within 1 min and calculating the chewing rate Counting the number of chewing cycles needed for the oral breakdown of food to the point of swallowing	Multiple linear regression was used for predicting average chewing cycles for soft chewable dosage forms, based on hardness, fat content, water content, stickiness, softening behaviour New dissolution method developed based on *in vivo* chewing data – attaching the samples to a steel tooth coupled with a texture analyzer, in order to mimic both squeezing and grinding that occur during the mastication process The new method allows differentiating distinct soft chewable formulations which appear to be similar following the methods of the European Pharmacopoeia	(Stomberg et al., 2017)
Films				
In vitro: thin film tribology. Stribeck curves were obtained. *In vivo*: ease of swallowing, sensory attributes (roughness, adhesiveness, slipperiness)	Rheometer (DHR-2) with a tribo-rheology cell, top geometry: rotating, 3-balls-on a plate,bottom geometry: stationary, Tegaderm™ hydrocolloid thin dressing (3 M™) attached to the bottom surface, F_{con} = 1 N, S_{test} = 0.001–10 rad/s	Ease of swallowing evaluation – swallowing tablet samples and assessing ease of swallowing on a 100 mm VAS.Sensory attributes (roughness, adhesiveness, slipperiness) evaluation – maintaining the tablet in the mouth for minimum 10 s, then spit/swallow, then assess with 100 mm VAS.	Correlations between thin film tribology and sensory attributes were not significant However, it has the potential to help in mouthfeel comprehension	(Hofmanová et al., 2021)

*DT – disintegration/dispersion time; COF_{10} – coefficient of friction at 10 s; COF_{30} – coefficient of friction at 30 s; CT – compression test; IVIVC – *in vitro - in vivo* correlation; F_{con}- contact force; F_{det} - detachment force; $S_{pretest}$- pretest speed; $S_{posttest}$- posttest speed; S_{test}- test speed of lowering the probe with the attached sample; TA- texture analyzer; T_{adh} – time of adhesion; T_{con}- contact time; VAS - visual analogue scale; W_{adh} - work of adhesion

* Device model (Maximum load / Force resolution): CT3-1000 (1 kg/0.10 g), CT3-4500 (4.5 kg/0.50 g), TA.XTplus (50 kg/0.1 g), TA.HDplus (750 kg/0.10 g), DHR-2 (50 N/0.5 mN).

characterization of the solid oral pharmaceutical form, but no IVIVC is performed (Alopaeus et al., 2020; Cilurzo et al., 2003; Wang et al., 2021).

Therefore, despite the limited number of research documents that correlate *in vitro* and *in vivo* data in comparison with the ones that describe *in vitro* analysis of sensory properties, our review includes the description of this important tool which, as previously mentioned, provides a quality control method, reduces the costs of oral dosage forms evaluation by using data from TA and offers the possibility to understand how texture characteristics can estimate the behaviour of dosage forms after oral administration (Asiri et al., 2021).

The solid oral dosage forms evaluated in the studies that met all the criteria to be included in this subsection mainly belong to the category of tablets, in particular ODTs, but also to coated tablets, buccal mucoadhesive tablets, soft chewable dosage forms and films. It is clear that there is a strong connection between the category of the studied pharmaceutical form and the types of the determined or measured parameters. In the case of ODTs, IVIVC are generally performed between the *in vitro* disintegration time and oral disintegration time.

For example, Dor and Fix were among the first researchers to attempt developing a disintegration method that mimics *in vivo* conditions of the oral cavity by using a texture analyzer and determining the time for complete tablet disintegration versus distance. An important disadvantage of this method is the fact that in the oral cavity, the tablet would be completely moistened, while in the method developed by Dor and Fix the sample is only partially in contact with the disintegration medium, because one side of the tablet is taped to the probe (Dor and Fix, 2000).

Abdelbary *et al.* also assessed the possibility to link the *in vitro* disintegration profile of rapidly disintegrating tablets with oral disintegration time by determining time versus distance profiles. The researchers concluded that the use of a perforated grid during the TA minimised the operating errors and simulated well the *in vivo* conditions, thus gaining a successful, convenient, and precise method. The *in vitro* results obtained with the texture analyzer were very well correlated with the oral disintegration time for all the studied tablet types: a porous solid rapidly disintegrating tablet obtained by lyophilisation of an oil-in-water emulsion (Spasfon®), a rapidly disintegrating tablet which incorporated a disintegrating agent and a swelling agent (FlashTab®), a compression-moulding tablet (Wowtab®) and two rapidly disintegrating tablets formulations prepared with a powerful disintegrating agent, croscarmellose (Abdelbary et al., 2005).

In the study of Gryczke et al., the TA experimental setup used a perforated grid to better simulate the *in vivo* conditions and to ensure tablet wetting on all sides, like the method developed by Abdelbary et al. The results of the study showed no significant differences between the *in vitro* and *in vivo* disintegration times, hence the demonstrating the success of the IVIVC (Gryczke et al., 2011).

Another study that aimed at predicting the oral disintegration time by means of TA and mathematical optimization of the parameters of the method not only revealed a good correlation between the *in vitro* and *in vivo* data, but also calculated a new *in vivo* disintegration time for a theoretical patient group suffering from mild xerostomia (Szakonyi and Zelkó, 2013).

Casian et al. reported a complex study which followed the prediction of *in vivo* ODTs softening and disintegration behavior, volume of residue and total palatability, by using TA data. The research used, by partial least squares (PLS) and multivariate calibration, the entire curve load vs. time, but also individual parameters to perform the relationship evaluation between the texture profiles and disintegration. This study showed that the effects of formulation factors strongly influenced the perception and acceptance of ODTs (Casian et al., 2018).

Regarding the coated tablets and films, a different yet similar method with TA was used, namely a tribological method. Tribological measurements are relevant in the development of pharmaceutical

formulations due to their ability to predict mouthfeel and ease of swallowing. To assess the correlation capacity of *in vitro* tribological measurements (coefficient of friction) with oral sensory evaluation (slipperiness, stickiness, ease of swallowing, smoothness) for pharmaceutical coatings and coating tablets, Hofmanova *et al.* used Pearson's correlation coefficient and Spearman's correlation coefficient. The study reported surface and thin film tribological assessment of coated tablets and coating films, but the latter did not show a significant correlation and could not be used as a predictor of oral sensory characteristics. Regarding surface tribology, correlations were found between the static coefficient of friction and stickiness, as well as for the higher speed coefficient of friction and slipperiness. The explanation for the interconnection between stickiness at reduced speeds and slipperiness at more elevated speeds could be that adhesion is mostly linked to static friction, while slipperiness is associated with dynamic friction (Hofmanová et al., 2021).

One of the first attempts to perform an IVIVC in the field of mucoadhesive dosage forms was the study of Bouckaert *et al.*, on buccal bioadhesive tablets. The parameters which they assessed were the *in vitro* detachment force and work of adhesion, while the study in human volunteers determined bioadhesive properties of tablets. The apparatus used for determining *in vitro* properties was a TTing machine. One-way analysis of variance was used to statistically evaluate the *in vitro* results, while nonparametric statistics was used to evaluate the *in vivo* results. Even though there was a difference regarding the work of adhesion or the detachment force between formulations, the biopharmaceutical parameters and *in vivo* adhesion time did not reveal the same significant difference, which led to the conclusion that the study did not clarify if and which of the two parameters studied *in vitro* are important for the *in vivo* characteristics (Bouckaert et al., 1993).

Chewable dosage forms are another pharmaceutical product for which texture is essential for the compliance of patients, particularly in special patient populations. Multiple linear regression was used to predict the chewing cycles of different edibles according to the following independent variables determined by TA: hardness, stickiness, fat/water content, and softening behaviour (Stomberg et al., 2017). This statistical technique, used to analyse the relationship between independent and dependent variables, is successfully applied in the field of IVIVC.

Among the parameters of interest studied with the help of TA, it is observed that the disintegration time is predominant, being correlated with the oral disintegration time. The working methodology for determining the disintegration time is similar for all studies – the CT, even if there are small differences, such as the type of texture analyzer and probe, speed etc. Regarding the prediction method used, the disintegration profile was recorded either as load vs. time curve (Casian et al., 2018; Szakonyi and Zelkó, 2013) or as time vs. distance curve (Abdelbary et al., 2005; Dor and Fix, 2000).

Concerning the prediction method of the *in vivo* properties based on *in vitro* characteristics, it can be observed that good results are obtained using mathematical models, such as linear regression analysis, Pearson's correlation coefficient or Spearman's correlation coefficient (Dor and Fix, 2000; Hofmanová et al., 2021). Additionally, the multivariate data analysis is a powerful tool that has been recently used in a multitude of fields and situations. Casian et al. applied a PLS method and managed to predict subjective characteristics perceived during oral disintegration of ODTs based on TA data (Casian et al., 2018).

As mentioned earlier, there are other studies that, although they do not fully fit the criteria selected for this review, are worth mentioning. For example, the research conducted by Wang *et al.* used TA and dissolution testing to predict the time of dispersion in the oral cavity of levetiracetam from 3D printed instant-dissolving tablets, but without performing an actual *in vivo* study. The research also evaluated, with the ASTREE electronic tongue, the palatability of various formulations developed by optimizing the sucralose and spearmint flavour amounts through design of experiments. The oral dispersion time was predicted to be rapid based on TA results, which indicated a 30 s dispersion time of instant-dissolving tablets and a reduction of this dispersion time with tablet strength decrease, and also on the *in vitro* drug release test, which showed an almost complete release after 2.5 min (Wang et al., 2021). Another scientific article which did not perform an *in vivo* study but formulated hypotheses regarding sensory attributes (ease of swallowing) of the tested preparation based on the TPA is the study of Ito et al. (Ito et al., 2019). The research group focused on obtaining acetaminophen mini-tablets using various water-soluble polymers (eg. carrageenan, ι-carrageenan, HPMC, CMCNa, sodium alginate, pectin) to achieve rapid swelling and gelling, elasticity and low adhesiveness, therefore an easy deglutition. Their results showed that mini-tablets prepared with 20–30% carrageenan presented appropriate characteristics for a comfortable oral administration.

Overall, IVIVC is a valuable instrument for the prediction of the *in vivo* sensory attributes of pharmaceutical products based on TA data of solid oral dosage forms, which can be exploited to develop pharmaceutical forms based on texture studies, without including the stages of *in vivo* evaluations, which would lead to saving time, but also financial resources. However, the number of these studies is very small, which means that this topic can be successfully exploited in the future.

7. Insight into practical details derived from the review

In the past years, TA has become widely used in the pharmaceutical development, deemed as a very customizable method, with a wide range of easily available and affordable accessories. As shown in Fig. 8, mechanical characterization through TA was reported for most of the solid oral dosage forms, while the other TA methodologies address subgroups of dosage forms depending on product characteristics and quality control needs. Based on the summarised information in this work several practical implications emerge to guide future research.

Regarding mechanical characterization, for some types of products (e.g. tablets, films, filaments), formulations can be assessed through multiple different tests to obtain an overview of the mechanical profile. As up to date there are no official acceptance criteria for pharmaceutical products tested through TA, researchers often compare results with other published reports, which is problematic because of the differences in the experimental conditions and in the results. In this respect, prior testing of reference materials or commercially available products could be helpful as it allows to define standard values obtained in the same experimental settings. The reproducibility of results is variable, some studies were performed with as few as three replicates to 15–20 replicates for a formulation. In this context, a useful experimental approach to overcome the variability issue is the design of experiments, a methodology that discriminates the real effects of input variables from the experimental error.

In addition to the challenges met with mechanical testing, bioadhesion measurements bring extra variability. The diversity of the substrates, and implicitly of their characteristics significantly increase the inconsistency of the results. Apart from the substrate types, the pretreatment steps of the substrates and the experimental setups are sometimes difficult to compare between the reported studies. Consequently, the acceptance criteria based on such methods are not very reliable.

In contrast to the high number of studies describing the mechanical and mucoadhesive properties, the IVIVC data obtained through TA is modest. Therefore, the prediction of the *in vivo* properties based on *in vitro* characteristics represents an open topic that could be the focus of future studies, of particular interest in early formulation design for research and development scientists. However, the standardization of the test protocol for *in vitro - in vivo* analysis is required.

In conclusion, the main challenge of TA arises from the difficulty to define of a set of general tests which enables the assessment of samples varying from raw materials to a broad spectrum of oral dosage forms with distinct characteristics. The choice of the testing protocol and parameters depends entirely on the characteristics of the product that is

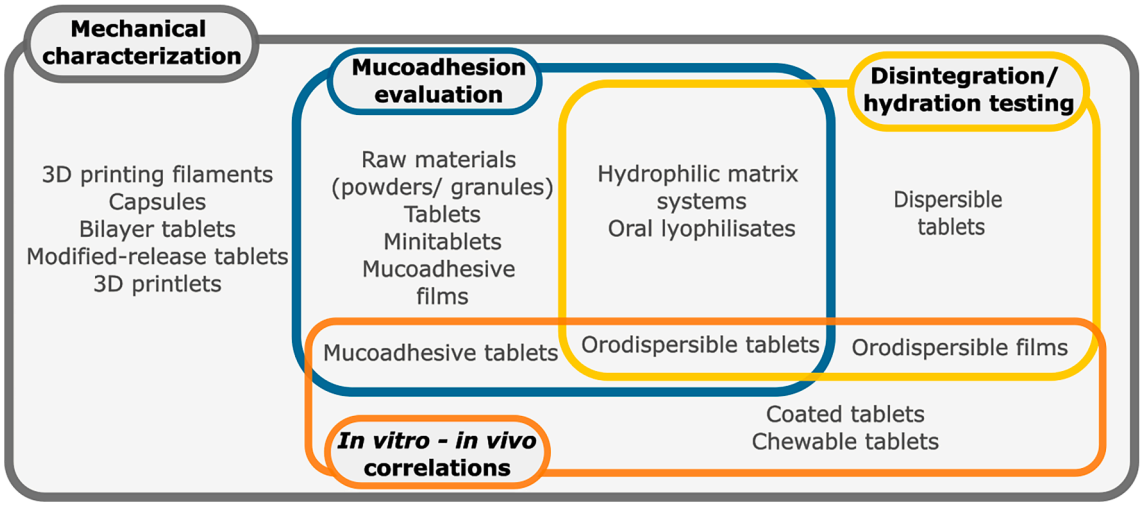


Fig. 8. Summary of texture analysis (TA) applications on solid oral dosage forms.

being tested and has a significant impact on the results. Therefore, a step ahead for researchers would be to standardize the tests and testing parameters as rigorously as possible, as well as the characteristics of the products that are being tested. Clear definitions of the texture attributes together with consistent terminology would enable the correspondence between studies and should be considered when developing texture methodologies.

As a versatile testing method, TA will evolve in accordance with the changes across the pharmaceutical industry, to fulfill the needs coming from emerging dosage forms, but also with the evolving regulatory requirements. The significant changes driven by the growing trend of enhanced drug products will require accurate testing methods. Thus, TA can provide multiple parameters describing the performance in improving dosage forms, such as through user friendly-dosage forms or 3D printed medicines.

8. Conclusion

Texture analysis is a testing method that constantly adapts, in order to meet the needs of the continous evolution and diversification of pharmaceutical dosage forms, trying to simulate the conditions in which a certain product is used. Several texture methods to characterize oral solid dosage forms have been published over the past decades. Among them, great emphasis is placed on mechanical testing; depending on the type and the characteristics of the samples various techniques such as compression, indentation, puncture, tensile, FT, and TPA were applied. Further, the parameters derived from mechanical testing were calculated to quantify the texture characteristics aiming to comprehensively describe the mechanical profile of the samples. In the current work, the applications of texture analysis in mechanical characterization are reviewed from the viewpoint of the suitability for various dosage forms, and comparability of experimental setups. Apart from mechanical characterization, different methods to evaluate the properties of mucoadhesive oral dosage forms have been summarized by discussing the test parameters but also the preliminary steps together with the interpretation of the experimental results for different sample types. In addition, reported studies to characterize the disintegration properties and the texture analysis experimental setups for disintegration testing are reviewed underlying the particularities of the methods and the advantages over traditional methods, but also the prediction of the *in vivo* sensory attributes of solid oral dosage forms based on texture analysis data.

CRediT authorship contribution statement

Cătălina Bogdan: Conceptualization, Writing – original draft. **Dana Hales:** Conceptualization, Writing – original draft. **Andreea Cornilă:** Conceptualization, Writing – original draft. **Tibor Casian:** Writing – review & editing. **Rareș Iovanov:** Writing – review & editing. **Ioan Tomuță:** Writing – review & editing. **Sonia Iurian:** Conceptualization, Writing – original draft, Writing – review & editing, Supervision, Project administration, Funding acquisition.

Declaration of Competing Interest

The authors declare that they have no known competing financial interests or personal relationships that could have appeared to influence the work reported in this paper.

Data availability

No data was used for the research described in the article.

Acknowledgements

This work was supported by a grant of the Romanian Ministry of Research, Innovation and Digitization, CCCDI - UEFISCDI, project number PN-III-P2-2.1-PED-2021-4198, within PNCDI III. The funding source had no involvement in the study design, in the collection, analysis and interpretation of data, in the writing of the report, or in the decision to submit the article for publication.

References

2.9. Pharmaceutical technical... - European Pharmacopoeia 11.0 [WWW Document], n.d. URL https://pheur.edqm.eu/app/11-0/content/11-0/20900E.htm (accessed 13.23).

Abdelbary, G., Eouani, C., Prinderre, P., Joachim, J., Reynier, J., Piccerelle, P., 2005. Determination of the in vitro disintegration profile of rapidly disintegrating tablets and correlation with oral disintegration. Int J Pharm 292, 29–41. https://doi.org/10.1016/J.IJPHARM.2004.08.019.

Abdel-Haq, M., Alyan, R., Abd-Rbo, K., Kasem, H., Aiman, A.A., 2021. Biomimetic clotrimazole-loaded PLGA films with enhanced adhesiveness for controlled drug release. Int J Pharm 601. https://doi.org/10.1016/j.ijpharm.2021.120578.

Accili, D., Menghi, G., Bonacucina, G., di Martino, P., Palmieri, G.F., 2004. Mucoadhesion dependence of pharmaceutical polymers on mucosa characteristics. European Journal of Pharmaceutical Sciences 22, 225–234. https://doi.org/10.1016/J.EJPS.2003.12.011.

Alaei, S., Omidi, Y., Omidian, H., 2021. In vitro evaluation of adhesion and mechanical properties of oral thin films. European Journal of Pharmaceutical Sciences 166, 105965. https://doi.org/10.1016/J.EJPS.2021.105965.

Alaei, S., Omidian, H., 2021. Mucoadhesion and Mechanical Assessment of Oral Films. European Journal of Pharmaceutical Sciences 159. https://doi.org/10.1016/j.ejps.2021.105727.

Alam, N., Beg, S., Rizwan, M., Ahmad, A., Ahmad, F.J., Ali, A., Aqil, M., 2015. Mucoadhesive elementary osmotic pump tablets of trimetazidine for controlled drug delivery and reduced variability in oral bioavailability. Drug Dev Ind Pharm 41, 692–702. https://doi.org/10.3109/03639045.2014.900076.

Alopaeus, J.F., Hellfritzsch, M., Gutowski, T., Scherließ, R., Almeida, A., Sarmento, B., Škalko-Basnet, N., Tho, I., 2020. Mucoadhesive buccal films based on a graft co-polymer – A mucin-retentive hydrogel scaffold. European Journal of Pharmaceutical Sciences 142. https://doi.org/10.1016/j.ejps.2019.105142.

Alzahrani, A., Narala, S., Adel Ali Youssef, A., Nyavanandi, D., Bandari, S., Mandati, P., Almotairy, A., Almutairi, M., Repka, M., 2022. Fabrication of a shell-core fixed-dose combination tablet using fused deposition modeling 3D printing. European Journal of Pharmaceutics and Biopharmaceutics 177, 211–223. 10.1016/j.ejpb.2022.07.003.

Antonyuk, S., Palis, S., Heinrich, S., 2011. Breakage behaviour of agglomerates and crystals by static loading and impact. Powder Technol 206, 88–98. https://doi.org/10.1016/J.POWTEC.2010.02.025.

Arpa, M.D., Ünükür, M.Z., Erim, Ü.C., 2021. Formulation, characterization and in vitro release studies of terbinafine hydrochloride loaded buccal films. Journal of Research in Pharmacy 25, 667–680. https://doi.org/10.29228/jrp.58.

Asiri, A., Hofmanová, J., Batchelor, H., 2021. A review of in vitro and in vivo methods and their correlations to assess mouthfeel of solid oral dosage forms. Drug Discov Today 26, 740–753. https://doi.org/10.1016/j.drudis.2020.12.015.

Awad, A., Trenfield, S.J., Basit, A.W., 2021. Solid oral dosage forms. Remington: The Science and Practice of Pharmacy 333–358. 10.1016/B978-0-12-820007-0.00019-2.

Baranauskaite, J., Ockun, M.A., Uner, B., Gungor, B., Duman, G., Tas, C., Yesilada, E., 2022. Development and In vitro characterization of pullulan fast dissolving films loaded with Panax ginseng extract, antioxidant properties and cytotoxic efficiency on lung and breast cancer cell lines. J Drug Deliv Sci Technol 76. https://doi.org/10.1016/j.jddst.2022.103701.

Basim, P., Haware, R. v., Dave, R.H., 2019. Tablet capping predictions of model materials using multivariate approach. Int J Pharm 569. 10.1016/j.ijpharm.2019.118548.

Baus, R.A., Haug, M.F., Leichner, C., Jelkmann, M., Bernkop-Schnürch, A., 2019. In Vitro-in Vivo Correlation of Mucoadhesion Studies on Buccal Mucosa. Mol Pharm 16, 2719–2727. https://doi.org/10.1021/acs.molpharmaceut.9b00254.

Bhatt, J.A., Bahl, D., Morris, K., Stevens, L.L., Haware, R. v., 2020. Structure-mechanics and improved tableting performance of the drug-drug cocrystal metformin:salicylic acid. European Journal of Pharmaceutics and Biopharmaceutics 153, 23–35. 10.1016/j.ejpb.2020.05.031.

Boateng, J.S., Auffret, A.D., Matthews, K.H., Humphrey, M.J., Stevens, H.N.E., Eccleston, G.M., 2010. Characterisation of freeze-dried wafers and solvent evaporated films as potential drug delivery systems to mucosal surfaces. Int J Pharm 389, 24–31. https://doi.org/10.1016/j.ijpharm.2010.01.008.

Bodini, R.B., Guimarães, J. das G.L., Monaco-Lourenço, C.A., Aparecida de Carvalho, R., 2019. Effect of starch and hydroxypropyl methylcellulose polymers on the properties of orally disintegrating films. J Drug Deliv Sci Technol 51, 403–410. 10.1016/j.jddst.2019.03.028.

Bonacucina, G., Cespi, M., Misici-Falzi, M., Palmieri, G.F., 2007. Mechanical characterization of pharmaceutical solids: A comparison between rheological tests performed under static and dynamic porosity conditions. European Journal of Pharmaceutics and Biopharmaceutics 67, 277–283. https://doi.org/10.1016/j.ejpb.2006.12.018.

Bouckaert, S., Lefebvre, R.A., Remon, J.P., 1993. In Vitro/in Vivo Correlation of the Bioadhesive Properties of a Buccal Bioadhesive Miconazole Slow-Release Tablet. Pharmaceutical Research: An Official Journal of the American Association of Pharmaceutical Scientists 10, 853–856. https://doi.org/10.1023/A:1018957126809/METRICS.

Brniak, W., Maślak, E., Jachowicz, R., 2015. Orodispersible films and tablets with prednisolone microparticles. European Journal of Pharmaceutical Sciences 75, 81–90. 10.1016/j.ejps.2015.04.006.

Buck, J., Huwyler, J., Kühl, P., Dischinger, A., 2016. Pediatric Dispersible Tablets: a Modular Approach for Rapid Prototyping. Pharm Res 33, 2043–2055. https://doi.org/10.1007/s11095-016-1946-9.

Caccavo, D., Cascone, S., Lamberti, G., Barba, A.A., 2015. Controlled drug release from hydrogel-based matrices: Experiments and modeling. Int J Pharm 486, 144–152. https://doi.org/10.1016/J.IJPHARM.2015.03.054.

Carvalho, F.C., Bruschi, M.L., Evangelista, R.C., Gremião, M.P.D., 2010. Mucoadhesive drug delivery systems. Brazilian Journal of Pharmaceutical Sciences 46, 1–17. https://doi.org/10.1590/S1984-82502010000100002.

Cascone, S., Lamberti, G., Titomanlio, G., D'Amore, M., Barba, A.A., 2014. Measurements of non-uniform water content in hydroxypropyl-methyl-cellulose based matrices via texture analysis. Carbohydr Polym 103, 348–354. https://doi.org/10.1016/J.CARBPOL.2013.12.060.

Casian, T., Bogdan, C., Tarta, D., Moldovan, M., Tomuta, I., Iurian, S., 2018. Assessment of oral formulation-dependent characteristics of orodispersible tablets using texture profiles and multivariate data analysis. J Pharm Biomed Anal 152, 47–56. https://doi.org/10.1016/j.jpba.2018.01.040.

Chachlioutaki, K., Karavasili, C., Mavrokefalou, E.E., Gioumouxouzis, C.I., Ritzoulis, C., Fatouros, D.G., 2022. Quality control evaluation of paediatric chocolate-based dosage forms: 3D printing vs mold-casting method. Int J Pharm 624. https://doi.org/10.1016/j.ijpharm.2022.121991.

Chandrasekhar, R., Hassan, Z., AlHusban, F., Smith, A.M., Mohammed, A.R., 2009. The role of formulation excipients in the development of lyophilised fast-disintegrating tablets. European Journal of Pharmaceutics and Biopharmaceutics 72, 119–129. https://doi.org/10.1016/j.ejpb.2008.11.011.

Chang, S., Li, J., Sun, C.C., 2017. Tensile and shear methods for measuring strength of bilayer tablets. Int J Pharm 523, 121–126. https://doi.org/10.1016/j.ijpharm.2017.03.010.

Chang, S.Y., Sun, C.C., 2019. Effect of particle size on interfacial bonding strength of bilayer tablets. Powder Technol 356, 97–101. https://doi.org/10.1016/j.powtec.2019.07.100.

Chatzitaki, A.T., Mystiridou, E., Bouropoulos, N., Ritzoulis, C., Karavasili, C., Fatouros, D.G., 2022. Semi-solid extrusion 3D printing of starch-based soft dosage forms for the treatment of paediatric latent tuberculosis infection. Journal of Pharmacy and Pharmacology 74, 1498–1506. https://doi.org/10.1093/JPP/RGAB121.

Chaud, M. v., Lima, A.C., Vila, M.M.D.C., Paganelli, M.O., Paula, F.C., Pedreiro, L.N., Gremião, M.P.D., 2013. Development and evaluation of praziquantel solid dispersions in sodium starch glycolate. Tropical Journal of Pharmaceutical Research 12, 163–168. 10.4314/tjpr.v12i2.5.

Chen, L., Opara, U.L., 2013. Texture measurement approaches in fresh and processed foods - A review. Food Research International 51, 823–835. https://doi.org/10.1016/j.foodres.2013.01.046.

Chen, L., He, Z., Kunnath, K.T., Fan, S., Wei, Y., Ding, X., Zheng, K., Davé, R.N., 2019. Surface engineered excipients: III. Facilitating direct compaction tableting of binary blends containing fine cohesive poorly-compactable APIs. Int J Pharm 557, 354–365. https://doi.org/10.1016/j.ijpharm.2018.12.055.

Chen, H., Zhang, J., Qiao, Q., Hu, E., Wei, Y., Pang, Z., Gao, Y., Qian, S., Zhang, J., Heng, W., 2022. A novel soluble lornoxicam-sodium chelate monohydrate with improved plasticity and tabletability. Int J Pharm 624. https://doi.org/10.1016/j.ijpharm.2022.122060.

Cheng, Y., Qin, H., Acevedo, N.C., Jiang, X., Shi, X., 2020. 3D printing of extended-release tablets of theophylline using hydroxypropyl methylcellulose (HPMC) hydrogels. Int J Pharm 591. https://doi.org/10.1016/j.ijpharm.2020.119983.

Chickering, D.E.I., Mathiowitz, E., 1999. Definitions, Mechanisms and Theories of Bioadhesion. In: Mathiowitz, E. (Ed.), Bioadhesive Drug Delivery Systems: Fundamentals, Novel Approaches, and Development. Marcel Dekker Inc, New York, pp. 1–10.

Cilurzo, F., Minghetti, P., Selmin, F., Casiraghi, A., Montanari, L., 2003. Polymethacrylate salts as new low-swellable mucoadhesive materials. Journal of Controlled Release 88, 43–53. https://doi.org/10.1016/S0168-3659(02)00459-5.

Ciper, M., Bodmeier, R., 2005. Preparation and characterization of novel fast disintegrating capsules (Fastcaps) for administration in the oral cavity. Int J Pharm 303, 62–71. https://doi.org/10.1016/J.IJPHARM.2005.07.004.

Crișan, A.G., Iurian, S., Porfire, A., Rus, L.M., Bogdan, C., Casian, T., Lucacel, R.C., Turza, A., Porav, S., Tomuță, I., 2022. QbD guided development of immediate release FDM-3D printed tablets with customizable API doses. Int J Pharm 613. https://doi.org/10.1016/j.ijpharm.2021.121411.

Croquelois, B., Girardot, J., Kopp, J.B., Cazautets, C., Tchoreloff, P., Mazel, V., 2017. Breaking pharmaceutical tablets with a hole: Reevaluation of the stress concentration factor and influence of the hole size. Powder Technol 317, 126–132. https://doi.org/10.1016/j.powtec.2017.04.033.

Croquelois, B., Girardot, J., Kopp, J.B., Tchoreloff, P., Mazel, V., 2020. Quantification of tablet sensitivity to a stress concentration: Generalization of Hiestand's approach and link with the microstructure. Powder Technol 369, 176–183. https://doi.org/10.1016/j.powtec.2020.05.002.

Texture Analyzer, Ametek Brookfield [WWW Document], n.d. URL https://www.scinteck.com/store/p1201/Brookfield.html (accessed 1.31.23).

CT3 TEXTURE ANALYZER Operating Instructions [WWW Document], n.d. URL https://www.brookfieldengineering.com/-/media/ametekbrookfield/manuals/texture/ct3%20manual%20m08-372-f1116.pdf (accessed 2.1.23).

de Backere, C., de Beer, T., Vervaet, C., Vanhoorne, V., 2022. Effect of feed frame on lubricant sensitivity during upscaling from a compaction simulator to a rotary tablet press. Int J Pharm 616. https://doi.org/10.1016/j.ijpharm.2022.121562.

de Spiegeleer, B., van Vooren, L., Voorspoels, J., Thoné, D., Rosier, J., 2001. Dissolution stability and IVIVC investigation of a buccal tablet. Anal Chim Acta 446, 343–349. https://doi.org/10.1016/S0003-2670(01)01074-1.

Desai, N., Masen, M., Cann, P., Hanson, B., Tuleu, C., Orlu, M., 2022. Modernising Orodispersible Film Characterisation to Improve Palatability and Acceptability Using a Toolbox of Techniques. Pharmaceutics 14. https://doi.org/10.3390/pharmaceutics14040732.

do Couto, R.O., Cubayachi, C., Calefi, P.L., Lopez, R.F.V., Pedrazzi, V., de Gaitani, C.M., de Freitas, O., 2017. Combining amino amide salts in mucoadhesive films enhances needle-free buccal anesthesia in adults. Journal of Controlled Release 266, 205–215. 10.1016/j.jconrel.2017.09.039.

Dor, P.J.M., Fix, J.A., 2000. In Vitro Determination of Disintegration Time of Quick-Dissolve Tablets Using a New Method. Pharm Dev Technol 5, 575–577. https://doi.org/10.1081/PDT-100102041.

Duchene, D., Touchard, F., Peppas, N.A., 2008. Pharmaceutical and Medical Aspects of Bioadhesive Systems for Drug Administration. Drug Dev Ind Pharm 14, 283–318. https://doi.org/10.3109/03639048809151972.

Dun, J., Osei-Yeboah, F., Boulas, P., Lin, Y., Sun, C.C., 2018. A systematic evaluation of dual functionality of sodium lauryl sulfate as a tablet lubricant and wetting enhancer. Int J Pharm 552, 139–147. https://doi.org/10.1016/j.ijpharm.2018.09.056.

Dun, J., Chen, H., Sun, C.C., 2020. Profound tabletability deterioration of microcrystalline cellulose by magnesium stearate. Int J Pharm 590. https://doi.org/10.1016/j.ijpharm.2020.119927.

Dvořák, J., Tomas, J., Lizoňová, D., Schöngut, M., Dammer, O., Pekárek, T., Beránek, J., Štěpánek, F., 2020. Investigation of tablet disintegration pathways by the combined

use of magnetic resonance imaging, texture analysis and static light scattering. Int J Pharm 587. https://doi.org/10.1016/j.ijpharm.2020.119719.
El-Arini, S.K., Clas, S.D., 2002. Evaluation of Disintegration Testing of Different Fast Dissolving Tablets Using the Texture Analyzer. Pharm Dev Technol 7, 361–371. https://doi.org/10.1081/PDT-120005732.
Eleftheriadis, G.K., Ritzoulis, C., Bouropoulos, N., Tzetzis, D., Andreadis, D.A., Boetker, J., Rantanen, J., Fatouros, D.G., 2019. Unidirectional drug release from 3D printed mucoadhesive buccal films using FDM technology: In vitro and ex vivo evaluation. European Journal of Pharmaceutics and Biopharmaceutics 144, 180–192. https://doi.org/10.1016/j.ejpb.2019.09.018.
Eleftheriadis, G.K., Monou, P.K., Bouropoulos, N., Boetker, J., Rantanen, J., Jacobsen, J., Vizirianakis, I.S., Fatouros, D.G., 2020. Fabrication of Mucoadhesive Buccal Films for Local Administration of Ketoprofen and Lidocaine Hydrochloride by Combining Fused Deposition Modeling and Inkjet Printing. J Pharm Sci 109, 2757–2766. https://doi.org/10.1016/j.xphs.2020.05.022.
El-Malah, Y., Nazzal, S., 2010. Preparation of delayed release tablet dosage forms by compression coating: Effect of coating material on theophylline release. Pharm Dev Technol 15, 305–310. https://doi.org/10.3109/10837450903188519.
El-Malah, Y., Nazzal, S., 2013. "Real-time" disintegration analysis and D-optimal experimental design for the optimization of diclofenac sodium fast-dissolving films. Pharmaceutical Development and Technology 18, 1355–1360. https://doi.org/10.3109/10837450.2012.700936.
Farias, S., Boateng, J.S., 2018. Development and functional characterization of composite freeze dried wafers for potential delivery of low dose aspirin for elderly people with dysphagia. Int J Pharm 553, 65–83. https://doi.org/10.1016/j.ijpharm.2018.10.025.
Farias, S., Boateng, J.S., 2020. In vitro, ex vivo and in vivo evaluation of taste masked low dose acetylsalicylic acid loaded composite wafers as platforms for buccal administration in geriatric patients with dysphagia. Int J Pharm 589. https://doi.org/10.1016/j.ijpharm.2020.119807.
Fell, J.T., Newton, J.M., 1970. Determination of Tablet Strength by the Diametral-Compression Test. J Pharm Sci 59, 688–691. https://doi.org/10.1002/jps.2600590523.
Flügel, K., Hennig, R., Thommes, M., 2020. Impact of structural relaxation on mechanical properties of amorphous polymers. European Journal of Pharmaceutics and Biopharmaceutics 154, 214–221. https://doi.org/10.1016/j.ejpb.2020.07.016.
Foegeding, E.A., Drake, M.A., 2007. Invited review: Sensory and mechanical properties of cheese texture. J Dairy Sci 90, 1611–1624. https://doi.org/10.3168/jds.2006-703.
Gennari, C.G.M., Sperandeo, P., Polissi, A., Minghetti, P., Cilurzo, F., 2019. Lysozyme Mucoadhesive Tablets Obtained by Freeze-Drying. J Pharm Sci 108, 3667–3674. https://doi.org/10.1016/j.xphs.2019.08.011.
Göbel, A., da Silva, J.B., Cook, M., Breitkreutz, J., 2021. Development of buccal film formulations and their mucoadhesive performance in biomimetic models. Int J Pharm 610. https://doi.org/10.1016/j.ijpharm.2021.121233.
Gong, X., Sun, C.C., 2015. A new tablet brittleness index. European Journal of Pharmaceutics and Biopharmaceutics 93, 260–266. https://doi.org/10.1016/j.ejpb.2015.04.007.
Gottschalk, N., Quodbach, J., Elia, A.G., Hess, F., Bogdahn, M., 2022. Determination of feed forces to improve process understanding of Fused Deposition Modeling 3D printing and to ensure mass conformity of printed solid oral dosage forms. Int J Pharm 614, 121416. https://doi.org/10.1016/J.IJPHARM.2021.121416.
Gryczke, A., Schminke, S., Maniruzzaman, M., Beck, J., Douroumis, D., 2011. Development and evaluation of orally disintegrating tablets (ODTs) containing Ibuprofen granules prepared by hot melt extrusion. Colloids Surf B Biointerfaces 86, 275–284. https://doi.org/10.1016/j.colsurfb.2011.04.007.
Gugulothu, D., Desai, P., Pandharipande, P., Patravale, V., 2015. Freeze drying: Exploring potential in development of orodispersible tablets of sumatriptan succinate. Drug Dev Ind Pharm 41, 398–405. https://doi.org/10.3109/03639045.2013.871551.
Guinard, J.-X., Mazzucchelli, R., 1996. The sensory perception of texture and mouthfeel. Trends Food Sci Technol 7, 213–219. https://doi.org/10.1016/0924-2244(96)10025-X.
Gültekin, H.E., Tort, S., Acartürk, F., 2019. An Effective Technology for the Development of Immediate Release Solid Dosage Forms Containing Low-Dose Drug: Fused Deposition Modeling 3D Printing. Pharm Res 36. https://doi.org/10.1007/s11095-019-2655-y.
Gültekin, H.E., Tort, S., Tuğcu-Demiröz, F., Acartürk, F., 2021. 3D printed extended release tablets for once daily use: An in vitro and in vivo evaluation study for a personalized solid dosage form. Int J Pharm 596. https://doi.org/10.1016/j.ijpharm.2021.120222.
Gurpreetarora, Malik, K., Rana, V., Singh, I., 2012. Gum ghatti - A pharmaceutical excipient: Development, evaluation and optimization of sustained release mucoadhesive matrix tablets of domperidone [WWW Document]. Acta Pol Pharm. URL https://www.researchgate.net/publication/230643748_Gum_ghatti_-_A_pharmaceutical_excipient_Development_evaluation_and_optimization_of_sustained_release_mucoadhesive_matrix_tablets_of_domperidone (accessed 2.2.23).
Hackl, E. v., Ermolina, I., 2016. Using Texture Analysis Technique to Assess the Freeze-Dried Cakes in Vials. J Pharm Sci 105, 2073–2085. 10.1016/j.xphs.2016.05.016.
Hackl, E., Ermolina, I., 2019. Application of Texture Analysis Technique in Formulation Development of Lyophilized Orally Disintegrating Tablets Containing Mannitol. Polyvinylpyrrolidone and Amino Acids. AAPS PharmSciTech 20. https://doi.org/10.1208/s12249-018-1269-8.
Hagen, E., Løding, F.S., Mattsson, S., Tho, I., 2016. Use of interactive mixtures to obtain mini-tablets with high dose homogeneity for paediatric drug delivery. J Drug Deliv Sci Technol 34, 51–59. https://doi.org/10.1016/j.jddst.2016.03.006.
Hagesaether, E., Hiorth, M., Sande, S.A., 2009. Mucoadhesion and drug permeability of free mixed films of pectin and chitosan: An in vitro and ex vivo study. European Journal of Pharmaceutics and Biopharmaceutics 71, 325–331. https://doi.org/10.1016/j.ejpb.2008.09.002.
Han, J.K., Kim, J.Y., Choi, D.H., Park, E.S., 2022. A formulation development strategy for dual-release bilayer tablets: An integrated approach of quality by design and a placebo layer. Int J Pharm 618. https://doi.org/10.1016/j.ijpharm.2022.121659.
Hejduk, A., Czajka, S., Lulek, J., 2021. Impact of co-processed excipient particles solidity and circularity on critical quality attributes of orodispersible minitablets. Powder Technol 387, 494–508. https://doi.org/10.1016/j.powtec.2021.03.063.
Hofmanová, J.K., Mason, J., Batchelor, H.K., 2021. Tribology provides an in vitro tool that correlated to in vivo sensory data on the mouthfeel of coated tablets. Int J Pharm 597. https://doi.org/10.1016/j.ijpharm.2021.120323.
Hu, Z., Xu, P., Zhang, J., Bandari, S., Repka, M.A., 2022. Development of controlled release oral dosages by density gradient modification via three-dimensional (3D) printing and hot-melt extrusion (HME) technology. J Drug Deliv Sci Technol 71, 103355. https://doi.org/10.1016/J.JDDST.2022.103355.
Iftimi, L.D., Edinger, M., Bar-Shalom, D., Rantanen, J., Genina, N., 2019. Edible solid foams as porous substrates for inkjet-printable pharmaceuticals. European Journal of Pharmaceutics and Biopharmaceutics 136, 38–47. https://doi.org/10.1016/j.ejpb.2019.01.004.
Ikeuchi-Takahashi, Y., Watanabe, N., Sasatsu, M., Onishi, H., 2013. Formulation and evaluation of matrix type mucoadhesive tablets aimed at treating oral aphtha. Drug Dev Ind Pharm 39, 1254–1261. https://doi.org/10.3109/03639045.2012.717297.
ISO - ISO 5492:2008 - Sensory analysis — Vocabulary [WWW Document], n.d. URL https://www.iso.org/standard/38051.html (accessed 1.31.23).
Ito, I., Ito, A., Unezaki, S., 2019. Preparation and evaluation of water-absorbing swollen mini-tablet aimed at improving ingestion. J Drug Deliv Sci Technol 50, 201–207. https://doi.org/10.1016/j.jddst.2019.01.009.
Iurian, S., Bogdan, C., Tomuță, I., Szabó-Révész, P., Chvatal, A., Leucuța, S.E., Moldovan, M., Ambrus, R., 2017a. Development of oral lyophilisates containing meloxicam nanocrystals using QbD approach. European Journal of Pharmaceutical Sciences 104, 356–365. https://doi.org/10.1016/j.ejps.2017.04.011.
Iurian, S., Dinte, E., Iuga, C., Bogdan, C., Spiridon, I., Barbu-Tudoran, L., Bodoki, A., Tomuță, I., Leucuța, S.E., 2017b. The pharmaceutical applications of a biopolymer isolated from Trigonella foenum-graecum seeds: Focus on the freeze-dried matrix forming capacity. Saudi Pharmaceutical Journal 25, 1217–1225. https://doi.org/10.1016/j.jsps.2017.09.006.
Kajthunyakarn, W., Khlibsuwan, R., Sakloetsakun, D., Pongjanyakul, T., 2019. Sodium caseinate films modified using halloysite: Physicochemical characterization and drug permeability studies. J Drug Deliv Sci Technol 54. https://doi.org/10.1016/j.jddst.2019.101235.
Karemore, M.N., Bali, N.R., 2021. Gellan gum based gastroretentive tablets for bioavailability enhancement of cilnidipine in human volunteers. Int J Biol Macromol 174, 424–439. https://doi.org/10.1016/J.IJBIOMAC.2021.01.199.
Karrout, Y., Neut, C., Wils, D., Siepmann, F., Deremaux, L., Flament, M., Dubreuil, L., Desreumaux, P., Siepmann, J., 2010. Enzymatically activated coated multiparticulates containing theophylline for colon targeting. J Drug Deliv Sci Technol 20, 193–199. https://doi.org/10.1016/S1773-2247(10)50029-7.
Kawano, Y., Sasatsu, M., Mizutani, A., Hirose, K., Hanawa, T., Onishi, H., 2016. Preparation and Evaluation of Stomatitis Film Using Xyloglucan Containing Loperamide. Chem. Pharm. Bull 564, 564–569. https://doi.org/10.1248/cpb.c15-00926.
Khan, D., Kirby, D., Bryson, S., Shah, M., Rahman Mohammed, A., 2022. Paediatric specific dosage forms: Patient and formulation considerations. Int J Pharm 616, 121501. https://doi.org/10.1016/J.IJPHARM.2022.121501.
Khuathan, N., Pongjanyakul, T., 2014. Modification of quaternary polymethacrylate films using sodium alginate: Film characterization and drug permeability. Int J Pharm 460, 63–72. https://doi.org/10.1016/j.ijpharm.2013.10.050.
Kilicarslan, M., Ilhan, M., Inal, O., Orhan, K., 2018. Preparation and evaluation of clindamycin phosphate loaded chitosan/alginate polyelectrolyte complex film as mucoadhesive drug delivery system for periodontal therapy. European Journal of Pharmaceutical Sciences 123, 441–451. https://doi.org/10.1016/j.ejps.2018.08.007.
Kiniwa, R., Miyake, M., Kimura, S. ichiro, Itai, S., Kondo, H., Iwao, Y., 2019. Development of muco-adhesive orally disintegrating tablets containing tamarind gum-coated tea powders for oral care. Int J Pharm X 1, 100012. 10.1016/J.IJPX.2019.100012.
Kottke, D., Burckhardt, B.B., Knaab, T.C., Breitkreutz, J., Fischer, B., 2021. Development and evaluation of a composite dosage form containing desmopressin acetate for buccal administration. Int J Pharm X 3. https://doi.org/10.1016/j.ijpx.2021.100082.
Kraisit, P., Limmatvapirat, S., Nunthanid, J., Sriamornsak, P., Luangtana-Anan, M., 2017. Preparation and characterization of hydroxypropyl methylcellulose/polycarbophil mucoadhesive blend films using a mixture design approach. Chem Pharm Bull (Tokyo) 65, 284–294. https://doi.org/10.1248/cpb.c16-00849.
Kuck, J., Breitkreutz, J., 2022. Impact of lubrication on key properties of orodispersible minitablets in comparison to conventionally sized orodispersible tablets. European Journal of Pharmaceutics and Biopharmaceutics 180, 71–80. https://doi.org/10.1016/j.ejpb.2022.08.023.
Kulinowski, P., Woyna-Orlewicz, K., Rappen, G.M., Haznar-Garbacz, D., Węglarz, W.P., Dorożyński, P.P., 2015. An understanding of modified release matrix tablets behavior during drug dissolution as the key for prediction of pharmaceutical product performance - Case study of multimodal characterization of quetiapine fumarate tablets. Int J Pharm 484, 235–245. https://doi.org/10.1016/j.ijpharm.2015.02.040.

LaFountaine, J.S., Prasad, L.K., Miller, D.A., McGinity, J.W., Williams, R.O., 2017. Mucoadhesive amorphous solid dispersions for sustained release of poorly water soluble drugs. European Journal of Pharmaceutics and Biopharmaceutics 113, 157–167. https://doi.org/10.1016/J.EJPB.2016.12.031.

Lee, J.H., Park, C., Song, I.O., Lee, B.J., Kang, C.Y., Park, J.B., 2022. Investigation of Patient-Centric 3D-Printed Orodispersible Films Containing Amorphous Aripiprazole. Pharmaceuticals 15. https://doi.org/10.3390/ph15070895.

Li, L., Wang, L., Li, J., Jiang, S., Wang, Y., Zhang, X., Ding, J., Yu, T., Mao, S., 2014. Insights into the mechanisms of chitosan-anionic polymers-based matrix tablets for extended drug release. Int J Pharm 476, 253–265. https://doi.org/10.1016/j.ijpharm.2014.09.057.

Limmatvapirat, S., Panchapornpon, D., Limmatvapirat, C., Nunthanid, J., Luangtana-Anan, M., Puttipipatkhachorn, S., 2008. Formation of shellac succinate having improved enteric film properties through dry media reaction. European Journal of Pharmaceutics and Biopharmaceutics 70, 335–344. https://doi.org/10.1016/J.EJPB.2008.03.002.

Liu, B., Wang, J., Zhou, Q., Zhao, L., Wang, Y., Shen, L., Feng, Y., Du, R., 2022. High shear wet granulation: Improved understanding of the effects of process variables on granule and tablet properties of a high-dose, high-hydrophobicity API based on quality by design and multivariate analysis approaches. Advanced Powder Technology 33. https://doi.org/10.1016/j.apt.2021.11.021.

Lura, A., Breitkreutz, J., 2022. Manufacturing of mini-tablets. Focus and impact of the tooling systems. J Drug Deliv Sci Technol 72. https://doi.org/10.1016/j.jddst.2022.103357.

Lura, A., Tardy, G., Kleinebudde, P., Breitkreutz, J., 2020. Tableting of mini-tablets in comparison with conventionally sized tablets: A comparison of tableting properties and tablet dimensions. Int J Pharm X 2. https://doi.org/10.1016/j.ijpx.2020.100061.

Lura, A., Elezaj, V., Kokott, M., Fischer, B., Breitkreutz, J., 2021. Transfer and scale-up of the manufacturing of orodispersible mini-tablets from a compaction simulator to an industrial rotary tablet press. Int J Pharm 602. https://doi.org/10.1016/j.ijpharm.2021.120636.

Machado, A.H.E., Kokubo, T., Dujovny, G., Jones, B., Scialdone, C., Bravo, R., Kuentz, M., 2016. A microstructural study of water effects in lipid-based pharmaceutical formulations for liquid filling of capsules. European Journal of Pharmaceutical Sciences 90, 64–75. https://doi.org/10.1016/j.ejps.2016.04.035.

Matulyte, I., Marksa, M., Bernatoniene, J., 2021a. Development of innovative chewable gel tablets containing nutmeg essential oil microcapsules and their physical properties evaluation. Pharmaceutics 13. https://doi.org/10.3390/pharmaceutics13060873.

Matulyte, I., Mataraite, A., Velziene, S., Bernatoniene, J., 2021b. The Effect of Myristica fragrans on Texture Properties and Shelf-Life of Innovative Chewable Gel Tablets. Pharmaceutics 13, 238. https://doi.org/10.3390/PHARMACEUTICS13020238.

Mazel, V., Guerard, S., Croquelois, B., Kopp, J.B., Girardot, J., Diarra, H., Busignies, V., Tchoreloff, P., 2016. Reevaluation of the diametral compression test for tablets using the flattened disc geometry. Int J Pharm 513, 669–677. https://doi.org/10.1016/j.ijpharm.2016.09.088.

Mazel, V., Diarra, H., Malvestio, J., Tchoreloff, P., 2018. Lamination of biconvex tablets: Numerical and experimental study. Int J Pharm 542, 66–71. https://doi.org/10.1016/j.ijpharm.2018.03.012.

Meruva, S., Thool, P., Gong, Y., Agrawal, A., Karki, S., Bowen, W., Mitra, B., Kumar, S., 2021. A Novel Use of Nanocrystalline Suspensions to Develop Sub-Microgram Dose Micro-Tablets. J Pharm Sci 110, 3276–3288. https://doi.org/10.1016/j.xphs.2021.05.025.

Mirdamadian, S.Z., Varshosaz, J., Minaiyan, M., Taheri, A., 2022. 3D printed tablets containing oxaliplatin loaded alginate nanoparticles for colon cancer targeted delivery. An in vitro/in vivo study. Int J Biol Macromol 205, 90–109. https://doi.org/10.1016/j.ijbiomac.2022.02.080.

Mitra, B., Hilden, J., Litster, J.D., 2015. Novel use of monodisperse granules to deconvolute impacts of granule size versus granule solid fraction on tablet tensile strength. Advanced Powder Technology 26, 553–562. https://doi.org/10.1016/J.APT.2015.01.004.

Mizrahi, B., Golenser, J., Wolnerman, J.S., Domb, A.J., 2004. Adhesive tablet effective for treating canker sores in humans. J Pharm Sci 93, 2927–2935. https://doi.org/10.1002/jps.20193.

Nazzal, S., Nazzal, M., El-Malah, Y., 2007. A novel texture-probe for the simultaneous and real-time measurement of swelling and erosion rates of matrix tablets. Int J Pharm 330, 195–198. https://doi.org/10.1016/j.ijpharm.2006.08.045.

Nep, E.I., Conway, B.R., 2011. Grewia gum 2: Mucoadhesive properties of compacts and gels. Tropical Journal of Pharmaceutical Research 10, 393–401. https://doi.org/10.4314/tjpr.v10i4.4.

Oladeji, S., Mohylyuk, V., Jones, D.S., Andrews, G.P., 2022. 3D printing of pharmaceutical oral solid dosage forms by fused deposition: The enhancement of printability using plasticised HPMCAS. Int J Pharm 616. https://doi.org/10.1016/j.ijpharm.2022.121553.

Oliver, W.C., Pharr, G.M., 2004. Measurement of hardness and elastic modulus by instrumented indentation: Advances in understanding and refinements to methodology. J Mater Res 19, 3–20. https://doi.org/10.1557/JMR.2004.19.1.3.

Owens, T.S., Dansereau, R.J., Sakr, A., 2005. Development and evaluation of extended release bioadhesive sodium fluoride tablets. Int J Pharm 288, 109–122. https://doi.org/10.1016/J.IJPHARM.2004.09.017.

Owusu-Ware, S.K., Boateng, J., Jordan, D., Portefaix, S., Tasseto, R., Ramano, C.D., Antonijević, M.D., 2016. Molecular mobility of hydroxyethyl cellulose (HEC) films characterised by thermally stimulated currents (TSC) spectroscopy. Int J Pharm 497, 222–227. https://doi.org/10.1016/j.ijpharm.2015.11.052.

Owusu-Ware, S.K., Boateng, J.S., Chowdhry, B.Z., Antonijevic, M.D., 2019. Glassy state molecular mobility and its relationship to the physico-mechanical properties of plasticized hydroxypropyl methylcellulose (HPMC) films. Int J Pharm X 1. https://doi.org/10.1016/j.ijpx.2019.100033.

Partheniadis, I., Athanasiou, K., Laidmäe, I., Heinämäki, J., Nikolakakis, I., 2022. Physicomechanical characterization and tablet compression of theophylline nanofibrous mats prepared by conventional and ultrasound enhanced electrospinning. Int J Pharm 616. https://doi.org/10.1016/j.ijpharm.2022.121558.

Patel, V.F., Liu, F., Brown, M.B., 2012. Modeling the oral cavity: In vitro and in vivo evaluations of buccal drug delivery systems. Journal of Controlled Release 161, 746–756. https://doi.org/10.1016/j.jconrel.2012.05.026.

Patel, S., Sun, C.C., 2016. Macroindentation hardness measurement—Modernization and applications. Int J Pharm 506, 262–267. https://doi.org/10.1016/J.IJPHARM.2016.04.068.

Paul, S., Baranwal, Y., Tseng, Y.C., 2021. An insight into predictive parameters of tablet capping by machine learning and multivariate tools. Int J Pharm 599. https://doi.org/10.1016/j.ijpharm.2021.120439.

Paul, S., Sun, C.C., 2018. Systematic evaluation of common lubricants for optimal use in tablet formulation. European Journal of Pharmaceutical Sciences 117, 118–127. https://doi.org/10.1016/j.ejps.2018.02.013.

Paul, S., Wang, C., Sun, C.C., 2022. An extended macroindentation method for determining the hardness of poorly compressible materials. Int J Pharm 624, 122054. https://doi.org/10.1016/J.IJPHARM.2022.122054.

Peerapattana, J., Ngamsupsiri, T., Cheucharoenvasuchai, N., Saikaew, C., 2015. Optimization of metronidazole sustained-release films using D-optimal design. Int J Pharm 484, 1–7. https://doi.org/10.1016/j.ijpharm.2015.02.019.

Pekoz, A.Y., Erdal, M.S., Okyar, A., Ocak, M., Tekeli, F., Kaptan, E., Sagirli, O., Araman, A., 2015. Preparation and in-vivo evaluation of dimenhydrinate buccal mucoadhesive films with enhanced bioavailability. Drug Dev Ind Pharm 42, 916–925. https://doi.org/10.3109/03639045.2015.1091470.

Perumalla, S.R., Sun, C.C., 2014. Enabling tablet product development of 5-fluorocytosine through integrated crystal and particle engineering. J Pharm Sci 103, 1126–1132. https://doi.org/10.1002/jps.23876.

Picart, L., Mazel, V., Moulin, A., Bourgeaux, V., Tchoreloff, P., 2022. Breaking patterns of press-coated tablets during the diametral compression test: Influence of the product, geometry and process parameters. Int J Pharm 612. https://doi.org/10.1016/j.ijpharm.2021.121371.

Pitt, K.G., Heasley, M.G., 2013. Determination of the tensile strength of elongated tablets. Powder Technol 238, 169–175. https://doi.org/10.1016/j.powtec.2011.12.060.

Pitt, K.G., Newton, J.M., Richardson, R., Stanley, P., 1989. The Material Tensile Strength of Convex-faced Aspirin Tablets. Journal of Pharmacy and Pharmacology 41, 289–292. https://doi.org/10.1111/J.2042-7158.1989.TB06458.X.

Pongjanyakul, T., Khuathan, N., 2016. Quaternary polymethacrylate-sodium alginate films: Effect of alginate block structures and use for sustained release tablets. Pharm Dev Technol 21, 487–498. https://doi.org/10.3109/10837450.2015.1022787.

Prakash, S., Tan, D.D.Y., Chen, J., 2013. Applications of tribology in studying food oral processing and texture perception. Food Research International 54, 1627–1635. https://doi.org/10.1016/j.foodres.2013.10.010.

Prasad, E., Islam, M.T., Goodwin, D.J., Megarry, A.J., Halbert, G.W., Florence, A.J., Robertson, J., 2019. Development of a hot-melt extrusion (HME) process to produce drug loaded Affinisol™ 15LV filaments for fused filament fabrication (FFF) 3D printing. Addit Manuf 29, 100776. https://doi.org/10.1016/J.ADDMA.2019.06.027.

Prasad, L.K., Keen, J.M., Lafountaine, J.S., Maincent, J., Williams, R.O., McGinity, J.W., 2015. Electrostatic powder deposition to prepare films for drug delivery. J Drug Deliv Sci Technol 30, 501–510. https://doi.org/10.1016/j.jddst.2015.08.011.

Preis, M., Gronkowsky, D., Grytzan, D., Breitkreutz, J., 2014a. Comparative study on novel test systems to determine disintegration time of orodispersible films. Journal of Pharmacy and Pharmacology 66, 1102–1111. https://doi.org/10.1111/jphp.12246.

Preis, M., Knop, K., Breitkreutz, J., 2014b. Mechanical strength test for orodispersible and buccal films. Int J Pharm 461, 22–29. https://doi.org/10.1016/j.ijpharm.2013.11.033.

Prodduturi, S., Manek, R. v., Kolling, W.M., Stodghill, S.P., Repka, M.A., 2004. Water vapor sorption of hot-melt extruded hydroxypropyl cellulose films: Effect on physico-mechanical properties, release characteristics, and stability. J Pharm Sci 93, 3047–3056. 10.1002/jps.20222.

Prodduturi, S., Manek, R. v., Kolling, W.M., Stodghill, S.P., Repka, M.A., 2005. Solid-state stability and characterization of hot-melt extruded poly(ethylene oxide) films. J Pharm Sci 94, 2232–2245. 10.1002/jps.20437.

Pund, S., Joshi, A., Vasu, K., Nivsarkar, M., Shishoo, C., 2011. Gastroretentive delivery of rifampicin: In vitro mucoadhesion and in vivo gamma scintigraphy. Int J Pharm 411, 106–112. https://doi.org/10.1016/j.ijpharm.2011.03.048.

Qi, X., Tester, R., Liu, Y., Mullin, M., 2012. Applications of β-limit Dextrin as a Matrix Forming Excipient for Fast Disintegrating Buccal Dosage Formats. Journal of Pharmacy & Pharmaceutical Sciences 15, 669–679. https://doi.org/10.18433/J3RC8M.

Radebaugh, G.W., Murtha, J.L., Julian, T.N., Bondi, J.N., 1988. Methods for evaluating the puncture and shear properties of pharmaceutical polymeric films. Int J Pharm 45, 39–46. https://doi.org/10.1016/0378-5173(88)90032-4.

Rahman, Z., Zidan, A.S., Korang-Yeboah, M., Yang, Y., Siddiqui, A., Shakleya, D., Khan, M.A., Cruz, C., Ashraf, M., 2017. Effects of excipients and curing process on the abuse deterrent properties of directly compressed tablets. Int J Pharm 517, 303–311. https://doi.org/10.1016/j.ijpharm.2016.12.015.

Rai, P.R., Tiwary, A.K., Rana, V., 2012. Optimization of an aqueous tablet-coating process containing carboxymethylated Cassia fistula gum. AAPS PharmSciTech 13, 431–440. https://doi.org/10.1208/s12249-012-9763-x.

Repka, M.A., Elsohly, M.A., Munjal, M., Ross, S.A., 2006. Temperature Stability and Bioadhesive Properties of Δ9-Tetrahydrocannabinol Incorporated Hydroxypropylcellulose Polymer Matrix Systems. Drug Dev Ind Pharm 32, 21–32. https://doi.org/10.1080/03639040500387914.

Rodríguez-Pombo, L., Awad, A., Basit, A.W., Alvarez-Lorenzo, C., Goyanes, A., 2022. Innovations in Chewable Formulations: The Novelty and Applications of 3D Printing in Drug Product Design. Pharmaceutics 14, 1732. https://doi.org/10.3390/PHARMACEUTICS14081732/S1.

Rongthong, T., Sungthongjeen, S., Siepmann, J., Pongjanyakul, T., 2013. Quaternary polymethacrylate–magnesium aluminum silicate films: Molecular interactions, mechanical properties and tackiness. Int J Pharm 458, 57–64. https://doi.org/10.1016/J.IJPHARM.2013.10.016.

Saab, M., Mehanna, M.M., 2019. Disintegration time of orally dissolving films: Various methodologies and in-vitro/in-vivo correlation. Pharmazie 74, 227–230. https://doi.org/10.1691/ph.2019.8231.

Sabri, A.H., Hallam, C.N., Baker, N.A., Murphy, D.S., Gabbott, I.P., 2018. Understanding tablet defects in commercial manufacture and transfer. J Drug Deliv Sci Technol 46, 1–6. https://doi.org/10.1016/j.jddst.2018.04.020.

Sakloetsakun, D., Preechagoon, D., Bernkop-Schnürch, A., Pongjanyakul, T., 2016. Chitosan–gum arabic polyelectrolyte complex films: physicochemical, mechanical and mucoadhesive properties. Pharm Dev Technol 21, 590–599. https://doi.org/10.3109/10837450.2015.1035727.

Salawi, A., Sonju, J.J., Kamal, M.M., Abu-Fayyad, A., al Hagbani, T., Nazzal, S., 2021. Preparation and characterization of aqueous vitamin E/Soluplus® dispersions for film coating applications. Drug Dev Ind Pharm 47, 1335–1341. 10.1080/03639045.2021.1991367.

Samaro, A., Janssens, P., Vanhoorne, V., van Renterghem, J., Eeckhout, M., Cardon, L., de Beer, T., Vervaet, C., 2020. Screening of pharmaceutical polymers for extrusion-Based Additive Manufacturing of patient-tailored tablets. Int J Pharm 586. https://doi.org/10.1016/j.ijpharm.2020.119591.

Samaro, A., Shaqour, B., Goudarzi, N.M., Ghijs, M., Cardon, L., Boone, M.N., Verleije, B., Beyers, K., Vanhoorne, V., Cos, P., Vervaet, C., 2021. Can filaments, pellets and powder be used as feedstock to produce highly drug-loaded ethylene-vinyl acetate 3D printed tablets using extrusion-based additive manufacturing? Int J Pharm 607. https://doi.org/10.1016/j.ijpharm.2021.120922.

Sankar, R., Jain, S.K., 2013. Development and characterization of gastroretentive sustained-release formulation by combination of swelling and mucoadhesive approach: A mechanistic study. Drug Des Devel Ther 7, 1455–1469. https://doi.org/10.2147/DDDT.S52890.

Scheuerle, R.L., Gerrard, S.E., Kendall, R.A., Tuleu, C., Slater, N.K.H., Mahbubani, K.T., 2015. Characterising the disintegration properties of tablets in opaque media using texture analysis. Int J Pharm 486, 136–143. https://doi.org/10.1016/j.ijpharm.2015.03.023.

Schmidt, L.M., dos Santos, J., de Oliveira, T.V., Funk, N.L., Petzhold, C.L., Benvenutti, E. V., Deon, M., Beck, R.C.R., 2022. Drug-loaded mesoporous silica on carboxymethyl cellulose hydrogel: Development of innovative 3D printed hydrophilic films. Int J Pharm 620. https://doi.org/10.1016/j.ijpharm.2022.121750.

Schreuders, F.K.G., Schlangen, M., Kyriakopoulou, K., Boom, R.M., van der Goot, A.J., 2021. Texture methods for evaluating meat and meat analogue structures: A review. Food Control 127. https://doi.org/10.1016/j.foodcont.2021.108103.

Şenel, S., Çapan, Y., Sargon, M.F., Giray, C.B., Hincal, A.A., 1998. Histological and bioadhesion studies on buccal bioadhesive tablets containing a penetration enhancer sodium glycodeoxycholate. Int J Pharm 170, 239–245. https://doi.org/10.1016/S0378-5173(98)00148-3.

Shakweh, M., Bravo-Osuna, I., Ponchel, G., 2007. Comparative in vitro study of oesophageal adhesiveness of different commercial formulations containing alendronate. European Journal of Pharmaceutical Sciences 31, 262–270. https://doi.org/10.1016/J.EJPS.2007.03.012.

Sharma, O.P., Shah, M. v., Parikh, D.C., Mehta, T.A., 2015. Formulation optimization of gastroretentive drug delivery system for allopurinol using experimental design. Expert Opin Drug Deliv 12, 513–524. 10.1517/17425247.2014.944861.

Shumeyko, C.M., Dunstan, M., Goins, P., Yin, D., Cline, J.E., Dunstan, M.K., Goins, P.E., Field, D.M., 2019. Snap, crackle and pop: breaking chocolate to understand composite design. Journal of Materials Education 41, 27–40.

Singh, I., Rana, V., 2013. Iron oxide induced enhancement of mucoadhesive potential of Eudragit RLPO: Formulation, evaluation and optimization of mucoadhesive drug delivery system. Expert Opin Drug Deliv 10, 1179–1191. https://doi.org/10.1517/17425247.2013.790361.

Singh, I., Rana, V., 2014. Exploiting the interaction of polymethacrylates with iron oxide for the enhancement of mucoadhesive strength. Pak J Pharm Sci 27, 343–350.

Speer, I., Lenhart, V., Preis, M., Breitkreutz, J., 2019. Prolonged release from orodispersible films by incorporation of diclofenac-loaded micropellets. Int J Pharm 554, 149–160. https://doi.org/10.1016/j.ijpharm.2018.11.013.

Stokes, J.R., Boehm, M.W., Baier, S.K., 2013. Oral processing, texture and mouthfeel: From rheology to tribology and beyond. Curr Opin Colloid Interface Sci 18, 349–359. https://doi.org/10.1016/j.cocis.2013.04.010.

Stomberg, C., Kanikanti, V.R., Hamann, H.J., Kleinebudde, P., 2017. Development of a New Dissolution Test Method for Soft Chewable Dosage Forms. AAPS PharmSciTech 18, 2446–2453. https://doi.org/10.1208/s12249-017-0729-x.

Szabó, B., Sebe, I., Kállai, N., Süvegh, K., Zelkó, R., 2013. Comparison of the micro- and macrostructural characteristics of biopolymer cast films. Eur Polym J 49, 2422–2425. https://doi.org/10.1016/J.EURPOLYMJ.2013.03.033.

Szakonyi, G., Zelkó, R., 2013. Prediction of oral disintegration time of fast disintegrating tablets using texture analyzer and computational optimization. Int J Pharm 448, 346–353. https://doi.org/10.1016/j.ijpharm.2013.03.047.

Szekalska, M., Amelian, A., Winnicka, K., 2015. Alginate microspheres obtained by the spray drying technique as mucoadhesive carriers of ranitidine. Acta Pharmaceutica 65, 15–27. https://doi.org/10.1515/acph-2015-0008.

TA.XTplus Texture Analyser | Stable Micro Systems Products [WWW Document], n.d. URL https://www.stablemicrosystems.com/TAXTplus.html (accessed 1.31.23).

Tabriz, A.G., Scoutaris, N., Gong, Y., Hui, H.W., Kumar, S., Douroumis, D., 2021. Investigation on hot melt extrusion and prediction on 3D printability of pharmaceutical grade polymers. Int J Pharm 604, 120755. https://doi.org/10.1016/J.IJPHARM.2021.120755.

Tamburic, S., Craig, D.Q.M., 1997. A comparison Research paper of different in vitro methods mucoadhesive performance for measuring. European Journal of Pharmaceutics and Biopharmaceutics 44, 159–167.

Texture Profile Analysis | Texture Technologies [WWW Document], n.d. URL https://texturetechnologies.com/resources/texture-profile-analysis#tpa-measurements (accessed 1.31.23).

Than, Y.M., Titapiwatanakun, V., 2021. Tailoring immediate release FDM 3D printed tablets using a quality by design (QbD) approach. Int J Pharm 599. https://doi.org/10.1016/j.ijpharm.2021.120402.

Thirawong, N., Nunthanid, J., Puttipipatkhachorn, S., Sriamornsak, P., 2007. Mucoadhesive properties of various pectins on gastrointestinal mucosa: An in vitro evaluation using texture analyzer. European Journal of Pharmaceutics and Biopharmaceutics 67, 132–140. https://doi.org/10.1016/j.ejpb.2007.01.010.

Tidau, M., Finke, J.H., 2022. Modified release kinetics in dual filament 3D printed individualized oral dosage forms. European Journal of Pharmaceutical Sciences 175, 106221. https://doi.org/10.1016/J.EJPS.2022.106221.

Tomas, J., Schöngut, M., Dammer, O., Beránek, J., Zadražil, A., Štěpánek, F., 2018. Probing the early stages of tablet disintegration by stress relaxation measurement. European Journal of Pharmaceutical Sciences 124, 145–152. https://doi.org/10.1016/j.ejps.2018.08.029.

Vanbillemont, B., de Beer, T., 2020. Application of polyvinyl acetate in an innovative formulation strategy for lyophilized orally disintegrating tablets. Int J Pharm 588. https://doi.org/10.1016/j.ijpharm.2020.119717.

Vanbillemont, B., Everaert, H., de Beer, T., 2020. New advances in the characterization of lyophilised orally disintegrating tablets. Int J Pharm 579. https://doi.org/10.1016/j.ijpharm.2020.119153.

Viidik, L., Vesala, J., Laitinen, R., Korhonen, O., Ketolainen, J., Aruväli, J., Kirsimäe, K., Kogermann, K., Heinämäki, J., Laidmäe, I., Ervasti, T., 2021. Preparation and characterization of hot-melt extruded polycaprolactone-based filaments intended for 3D-printing of tablets. European Journal of Pharmaceutical Sciences 158. https://doi.org/10.1016/j.ejps.2020.105619.

Vo, A.Q., Zhang, J., Nyavanandi, D., Bandari, S., Repka, M.A., 2020. Hot melt extrusion paired fused deposition modeling 3D printing to develop hydroxypropyl cellulose based floating tablets of cinnarizine. Carbohydr Polym 246. https://doi.org/10.1016/j.carbpol.2020.116519.

Volod'ko, A. v., Davydova, V.N., Petrova, V.A., Romanov, D.P., Pimenova, E.A., Yermak, I.M., 2021. Comparative Analysis of the Functional Properties of Films Based on Carrageenans, Chitosan, and Their Polyelectrolyte Complexes. Mar Drugs 19, 704. 10.3390/MD19120704.

Vreeman, G., Sun, C.C., 2022a. A powder tabletability equation. Powder Technol 408. https://doi.org/10.1016/j.powtec.2022.117709.

Vreeman, G., Sun, C.C., 2022b. Air entrapment during tablet compression – Diagnosis, impact on tableting performance, and mitigation strategies. Int J Pharm 615. https://doi.org/10.1016/j.ijpharm.2022.121514.

Walicová, V., Gajdziok, J., Pavloková, S., Vetchý, D., 2016. Design and evaluation of mucoadhesive oral films containing sodium hyaluronate using multivariate data analysis. Pharm Dev Technol 22, 229–236. https://doi.org/10.1080/10837450.2016.1194857.

Wang, C., Hu, S., Sun, C.C., 2017a. Expedited development of a high dose orally disintegrating metformin tablet enabled by sweet salt formation with acesulfame. Int J Pharm 532, 435–443. https://doi.org/10.1016/j.ijpharm.2017.08.100.

Wang, C., Hu, S., Sun, C.C., 2017b. Expedited Development of Diphenhydramine Orally Disintegrating Tablet through Integrated Crystal and Particle Engineering. Mol Pharm 14, 3399–3408. https://doi.org/10.1021/ACS.MOLPHARMACEUT.7B00423/SUPPL_FILE/MP7B00423_SI_001.PDF.

Wang, Z., Li, J., Hong, X., Han, X., Liu, B., Li, X., Zhang, H., Gao, J., Liu, N., Gao, X., Zheng, A., 2021. Taste Masking Study Based on an Electronic Tongue: the Formulation Design of 3D Printed Levetiracetam Instant-Dissolving Tablets. Pharm Res 38, 831–842. https://doi.org/10.1007/S11095-021-03041-9/FIGURES/12.

Wening, K., Breitkreutz, J., 2010. Novel delivery device for monolithical solid oral dosage forms for personalized medicine. Int J Pharm 395, 174–181. https://doi.org/10.1016/j.ijpharm.2010.05.036.

Woertz, C., Preis, M., Breitkreutz, J., Kleinebudde, P., 2013. Assessment of test methods evaluating mucoadhesive polymers and dosage forms: An overview. European Journal of Pharmaceutics and Biopharmaceutics 85, 843–853. https://doi.org/10.1016/J.EJPB.2013.06.023.

Xu, P., Li, J., Meda, A., Osei-Yeboah, F., Peterson, M.L., Repka, M., Zhan, X., 2020. Development of a quantitative method to evaluate the printability of filaments for fused deposition modeling 3D printing. Int J Pharm 588. https://doi.org/10.1016/j.ijpharm.2020.119760.

Zhang, J., Feng, X., Patil, H., Tiwari, R. v., Repka, M.A., 2017. Coupling 3D printing with hot-melt extrusion to produce controlled-release tablets. Int J Pharm 519, 186–197. 10.1016/J.IJPHARM.2016.12.049.

Zhang, Y., Li, Y.P., Wu, F., Hong, Y.L., Shen, L., Lin, X., Feng, Y., 2021. Texture and surface feature-mediated striking improvements on multiple direct compaction properties of Zingiberis Rhizoma extracted powder by coprocessing with nano-silica. Int J Pharm 603. https://doi.org/10.1016/j.ijpharm.2021.120703.

Zhang, Y., Li, J., Gao, Y., Wu, F., Hong, Y., Shen, L., Lin, X., 2022c. Improvements on multiple direct compaction properties of three powders prepared from Puerariae Lobatae Radix using surface and texture modification: Comparison of microcrystalline cellulose and two nano-silicas. Int J Pharm 622. https://doi.org/10.1016/j.ijpharm.2022.121837.

Zhang, B., Teoh, X.Y., Yan, J., Gleadall, A., Belton, P., Bibb, R., Qi, S., 2022a. Development of combi-pills using the coupling of semi-solid syringe extrusion 3D printing with fused deposition modelling. Int J Pharm 625. https://doi.org/10.1016/j.ijpharm.2022.122140.

Zhang, J., Xu, P., Vo, A.Q., Bandari, S., Yang, F., Durig, T., Repka, M.A., 2019. Development and evaluation of pharmaceutical 3D printability for hot melt extruded cellulose-based filaments. J Drug Deliv Sci Technol 52, 292–302. https://doi.org/10.1016/j.jddst.2019.04.043.

Zhang, J., Thakkar, R., Zhang, Y., Maniruzzaman, M., 2020. Structure-function correlation and personalized 3D printed tablets using a quality by design (QbD) approach. Int J Pharm 590. https://doi.org/10.1016/j.ijpharm.2020.119945.

Zhang, P., Xu, P., Chung, S., Bandari, S., Repka, M.A., 2022b. Fabrication of bilayer tablets using hot melt extrusion-based dual-nozzle fused deposition modeling 3D printing. Int J Pharm 624. https://doi.org/10.1016/j.ijpharm.2022.121972.

Zhao, H., Yu, Y., Ni, N., Zhao, L., Lin, X., Wang, Y., Du, R., Shen, L., 2022. A new parameter for characterization of tablet friability based on a systematical study of five excipients. Int J Pharm 611. https://doi.org/10.1016/j.ijpharm.2021.121339.

Zhou, Z., Li, W., Sun, W.J., Lu, T., Tong, H.H.Y., Sun, C.C., Zheng, Y., 2016. Resveratrol cocrystals with enhanced solubility and tabletability. Int J Pharm 509, 391–399. https://doi.org/10.1016/j.ijpharm.2016.06.006.

Drug Development and Industrial Pharmacy

ISSN: (Print) (Online) Journal homepage: www.tandfonline.com/journals/iddi20

Design, optimization and pharmaceutical characterization of wound healing film dressings with chloramphenicol and ibuprofen

Ioana Savencu, Sonia Iurian, Cătălina Bogdan, Nicoleta Spînu, Maria Suciu, Anca Pop, Alexandru Țoc & Ioan Tomuță

To cite this article: Ioana Savencu, Sonia Iurian, Cătălina Bogdan, Nicoleta Spînu, Maria Suciu, Anca Pop, Alexandru Țoc & Ioan Tomuță (15 Apr 2024): Design, optimization and pharmaceutical characterization of wound healing film dressings with chloramphenicol and ibuprofen, Drug Development and Industrial Pharmacy, DOI: 10.1080/03639045.2024.2339306

To link to this article: https://doi.org/10.1080/03639045.2024.2339306

Published online: 15 Apr 2024.

Submit your article to this journal

View related articles

View Crossmark data

Full Terms & Conditions of access and use can be found at
https://www.tandfonline.com/action/journalInformation?journalCode=iddi20

DRUG DEVELOPMENT AND INDUSTRIAL PHARMACY
https://doi.org/10.1080/03639045.2024.2339306

Taylor & Francis
Taylor & Francis Group

RESEARCH ARTICLE

Check for updates

Design, optimization and pharmaceutical characterization of wound healing film dressings with chloramphenicol and ibuprofen

Ioana Savencu[a], Sonia Iurian[a], Cătălina Bogdan[b], Nicoleta Spînu[a], Maria Suciu[c,d], Anca Pop[e], Alexandru Țoc[f] and Ioan Tomuță[a]

[a]Department of Pharmaceutical Technology and Biopharmacy, Faculty of Pharmacy, 'Iuliu Hațieganu' University of Medicine and Pharmacy, Cluj-Napoca, Romania; [b]Department of Dermopharmacy and Cosmetics, Faculty of Pharmacy, 'Iuliu Hațieganu' University of Medicine and Pharmacy, Cluj-Napoca, Romania; [c]Electron Microscopy Center 'C.Craciun', Biology and Geology Faculty, Babes-Bolyai University, Cluj-Napoca, Romania; [d]LIME-CETATEA, National Institute for R&D of Isotopic and Molecular Technologies (INCDTIM), Cluj-Napoca, Romania; [e]Department of Toxicology, Faculty of Pharmacy, 'Iuliu Hațieganu' University of Medicine and Pharmacy, Cluj-Napoca, Romania; [f]Department of Microbiology, Faculty of Medicine, 'Iuliu Hațieganu' University of Medicine and Pharmacy, Cluj-Napoca, Romania

ABSTRACT

Objective: The aim of the present study was to develop and optimize a wound dressing film loaded with chloramphenicol (CAM) and ibuprofen (IBU) using a Quality by Design (QbD) approach.

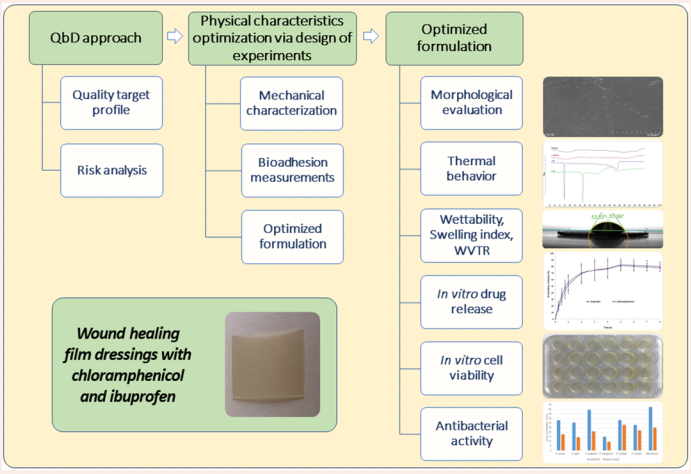
Significance: The two drugs have been combined in the same dressing as they address two critical aspects of the wound healing process, namely prevention of bacterial infection and reduction of inflammation and pain related to injury.

Methods: Three critical formulation variables were identified, namely the ratios of Kollicoat SR 30D, polyethylene glycol 400 and polyvinyl alcohol. These variables were further considered as factors of an experimental design, and 17 formulations loaded with CAM and IBU were prepared *via* solvent casting. The films were characterized in terms of dimensions, mechanical properties and bioadhesion. Additionally, the optimal formulation was characterized regarding tensile properties, swelling behavior, water vapor transmission rate, surface morphology, thermal behavior, goniometry, *in vitro* drug release, cell viability, and antibacterial activity.

Results: The film was optimized by setting minimal values for the folding endurance, adhesive force and hardness. The optimally formulated film showed good fluid handling properties in terms of swelling behavior and water vapor transmission rate. IBU and CAM were released from the film up to 80.9% and 82.5% for 8 h. The film was nontoxic, and the antibacterial activity was prominent against *Micrococcus spp*. and *Streptococcus pyogenes*.

Conclusions: The QbD approach was successfully implemented to develop and optimize a novel film dressing promising for the treatment of low-exuding acute wounds prone to infection and inflammation.

GRAPHICAL ABSTRACT



ARTICLE HISTORY

Received 16 December 2023
Revised 6 March 2024
Accepted 13 March 2024

KEYWORDS

Film dressings; wound healing; ibuprofen; chloramphenicol; quality by design

CONTACT Cătălina Bogdan catalina.bogdan@umfcluj.ro Department of Dermopharmacy and Cosmetics, Faculty of Pharmacy, 'Iuliu Hațieganu' University of Medicine and Pharmacy, Cluj-Napoca, Romania

© 2024 Informa UK Limited, trading as Taylor & Francis Group

Introduction

Wounds may represent access for microorganisms into the body, which can lead to infections in the wound bed. Gram-positive bacteria, such as *Staphylococcus aureus* and *Streptococcus pyogenes* are the main bacteria involved in the early phases of the infectious process, while Gram-negative bacteria are characteristic for chronic wounds [1]. Since the wound healing process involves inflammation, proliferation and remodeling, one concern for clinicians is a prolonged inflammatory stage because it delays the healing process, leading to chronic wounds [2].

Wound healing is promoted when a moist environment is provided [3]. Traditional passive wound dressings such as gauze, gauze composites, cotton wool or bandages are used to dry, cover and protect the wound, but are not moisture retentive [4,5]. On the other hand, moist dressings which include films, hydrogels, hydrocolloids, hydroactives, foams, alginates and hydrofibers, facilitate healing by keeping a moist environment on the wound bed [2,3]. Their selection depends on the wound depth and amount of exudate [2].

Film dressings are widely used as primary dressings for minor skin wounds, to waterproof a primary dressing (e.g. foam), or as postoperative layers over sutures [3]. Among their benefits, we mention their high flexibility, ease of application, pain reduction, water semipermeability, and a facile inspection of the wound site due to their transparency [6]. Compared to conventional transdermal patches, transdermal films are less irritative to the skin due to less occlusive properties which promote water vapor permeation and do not confer a sticky sensation on the application site [7]. Film dressings also have high clinical potential for the treatment of low-exuding wounds and have been explored by researchers in the recent years [8–10]. They may possess intrinsic therapeutic activity (e.g. antimicrobial, restorative, antioxidant) due to the properties of the constituent film-forming polymers or can be loaded with active pharmaceutical ingredients (APIs), which makes them promising drug delivery systems for cutaneous applications [6].

Polymers are often combined in film dressing formulations as this enhances the benefits of each part while reducing the limitations of each individual polymer [11]. Numerous research groups have proposed various combinations of polymers for wound healing purposes, either drug-loaded or not [11–18]. Alginate films with gentamicin and xylitol were found to have superior antibacterial activity against *Staphylococcus aureus* and *Pseudomonas aeruginosa* compared to a commercial gentamicin cream, due to the antibiofilm properties of xylitol [18]. Pawar et al. obtained films with potential for wound healing by combining Polyox® with carrageenan plasticized with glycerol and loaded with streptomycin and diclofenac. Soft and tough films were obtained, and it was revealed that the plasticizer increased the swelling capacities of the films as well as the cumulative release of the APIs [11]. Another study reported polymeric bioadhesive films loaded with vitamin E acetate and *Aloe vera* containing different amounts of PVA and sodium alginate and constant amounts of hyaluronate, sorbitol and polyethylene oxide water soluble resin. Vitamin E acetate was released around 30% from the polymeric films for 12 h [17].

In the present study, a cumulative sustained release of the APIs as high as possible was desired, therefore two hydrophilic film-forming agents with extended-release properties were chosen: Kollicoat SR 30D and Methocel. Kollicoat SR 30D is a polyvinyl acetate aqueous dispersion stabilized with povidone and sodium lauryl sulfate. It is an excellent film-former and is used for the fabrication of pH-independent sustained-release dosage forms [19]. Methocel (hydroxypropyl methylcellulose, HPMC) is widely used in pharmaceutical formulations. It is a film-forming agent, among others, and can be used as a hydrophilic matrix with extended-release properties [20]. Another polymer of choice was polyvinyl alcohol (PVA) because it is a synthetic polymer commonly used for wound healing purposes as it is biocompatible, biodegradable, non-carcinogenic, easily processable and inexpensive [6]. In addition, it has adhesive properties, beneficial when application on the skin is intended [21]. Due to its water solubility, it maintains a moist wound environment, thus promoting wound healing. Yet, PVA formulations do not have elasticity and have limited hydrophilicity, therefore it cannot be used as the only material within a wound dressing formulation [22]. To overcome this limitation, polyethylene glycol (PEG) 400 was used as plasticizer, enhancing the flexibility and hydrophilic character of the films.

As for the APIs chosen in our designed wound healing dressings, chloramphenicol and ibuprofen were considered because of their reputed antibacterial and anti-inflammatory activities. Chloramphenicol (CAM) is a bacteriostatic broad-spectrum antibiotic derived from *Streptomyces venezuelae*. Its use in clinical practice has been limited to topical applications, mostly for the treatment of eye and ear infections, due to its systemic toxicity associated with aplastic anemia and bone marrow suppression. CAM's limited use makes it still efficient against certain bacteria such as methicillin-resistant *Staphylococcus aureus* [23]. Ibuprofen (IBU) is a non-steroidal anti-inflammatory drug (NSAID) with a beneficial effect on wound healing by preventing excessive inflammation [24].

Pharmaceutical Quality by Design (QbD) is a systematic and scientific concept regarding product development, which begins with predefined objectives. It is based on a thorough product and process understanding and control, making use of scientific methods and quality risk management. QbD elements include a quality target product profile (QTPP) that identifies the critical quality attributes (CQAs) of the product. Risk assessment is performed before the development studies and its purpose is to identify potentially high-risk formulation and process variables which might influence the quality of the final product [25]. Afterwards, levels or ranges of the identified high-risk variables are established, and experimental work is performed according to the Design of Experiments (DoE). The experimental data is eventually analyzed, and results are interpreted, followed by the optimization step. This approach is highly advantageous because it facilitates the obtaining of an optimal formulation with minimal effort, time and developmental cost compared to the traditional 'one factor at a time' approach [26].

The aim of this study was to develop and optimize wound dressing films with antibacterial and anti-inflammatory activity, using a QbD approach. To the best of our knowledge, so far there are neither reports of CAM and IBU loaded film dressings, nor combinations of the polymers used in this study being integrated in a QbD approach. A multi-target and accelerating wound healing effect was envisaged due to the two APIs which have been combined in the same film dressing as they address two critical aspects of the process (preventing bacterial infection and reducing inflammation and pain related to injury). In addition, PVA maintained a moist environment which favors wound healing. Kollicoat SR 30D and HPMC were chosen to ensure a sustained release of the APIs from the polymeric matrix while PEG 400 was used to improve the flexibility of the films.

Materials and methods

Materials

PVA 87–90% hydrolyzed with an average molecular weight of 30000–70000 was purchased from Sigma-Aldrich (St. Louis, MO,

USA) and PEG 400 from Merck (Darmstadt, Germany). Kollicoat SR 30D (polyvinyl acetate) was obtained from BASF SE (Ludwigshafen, Germany), HPMC (Methocel E6 Premium LV) from Colorcon (London, UK), IBU from Shandong Xinhua Pharmaceutical (Zibo, China) and CAM from PI Chemicals Ltd. (China).

Dulbecco's modified Eagle medium (DMEM) was acquired from Gibco (Paisley, UK), while fetal bovine serum (FBS) and resazurin were obtained from Sigma Aldrich (Steinheim, Germany). The HaCaT cell line was procured from CLS Cell Lines Service (Eppelheim, Germany). The cells were sustained in DMEM medium supplemented with 10% FBS, as instructed by the provider. Harvesting occurred at 70–80% confluence for subculturing or subsequent use in experiments.

All the ATCC bacterial strains used for assessing the antibacterial activity of the films (*Staphylococcus aureus* ATCC25923, *Streptococcus pyogenes* ATCC 19615, *Enterococcus faecalis* ATCC29212, *Micrococcus spp* ATCC700405, *Salmonella typhi* ATCC14028, *Pseudomonas aeruginosa* ATCC 27853 and *Proteus mirabilis* ATCC12453) were purchased from Thermo Fisher Scientific (Lenexa, USA).

Film preparation

Films were prepared using the solvent casting method as previously reported [27]. Stock solutions were initially made for an easier preparation of the formulations according to the experimental design. Distilled water was used as a solvent for the preparation of stock solutions of the excipients: Kollicoat SR 30D (30% w/v), PVA (5% w/v), PEG 400 (10% w/v), HPMC (10% w/v). Different volumes of each solution (corresponding to the ratios indicated in the experimental design) were mixed together, starting by mixing the largest volumes, then adding the smaller ones. This resulted in a polymeric viscous dispersion which was sonicated to remove the bubbles.

IBU and CAM were dissolved in ethanol, resulting in stock solutions of 2% w/v each. Volumes of the API stock solutions were eventually mixed with a defined volume of the previously obtained polymeric dispersion, followed by sonication for bubble removal.

The prepared hydro-alcoholic dispersions were then cast onto polystyrene Petri dishes (8.5 cm diameter with 21.7 ml of hydro-alcoholic dispersion/dish), and dried at room temperature for 72 h. The obtained dry films were peeled off and stored for further analysis.

Quality by design (QbD) approach

Identification of the quality target product profile (QTPP), critical quality attributes (CQAs) of films and the risk analysis of CQAs

The first step of the study was to define the QTPP according to the guidelines developed by the International Council of Harmonization (ICH) Expert Working Group [28]. The QTPP included the CQAs, represented by the physical characteristics of the films which should lay within the defined range to ensure the quality of the final product (Table 1). The CQAs were further assessed *via* the Ishikawa diagram to identify the potential variables which may influence the desired quality of the product [28].

Risk assessment by failure mode effects analysis (FMEA)

FMEA is a powerful tool which relies on product and process understanding, breaking down the analysis of complex processes into manageable steps [29]. In this study, FMEA was applied to identify and classify the failure modes which are most likely to cause a process failure and thus lead to an inappropriate product [30].

The overall failure risk was evaluated based on the following three criteria: severity (S), occurrence (O) and detectability (D), each of them being ranked on a scale from 1–5 (1- representing the lowest level and 5-representing the highest level of the above-mentioned criteria). The final score, namely the Risk Priority Number (RPN) was then obtained by multiplying the individual scores registered for each one of these criteria. The parameters which had the highest scores were further studied in detail in the DoE.

Design of Experiments

A DoE was used to thoroughly understand the product and the process. The films (F1-F17) were prepared according to a Box-Wilson central composite face centered experimental design with 3 factors and 3 levels. The Modde 13.0 software (Umetrics, Sweden) was used to create the experimental design. It was also used for the calculation of coefficients and statistical parameters as well as for the data fitting necessary to evaluate the results. The independent variables (factors) with their variation levels together with the dependent variables (responses) are presented in Table 2.

Film dimensions

Films were characterized regarding the mass uniformity by determining the average mass of 20 random square-shaped units of films of 1.8 cm x 1.8 cm, according to the European Pharmacopeia

Table 1. QTPP Of the wound healing film dressings.

QTPP element		Target
Appearance		Transparent colorless film
Route of administration	Topical	Aimed to be applied to the wound
Final product quality attributes	Mass uniformity (g)	Average weight ± 10%
	Thickness (mm)	0.15–0.25
	Folding endurance	>100
	Adhesive force (g)	10–35
	Adhesiveness (mJ)	> 0.3
	Hardness (g)	> 2000
	Deformation at hardness (mm)	> 3
	First fracture work done (mJ)	> 25
Efficacy	Antibacterial activity	Against Gram-positive and Gram-negative bacteria
	Cell viability	Minimum 80% viability of the HaCat cells after exposure
	In vitro drug release	Sustained release over 8 h

Table 2. The factors and responses of the DoE.

Factors		Levels		
	Symbol	−1	0	1
Kollicoat SR 30D ratio	X_1	23	30	37
PEG 400 ratio	X_2	5	15	25
PVA ratio	X_3	13	20	27
Responses				
	Symbol			Symbol
Weight (g)	Y_1		**Stringiness length (mm)**	Y_6
Thickness (mm)	Y_2		**Hardness (g)**	Y_7
Folding endurance	Y_3		**Deformation at hardness (mm)**	Y_8
Adhesive force (g)	Y_4		**First fracture work done (mJ)**	Y_9
Adhesiveness (mJ)	Y_5			

11.2 provisions for uniformity of mass of single-dose preparations [31]. The thickness was measured using a digital caliper at 20 different points and an average value was reported.

Mechanical characterization

The folding endurance was determined by repeatedly folding square-shaped units of films of 1.8 cm x 1.8 cm at 180° of the plane at the same place until obtaining a visible fissure. The measurement was performed in triplicate and the average value was reported [7].

The texture properties consisting of hardness, deformation at hardness and first fracture work done were determined by the CT3 Brookfield Texture Analyzer (Brookfield Engineering Laboratories, USA) *via* the Rupture Test. The sample was placed into the TA-FSF Film Support Fixture for puncture test. The force and work required to penetrate the film as well as deformation was recorded. The settings were as follows: trigger load-10 g and test speed 0.2 mm/s. All measurements were performed in triplicate and the mean ± standard deviation was reported.

The optimal formulation (blank and loaded film) was additionally assessed in tensile mode, using the Tension Test of the CT3 Brookfield Texture Analyzer equipped with a 50000 gram unit load cell. Samples having dimensions of 4 cm x 2 cm were fixed in the TA-DGF Dual Grip Fixture and stretched at a test speed of 0.5 mm/s until films broke. The following equations were used to calculate the tensile strength (TS, MPa) and percent elongation at break (EAB, %) [32]:.

$$Tensile\ Strength = \frac{Peak\ load\ at\ break}{Cross-sectional\ area\ of\ the\ film} \quad (1)$$

$$Elongation\ at\ break = \frac{Deformation\ at\ peak\ load}{Initial\ film\ length} \times 100 \quad (2)$$

Young's Modulus (YM, MPa) was calculated by plotting the stress-strain curve in Microsoft Excel. The slope corresponding to the elastic deformation (e. g., the initial linear region of stress-strain curve) indicated the YM [33].

All measurements were performed in triplicate and the mean ± standard deviation was reported.

Bioadhesion measurements

The adhesive behavior of the films expressed as adhesive force, adhesiveness and stringiness length was determined *via* the Compression Test of the CT3 Brookfield Texture Analyzer. The sample was placed into the TA-BT-KIT fixture and eventually wetted with 200 µl of distilled water for 2 min. The TA-AACC36 probe was covered with the porcine small intestinal mucosal tissue, and it was lowered until the contact with the sample. After a predefined time of 10 s the probe returned to the initial position. The force and work required for the detachment as well as the stringiness length were reported. The settings were as follows: the target value-100 g, hold time-10 s, trigger load-0.5 g, test speed 1 mm/s. Measurements were performed in quadruplicate and the mean ± standard deviation was reported.

Swelling behavior

Samples with dimensions of 1.8 cm x 1.8 cm were cut from the blank and loaded optimally formulated film and weighted. Each was completely immersed into a Petri dish with 26 ml Buffer solution with pH = 7.2 prepared according to European Pharmacopeia 10, at 23 ± 2 °C. According to ISO 175:2010, the amount of test liquid used should be at least 8 ml per square centimeter of the total surface area of the specimen [34]. After 15 min, the samples were taken out and the excess moisture was removed with a tissue paper. Finally, the samples were weighted and the swelling index (SI, %) was determined using Equation (3). Measurements were performed in triplicate and the mean ± standard deviation was reported.

$$Swelling\ index = \frac{W_s - W_0}{W_0} \times 100 \quad (3)$$

where Ws = weight of film after swelling and W_0 = initial film weight.

Water vapor transmission rate (WVTR)

The test was performed based on the method proposed by Muthuramalingam et al. [35] with a few changes. Circular shapes cut from the optimally formulated blank and loaded film were fixed on the mouth of a Franz diffusion cell (having the inner diameter of 18 mm) which was filled with 10 ml of distilled water allowing an air gap of 10 mm between the surface of the water and the films. The arm of the cell was covered with the plastic cap and sealed with Parafilm to prevent evaporation. This assembly was weighted and then incubated at 33 °C in the heating block of the Phoenix diffusion cell system (Teledyne Hanson, USA) for 24 h. After 24 h, the assembly was weighted again and the WVTR (g/m^2/day) was determined as follows:.

$$WVTR = \frac{W_i - W_f}{A} \quad (4)$$

where W_i is the initial weight of the assembly, W_f is the weight of the assembly after 24 h and A is the area of the membrane under study.

Measurements were performed in triplicate and the mean ± standard deviation was reported.

Scanning electron microscopy

The scanning electron microscope (SEM) (Hitachi SU8230, Japan) analysis was used to determine the optimally formulated films' topography. Samples of blank and loaded film were mounted on carbon sticky tape and sputter coated with 10 nm of Pt/Pd. The SEM analysis was done at 30 kV and 8 mm working distance, with magnifications ranging from 40 to 50000x in three different regions of interest for each sample.

Thermal behavior

The thermal behavior of the blank and loaded optimally formulated film as well as the pure APIs was assessed using the differential scanning calorimetry (DSC) technique. A DSC 3 thermal analyzer (Mettler Toledo, USA) and the STARe Software were employed. The samples (5–8 mg) were weighted in aluminum pans which were sealed with pierced lids and were heated from 25 to 400 °C with a heat rate of 10 °C/min, under nitrogen flow (50 ml/min).

Static contact angle measurement

The wettability of the optimally formulated film (blank and loaded) was assessed by measuring the water contact angle at room temperature by the drop method (OCA 25, Dataphysics, Germany). Briefly, a double distilled water droplet was placed on the film surface and a picture was taken. The contact angle was calculated *via* the software DpiMAX. Each reported contact angle was the mean ± standard deviation of 18 measurements (6 measurements taken in 3 different areas of the film).

In vitro drug release study

The release of IBU and CAM from the optimally formulated films was assessed using an automated Phoenix diffusion cell system (Teledyne Hanson, USA). The donor and receptor compartment were separated by a RephiLe PES Membrane (0.45 µm pore size, 25 mm diameter). The release medium was the Buffer solution with a pH of 7.2 prepared according to the European Pharmacopeia 10. The temperature was set to 33 °C. The measurement was performed in quadruplicate. Small disks with a diameter of 9 mm were randomly cut from the film and carefully placed on the membrane situated on the cell cap. The cell cap was then covered with a glass cover to prevent evaporation. The released amount of IBU and CAM was determined by collecting 0.2 ml of medium from the receptor compartment at predefined intervals of time (15, 30, 45 min, and then from hour to hour for 8 h) *via* autosampler. The withdrawn volume was immediately replaced by the same volume of fresh medium. The withdrawn aliquots were injected into HPLC for the quantification of the APIs released from films using a RP-HPLC method. The column used was Luna® 5 µm C18(2) 100 Å, 150 × 4.6 mm (Phenomenex, USA), while the mobile phase was a mixture of Buffer phosphate: Acetonitrile = 70:30 (v:v), with the UV detector set at λ = 222 nm. The cumulative release of the APIs was plotted against time, using a calibration curve of pure IBU and CAM.

In vitro cell viability assay

24 well plates were used for this protocol, the film was placed at the bottom of each well. The HaCaT cells were seeded on top of the films and were left to attach for 24 h. The seeding number of cells was calculated to have 80% confluence in the following 24 h. A blank film without any active compounds was used for comparison. After the 24-h period, the cells underwent exposure to a resazurin solution for 1–3 h. The Synergy 2 Multi-Mode Microplate Reader was used to measure the conversion of resazurin to resorufin, a pink, fluorescent dye, by metabolically active cells. Each experiment comprised three biological replicates, with each one incorporating three technical replicates. The results were expressed as relative values in comparison to the blank film containing no active compounds (100%).

Antibacterial activity

The antibacterial activity of the optimized film formulation was tested against Gram-positive bacteria (*Staphylococcus aureus* ATCC25923, *Streptococcus pyogenes* ATCC 19615, *Enterococcus faecalis* ATCC29212 and *Micrococcus spp* ATCC700405) and Gram-negative bacteria (*Salmonella typhi* ATCC14028, *Pseudomonas aeruginosa* ATCC 27853 and *Proteus mirabilis* ATCC12453) using a modified Kirby-Bauer disk diffusion method. A 0,5 McFarland dilution of bacteria using 0,9% NaCl was prepared. The solution was streaked using the spread plate technique on Mueller-Hinton agar. A 5.49 mm round cut was made on the polymeric film and then disposed on the plated agar. A blank formulation was used as negative control whereas the antibiotic paper disk Chloramphenicol (30 µg, diameter of 6 mm) from Biomaxima, Lublin, Poland was used as positive control. The media were incubated at 37 °C for 24 h, and the zones of inhibition (ZOIs) were measured thereafter. The experiments were performed in triplicate and the mean ± standard deviation was reported.

Statistical analysis

The experimental data from the DoE were analyzed by ANOVA using the Modde 13.0 software. The data post DoE were analyzed by ANOVA Single Factor using Microsoft Excel. P-values below 0.05 were considered statistically significant.

Results

QTPP and risk analysis

The QTPP was established based on literature research and preliminary studies on this topic. Favorable physical and mechanical properties were considered essential features of the films in order to ensure their easy manipulation and application. Therefore, in a first step, the risk factors related to the mechanical profile of the films were identified and analyzed and are summarized in an Ishikawa diagram (Figure 1). The critical material attributes (CMA) and critical process parameters (CPP) were further analyzed by the FMEA approach (Table 3) because once failure modes are established, risk reduction can be used to eliminate, reduce or control the potential failures [29]. The RPN score was considered as the risk score. Ratios of the plasticizer (PEG 400) and the bioadhesive agent (PVA) registered the highest risk since their improper proportion could lead to a failed product being either too soft or too rigid and having variable mechanical properties. A high risk was also registered for the ratio of the film-forming agent (Kollicoat SR 30D), following the

previous two. This was attributed to the fact that an improper amount may prevent a good film formation and also interfere with the APIs release from the final product. HPMC ratio revealed a moderate risk which could arise due to physicochemical differences in selected sort. The above-mentioned considerations were based on previous literature reports which revealed a high impact of the plasticizer [36], bioadhesive agent [37] and film-forming agent [38] on the final product. Moreover, a previous study of our research group revealed a similar impact of the three components (plasticizer, bioadhesive and film-forming agent) on the final product [27]. Regarding the formulation steps, the highest risk was registered by the mixing and homogenization of stock solutions because, if not performed accordingly, it could generate an inhomogeneous structure of the final product, with thickness variations and uneven APIs distribution into the polymeric matrix. However, it was not such of a high magnitude as the material attributes, thus being considered a medium-risk factor. The concentration of the stock solutions and film solution impacted the final product in a similar manner. Parameters related to the drying step were deemed to have a low influence on CQAs of the product because films were dried in ambient air, in an atmosphere with relatively constant temperature and humidity, where fluctuations could be easily detected. The extent to which the films were dried could also be easily assessed visually therefore these parameters had low RPNs. Since parameters registering the highest scores were the ratios of the plasticizer (i.e. PEG 400), bioadhesive agent (i.e. PVA) and film forming agent (i.e. Kollicoat SR 30D), their impact on the final product was further studied in the DoE, based on their variation levels.

Physical characteristics optimization via design of experiments

The DoE approach was used both to thoroughly investigate the impact of the highest risk factors on the mechanical profile of the films and predict an optimal formulation based on these results. After the optimization step, the final product was tested in terms of film dimensions, adhesive properties, mechanical profile. In addition, it was tested in detail regarding tensile properties, swelling behavior, WVTR, surface morphology, thermal behavior, wettability, *in vitro* release of APIs, *in vitro* cell viability, and antibacterial activity.

Experimental data fitting

The results obtained based on the set domain of the DoE were eventually centralized and introduced into the design matrix. The fitting of the experimental data with the experimental design was done according to the Partial Least Squares (PLS) method, using R2, Q2 and the ANOVA (analysis of variance) test as statistical parameters. The model validity and reproducibility were also calculated for all the responses and are displayed in Table 4.

The selected model indicated a great quality for y8 with $R2 > 0.95$ and $Q2 > 0.85$. A good fit of the model was also revealed for y1, y2, y3 and y9 with $R2 > 0.8$. A good model validity (values higher than 0.25) was observed for all responses, as well as a good reproducibility (values higher than 0.5). All the p values of the ANOVA test for the responses were lower than 0.05, whereas all the p values were higher than 0.08 for the lack of fit. These results indicate that the factors significantly influence the responses and that the model has no lack of fit.

The effect of independent variables on film properties

The coefficients of the regression equations mark the influence of the formulation factors on film properties and are presented as histograms and representative response surfaces below (Figure 2).

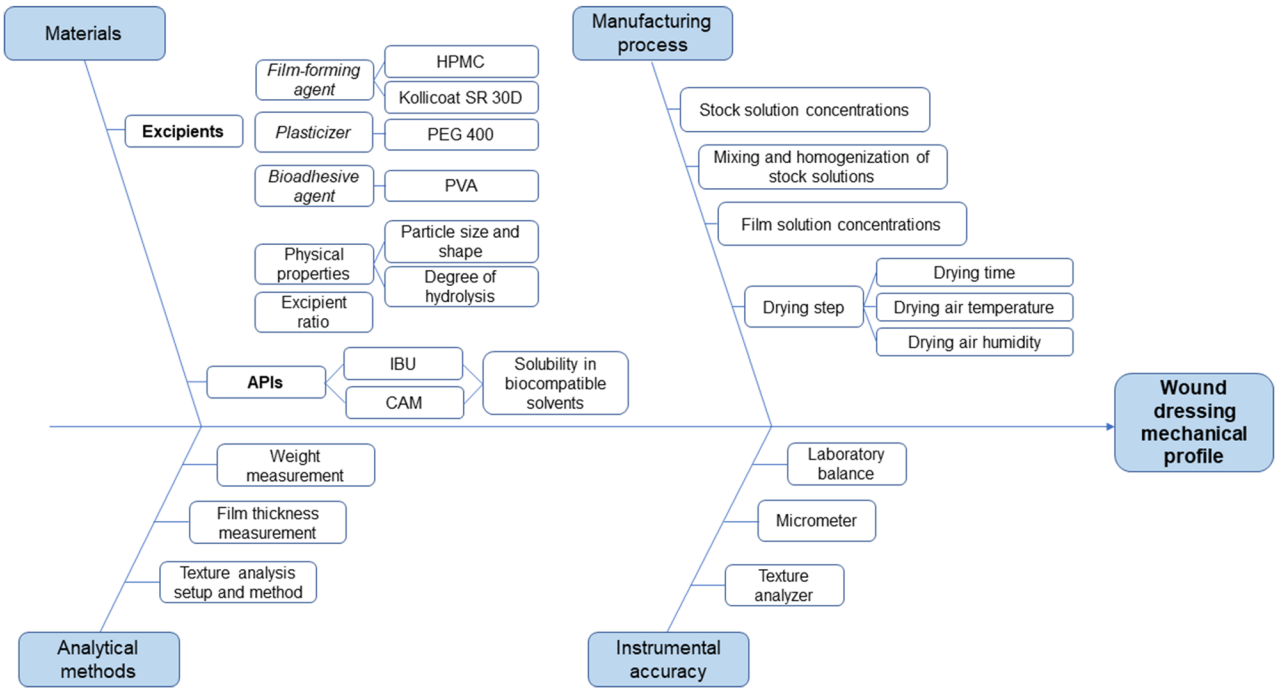


Figure 1. Ishikawa diagram presenting the parameters with potential influence on the final product.

Table 3. Overview of the risk assessment of the failure mode effects analysis.

Nr.	CMA/CPP	Potential causes	Failure Mode	Failure effects	Control methods	Severity	Occurrence	Detectability	RPN
				Film forming agents					
1	Kollicoat SR 30D ratio	Physicochemical differences in selected sorts	Solubility issues and slight variations of polymer viscosity	Variable mechanical properties (hardness, folding endurance); thickness variations	DoE	4	2	4	**32**
2	HPMC ratio	Physicochemical differences in selected sorts	Solubility issues and slight variations of polymer viscosity	Variable mechanical properties (adhesiveness/ too sticky, hardness, folding endurance)	DoE	4	2	3	24
				Plasticizer					
3	PEG 400 ratio	Low correlation between plasticizer and polymer mixture	Variations of polymer viscosity	Too rigid/soft films, thickness variations	DoE	4	3	3	**36**
				Bioadhesive agent					
4	PVA ratio	Physicochemical differences in selected sorts	Solubility issues and slight variations of polymer viscosity	Variable mechanical properties (adhesiveness/ too sticky, hardness, folding endurance)	DoE	4	3	3	**36**
				Manufacturing process					
5	Stock solutions concentrations	Human and instrumental errors	Homogeneity issues; formulation errors	Variable mechanical properties (adhesiveness/ too sticky, hardness, folding endurance)	A careful weighting and measuring of solid and liquid ingredients	3	1	4	12
6	Film solution concentrations	Human and instrumental errors	Homogeneity issues; formulation errors	Variable mechanical properties (adhesiveness/ too sticky, hardness, folding endurance)	A careful weighting and measuring of solid and liquid ingredients	3	2	3	18
7	Mixing and homogenization of stock solutions	Human and instrumental errors	Homogeneity issues; formulation errors	Nonuniform films, variations of films' characteristics	Timing of the mixing step and monitorization of the mixing rate	5	2	2	20
8	Drying time	Human errors	Too long/short drying time	Too rigid/tacky films	Monitorization and timing of the drying step	2	2	2	8
9	Drying temperature	Temperature fluctuations				3	1	1	3
10	Drying air humidity	Humidity fluctuations				3	1	1	3

Table 4. Statistical parameters for the DoE work set.

Response	R2	Q2	Validity	Reproducibility	*p*-value ANOVA Regression	p-value ANOVA Lack of fit
Y1	0.848	0.410	0.544	0.987	0.003	0.162
Y2	0.812	0.458	0.687	0.950	0.007	0.287
Y3	0.940	0.495	0.374	0.999	0.000	0.082
Y4	0.658	0.483	0.715	0.797	0.008	0.320
Y5	0.694	0.450	0.895	0.893	0.031	0.163
Y6	0.615	0.189	0.480	0.910	0.038	0.125
Y7	0.741	0.267	0.621	0.960	0.026	0.220
Y8	0.959	0.851	0.867	0.934	0.000	0.589
Y9	0.910	0.597	0.892	0.917	0.036	0.651

Optimized formulation

The optimal formulation was predicted by introducing a set of constraints and target values according to the QTPP and taking into consideration the following responses: maximization for folding endurance (y3) with a minimum value of 200, maximization for adhesive force (y4) with a minimum value of 20 g, and maximization for hardness (y7) with a minimum value of 2600 g. These three were considered of paramount importance because the envisaged final product should be both firm and flexible to ensure easy manipulation and application and possess adhesive properties. The other responses were also important and were taken into consideration when characterizing the optimal formulation.

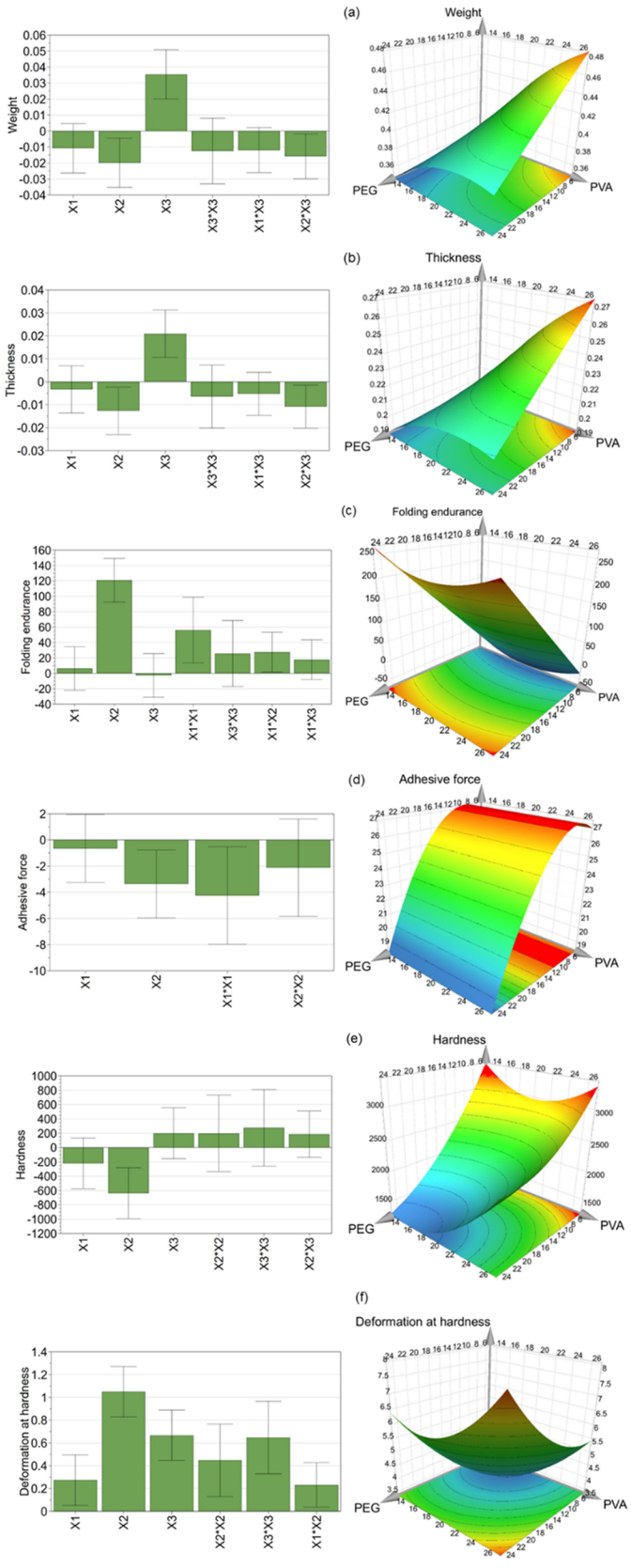


Figure 2. Regression coefficients displayed as histograms and response surfaces for weight (a), thickness (b), folding endurance (c), adhesive force (d), hardness (e), deformation at hardness (f).

Based on the established values, the DoE software predicted the composition of an optimal formulation, as seen in Table 5 which also includes DoE predicted values as well as experimental data obtained for the responses. The optimized film formulation was additionally characterized regarding tensile properties, swelling behavior, WVTR, by SEM, DSC, goniometry, *in vitro* drug release study, *in vitro* cell viability assay, and antibacterial activity.

The tensile properties of the optimal blank and loaded film expressed as TS, EAB and YM are presented in Table 6. Similar values of the TS for the blank (48.54 ± 4.22 MPa) and loaded (50.30 ± 2.63 MPa) formulation were observed, without a statistically significant difference ($p = 0.572$). EAB registered approximately the same values both for the blank and loaded film (16.88 ± 4.43%, 16.94 ± 1.05%, respectively; $p = 0.981$). YM of the loaded film (3012.63 ± 235.70 MPa) was significantly higher than the YM of the blank film (2456.63 ± 82.36 MPa, $p = 0.018$).

Swelling behavior

The results of the swelling study are presented in Table 7. It was observed that the SI of the blank and loaded film are similar, without a statistically significant difference between the values ($p = 0.704$). The SI of the blank film (455.80% ± 21.13) was slightly higher than the SI of the loaded film (448.75% ± 21.10).

Water vapor transmission rate (WVTR)

The WVTR of the blank and loaded optimally formulated films are presented in Table 7. The WVTR of the blank film was higher (1407.41 g/m^2/day ± 68.24) than for the loaded film (1361.16 g/m^2/day ± 32.13), but no statistically significant difference was observed ($p = 0.348$).

Morphological evaluation of the films

SEM was used to investigate the aspect of the film surface, identify the APIs distribution and the potential APIs recrystallization into the optimally formulated film. The SEM images of the blank and loaded film are shown in Figure 3. The blank film had a smooth surface and no structures could be observed in it (Figure 3(a)). On the other hand, the loaded film showed a smooth wavy surface with areas of small depressions, similar to popped bubbles (Figure 3(b)).

Thermal behavior

DSC was used to examine the state of the APIs inside the film. The melting of the pure IBU and CAM was observed as an endothermic event with a peak around 76 °C and 150 °C, respectively, suggesting the crystalline nature of the APIs. The blank and loaded film did not show any sharp peaks but displayed an endotherm around 90 °C which was attributed to the presence of entrapped water into the film structure (Figure 4).

Wettability (hydrophilicity)

The contact angle of the loaded film was 54.70 ± 9.60°, while for the blank film it was 47.59 ± 6.71°, both indicating hydrophilic

Table 5. Optimized formulation.

Composition			Responses				
Name		Values (%)	Name		Predicted values	Obtained values	Bias (%)
Kollicoat SR 30D ratio	X_1	23.05	Weight (g)	Y_1	0.343	0.358	4.37
			Thickness (mm)	Y_2	0.19	0.22	15.79
			Folding endurance	Y_3	195	226	15.90
PEG 400 ratio	X_2	12.58	Adhesive force (g)	Y_4	20.83	21.30	2.26
			Adhesiveness (mJ)	Y_5	0.43	0.51	18.60
			Stringiness length (mm)	Y_6	3	3.33	11
PVA ratio	X_3	13.00	Hardness (g)	Y_7	2600	2617	0.65
			Deformation at hardness (mm)	Y_8	3.80	3.40	−10.53
			First fracture work done (mJ)	Y_9	39.30	31.80	−19.08

Table 6. Tensile properties of the blank and loaded optimal formulation[a].

Tensile strength (MPa)		Elongation at break (%)		Young's Modulus (MPa)*	
Blank	Loaded	Blank	Loaded	Blank	Loaded
48.54 ± 4.22	50.30 ± 2.63	16.88 ± 4.43	16.94 ± 1.05	2456.63 ± 82.36	3012.63 ± 235.70

[a](Mean ± SD, $n = 3$), *significant difference between the blank and loaded film ($p = 0.018$).

surfaces (angles < 90°), as seen in Figure 5, without any statistically significant difference ($p = 0.353$).

In vitro drug release

The results of the *in vitro* release study are presented in Figure 6. The results indicate that 55.8% and 51.3% of IBU and CAM, respectively, were released within the first hour, whereas a maximum release of 80.9% and 82.5% of IBU and CAM, respectively, was observed after 5 h.

In vitro cell viability assay

The Alamar Blue assay was performed to evaluate whether the loaded film may alter the viability of the HaCaT cells when compared to the blank film. The viability of the cells exposed to the optimized film reached 80% of the cells exposed to the control, indicating that the 20% reduction in viability is not substantial enough to classify the film as toxic (Figure 7).

Antibacterial activity

The aim of this investigation was to test whether CAM maintained its antibacterial effect against Gram- positive and Gram-negative bacteria when incorporated into films. The antibacterial activity of the loaded film against Gram-positive bacteria was evident for *Streptococcus pyogenes* ATCC 19615 and *Micrococcus spp* ATCC700405, both displaying an inhibition zone above 40 mm diameter on average (Figure 8). However, *Staphylococcus aureus* ATCC25923 and *Enterococcus faecalis* ATCC29212 presented an inhibition zone of only around 30 mm diameter on average, suggesting that the antibacterial activity of the loaded film against these strains is of a lesser extent. Regarding the Gram-negative bacteria, the antibacterial activity was observed against *Salmonella typhi* ATCC14028 and *Proteus mirabilis* ATCC12453 with an average diameter of the inhibition zone of around 30 mm. Unfortunately, the loaded film did not show a convincing diameter of the inhibition zone against *Pseudomonas aeruginosa* ATCC 27853, which was not surprising since it is reported to be usually resistant to CAM [39]. The positive control displayed inhibition zones significantly smaller than those of the loaded film ($p = 0.014$), as seen in Figure 8, while the blank film did not display any inhibition zone.

Table 7. Swelling behavior and water vapor transmission rate (WVTR) of the blank and loaded optimal formulation[a].

Swelling index (%)		WVTR (g/m²/day)	
Blank	Loaded	Blank	Loaded
455.80 ± 21.13	448.75 ± 21.10	1407.41 ± 68.24	1361.16 ± 32.13

[a](Mean ± SD, $n = 3$).

Discussion

It was observed that the weight (y1) and the thickness (y2) of the films were positively influenced by an increase in the PVA ratio (x3). Interestingly, an increase in the PEG400 ratio led to a decrease of y1 and y2. This could be explained by the fact that the plasticizer was embedded in the polymeric matrix of film-forming agents (namely Kollicoat SR 30 D, HPMC), thus reducing the thickness of the films [27]. Blending the plasticizer with the bioadhesive agent also revealed a negative influence on weight and thickness. The folding endurance (y3) was the most significantly influenced by the increase of the PEG 400 ratio. This comes as no surprise due to the fact that the plasticizer improves the flexibility of films [6]. For example, PEG 400 increased the flexibility of tenoxicam-loaded transdermal films [12] and a similar effect was observed when incorporating PEG 400 combined with glycerol to study the effects of HPMC, PVP mannitol and microcrystalline cellulose on the physical properties of orally disintegrating films [40]. A non-linear positive influence of Kollicoat SR 30D on the folding endurance was also observed, meaning an increase of the response when a ratio of Kollicoat SR 30D higher than 30 was involved. The adhesive force (y4) was decreased by PEG 400 which could be probably ascribed to the fact that the plasticizer increases the free volume between the polymer network of HPMC and Kollicoat SR 30D and the mobility of the polymer chains [41], thus promoting their separation from the tissue. A non-linear negative influence of Kollicoat SR 30D was noted, suggesting an increase of y4 in the range of 23–30 followed by a decrease of y4 in the range of 23–30. A similar influence of the plasticizer (glycerol) on adhesive strength was reported by a study about bioadhesive okra polymer-based buccal patches, where increasing the concentration of the plasticizer was correlated to an increase of adhesion until a certain point beyond which an abrupt decrease of the adhesive strength occurred, possibly due to overhydration of film formulations [42]. None of the factors showed any significant effect on adhesiveness (y5) and stringiness

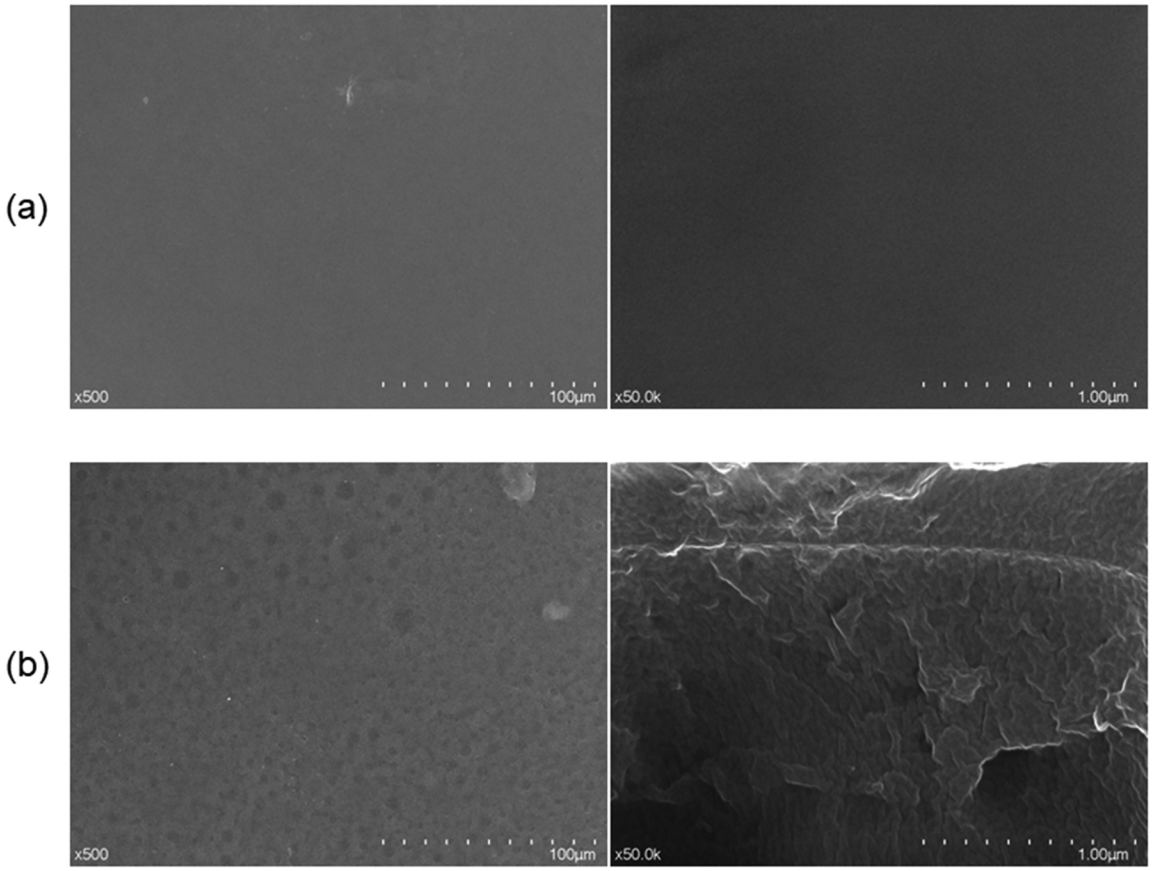


Figure 3. SEM images of the blank (a) and loaded (b) film captured with magnification of 500x and 50000x. Scales represent 100 µm and 1 µm, respectively.

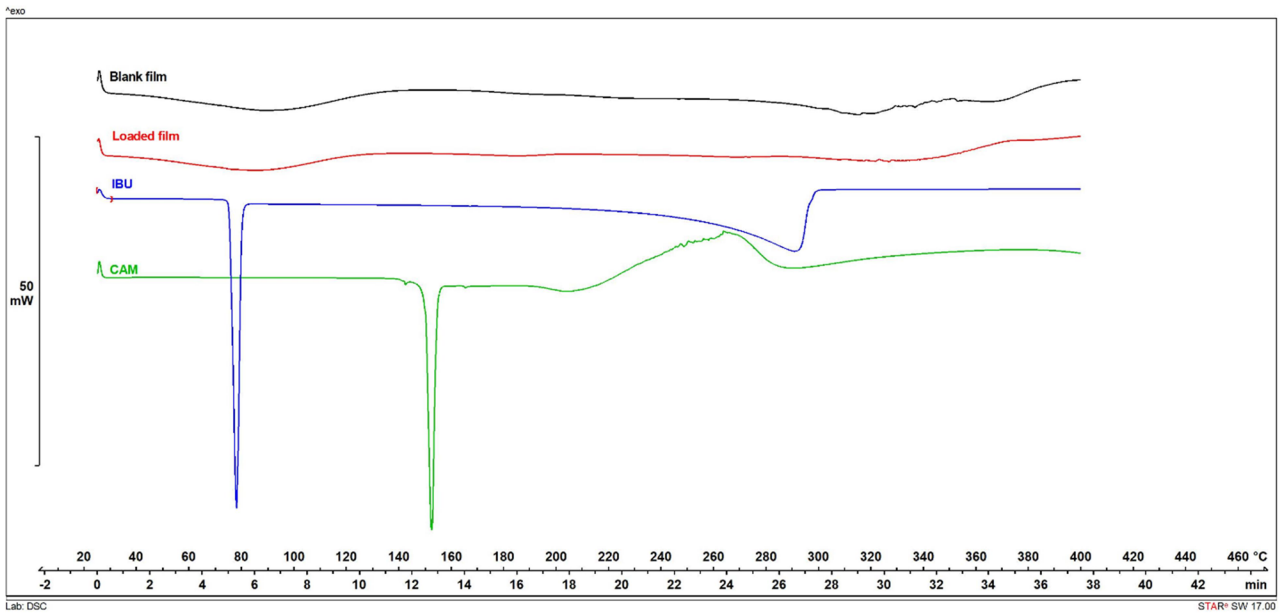


Figure 4. Thermograms of blank and loaded film, IBU and CAM.

length (y6). Regarding mechanical properties, it was shown that the plasticizer decreased the hardness (y7) of the films. It has been reported that the addition of the plasticizer may soften the films, by reducing the intermolecular forces in their structure [7]. Deformation (y8) was significantly influenced by all the 3 factors in a positive manner, of which the plasticizer revealed the highest impact. Mixing the film-forming agent with the plasticizer also increased deformation. A higher deformation indicates a higher flexibility of the film since flexibility is defined as the ratio of deformation to force. Deformation is therefore correlated with the

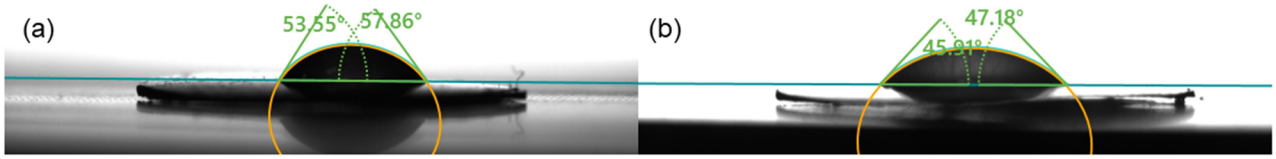


Figure 5. Water contact angles (representing one measurement) of loaded (a) and blank (b) films.

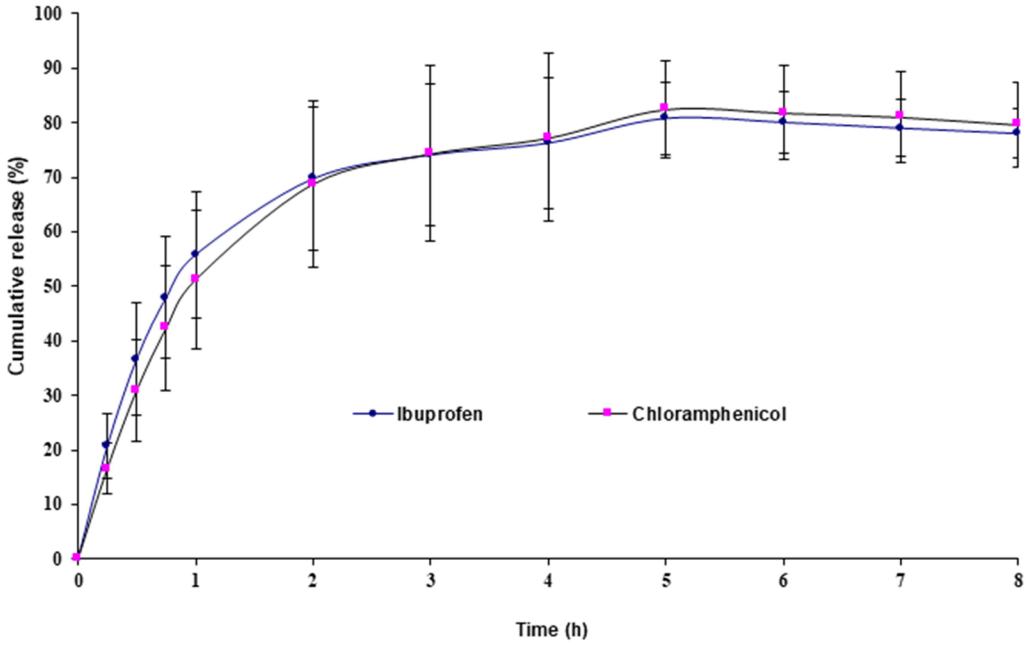


Figure 6. In vitro release profile of IBU and CAM (mean ± SD, n = 4).

folding endurance, and this can be evidenced by the strong impact of the plasticizer on both responses. Another study also reported that the plasticizer (glycerol) enhanced the flexibility of the films and enabled them to extend a longer time before breaking [43]. An explanation for this could be the fact that plasticizers can disrupt intermolecular and intramolecular hydrogen bonds by placing themselves between the polymer molecules. The free motion of the polymer is thus increased followed by an implicit increase of the flexibility of the film [44]. For the first fracture work done (y9), no significant effects of the factors were observed.

Based on the discussion above, it was observed that the most influential factors were PEG 400, followed by PVA and Kollicoat SR 30D, while the most impacted responses were: deformation, folding endurance, weight, thickness, hardness, and adhesive force.

The tensile properties of the optimally formulated blank and loaded film revealed tough and stiff films due to the high values of the TS and YM. TS and YM increased with the incorporation of the APIs into the polymeric matrix, in line with the results reported by Ahmad et al. [8]. This may be explained by the fact that the APIs decreased the free volume in the polymeric matrix, thus stiffening the film. Literature reports of tensile properties vary a lot among different research groups. For example, similar results were obtained by Gomes Neto et al. who also reported TS values above 40 MPa [45]. On the contrary, Ahmed and Boateng reported values in the range of 5–15 MPa for TS, and a maximum value of 78 MPa for YM [46]. EAB represents the elasticity of the blank and loaded film and was similar compared to the values

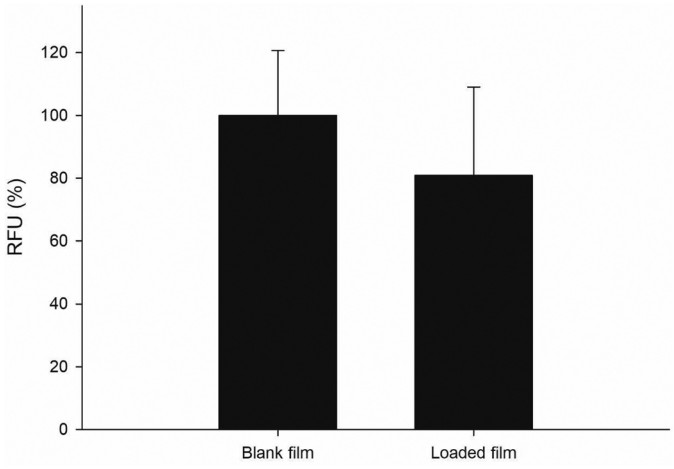


Figure 7. Viability was evaluated using Alamar Blue assay on HaCaT cell line after a 24 h exposure. The results are presented as the mean ± SD, n = 3, each one including 3 technical replicates. The values were expressed as relative values (RFU) compared to the control (100%).

below 20% reported by some researchers [45], but low compared to other studies, where values above 30% [41] or even 80% [8] were reported.

The tensile properties presented in the current study are advantageous as they ensure a facile manipulation of the films without any concern that they may break. In addition, they can easily resist

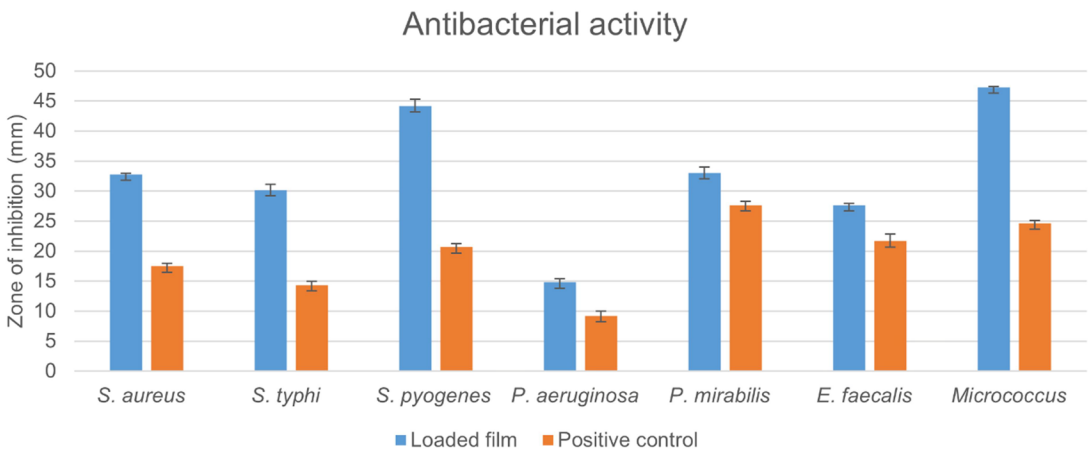


Figure 8. Antibacterial activity of the optimally formulated loaded film vs positive control (mean ± SD, $n = 3$).

to the deformations of the human skin which was reported to have TS in the range of 2.5–16 MPa [47]. On the other hand, since the human skin was reported to have EAB values around 70% in the most flexible zones [47], they may be perceived as uncomfortable due to their limited capacity to conform to the patient's body. However, when in contact with liquid/exudate, as revealed by the swelling behavior and contact angle measurements, films rapidly hydrate and this limitation can be overcome.

The swelling capacity of the optimally formulated loaded film was slightly lower than that of the blank film. This could be due to the fact that the APIs incorporation led to more rigid films (also revealed by the tensile properties) with a smaller free volume between the polymers, therefore lower water intake [46]. The high swelling capacity of both the blank and loaded film can be attributed to their hydrophilic nature (also revealed by the contact angle measurements). The values of the SI are similar to results reported by Okeke and Boateng, whose HPMC and sodium alginate-based films had SI in the range of 300–400% after 15 min [41].

The WVTR value was decreased by the APIs incorporation which is in accordance with the swelling behavior and contact angle measurements. This can be ascribed to the hydrophobic structure of the APIs which hindered water vapor transmission. Close values as well as a similar influence of the drug incorporation on the WVTR of films were reported by Ahmad et al. whose gentamicin loaded films registered WVTR in the range of 1665–1850 g/m^2/day [8]. Commercially available wound dressings have WVTR ranging from 90–3350 g/m^2/day, while for the injured skin values range from 279 to 5138 g/m^2/day [48].

The small depressions observed in the structure of the optimally formulated loaded film could be attributed to the small air bubbles entrapped in the casting dispersion that have not been completely removed by sonication. Since no particles of APIs were observed on the film surface, this indicates a homogeneous amorphous solid dispersion into the polymeric matrix. These observations are in accordance with the results of the DSC study consequently presented. The plasticizer may also contribute to the formation of a homogeneous system with a smooth aspect and wavy structures on the surface. Similar results were reported by Llabot et al. when studying the influence of PEG 400 on the surface morphology and crystallinity of some antifungal mucoadhesive films [49].

The DSC results reveal that the APIs are in an amorphous state inside the loaded film, therefore no recrystallization phenomena occurred after the film preparation. An amorphous state renders a higher solubility, which is advantageous for the APIs release from the dosage form. On the other hand, the amorphous state comes with an instability limitation due to the potential of converting back to the crystalline form during storage if conditions are not properly controlled. The similarity between the thermograms of the blank and loaded optimally formulated film also indicates the compatibility of the APIs with the other film components.

The contact angle measurements are as expected, due to the hydrophobic structures of IBU and CAM which slightly increased the contact angle. A hydrophilic surface is desired because it allows films to absorb humidity in the wound area [6]. It has also been reported that good surface wettability is related to antibacterial adhesion. This is due to the formation of a water layer which interacts with the polymer and acts as a physical barrier preventing the bacteria adsorption onto the surface [50]. Moreover, it has been proposed that an optimal range for water contact angles of materials implied in cell adhesion and protein adsorption should be 40–65° [51], therefore both the blank and loaded optimally formulated film fall in the desired range.

Drug release from the polymeric matrix is influenced by the hydration of the dried polymeric matrix, swelling and formation of gel, diffusion of APIs through the swollen gel, and degradation of the polymeric matrix [52]. For wounds prone to infection and inflammation, an initial rapid release of the antibiotic and the NSAID is desired as it prevents infection and provides comfort to the patient by relieving pain. Following the rapid release, it is then useful to have a sustained release of the APIs which ensures the therapeutic effect for a longer time. The data of the release study together with the swelling behavior suggest that the prepared films could be used as primary dressings for low-exuding acute wounds either infected and inflamed or prone to infection and inflammation.

Testing films on cells derived from human skin, such as HaCaT cell line, represents a relevant phase in studying dermatological treatments. By exposing these cells to films containing compounds such as CAM and IBU designed to combat skin infections and inflammation, the efficacy and safety of novel formulations could be assessed. The HaCaT cells were seeded on top of the films, allowing the cells to grow and interact directly with the film's surface, but also with the compounds released from the film. By using this method, we were able to establish that the optimized film does not impact the viability of the HaCaT cell line in a significant manner, therefore this novel film dressing formulation could be further tested for its therapeutic effects in wound healing process.

The microbiological investigation proves that the antibacterial activity of the antibiotic was not altered by its incorporation into films but was significant both against Gram-positive and Gram-negative bacteria, thus making the films promising candidates for wound healing purposes when antibacterial activity is necessary.

Conclusions

The QbD approach was successfully implemented to develop and optimize a novel film dressing formulation loaded with IBU and CAM. The optimal dry film formulation consisted of Kollicoat SR 30D (23.05%), PEG 400 (12.58%), PVA (13.00%), HPMC (50.37%), IBU (0.5%) and CAM (0.5%). Of the 3 factors investigated due to their potential impact on the final product, the plasticizer (PEG 400) influenced the responses the most, followed by the bioadhesive agent (PVA) and the film-forming agent (Kollicoat SR 30D). The films prepared according to the optimal formulation had good mechanical and tensile properties, being both firm and flexible, and possessing adhesive properties when prewetted. The SI of 448.75% ± 21.10 and WVTR of 1361.16 ± 32.13 indicated that the films can remove wound exudates while allowing an adequate transmission of water vapors. The contact angle of 54.7° indicated a hydrophilic surface which is proper for their use as wound dressings. SEM and DSC studies did not reveal any recrystallization of the APIs inside the film. The *in vitro* drug release profile indicated a sustained release of up to 80.9% and 82.5% for IBU and CAM, respectively, for 8 h. The cell viability of 80% indicated that films were nontoxic, and the antibacterial activity of CAM was preserved when incorporated into films, being highly effective against *Micrococcus spp*., *S. pyogenes, P. mirabilis* and *S. aureus*.

The above-mentioned features make this novel film dressing formulation a promising candidate for wound healing purposes, namely for low-exuding acute wounds prone to infection and inflammation. The release profiles of the APIs allow film application on the injured skin up to three times a day, ensuring the antibacterial and anti-inflammatory effect of the APIs and maintaining a wet environment due to the presence of PVA.

Disclosure statement

No potential conflict of interest was reported by the author(s).

Funding

This study was supported by the 'Iuliu Haţieganu' University and Medicine and Pharmacy through the internal doctoral research grant 771/56/11.01.2023.

References

[1] Cardona AF, Wilson SE. Skin and Soft-Tissue infections: a critical review and the role of telavancin in their treatment. Clin Infect Dis. 2015;61(suppl 2):S69–S78. doi:10.1093/cid/civ528.

[2] Broussard KC, Powers JG. Wound dressings: selecting the most appropriate type. Am J Clin Dermatol. 2013;14(6):449–459. doi:10.1007/s40257-013-0046-4.

[3] Weller CD, Team V, Sussman G. First-Line interactive wound dressing update: a comprehensive review of the evidence. Front Pharmacol. 2020;11:155. doi:10.3389/fphar.2020.00155.

[4] Özcan Bülbül E, Okur ME, Üstündağ Okur N, et al. Chapter 2 - Traditional and advanced wound dressings: physical characterization and desirable properties for wound healing. In: Sah MK, Kasoju N, Mano JF, editors. Natural polymers in wound healing and repair. Amsterdam: Elsevier; 2022. p. 19–50.

[5] Rezvani Ghomi E, Niazi M, Ramakrishna S. The evolution of wound dressings: from traditional to smart dressings. Polymers Adv Techs. 2023;34(2):520–530. doi:10.1002/pat.5929.

[6] Savencu I, Iurian S, Porfire A, et al. Review of advances in polymeric wound dressing films. React Funct Polym. 2021;168:105059. doi:10.1016/j.reactfunctpolym.2021.105059.

[7] Karki S, Kim H, Na S-J, et al. Thin films as an emerging platform for drug delivery. Asian J Pharm Sci. 2016;11(5):559–574. doi:10.1016/j.ajps.2016.05.004.

[8] Ahmad N, Tayyeb D, Ali I, et al. Development and characterization of Hemicellulose-Based films for antibacterial wound-dressing application. Polymers. 2020;12(3):548. doi:10.3390/polym12030548.

[9] Amalraj A, Haponiuk JT, Thomas S, et al. Preparation, characterization and antimicrobial activity of polyvinyl alcohol/gum arabic/chitosan composite films incorporated with black pepper essential oil and ginger essential oil. Int J Biol Macromol. 2020;151:366–375. doi:10.1016/j.ijbiomac.2020.02.176.

[10] Genesi BP, de Melo Barbosa R, Severino P, et al. Aloe vera and copaiba oleoresin-loaded chitosan films for wound dressings: microbial permeation, cytotoxicity, and in vivo proof of concept. Int J Pharm. 2023;652:123823. doi:10.1016/j.ijpharm.2023.122648.

[11] Pawar HV, Tetteh J, Boateng JS. Preparation, optimisation and characterisation of novel wound healing film dressings loaded with streptomycin and diclofenac. Colloids Surf B Biointerfaces. 2013;102:102–110. doi:10.1016/j.colsurfb.2012.08.014.

[12] Nesseem DI, Eid SF, El-Houseny SS. Development of novel transdermal self-adhesive films for tenoxicam, an anti-inflammatory drug. Life Sci. 2011;89(13-14):430–438. doi:10.1016/j.lfs.2011.06.026.

[13] Costa NN, de Faria Lopes L, Ferreira DF, et al. Polymeric films containing pomegranate peel extract based on PVA/starch/PAA blends for use as wound dressing: in vitro analysis and physicochemical evaluation. Mater Sci Eng C Mater Biol Appl. 2020;109:110643. doi:10.1016/j.msec.2020.110643.

[14] Das A, Uppaluri R, Das C. Feasibility of poly-vinyl alcohol/starch/glycerol/citric acid composite films for wound dressing applications. Int J Biol Macromol. 2019;131:998–1007. doi:10.1016/j.ijbiomac.2019.03.160.

[15] Arthe R, Arivuoli D, Ravi V. Preparation and characterization of bioactive silk fibroin/paramylon blend films for chronic wound healing. Int J Biol Macromol. 2020;154:1324–1331. doi:10.1016/j.ijbiomac.2019.11.010.

[16] Sakthiguru N, Sithique MA. Fabrication of bioinspired chitosan/gelatin/allantoin biocomposite film for wound dressing application. Int J Biol Macromol. 2020;152:873–883. doi:10.1016/j.ijbiomac.2020.02.289.

[17] Pereira GG, Guterres SS, Balducci AG, et al. Polymeric films loaded with vitamin E and aloe vera for topical application in the treatment of burn wounds. Biomed Res Int. 2014;2014:641590–641599. (Electronic)). doi:10.1155/2014/641590.

[18] Ng S-F, Leow H-L. Development of biofilm-targeted antimicrobial wound dressing for the treatment of chronic wound infections. Drug Dev Ind Pharm. 2015;41(11):1902–1909. doi:10.3109/03639045.2015.1019888.

[19] Kollicoat® SR 30 D. 2023. https://pharma.basf.com/products/kollicoat-sr-30-d

[20] Hypromellose. In: Rowe RC, Sheskey PJ, Quinn ME, editors. Handbook of pharmaceutical excipients. 6th ed. London: Pharmaceutical Press; 2009. p. 326–329.
[21] Muppalaneni S, Omidian H. Polyvinyl alcohol in medicine and pharmacy: a perspective. J Dev Drugs. 2013;02(03):112. doi:10.4172/2329-6631.1000112.
[22] Jin SG. Production and application of biomaterials based on polyvinyl alcohol (PVA) as wound dressing. Chem Asian J. 2022;17(21):e202200595. doi:10.1002/asia.202200595.
[23] Ingebrigtsen SG, Didriksen A, Johannessen M, et al. Old drug, new wrapping – a possible comeback for chloramphenicol? Int J Pharm. 2017;526(1-2):538–546. doi:10.1016/j.ijpharm.2017.05.025.
[24] Aycan D, Selmi B, Kelel E, et al. Conductive polymeric film loaded with ibuprofen as a wound dressing material. Eur Polym J. 2019;121:109308. doi:10.1016/j.eurpolymj.2019.109308.
[25] Yu LX, Amidon G, Khan MA, et al. Understanding pharmaceutical quality by design. Aaps J. 2014;16(4):771–783. doi:10.1208/s12248-014-9598-3.
[26] Gilani SJ, Rizwanullah M, Imam SS, et al. Chapter 7 - QbD considerations for topical and transdermal product development. In: Beg S, Hasnain MS, editors. Pharmaceutical quality by design. Cambridge, MA: Academic Press; 2019. p. 131–150.
[27] Colobatiu L, Gavan A, Mocan A, et al. Development of bioactive compounds-loaded chitosan films by using a QbD approach – a novel and potential wound dressing material. React Funct Polym. 2019;138:46–54. doi:10.1016/j.reactfunctpolym.2019.02.013.
[28] ICH Harmonized Tripartite Guideline - Pharmaceutical Development Q8 (R2). 2009. https://database.ich.org/sites/default/files/Q8_R2_Guideline.pdf
[29] ICH guideline Q9 on quality risk management: European Medicines Agency. 2015. https://www.ema.europa.eu/en/documents/scientific-guideline/international-conference-harmonisation-technical-requirements-registration-pharmaceuticals-human-use-ich-guideline-q9-quality-risk-management-step-5-first-version_en.pdf
[30] IEC 60812. 2018 Failure modes and effects analysis (FMEA and FMECA). 2018.
[31] European Pharmacopoeia 11.2 Section 2.9.5. Uniformity of mass of single-dose preparations. 2023.
[32] Baranauskaite J, Ockun MA, Uner B, et al. Development and in vitro characterization of pullulan fast dissolving films loaded with panax ginseng extract, antioxidant properties and cytotoxic efficiency on lung and breast cancer cell lines. J Drug Delivery Sci Technol. 2022;76:103701. doi:10.1016/j.jddst.2022.103701.
[33] Nair AB, Kumria R, Harsha S, et al. In vitro techniques to evaluate buccal films. J Control Release. 2013;166(1):10–21. doi:10.1016/j.jconrel.2012.11.019.
[34] ISO 175:2010 Plastics. Methods of test for the determination of the effects of immersion in liquid chemicals 2010. https://www.iso.org/standard/55483.html.
[35] Muthuramalingam K, Choi SI, Hyun C, et al. β-Glucan-Based wet dressing for cutaneous wound healing. Adv Wound Care. 2019;8(4):125–135. doi:10.1089/wound.2018.0843.
[36] Krull SM, Patel HV, Li M, et al. Critical material attributes (CMAs) of strip films loaded with poorly water-soluble drug nanoparticles: i. Impact of plasticizer on film properties and dissolution. Eur J Pharm Sci. 2016;92:146–155. doi:10.1016/j.ejps.2016.07.005.
[37] Gómez-Aldapa CA, Velazquez G, Gutierrez MC, et al. Effect of polyvinyl alcohol on the physicochemical properties of biodegradable starch films. Mater Chem Phys. 2020;239:122027. doi:10.1016/j.matchemphys.2019.122027.
[38] El-Bary AA, Al Sharabi I, Haza'a BS. Effect of casting solvent, film-forming agent and solubilizer on orodispersible films of a polymorphic poorly soluble drug: an in vitro/in silico study. Drug Dev Ind Pharm. 2019;45(11):1751–1769. doi:10.1080/03639045.2019.1656733.
[39] Morita Y, Tomida J, Kawamura Y. Responses of Pseudomonas aeruginosa to antimicrobials. Front Microbiol. 2014;4:422. doi:10.3389/fmicb.2013.00422.
[40] Liew KB, Tan YTF, Peh K-K. Effect of polymer, plasticizer and filler on orally disintegrating film. Drug Dev Ind Pharm. 2014;40(1):110–119. doi:10.3109/03639045.2012.749889.
[41] Okeke OC, Boateng JS. Composite HPMC and sodium alginate based buccal formulations for nicotine replacement therapy. Int J Biol Macromol. 2016;91:31–44. doi:10.1016/j.ijbiomac.2016.05.079.
[42] Kaur G, Singh D, Brar V. Bioadhesive okra polymer based buccal patches as platform for controlled drug delivery. Int J Biol Macromol. 2014;70:408–419. doi:10.1016/j.ijbiomac.2014.07.015.
[43] Boateng JS, Stevens HNE, Eccleston GM, et al. Development and mechanical characterization of solvent-cast polymeric films as potential drug delivery systems to mucosal surfaces. Drug Dev Ind Pharm. 2009;35(8):986–996. doi:10.1080/03639040902744704.
[44] Maulana DS, Mubarak AS, Pujiastuti DY. The concentration of polyethylen glycol (PeG) 400 on bioplastic cellulose based carrageenan waste on biodegradability and mechanical properties bioplastic. IOP Conf Ser Earth Environ Sci. 2021;679(1):012008. doi:10.1088/1755-1315/679/1/012008.
[45] Gomes Neto RJ, Genevro GM, Paulo L, et al. Characterization and in vitro evaluation of chitosan/konjac glucomannan bilayer film as a wound dressing. Carbohydr Polym. 2019;212:59–66. doi:10.1016/j.carbpol.2019.02.017.
[46] Ahmed A, Boateng J. Calcium alginate-based antimicrobial film dressings for potential healing of infected foot ulcers. Ther Deliv. 2018;9(3):185–204. doi:10.4155/tde-2017-0104.
[47] Pereira R, Carvalho A, Vaz DC, et al. Development of novel alginate based hydrogel films for wound healing applications. Int J Biol Macromol. 2013;52:221–230. doi:10.1016/j.ijbiomac.2012.09.031.
[48] Rezvanian M, Ahmad N, Mohd Amin MCI, et al. Optimization, characterization, and in vitro assessment of alginate-pectin ionic cross-linked hydrogel film for wound dressing applications. Int J Biol Macromol. 2017;97:131–140. doi:10.1016/j.ijbiomac.2016.12.079.
[49] Llabot JM, Palma SD, Manzo RH, et al. Design of novel antifungal mucoadhesive films: part II. Formulation and in vitro biopharmaceutical evaluation. Int J Pharm. 2007;336(2):263–268. doi:10.1016/j.ijpharm.2006.12.001.
[50] Francolini I, Donelli G, Vuotto C, et al. Antifouling polyurethanes to fight device-related staphylococcal infections: synthesis, characterization, and antibiofilm efficacy. Pathog Dis. 2014;70(3):401–407. doi:10.1111/2049-632X.12155.
[51] Gultekin G, Atalay-Oral C, Erkal S, et al. Fatty acid-based polyurethane films for wound dressing applications. J Mater Sci Mater Med. 2009;20(1):421–431.
[52] Alavi T, Rezvanian M, Ahmad N, et al. Pluronic-F127 composite film loaded with erythromycin for wound application: formulation, physicomechanical and in vitro evaluations. Drug Deliv Transl Res. 2019;9(2):508–519. doi:10.1007/s13346-017-0450-z.

gels

MDPI

Article

QbD Approach in Cosmetic Cleansers Research: The Development of a Moisturizing Cleansing Foam Focusing on Thickener, Surfactants, and Polyols Content

Cătălina Bogdan [1], Diana Antonia Safta [1,*], Sonia Iurian [2], Dyana Roxana Petrușcă [1] and Mirela-Liliana Moldovan [1,*]

[1] Department of Dermopharmacy and Cosmetics, Faculty of Pharmacy, "Iuliu Hațieganu" University of Medicine and Pharmacy, 12 I. Creangă St., 400010 Cluj-Napoca, Romania; catalina.bogdan@umfcluj.ro (C.B.); dyana.roxa.petrusca@elearn.umfcluj.ro (D.R.P.)

[2] Department of Pharmaceutical Technology and Biopharmacy, Faculty of Pharmacy, "Iuliu Hațieganu" University of Medicine and Pharmacy, 41 V. Babeș St., 400012 Cluj-Napoca, Romania; sonia.iurian@umfcluj.ro

* Correspondence: diana.an.safta@elearn.umfcluj.ro (D.A.S.); mmoldovan@umfcluj.ro (M.-L.M.)

Abstract: Cleansing products, particularly innovative cosmetic foams, must efficiently remove impurities with minimal impact on the skin barrier and have a favorable sensory profile. The choice of product ingredients is crucial to ensure the optimal characteristics. The current study aims to provide a comprehensive framework for understanding the variability in the characteristics of a cleansing foam to achieve desired properties. The novelty of this study lies in the combination of ingredients for their potential synergistic and complementary effects in cleansing dry skin, as well as the application of Quality by Design (QbD) elements to develop and optimize the formulation of cleansing foam. The effects of varying the concentration of mild surfactants, polyols, and gel-forming agents on the properties of the gels and of the generated foams were studied. Significant influences of the formulation factors were observed: an increased ratio of xanthan gum positively impacted the texture properties of the gel, whereas higher concentrations of surfactants had a negative impact on these parameters. Additionally, increasing the polyols ratio was found to negatively influence the foaming property and stability of the foam. The study established an optimal formulation of a cleansing foam with a ratio of 0.45% xanthan gum, 26.19% surfactants and 2.16% polyols to be used for dry skin hygiene.

Keywords: cleansing foams; DoE; dry skin hygiene; mild surfactants; xanthan gum; polyols

check for updates

Citation: Bogdan, C.; Safta, D.A.; Iurian, S.; Petrușcă, D.R.; Moldovan, M.-L. QbD Approach in Cosmetic Cleansers Research: The Development of a Moisturizing Cleansing Foam Focusing on Thickener, Surfactants, and Polyols Content. *Gels* **2024**, *10*, 484. https://doi.org/10.3390/gels10080484

Academic Editor: Jean-Michel Guenet

Received: 14 June 2024
Revised: 18 July 2024
Accepted: 19 July 2024
Published: 23 July 2024

Copyright: © 2024 by the authors. Licensee MDPI, Basel, Switzerland. This article is an open access article distributed under the terms and conditions of the Creative Commons Attribution (CC BY) license (https://creativecommons.org/licenses/by/4.0/).

1. Introduction

The performance requirements of cleansing products encompass efficient removal of environmental pollutants, make-up, sebum, and microorganisms from the skin's surface [1]. The cleansing action is primarily attributed to surfactants or "surface acting agents", amphiphilic compounds used to clean skin through chemical or physical mechanisms. Surfactants clean the skin's surface by emulsifying the lipids, which are further easily washed, while physical cleansing involves the mechanical removal of the impurities from the surface of the skin. Surfactants should have a minimal impact on the barrier function of the skin [2]. Particularly for dry skin, it is crucial to use cleansers with minimal defatting activity and a neutral to slightly acidic pH to avoid further damage [3].

Progress in surfactant technology led to the formulation of affordable and performant cleansers. Among the high variety of cleansing products, cosmetic foams represent an innovative category for skin hygiene, with various advantages such as ease of application and effective and fast removal of both hydrophilic and lipophilic impurities. According to European Pharmacopoeia's definition, foams are obtained at the moment of administration by dispersing a significant volume of gas in a liquid [4]. Generally, foam-based delivery

systems contain the active ingredients and the dispersed solid or liquid components that become gaseous by pressing the valve of the conditioning bottle, due to the contained surfactants. Foams can be obtained from non-aerosol recipients, as well as by releasing the ready-to-use product upon pump activation [5]. The easy application and good spreadability of foams lead to increased acceptability and consumer satisfaction [1,2,5].

The main disadvantage of the foams is the fact that they are thermodynamically unstable, so formulation studies are needed to ensure foam stability. Moreover, their composition must be well chosen to guarantee efficiency and sensorial properties. To fully understand various formulation components and processes affecting the final product, a Quality by Design (QbD) approach is therefore very important, helping to achieve a quality-based development [1,5].

One of the main challenges of the cosmetic industry is to ensure consistent product quality during the manufacturing process, given its importance for maintaining safety, efficacy, and regulatory compliance, while also achieving cost-effective production. Therefore, the adaptation of QbD principles into cosmetic development plays a crucial role in producing high-quality products that meet safety requirements and fulfill user expectations. Moreover, the integration of QbD elements yields additional environmental advantages, since the industry is increasingly focused on sustainability, aiming to reduce energy and material usage and generate less waste in the production of cosmetics.

The development of cosmetic foams within the QbD framework considers the specific characteristics of these formulations and accelerates the development process. The development of a product through QbD involves the profiling step with the selection of a quality target product profile (QTPP) and determining the Critical Quality Attributes (CQAs) [1]. Appearance and bubble size, viscosity of the liquid formulation, foamability, foam density, consistency and texture, or drug content and drug release for medicated foams are just a few of the features with important for foam quality [1,6]. Further, the identification of risk factors is conducted to establish potential risk variables both in the early stages of development and throughout the development process, as additional knowledge about the product is obtained. In line with the QbD principles, Falusi et al. (2022) identified and categorized the CQAs with the highest potential impact in the quality profile, followed by determining the material attributes and the process parameters that exert the highest risk on the CQAs. The type and ratio of polymers, as well as the stirring speed and time, were deemed as the most impactful factors on properties like foam volume stability, foam expansion, or cross point [5].

However, the QbD approach usually involves the use of Design of Experiments (DoE) as a risk mitigation tool, which can lead to a Design Space described as a multidimensional combination and interaction of input variables shown to guarantee the product's quality [7,8]. The development of cosmetic products using DoE has as an advantage the ability to quantify the relationships between the risky variables and the properties of the product, allowing the prediction of the experimental conditions that lead to the desired characteristics [9].

Therefore, the current study aims to provide a framework to assess and understand the variability of the characteristics of a cleansing foam containing mild surfactants and suitable excipients to ensure adequate properties for dry skin hygiene. The factors influencing its quality attributes were analyzed through DoE leading to the development of an optimal formulation. The novelty of this study lies in the combination of ingredients chosen for their potential synergistic and complementary effects in cleansing dry skin, and in the application of the QbD approach to set the optimum factors for an improvement in product performance. Moreover, this study is one of the few in the literature that use QbD elements to develop a cleansing foam, studying both the gel and generated foam characteristics.

2. Results and Discussion

A thorough understanding of the interactions between surfactants and the compromised stratum corneum barrier is necessary for the formulation of cleaning products for

dry skin. Due to their many advantages over conventional skincare products, foams are becoming more attractive. They are also considered a user-friendly solution. The product is delivered in an exact amount thanks to the dispenser pump, which also lowers the risk of microbial contamination.

To develop the foam, mild surfactants like lauryl glucoside, decyl glucoside, and sodium cocoyl isethionate were chosen due to their excellent cleansing efficacy and skin tolerance. Lauryl glucoside and decyl glucoside are nonionic surfactants with good foaming properties and soft caring after feeling [6]. They do not produce a significant decrease in skin moisture [10]. Sodium cocoyl isethionate is an anionic surfactant with high foaming power [11] and produces rich creamy foam with a moisturizing and soothing feeling [6,12].

Foams are characterized by a low density and are influenced significantly by surface tension gradient. Three steps characterize the foaming process: initiation and formation, stability, drainage and rupture. Initially, foam formation is due to large gas voids which create a high liquid-gas interface. Surfactant solutions stabilize this interface, creating a surface tension gradient that prevents liquid drainage and favors the persistence of the foam. While the foam formation is influenced by the dynamic surface pressure, foam stability is influenced by the surface dilatational rheology. Thus, low concentrations of surfactants create elastic monolayers that prevent foam formation and higher concentrations yield a viscoelastic surface necessary for the stability of the foams. Initially, during the foam formation, the foam is predominantly liquid, afterward the foam coarsens as bubble size increases and lamellar distances decrease. Increasing the viscosity of the interlamellar liquid by adding water-soluble polymers limits the film drainage [13].

The active ingredients: sodium PCA (pyrrolidone carboxylic acid), *Aloe vera* oil, *Cedrus atlantica* bark oil, *Cupressus sempervirens* oil and *Copaifera officinalis* resin oil were chosen for their interesting properties to restructure the barrier and enhance the appearance of dry skin. The selected ingredients may act synergistically and complementary to gently clean the skin and provide the hydration needed for dry skin.

Aloe vera L. (*Asphodelaceae* family) is considered one of the most potent, commercially important, and popular plants in the research field of skin products. Different parts of the plant contain about 200 active phytocompounds, namely amino acids, polysaccharides, enzymes, vitamins, minerals, saponins, anthraquinones, lignin, and salicylic acid [14]. In addition to providing a protective barrier for the skin and retaining moisture, *Aloe vera* may promote the healing of skin damage which may be associated with dry skin [14,15].

Cedrus atlantica (Endl.) Manetti ex Carriere (*Pinaceae* family) contains several bioactive compounds, including oxygenated sesquiterpenes and sesquiterpene hydrocarbons. The major compounds encountered are α-pinene, himachalene, β-himachalene, cis-α-atlantone, himachalol, germacrene D, and β-copaene [16,17] *Cedrus atlantica* oil exhibits high antibacterial and antifungal activity, remarkable antioxidant activity, good anti-inflammatory, and important depigmenting activity through tyrosinase inhibition [16].

Copaifera officinalis (Fabaceae family) contains volatile compounds like sesquiterpenes e.g., β-caryophyllene, α-copaene, β-bisabolene, trans-α-bergamotene with anti-inflammatory, antioxidant, and antimicrobial actions, being used traditionally in the treatment of wounds [18,19].

Cupressus sempervirens L. (*Cupressaceae* family) contains volatile oils such as α-pinene, δ-3-carene, limonene, and α-terpinolene that possess antioxidant, antimicrobial, and antibiofilm properties [20,21].

As regards the impact of oil inclusion on foaming systems, the stability of the foams can be reduced by changing the surface tension and increasing liquid drainage [22].

In addition to herbal extracts and vegetal oils, sodium PCA was added to lessen the dryness usually associated with the washing procedure. Sodium PCA, a salt of pyrrolidone carboxylic acid), is naturally present in the stratum corneum as a component of the natural moisturizing factor (NMF). There are many reports of topical PCA applications being effective in treating symptoms of dry skin [23,24]. Furthermore, glycerin, the most well-known humectant, and moisturizer, can keep the skin smooth and thus help to preserve hydration in the top layers of the skin [25]. Xylitol has also been documented for its skin-

hydrating effect [26]. As concluded by Korponyai et al., using a combination of glycerol and xylitol can be a useful approach for treating dry skin, by increasing the skin hydration, the quantity of filaggrin, the interdigitation index, decreasing the TEWL (transepidermal water loss) and improving the biomechanical properties of the skin [26]. Moreover, as demonstrated by Szel et al., xylitol can exert anti-irritant and anti-inflammatory effects even at a lower concentration compared to glycerol [27]. In a study conducted by Sagitani et al., the effect of polyols on the formation of the lamellar gel phase for the stability of cream soaps was investigated. The results showed that glycerol was more advantageous than other polyols, such as 1,3-butylene glycol, PEG 400, or dipropylene glycol, in obtaining stable cream soaps [28].

Xanthan gum is a thickening natural-derived agent, that is widely used in cosmetic formulations due to its beneficial properties. It is highly compatible with anionic, amphoteric, and nonionic surfactants and stabilizes foams against separation [11,29]. The addition of different polymers such as xanthan gum, alginates, or cellulose derivatives in foam preparations can be used to enhance the stability of the foams, through the formation of a surfactant-polymer complex [22].

Lathering products are generally more popular among users, but they are not typically recommended for dry skin [30]. However, by combining the appropriate level of surfactants that ensure effective cleansing without damaging skin barrier lipids, along with humectants and plant extracts with antioxidant and anti-inflammatory properties, a balanced product that mitigates the negative effects commonly associated with lathering products can be obtained.

Recently, Falusi et al. developed foams using the QbD concept, studying the influence of different polymers on the quality of the foams. They also noted the good properties of xanthan gum in foam development, specifying that the type and concentrations of different polymers can impact the properties of the product in different ways [5]. Despite the significant contributions of this research, the literature remains scarce on this topic, this article being the only one found on foam development using the QbD approach. Thus, to the best of our knowledge, our article is one of the few publications to explore QbD in the formulation of cleansing foams, underscoring the novelty and importance of our findings. In addition to the research of Falusi et al., the current study aimed to investigate some other factors affecting both the gel and the foam formed, such as surfactants and polyol concentrations, contributing to providing a comprehensive framework for enhancing product quality.

2.1. QbD Approach

2.1.1. Definition of QTPP, CQAs

QbD involves identifying and understanding the critical quality attributes (CQAs) of the cleansing foam from the elements that compose the QTPP (Table 1). By defining these early in the development process, manufacturers can ensure the final product meets the desired specifications and performance standards. As outlined in Table 1, the key attributes of successful cleansing products include the following characteristics: easy to spread with appropriate foaming properties, pleasant feeling during the application, non-greasy feeling, residue-free, and additional moisturizing properties while cleaning [30].

Table 1. QTPP and CQAs of foam dosage forms.

QTPP	Target	CQAs	Justification
Cosmetic dosage form	Cleansing foam	Yes	Surfactant-based product for dry skin cleansing
Application site	Face hygiene	-	
Product design	Foam	-	Impact on ease of use and spreading
Appearance	Smooth foam	-	Impact on users' acceptability
Color	White	-	Impact on users' acceptability
Odor	Specific for the herbal ingredients; fragrance-free	-	Impact on users' acceptability
Physical properties:			
The gel from the non-aerosol container			Impact on the stability, foaming properties, and sensory performance
Firmness (g)—Y1	Low	Yes	Impact on the formation of the foam from the gel at the moment of product release
Consistency (mJ)—Y2	Low	Yes	
Stringiness length (mm)—Y3		-	Impact on the sensorial profile of the foaming product
Stringiness work done (mJ)—Y4		-	Influences the ease of pick-up from the recipient
Adhesive force (g)—Y5	Low	Yes	Impact on users' acceptability
Adhesiveness (mJ)—Y6	Low	Yes	
Formed foam			
Foaming property (mL)—Y7	High	Yes	Influences users' satisfaction
Foam stability (mL)—Y8	High	Yes	Influences the performance of the formulation
Dirt dispersion—Y9	High	Yes	
Firmness (g)—Y10			Influences the handling properties, the lightweight texture, and the even application
Consistency (mJ)—Y11			
Adhesive force (g)—Y12			Influences users' acceptability
Adhesiveness (mJ)—Y13			
Stringiness length (mm)—Y14			
Stringiness work done (mJ)—Y15			
pH value	4–7		
Content uniformity	Homogenous Product		Maintenance of resident flora and barrier function
Container	Foam container	-	Influences the formation of the foam/User- friendly delivery system

2.1.2. Risk Analysis

In Figure S1 and Table S1 (Supplementary Materials), the risk assessment and management of foaming-gels development are highlighted. The potential risks were identified, and the control methods were established. By addressing these risks proactively, the likelihood of product failure or defects is significantly reduced. The factors that had the greatest RPN were the most important in assuring the quality of the final product [1]. Thus, the concentrations of surfactants, polyols, and the gel-forming agent, were further chosen as variation factors in the experimental plan.

2.1.3. Experimental Design

The results obtained after preparing and analyzing the formulations are presented in Table 2.

As the design of experiments selected for this study was a D-Optimal screening design, the mathematical model was able to quantify the independent effects and the second-order interactions. The theoretical model applied to each of the responses is presented below:

$$Y = const + a1X1 + a2X2 + a3X3 + a4X1X2 + a5X1X3 + a6X2X3$$

where Const—constant, intercept, a—regression equation coefficients that show the effect of each factor, Y is the response, X1-X3 represent the individual effects, while X1X2, X1X3, and X2X3 are the interactions effects, which show the variation of the response when two factors are changed simultaneously.

Table S2 (Supplementary Materials) presents the revised quantitative factor effects and the associated *p*-values.

Table 2. The results of selected output responses.

Exp	Y1 (g)	Y2 (mJ)	Y3 (mm)	Y4 (mJ)	Y5 (g)	Y6 (mJ)	Y7 (mL)	Y8 (mL)	Y9	Y10 (g)	Y11 (mJ)	Y12 (g)	Y13 (mJ)	Y14 (mm)	Y15 (mJ)
N1	83.20 ± 9.80	13.52 ± 2.12	11.87 ± 0.33	5.51 ± 0.82	54.80 ± 6.40	8.44 ± 0.98	22.00 ± 0.57	20.00 ± 1.52	1.00 ± 0.57	6.80 ± 2.00	1.07 ± 0.46	6.70 ± 2.60	0.98 ± 0.43	34.21 ± 7.65	0.66± 0.33
N2	126.3 ± 3.80	22.77 ± 1.06	9.77 ± 0.39	8.05 ± 0.70	99.00 ± 3.60	14.95 ± 0.51	20.00 ± 0.57	19.00 ± 0.00	1.00 ± 0.57	6.30 ± 11.30	1.09 ± 0.47	3.80 ± 1.00	0.34 ± 0.27	37.04 ± 10.01	0.08± 0.27
N3	31.20± 4.00	4.12 ± 0.22	1.66 ± 0.74	0.08 ± 0.05	10.50 ± 3.00	0.64 ± 0.11	25.00 ± 0.57	23.00 ± 0.57	4.00 ± 0.57	6.30 ± 0.30	1.81 ± 0.22	3.50 ± 0.50	0.17 ± 0.11	56.27 ± 3.81	0.10± 0.16
N4	25.70 ± 2.00	4.30 ± 0.49	15.08 ± 20.00	0.22 ± 0.30	8.5 ± 0.00	0.66 ± 0.07	25.00 ± 2.00	23.00 ± 2.51	3.00 ± 0.57	8.20 ± 0.30	2.22 ± 0.3	3.20 ± 0.30	0.06 ± 0.05	56.94 ± 3.74	0.27± 0.07
N5	96.30 ± 6.50	17.47 ± 1.22	11.18 ± 0.95	6.21 ± 0.24	69.30 ± 6.10	11.21 ± 0.88	20.00 ± 2.00	19.00 ± 2.51	3.00 ± 0.57	5.70 ± 1.30	1.33 ± 0.35	5.00 ± 1.70	0.66 ± 0.37	52.79 ± 11.17	0.38± 0.08
N6	143.00 ± 1.80	26.12 ± 0.76	9.83 ± 0.73	9.08 ± 0.98	113.20 ± 3.20	16.88± 0.40	17.00 ± 0.57	18.00 ± 1.15	3.00 ± 1.00	6.50 ± 0.50	1.74 ± 0.26	3.30 ± 0.30	0.07 ± 0.08	50.05 ± 7.27	0.41± 0.17
N7	31.20 ± 4.90	4.13 ± 0.29	1.83 ± 0.59	0.10± 0.05	12.00 ± 3.50	0.83 ± 0.20	21.00 ± 1.52	19.00 ± 1.15	1.00 ± 0.57	5.20 ± 0.30	1.42 ± 0.19	5.00 ± 0.00	0.47 ± 0.14	58.71 ± 0.85	0.36± 0.20
N8	63.70 ± 6.40	9.11 ± 2.81	12.01 ± 8.11	2.96 ± 1.83	33.80 ± 2.30	4.66 ± 0.56	19.00 ± 1.15	18.00 ± 1.00	1.00 ± 0.00	9.00 ± 0.50	2.87± 0.26	3.30 ± 0.60	0.14 ± 0.09	57.74 ± 1.33	0.03± 0.15
N9	36.70 ± 5.30	3.61 ± 0.23	3.16 ± 2.28	0.21 ± 0.05	19.70 ± 2.80	0.77 ± 0.07	21.00 ± 1.00	20.00 ± 0.57	3.00 ± 0.57	6.20 ± 0.30	1.39 ± 0.35	5.00 ± 0.50	0.76 ± 0.26	58.46 ± 1.77	0.71± 0.28
N10	57.80 ± 6.90	7.55 ± 1.86	8.09 ± 5.08	1.72 ± 0.88	29.00 ± 4.30	3.96 ± 0.87	20.00 ± 0.57	20.00 ± 0.57	1.00 ± 0.00	5.20 ± 0.80	1.33 ± 0.18	4.30 ± 0.30	0.26 ± 0.08	56.74 ± 1.82	0.01± 0.13
N11	43.50 ± 2.00	7.96 ± 0.44	15.68 ± 0.97	2.10 ± 0.37	19.20 ± 1.00	3.28 ± 0.11	20.00 ± 0.00	19.00 ± 0.00	2.00 ± 0.57	5.70 ± 0.30	1.50 ± 0.07	3.50 ± 0.05	0.13 ± 0.03	53.42 ± 6.66	0.30± 0.04
N12	49.20 ± 3.50	9.00 ± 0.63	15.00 ± 1.07	2.56 ± 0.61	23.50 ± 3.30	3.78 ± 0.46	20.00± 0.00	20.00 ± 0.00	1.00 ± 0.57	6.70 ± 2.10	1.34 ± 0.21	4.70 ± 0.60	0.46± 0.11	57.37 ± 2.34	0.32± 0.15
N13	74.00 ± 5.20	13.30 ± 1.03	13.90 ± 1.12	5.34 ± 1.03	47.70 ± 4.50	7.50 ± 0.90	21.00 ± 0.57	21.00 ± 0.57	2.00 ± 0.00	4.30 ± 0.30	1.11 ± 0.12	4.80 ± 0.30	0.44 ± 0.06	54.09 ± 8.45	0.26 ± 0.19

Quantitative variables and their variation levels: X1—% xanthan gum, X2—% surfactants (lauryl glucoside, decyl glucoside. sodium cocoyl isethionate). X3—% polyols (glycerin:xylitol); Characterization of the gel: Y1—firmness (g), Y2—consistency (mJ), Y3—stringiness length (mm), Y4—stringiness work done (mJ), Y5—adhesive force (g), Y6—adhesiveness (mJ), Characterization of the foam: Y7—foaming property (mL), Y8—foam stability (mL), Y9—dirt dispersion, Y10—firmness (g), Y11-consistency (mJ), Y12—adhesive force (g), Y13—adhesiveness (mJ), Y14—stringiness length (mm), Y15—stringiness work done (mJ).

2.1.4. Statistical Analysis

For each of the fifteen responses, mathematical models were fitted. According to Table 3, the results obtained show an appropriate fitting of the experimental data with the chosen models. R^2, the percentage of the variation of the response explained by the model, indicates a good fit, with values above 0.55. The values of Q^2, defined as the percent of the variation of the response predicted by the model, were higher than 0.45. Consequently, the high values of these two parameters for most response factors indicate a good model. The difference between the two values should be smaller than 0.2–0.3, as smaller differences indicate an appropriately selected model. When the model validity values are higher than 0.25, there is no lack of fit of the model (the model error is in the same range as the pure error) and the values are considered acceptable. The model validity parameter indicates whether the appropriate model type has been chosen. In this case, the validity was good for all answers. The reproducibility, a measure of the systematic error, reflects the variation of the response under identical conditions (pure error), often at the center points, compared to the total variation of the response and it reached values above 0.35. The equations used by the software to calculate the validity and reproducibility are presented below. Table 3 presents the statistical parameters for the ANOVA test and the quality of fit. Excepting Y10, the *p*-value was below 0.05, which indicates a statistically significant model [7,9,31,32].

$$\text{Validity} = 1 + 0.57647 \times \log10(p),$$

(available only when replicated experiments have been performed).

Reproducibility is a measure of the systematic error, calculated using the following equation [32]:

$$\text{Reproducibility} = 1 - (\text{MSPure error}/\text{MSTotal corrected})$$

Table 3. Statistical parameters for ANOVA test and quality of fit.

Response	R^2	Adjusted R^2	Q^2	*p*-Value Regression	*p*-Value Lack of Fit	Model Validity	Reproducibility
Y1	0.847	0.796	0.710	0.001	0.322	0.715	0.872
Y2	0.899	0.879	0.846	0.000	0.658	0.895	0.854
Y3	0.714	0.619	0.693	0.008	0.693	0.908	0.510
Y4	0.837	0.783	0.677	0.001	0.168	0.553	0.917
Y5	0.837	0.783	0.712	0.001	0.322	0.716	0.863
Y6	0.847	0.817	0.778	0.000	0.362	0.745	0.876
Y7	0.799	0.733	0.625	0.002	0.067	0.322	0.948
Y8	0.868	0.824	0.775	0.000	0.776	0.936	0.741
Y9	0.764	0.685	0.624	0.003	0.493	0.822	0.714
Y10	0.490	0.321	0.342	0.095	0.521	0.836	0.349
Y11	0.682	0.576	0.414	0.013	0.086	0.387	0.901
Y12	0.766	0.650	0.384	0.012	0.517	0.834	0.661
Y13	0.732	0.598	0.403	0.020	0.384	0.760	0.699
Y14	0.888	0.850	0.840	0.000	0.180	0.570	0.940
Y15	0.657	0.486	0.404	0.050	0.660	0.895	0.369

R^2—the percentage of the variation of the response explained by the model; Q^2—the percent of the variation of the response predicted by the model; Characterization of the gel: Y1—firmness (g), Y2—consistency (mJ), Y3—stringiness length (mm), Y4—stringiness work done (mJ), Y5—adhesive force (g), Y6—adhesiveness (mJ), Characterization of the foam: Y7—foaming property (mL), Y8—foam stability (mL), Y9—dirt dispersion, Y10— firmness (g), Y11—consistency (mJ), Y12—adhesive force (g), Y13—adhesiveness (mJ), Y14—stringiness length (mm), Y15—stringiness work done (mJ).

2.1.5. The Influence of the Formulation Factors on the Physical Characteristics of the Cleansing Foams

The scaled and centered histograms showing the mathematical model coefficients that further indicate the influence of the formulation factors on the parameters of the gels and foams are presented in Figure 1. To a better understanding of the interactions and

nonlinear effects, contour plots were also included in Figure S2 (Supplementary Materials). The significant influences are discussed further.

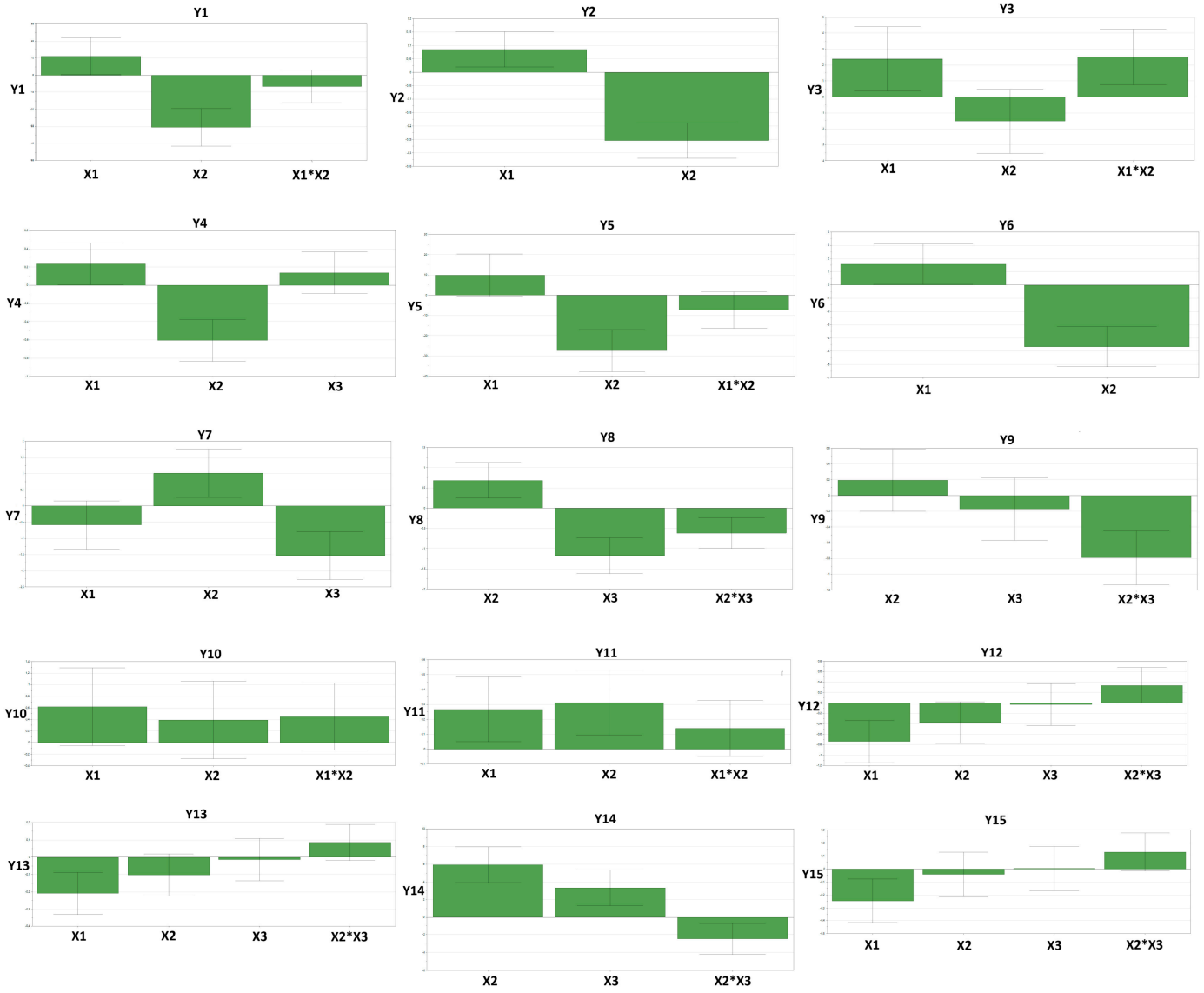


Figure 1. Scaled and centered histograms. Quantitative variables and their variation levels: X1—% xanthan gum, X2—% surfactants (lauryl glucoside, decyl glucoside, sodium cocoyl isethionate), X3—% polyols (glycerin: xylitol); Characterization of the gel: Y1—firmness (g), Y2—consistency (mJ), Y3—stringiness length (mm), Y4–stringiness work done (mJ), Y5—adhesive force (g), Y6—adhesiveness (mJ), Characterization of the foam: Y7—foaming property (mL), Y8—foam stability (mL), Y9—dirt dispersion, Y10—firmness (g), Y11—consistency (mJ), Y12—adhesive force (g), Y13—adhesiveness (mJ), Y14—stringiness length (mm), Y15—stringiness work done (mJ).

Xanthan gum was selected as an input variable to observe the influences on the physical characteristics of the final products because it is well-known that viscosity-enhancing agents modify the foaming properties in surfactant-based formulations [11]. By increasing the xanthan gum ratio (X1), a positive influence was observed on the values of gel parameters: firmness (Y1), consistency (Y2), stringiness length (Y3), stringiness work done (Y4), and adhesiveness (Y6). These influences can be explained by the thickening and gel network-forming properties of the xanthan gum, which lead to the forming of a more viscous, stickier gel, with an increase in the difficulty in stretching and deforming [29]. Regarding the foam characteristics, an increase in the xanthan gum ratio had also a positive

influence on foam consistency (Y11), but a negative influence on the adhesive force (Y12), adhesiveness (Y13), and stringiness work done (Y15). The greater consistency of the foam given by the xanthan gum can be explained by its thickening properties, as for the gel [29]. Inversely as for the gel, xanthan gum decreased the adhesive properties of the foam, probably due to some interactions between the air bubbles and the gel network. Moreover, as the foam network was modified, this led to a decrease in the work needed to stretch the foam.

Increased concentrations of foaming agents and higher viscosities were observed to enhance foam stabilization [22]. Thus, favorable rheological properties and stable foam obtention were observed in the study conducted by Falusi et al., when xanthan gum was used in the preparation of a dermal foam [5].

Generally, self-foaming compositions contain surfactant amounts ranging from 10% to about 35% [33]. In our study, we used a percentage between 15% and 30%, which falls in the previously mentioned interval. A wide experimental range was chosen to observe the impact of extreme surfactant ratios on foam properties. The use of higher ratios of surfactants (X2) determined a negative influence on the values of gel parameters: firmness (Y1), consistency (Y2), stringiness work done (Y4), adhesive force (Y5), and adhesiveness (Y6). These effects can be attributed to the surfactants' amphiphilic nature, which disrupts the gel network structure. Furthermore, by lowering the surface tension between the substrate and the gel matrix [34], surfactants might lessen the adhesiveness. Higher ratios of surfactants provided higher foaming properties and foam stability and positively influenced the consistency and stringiness length of the foams. As expected, due to the lowering of the surface tension of the liquids and absorbing the air-liquid interface, the surfactants improved foam quality [34]. Subsequently, a high ratio of surfactants had a better ability to stabilize the foam and led to a stronger and more interconnected air bubbles network and a higher consistency and resistance to deformation of the foam. Possible effects on the skin barrier induced by the high ratio of surfactants are reduced through a limited contact time between the surfactant and the skin, as the foam is already formed. Moreover, the selected surfactants are recognized for their mild and skin-friendly properties. Previous studies have shown that mild cleansers do not significantly change TEWL, stratum corneum hydration, or skin surface pH when using such products [30].

Together with the surfactants, the humectants represent the primary ingredients of aqueous-based cleaners. A high percentage of polyols (X3) led to an increase in the values of the stringiness length of the foam (Y14) and a decrease in the values of the foaming property (Y7) and stability of the foam (Y8). The positive effects in stringiness length could be the result of the humectant and plasticizing effect of the polyols, which led to the increase in the hydration level and flexibility of the product and thus to a more stretchable foam [35]. The negative effects on the foam can be explained by the fact that the polyols can increase the viscosity and stickiness of the product, increasing the difficulty of the bubbles forming and maintaining their structure. Additionally, polyols—as hydrophilic molecules—may compete with surfactants and water molecules at the air-liquid interface and inhibit the foam formation or disrupt the foam network [36].

The simultaneous increase in the xanthan gum and surfactant ratios (X1*X2) led to an increase in the stringiness length of the gel (Y3). As previously discussed, the network structure formed by xanthan gum became more robust, while the surfactants facilitated better dispersion and interaction of the ingredients, leading to a more cohesive and elastic texture of the gel. Regarding the simultaneous increase of the surfactants and polyols ratios (X2*X3), their above-explained disruption of the foam network caused by polyols induced a negative influence on the foam stability (Y8), dirt dispersion (Y9) and stringiness length of the foam (Y14).

2.1.6. The pH Determination

The final pH range should be considered when selecting raw materials. For our products, the pH values ranged between 6.4 and 6.8 ensuring good skin compatibility and tolerance. Respecting the skin's pH is important, especially for cleansing products for dry skin, because of their frequent use and their aggressive potential on sensitive skin. The use

of cleansing products at neutral pH is preferred [12]. High pH values of skincare products negatively impact processes like desquamation, the skin's ability to maintain the normal microbiome, and lipid synthesis, essential for maintaining skin health and integrity [37].

2.1.7. Optimization Process

Optimization was based on the previously developed mathematical responses included as CQAs. It aimed at obtaining a suitable product that fulfills the characteristics of the previously established QTPP and was performed using Modde software. Optimization involved applying a set of constraints on the selected responses/CQAs to get the desired quality features. Thus, the consistency and adhesive properties of the gel were minimized, to facilitate the release from the container and to avoid the sticky feeling of the product. Moreover, the foaming property and the stability of the foam were maximized, to achieve a high-quality foam. All these characteristics were chosen to obtain increased cleansing effectiveness and a favorable sensory profile to guarantee the users' acceptability, given the intended use for dry skin cleansing. The optimal formulation was generated, and then prepared and characterized. The theoretical values predicted, and the practical results obtained after preparation and analysis are close, revealing the good choice of the proposed model (Table 4).

Table 4. Composition of the optimal formulation of the cleansing foam and the results of the analysis.

Ingredients (INCI)	Role	%	Characterization	Theoretical Values	Practical Values	Difference %
Lauryl Glucoside	Mild surfactant [6,10]	8.73	Firmness (g) (Y1)	23.50	20.30	13.61
Decyl Glucoside	Mild surfactant [6,10]	8.73				
Sodium Cocoyl Isethionate	Mild surfactant [6,12]	8.73	Consistency (mJ) (Y2)	3.70	3.15	14.86
Glycerin	Humectant [26,27]	1.80				
Xylitol	Humectant [26,27]	0.36	Adhesive force (g) (Y5)	5.80	5.10	12.06
Xanthan Gum	Thickening agent [29]	0.45				
Sodium PCA	Moisturizer [23,24]	1.00	Adhesiveness (mJ) (Y6)	1.00	0.86	14.00
Aloe Vera Oil	Moisturizer, wound healing [14,15,38]	2.00				
Cedrus Atlantica Bark Oil	Antimicrobial, antioxidant, anti-inflammatory [16,17]	0.10	Foaming property (mL) (Y7)	23.60	22.10	6.35
Cupressus Sempervirens Oil	Antimicrobial, antioxidant [20]	0.10				
PEG-40 Hydrogenated Castor Oil	Solubilizer for oils, emollient [39]	3.00	Foam stability (mL) (Y8)	22.50	19.80	12.00
Copaifera Officinalis Resin Oil	Antimicrobial, antioxidant, anti-inflammatory, wound healing [18]	0.10				
Benzyl Alcohol, Salicylic Acid, Glycerin, Sorbic Acid (Cosgard®)	Preservative [40]	1.00	Dirt dispersion (Y9)	2.40	2.10	12.50
Aqua	Solvent	qs ad 100				

In conclusion, the main advantages of the optimal formulation are emphasized by the following characteristics:

(1) The innovative formulation concept, this study being among the limited research using the QbD approach to develop a cleansing foam.
(2) The content of mild surfactants in optimized concentration ensures effective cleansing while minimizing potential irritation and ensuring suitability for dry skin.
(3) The optimized ratio of polyols increases skin hydration and contributes to the overall efficacy of the cleansing foam.
(4) The optimized ratio of xanthan gum contributes to a better stability of the foam.
(5) The vegetal oils that provide additional moisturizing effects make the product particularly beneficial for dry skin.
(6) Foam for delivery of cosmetic actives: the optimized formulation produces a rich, stable foam and it is designed to clean the skin easily and quickly, ensuring efficient cleansing with minimal contact time between surfactants and skin, thereby reducing the risk of skin dryness or irritation.

The developed cleansing foam is designed to clean the facial skin, carefully avoiding the eye area as it is not intended for the periocular region. For optimal results, it should be used twice daily and gently applied in circular motions to wet skin. The product is thoroughly rinsed with warm water and a moisturizing cream for dry skin should be applied afterward.

2.1.8. Characterization of the Optimal Formulation

pH measurement

The pH of the optimal formulation was 6.58 ± 0.01, a premise to ensure good skin tolerance. The difference in the chemical structure of the synthetic surfactants when compared to traditional soaps, and the pH value of the final product below 7 contributes to the milder nature of the cleansing product [5].

Viscosity measurement

Viscosity significantly affects the rheological behavior of cosmetic cleansers, making its measurement important in product development. The optimal formulation had a viscosity of 71.5 ± 2.29 cPs, a low value necessary for foam generation when using a pump-type dispenser; thicker products risk blocking the dispenser cap and failing to discharge the product properly. Our results were lower than those recorded for other cleansing products (i.e., facial gels or shampoos) due to the presence of thickeners such as gums or cellulose derivates in lower concentrations [38,41]. To ensure the easy release of foam upon activation of the pump, the conditioned product needs to maintain appropriate viscosity.

Regarding the correlation between viscosity and foaming ability, Sheng et al. found that higher viscosities resulted in reduced foamability. They also observed that an increased concentration of xanthan gum increased the viscosity, which led to a decrease in foam height [29].

Foam structure

The microscopic image of the optimal formulation of the gel (Figure 2A) displayed a dense, interconnected network of polymer strands forming a three-dimensional matrix. The gel structure was homogenous, and well-formed, with no visible conglomerates or precipitates, assuring the homogeneity of the further foam. The presence of aggregated particles can affect foaming ability, making it essential to ensure the product is homogeneous [12].

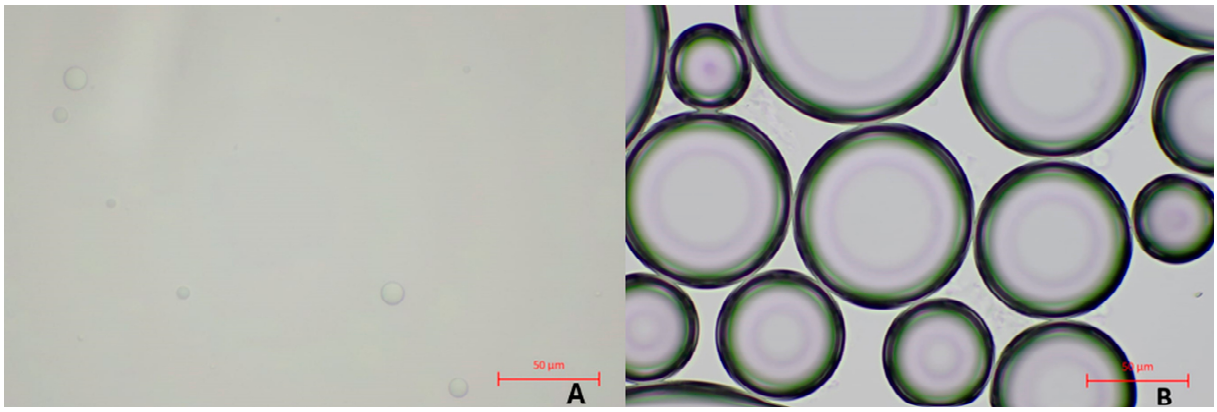


Figure 2. Microscopical image of the gel (**A**) and foam (**B**) at 40× magnification (scale bar 50 µm).

The microscopic image of the optimal formulation of foam (Figure 2B) revealed a network of closely packed homogenous bubbles with spherical shapes. The foam structure was uniform and stable, with thin films separating the bubbles. The overall texture was consistent, indicating a well-formed and stable foam matrix. The size distribution was good, slightly varying from approximately 50 µm or below. The obtention of small bubbles was desired to ensure good stability of the foam. To preserve the foam structure and lessen water drainage, smaller foam bubbles raise the air-water contact, enabling the membrane to store significantly more water.

When compared to pressurized aerosol foams, the foam quality generated by foam dispensers that mix air and liquid to create foam differs significantly from that produced by propellant-based methods. Aerosol foams are finer-pored and more viscous than those generated without a gas propellant [22].

Actuation force

The actuation force is represented by the force necessary to release the foam from the pump-head dispenser [30]. The results of this imitative test depend on different features such as consistency and viscosity of the conditioned gel, influencing the generation of the foam and posing challenges from the manufacturing standpoint. The actuation force vs. time graph shows comparative profiles of the optimal formulation and a commercial foam (Figure 3). As observed, both products exhibit similar profiles, indicating comparable behavior.

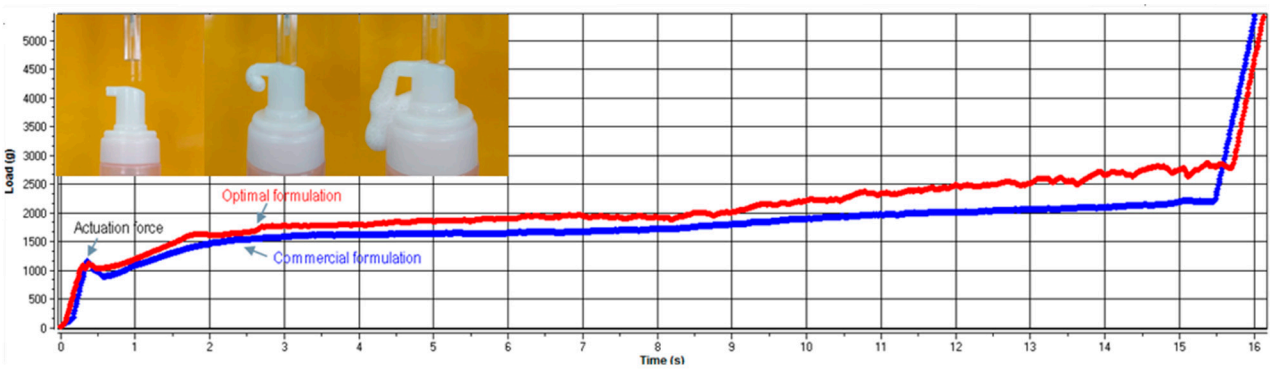


Figure 3. Actuation force measurements for the optimal formulation and a commercial product.

3. Conclusions

Cleansing products technology is evolving rapidly due to increasing consumer demand for more interesting texture profiles and environmentally sustainable products. In recent years, foams have gained attention due to their several advantages over traditional cleansers. The ease of use, effective cleaning properties, and silky texture make them popular among consumers. However, stability issues and the risk of skin dryness due to the surfactant content pose formulation challenges. Nevertheless, the amount of surfactants is critical for foam formation, making the selection of the appropriate amount essential. Other ingredients such as thickeners and polyols, also impact foam generation and stability. The current study focused on the development of a cosmetic cleansing foam by implementing a systematic DoE as a proof of concept to demonstrate the feasibility of cosmetic development within the QbD framework. The ratios of xanthan gum, surfactants, and polyols were investigated as the most influential factors for the foams. Eleven formulations were obtained by careful choice of the ingredients and the physicochemical properties of both gels and the generated foams were evaluated. All ingredients were selected to be effective and beneficial for the cleansing of dry skin. Their effects on the quality characteristics of the gel and foam were investigated, revealing significant influences of the formulation factors on product characteristics. An optimal formulation of cleansing foam containing 0.45% xanthan gum, 26.19% surfactants, and 2.16% polyols, with suitable characteristics for dry skin, was obtained. These findings provide valuable insights into the formulation of effective cleansing foams for dry skin, highlighting the critical balance between ingredient ratios to achieve optimal product performance. Future studies should assess more formulation factors, such as the ratio of oils or other emollients and different process parameters, to provide a more complete picture of this product category. Additionally, in vitro tests carried out in cell cultures, in vivo performance, skin dryness, and sensory attributes should be explored in subsequent research.

4. Materials and Methods

4.1. Materials

Aloe vera oil, *Cedrus atlantica* bark oil, *Cupressus sempervirens* oil, *Copaifera officinalis* resin oil, lauryl glucoside, decyl glucoside, sodium cocoyl isethionate, glycerin, xylitol, xanthan gum, sodium PCA, and Cosgard (INCI: Benzyl Alcohol, Salicylic Acid, Glycerin, Sorbic Acid), were purchased from Ellemental, Oradea, Romania. PEG-40 hydrogenated castor oil was purchased from Clariant, Muttenz, Switzerland.

4.2. Preparation of the Cleansing Foams

The initial step of the process involved the dispersing of xanthan gum in glycerol. Separately, the aqueous phase was prepared by solubilization and gentle mixing of lauryl glucoside, decyl glucoside, sodium cocoyl isethionate, xylitol, and sodium PCA in hot distilled water (70 °C ± 2 °C) on the water bath (BAC-1, Raypa, Barcelona, Spain). The aqueous phase was added to previously obtained xanthan gel and mixed gently until a homogeneous gel was obtained. The ingredients of the oily phase, comprised of *Aloe vera* oil, *Cedrus atlantica* bark oil, *Cupressus sempervirens* oil, *Copaifera officinalis* resin oil, and PEG-40 hydrogenated castor oil, were mixed. Then, the oily phase was added under continuous manual stirring in the aqueous phase previously cooled at room temperature. In the last step, the preservative system was added, and the gel was manually homogenized and conditioned in a foam container. All the formulations, as well as the optimal formulation, were prepared using the same preparation method.

4.3. Characterization of the Gels and Foams

To evaluate the quality of foaming cleansing products, several characteristics are commonly tested: texture parameters, foaming property, foam stability, foam structure, viscosity, and pH.

4.3.1. Characterization of the Gels

The texture analysis of both the gel and the generated foam was assessed using the CT3 Texture Analyzer (Brookfield Engineering Laboratories, Middleboro, MA, USA). The accessories of the texture analyzer were chosen based on the sample type and the test performed, considering the very distinct characteristics of gels and foams. Thus, the TA-DEC probe and TA-BT-KIT fixture are generally used for testing semisolids, such as gels, while the TA10 probe has been considered the most suitable to analyze foam texture properties. These setups were selected to reflect how small variations in composition could impact the features of the final product [42].

The gel's properties, such as firmness, consistency, adhesiveness, adhesive force, stringiness length, and stringiness work, were assessed using the TA-DEC probe and TA-BT-KIT fixture. The test parameters were the following: Test type—Compression, Pre-test speed—1.0 mm/s, Test speed—2.0 mm/s, Post-test speed—2.0 mm/s, Trigger load—10 g, Target value -10 mm. The results were recorded, and the texture parameters were calculated by using Texture ProCT Software 1.9 (Brookfield Engineering Laboratories, Middleboro, MA, USA). Firmness was calculated as the peak of the positive force (hardness) on the load vs. time graph, while consistency was determined as the area under the positive part of the graph (hardness work done). Adhesiveness refers to the work needed to overcome the attractive forces between the product's surface (gel or foam) and the materials it comes in contact with. Adhesive force represents the force required to pull the probe from the product and it was measured as the total negative area and the adhesive force as the peak negative force. Stringiness length was calculated as the distance to which the gel extends before it breaks away from the probe while the stringiness work represents the work necessary to stretch the gel until the breaking point. The stringiness parameters give information about the gel behavior during stretching [42,43].

Foaming property (Foamability)

When talking about foaming cleansing products, the volume, stability, and density of the foam are important to consumers. Since most consumers correlate foamability with cleansing

ability, they search for well-lathering formulations that generate stable and dense foam [30]. Foamability was assessed using the Cylinder shake method. A 50 mL sample from a 1% solution was placed in a 100 mL graduated cylinder (30 mm diameter × 250 mm height), inverted 20 times to generate foam, and the foam volume (mL) was measured. Three measurements were made for each formulation [30,44].

Foam stability

Foam stability was assessed by measuring the foam volume (mL) over time. Thus, the solutions used in the determination of foaming property were observed for 3 min, and the foam volume was recorded. Three experiments were conducted for each formulation and the mean value was recorded.

Dirt dispersion was evaluated by using the method previously described by AlQuadeib et al. [41] with small modifications. Briefly, 10 mL of distilled water, one drop of Indian ink, and one drop of cleansing product were added to a test tube and vigorously shaken 10 times. The amount of dye that passes into the foam immediately after shaking (the coloration of the foam) was rated on a scale from 1 to 4. To produce adequate cleansing products, it is beneficial to ensure that dirt remains in the water portion during the rinsing process. Lower values indicate better dirt dispersion, meaning the dirt remains in the water portion and is easier to rinse away.

pH measurement

The pH assessment was performed by using the pH meter (HI 8424, Hanna Instruments, Cluj-Napoca, Romania). The measurements were performed in triplicate, at 25 ± 0.2 °C.

Viscosity measurement

The viscosity of the optimal formulation at different shear rates was recorded using a rotational rheometer DV-III Ultra (Brookfield Engineering Laboratories, Middleborough, MA, USA, spindle 62). Measurements were performed in triplicate at 25 ± 0.2 °C and mean values ± standard deviation were reported.

4.3.2. Characterization of the Foams

The foam was obtained through the Cylinder shake method from a 20 mL of 10% product solution placed in a 50 mL glass cylinder (20 mm diameter × 200 mm height), covered with a Parafilm® type membrane, and shaken vigorously 20 times. The firmness, consistency, adhesiveness, adhesive force, stringiness length, and stringiness work done on the generated foam were determined using the Brookfield CT3 texture analyzer equipped with a TA10 probe. The recorded parameters were the following: Test type—Compression, Pre-test speed—1.0 mm/s, Test speed—2.0 mm/s, Post-test speed—2.0 mm/s, Trigger load—0.1 g, Target value—20 mm. All the determinations were performed in triplicate, and the mean value and standard deviation were reported.

Actuation force

The actuation force test was measured using a CT3 Texture Analyzer (Brookfield Engineering Laboratories, Middleboro, MA, USA) equipped with a TA10 probe. The recorded parameters were the following: Test type—Compression, Test speed—1.0 mm/s Trigger load—2 g, Target value—20 mm. The determinations were conducted in triplicate, in comparison with a commercial product.

The foam structure of the optimal formulation was determined using a Zeiss Primostar 3 Axiocam 208 color microscope (Zeiss, Jena, Germany) capturing at least three images of different samples of gel and foam with the Labscope application.

4.4. QbD Approach

4.4.1. Definition of QTPP, CQA

Establishing the Quality Target Product Profile (QTTP), or the final objective of formulation development, is the first stage in the QbD process. The next action is to determine critical quality attributes (CQAs), critical material attributes (CMAs), and critical process parameters (CPPs), after which risk assessment is used to choose parameters that could have an impact on the quality of the final product [7].

4.4.2. Risk Analysis

A Fishbone Diagram, also known as an Ishikawa or Cause-and-Effect Diagram, is a visual tool used to systematically identify the risks and the potential problems and root causes in a process. The factors noticed during the diagram development were then further analyzed and prioritized in a risk assessment [7].

Failure Modes and Effects Analysis (FMEA) is a systematic method for evaluating different processes to identify where and how they might fail and to assess the relative impact of the failures. The FMEA risk assessment involves calculating the Risk Priority Number (RPN) for each potential failure mode, which helps prioritize the risk factors. RPN is calculated by multiplying the values given for each parameter: severity (S), occurrence (O), and detection (D) of each factor. Each of them uses a scale from 1 to 10, where for S, 1 indicates insignificant impact while 10 indicates catastrophic impact on the user or process, respectively for O, 1 indicates extremely unlikely and 10 indicates very frequently. For D, 1 indicates a high likelihood of detection and 10 indicates a very low likelihood of detection [7].

4.4.3. Experimental Design

Following the FMEA risk assessment, the variables with the greatest impact on the quality of the product were included as formulation variables in the experimental plan (concentrations of surfactants, polyols, and the gel-forming agent). The types and concentrations studied were established after multiple preliminary formulations to guarantee that the formulations subsequently generated by the experimental plan were organoleptically adequate and could be further analyzed. As response variables, both gel and foam properties were studied for a comprehensive understanding of how these factors influence the product, paving the way for future research and development in this field. Based on the formulation variables and responses presented in Table 5, a D-optimal experimental design with N = 13 experiments was generated (Table 6). Accordingly, the experiments were performed and the effects of independent variables on the responses were analyzed. Quality-of-fit assessment, coefficient calculation, and statistic parameters evaluation were performed with Modde 12.1 software (Sartorius, Germany).

Table 5. Input and output variables of the experimental plan.

Quantitative Variables and Their Variation Levels (%)				**Response Variables**	
X1—% xanthan gum	0.4	0.6	0.8	Gel Y1—firmness (g), Y2—consistency (mJ), Y3—stringiness length (mm), Y4—stringiness work done (mJ), Y5—adhesive force (g), Y6—adhesiveness (mJ)	Foam Y7—foaming property (mL), Y8—foam stability (mL), Y9—dirt dispersion, Y10— firmness (g), Y11—consistency (mJ), Y12—adhesive force (g), Y13— adhesiveness (mJ), Y14—stringiness length (mm), Y15—stringiness work done (mJ)
X2—% surfactants (lauryl glucoside: decyl glucoside: sodium cocoyl isethionate = 1:1:1)	15	22.5	30		
X3—% polyols (glycerin:xylitol = 5:1)	2	7	12		

Table 6. Experimental design matrix.

Experiment	**X1**	**X2**	**X3**
N1	0.4	15	2
N2	0.8	15	2
N3	0.4	30	2
N4	0.8	30	2
N5	0.4	15	12

Table 6. *Cont.*

Experiment	X1	X2	X3
N6	0.8	15	12
N7	0.4	30	12
N8	0.8	30	12
N9	0.4	30	7
N10	0.6	22.5	7
N11	0.6	22.5	7
N12	0.6	22.5	7
N13	0.6	22.5	7

Quantitative variables and their variation levels: X1—% xanthan gum, X2—% surfactants (lauryl glucoside, decyl glucoside, sodium cocoyl isethionate). X3—% polyols (glycerin:xylitol).

4.4.4. Statistical Analysis

The Modde 12 software was used to process the data from the experimental plan. The data was statistically analyzed by ANOVA test and a *p*-value below 0.05 was considered statistically significant.

Supplementary Materials: The following supporting information can be downloaded at: https://www.mdpi.com/article/10.3390/gels10080484/s1, Figure. S1. Fishbone diagram of cleansing foams development; Figure S2. Contour plots. Table S1. FMEA analysis of cleansing foams development, Table S2. The revised quantitative factor effects and the associated p-values.

Author Contributions: Conceptualization, C.B. and M.-L.M.; methodology, C.B., D.R.P. and D.A.S.; software, S.I.; validation, S.I.; formal analysis, C.B. and S.I.; investigation, C.B., D.R.P. and D.A.S.; data curation, C.B. and D.A.S.; writing—original draft preparation, D.R.P., D.A.S. and C.B.; writing—review and editing, C.B., D.R.P., D.A.S., S.I. and M.-L.M.; supervision, C.B. All authors have read and agreed to the published version of the manuscript.

Funding: This research received no external funding.

Institutional Review Board Statement: Not applicable.

Informed Consent Statement: Not applicable.

Data Availability Statement: The raw data supporting the conclusions of this article will be made available by the authors upon request.

Conflicts of Interest: The authors declare no conflicts of interest.

References

1. Kumar, M.; Kumar, D.; Singh, S.; Chopra, S.; Mahmood, S.; Bhatia, A. Quality by Design Perspective for Designing Foam-based Formulation: Current State of Art. *Curr. Pharm. Des.* **2024**, *30*, 410–419. [CrossRef] [PubMed]
2. Hasenoehrl, E.J. Facial Cleansers and Cleansing Cloths. In *Cosmetic Dermatology: Products and Procedures*, 2nd ed.; Draelos, Z., Ed.; John Wiley & Sons, Ltd.: Chichester, UK, 2010; pp. 95–101.
3. Ersser, S.J.; Nicol, N.H. Educational Interventions for the Management of Children with Dry Skin. In *Treatment of Dry Skin Syndrome: The Art and Science of Moisturizers*, 1st ed.; Lodén, M., Maibach, H.I., Eds.; Springer: Berlin/Heidelberg, Germany, 2012; pp. 1–591.
4. European Pharmacopeia (Ed.) 11.5. 2024. Available online: https://pheur.edqm.eu/home (accessed on 9 July 2024).
5. Falusi, F.; Budai-Szűcs, M.; Csányi, E.; Berkó, S.; Spaits, T.; Csóka, I.; Kovács, A. Investigation of the effect of polymers on dermal foam properties using the QbD approach. *Eur. J. Pharm. Sci.* **2022**, *173*, 106160. [CrossRef] [PubMed]
6. Rocafort, C.M. Functional Material for Hair. In *Cosmetic Science and Technology: Theoretical Principles and Applications*; Fedor, J., Ed.; Elsevier: Amsterdam, The Netherlands, 2017; pp. 321–335.
7. Safta, D.A.; Ielciu, I.; Șuștic, R.; Hanganu, D.; Niculae, M.; Cenariu, M.; Pall, E.; Moldovan, M.L.; Achim, M.; Bogdan, C.; et al. Chemical Profile and Biological Effects of an Herbal Mixture for the Development of an Oil-in-Water Cream. *Plants* **2023**, *12*, 248. [CrossRef]
8. Simões, A.; Veiga, F.; Figueiras, A.; Vitorino, C. A practical framework for implementing Quality by Design to the development of topical drug products: Nanosystem-based dosage forms. *Int. J. Pharm.* **2018**, *548*, 385–399. [CrossRef] [PubMed]

9. Bogdan, C.; Iurian, S.; Tomuta, I.; Moldovan, M. Improvement of skin condition in striae distensae: Development, characterization and clinical efficacy of a cosmetic product containing *Punica granatum* seed oil and *Croton lechleri* resin extract. *Drug Des. Dev. Ther.* **2017**, *11*, 521–531. [CrossRef] [PubMed]
10. MacFarlane, B. Common Cosmetic Ingredients: Chemistry, Actions, Safety and Products. In *Cosmetic Formulation Principles and Practice*; Benson, H., Roberts, M., Leite-Silva Rodrigues, V., Walters, K., Eds.; CRC Press, Taylor & Francis Group: Boca Raton, FL, USA, 2019; pp. 105–118.
11. Garcia, R.D. AO and VRLS. Thickening Agents. In *Cosmetic Formulation Principles and Practice*; Benson, H., Roberts, M., Leite-Silva Rodrigues, V., Walters, K., Eds.; CRC Press, Taylor & Francis Group: Boca Raton, FL, USA, 2019; pp. 119–128.
12. Sakai, T. Body Care Cosmetics. In *Cosmetic Science and Technology: Theoretical Principles and Applications*; Fedor, J., Ed.; Elsevier: Amsterdam, The Netherlands, 2017; pp. 561–570.
13. Lochhead, R. Chapter 3. Basic Physical Sciences for the Formulation of Cosmetic Products. In *Cosmetic Science and Technology*, 1st ed.; Kazutami, S., Lochhead, R., Maibach, H., Yamashita, Y., Eds.; Elsevier Inc.: Amsterdam, The Netherlands, 2017; pp. 39–76.
14. Maan, A.A.; Nazir, A.; Khan, M.K.; Ahmad, T.; Zia, R.; Murid, M.; Abrar, M. The therapeutic properties and applications of *Aloe vera*: A review. *J. Herb. Med.* **2018**, *12*, 1–10. [CrossRef]
15. Hekmatpou, D.; Mehrabi, F.; Rahzani, K.; Aminiyan, A. The Effect of Aloe Vera Clinical Trials on Prevention and Healing of Skin Wound: A Systematic Review. *Iran. J. Med. Sci.* **2019**, *44*, 1. [PubMed]
16. El Hachlafi, N.; Mrabti, H.N.; Al-Mijalli, S.H.; Jeddi, M.; Abdallah, E.M.; Benkhaira, N.; Hadni, H.; Assaggaf, H.; Qasem, A.; Goh, K.W.; et al. Antioxidant, Volatile Compounds; Antimicrobial, Anti-Inflammatory, and Dermatoprotective Properties of *Cedrus atlantica* (Endl.) Manetti Ex Carriere Essential Oil: In Vitro and In Silico Investigations. *Molecules* **2023**, *28*, 5913. [CrossRef] [PubMed]
17. Saab, A.M.; Gambari, R.; Sacchetti, G.; Guerrini, A.; Lampronti, I.; Tacchini, M.; El Samrani, A.; Medawar, S.; Makhlouf, H.; Tannoury, M.; et al. Phytochemical and pharmacological properties of essential oils from Cedrus species. *Nat. Prod. Res.* **2018**, *32*, 1415–1427. [CrossRef]
18. Paranhos, S.B.; Ferreira, E.D.; Canelas, C.A.; da Paz, S.P.; Passos, M.F.; da Costa, C.E.; da Silva, A.C.; Monteiro, S.N.; Candido, V.S. Chitosan Membrane Containing Copaiba Oil (Copaifera spp.) for Skin Wound Treatment. *Polymers* **2022**, *14*, 35. [CrossRef]
19. Pascoal, D.R.C.; Velozo, E.S.; Braga, M.E.M.; Sousa, H.C.; Cabral-Albuquerque, E.C.M.; Vieira de Melo, S.A.B. Bioactive compounds of *Copaifera* sp. impregnated into three-dimensional gelatin dressings. *Drug Deliv. Transl. Res.* **2020**, *10*, 1537–1551. [CrossRef] [PubMed]
20. Galovičová, L.; Čmiková, N.; Schwarzová, M.; Vukic, M.D.; Vukovic, N.L.; Kowalczewski, P.Ł.; Bakay, L.; Kluz, M.I.; Puchalski, C.; Obradovic, A.D.; et al. Biological Activity of Cupressus sempervirens Essential Oil. *Plants* **2023**, *12*, 1097. [CrossRef] [PubMed]
21. Selim, S.A.; Adam, M.E.; Hassan, S.M.; Albalawi, A.R. Chemical composition, antimicrobial and antibiofilm activity of the essential oil and methanol extract of the Mediterranean cypress (*Cupressus sempervirens* L.). *BMC Complement. Altern. Med.* **2014**, *14*, 1–8. [CrossRef]
22. Arzhavitina, A.; Steckel, H. Foams for pharmaceutical and cosmetic application. *Int. J. Pharm.* **2010**, *394*, 1–17. [CrossRef] [PubMed]
23. Fowler, J. Understanding the Role of Natural Moisturizing Factor in Skin Hydration. *Pract. Dermatol.* **2012**, *9*, 36–40.
24. Spada, F.; Barnes, T.M.; Greive, K.A. Skin hydration is significantly increased by a cream formulated to mimic the skin's own natural moisturizing systems. *Clin. Cosmet. Investig. Dermatol.* **2018**, *11*, 491–497. [CrossRef]
25. Ash, M.; Ash, I. *Handbook of Cosmetic and Personal Care Additives*; Synapse Information Resources: New York, NY, USA, 2013; Volume 1–2.
26. Korponyai, C.; Szél, E.; Behány, Z.; Varga, E.; Mohos, G.; Dura, Á.; Dikstein, S.; Kemény, L.; Erős, G. Effects of Locally Applied Glycerol and Xylitol on the Hydration, Barrier Function and Morphological Parameters of the Skin. *Acta Derm. Venereol.* **2017**, *97*, 182–187. [CrossRef]
27. Szél, E.; Polyánka, H.; Szabó, K.; Hartmann, P.; Degovics, D.; Balázs, B.; Németh, I.B.; Korponyai, C.; Csányi, E.; Kaszaki, J.; et al. Anti-irritant and anti-inflammatory effects of glycerol and xylitol in sodium lauryl sulphate-induced acute irritation. *J. Eur. Acad. Dermatol. Venereol.* **2015**, *29*, 2333–2341. [CrossRef] [PubMed]
28. Sagitani, H.; Komoriya, M. Stability conditions and mechanism of cream soaps: Effect of polyols. *J. Oleo Sci.* **2015**, *64*, 809–816. [CrossRef]
29. Sheng, Y.; Zhang, H.; Ma, L.; Wang, Z.; Hu, D.; Zhang, S. Rheological Properties of Gel Foam Co-Stabilized with Nanoparticles, Xanthan Gum, and Multiple Surfactants. *Gels* **2023**, *9*, 534. [CrossRef]
30. Baki, G.; Alexander, K. *Introduction to Cosmetic Formulation and Technology*, 1st ed.; John Wiley & Sons, Inc.: Hoboken, NJ, USA, 2015; pp. 1–697.
31. Iurian, S.M.; Adespei, D.R.; Pop, A.; Fizeșan, I.; Carpa, R.; Moldovan, M.L.; Loghin, F.; Achim, M.; Bogdan, C. Development of a Mouthwash Using Freeze-Drying Technique: An Optimization Study. *Appl. Sci.* **2021**, *11*, 9609. [CrossRef]
32. Sartorius Stedim Data Analytics AB. MODDE® 12 User Guide. 2017. Available online: https://www.sartorius.com/download/544636/modde-12-user-guide-en-b-00090-sartorius-data.pdf (accessed on 9 July 2024).
33. WO2002005758A2—Self Foaming Cleansing Gel—Google Patents. Available online: https://patents.google.com/patent/WO2002005758A2/en (accessed on 9 July 2024).
34. Pradhan, A.; Bhattacharyya, A. Shampoos Then and Now: Synthetic versus Natural. *J. Surf. Sci. Technol.* **2014**, *30*, 59–76.

35. Antoniou, J.; Liu, F.; Majeed, H.; Qazi, H.J.; Zhong, F. Physicochemical and thermomechanical characterization of tara gum edible films: Effect of polyols as plasticizers. *Carbohydr. Polym.* **2014**, *111*, 359–365. [CrossRef] [PubMed]
36. Nakama, Y. Surfactants. In *Cosmetic Science and Technology: Theoretical Principles and Applications*; Fedor, J., Ed.; Elsevier: Amsterdam, The Netherlands, 2017; pp. 231–244.
37. Ananthapadmanabhan, K.P.; Hawkins, S. Bar Cleansers. In *Cosmetic Dermatology Products and Procedures*, 3rd ed.; Draelos, Z.D., Ed.; Wiley Blackwell: Hoboken, NJ, USA, 2022; pp. 83–95.
38. Wulandini, R.; Irwansyah, F.S.; Windayani, N. Formulation of facial cleansing gels using aloe vera as natural surfactant. *J. Phys. Conf. Ser.* **2019**, *1402*, 1402055069. Available online: https://iopscience.iop.org/article/10.1088/1742-6596/1402/5/055069 (accessed on 9 July 2024). [CrossRef]
39. PEG-40 Hydrogenated Castor Oil. Available online: https://inci.guide/essential-oils-fixed-plant-oils/peg-40-hydrogenated-castor-oil (accessed on 9 July 2024).
40. Cosgard | ELLEMENTAL. Available online: https://www.ellemental.ro/905-cosgard-conservant-cosmetic.html (accessed on 9 July 2024).
41. AlQuadeib, B.T.; Eltahir, E.K.D.; Banafa, R.A.; Al-Hadhairi, L.A. Pharmaceutical evaluation of different shampoo brands in local Saudi market. *Saudi Pharm. J.* **2018**, *26*, 98–106. [CrossRef] [PubMed]
42. Bogdan, C.; Hales, D.; Cornilă, A.; Casian, T.; Iovanov, R.; Tomuță, I.; Iurian, S. Texture analysis—A versatile tool for pharmaceutical evaluation of solid oral dosage forms. *Int. J. Pharm.* **2023**, *638*, 122916. [CrossRef]
43. Brookfield Ametek I and SCD. CT3 Texture Analyzer Operating Instructions Manual. pp. 1–64. Available online: https://www.brookfieldengineering.com/-/media/ametekbrookfield/manuals/texture/ct3%20manual%20m08-372-f1116.pdf (accessed on 9 July 2024).
44. Klein, K. Evaluating Shampoo Foam. *Cosmet. Toilet.* **2004**, *119*, 32–35.

Disclaimer/Publisher's Note: The statements, opinions and data contained in all publications are solely those of the individual author(s) and contributor(s) and not of MDPI and/or the editor(s). MDPI and/or the editor(s) disclaim responsibility for any injury to people or property resulting from any ideas, methods, instructions or products referred to in the content.

pharmaceutics

MDPI

Review

SLNs and NLCs for Skin Applications: Enhancing the Bioavailability of Natural Bioactives

Diana Antonia Safta, Cătălina Bogdan * and Mirela-Liliana Moldovan

Department of Dermopharmacy and Cosmetics, Faculty of Pharmacy, "Iuliu Hatieganu" University of Medicine and Pharmacy, 12 I. Creanga Street, 400010 Cluj-Napoca, Romania;
diana.an.safta@elearn.umfcluj.ro (D.A.S.); mmoldovan@umfcluj.ro (M.-L.M.)
* Correspondence: catalina.bogdan@umfcluj.ro

Abstract: Natural bioactives are mixtures of compounds extracted from plants with physicochemical properties that are usually not favorable for penetrating the skin`s complex barrier. Nanoparticles have important advantages both in dermatology and cosmetology: improved solubility and stability of encapsulated phytocompounds, controlled and sustained skin delivery, and enhanced skin permeation, leading to an improved bioavailability. This review focuses on two generations of lipid-based nanoparticles: solid lipid nanoparticles (SLNs) and nanostructured lipid carriers (NLCs). An extensive overview on the recent studies on SLNs and NLCs entrapping essential oils, oils, herbal extracts, and phytocompounds for topical applications is presented, emphasizing their composition, physicochemical characterization, efficacy, and methodologies used to evaluate them. This review also summarizes topical systems containing natural bioactives incorporated into SLNs and NLCs, commercially available products and registered patents in the field. SLNs and NLCs turn out to be effective nanocarriers for skin applications, offering significantly improved encapsulation efficiency, stability, and bioactives delivery. However, their full potential is underexplored. Future applications should study the encapsulation potential of new natural bioactives and show more specialized solutions that address specific requirements; an improved product performance and a pleasant sensory profile could lead to increased customer compliance with the product use.

Keywords: solid lipid nanoparticles; nanostructured lipid carriers; herbal extracts; essential oils; phytocompounds

Citation: Safta, D.A.; Bogdan, C.; Moldovan, M.-L. SLNs and NLCs for Skin Applications: Enhancing the Bioavailability of Natural Bioactives. *Pharmaceutics* **2024**, *16*, 1270. https://doi.org/10.3390/pharmaceutics16101270

Academic Editors: Heather Benson, Lenuța Șuta and Claudia-Geanina Watz

Received: 22 August 2024
Revised: 20 September 2024
Accepted: 26 September 2024
Published: 28 September 2024



Copyright: © 2024 by the authors. Licensee MDPI, Basel, Switzerland. This article is an open access article distributed under the terms and conditions of the Creative Commons Attribution (CC BY) license (https://creativecommons.org/licenses/by/4.0/).

1. Introduction

The entrapment of herbal extracts (HEs), essential oils (EOs), or phytocompounds (PCs) in novel pharmaceutical nanostructures for skincare represents a blend of traditional knowledge with modern technology, aligning with the growing consumers' preference for natural products. Their effectiveness and safety, along with the current trend towards eco-friendly products, encourage this nature-inspired approach. Thus, according to the World Health Organization (WHO), over 80% of people worldwide obtain their primary healthcare from traditional medicine, based on natural-origin products [1,2].

HEs and EOs are rich in bioactive PCs such as polyphenols, flavonoids, and terpenoids, which have been shown to possess potent antioxidant, anti-inflammatory, and antimicrobial properties. Thus, as they can offer a wide range of important effects and can be useful to various skin types and conditions, they are highly versatile in cosmetic and dermatological formulations. Nanotechnology can help unlock the full potential of traditional herbal extracts by improving their stability, bioavailability, and delivery, expanding their use in modern dermatology and cosmetology [3].

2. Skin Delivery of SLNs and NLCs

The skin, as the external covering of the body, has multiples roles, with the primary function being to protect it against environmental factors and maintain body homeostasis. For many years, the skin was considered as an impenetrable barrier; however, nowadays it is known that skin is permeable to various substances, depending mainly on their physicochemical properties and on the skin integrity. Due to its selective permeability, the skin can also be considered a therapeutic interface and a target for drug delivery at three levels: on the skin surface (e.g., for antiseptic effect, repellent effect against insects, skin protection effect), at the epidermis and dermis levels (e.g., for anti-inflammatory, antimicrobial, antineoplastic effects), and for transdermal delivery when the drug is expected to reach systemic circulation to provide a systemic effect, representing an alternative to oral administration [4,5].

2.1. Pathways of Skin Absorption

The penetration of actives through intact skin is obtained through two pathways: transepidermal penetration and transappendageal penetration (via sweat glands, sebaceous glands, and hair follicles). In transepidermal penetration, the stratum corneum governs the penetration of active ingredients either through intracellular or intercellular pathways, acting as a barrier for molecules with high molecular weight (MW) and hydrophilic molecules [6,7]. Skin absorption involves three successive phases: the penetration phase, consisting of a passive diffusion into the *stratum corneum* of the active ingredient from the topical product applied to the skin surface, followed by a permeation phase where the active ingredient passes through the viable epidermis to dermis, and the resorption phase, when the active ingredient passes from the dermis into the skin's microcirculation and subsequently into deeper skin layers or into systemic circulation [8].

2.2. Skin Permeability of Active Ingredients

The penetration across the skin is influenced by several factors like the physiological properties of the skin, the physicochemical properties of the incorporated active ingredient, and the properties of the vehicle. Regarding skin properties, one of the most important features is the quality of *stratum corneum* (its integrity, thickness, and hydration state), along with the skin temperature, which has a direct influence on skin microcirculation. Other factors such as age, gender, anatomical site, and application method (e.g., massage) are also mentioned [9].

Among the physicochemical properties of the actives, the skin penetration may be increased when the active's solubility is increased, either by reducing particle size or by obtaining supersaturated vehicles. According to Bos et al., small molecules with an MW under 500 Dalton can pass intracellularly, while lipophilic actives can pass into skin via intercellular lipids, following the intercellular route. The penetration of actives into the skin is largely dependent also by the lipid–water partition coefficient, as molecules with strong hydrophilic or lipophilic character tend to have small permeation across the skin, while a good solubility in aqueous and lipophilic environments will ensure a good penetration ability. Usually, a value of the octanol–water partition coefficient of 1–3 will ensure a good permeability through skin. Additionally, the melting point of the active should be below 200 °C to facilitate its skin permeation [7,10–13].

The vehicle used to deliver the actives impacts skin penetration by ensuring good skin contact and providing occlusion. For some active ingredients, the pH of the vehicle is important to facilitate the active permeation through the skin, as it influences the ionization state of the active; thus, its permeation across *stratum corneum* lipids is influenced. Knowing that only the unionized form of an active ingredient can permeate the skin, for an active in unionized form, the diffusion coefficient may be higher [14]. Occlusion usually reduces transepidermal water loss (TEWL) and increases skin hydration by up to 50%, leading to swollen corneocytes and facilitating water retention in intercellular lipids. This

can affect the skin barrier and may increase the permeability of lipophilic active ingredients, while for hydrophilic active ingredients the influence of occlusion on skin permeation is less important [15]. Histological changes such as the expanding of the intercellular space of the stratum spinosum were recorded at 6 h of occlusion. After 24 h of occlusion, additional changes include the appearance of perinuclear vacuoles in the keratinocytes (excluding the stratum granulosum) and the presence of vesicles and vacuoles in the cytoplasm in the cellular periphery. Microbiological modifications in skin microbiota were also noticed in occluded skin, usually the increase in bacterial colonies, namely, *Staphyococcus* sp., *Corynebacterium* sp., and of the yeast *Pityrosporum orbiculare* [16]. The occlusion effect of topical products may be modulated by choosing the right ingredients and the galenic formulation. Vehicles with different degrees of occlusion may be obtained when using mineral and vegetal oils, paraffin, waxes, and other fats. Regarding the galenical formulations, the ointments are the most occlusive, followed by water-in-oil emulsions, while the oil-in-water emulsions are less occlusive [17]. Vehicles may also influence skin permeation through specific ingredients known as permeation enhancers. There are well-known substances like alcohols (ethanol, butanol, propanol, decanol, lauryl alcohol), esters (glyceryl monocaprylate, glyceryl monooleate), and surfactants, which enhance skin permeation of polar and nonpolar actives by lipid extraction; ethanol enhances skin permeation also by fluidization of intercellular lipid matrix, soap-like detergents enhance skin permeation through the disorganization of the *stratum corneum* lipid lamellae; other ingredients like proteins, lipids, and surfactants act by disintegration of the tight junctions structure [18,19]. Other chemical penetration enhancers belong to ethers (Diethylene glycol monoethyl ether or Transcutol®), terpenes (D-limonene, menthol), sesquiterpenes (farnesol, neridol), glycols (propylene glycol, dipropylene glycol), sulfoxides (dimethyl sulfoxides, decyl methyl sulfoxides), amides (azone), carboxylic acids and esters (oleic acid, geranic acid, caprylic acid, lauric acid) pyrrolidone derivatives (N-methyl-2-pyrrolydone), and amino acids derivatives [18]. Other ingredients like pyrrolidone carboxylic acid, proline, and 4-hydroxyproline act like transdermal permeation enhancers, but with reversible effect [20]. Some of these permeation enhancers may be used in the composition of the SLNs and NLCs.

3. Fundamental Insights into SLNs and NLCs

Nanosystems have emerged as revolutionary platforms for encapsulating both synthetic and natural bioactives (HEs, EOs, PCs), enhancing their efficacy and bioavailability [21]. During the last decades, a wide range of inorganic- and organic-based delivery systems were developed, with their classification being presented as a schematic diagram in Figure 1. From the organic delivery systems, the lipid-based ones are considered the most appropriate systems for topical applications due to their structure, biocompatibility, and resemblance to skin components [22,23]. Lipid-based nanoparticles consist of vesicular systems (liposomes and derivates), lipid nanoparticles—SLNs, NLCs, and the hybrids between lipid- and polymer-based nanoparticles, lipid–polymer hybrid nanoparticles (LPHNPs), respectively [24,25]. SLNs and NLCs loading natural bioactives, according to their lipophilicity, are also represented in Figure 1, emphasizing their main structural components.

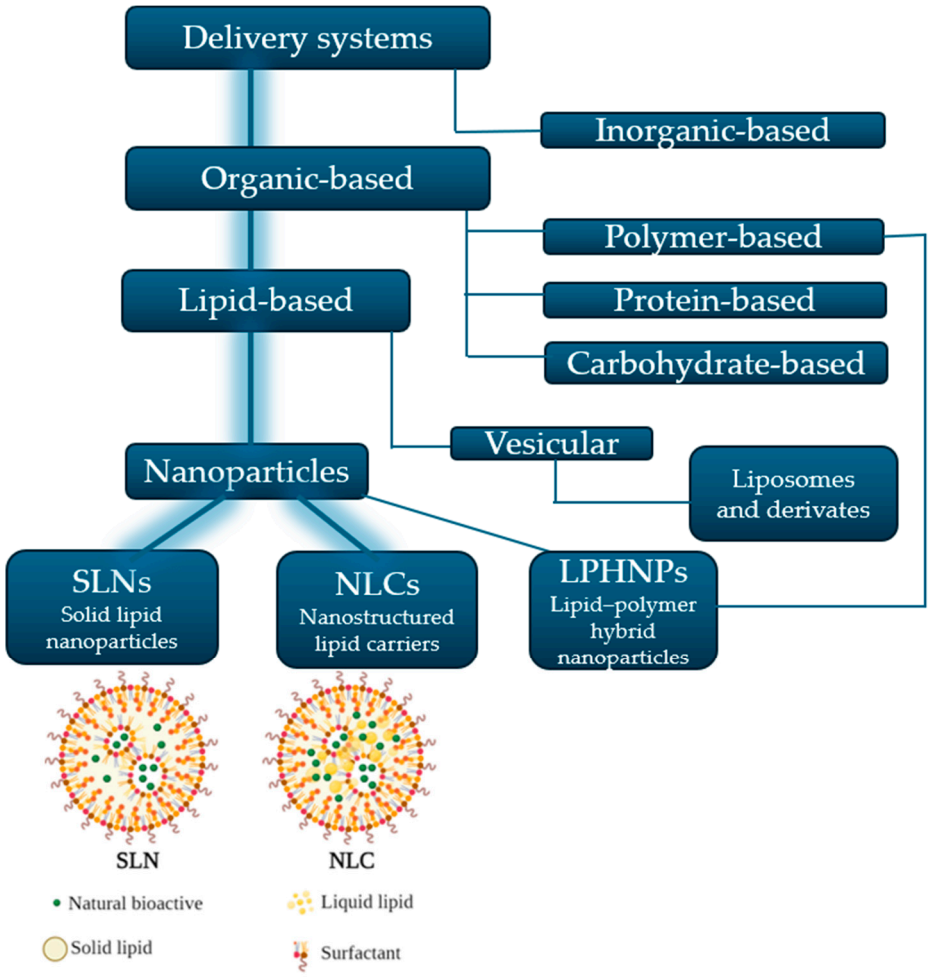


Figure 1. The classification of delivery systems, emphasizing the subcategories of lipid-based nanoparticles (image created using Biorender.com, accessed on 16 September 2024).

SLNs and NLCs are considered a better alternative than vesicular systems because they can penetrate the deeper layers of the epidermis and can ensure higher stability and prolonged and sustained release of the incorporated actives [1,25]. Moreover, while liposomes have been extensively studied so far to incorporate HEs or PCs, lipid nanoparticles are more recently used for this purpose and, therefore, this topic is less covered. SLNs and NLCs can entrap various types of active ingredients, both lipophilic and hydrophilic, within their lipid matrix [1]. According to their lipophilicity, the active ingredients are dissolved or molecularly dispersed in the solid lipid matrix (Figure 1), restricting their mobility, thus providing a controlled and sustained release profile [26].

SLNs and NLCs are typically composed of solid and/or liquid lipids (0.1–30%), water, and surfactants or emulsifiers (0.5–5% *w*/*w*), as represented in Figure 1 [26]. They have the major advantage of being safer than polymeric nanoparticles both for the skin and for the environment, since organic solvents are not used during the synthesis phase [1,25], leading to a natural and sustainable fabrication [27].

SLNs consist of solid lipids and surfactants (Figure 1). They are solid colloidal particles both at room and body temperature and have better target capability, lower toxicity due to the presence of physiological lipids, enhanced bioavailability, and better ability to protect drugs or natural bioactives [1]. SLNs have good physical and chemical stability that makes them a preferable alternative for emulsions and liposomes [28]. Since their development, at the beginning of the 1990s, parenteral, oral, and ocular delivery of SLNs have been the subject of extended research, proving better bioavailability of entrapped active ingredients. SLNs are regarded as promising carriers for topical application also,

due to their capacity to improve drug penetration into the skin. Particularly, they are well suited for usage in injured or inflamed skin, because the lipids used to prepare SLNs are nontoxic and nonirritating [29]. However, SLNs may have some disadvantages such as instability during storage, potential particle aggregation or low encapsulation efficiency for some natural bioactives [30].

NLCs are considered the second generation of SLNs, due to their better encapsulation efficiencies and improved stability. NLCs are formed by surfactants and solid and liquid lipids (Figure 1), but their aggregate state also remains solid at the room and body temperature [1]. The lipids from NLCs have a less ordered crystalline arrangement than SLNs, which is useful to prevent the leakage of the entrapped active ingredients [1,25]. The structural differences between SLNs and NLCs could be explained considering the key role of the oil phase (liquid lipid) allowing them to retain the active ingredients inside the NLC matrix and to release them in a controlled manner. The inclusion of oils is useful to hold higher amounts of an active ingredient because the oils, behaving as an impurity in the solid lipids, reduce the particle crystallinity, ensuring better stability and a higher suitability for a controlled release [31]. Moreover, San et al. mentioned that NLCs with a higher ratio of liquid lipids led to a better physical stability. Conversely, NLCs with lower liquid lipid ratio may have lower physical stability; however, they can show potential for topical application due to their better skin absorption [32].

SLNs and NLCs can be used to entrap active ingredients by encapsulation, incorporation, or/and surface attachment, and to deliver them to target tissues [1]. Depending on the preparation method and the type of loading of active ingredients in the lipidic network, three types of SLNs and NLCs can be distinguished, as summarized in Table 1, together with their key features [30,33].

Table 1. The main SLNs and NLCs categories and their key features.

SLNs and NLCs Categories		Characteristics
SLNs	Type I (homogenous matrix model)	The bioactive is dispersed in the lipid core.
	Type II (drug-enriched shell model)	The lipid core is bioactive-free, and the exterior solid shell has both lipids and bioactive.
	Type III (drug-enriched core model)	The active ingredient is precipitated in the core with a lipid coverage (the active concentration is close to its saturation solubility in the lipid).
NLCs	Type I (imperfect crystal model)	The mixture of lipids has a great number of voids and imperfections where the bioactive can be placed.
	Type II (amorphous/structureless model)	The special lipids do not recrystallize after homogenization and cooling and an amorphous lipid matrix that minimizes drug expulsion.
	Type III (multiple model)	Small oil nanoparticles that are inside the solid lipid matrix due to a phase separation (mixing solid lipids with higher amounts of oils in a ratio where the solubility of the oil in the solid lipid is exceeded).

Small changes in formulation can influence SLNs and NLCs structure and, consequently, their applicability. To achieve a prolonged drug release, for instance, SLNs type III is adequate, while SLNs type II is not appropriate for this purpose. In contrast, SLNs type I can exhibit controlled release qualities [30,33,34].

SLNs and NLCs are primarily intended to deliver lipophilic active ingredients, whereas the vesicular carriers are primarily intended to deliver hydrophilic active ingredients. Particularly, SLNs have a greater affinity for lipophilic active ingredients than for hydrophilic ones because their fundamental matrix is solid lipid-based. Because of this, it has been observed that SLNs containing hydrophilic active ingredients exhibit limited

stability or low entrapment efficiency. During the preparation process, hydrophilic active ingredients have a high tendency to partition into the outer aqueous phase because they lack affinity for the lipid matrix but, hydrophilic drug-loaded SLNs with good entrapment efficiency may be obtained as well, even if it is considered a challenging objective [35].

The HEs often contain a mixture of both hydrophilic (phenolic acids, flavonoids, glycosides, some alkaloids) and lipophilic compounds (terpenoids, essential oils, fatty acids, steroids); their composition varies according to the plant species, to the extraction method and the solvents used [2]. PCs from the HEs will be loaded in the SLNs and NLCs according to their lipophilicity (Figure 1).

4. Overview on SLNs and NLCs Entrapping Natural Bioactives for Skin Health

4.1. Delivery of Natural Bioactives from SLNs and NLCs

The advantages of entrapping natural bioactives in SLNs and NLCs are summarized in Figure 2 [23,36–38].

Natural bioactives are known to have poor bioavailability caused by their large molecular weight and poor skin permeability, along with their low stability to environmental factors. These drawbacks make natural bioactives good candidates for entrapment in nanoparticles, because they can improve their stability and bioavailability. Moreover, nanoparticles such as SLNs and NLCs may modulate the release of entrapped natural bioactives by adjusting the formulation factors and nanoparticles' properties, to assure a targeted and controlled release. The increase in skin bioavailability is due to small particle size and also to their property of film formation, occlusion factor, and adherence on the skin. Thus, by increasing skin hydration and protection, the penetration of the nanoparticles loading natural bioactives is improved. Consequently, the enhanced effects of natural bioactives for skin health come as a huge benefit of consumers, as the preference for more natural products was recently observed. All in all, the innovative combination of natural bioactives extracted from plants with nanotechnology has opened new opportunities for developing cutting-edge topical products with enhanced skin delivery and, therefore, better anti-inflammatory, antioxidant, antimicrobial, or wound healing properties [23,36–38].

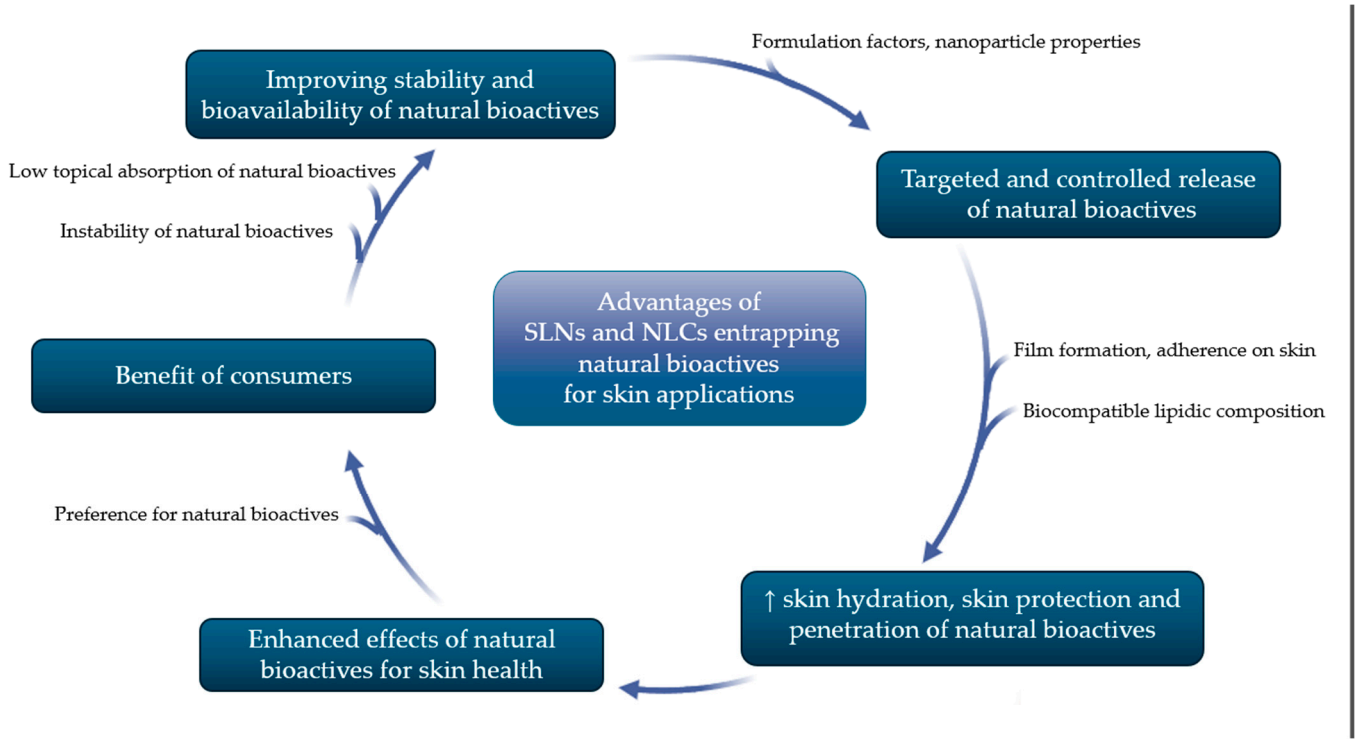


Figure 2. Summary of advantages of SLNs and NLCs entrapping natural bioactives for skin applications (image created using Biorender.com, accessed on 22 July 2024). ↑—increasing.

SLNs and NLCs seem to improve natural bioactives' skin permeation by sticking to the skin surface, forming an adhesive film that increases skin hydration and promotes penetration of natural bioactives and of the carrier into the *stratum corneum* due to a reduced corneocyte packing and enlarged intercorneocyte space [39]. Here, lipid particles form a depot from which the natural bioactive is slowly released [40]. Surfactants' presence in SLNs and NLCs may also increase the permeation of the loaded natural bioactives interfering with the lipid layer of *stratum corneum* through the fluidization and reorganization of its lipids [12]. The occlusion potential is the result of the surface lipidic film provided by the lipid nanoparticles and is related to the type of solid lipid and to the concentration of the surfactant used to formulate these nanocarriers [39].

The physicochemical properties of SLNs and NLCs, such as their shape, size, surface properties, and the diffusion coefficient, are important parameters which influence their permeation into the skin. The spherical shape, the small particle size, and the high surface area ensure their higher efficacy as delivery systems. The electrical charge of the lipid nanoparticles' surface influences their aggregation and skin penetration pathways and diffusion [12,41].

4.2. The Advantages of Natural Bioactives Incorporation in SLNs and NLCs

The ability to entrap both hydrophilic and lipophilic actives, their remarkable biodegradability, biocompatibility, a good protection of the entrapped active, and good stability of nanoparticles, along with the controlled release of the entrapped active, represent some of the advantages of using SLNs and NLCs as carriers. The active ingredients loading capacity and their retention over time, lower in the case of SLNs, was improved for NLCs [42]. The improvement of the photostability of light-sensitive natural bioactives is another advantage of the encapsulation in SLNs and NLCs. Cordenonsi et al. demonstrated the increase in the photostability of fucoxanthin and conferred protection against its degradation after UVA light exposure, as compared to free fucoxanthin [43]. Mitri et al. showed the photoprotection of lutein incorporated in NLCs and SLNs, being higher for SLNs, at a radiation dose of 10 minimal erythema dose (MED) provided by a solar simulator [44].

These advantages led to the improvement of the biological effects. Thus, the enhancement of the antioxidant activity of the SLNs- and NLCs-loaded natural bioactives was demonstrated in a study conducted by Soldati et al., where higher antioxidant activity of SLNs-loaded resveratrol compared to free resveratrol and empty SLNs was observed through the DPPH (2,2-Diphenyl-1-picrylhydrazyl) test [45]. In another study, Okonogi et al. also observed a high antioxidant activity of NLCs containing lycopene compared to NLC base, after performing ABTS [2,2′-azino-bis (3-ethylbenzothiazoline-6-sulfonic acid)] and DPPH assays [46]. The antioxidant activity of sesamol was preserved and prolonged for up to 40 h after including sesamol in SLNs and NLCs, being higher in NLCs [31].

Gad et al. studied the wound healing effects of SLNs with *Chamomilla recutita* oil, observing the increase in wound area contraction, re-epithelization rate, collagen deposition, restoration of the normal skin architecture, and skin tensile strength [47]. Wound healing applications were also studied by Ghodrati et al., after incorporation of *Mentha piperita* EO in NLCs, by increasing neovascularization, fibroblasts infiltration, collagen synthesis, re-epithelization, and wound contraction ratio with better results after loading of EO in NLCs than free EO [48]. Navabhatra et al. also demonstrated the potential in wound care of these nanosystems, by loading *Cratoxylum formosus* extract in NLCs. It was found that the irritation potential of the free HE was decreased by loading the HE in NLCs [49].

Anti-inflammatory effects were also demonstrated by Gad et al., by increasing the transforming growth factor-β1 (TGF-β) levels and decreasing the interleulin-1β (IL-1β) levels and metalloproteinases-9/tissue inhibitor metalloproteinase-1 ratio. For all these assessments, better results were found for the creams with SLNs loading *Chamomilla recutita* oil followed by SLNs loading *Chamomilla recutita* oil and then the free oil [47]. Anti-inflammatory effects were also demonstrated by Rahmanian-Devin et al., when studying formulations to treat psoriasis-like lesions through histopathological assays on mice. SLNs

loading noscapine considerably reduced tumor necrosis factor (TNF-α), transforming growth factor-beta (TGF-β1), and interleukin 17 (IL-17) levels compared to conventional cream with noscapine. Decreases in inflammation score, psoriasis area, and severity index (PASI), parakeratosis, hyperkeratosis, acanthosis were also observed [50].

The antimicrobial effects of natural bioactives have also been studied after incorporation in SLNs or NLCs. Ghodrati et al. showed the decrease in the total bacterial count in an in vivo infected wound model by application of *Mentha piperita* EO loaded in NLCs. It seems that the EO-loaded NLCs had the same antibacterial activity as the free EO [48]. After loading *Eucalyptus globulus* and *Rosmarinus officinalis* EOs in SLNs, Saporito et al. also noted the same inhibition of bacterial strains as the free EOs. Moreover, regarding the incorporation of EOs in NLCs, an increased inhibition compared to free EOs was observed [51]. Folle et al. found that NLCs loading thymol had higher antimicrobial activity on *Cutibacterium acnes*, but lower antimicrobial activity against *Staphylococcus epidermidis*, compared to free thymol [27].

Other notable applications of natural bioactives loaded in SLNs or NLCs and then incorporated in creams or gels consist of antiacne effects, where a decrease in the number of inflammatory acne lesions and in sebum rate were observed [52], along with an increase in skin hydration and skin elasticity [52,53], wrinkles reduction, and skin whitening [54].

Moreover, SLNs and NLCs are suitable carriers to deliver natural bioactives to skin appendages like hair follicles. Nanoparticles penetrate preferentially through the follicular pathway, facilitated by their smaller size [41]. The hair follicles serve as long-term reservoirs for topically applied substances, being able to store them for up to 10 days, which is 10 times longer than the reservoir of the *stratum corneum* [26,41]. Daneshmand et al. showed that SLNs with *Platycladus orientalis* L. extract allowed better absorption of cedrol, the marker molecule of this extract, to the hair follicle to prevent hair loss. A slow-release action was reported for SLN, as lipid nanodots were detected in the hair follicle even after 24 h of use [41]. Riangjanapatee et al. prepared *Camellia oleifera* seed oil-loaded NLCs, which showed better hair growth effect and a better localization of the active into the hair follicle than the oil itself [55].

Recently developed SLNs and NLCs entrapping HEs, Eos, or PCs for skin or hair applications are presented in Table 2. Their classification was made according to the type of nanosystems and the loaded natural bioactives, then specifying their composition, method of preparation, results of characterization, evaluation, effects reported, and applications. This classification may be used as a reference for future research in this innovative field.

Table 2. SLNs and NLCs entrapping EOs, HEs, and PCs for topical applications.

SLNs							
Entrapped Natural Bioactives	**Lipids**	**Surfactants**	**Method of Preparation**	**Characterization**	**Applications**	**Evaluation: Samples and Test Type (In Vitro/Ex Vivo/In Vivo Studies)**	**Effects Reported**	**Ref.**
Oils and EOs								
Chamomila recutita oil	Stearic acid	Tween® 80	Hot homogenization.	Size 542.1–956.5 nm PDI: 0.273–0.723, ZP: (−25.6)–(−35.9) mV, Occlusion factor: 38.46–56.41%, Viscosity: 1.70–5.80 Pa s.	Wound healing	SNLs and cream with SLNs: In vivo wound healing study (Wistar rats), Ex vivo IL-1β and TGF-β1, MMP-9 and TIMP-1 levels and collagen deposition.	↑ Wound area contraction, ↑ re-epithelization grade, ↑ collagen deposition, skin architecture, ↑ tensile strength, ↑ TGF-β levels, ↓ IL-1β levels and MMP-9 activity (better results in cream with SLNs with oil > SLNs with oil > oil).	[47]
HEs								
Platycladus orientalis methanolic extract	Precirol® Compritol® Glucire® Glyceryl monostearate	Tween® 80, Labrasol®, Poloxamer®	High-shear homogenization and sonication.	Size: 34.32–1420 nm. PDI: 0.159–0.921. ZP: (−651)–(−4.35) mV. EE: 71%. Stability for 6 M.	Hair growth	SLNs: biofilm formation assay (*P. aeruginosa*, *P. mirabilis*, *E. coli*, *S.s aureus*, *E. fecalis*, *S. pneumoniae*), 5-α reductase activity.	↓ Biofilm development compared to control sample. ↑ 5-α reductase inhibitor activity.	[41]
Withania somnifera leaves ethanolic, hydroethanolic and aqueous extract	Compritol® 888ATO, L-α-phosphatidylcholine	Tween® 80, Span®80	Solvent injection method and sonication.	Size: 186.8–260.8 nm. PDI: 0.48–0.74. ZP: 16.7–27.3 mV. EE withaferin A: 35.4–70.0%. EE withanolide A: 81.5–95.3%. pH: 5.0–5.3. Stability for 3 M, room temperature.	Antimelanoma	SNLs: ex vivo skin diffusion and tape-stripping studies (human skin).	Relatively low concentrations of withaferin A and withanolide A diffused into the skin during 12 h. High EE, not correlated with a high release and skin permeation.	[56]

Elaeis guineensis fruits concentrated ethanolic extract	Glyceryl monostearate	Span® 80, Tween® 80	Hot homogenization.	Size: 609.70 nm. PDI: 0.22. ZP: −28.3 mV. pH: 4.77. Stability for 1 M (better at 4 °C than at room temperature).	Skin hydration	Creams with SLNs: skin hydration, TEWL, skin elasticity, melanin index, skin texture and satisfactory survey on human volunteers.	↑ Skin hydration, TEWL, cutaneous elasticity, and melanin index, skin moisturizing, ↓ wrinkles, ↑ elasticity, and skin whitening.	[54]
Aloe vera powder	Stearic acid, cetosteryl alcohol, and glyceryl monostearate	Tween® 80	Modified solvent emulsification technique and sonication.	Size: 96.36–209.86 nm. PDI: 0.28–0.66. ZP: (−19.18)–(−11.02) mV. EE: 64.78 to 86.27%.	Photoprotective potential	Cream with SLNs: in vitro release profile dialysis bag (cellophane membrane), ex vivo permeation study (Albino rats' skin) Determination of SPF: in vitro method and in vivo (Albino rats) Skin irritation test (Albino rats).	Improved topical retention of *Aloe vera* up to 12 h SPF 14.6–16.9 *(in vitro*) and 14.81 (*in vivo*) 80.10% permeation over 8 h. No irritation or sensitivity.	[57]
PCs								
Rutin	Beeswax, Carnauba wax	Tween® 80, phosphatidylcholine	Hot melt microemulsion technique.	Size: 74.22 nm. PDI: 0.16. ZP: –53.00 mV. EE: 98.9%.	Photoprotective	SNLs: photochemopreventive effect against UVB radiation in ex vivo skin explants and 3D tissue engineering skin.	Efficient protection against UVB induced damage, inhibition of lipid peroxidation and metalloproteinase formation.	[58]
Noscapine	Precirol®, glyceryl monostearate, stearic acid, Campritol® 888 ATO, cetyl palmitate	Poloxamer® 188, Tween® 80	High-shear homogenization method.	Size: 99.8–384 nm. PDI: 0.215–0.412. ZP: (−12.6)–(−32) mV. EE: 86.45–94.15%. Stability for 6 M, 30°, and 40° C.	Psoriasis	SNLs: in vitro release profile, in vivo: inflammation degree, PASI on mice, histological analysis of ear samples, ELISA.	Cumulative release at pH 7.4 and 5.8 (72 h) ↓ inflammation degree and PASI, ↓ IL-17, TNF- α, TGF-β levels, ↑ IL-10 levels ↓ parakeratosis, hyperkeratosis, acanthosis.	[50]
Auraptene	Glyceryl monostearate Precirol® ATO 5, stearic acid, glyceryl behenate	Poloxamer® 188, Span®80	Hot homogenization and ultrasound method.	Size: 130.1–401.2 nm. PDI: 0.21–0.40. ZP: (−29.1)–19.4 mV. EE: 84.11%. Stability for 3 M, 25°, and 4 °C.	Anti-inflammatory	SNLs: in vitro release profile and skin retention study (mice skin). Anti-inflammatory activity (ear edema inflammation method), histopathological studies (mice)	Biphasic release (burst release: 30–60 min, then sustained release until 24 h). ↑ cutaneous uptake and skin targeting.	[59]

						Skin sensitization study (Guinea pigs).	Improvement of the anti-inflammatory activity, no skin sensitization.	
Tetrahydrocurcumin	Compritol® 888 ATO	Tween® 80, phosphatydylcholine	Microemulsification technique.	Size: 96.6 nm. PDI: 0.252. ZP: −22 mV. EE: 69.56% Stability for 2 M, 4 °C, and 40° C.	Anti-inflammatory, wound healing	SLNs and hydrogel with SNLs: in vitro release profile (dialysis membrane). Ex vivo permeation studies (pig ear skin). Hydrogel with SNLs: acute dermal irritation studies.	↑ Drug release for 24 h. ↑ Skin permeation. No erythema or edema.	[60]
Curcuminoids	Beeswax	Tween® 80, phosphatidylcholine	Hot melt emulsion technique, high-shear homogenization.	Size: 32.7–481.9 nm. PDI: 0.179–1.000. ZP: (−34.0)–(−21.2) mV. EE curcumin: 41.4–62.0%. EE total curcuminoids: 31.0–58.78%.	Anti-inflammatory, radiodermitis	SLNs: in vitro release profile. Gel with SNLs: ex vivo permeation study (pig ear skin), retention in the epidermis and dermis.	Sustained and slow release for 16 h, reduced permeation in epidermis/dermis for 18 h.	[61]
Curcumin	Precirol® ATO 5	Tween® 80, Span® 80	Pre-emulsion technique and sonication.	Size: 51.8–107.0 nm. PDI: 0.211–0.462. EE: 85–93%. DL: 5.05–9.51%.	Contact dermatitis (pigmentation, irritation)	Gel with SNLs: ex vivo drug diffusion, drug deposition studies, antioxidant activity (DPPH assay), in vitro tyrosinase inhibition assay skin irritation test, efficacy against irritant contact dermatitis (BALB/c mice ears).	Controlled drug release up to 24 h, potential in skin depigmentation, ↑ antioxidant activity, proficient suppression of ear swelling and reduction in skin water content in the BALB/c mouse.	[62]
Resveratrol	*Theobroma grandiflorum* seed butter	Pluronic® F-127	High shear homogenization technique and sonication.	Size: 195.30 nm. PDI: 0.16. ZP: −19.54 mV. DL: 3.36%. EE: 74.12%.	Antioxidant	SLNs: in vitro release profile (polysulfone membrane), in vitro permeation (human skin), antioxidant activity (DPPH assay).	Slow and sustained release for 24 h. ↑ Concentration of resveratrol retained in the skin.	[45]
NLCs								
Oils and EOs								
Rosmarinus officcinalis EO	Cetyl palmitate	Oleth-20, Glyceryl Oleate	Phase inversion temperature method.	Size: 26.90–171.70 nm. PDI: 0.171–0.495. ZP: (−1.55)–(−2.19) mV.	Skin hydration	Gels with NLCs: skin hydration and elasticity on human volunteers.	↑ Skin hydration and elasticity.	[53]

				Stability for 2 M, room Temperature.			
Menta piperita EO	Precirol ® -ATO 5, Miglyol ® -812	Poloxamer®	Hot melt homogenization technique.	Size: 40–250 nm. PDI: ~0.4. ZP: (−10)–(−15) mV. EE 93.2%. DL 9.3%.	Antibacterial, wound healing	NLCs: wound area rate, histopathological studies, molecular analysis, antimicrobial activity, total tissue bacterial count.	↑ Wound contraction rate, fibroblast infiltration, collagen deposition, and re-epithelialization, positive effects on the FGF-2 and EGF mRNA levels expressions, antibacterial activity against *S. epidermidis*, *S. aureus*, *L. monocytogenes*, *E. coli*, and *P. aeruginosa*.	[48]
Piper aduncum oil	Caprylic/capric triglycerides, *Theobroma grandiflorum* (Cupuaçu) butter	Tween 20®, Span 80®	Ultra-turrax homogenization and high-pressure homogenization.	Size: ~130 nm. PDI: 0.17. ZP: −40.50 mV. EE: 89.42%.	Anti-inflammatory	NLCs and hydrogels with NLCs: In vitro release profile (cellulose ester membrane), in vitro permeation/retention studies on porcine skin, HET-CAM Toxicity Test.	Controlled and constant release: initial burst for 2 h, then slower and continuous release for 12 h Delivery of dillapiole to dermis, low irritation potential.	[63]
Camellia oleifera seed oil	Olivem® 1000	Tween® 80, Varisoft®442	High-speed homogenization technique.	Size 80–290 nm. PDI 0.15–0.8. EE 96.26%. Stability for 3 M, 4°, 25°, and 40° C.	Hair growth	NLCs: In vitro cell viability (HFDP cells).	Certain NLCs ↓ and other ↑ cell viability, depending on the surfactant and on the physicochemical properties. Hair growth stimulating effect and a better localization of the active into hair follicle.	[55]
Rosa canina oil, *Nigella sativa* oil, *Daucus carota* extract, *Calendula officinalis* extract	Glycerol monostearate, cetyl palmitate	Tween® 20, Poloxamer® 188, phosphatidylcholine	Melt-emulsification and high-pressure homogenization.	Size: 118–158 nm. PDI: 0.108–0.189. ZP: (−41.6)–(−64.3) mV. EE β-carotene: 94.37–97.88%. EE azelaic acid: 91.76–93.48%.	Antioxidant, anti-inflammatory, antiacne, skin hydration	Hydrogels with NLCs: in vitro release profile (cellulose nitrate membrane), in vitro antioxidant action (chemiluminescence and TEAC methods), antimicrobial activity. Studies on cell lines: cytotoxicity, in vitro anti-inflammatory activity, in vivo hydration degree, antiacne	Sustained release during for 8 h, ↑ antioxidant activity, antimicrobial activity on *S. epidermidis*, *C. acnes*, *C. albicans*. Biocompatibility with fibroblasts, ↓ IL-1β and TNF-α,	[52]

						potential (human volunteers), anti-inflammatory (Wistar rats).	↑ skin hydration and skin elasticity, ↓ number of inflammatory acne lesions, ↓ sebum rate.	
HEs								
Cratoxylum formosum leaf ethanolic extract, lyophilized	Glyceryl behenate, glyceryl monostearate, caprylic/capric triglycerides	Tween® 80, Poloxamer® 188	High-shear ultrasonic Homogenization.	Size: 57.68–489.33 nm. PDI: 0.16–0.45. ZP: (−15.06)–(−5.76) mV. EE: 40.30–80.76%. Stability for 3 M, 4°, 25°, and 40° C.	Skincare	NLCs: in vitro release profile (dialysis bag), skin permeation (porcine ear skin), cell viability (HDFn).	↑ Skin absorption and biocompatibility, ↓ irritation potential than the free extract solution.	[49]
PCs								
Curcumin	Medium chain triglycerides, glyceryl monostearate, Span® 80	Tween® 80	High-pressure homogenization.	Size: ~200 nm. PDI: ~0.25. ZP: ~>−20 mV. EE: >90%. Stability for 4 M, 4°, 25°, and 37 °C.	Skin burns	NLCs: in vitro release profile (dialysis bags), ex vivo skin permeation and retention studies (porcine ear skin), cell viability on human skin fibroblasts (HFF-1 line), antimicrobial activity.	Release of curcumin in 72 h (51.64%). No toxicity on cells. ↑ Antimicrobial activity on *Pseudomonas aeruginosa.*	[64]
Curcumin and caffeine	Stearic acid, oleic acid	Soya lecithin, polyvinyl alcohol	Hot homogenization and ultrasonication.	Size: 98–169 nm. PDI: 0.23–0.58. EE: 44.14–63.92%.	Psoriasis	NLCs: in vitro release profile (dialysis bag), gels with NLCs: in vitro drug diffusion studies (cellophane dialysis membrane), in vivo studies (mice with induced psoriasis), skin irritation, skin inflammation, ex vivo permeation studies, PCs retention in the skin layers.	Initial burst release followed by prolonged release of drug for 12 h, gels with NLCs: compatibility and nonirritant effect. ↓ Inflammation, ↑ efficacy of psoriasis treatment.	[65]
Thymol	Glyceryl behenate, PEG-8,	Tween® 20	High-pressure homogenization and sonication.	Size: 123.8–360.0 nm. PDI: 0.113–0.359. ZP: (−13.02)–30.81 mV. EE: 76.38–81.41%.	Anti acne	NLCs and gels with NLCs: in vitro release profile (methylcellulose membranes), cell viability on HaCaT, ex vivo skin permeation	Prolonged release for 72 h cytotoxic at high doses, at lower doses and removal of excess free Tween® 20 from the formulation, cell viability ↑ significantly	[27]

	caprylic/capric triglycerides,			Stability for 6 M, room temperature.		studies (human skin explants), antimicrobial activity.	↑ antimicrobial activity on *C. acnes, S.s epidermidis.*	
Naringenin, nordihydroguaiaretic acid, kaempferol	Gelucire® 50/13, Apifil®, Miglyol® 812, Labrafac® WL1349	Tween® 80, Pluronic® F-127	High shear homogenization and sonication.	Size: 176–213 nm. PDI: 0.205–0.234. ZP: (−22.9)–(−8.9) mV. EE: 89.9–98.8%. Stability for 1 M.	Antioxidant, cancer prevention	NLCs: in vitro release profile, antioxidant activity (DPPH assay), cell viability and antioxidant activity (HaCaT).	Slow and sustained release for 19 days. No significant cytotoxicity. Good antioxidant activity.	[66]
Lycopene	*Citrus sinensis* wax, *Oryza sativa* bran oil	Eumulgin® SG	High pressure homogenization.	Size: 158–166 nm. PDI: 0.13–0.15. ZP: (−74.6)–(−74.2). pH: 6.6, EE: >99%. Stability for 4 M, 4°, 30°, and 40 °C.	Antioxidant	NLCs: in vitro release profile a.	Biphasic release profile: fast release for 6 h, then sustained release for 18 h.	[46]
SLNs and NLCs								
Oils and EOs								
Eucalyptus globulus or *Rosmarinus officinalis* oils	*Theobroma cacao* butter, *Olea europaea* oil, *Sesamum indicum* oil	L-α-phosphatidylcholine	High shear homogenization and sonication.	Size: 50–60 nm. PDI: ~0.5. ZP: −22.07 mV. Good bioadhesive properties. Stability 3 M, 2–8 °C.	Wound healing	SLNs and NLCs: antimicrobial activity cytocompatibility, in vitro proliferation enhancement, and wound healing properties in human dermal fibroblasts, in vivo wound healing efficacy (Wistar rats).	Same inhibition on *Staphylococcus aureus* and *Streptococcus pyogenes* as the free oils for SLNs and ↑ inhibition than free oils for NLCs, good biocompatibility, ↑ cell proliferation.	[51]
PCs								
Orobol	*Theobroma cacao* butter, *Butyrospermum parkii* butter, Capmul® MCM EP	Transcutol® HP, Tween® 20	Hot homogenization and sonification.	Size: 133–498 nm. PDI: 0.140–0.211. EE: 95.7–97.2%. DL: 0.91–0.97%. Stability 28 days, room temperature.	Antiaging	SLNs and NLCs: deposition study (Strat-M membranes and human cadaver skin), skin irritation (human volunteers).	Better results on NLCs: ↑ membrane/skin deposition of orobol, no significant skin irritation.	[67]

Sesamol	Compritol®888 ATO, Miglyol® 812, *Sesamum indicum* oil	Poloxamer® 188	Hot homogenization and sonification.	Size: 169.2–224.7 nm. PDI: 0.277–0.317. ZP: (−35)–(−38) mV. EE: 78.5–91.2%.	Antioxidant	Hydrogel with SLNs and NLCs: in vitro percutaneous absorption (human skin), in vitro skin permeation (human SCE membranes), in vitro antioxidant efficiency (ORAC assay).	↓ Permeation from NLCs, controlled diffusion through the skin, prolonged antioxidant activity.	[31]
Resveratrol	Octyl and decyl glycerate, glycerol monosterate	Cremophor® A25 and A6	Hot high-pressure homogenization.	Size: 297.9–336.4 nm. PDI: 0.352–0.405. ZP: 4.9–6.8 mV. EE: 94.8–96.2%. Stability for 6 weeks, 2–6 °C.	N.A.	SLNs and NLCs: in vitro release profile (dialysis bags), in vitro penetration study.	Biphasic drug release profile (burst release at the initial stage, then controlled release for 24 h) ↑ Penetration of SLNs compared. to NLCs.	[32]

↑—increasing , ↓—decreasing, HEs—herbal extracts, EOs—essential oils, PCs—phytocompounds, N.A.: not available, ZP—zeta potential, EE—encapsulation efficiency, DL—drug loading, M—months, HDFn—primary human dermal fibroblasts, PIT-phase inversion temperature, DPPH (2,2-Diphenyl-1-picrylhydrazyl), TEWL—transepidermal water loss, TEAC—Trolox Equivalent Antioxidant Capacity, HSV1—Herpes simplex virus 1, SPF—sun protection factor, LMW—low molecular weight, HFF—human foreskin fibroblasts, Hen's Egg Chorioallantoic Membrane Test (HET-CAM, Eumulgin SG (sodium stearoyl 69 glutamate), SPF—sun protection factor, PASI—Psoriasis Area and Severity Index, ELISA—enzyme-linked immunosorbent assay, Substances: Precirol®-ATO 5—Glyceryldistearate, Miglyol®-812—caprylic/capric triglycerides, Labrasol®-PEG-8 caprylic/capric glycerides, Compritol® CG 888 ATO—Glyceryl behenate, Transcutol P®—Diethylene glycol monoethyl ether, Poloxamer® 188—a -Hydro-o-hydroxypoly(oxyethylene)poly(oxypropylene) poly-(oxyethylene), Tween® 80—polyoxyethylene sorbitan monooleate, Span® 80-Sorbitan monooleate, Olivem® 1000—Cetearyl olivate, sorbitan olivate, Varisoft 442 100P.-Quaternium-18 Miglyol® 812-Caprylic/Capric Triglyceride, Capmul® MCM EP-Glyceryl Caprylate/Caprate, Cremophor® A25—Ceteareth 25, Cremophor® A6—ceteareth 6, stearyl alcohol.

To address skincare applications related both to dermatology and cosmetics such as wound healing, antibacterial, anti-inflammatory, antimelanoma, photoprotective, skin hydration, skin whitening, and the treatment of psoriasis, acne, and hair loss, a variety of EOs, oils, HEs, and PCs have been loaded in SLNs and NLCs. Of the many encapsulated natural bioactives, curcuminoids were often used, due to their multifaceted potential therapeutic properties, as well as their poor bioavailability, which makes them interesting to include in SLNs and NLCs [68]. A variety of lipids were used to obtain SLNs and NLCs, of which the most common was glyceryl monostearate, stearic acid, and Compritol® 888 ATO (Glyceryl behenate). Regarding the NLCs, the most used liquid lipids were caprylic/capric triglycerides and various natural oils. The lipids were chosen as a function of their compatibility with the bioactive ingredient and biocompatibility with the skin [34]. The most used surfactants were Tween® 80 (polyoxyethylene sorbitan monooleate), Poloxamer 188 (a-Hydro-o-hydroxypoly(oxyethylene)poly(oxypropylene) poly-(oxyethylene), and Span® 80 (Sorbitan monooleate). Due to their amphiphilic structure, surfactants lower the surface tensions and promote partitioning into hydrophilic and hydrophobic groups from the dispersion, preserving the stability of the SLNs and NLCs. The selection of surfactants must be chosen to avoid irritation and sensitivity of the skin [34]. Methods of preparation of SLNs and NLCs such as hot homogenization and high-shear homogenization, usually followed by sonication, are commonly employed.

The characterization of SLNs and NLCs loaded with natural bioactives is important to ensure the efficacy and the delivery to the desired skin layer. Further, the parameters used for the characterization of nanosystems presented in Table 2 are discussed below. As can be seen in Table 2, the particle sizes of SLNs and NLCs entrapping natural bioactives ranged from 32.7 to 1420 nm. SLNs and NLCs typically have diameters between 40 to 800 nm, which enables them to attach to the *stratum corneum*'s lipid matrix and increase the quantity of active ingredients that reach the skin's deeper layers. In general, nanosystems with a diameter of 600 nm or higher are unable to deliver loaded bioactive substances to deeper skin layers; they tend to remain on or in the *stratum corneum*, where they can form a lipid layer after drying [26]. It is generally acknowledged that the particle size should be smaller than 300 nm to allow efficient skin penetration, while maximum deposition of actives in both viable dermal and epidermal layers is obtained when particle size is below 70 nm [23]. It was reported that particles with size below 200 nm or 300 nm can also enter the skin via the hair follicles [25,26]. The particle size of the SLNs and NLCs can be influenced by the lipid matrix's composition. It was reported that size decreased with increasing oil content of the NLCs, probably due to lower viscosity of the melted droplets, thus easing dispersion and resulting in smaller sizes [44]. The particle size of SLNs and NLCs may also depend on the concentration of surfactant required to form an adsorption monolayer on the particles [57]. It was found that particle size significantly decreased with increasing concentration of Tween® 80 [62]. Another parameter important for particle characterization is the homogeneity of particle size, evaluated through the determination of the polydispersity index (PDI). The PDI of SLNs and NLCs with natural bioactives varied widely between 0.16 and 1.00 (Table 2). Particle monodispersity is obtained when PDI has values lower than 0.3. PDI can be narrowed and the particle size of SLNs and NLCs can be reduced by sonication or by increasing the number of homogenization cycles when obtained by the high-pressure homogenization method. However, the application of too many cycles may determine the agglomeration of coalescence of particles, due to the additional energy input and higher kinetic energy [23,44,62]. The zeta potential (ZP) is influenced by the net charge of the lipids and surfactants from the structure of the SLNs and NLCs. If the particles are uncharged, so the closer the ZP values are to zero, they are prone to flocculation. Ideally, ZP should reach values below −25 mV or greater than 25 mV, but, as it seems from the research results, this is quite difficult to achieve. For SLNs and NLCs loading natural bioactives, ZP varied between −651.0 to 27.3 mV, with most of the values being below −25 mV (Table 2), as is necessary for ensuring a high stability, due to the repulsive forces that have the natural tendency to aggregate [23]. Encapsulation efficiency

(EE) is represented by the amount of entrapped active ingredient from the total amount of the active which was initially added to the dispersion of natural bioactives [34]. For SLNs and NLCs entrapping natural bioactives, EE ranged between 31.0% and 99% (Table 2), indicating the effectiveness of different preparation methods in their encapsulation. Drug loading (DL) or loading content of natural bioactives is calculated by dividing the amount of entrapped natural bioactives by the amount of lipid used [45]. DL varied from 0.91 to 9.51% (Table 2), even though it was not reported in most studies. SLNs and NLCs with natural bioactives exhibited physical stability for a period between 1 and 6 months, analyzing the parameters presented above. They were stable when stored at room temperature and had even better stability at 4 °C (Table 2).

The kinetic studies on SLNs and NLCs containing natural bioactives were performed in vitro using synthetic membranes or ex vivo studies using skin explants (Table 2). These studies have documented the release profile, percutaneous absorption, deposition in different skin layers, or permeation characteristics of these parameters. The most performed test was the in vitro release profile assessment, which demonstrated the sustained or prolonged release of the bioactives [32]. The bioactives' solubility in the lipid matrix is the first major factor influencing their release [43,46]. Additionally, the increased concentration of lipids and surfactants in the SLNs and NLCs formulation ensures a faster diffusion of loaded bioactives and, consequently, a better release [57]. Interestingly, some studies revealed a biphasic pattern, a relatively fast release during the first hours followed by a sustained release during the next many hours [46,59,63]. A fast release at the initial stage was due to the high amount of lipophilic bioactive dissolved in this liquid lipid shell. This phenomenon was found for NLCs, due to some lipids that can lead to accumulation of the lipophilic bioactive in the outer shell after lipid crystallization, because of the distribution of liquid lipid in the solid lipid matrix and their different melting behavior. The wide surface area of the NLCs and a high diffusion coefficient resulting from the low viscosity of the matrix are the other elements that promote the observed quick release in the first stage. Additionally, it has been found that decreasing the liquid lipid ratio can accelerate the release rate during the burst release stage [32]. In most studies, a sustained release for 72 h was reported, while in the study reported by Gonçalves et al., a slow and sustained release for 19 days was observed [66].

Skin permeation and skin retention studies were performed using dialysis method with Franz diffusion cells and ear porcine skin as the membrane, comparing nanoemulsions (NEs) and NLCs loaded with curcumin. The results showed that curcumin from NLCs was retained in the epidermis at levels 1.25 times higher (μg/cm^2) than from NEs, while in the dermis its concentration was 1.37 times lower than from NEs. No curcumin was detected in the acceptor fluid, indicating that these nanocarriers were preferentially retained in the skin layers, without penetrating the systemic circulation [64]. The release of dillapiole from NEs and NLCs loaded with *Piper aduncum* EO rich in dillapiole was performed using Franz diffusion cells and a synthetic cellulose ester membrane. The percentage of the released dillapiole from NLCs was about three times lower than from NEs, probably due to the solid core of NLCs. The skin permeation and retention studies performed using porcine ear skin showed that dillapiole has a good ability to penetrate the deeper layers of skin, as it was not retained in the epidermis, but was retained in an important amount in the dermis, where an important cumulative amount permeated was determined both from NEs and NLCs. This finding showed an important potential of these nanocarriers for the management of topical inflammatory diseases [63]. The release profile and the skin retention ability were also studied using Franz diffusion cells and methylcellulose membranes, comparing an aqueous formulation, NLCs encapsulating thymol, and gels containing NLCs entrapping thymol. The aqueous solution of thymol reached a steady state around 12 h, while both NLCs and gel formulations of NLCs exhibited a prolonged release for 72 h. Ex vivo permeation studies realized using human abdominal skin obtained from plastic surgery indicated that thymol from the aqueous formulation reached the systemic circulation faster and its retention at skin levels was lower

than from the NLCs carrier. This finding suggested that NLCs encapsulation of thymol was a more effective approach for the therapy of topical conditions [27].

Other studies, conducted in vitro on cell cultures (e.g., fibroblasts, keratinocytes) and in vivo studies in animals (mice or rats) or human volunteers, indicated enhanced biological effects when using SLNs and NLCs compared to free bioactives (Table 2).

With regard to the potential drawbacks of these nanosystems, there were studies that reported cytotoxicity of NLCs in HaCaT cells, depending on surfactant type and increasing with its concentration, knowing that some surfactants may have cytotoxic potential at high doses. For example, in a study conducted by Folle et al., the cell viability increased after removing the free Tween® 20 (Polyoxyethylene (20) sorbitan monolaurate) from the samples. Other authors have stated that the cytotoxicity of SLNs and NLCs may be attributed also to lipid peroxidation and generation of oxygen free radical species, depending on the cell type and concentration used [27,69,70].

5. Formulation of SLNs and NLCs into Semisolid Systems and Use as Dispersions: Revealing Their Properties for Specific Applications

Products applied on skin must have desirable viscosity, texture, and sensory properties according to their specific applications and conditions of usage. For example, in some applications when large skin surfaces are targeted, low viscosity is desired, ensuring the fluidity needed for an easy application [24], while in other cases, when a small skin surface is targeted, a reduced viscosity can be less attractive or even a disadvantage [43].

SLNs and NLCs can be used as dispersions, per se, or incorporated into semisolid formulations, e.g., creams or gels.

5.1. SLNs and NLCs Used as Dispersion Per Se

SLNs and NLCs may have good bioadhesive properties, probably determined by their flexibility, which could promote interaction with the biologic substrate and the consequent bioadhesive joint formation. To be used in topical administration, this represents an important feature to allow an intimate contact between formulation and the skin, to assure treatment efficacy. The bioadhesive properties can be evaluated using a texture analyzer and a biologic substrate [51].

When nanoparticles come into contact with skin, they generally attach excellently due to a film-forming property generating an occlusive film (at a minimal concentration of 2–4% of NLCs) which promotes the penetration of actives. Additionally, the lipids from the SLNs and NLCs structure can interact with matrix lipids from the stratum corneum when the melting point of the lipids is close to the temperature of the skin ($t < 32$ °C). If the melting temperature of the lipids is higher, the particles remain on the skin surface, and they can be slightly deformed during application [39]. The film-forming property results from the adsorption of these particles on skin, which lowers the surface free energy, and, hence, the thermodynamic driving force of the resulting system. Another explanation of this phenomenon is represented by the property of ultrafine materials to form high van der Waals forces between the particles and contact surface. If a monolayer of lipophilic coating occludes the skin, the evaporation-induced loss of moisture may be postponed. Moreover, the pressure obtained during skin application causes the fusion of the particles, forming a dense coating on the skin, with this fusion also being supported by the capillary forces involved in water evaporation [24,46]. The occlusive effect depends on the lipids' ratio, the sample volume of the product applied, particle size, and crystallinity of particles [26]. Depending on the particle size of the SLNs and NLCs, the moisture barrier's properties reveal different degrees of occlusion. Thus, the barrier against evaporation increases with a decrease in their particles size, while the evaporated amount of water will increase with their particle size [24]. An increase in the occlusion factor over time has been demonstrated as well [46]. The ability to form an occlusive film by the SLNs and NLCs or their formulations (after including in gels and creams) can be measured using an occlusion study [24,46,47,57,60,62]. Moreover, it was shown that SLNs and NLCs provide good skin

lubrication and smoothness due to their spherical-like shape. The lubricating effect assessment could be conducted using rheological analysis [24].

Using different types and concentrations of lipids and surfactants, the formulators can adjust the SLNs and NLCs properties depending on their usage particularities [1,24]. The choice of the ingredients should start with compatibility studies between the active substances and excipients [32,66]. DSC (differential scanning calorimetry analysis) and FTIR (Fourier transform infrared spectroscopy) of the lipids, surfactants, and bioactives intended to be used, as well as their physical mixture, can be evaluated to observe the interactions between the ingredients [65]. The study of the influence of multiple formulation variables (type and concentration of lipids, surfactants, and active substances contained) on the SLNs and NLCs properties (e.g., particle size, PDI, zeta potential, encapsulation efficiency, etc.) can be assessed using a design of experiment approach, a systematic method with the advantages of minimal number of experimental runs and reduced consumption of raw materials [27,28,49,50,59,62,65,71,72]. Moreover, process formulation factors can be also varied (e.g., homogenization time) and then their influences on the quality characteristics of the SLNs and NLCs can be studied [61].

5.2. SLNs and NLCs Used after Incorporation in Topical Vehicles

Table 3 presents an overview of the SLNs and NLCs entrapping HEs, oils, Eos, and PCs included in topical application systems. To facilitate topical application, SLNs and NLCs can be dispersed into several vehicles to form semisolid formulations, also improving the acceptability and user compliance, and even increasing their stability [27,43,60]. Thus, a convenient choice for vehicles can be represented by gels or hydrogels, e.g., Carbopol® (Carbomer) or cellulose derivates gels, because of the forming gel threads with SLNs and NLCs embedded within them. In a study conducted by Folle et al., NLCs were included in three different types of gels; carbomer and hydroxypropyl methyl cellulose (HPMC) gels containing NLCs provided an easy spreading application onto the skin and Pluronic®F127 (Poloxamer 407, Oxirane, methyl-, polymer with oxirane) gel containing NLCs provided a more dried touch and non-easy spreadable formulation. The investigation of transmission electron microscopy (TEM) images revealed that gel threads had a lipidic appearance, where the NLCs were embedded. It presented an amorphous lipidic (waxy-like) appearance, like an emulgel (nongreasy, easy spreadable, and easily removable). The NLCs dispersion was found to be stabilized after inclusion in gels, making them suitable for storage to avoid creaming or flocculation phenomena. Carbopol® and HPMC gels loaded with NLCs had higher and similar amount of active compound retained inside the skin compared to Pluronic®F127 gels containing NLCs, which exhibited a very slow penetration rate of the natural bioactive. Carbopol® gels containing NLCs have been shown to be highly retained in skin tissues, provided a low permeation rate and a prolonged release up to 72 h [27]. Moreover, SLNs and NLCs can be formulated as hydrogels by including hydroxyethyl cellulose or Carbopol ® in the dispersion. In the study conducted by Caneiro et al., the resulting hydrogels-thickened NE and NLCs exhibited pseudoplastic behavior and bioadhesive properties. The hydrogels-thickened nanosystems proved to be more bioadhesive since the work of adhesion and the force of detachment were about eight times and three times higher in comparison with the NE and NLCs without hydroxyethyl cellulose. Additionally, a lower retention of active substance in the dermis was observed from hydrogels-thickened nanosystems in comparison with NE and NLCs without hydroxyethyl cellulose. Due to the higher viscosity of the system, the hydrogels-thickened nanosystems may hinder the delivery of active compounds, because they should leave the polymeric network and then penetrate the skin [63]. In another study by Kakkar et al., Carbopol® gel was added in the SLNs dispersion to obtain a hydrogel. The release of the active from the Carbopol ® gel-loading SLNs and SLNs dispersion was almost 16–17 times higher than the free substance hydrogel during the ex vivo permeation studies [60]. Gels containing Rosmarinus officinalis EO-loaded NLCs showed a significant increase in skin hydration and a lesser increase in skin elasticity in comparison with gels containing free

Rosmarinus essential oil [53]. In a study conducted by Riangjanapatee et al., NLCs loading Camellia oleifera seed oil were incorporated in serums, which reduced the sticky, oily, and greasy feeling, while ensuring an easier application (better spreadability and reduction in firmness) [55].

SLNs and NLCs can also be included in creams. Their incorporation requires careful formulation to ensure uniform distribution, prevent phase separation, and ensure their overall stability. SLNs and NLCs are usually incorporated in the final step, by gently stirring them into water-based products, when the temperature is around 30 °C [39]. The stability of topical products with SLNs and NLCs was evaluated by specific methods. For example, in the study conducted by Plyduang et al., SLNs loading *Elaeis guineensis* fruit extract included in creams were stable after six cycles of freeze–thaw and after storage at 30 °C/75% RH for 6 months, in terms of pH, viscosity, and PCs content (tocopherol, tocotrienol, and beta-carotene) [54].

Figure 3 schematically represents the skin bioavailability enhancement of the natural bioactive substances loaded in SLNs and NLCs from a topical product, as described above, in Sections 5.1. and 5.2. The adhesion and occlusion formed by SLNs and NLCs included in a topical product determine film formation, which increases skin hydration and, furthermore, increases the skin penetration of SLNs and NLCs and the natural bioactives contained. The skin absorption of SLNs and NLCs through transepidermal and transappendageal routes are also illustrated.

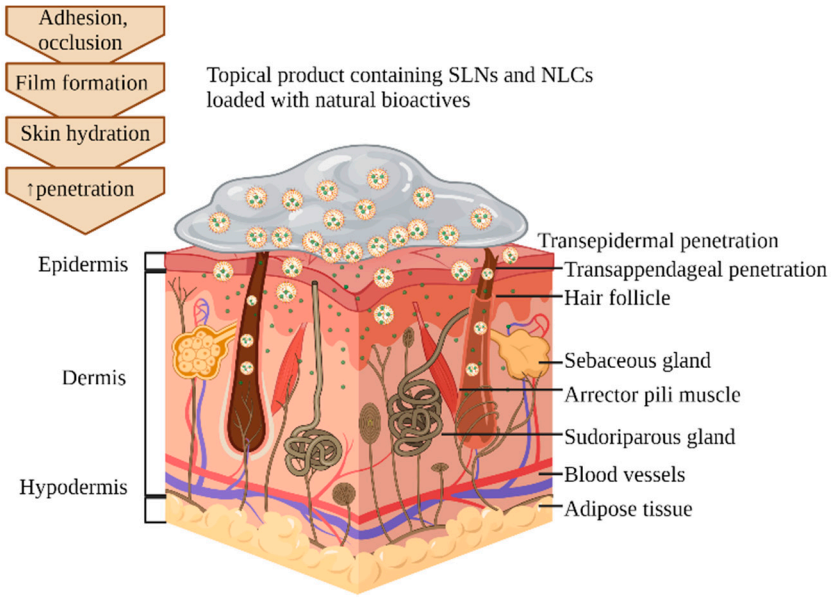


Figure 3. Skin bioavailability enhancement of the natural bioactive substances loaded in SLNs and NLCs from a topical product (image created using Biorender.com, accessed on 2 August 2024).

Table 3. Overview of SLNs and NLCs loading HEs, EOs, or PCs, included in topical application systems.

Entrapped EOs, HEs, PCs	Concentration of the Natural Bioactives in the Final Topical System	Composition of the Topical System	Ref.
		SLNs	
Chamomilla recutita oil	N.A.	Camisan® cream (EIPICO, Egypt)	[47]
Rosmarinus officinalis essential oil	N.A.	Carbopol® hydrogel (Carbopol® Ultrez 21®, TEA, Imidazolidinyl urea, Methylchloroisothiazolinone, Methylisothiazolinone)	[53]
Aloe vera powder	N.A.	Sunscreen cream (Cetosteryl alcohol, Stearic acid, TEA, Glycerol, Liquid paraffin)	[57]
Elaeis guineensis fruit extract	3%	Day and night creams (Liquid paraffin, White soft paraffin, Isopropyl myristate, Glyceryl monostearate, Cetyl alcohol, Stearic acid, Carbomer 940, Glycerin, Propylene glycol, Polysorbate 80, Tocopherol acetate, Disodium EDTA, Phenoxyethanol, Titanium dioxide, Octyl methoxycinnamate, Grape seed extracts)	[54]
		NLCs	
Piper aduncum oil	N.A	Hydroxyethyl cellulose hydrogels	[63]
Curcuminoids	N.A.	Natrosol® gel (Via Pharma Ltda, Brazil)	[61]
Sesamol	0.1%	Sodium polyacrylate hydrogels	[31]
Rosa canina oil, *Nigella sativa* oil, *Daucus carota* extract, *Calendula officinalis* extract	6% *Daucus carota* extract/*Calendula officinalis* extract, 2% azelaic acid and 12% *Rosa canina* oil/*Nigella sativa* oil	Carbopol® hydrogel (Carbopol® 940, ethanol, glycerin, TEA)	[52]
Thymol	0.1%, 0.25%	Carbopol® hydrogel (Carbopol® 934, glycerin, propylene glycol) Hydroxypropyl methylcellulose gel (HPMC, glycerin, propylene glycol) Pluronic® gel (poloxamer 407/Pluronic®F127, glycerin, propylene glycol)	[27]
Tetrahydrocumarin	0.2%	Carbopol® hydrogel (Carbopol® 934, TEA)	[60]
Curcumin	N.A.	Carbopol® hydrogel (Carbopol 940®, propylene glycol, TEA, methyl and propylparaben)	[62]
Curcumin and caffeine	N.A.	Carbopol gel (Carbopol-934, propylene glycol, TEA, propyl paraben)	[65]
Camellia oleifera seed oil	N.A.	Serum (Ammonium acryloyldimethyltaurate/VP copolymer, glycerin, phenoxyethanol, and chlorphenesin)	[55]

HEs—herbal extracts, EOs—essential oils, PCs—phytocompounds, N.A.—not available, Carbopol®—Carbomer, TEA—triethanolamine, EDTA—Ethylenediaminetetraacetic acid.

6. Key Features of Commercial Products Incorporating SLNs and NLCs

The range of commercially available products with SLNs and NLCs has significantly widened in recent years due to their functional benefits. From the perspective of the cosmetic industry, the cost-effective manufacturing process by high-pressure homogenization and the ease of incorporating nanoparticles in the final formulations provide significant advantages. The possibility to use various natural oils such as *Argania spinosa* kernel oil, *Aleurites moluccana* seed oil, *Macadamia ternifolia* seed oil, *Olea europea* oil, *Ribes nigrum* seed oil, and *Prunus amygdalus* dulcis oil, as well as herbal extracts (*Panax ginseng* root, *Equisetum arvense*, *Camelia sinensis* leaf, *Viola tricolor* extract) or different active ingredients (coenzyme Q10, fatty acids), allows for personalized formulations and additional marketing claims [37,39]. SLNs and NLCs improve the efficacy and tolerance of sunscreens, acting as penetration enhancers, thus allowing for smaller ratios of actives and minimizing side effects. They provide excellent photoprotective action and enhanced active ingredient EE, depending on the choice of the lipids used [73].

The first cosmetic product incorporating NLCs (Cutanova Nanorepair Q10) was launched in the market in 2005 [74]. Since then, these nanoparticles have been used in a variety of cosmetic formulations, mainly in restructuring antiaging creams (e.g., Nanorepair Q10 cream and serum and Nanovital Q10 cream, Dr. Rimpler GmbH) or moisturizing products (e.g., Surmer masque crème hydratante, Surmer crème legère nanoprotection, Isabelle Lancray). NLC concentrates such as NanoLipid Restore CLR™ (Ribes Nigrum (Black Currant) Seed Oil (and) Copernicia Cerifera (Carnauba) Wax (and) Decyl Glucoside (and) Water) are also available and facilitate the development of tailormade formulations according to cosmetic companies' strategies [39].

Even if it is estimated that more than 500 cosmetic products containing NLCs are available, these products are not explicitly listed as NLCs in the INCI nomenclature, only the individual components of NLCs, such as actives, lipids, and surfactants [39].

7. Recent Patents and Patent Applications with SLNs and NLCs

The advantages offered by SLNs and NLCs in applications for the cosmetic industry have been intensively investigated, and numerous patent applications on this topic have been filed in the last years. Some recently filed patents, summarized in Table 4, highlight the potential applications of SLNs and NLCs in cosmetic and therapeutical fields. These patents emphasize the abovementioned advantages in the previous subsections, mainly the efficient delivery of active ingredients, enhanced bioavailability, and improved stability in various formulations.

Patents related to cosmetic products for face care include skin whitening, antiaging, moisturizing, and antiacne formulations, and incorporate different actives such as phenethyl resorcinol, ceramides, and azelaic acid. The preparation of SLNs and NLCs with PCs such as curcumin, astaxanthin, glabridin, and arbutin has been addressed in a few patents [75,76]. The incorporation of antioxidants such as curcumin ensures a good entrapment efficacy and superior solubilization (10,000 times higher than the free active) through an easy scalable preparation method with potential industrial application [77]. For another powerful antioxidant molecule, astaxanthin, an improved solubility and better stability were obtained when this phytocompound was entrapped in SLNs, with a mass ratio of the lipid material and water of 1:11, a lipid phase consisting of solid lipid 1–15%, vegetable oil 85–98.9%, and astaxanthin, 0.1%; in the aqueous phase, a ratio of 1–10% surfactant was used. The entrapment of essential oils in solid-lipid nanostructures is particularly advantageous for improving the physical and chemical stability of the phytocomplex. Thus, in the case of α-tocopheryl stearate-SLNs loaded with bergamot oil, stability studies showed that after two and six months of light exposure, the level of active ingredients decreased by only 10% and 18%, respectively, and no further degradation was observed at twelve months [78].

The use of plant extracts in SLNs and NLCs has potential applications that can be valorized into patent applications related to unique combinations of plant extracts with synergistic effects. Thus, patent CN116211777A describes preparation of SLNs with concentrated extracts of *Angelica dahurica*, *Scutellaria baicalensis*, and *Forsythia chinensis* and, further, the incorporation in a semisolid vehicle. The product displayed in vitro antioxidant, tyrosinase inhibitory activity, and antibacterial activity on *Cutibacterium acnes* strains [79].

Patents related to body care products employ NLCs in noninvasive approaches targeting fat deposits, emphasizing their potential in body contouring and lipolysis treatments [80]. In sunscreen formulations, the sunscreen filters encapsulated NLCs demonstrated an increase in the photoprotection effect [81].

Patents related to hair care products describe SLNs and NLCs to improve hair fiber properties, emphasizing the suitability of NLCs and SLNs as vehicles for releasing active ingredients on hair and scalp surfaces [82].

The abovementioned patents describe several innovative products and preparation methods and show the advancements achieved within the lipid nanoparticles field. Recent applications describe specialized formulations such as pH-responsive or mucoadhesive SLNs, offering solutions for an efficient delivery of active substances [83,84].

Table 4. Selection of recent patents and patent applications with SLNs and NLCs.

No	Patent No	Title	Filing Date	Description	Ref.
1	CN104257632A	Solid lipid nanometer particle for astaxanthin and preparation method of solid lipid nanometer particle.	2014-10-24	Astaxanthin SLNs.	[76]
2	CA2872279A1	Topical lipolysis compositions and methods.	2014-11-25	NLCs targeting fat deposits for noninvasive therapy of aggregated deposits of adipose tissue.	[80]
3	KR101860555B1	Solid lipid nanoparticles composition for skin-whitening effect comprising MHY498 and preparation method thereof.	2016-09-12	Skin-whitening SLNs composed of a core layer made of MHY498 and a lipid matrix, and a shell layer made off Poloxamer 188 as an active ingredient.	[85]
4	JP7010823B2	Compounds useful in the treatment and/or care of skin, hair, nails and / or mucous membranes.	2016-12-08	SLNs and NLCs incorporated in cosmetic delivery systems for antiaging properties.	[86]
5	US2021069121A1	Solid lipid nanoparticle for intracellular release of active substances and method for production the same.	2017-12-12	SLNs containing a lipid (natural plant or synthetic wax), a surface acting agent (d-α-Tocopheryl polyethylene glycol 1000 succinate), water and an active compound.	[87]
6	US2021353553A1	Mucoadhesive dispersion nanoparticle system and method for production the same.	2018-09-11	Mucoadhesive dispersion nanoparticle system for the transport and delivery of actives entrapped in SLNs.	[84]
7	US2022151945A1	Solid lipid nanoparticles of curcumin.	2018-11-26	Curcumin-loaded SLNs using generally recognized as safe (GRAS) components.	[77]
8	KR20200094871A	Lipid-protein nanocomposites comprising ginsenoside and use thereof.	2019-01-30	Lipid nanocomplex containing ginsenoside, phosphatidylcholine, sucrose fatty acid ester, surfactant, and positively charged protein.	[88]
9	JP7377813B2	Hair modification composition and method thereof.	2019-04-11	Hair care products with SLNs and NLCs.	[82]
10	CN111988999A	Pigment-loaded solid lipid nanoparticles.	2019-04-16	SLNs containing oil-soluble pigments and high melting point lipids in the core and a surfactant system formed by polysorbate and phospholipids.	[89]
11	CN112691044A	Positive charge modified solid lipid nanoparticle and preparation method thereof.	2019-10-22	SLNs for transdermal administration of cosmetic actives.	[90]
12	CN110974712A	Whitening acid nanostructure lipid carrier as well as preparation method and application thereof.	2019-12-27	Whitening acid nanostructured lipid carrier including the following components: fat-soluble acid, emulsifier, water-soluble acid, emulsion stabilizer, water.	[91]
13	US2022265565A1	Nanotechnology-based delivery system of bergamot essential oil, method of preparation of the system and uses thereof.	2020-07-29	α-tocopheryl stearate-solid lipid nanostructures loaded with bergamot essential oil without psoralens.	[78]

14	CN114515258A	Phenylethyl resorcinol nanostructure lipid carrier, preparation method, and application in cosmetics.	2020-11-20	Phenethyl resorcinol nanostructure lipid carrier for cosmetic applications.	[92]
15	KR102577778B1	pH-responsive capsosome using chitosan-coated solid lipid nanoparticles as core.	2020-12-24	pH-responsive-release-controlled capsosome prepared by reacting liposomes with chitosan-coated SLNs.	[83]
16	EP4169509A1	Particle containing lipid nanoparticles and method for producing same.	2021-05-18	SLNs included in functional cosmetics.	[93]
17	WO2022112527A1	Method for preparing nanosystems.	2021-11-26	Lipid-based nanoparticulate carriers, preferably SLNs or NLCs that be entrapped in vehicles for cosmetic use.	[94]
18	CN112868816A	Preparation method of water-in-oil emulsion gel based on diglyceride solid lipid nanoparticles.	2021-01-26	W/O emulsion gel based on diglyceride SLNs.	[95]
19	TWM639079U	Mist spray container bottle with nanostructured lipid carrier suspension.	2021-09-29	Spray container bottle with NLC suspension.	[96]
20	CN113876642A	Face cream composition containing lipid nanoparticles with moisturizing and hydrating effects and preparation method thereof.	2021-11-12	Face cream composition containing lipid nanoparticles with moisturizing effect.	[97]
21	KR20230149537A	Solid lipid nanoparticles comprising cosmetic composition and cosmetics comprising the same.	2022-04-20	SLNs containing 4-alkylresorcinol and cosmetic compositions containing SLNs with 4-alkylresorcinol.	[98]
22	WO2023137532A1	Nanostructured lipid carrier, use of the nanostructured lipid carrier, photoprotective composition and method for skin photoprotection.	2022-01-19	NLCs consisting of at least one solid natural lipid, at least one liquid natural lipid, and at least one surfactant, which are combined to encapsulate sunscreen filters and enhance photoprotection in a sunscreen formulation.	[81]
23	CN116139025A	Preparation and application of multi-repeat-matching nanostructure lipid carrier.	2022-08-26	Multiple complex type NLC with glabridin and arbutin.	[75]
24	CN115517988A	Azelaic acid nano lipid particle, freeze-dried powder, preparation method and application.	2022-10-12	Nanolipid particles containing azelaic acid, cetyl palmitate, oleic acid, emulsifier (Tween 80 or poloxamer), glycerin, and water.	[99]
25	CN116211777A	Whitening and acne-removing cosmetic and preparation process thereof.	2023-04-24	SLNs with concentrated extracts of Angelica dahurica, Scutellaria baicalensis, and Forsythia chinensis.	[79]
26	CN116327662A	Antiaging solid lipid nanoparticle emulsion and preparation method thereof.	2023-05-06	Antiaging SLN emulsion containing 3,3,5-trimethylcyclohexyl dimethylamide succinate.	[100]
27	CN116725918A	Preparation method and application of diglyceride nanostructure lipid carrier hydrogel.	2023-05-31	Diglyceride caprylic acid NLC and diglyceride caprylic acid NLC hydrogel containing vegetable oil, diglyceride, soybean lecithin, tea saponin and glycerin.	[101]

28	CN117137825A	Ceramide lipid nanoparticles as well as preparation method and application thereof.	2023-09-07	Ceramide lipid nanoparticles.	[102]
29	CN117398294A	Chitosan interface modified ellagic acid nanostructure lipid carrier and preparation method thereof.	2023-10-16	NLCs loaded containing ellagic acid, solid lipids, liquid lipids, and emulsifier sodium caseinate.	[103]
30	WO2024102798A1	Lipid nanoparticles as active molecule carriers in ophthalmic, dermatological, and/or cosmetic applications, and process for production thereof.	2023-11-08	NLCs containing solid lipids (glyceryl distearate, cocoa butter, and combinations thereof), liquid lipids (Linoleoyl Polyoxyl-6 glycerides, Oleoyl Polyoxyl-6 glycerides and combinations thereof) and nonionic surfactants (Polyethylene glycol 660 12-hydoxystearate, Polysorbate 80, and combinations thereof).	[104]

8. Conclusions

There is growing interest in SLNs and NLCs development, to explore their potential for topical applications such as cosmetics or dermatological systems, being recognized as efficient carriers and having advantages for large-scale industrial production. They offer significant benefits in enhancing the stability and bioavailability of natural bioactives due to their protection and improved stability. Moreover, SLNs and NLCs may enhance the delivery and penetration of HEs, EOs, oils, and PCs, ensuring targeted and controlled release. The film formation and adherence on the skin of the SLNs and NLCs can increase the hydration and protection of the skin and, consequently, the penetration of natural bioactives. All of these can enhance the effects of bioactives for skin health for the benefit of patients or consumers. Recent research and patent applications in the field of SLNs and NLCs loading natural bioactives for skin health have shown significant advancements in encapsulation efficiency, stability, and bioactives delivery. The choice of lipids, surfactants, and preparation methods critically influenced the physicochemical properties and efficacy of the final formulations. In vitro and in vivo studies evaluated the potential of these nanoparticles to enhance the therapeutic outcomes of natural bioactives, providing promising opportunities for advanced skincare and dermatological treatments. Further research could focus on optimizing formulations for specific conditions, improving efficacy, and conducting extensive in vivo studies to validate these findings. However, their full potential has not been fully explored yet, while new natural bioactives can be encapsulated in these nanosystems; consequently, this research field will be continuously growing to create more appealing products.

Author Contributions: Conceptualization, D.A.S., C.B., and M.-L.M.; writing—original draft preparation, D.A.S., C.B., and M.-L.M.; writing—review and editing, D.A.S., C.B., and M.-L.M. All authors have read and agreed to the published version of the manuscript.

Funding: This research received no external funding.

Institutional Review Board Statement: Not applicable.

Informed Consent Statement: Not applicable.

Conflicts of Interest: The authors declare no conflicts of interest.

References

1. Qadir, A.; Jahan, S.; Aqil, M.; Warsi, M.H.; Alhakamy, N.A.; Alfaleh, M.A.; Khan, N.; Ali, A. Phytochemical-based nanopharmacotherapeutics for management of burn wound healing. *Gels* **2021**, *7*, 209.
2. Sasidharan, S.; Chen, Y.; Saravanan, D.; Sundram, K.M.; Latha, L.Y. Extraction, isolation and characterization of bioactive compounds from plants' extracts. *Afr. J. Tradit Complement. Altern. Med*. **2011**, *8*, 1–10.
3. de Souza Guedes, L.; Martinez, R.M.; Bou-Chacra, N.A.; Velasco, M.V.R.; Rosado, C.; Baby, A.R. An overview on topical administration of carotenoids and coenzyme Q10 loaded in lipid nanoparticles. *Antioxidants* **2021**, *10*, 1034.
4. Lopez-Ojeda, W.; Pandey, A.; Alhajj, M.; Oakley, A.M. Anatomy, skin (Integument) [Updated 17 October 2022]. In *StatPearls [Internet]*; StatPearls Publishing: Treasure Island, FL, USA, 2024. Available online: https://www.ncbi.nlm.nih.gov/books/NBK441980/ (accessed on 13 August 2024).
5. Romero, E.L.; Morilla, M.J. Ultradeformable phospholipid vesicles as a drug delivery system: A review. *Res. Rep. Transdermal Drug Deliv.* **2015**, *4*, 55.
6. Alkilani, A.Z.; McCrudden, M.T.C.; Donnelly, R.F. Transdermal drug delivery: Innovative pharmaceutical developments based on disruption of the barrier properties of the stratum corneum. *Pharmaceutics* **2015**, *7*, 438–470.
7. Murthy, S.N. Approaches for Delivery of Drugs Topically. *AAPS PharmSciTech* **2020**, *21*, 30.
8. Nielsen, J.B.; Benfeldt, E.; Holmgaard, R. Penetration through the skin Barrier. *Curr. Probl. Dermatol*. **2016**, *49*, 103–111.
9. Pandey, A.; Ashu, M.; Nitesh, C.; Sanjar, A. Role of surfactants as penetration enhancer in transdermal drug delivery system. *J. Mol. Pharm. Org. Process Res*. **2014**, *2*, 2–7.
10. Bolzinger, M.A.; Briançon, S.; Pelletier, J.; Chevalier, Y. Penetration of drugs through skin, a complex rate-controlling membrane. *Curr. Opin. Colloid Interface Sci*. **2012**, *17*, 156–165.
11. Yu, Y.Q.; Yang, X.; Wu, X.F.; Fan, Y.B. Enhancing permeation of drug molecules across the skin via delivery in nanocarriers: Novel strategies for effective transdermal applications. *Front. Bioeng. Biotechnol*. **2021**, *9*, 646554.

12. Souto, E.B.; Baldim, I.; Oliveira, W.P.; Rao, R.; Yadav, N.; Gama, F.M.; Mahant, S. SLN and NLC for topical, dermal, and transdermal drug delivery. *Expert Opin. Drug Deliv.* **2020**, *17*, 357–377.
13. Ng, K.W.; Lau, W.M. Skin deep: The basics of human skin structure and drug penetration. In *Percutaneous Penetration Enhancers Chemical Methods in Penetration Enhancement: Drug Manipulation Strategies and Vehicle Effects*; Dragicevic, N., Maibach, H.I., Eds.; Springer: Berlin/Heidelberg, Germany, 2015; pp. 3–11.
14. Gaohua, L.; Miao, X.; Dou, L. Crosstalk of physiological pH and chemical pKa under the umbrella of physiologically based pharmacokinetic modeling of drug absorption, distribution, metabolism, excretion, and toxicity. *Expert. Opin. Drug Metab. Toxicol.* **2021**, *17*, 1103–1124.
15. Hafeez, F.; Maibach, H. Occlusion effect on in vivo percutaneous penetration of chemicals in man and monkey: Partition coefficient effects. *Skin Pharmacol. Physiol*. **2013**, *26*, 85–91.
16. Osman, N.; Maibach, H.I. Effects of Occlusion on Dermal Drug Delivery: Implications for Bioequivalence Measurement. In *Topical Drug Bioavailability, Bioequivalence, and Penetration*; Shah, V.P., Maibach, H., Jenner, J., Eds.; Springer Science+Business Media: New York, NY, USA, 2014; pp. 351–359.
17. Barnes, T.M.; Mijaljica, D.; Townley, J.P.; Spada, F.; Harrison, I.P. Vehicles for drug delivery and cosmetic moisturizers: Review and comparison. *Pharmaceutics* **2021**, *13*, 2012.
18. Lopes, L.B.; Garcia, M.T.J.; Lb Bentley, M.V. Chemical penetration enhancers. In *Therapeutic Delivery*; Future Science Ltd.: London, UK, 2015; Volume 6, pp. 1053–1061.
19. Roussel, L.; Gilbert, E.; Pirot, F. Influence of Excipients on Two Elements of the Stratum Corneum Barrier: Intercellular Lipids and Epidermal Tight Junctions. In *Percutaneous Penetration Enhancers Chemical Methods in Penetration Enhancement: Drug Manipulation Strategies and Vehicle Effects*; Springer: Berlin/Heidelberg, Germany, 2015; pp. 69–90. Available online: https://link.springer.com/chapter/10.1007/978-3-662-45013-0_7 (accessed on 27 September 2024)
20. Kopečná, M.; Macháček, M.; Roh, J.; Vávrová, K. Proline, hydroxyproline, and pyrrolidone carboxylic acid derivatives as highly efficient but reversible transdermal permeation enhancers. *Nat. Sci. Rep*. **2022**, *12*, 19495.
21. Dhiman, N.; Awasthi, R.; Sharma, B.; Kharkwal, H.; Kulkarni, G.T. Lipid Nanoparticles as Carriers for Bioactive Delivery. *Front. Chem*. **2021**, *9*, 580118.
22. Kyriakoudi, A.; Spanidi, E.; Mourtzinos, I.; Gardikis, K. Innovative delivery systems loaded with plant bioactive ingredients: Formulation approaches and applications. *Plants* **2021**, *10*, 1238.
23. Safta, D.A.; Bogdan, C.; Moldovan, M.L. Vesicular Nanocarriers for Phytocompounds in Wound Care: Preparation and Characterization. *Pharmaceutics* **2022**, *14*, 991.
24. Assali, M.; Zaid, A.N. Features, applications, and sustainability of lipid nanoparticles in cosmeceuticals. *Saudi Pharm. J.* **2022**, *30*, 53–65.
25. Farasati Far, B.; Naimi-Jamal, M.R.; Sedaghat, M.; Hoseini, A.; Mohammadi, N.; Bodaghi, M. Combinational system of lipid-based nanocarriers and biodegradable polymers for wound Healing: An updated review. *J. Funct. Biomater*. **2023**, *14*, 115.
26. Akombaetwa, N.; Ilangala, A.B.; Thom, L.; Memvanga, P.B.; Witika, B.A.; Buya, A.B. Current Advances in Lipid Nanosystems Intended for Topical and Transdermal Drug Delivery Applications. *Pharmaceutics* **2023**, *15*, 656.
27. Folle, C.; Marqués, A.M.; Díaz-Garrido, N.; Carvajal-Vidal, P.; Sánchez López, E.; Suñer-Carbó, J.; Halbaut, L.; Mallandrich, M.; Espina, M.; Badia, J.; et al. Gel-Dispersed Nanostructured Lipid Carriers Loading Thymol Designed for Dermal Pathologies. *Int. J. Nanomed.* **2024**, *19*, 1225–1248.
28. Sabapati, M.; Palei, N.N.; Ashok, A.K.; Molakpogu, R.B. Solid lipid nanoparticles of Annona muricata fruit extract: Formulation, optimization and in vitro cytotoxicity studies. *Drug Dev. Ind. Pharm*. **2019**, *45*, 577–586.
29. Ryan, A.; Patel, P.; Ratrey, P.; O'Connor, P.M.; O'Sullivan, J.; Ross, R.P.; Hill, C.; Hudson, S.P. The development of a solid lipid nanoparticle (SLN)-based lacticin 3147 hydrogel for the treatment of wound infections. *Drug Deliv. Transl. Res*. **2023**, *13*, 2407–2423.
30. Viegas, C.; Patrício, A.B.; Prata, J.M.; Nadhman, A.; Chintamaneni, P.K.; Fonte, P. Solid Lipid Nanoparticles vs. Nanostructured Lipid Carriers: A comparative review. *Pharmaceutics* **2023**, *15*, 1593.
31. Puglia, C.; Lauro, M.R.; Offerta, A.; Crascì, L.; Micicchè, L.; Panico, A.M.; Bonina, F.; Puglisi, G. Nanostructured lipid carriers (nlc) as vehicles for topical administration of sesamol: In vitro percutaneous absorption study and evaluation of antioxidant activity. *Planta Medica* **2017**, *83*, 398–404.
32. Sun, R.; Zhao, G.; Ni, S.; Xia, Q. Lipid based nanocarriers with different lipid compositions for topical delivery of resveratrol: Comparative analysis of characteristics and performance. *J. Drug Deliv. Sci. Technol*. **2014**, *24*, 591–600.
33. Borges, A.; de Freitas, V.; Mateus, N.; Fernandes, I.; Oliveira, J. Solid lipid nanoparticles as carriers of natural phenolic compounds. *Antioxidants* **2020**, *9*, 998.
34. Fitriani, E.W.; Avanti, C.; Rosana, Y.; Surini, S. Nanostructured lipid carriers: A prospective dermal drug delivery system for natural active ingredients. *Pharmacia* **2024**, *71*, 1–15.
35. Mirchandani, Y.; Patravale, V.B.; Brijesh, S. Solid lipid nanoparticles for hydrophilic drugs. *J. Control. Release* **2021**, *335*, 457–464.
36. Ahmad, A.; Abuzinadah, M.F.; Alkreathy, H.M.; Banaganapalli, B.; Mujeeb, M. Ursolic acid rich Ocimum sanctum L leaf extract loaded nanostructured lipid carriers ameliorate adjuvant induced arthritis in rats by inhibition of COX-1, COX-2, TNF-α and IL-1: Pharmacological and docking studies. *PLoS ONE* **2018**, *13*, e0193451.
37. Puri, D.; Anil, B.; Sharma, P.; Choudhary, D. Lipid nanoparticles (SLN, NLC): A novel approach for cosmetic and dermal pharmaceutical. *J. Global Pharma Technol*. **2010**, *2*, 1–15.

38. Patel, P.; Garala, K.; Singh, S.; Prajapati, B.G.; Chittasupho, C. Lipid-based nanoparticles in delivering bioactive compounds for improving therapeutic efficacy. *Pharmaceuticals* **2024**, *17*, 329.
39. Müller, R.H.; Alexiev, U.; Sinambela, P.; Keck, C.M. Nanostructured lipid carriers (NLC): The second generation of solid lipid nanoparticles. In *Percutaneous Penetration Enhancers Chemical Methods in Penetration Enhancement: Nanocarriers*; Springer: Berlin/Heidelberg, Germany, 2016; pp. 161–185.
40. Jacob, S.; Nair, A.B.; Shah, J.; Gupta, S.; Boddu, S.H.S.; Sreeharsha, N.; Joseph, A.; Shinu, P.; Morsy, M.A. Lipid Nanoparticles as a Promising Drug Delivery Carrier for Topical Ocular Therapy—An Overview on Recent Advances. *Pharmaceutics* **2022**, *14*, 533.
41. Daneshmand, S.; Niazi, M.; Fazeli-Nasab, B.; Asili, J.; Golmohammadzadeh, S.; Sayyed, R.Z. Solid lipid nanoparticles of *Platycladus orientalis* L. possessing 5-alpha reductase inhibiting activity for treating hair Loss and Hirsutism. *J. Med. Plants By-Prod.* **2024**, *13*, 233–246.
42. Xu, L.; Wang, X.; Liu, Y.; Yang, G.; Falconer, R.J.; Zhao, C.X. Lipid nanoparticles for drug delivery. *Adv. Nanobiomed Res.* **2022**, *2*, 2100109.
43. Cordenonsi, L.M.; Santer, A.; Sponchiado, R.M.; Wingert, N.R.; Raffin, R.P.; Schapoval, E.E.S. Amazonia products in novel lipid nanoparticles for fucoxanthin encapsulation. *AAPS PharmSciTech*. **2020**, *21*, 32.
44. Mitri, K.; Shegokar, R.; Gohla, S.; Anselmi, C.; Müller, R.H. Lipid nanocarriers for dermal delivery of lutein: Preparation, characterization, stability and performance. *Int. J. Pharm*. **2011**, *414*, 267–275.
45. Soldati, P.P.; Polonini, H.C.; Paes, C.Q.; Restrepob, J.A.S.; Creczynksi-Pasa, T.B.; Chaves, M.G.A.M.; Brandão, M.A.; Pittella, F.; Raposo, N.R. Controlled release of resveratrol from lipid nanoparticles improves antioxidant effect. *IFAC-PapersOnLine* **2018**, *51*, 16–21.
46. Okonogi, S.; Riangjanapatee, P. Physicochemical characterization of lycopene-loaded nanostructured lipid carrier formulations for topical administration. *Int. J. Pharm*. **2015**, *478*, 726–735.
47. Gad, H.A.; Abd El-Rahman, F.A.A.; Hamdy, G.M. Chamomile oil loaded solid lipid nanoparticles: A naturally formulated remedy to enhance the wound healing. *J. Drug Deliv. Sci. Technol*. **2019**, *50*, 329–338.
48. Ghodrati, M.; Farahpour, M.R.; Hamishehkar, H. Encapsulation of Peppermint essential oil in nanostructured lipid carriers: In-vitro antibacterial activity and accelerative effect on infected wound healing. *Colloids Surf. A Physicochem. Eng. Asp*. **2019**, *564*, 161–169.
49. Navabhatra, A.; Brantner, A.; Yingngam, B. Artificial Neural Network Modeling of Nanostructured Lipid Carriers Containing 5-O-Caffeoylquinic Acid-Rich Cratoxylum formosum Leaf Extract for Skin Application. *Adv. Pharm. Bull*. **2022**, *12*, 801–817.
50. Rahmanian-Devin, P.; Askari, V.R.; Sanei-Far, Z.; Baradaran Rahimi, V.; Kamali, H.; Jaafari, M.R.; Golmohammadzadeh, S. Preparation and characterization of solid lipid nanoparticles encapsulated noscapine and evaluation of its protective effects against imiquimod-induced psoriasis-like skin lesions. *Biomed. Pharmacother.* **2023**, *168*, 115823.
51. Saporito, F.; Sandri, G.; Bonferoni, M.C.; Rossi, S.; Boselli, C.; Cornaglia, A.I.; Ferrari, F. Essential oil-loaded lipid nanoparticles for wound healing. *Int. J. Nanomed.* **2018**, *13*, 175–186.
52. Lacatusu, I.; Istrati, D.; Bordei, N.; Popescu, M.; Seciu, A.M.; Panteli, L.M.; Badea, N. Synergism of plant extract and vegetable oils-based lipid nanocarriers: Emerging trends in development of advanced cosmetic prototype products. *Mater. Sci. Eng. C* **2020**, *108*, 110412.
53. Montenegro, L.; Pasquinucci, L.; Zappalà, A.; Chiechio, S.; Turnaturi, R.; Parenti, C. Rosemary essential oil-loaded lipid nanoparticles: In vivo topical activity from gel vehicles. *Pharmaceutics* **2017**, *9*, 48.
54. Plyduang, T.; Atipairin, A.; Yoon, A.S.; Sermkaew, N.; Sakdiset, P.; Sawatdee, S. Formula development of red palm (*Elaeis guineensis*) fruit extract loaded with solid lipid nanoparticles containing creams and its anti-aging efficacy in healthy volunteers. *Cosmetics* **2022**, *9*, 3.
55. Riangjanapatee, P.; Khongkow, M.; Treetong, A.; Unger, O.; Phungbun, C.; Jaemsai, S.; Bootsiri, C.; Okonogi, S. Development of tea seed oil nanostructured lipid carriers and in vitro studies on their applications in inducing human hair growth. *Pharmaceutics* **2022**, *14*, 984.
56. Chinembiri, T.N.; Gerber, M.; Du Plessis, L.H.; Du Preez, J.L.; Hamman, J.H.; Du Plessis, J. Topical delivery of Withania somnifera crude extracts in niosomes and solid lipid nanoparticles. *Pharmacogn. Mag*. **2017**, *13*, S663–S671.
57. Rodrigues, L.R.; Jose, J. Exploring the photo protective potential of solid lipid nanoparticle-based sunscreen cream containing Aloe vera. *Environ. Sci. Pollut. Res.* **2020**, *27*, 20876–20888.
58. Martins, R.M.; de Siqueira Martins, S.; Barbosa, G.L.F.; Fonseca, M.J.V.; Rochette, P.J.; Moulin, V.J.; de Freitas, L.A.P. Photoprotective effect of solid lipid nanoparticles of rutin against UVB radiation damage on skin biopsies and tissue-engineered skin. *J. Microencapsul*. **2022**, *39*, 668–679.
59. Daneshmand, S.; Jaafari, M.R.; Movaffagh, J.; Malaekeh-Nikouei, B.; Iranshahi, M.; Seyedian Moghaddam, A.; Najaran, Z.T.; Golmohammadzadeh, S. Preparation, characterization, and optimization of auraptene-loaded solid lipid nanoparticles as a natural anti-inflammatory agent: In vivo and in vitro evaluations. *Colloids Surf B Biointerfaces* **2018**, *164*, 332–339.
60. Kakkar, V.; Kaur, I.P.; Kaur, A.P.; Saini, K.; Singh, K.K. Topical delivery of tetrahydrocurcumin lipid nanoparticles effectively inhibits skin inflammation: In vitro and in vivo study. *Drug Dev. Ind. Pharm*. **2018**, *44*, 1701–1712.
61. Zamarioli, C.M.; Martins, R.M.; Carvalho, E.C.; Freitas, L.A.P. Nanoparticles containing curcuminoids (*Curcuma longa*): Development of topical delivery formulation. *Rev. Bras. De Farmacogn.* **2015**, *25*, 53–60.
62. Shrotriya, S.; Ranpise, N.; Satpute, P.; Vidhate, B. Skin targeting of curcumin solid lipid nanoparticles-engrossed topical gel for the treatment of pigmentation and irritant contact dermatitis. *Artif. Cells Nanomed. Biotechnol*. **2018**, *46*, 1471–1482.

63. Carneiro, S.B.; Kreutz, T.; Limberger, R.P.; Teixeira, H.F.; da Veiga Júnior, V.F.; Koester, L.S. Piper aduncum essential oil rich in dillapiole: Development of hydrogel-thickened nanoemulsion and nanostructured lipid carrier intended for skin delivery. *Pharmaceutics* **2022**, *14*, 1–20.
64. de Araújo, G.M.S.; Loureiro, A.I.S.; Rodrigues, J.L.; Barros, P.A.B.; Halicki, P.C.B.; Ramos, D.F.; Marinho, M.A.G.; Vaiss, D.P.; Vaz, G.R.; Yurgel, V.C.; et al. Toward a platform for the treatment of burns: An assessment of nanoemulsions vs. nanostructured lipid carriers loaded with curcumin. *Biomedicines* **2023**, *11*, 3348.
65. Iriventi, P.; Gupta, N.v. Topical delivery of curcumin and caffeine mixture-loaded nanostructured lipid carriers for effective treatment of psoriasis. *Pharmacogn. Mag*. **2020**, *16*, 206.
66. Gonçalves, C.; Ramalho, M.J.; Silva, R.; Silva, V.; Marques-Oliveira, R.; Silva, A.C.; Pereira, M.C.; Loureiro, J.A. Lipid nanoparticles containing mixtures of antioxidants to improve skin care and cancer prevention. *Pharmaceutics* **2021**, *13*, 2042.
67. Kim, M.H.; Jeon, Y.E.; Kang, S.; Lee, J.Y.; Lee, K.W.; Kim, K.T.; Kim, D.-D. Lipid nanoparticles for enhancing the physicochemical stability and topical skin delivery of orobol. *Pharmaceutics* **2020**, *12*, 845.
68. Kasprzak-Drozd, K.; Niziński, P.; Hawrył, A.; Gancarz, M.; Hawrył, D.; Oliwa, W.; Pałka, M.; Markowska, J.; Oniszczuk, A. Potential of curcumin in the management of skin diseases. *Int. J. Mol. Sci*. **2024**, *25*, 3617.
69. Maupas, C.; Moulari, B.; Béduneau, A.; Lamprecht, A.; Pellequer, Y. Surfactant dependent toxicity of lipid nanocapsules in HaCaT cells. *Int. J. Pharm*. **2011**, *411*, 136–141.
70. Szwed, M.; Torgersen, M.L.; Kumari, R.V.; Yadava, S.K.; Pust, S.; Iversen, T.G.; Skotland, T.; Giri, J.; Sandvig, K. Biological response and cytotoxicity induced by lipid nanocapsules. *J. Nanobiotechnology* **2020**, *18*, 5.
71. Badawi, N.M.; Hteaima, M.H.; El-Say, K.M.; Aattia, D.A.; Ael-Nabarawi, M.A.; Elmazar, M.M. Pomegranate extract-loaded solid lipid nanoparticles: Design, optimization, and in vitro cytotoxicity study. *Int. J. Nanomed.* **2018**, *13*, 1313–1326.
72. Safta, D.A.; Ielciu, I.; Șuștic, R.; Hanganu, D.; Niculae, M.; Cenariu, M.; Tomuță, I. Chemical Profile and Biological Effects of an Herbal Mixture for the Development of an Oil-in-Water Cream. Plants **2023**, *12*, 248.
73. Jose, J.; Netto, G. Role of solid lipid nanoparticles as photoprotective agents in cosmetics. *J. Cosmet. Dermatol*. **2019**, *18*, 315–321. Available online: https://pubmed.ncbi.nlm.nih.gov/29441672/ (accessed on 27 September 2024).
74. Pardeike, J.; Schwabe, K.; Müller, R.H. Influence of nanostructured lipid carriers (NLC) on the physical properties of the Cutanova Nanorepair Q10 cream and the in vivo skin hydration effect. *Int. J. Pharm*. **2010**, *396*, 166–173.
75. Preparation and Application of Multi-Repeat-Matching Nano-Structure Lipid Carrier [Internet]. CN116139025A. Available online: https://worldwide.espacenet.com/patent/search/family/086360620/publication/CN116139025A?q=pn%3DCN116139025A (accessed on 13 August 2024).
76. Solid Lipid Nanometer Particle for Astaxanthin and Preparation Method of Solid Lipid Nanometer Particle [Internet]. CN104257632A. Available online: https://worldwide.espacenet.com/patent/search/family/052149294/publication/CN104257632A?q=pn%3DCN104257632A (accessed on 13 August 2024).
77. Solid Lipid Nanoparticles of Curcumin [Internet]. US2022151945A1. Available online: https://worldwide.espacenet.com/patent/search/family/070852435/publication/US2022151945A1?q=pn%3DUS2022151945A1 (accessed on 13 August 2024).
78. Nanotechnology-Based Delivery System of Bergamot Essential Oil, Method of Preparation of the System and Uses Thereof [Internet]. US2022265565A1. Available online: https://worldwide.espacenet.com/patent/search/family/068733546/publication/US2022265565A1?q=pn%3DUS2022265565A1 (accessed on 13 August 2024).
79. Whitening and Acne-Removing Cosmetic and Preparation Process Thereof [Internet]. CN116211777A. Available online: https://worldwide.espacenet.com/patent/search/family/086589507/publication/CN116211777A?q=pn%3DCN116211777A (accessed on 13 August 2024).
80. Topical Lipolysis Compositions and Methods—Google Patents [Internet]. CA2872279A1. Available online: https://patents.google.com/patent/CA2872279A1/en?q=(nanostructured+lipid+carriers+for+skin+delivery)&oq=nanostructured+lipid+carriers+for+skin+delivery (accessed on 13 August 2024).
81. Nanostructured Lipid Carrier, Use of the Nanostructured Lipid Carrier, Photoprotective Composition and Method for Skin Photoprotection [Internet]. WO2023137532A1. Available online: https://worldwide.espacenet.com/patent/search/family/087347490/publication/WO2023137532A1?q=pn%3DWO2023137532A1 (accessed on 13 August 2024).
82. Hair Modification Composition and Method Thereof—Google Patents [Internet]. JP7377813B2. Available online: https://patents.google.com/patent/JP7377813B2/en?q=(nanostructured+lipid+carriers)&oq=nanostructured+lipid+carriers (accessed on 13 August 2024).
83. pH—pH-Responsive Capsosome Using Chitosan-Coated Solid Lipid Nanoparticles as Core [Internet]. KR102577778B1. Available online: https://worldwide.espacenet.com/patent/search/family/082396913/publication/KR102577778B1?q=pn%3DKR102577778B1 (accessed on 13 August 2024).
84. Mucoadhesive Dispersion Nanoparticle System and Method for Production the Same [Internet]. US2021353553A1. Available online: https://worldwide.espacenet.com/patent/search/family/063857975/publication/US2021353553A1?q=pn%3DUS2021353553A1 (accessed on 13 August 2024).
85. MHY498 Solid Lipid Nanoparticles Composition for Skin-Whitening Effect Comprising MHY498 and Preparation Method Thereof [Internet]. KR101860555B1. Available online: https://worldwide.espacenet.com/patent/search/family/061900412/publication/KR101860555B1?q=pn%3DKR101860555B1 (accessed on 13 August 2024).

86. Compounds Useful in the Treatment and/or Care of Skin, Hair, Nails and/or Mucous Membranes [Internet]. JP7010823B2. Available online: https://patents.google.com/patent/JP7010823B2/en?q=(nanostructured+lipid+carriers+skin)&oq=nanostructured+lipid+carriers+skin+ (accessed on 13 August 2024).
87. Solid Lipid Nanoparticle for Intracellular Release of Active Substances and Method for Production the Same [Internet]. US2021069121A1. Available online: https://worldwide.espacenet.com/patent/search/family/060937800/publication/US2021069121A1?q=pn%3DUS2021069121A1 (accessed on 13 August 2024).
88. Lipid-Protein Nanocomposites Comprising Ginsenoside and Use Thereof [Internet]. KR20200094871A. Available online: https://worldwide.espacenet.com/patent/search/family/072049304/publication/KR20200094871A?q=pn%3DKR20200094871A (accessed on 13 August 2024).
89. Pigment-Loaded Solid Lipid Nanoparticles [Internet]. CN111988999A. Available online: https://worldwide.espacenet.com/patent/search/family/062152298/publication/CN111988999A?q=pn%3DCN111988999A (accessed on 13 August 2024).
90. Positive Charge Modified Solid Lipid Nanoparticle and Preparation Method Thereof [Internet]. CN112691044A. Available online: https://worldwide.espacenet.com/patent/search/family/075504579/publication/CN112691044A?q=pn%3DCN112691044A (accessed on 13 August 2024).
91. Whitening Acid Nanostructure Lipid Carrier as well as Preparation Method and Application Thereof [Internet]. CN110974712A. Available online: https://worldwide.espacenet.com/patent/search/family/070077776/publication/CN110974712A?q=pn%3DCN110974712A (accessed on 13 August 2024).
92. Phenylethyl Resorcinol Nanostructure Lipid Carrier, Preparation Method and Application in Cosmetics [Internet]. CN114515258A. Available online: https://worldwide.espacenet.com/patent/search/family/081594908/publication/CN114515258A?q=pn%3DCN114515258A (accessed on 13 August 2024).
93. Particle Containing Lipid Nanoparticles, and Method for Producing Same—Google Patents [Internet]. EP4169509A1. Available online: https://patents.google.com/patent/EP4169509A1/ja (accessed on 13 August 2024).
94. Method for Preparing Nanosystems—Google Patents [Internet]. WO2022112527A1. Available online: https://patents.google.com/patent/WO2022112527A1/en (accessed on 13 August 2024).
95. Preparation Method of Water-in-Oil Emulsion Gel Based on Diglyceride Solid Lipid Nanoparticles [Internet]. CN112868816A. Available online: https://worldwide.espacenet.com/patent/search/family/076051915/publication/CN112868816A?q=pn%3DCN112868816A (accessed on 13 August 2024).
96. Mist Spray Container Bottle with Nanostructured Lipid Carrier Suspension [Internet]. TWM639079U. Available online: https://worldwide.espacenet.com/patent/search/family/086943529/publication/TWM639079U?q=pn%3DTWM639079U (accessed on 13 August 2024).
97. Face Cream Composition Containing Lipid Nanoparticles with Moisturizing and Hydrating Effects and Preparation Method Thereof [Internet]. CN113876642A. Available online: https://worldwide.espacenet.com/patent/search/family/079017962/publication/CN113876642A?q=pn%3DCN113876642A (accessed on 13 August 2024).
98. 4- Solid Lipid Nanoparticles Comprising 4-Alkylresorcinol Cosmetic Composition and Cosmetics Comprising the Same [Internet]. KR20230149537A. Available online: https://worldwide.espacenet.com/patent/search/family/088514246/publication/KR20230149537A?q=pn%3DKR20230149537A (accessed on 13 August 2024).
99. Azelaic Acid Nano Lipid Particle, Freeze-Dried Powder, Preparation Method and Application [Internet]. CN115517988A. Available online: https://worldwide.espacenet.com/patent/search/family/084702246/publication/CN115517988A?q=pn%3DCN115517988A (accessed on 13 August 2024).
100. Anti-Aging Solid Lipid Nanoparticle Emulsion and Preparation Method Thereof [Internet]. CN116327662A. Available online: https://worldwide.espacenet.com/patent/search/family/086889668/publication/CN116327662A?q=pn%3DCN116327662A (accessed on 13 August 2024).
101. Preparation Method and Application of Diglyceride Nanostructure Lipid Carrier Hydrogel [Internet]. CN116725918A. Available online: https://worldwide.espacenet.com/patent/search/family/087908965/publication/CN116725918A?q=pn%3DCN116725918A (accessed on 13 August 2024).
102. Ceramide Lipid Nanoparticles as well as Preparation Method and Application Thereof [Internet]. CN117137825A. Available online: https://worldwide.espacenet.com/patent/search/family/088885206/publication/CN117137825A?q=pn%3DCN117137825A (accessed on 13 August 2024).
103. Chitosan Interface Modified Ellagic Acid Nanostructure Lipid Carrier and Preparation Method Thereof [Internet]. CN117398294A. Available online: https://worldwide.espacenet.com/patent/search/family/089486458/publication/CN117398294A?q=pn%3DCN117398294A (accessed on 13 August 2024).
104. Lipid Nanoparticles as Active Molecule Carriers in Ophthalmic, Dermatological, and/or Cosmetic Applications, and Process for Production Thereof [Internet]. WO2024102798A1. Available online: https://worldwide.espacenet.com/patent/search/family/090220679/publication/WO2024102798A1?q=pn%3DWO2024102798A1 (accessed on 13 August 2024).

Disclaimer/Publisher's Note: The statements, opinions and data contained in all publications are solely those of the individual author(s) and contributor(s) and not of MDPI and/or the editor(s). MDPI and/or the editor(s) disclaim responsibility for any injury to people or property resulting from any ideas, methods, instructions or products referred to in the content.

pharmaceutics

MDPI

Review

Marine Macroalgae in Topical Formulations: Bioactive Compounds, Variability, Analytical Challenges and Skin Benefits

Cătălina Bogdan [1,2], Mara Molnar [1], Elena Ines Dima [3,*], Andreea Alexandra Olteanu [4], Diana Antonia Safta [1] and Mirela-Liliana Moldovan [1]

[1] Department of Dermopharmacy and Cosmetics, Faculty of Pharmacy, "Iuliu Haţieganu" University of Medicine and Pharmacy, 12 I. Creangă St., 400010 Cluj-Napoca, Romania; catalina.bogdan@umfcluj.ro (C.B.); pop.molnar.mara@elearn.umfcluj.ro (M.M.); diana.an.safta@elearn.umfcluj.ro (D.A.S.); mmoldovan@umfcluj.ro (M.-L.M.)
[2] Department of Nutrition and Medical Cosmetics, Faculty of Nursing and Health Sciences, "Iuliu Haţieganu" University of Medicine and Pharmacy, 12 I. Creangă St., 400010 Cluj-Napoca, Romania
[3] Department of Toxicology, Faculty of Pharmacy, "Carol Davila" University of Medicine and Pharmacy, 6 Traian Vuia St., 020956 Bucharest, Romania
[4] Department of Analytical Chemistry, Faculty of Pharmacy, "Carol Davila" University of Medicine and Pharmacy, 6 Traian Vuia St., 020956 Bucharest, Romania; andreea.olteanu@umfcd.ro
* Correspondence: elena.dima@umfcd.ro

Abstract

Marine macroalgae, classified into three major groups, brown (Phaeophyceae), red (Rhodophyta), and green (Chlorophyta), represent a source of structurally diverse compounds relevant for topical applications. This narrative review of the peer-reviewed literature and regulatory databases targets macroalgae-derived active ingredients in cosmetic formulations and in wound-healing applications. It outlines major compound classes (polyphenols, sulfated polysaccharides, carotenoids, fatty acids, and peptides), along with their documented biological effects on skin (antioxidant, anti-inflammatory, moisturizing, photoprotective, and anti-aging activity) and regulatory/safety aspects with formulation strategies. This review also addresses the variability in compound concentrations resulting from species, environmental conditions, and seasonal factors, which impacts reproducibility and standardization. Common extraction techniques like solvent extraction, ultrasound-assisted extraction, supercritical fluid extraction, and enzyme-assisted methods are described in relation to compound class and yield. Analytical methods used for the identification and quantification of these compounds, including HPLC, GC-MS, and FTIR, are then summarized. Additionally, recent in vitro and in vivo studies evaluating the bioactivity and safety of macroalgae-derived ingredients are discussed. This review compiles relevant evidence to inform formulation strategies and ingredient evaluation in the context of marine-based topical products.

Keywords: macroalgae extracts; macroalgal bioactives; skin health; environmental influence; extraction methods; quantitative analysis; algae-based topical formulations; cosmetics; wound healing

check for updates

Academic Editors: Carolina Martinez and María Jimena Prieto

Received: 29 July 2025
Revised: 23 August 2025
Accepted: 28 August 2025
Published: 31 August 2025

Citation: Bogdan, C.; Molnar, M.; Dima, E.I.; Olteanu, A.A.; Safta, D.A.; Moldovan, M.-L. Marine Macroalgae in Topical Formulations: Bioactive Compounds, Variability, Analytical Challenges and Skin Benefits. *Pharmaceutics* **2025**, *17*, 1143. https://doi.org/10.3390/pharmaceutics17091143

Copyright: © 2025 by the authors. Licensee MDPI, Basel, Switzerland. This article is an open access article distributed under the terms and conditions of the Creative Commons Attribution (CC BY) license (https://creativecommons.org/licenses/by/4.0/).

1. Introduction

In recent years, there has been an important increase in consumer interest in natural-based cosmetic products, especially for the valorization of natural origin ingredients. In this context, the European Green Deal represents a priority of the European Union, supporting the critical role of sustainable products and technologies in reaching climate

neutrality by 2050. Achieving this objective will require the active involvement of all industrial sectors, including the cosmetic industry, which are expected to contribute significantly across their entire value chains. One of the main goals of this sustainability-driven approach is to promote the responsible and efficient use of natural resources. Among these, marine-derived ingredients, especially algae, represent a valuable source of cosmetic ingredients due to their rich content of bioactive compounds [1]. To date, numerous studies have described various applications of algal compounds, which are mainly due to their biochemical variety, sustainability and availability. Despite these advantages, only a limited number of studies have systematically presented this information. This review focuses specifically on macroalgae by presenting the extraction challenges of bioactive compounds, the environmental variability in their chemical composition, the quantitative analysis of bioactives, and their applications in skin health. To establish this context, general insights about biochemical diversity and classification that provide the framework for understanding dermatological applications of the macroalgal compounds are also presented.

Algae can be either prokaryotic or eukaryotic and display a wide range of forms and structures; structurally, they are divided into unicellular (microalgae) or multicellular (macroalgae) organisms. Over a period of 2.45 billion years, algae have evolved specific features that enable them to thrive in harsh and competitive environments, including the synthesis of a variety of biologically active molecules and secondary metabolites, with protective and adaptive functions in diverse ecosystems [2]. The biochemical diversity of algae represents a sustainable and potent resource for innovative cosmetic products [3]. Structurally, algae's cell walls are mainly made of cellulose, hemicellulose, mucilage and pectin, while brown and red algae are rich in polysaccharides such as alginic acid, fucoidan and fucan. Photosynthetic pigments, particularly chlorophyll a and chlorophyll b, are involved in energy conversion, generating oxygen and various sugars, mainly glucose, which are further converted to starch and biomass. Another important characteristic is that algae are very resilient to extreme environmental conditions such as extreme pH levels, temperatures, osmotic stress, salinity, ultraviolet radiation, and low-oxygen conditions. In these difficult environmental conditions, algae produce metabolites such as carotenoids (lutein and zeaxanthin), vitamin E, and fatty acids like oleic acids, which protect their cellular structures. Additionally, under severe stress conditions, they synthesize secondary compounds with antimicrobial properties effective against fungi and viruses [4]. The biochemical diversity of compounds found in algae is estimated as ten times higher than that of terrestrial plants and their flavonoid profile is completely different than that of terrestrial plants [5]. The resilience of algae, together with their diverse range of bioactive compounds, demonstrates their potential in cosmetic and dermatological formulations, providing antioxidant, antibacterial, and skin-revitalizing characteristics for novel applications.

One of the earliest systematic efforts to categorize algae was made by W. H. Harvey, who played an important role in the classification of algae. Since his contributions, a variety of classifications were proposed, incorporating morphological and physiological parameters, and biochemical or molecular characteristics [6].

Beginning in the 1830s, algae were divided into main groups based on their chromatic distinctions (red, brown, and green), which correspond to different pigments found in chloroplasts, including phycobiliproteins, carotenoids, and chlorophylls. These categories reflect chromatic differences but also metabolic profiles that influence their bioactive potential. This classification led to the description of major algal classes: Phaeophyceae (brown algae), Rhodophyceae (red algae), and Chlorophyceae (green algae). Overall, it is estimated that approximately 59% of known algal species are brown, and red algae comprise

about 40%, while green algae represent less than 1%. In 1989, Robert E. Lee proposed a classification system for algae based on the evolution of the chloroplast, dividing them into 4 groups and further into 15 divisions (*phyta*). The revised system, updated in 2008, reflects advancements in phycological research and taxonomy. Modern approaches also integrate morphological and molecular characteristics, including pigment composition (e.g., phycocyanin), genetic markers, fatty acid profiles, and secondary metabolite profiles, as well as biophysical parameters derived from diffraction patterns, light scattering, and fluorescence measurements [7].

2. Sources of Macroalgal Bioactives

Because most of the algae used in skin products come from the groups Phaeophyceae (brown algae), Chlorophyceae (green algae), Rhodophyceae (red algae), this section highlights the most important species from these groups, focusing on their specific compounds and effects on skin health. The incorporation of numerous algal species into topical formulations reflects their biochemical diversity, each addressing dermatological needs.

2.1. Phaeophyceae (Brown Algae) as Sources of Bioactive Compounds

Laminaria, one of the best-known genera, belongs to the brown algae group, which are distinguished by their high quantities of iodine, alginic acid, laminarin, potassium, and other active compounds. Oily extracts obtained from *Laminaria ochroleuca*, *Laminaria cloustoni* and *Laminaria digitata* have demonstrated protective effects against photoallergic reactions and enhance cellular metabolism. Aqueous extracts derived from *Laminaria saccharina and Laminaria hyperborea* possess anti-seborrheic properties, which are useful for oily skin. Rich in iodine, these brown algae enhance lipase activity, this effect making them valuable components in anti-cellulite cosmetic products. *Laminaria digitata* is particularly rich in proline, lysine, and glycine (constituents also found in human elastin), which makes its extracts useful to be incorporated in hair conditioners and products for improving skin elasticity. All species are characterized by a greenish brown trisected thallus. Among them, *Fucus vesiculosus* is the most frequently used species in the cosmetic industry, followed by *Fucus spiralis* and *Fucus serratus*. These species have a high content in iodine, zinc, laminarin, magnesium, manganese, and vitamin C. *Fucus vesiculosus* is often used in products for photoprotection. Moreover, this genus is also an excellent source of bioactive compounds such as fucoidans, phlorotannins and fucoxanthin, compounds with documented potential in a wide spectrum of conditions. Another species of brown algae used in cosmetic formulations is *Pylaiella*, which grows in the cold sea regions. It is extracted from the species *Pylaiella littoralis*, *Pylaiella ochotensis*, *Pylaiella flexilis*, *and Pylaiella seriata. Pylaiella* is rich in alginic acid, mannitol, laminarin, fucoidan, vitamins, polysaccharides; this extract has moisturizing and antioxidant effects, and skin renewal and skin metabolism stimulation, which will be further detailed in Section 8 [8].

Table 1 summarizes examples of cosmetic ingredients derived from brown algae, showing the industrial and formulation potential of brown algal bioactives. As can be observed, many extracts from *Laminaria* spp. are employed as humectants and skin conditioning agents, while various extracts from *Fucus* spp. have emollient, soothing, and skin-protecting functions. Additionally, genera such as *Ascophyllum nodosum*, *Hizikia fusiforme*, *Lessonia nigrescens*, and *Saccharina japonica* provide skin conditioning and protective effects in cosmetic formulations.

Table 1. Examples of cosmetic ingredients obtained from brown algae [9].

INCI Name/Description	Function
Fucoidan (Sulfated polysaccharide)	Antioxidant Skin conditioning
Fucoxanthin (Carotenoid from *Sargassum siliquastrum*)	Skin conditioning
Sargachromanol F (Chromene from *Sargassum siliquastrum*)	Skin conditioning
Sargachromanol D (Chromene from *Sargassum siliquastrum*)	Skin conditioning
Sargachromanol E (Chromene from *Sargassum siliquastrum*)	Skin conditioning
Sargassum filipendula extract	Skin protecting
Sargassum fusiforme extract	Skin protecting
Pylaiella littoralis extract (Extract of the whole plant)	Skin protecting
Laminaria longissima extract	Humectant
Laminaria digitata extract	Skin protecting
Laminaria diabolica extract	Humectant Skin conditioning
Laminaria hyperborea extract	Skin protecting
Laminaria ochroleuca extract	Skin conditioning
Laminaria cloustoni extract (Kelp extract)	Skin protecting
Laminaria saccharina extract (Extract of the thallus of *Laminaria saccharina*)	Skin protecting
Laminaria japonica extract (Extract of the Japan kelp/seaweed, *Laminaria japonica*)	Skin protecting
Deaminated *Laminaria japonica* extract (Extract of *Laminaria japonica* extract enzymatically deaminated)	Skin conditioning
Laminaria digitata powder (Powder from the dried and ground thallus of *Laminaria digitata*)	Skin conditioning
Laminaria japonica powder (Powder from the dried and ground alga of *Laminaria japonica*)	Skin conditioning
Laminaria digitata water (Aqueous solution of the steam distillate obtained from *Laminaria digitata*)	Skin protecting Skin conditioning
Fucus vesiculosus (The algae *Fucus vesiculosus*, Fucaceae)	Skin conditioning
Fucus spiralis extract	Skin conditioning—emollient
Fucus serratus extract	Skin protecting
Fucus vesiculosus extract (Extract of the dried thallus of the Bladderwrack, *Fucus vesiculosus* L., Fucaceae)	Skin conditioning—emollient Smoothing Soothing
Fucus vesiculosus powder (Powder obtained from Bladderwrack, *Fucus vesiculosus* L., Fucaceae)	Skin conditioning
Fucus crispus thalle extract (Extract from the dried thallus of *Fucus crispus*, Fucaceae)	Perfuming
Hydrolyzed *Fucus vesiculosus* extract (Hydrolyzed iodinated extract from the Bladderwrack, *Fucus vesiculosus* L., Fucaceae)	Skin conditioning Smoothing Soothing
Fucus crispus thalle oil/(Essential oil from the dried thallus of *Fucus crispus*, Fucaceae)	Perfuming

Table 1. *Cont.*

INCI Name/Description	Function
Fucus vesiculosus thale oil (Essential oil obtained from the dried thallus of the Bladderwrack, *Fucus vesiculosus* L., Fucaceae)	Perfuming
Hydrolyzed *Fucus vesiculosus* protein(Hydrolysate of the protein obtained from the Bladderwrack, *Fucus vesiculosus* L., Furaceae, derived by acid, enzyme or other methods of hydrolysis)	Skin conditioning
Macrocystis pyrifera extract	Skin conditioning
Macrocystis pyrifera juice(Juice expressed from the whole plant)	Skin conditioning
Macrocystis pyrifera protein (Protein from the Giant Kelp, *Macrocystis pyrifera* L., Lessoniaceae)	Skin conditioning
Macrocystis pyrifera	Viscosity controlling
Kelp sulfated oligosaccharides (Obtained from the seaweed kelp (*Macrocystis pyrifera*, Lessoniaceae) hydrolysate)	Hair conditioning
Sargassum horneri powder (Powder from the dried and ground *Sargassum horneri*)	Humectant Skin conditioning—humectant
Sargassum fulvellum extract	Skin conditioning
Sargassum macrocarpum extract	Skin conditioning—emollient
Sargassum aquifolium extract	Skin conditioning—miscellaneous
Sargassum ilicifolium extract	Skin conditioning—miscellaneous
Sargassum oligocystum extract	Skin conditioning—humectant
Sargassum hemiphyllum extract	Antioxidant Skin protecting Skin conditioning—miscellaneous
Sargassum yezoense extract	Antimicrobial
Sargassum serratifolium extract	Antioxidant
Sargassum vulgare extract	Skin conditioning
Sargassum muticum extract	Skin protecting
Sargassum glaucescens extract	Antioxidant
Sargassum thunbergii extract	Antimicrobial
Sargassum siliquastrum extract	Skin conditioning
Sargassum fusiforme extract	Skin protecting
Sargassum pacificum thallus extract	Skin conditioning—emollient
Sargassum fluitans/Natans extract	Emulsion stabilizing
Hydrolyzed *Sargassum horneri* extract/Hydrolysate of *Sargassum horneri* extract derived by acid, enzyme, or other methods of hydrolysis)	Skin conditioning—miscellaneous
Hydrolyzed *Sargassum thunbergii* extract (Hydrolysate of *Sargassum thunbergii extract* derived by acid, enzyme or other methods of hydrolysis)	Antimicrobial Hair conditioning Humectant Skin protecting Skin conditioning—humectant
Ecklonia/Laminaria extract (Extract of mixture of *Ecklonia* and *Laminaria* algae)	Skin conditioning
Ascophyllum nodosum/*Fucus vesiculosus* extract	Humectant Skin conditioning

Table 1. *Cont.*

INCI Name/Description	Function
Ascophyllum nodosum/*Fucus vesiculosus*/*Laminaria cloustoni*/*Laminaria digitata* extract	Skin conditioning—emollient
Ascophyllum nodosum/*Fucus vesiculosus*/*Hizikia fusiforme*/*Kjellmaniella gyrata*/*Lessonia nigrescens*/*Saccharina angustata*/*Saccharina japonica*/*Undaria pinnatifida* extract	Skin conditioning

2.2. Chlorophyceae (Green Algae) as Sources of Bioactive Compounds

Species from the *Ulva* genus are among the most used green macroalgae in the cosmetic industry. These algae can have two different morphological forms: one with blistered thallus characteristic to adult thalli, and another with corrugated thalli typical of juvenile organisms. Among them, *Ulva lactuca* is the most frequently used alga in the cosmetic industry. This species contains vitamins A, B, C, E, magnesium, iron and aosaine, a protein that contains the same amino acids as human elastin (glycine, proline, lysine) and that is used in cosmetic formulations targeting aging-skin problems like wrinkles and reduced firmness [8]. *Ulva* extracts and their hydrolyzed derivatives, such as *Ulva lactuca*, *Ulva linza*, and *Ulva australis*, are officially recognized for functions like skin conditioning, emollient, and humectant activities, as shown in Table 2.

Table 2. Examples of cosmetic ingredients obtained from green algae [9].

INCI Name/Description	Function
Cladophora wrightiana extract	Skin conditioning
Ulva australis extract	Skin conditioning—emollient
Ulva rigida extract	Skin conditioning
Ulva linza extract	Skin conditioning—emollient
Ulva lactuca extract	Skin conditioning Skin protecting
Ulva ramulosa callus culture extract	Skin conditioning
Ulva lactuca powder (Powder obtained from dried and ground *Ulva lactuca*, Cyperaceae)	Absorbent Binding Viscosity controlling
Hydrolyzed *Ulva pertusa* extract (Hydrolysate of *Ulva pertusa* extract derived by acid, enzyme or other methods of hydrolysis)	Skin conditioning
Hydrolyzed *Ulva lactuca* extract (Hydrolysate of *Ulva lactuca* extract derived by acid, enzyme or other methods of hydrolysis)	Skin conditioning
Hydrolyzed *Ulva linza* leaf extract (Hydrolysate of *Ulva linza* extract derived by acid, enzyme or other methods of hydrolysis)	Skin conditioning—emollient Skin conditioning—humectant

Another relevant genus for skin applications is *Cladophora* which grows in marine and freshwater environments, but it mostly grows in warm seas. The thallus of these algae is identified by its threadlike appearance and extensive branching; the cell walls are occasionally coated with calcium compounds. These algae contain siphonoxanthin, a rare carotenoid pigment. The most relevant species from this genus are *Cladophora glomerata*, *C. brasiliana*, *C. columbiana*, *C. dalmatica*, *C. fracta* and *Aegagropila linnaei.* Particularly, the extract from *C. glomerata* is widely used in cosmetic formulation. The extracts from *C. glomerata* contain high concentrations of phenolic and polyphenolic compounds that are responsible for its strong antioxidant action. Additionally, this species has demonstrated

antimicrobial activity against several bacterial strains, such as *Bacillus subtilis*, *Proteus mirabilis*, and *Staphylococcus aureus* [10].

2.3. Rhodophyceae (Red Algae) as Sources of Bioactive Compounds

The phylum Rhodophyta, comprising more than 6000 species, exhibits a wide range of morphological characteristics, including filamentous, branched, feathered, and sheet-like thalli. In recent years, red algae have begun to be used in cosmetic applications due to their bioactive potential. Species from the genus *Ceramium* contain high ratios of amino acids, proteins, vitamins, mineral salts, and agar. Among them, *Ceramium rubrum* is frequently used in body care products. Extracts from *Ceramium rubrum* and *Ceramium kondoi* are employed in body and skin care products, as humectants, emollients, and skin conditioning agents, as summarized in Table 3. Furthermore, extracts from these algae have been shown to have antimicrobial activity. Furthermore, *Polysiphonia* sp. shows potential in cosmetic applications due to its strong antioxidant activity demonstrated by FRAP assay, which may support activity related to age-related skin problems [2,8,11].

In conclusion, green, brown, and red algae are valuable sources of bioactive compounds with a wide range of applications in skin health, which will be further explored in the following sections. Each algal group offers specific benefits, including moisturizing, antioxidant, anti-inflammatory and antibacterial effects, which justify their growing use in modern topical formulations adapted to various dermatological needs. These skin health benefits of the main algal groups are summarized in Figure 1. The following sections will provide an in-depth overview of the key active compounds, extraction and quantification methods, as well as the influence of environmental factors on the quality and efficacy of algal-derived ingredients.

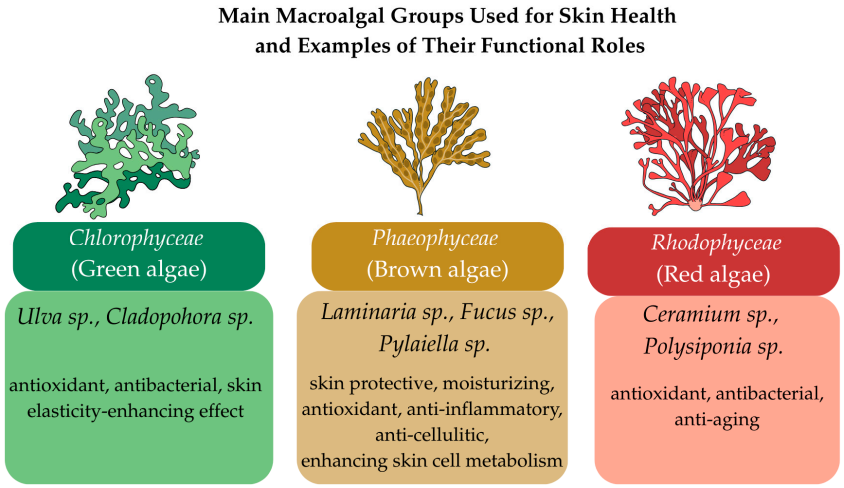


Figure 1. Overview of the main macroalgal groups and species used in skin health and their functional roles (image created using Canva.com, accessed on 23 May 2025).

Table 3. Examples of cosmetic ingredients obtained from red algae [9].

INCI Name/Description	Function
Ceramium kondoi extract	Humectant Skin conditioning
Ceramium rubrum extract	Skin conditioning—emollient Humectant Skin conditioning
Polysiphonia brodiei extract	Skin conditioning

Table 3. *Cont.*

INCI Name/Description	Function
Polysiphonia lanosa extract	Skin conditioning
Polysiphonia elongata extract	Humectant Skin conditioning
Polysiphonia morrowii extract	Antioxidant

3. Macroalgal Bioactives

Particular interest has been directed to the active compounds originating in algae, as their proven antioxidant, anti-inflammatory, moisturizing, and anti-aging effects made them relevant to the cosmetic industry, but also for other applications such as wound care. The main compoundsinclude polysaccharides, pigments (chlorophylls, carotenoids) or structures such as mycosporine-like amino acids (MAAs). Nowadays, there are many categories of skincare products formulated with different algae-derived ingredients with various roles, such as moisturizers, anti-wrinkle agents, texture-enhancing agents, and sunscreens [12].

3.1. Polysaccharides

Polysaccharides are large, water-soluble carbohydrates composed of long chains of monosaccharide units connected by glycosidic bonds. Polysaccharides are the most notable compounds found in algae, each type of seaweed being correlated with a specific qualitative and quantitative profile of these macromolecules: alginate, laminarin and fucoidan being predominant in Phaeophyta, agar and carrageenan in Rhodophyta, and ulvan in Chlorophyta. Within the latter, *Ulva* can contain up to 65% polysaccharides (dry weight). Other genera rich in polysaccharide are *Ascophyllum*, *Porphyra*, and *Palmaria* [12].

3.1.1. Alginates

Alginates are predominant in Phaeophyta species such as *Ascophyllum*, *Durvillaea*, *Ecklonia*, *Laminaria*, *Lessonia*, *Macrocystis*, *Saccharina*, *Sargassum* and *Turbinaria*. Alginates are composed of anionic polysaccharides. There are mainly two types of uronic acid residues: β-D-mannuronic acid and α-L-guluronic acid. These exhibit anti-allergic and antimicrobial properties and are widely used in cosmetic product formulations for their film-forming, rheological, and skin-conditioning benefits [12].

3.1.2. Laminarin

Laminarin is most abundantly found in brown algae, with the highest amounts recorded in species from the Laminariaceae family. Current sources of laminarin are *Laminaria digitata and japonica*, *Eisenia bicyclis*, *Saccharina latissima*, *Ecklonia kurome*, but also species with lower concentrations, such as *Fucus* or *Ascophyllum* and *Undaria*. Usually, laminarin represents around 35% of dry weight; however, this proportion may vary depending on factors like the season, the ecological growth conditions or the species itself. Laminarin has antioxidant activity, linked to an anti-inflammatory effect, and has shown antitumor potential in studies. Moreover, by degrading through irradiation, its ability to scavenge free radicals and inhibit melanin synthesis in melanoma cells is enhanced [13].

3.1.3. Fucoidans

Fucoidans are sulfated polysaccharides composed primarily of fucose and other sugars such as xylose, galactose, mannose, and glucuronic acid. They also include sulfates, uronic acids, and acetyl groups. Fucoidans exhibit a variety of biological activities, including

antioxidant effects through an antiradical mechanism, which vary depending on their molecular weight and sulfate content. In topical applications, fucoidans can prevent and treat skin photoaging by inhibiting UVB-induced collagenase and gelatinase activities in vitro and reducing elastase *activity* ex vivo in human skin. Additionally, they inhibit wrinkle-related enzymes, enhance collagen synthesis in human dermal fibroblasts, and provide anti-inflammatory effects by preventing extracellular matrix degradation by matrix metalloproteinases (MMP) [14].

3.1.4. Ulvan

Ulvan sulfated polysaccharides represent a major component of green algae, most often being the predominant ones, varying from 8% to 29% of the algae dry weight. The main components of ulvan are rhamnose, xylose, glucose, glucuronic acid, iduronic acid, and sulfate. If divalent cations (e.g., Ca^{2+}, Cu^{2+}, Zn^{2+}) are present in the medium, ulvan has gelling properties at pH 7.5–8.0, and remains stable up to 180 °C. Both the rheological (gelling) and biofunctional (anti-aging) properties of ulvan make it relevant as an ingredient for the formulation of cosmeceuticals. In addition, it was linked with anti-hyperlipidemic and antiherpetic effects [14].

3.1.5. Agar

Agar is a gelatinous hydrocolloid structurally containing residues of two carbohydrates, agarose and agaropectin, extracted from various red algae species. Agarose accounts for 50 to 90% of agar, conferring its gelling properties. It is stable up to 250 °C and it maintains its properties even at high, near-boiling temperatures. Agar is widely used in cosmetic formulations for its thickening, emulsifying, and stabilizing properties. It is commonly incorporated into a variety of products, including moisturizers, creams, liquid soaps, cleansers, and deodorants, especially those designed for anti-aging and acne treatments [14,15].

3.1.6. Carrageenan

Carrageenan is mostly present in red algae, especially in strains belonging to the order *Gigartinales*, which, for this reason, are also called carrageenophytes. These organisms generate a distinct polysaccharide known as carrageenin, which, in its natural form, is unstable and challenging to isolate. To enhance its stability, carrageenin interacts with cations, resulting in the formation of different carrageenan salts, collectively referred to as carrageenan. This compound can constitute 30% to 75% of the seaweed's dry mass. Carrageenan exists primarily in three forms: kappa (κ), iota (ι), and lambda (λ). The kappa and iota variants are capable of forming gels, whereas the lambda type is primarily used as a thickening agent. Hence, they may be considered an alternative to cosmetic synthetic thickeners like polyethylene glycol (PEG) and carbomer [14,16].

Several of the bioactive compounds derived from macroalgae exhibit structure-dependent effects. Laminarin, a β-(1→3)-glucan with β-(1→6) branches, has a hydroxyl-rich polysaccharide backbone that provides high water-binding capacity, which confers moisturizing and barrier support properties [17]. Fucoidans, sulfated fucose-containing polysaccharides, display antioxidant, anti-inflammatory and photoprotective activities; their degree of sulfation and molecular weight determine free radical scavenging ability and inhibition of melanogenesis, thereby contributing to skin-brightening and anti-aging effects [18]. Phlorotannins, polyphenolic compounds unique to brown algae, consist of oligomeric phloroglucinol units with abundant hydroxyl groups, which confer strong radical-scavenging and tyrosinase-inhibiting activity, reducing oxidative stress, which results in anti-pigmentation and anti-aging outcomes [19].

3.2. Proteins, Peptides and Amino Acids

The natural moisturizing factor (NMF) has a key role in preserving the hydration, barrier function, desquamation, and flexibility of the stratum corneum. Among its key constituents, amino acids are particularly important, as they significantly contribute to maintaining the skin's moisture balance and supporting the stratum corneum's optimal hydration levels [16]. All macroalgae contain both essential and non-essential amino acids. Regarding the protein content, red algae have a higher content, up to 47%, compared to green algae, with a level of 9% to 26%. The lowest protein concentrations are found in brown algae, from 3% to 15%. Seaweed-derived proteins and bioactive peptides were proven to have powerful antioxidant effects, particularly the low-molecular-weight compounds. Seaweeds are rich in amino acids such as alanine, proline, arginine, serine, histidine, and tyrosine. High concentrations of arginine are found in *Palmaria* sp. and *Porphyra* sp., which acts as an NMF and is relevant in the composition of the cosmetic products. Bioactive peptides in seaweeds typically contain 3–20 amino acid residues, which contribute, according to their content and sequence, to the antioxidant and antimicrobial properties. Peptides like carnosine, glutathione, and taurine exhibit antioxidant and chelating properties, though taurine is not a "true" amino acid due to its lack of a carboxyl group. Taurine is abundant in the thalli of several red algae, such as *Ahnfeltia plicata*, *Euthora cristata*, and *Ceramium virgatum.* A relatively new peptide is PPY1, obtained from *Pyropia yezoensis* (red algae) through enzymatic hydrolysis, which has demonstrated anti-inflammatory effects by suppressing inflammatory cytokines. Additionally, peptides PYP1-5 and porphyra-334 from *Pyropia yezoensis* reduce the expression of MMP, thereby enhancing elastin and collagen production [13].

Mycosporine-like Amino Acids

Mycosporine-Like Amino Acids (MAAs) represent a natural means of protection against UV radiation, a relevant feature for sunscreen formulation. These small molecules with a molecular weight of less than 400 Da are found in the cell cytoplasm. Their chemical structure includes a cyclohexenone or cyclohexenimine ring connected to amino acid substitutes. The ring-substituent bonds allow MAAs to absorb a wide range of UV wavelengths, while the type of substituent influences the absorption properties [14,20].

3.3. Pigments

3.3.1. Phycobillins

These compounds can be isolated from cytoplasm or cell stroma. They are connected by covalent bonds, which are responsible for the color, and the resulting complexes, which belong to three categories: phycoerythrin, phycocyanin and allophycocyanin. R-phycoerythrin is commonly found in Rhodophyta, but its concentration varies between species. This pigment has been widely used as a natural coloring agent in food products, cosmetics, and pharmaceutical formulations, along with other phycobiliproteins. Natural colorants are stable, and resistant to exposure to light, high temperatures, and pH changes. At present, pigments including C-phycocyanin, R-phycoerythrin, and B-phycoerythrin are incorporated into everyday coloring makeup products like eyeliners and lipsticks [14].

3.3.2. Chlorophylls

Chlorophylls, the green pigments essential for photosynthesis, are located within the chloroplasts and universally present in all seaweed species, regardless of their external coloration. The visual diversity observed among seaweeds arises from varying compositions of photosynthetic pigments, with the predominant pigment determining

their taxonomic classification into Chlorophyta (green algae), Rhodophyta (red algae), or Phaeophyceae (brown algae). Among these, chlorophylls are typically the most abundant pigment group. Owing to their strong antioxidant and antimutagenic effects, chlorophylls are widely utilized across food, pharmaceutical, and cosmetic industries. Their ability to absorb red and blue light while reflecting green makes them effective natural colorants. Furthermore, their documented deodorizing and antimicrobial actions, combined with their antioxidative potential, underscore their relevance as functional bioactives in cosmetic formulations [14].

3.3.3. Carotenoids

Carotenoids represent a broad class of naturally occurring pigments, subdivided into carotenes—comprising α-carotene, β-carotene, and lycopene—and xanthophylls, including lutein, zeaxanthin, violaxanthin, astaxanthin, and fucoxanthin. These compounds exhibit important effects, notably antioxidant, anti-inflammatory, and anticarcinogenic actions, which support their use in natural coloring products. Their provitamin A activity is notably more stable, especially under low-oxygen conditions, compared to vitamin C. Additionally, carotenoids are capable of modulating UVA-induced gene expression, thereby providing protection against photooxidative stress, a capability particularly studied for the skin and ocular tissues. Among these, a special focus in the cosmetic industry is on astaxanthin due to its excellent safety profile and diverse biological functions, including immunomodulation, anticancer activity, and potent free radical scavenging capacity, superior to that of β-carotene. Its vibrant red pigmentation also enhances its use as a dual-purpose cosmetic additive—both functional and aesthetic. Fucoxanthin is the dominant pigment found in brown seaweeds, responsible for their characteristic olive-green to yellow-brown coloration. It is characterized by a rich pharmacological profile, including antioxidant, anti-obesity, antidiabetic, anti-inflammatory, anticancer, antimalarial, and antiangiogenic effects, making it a promising candidate for various therapeutic and nutraceutical applications [14].

3.4. Phenolic Compounds

Phenolic compounds are water-soluble molecules characterized by the presence of one or more hydroxyl groups attached to an aromatic hydrocarbon ring, with molecular weights ranging from 126 to 65,000 Da, according to their biotransformation through the acetate–malonate pathway. These compounds are secondary metabolites, synthesized as part of defense mechanisms against environmental stressors. According to the number of substituents, these structures can be simple phenolic compounds or polyphenols. Polyphenols include terpenoids, flavonoids, phlorotannins and bromophenols, representing a differentiation criterion from polyphenols of terrestrial origin, which mainly consist of flavonoids and gallic acid. Brown algae contain higher levels of phlorotannins, while the predominant phenolic compounds in green and red algae are bromophenols, flavonoids, phenolic acids, terpenoids and MAAs [21].

3.4.1. Phlorotannins

Phlorotannins constitute an important class of polyphenolic compounds, found mainly in marine brown algae, comprising 5–12% of their dry weight. With a 1,3,5-trihydroxybenzene primary structure, they result from the polymerization of phloroglucinol units. Based on their degree of polymerization and structural variations, phlorotannins are classified into six distinct categories: phloroethols, fuhalols, fucophloroethols, fucols, eckols, and carmalols. Each class represents a unique structural form and sets of chemical properties within this group of compounds. They are able to inhibit tyrosinase activity and exhibit antidiabetic properties. The strong antioxidative, anti-allergic, and

anti-inflammatory effects support the benefits these compounds can provide to cosmetic formulations. Additionally, studies using mouse skin models have demonstrated their protective effects against UV radiation. Furthermore, phlorotannins have been observed to reduce the expression of MMP-1, an enzyme involved in the breakdown of dermal collagen during skin aging [22,23].

3.4.2. Phenolic Terpenoids

Phenolic terpenoids, a structurally diverse group of natural compounds, have been isolated from both brown and red macroalgae. In red algae, the most frequent types are diterpenes and sesquiterpenes, whereas in brown algae, the major representatives are meroditerpenoids, which consist of a hydroquinone core linked to a polyprenyl side chain. This class includes molecules such as plastoquinones, chromanols, and chromenes, which exhibit a range of bioactive functions. Meroditerpenoids are particularly noted for their strong antioxidant capacity and their potential to inhibit skin photoaging, but also for their good safety profile. Some derivatives have shown efficacy in minimizing UVA-induced cellular damage and mitigating photodamage in exposed skin cells, which supports their inclusion in dermatological and cosmetic formulations. Additionally, certain meroditerpenoids from brown algae have demonstrated skin-lightening or hypopigmenting effects, leading to their use as multifunctional cosmetic ingredients [14].

3.5. Lipids

Seaweeds generally have a low lipid content, typically of less than 5%, which is considered beneficial as lipids are highly unsaturated, consisting of ω-3 to ω-6 fatty acids. Notable polyunsaturated fatty acids (PUFAs) include α-linolenic acid (18:3$n-3$), octadecatetraenoic acid (18:4$n-3$), arachidonic acid (20:4$n-6$), and eicosapentaenoic acid (20:5$n-3$). Linoleic acid (LA) is the most prevalent PUFA in human skin, playing a crucial role in maintaining the epidermal water barrier, whose disruptions are a significant consequence of essential fatty acid deficiency. The second most prominent PUFA in the skin is arachidonic acid, which constitutes approximately 9% of the total fatty acids found in the epidermal phospholipids [23]. Additionally, seaweeds contain other lipid categories such as sterols and phospholipids. The primary sterols identified are fucosterol, isofucosterol, and clionasterol [15].

Seaweed-derived lipids have shown various beneficial activities that make them valuable in cosmeceutical formulations. For instance, E-10-oxooctadec-8-enoic acid and E-9-oxooctadec-10-enoic acid from *Gracilaria verrucosa* are recognized for their anti-inflammatory properties. Essential oils from *L. japonica*, containing compounds like tetradecanoic acid, hexadecanoic acid, (9Z,12Z)-9,12-octadecadienoic acid, and (9Z)-hexadec-9-enoic acid, exhibit significant antibacterial activity against *Staphylococcus aureus* and *Bacillus cereus*, as well as antioxidant effects through radical scavenging mechanisms (DPPH, superoxide, ABTS). Fucosterol, found in *Pelvetia siliquosa*, also enhances antioxidant defenses, this time by boosting the enzymatic activity of superoxide dismutase, catalase, and glutathione peroxidase. Studies on *Hizikia fusiformis* have revealed that fucosterol contributes to defense against UVB-related skin damage by downregulating MMPs and promoting procollagen synthesis, in addition to exhibiting significant anti-inflammatory properties. Meanwhile, the brown alga *Laminaria ochroleuca* is known for producing hydrating agents frequently incorporated into skincare formulations. Extracts from this species are particularly rich in unsaturated fatty acids, accounting for approximately 55% of their composition, and include linoleic, oleic, linolenic, and palmitoleic acids. The lipid composition of various macroalgae—such as *Ulva rigida*, *Gracilaria* spp., *Fucus vesiculosus*, and *Saccharina latissima*—has been related to their antioxidant capacity and enzyme inhibitory effects. Additionally,

unsaturated lipids derived from brown seaweeds are associated with free radical scavenging properties, while the fatty acid profiles of species like *Pterocladia capillacea*, *Sargassum hornschuchii*, and *Ulva lactuca* have been explored as biomarkers for chemical stress exposure in marine environments [15,24].

3.6. Vitamins and Minerals

Algae are rich in vitamin A and a range of B vitamins (B1, B2, B3, B5, B7, and B12), as well as vitamins C, D, E, and K. These vitamins play essential roles in metabolic processes, often functioning as enzyme co-factors. Vitamin A is known for its antioxidant and anti-wrinkle properties, making it a popular ingredient in cosmetics aimed at reducing fine lines and hyperpigmentation. The B vitamin complex, particularly niacinamide (B3), is widely used in skincare for its ability to strengthen the skin barrier by reducing water loss and promoting the production of proteins like keratin and ceramides. Red algae and other seaweeds are excellent sources of vitamin B12, which supports hair and nail growth and has anti-aging benefits. Vitamin E, another powerful antioxidant abundant in many seaweeds, helps protect against UV damage and photoaging, especially in its non-esterified form. It is often combined with vitamin C, which regenerates oxidized vitamin E. Vitamin C, commonly sourced from red algae like *Ceramium rubrum* and *Porphyra leucosticta*, offers antioxidant, anti-inflammatory, and antimicrobial benefits. It is widely used in cosmetics to reduce pigmentation and fine lines, repair blood vessels, and promote tissue regeneration. It inhibits tyrosinase activity, reducing melanogenesis by interacting with copper ions. On the other hand, vitamin K has a protective effect on tissues, supporting wound healing and reducing bruises and scars. Together, these vitamins extracted from algae provide numerous skin benefits, making them valuable in modern cosmeceutical products [15,25].

Algae have the ability to absorb a variety of trace elements and micronutrients due to the permeability of their cell walls to small molecules. This allows them to contain elements like zinc, aluminum, magnesium, silica, copper, iodine, selenium, iron, and manganese. Additionally, they can accumulate nutrients such as calcium, sodium, phosphorus, potassium, and chlorine, but their presence and/or concentrations in algae are influenced by habitat. These minerals are crucial for metabolic processes, acting as cofactors for different catalytic enzymes [26].

In conclusion, algae represent a rich and versatile source of bioactive compounds with significant potential for skin health. Their primary metabolites, such as polysaccharides, amino acids, and lipids, play essential structural and physiological roles and contribute to moisturizing, regenerating, and barrier-protective effects. On the other hand, secondary metabolites, including phenolic compounds, pigments, and certain peptides, are mainly responsible for antioxidant, anti-inflammatory, photoprotective, and anti-aging activities. The specific chemical composition corresponding to the different species of brown, red, and green algae contributes to a wide spectrum of functional ingredients suitable for topical formulations. The increasing demand for sustainable and natural topical products has an answer in algae-derived ingredients as biodegradable and biocompatible alternatives to synthetic compounds, at the same time providing undoubtable cosmetic effects. Continued exploration of their structures, mechanisms of action, and bioavailability will further expand their applications and efficacy in the cosmeceutical field. Figure 2 summarizes the main extraction methods and highlights the most important primary and secondary metabolites obtained from different algae species, as well as their cosmetic relevance.

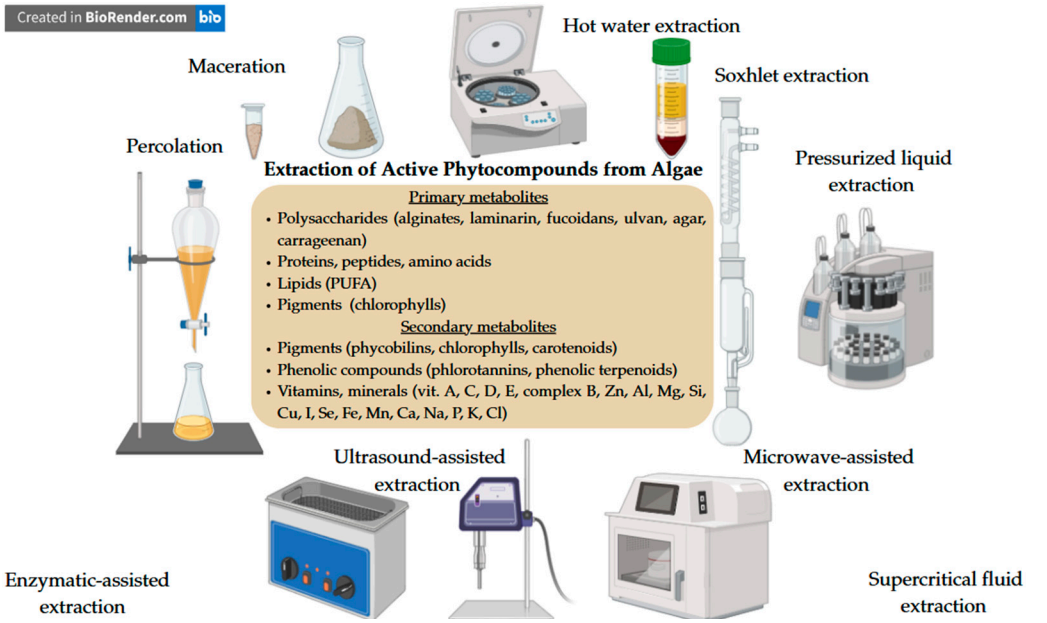


Figure 2. Extraction methods and active phytocompounds extracted from algae (image created using Canva.com and BioRender.com, accessed on 19 May 2025).

4. Environmental Influence on Macroalgal Chemical Composition and Toxicity

4.1. Habitat

The complexity of macroalgae habitat influences the chemical composition of Chlorophyceae, Phaeophyceae and Rhodophyceae. Habitat complexity in reefs enhances herbivory, prompting macroalgae to develop defenses like calcification, toxic chemicals as secondary metabolites, or both. In contrast, algae in simpler habitats (e.g., rocky shores or lagoons) show an unclear chemical defense. In total, 6 species of green algae, 7 of brown and 18 of red were collected from different places, which were a coral reef in the Mexican Caribbean, three myxohaline areas in the Yucatán peninsula and six rocky intertidal regions (four in the Mexican Pacific, two in the Gulf of Mexico). Toxicity was interpreted in correlation with lethality caused to the goldfish *Carasius auratus auratus.* All Chlorophyceae species were highly toxic, as were four of Phaeophyceae and half of Rhodophyta (nine species). The highest toxicity was exhibited by *Caulerpa cupressoides*, *Dictyopteris delicatula*, and *Ceramium nitens*. A gradient of toxicity related to the complexity of the habitat was detected; the more toxic macroalgae extracts were found in reefs, followed by a rocky intertidal environment, and lastly in myxohaline environments. A significant relationship between habitat complexity and toxicity potency was established for Chlorophyta and Rhodophyta species [27]. Besides the secondary metabolites produced as means of defense against grazers, macroalgae may host the benthic dinoflagellate *Gambierdiscus toxicus*, which produces polyether toxins ciguatoxins, which determine ciguatera poisoning in humans, known to be mostly caused by fish consumption. Palatable macroalgae, those more likely to be harvested for food, may host *Gambierdiscus* populations if they are collected in tropical reef regions where the dinoflagellate thrives. The risk is higher for wild-harvested macroalgae in endemic ciguatera regions (Pacific Islands, Caribbean). Of special concern is the Phaeophyceae genus *Dictyota*, which hosts large populations of *G. toxicus*; it is widespread in tropical areas and produces strong chemical compounds used for defense. Similarly, the *Rodophyceae* palatable genus *Acanthopora* is consumed by various marine organisms and humans, while *Laurencia* and *Asparagopsis* are sometimes used in nutraceuticals, cosmetics, or condiments; all of them were found to host moderate levels of *G. toxicus*. Despite the

relatively low dinoflagellate densities hosted by palatable turfs, as fast-growing algae, they could be linked to most of the toxin flux because of the fast resource turnover [28]. Intrinsic production of chemical compounds for defense purposes is documented for *Dictyotaceae* and *Caulerpaceae*, which are known for their high number of secondary metabolites [29].

Apart from the identification of potentially toxic compounds, the nutritional characterization of macroalgae is also relevant for oral or dermal exposure. From this point of view, Dromard et al. quantitatively assessed the concentrations of proteins, lipids, soluble and insoluble carbohydrates, as well the amount of ash, in several species of macroalgae. Although they possess great concentrations of lipids, which generate high quantities of energy, *Dictyota pulchella*, *Caulerpa cupressoides*, *Caulerpa sertularioides* and *Sargassum polyceratium* were found to have average nutritional properties because of their content in insoluble carbohydrates, which are considered low energetic compounds. On the other hand, the chemical composition of *Ceramium nitens*, *Ulva lactuca* and *Lobophora variegata*, consisting of abundant protein and soluble carbohydrates levels, provides them with high nutritional quality [29]. The specific carbon metabolism of green, brown and red algae was evaluated using a carbon stable isotope. Low values were recorded for *Rhodophyta* species, which are known for the absence of carbon-concentrating mechanisms, unlike the strong ones in *Chlorophyta* studies' samples. The biochemical profiles varied among the groups, as red algae were rich in soluble carbohydrates, while brown algae contained higher levels of lipids and proteins, and green algae exhibited elevated concentrations of insoluble carbohydrates [30].

4.2. Season

It was observed that the concentration of chemical constituents of the essential oil from the brown algae *Cystoseira compressa* varied from May to August. The volatile fraction of these algae contained 104 identified compounds, that summed up 84.37–89.43% of the total oil. In the samples harvested in May, June and July, there was a high proportion of fatty acids (56, 69, and 34%, respectively), mostly palmitic acid, while the samples collected in August had a high content of alcohols, especially phytol and oleyl alcohol. Ketones had the highest concentration in July (17%), decreasing in August (13%), May (9%) and June (only 2%). Aldehydes with higher molecular weight were also assessed; tridecanal had a minimum level in June (0.37%) and a maximum level in July (0.81%), while tetradecanal was not found in June and had its maximum concentration in August (0.20%). Esters, mainly methyl arachidonate, varied from 4% in August to 10% in May and June. The contents of tri, tetra, and penta-decyl esters had a peak in June, followed by July, May and the lowest levels were recorded in August [31].

4.3. CO_2 Concentration and Ocean Acidification

Ocean acidification (OA) influenced the pigment level; for example, in the red alga *Pyropia haitanensis*, it led to increased chlorophyll and phycoerythrin contents, suggesting enhanced photosynthetic pigment synthesis, possibly to optimize light capture under altered CO_2 and pH conditions.

Increased availability of inorganic carbon enhances photosynthesis, leading to greater carbon fixation and more sugar production. The content of carbon was also modified by elevated CO_2, as was observed in *Ulva linza*, which showed higher soluble carbohydrate accumulation. On the other hand, in *Saccharina japonica* (brown), OA induced a decrease in total soluble carbohydrates and alginate content, indicating altered energy storage and structural polysaccharide synthesis [32]. A two-week exposure of *Dictyota* spp. to OA induced an increase in macroalgal production, and the consistent carbon content was not linked to high rates of photosynthesis. Thus, *Dictyota* spp. may

adjust its carbon uptake strategy to offset decreased photosynthesis, obtaining greater biomass production under acidified conditions [33]. Nevertheless, it seems that the change in chemical composition as a result of OA influence is species-specific, with some macroalgae showing little or no change, while others exhibiting strong biochemical shifts. OA can interfere with intracellular acid–base regulation, which indirectly impacts the synthesis of metabolites, proteins, and lipids. This variability is often due to the presence or absence of carbon concentrating mechanisms and the species' tolerance to pH changes. For example, *Neosiphonia japonica* exhibited no significant change in growth under OA, indicating relative resilience [32].

The environmental pH variation, alone or combined with temperature variation, was assessed on two brown algae species, *Desmarestia anceps* and *Desmarestia menziesii*, in a 39-day experiment. Reduced pH (7.6) alone induced a significant decrease compared to ambient conditions (pH = 8) in the protein content of *D. anceps* tissues, while lipid levels were greatest under ambient conditions (1.5 °C) and lowest under elevated-temperature conditions (3.5 °C). Compared to the latter, a smaller reduction in the lipid content was caused by the joint effects of temperature and pH, proving an antagonistic influence. On *D. menziesii*, reduced pH and combined elevated temperature-reduced pH caused no significant alteration to the protein concentration, but reduced pH seemed to be beneficial as it led to an increase in the lipid level [34].

4.4. UV Radiation

UV radiation induces a reduction in CO_2 fixation and effective quantum yield in macroalgae. Although the intended use of UVA enhances morphogenesis and growth in some species, increased levels decrease the maximum quantum yield and inhibit photosynthesis. UVB determines damage that takes a lot of energy for restauration, which eventually implies a decrease in the growth rate. It may also determine photoinhibition and certain parameters related to the photosynthesis process.

Regarding the specific chemical composition variation caused by UV radiation, an interesting mechanism is the increase in UV-absorbing compounds as photoprotective metabolites. Mycosporine-like amino acids (MAAs), UVA and UVB-absorbing water-soluble secondary metabolites, protect cells from radiation damage. An increase in MAAs under UVB exposure was observed in *Chondrus crispus* and *Palmaria palmata* (both red), and high levels of MAAs were noticed in different species of *Porphyra* (red). Phenolic compounds that act as antioxidants and UV screens were increased in other species, like phlorotannins in *Fucus vesiculosus*. UV exposure determines alterations in pigment content, such as the degradation of chlorophyll a and carotenoids in *Ulva pertusa*. Chlorophyll loss was detected in *Enteromorpha intestinalis* or *Laminaria japonica*, along with a drop in fucoxanthin level in the latter. The typical markers of oxidative stress were identified in certain macroalgae species as a result of UV exposure. In terms of lipid peroxidation, increased malondialdehyde (MDA) levels were detected in *Gracilaria lemaneiformis* and oxidation of membrane lipids in *Porphyra haitanensis*. Species-specific chemically qualitative profile changes in response to UV exposure were recorded, as in *Gelidium pusillum*, which also experienced DNA and pigment damage, and had weak production of MAAs compared to other red algae [32].

4.5. Pollution

Different mechanisms for element sequestration were recorded for brown algae. *Cystoseira*, for example, a perennial alga, uptakes the chemicals from the polluted environment unrestrictedly, which may imply poor exclusion mechanism and low adaptability to polluted marine habits. *Cystoseira* included the greatest amount of the 60 analyzed metal

elements, from all types of macroalgae included in this study. On the other hand, annual algae may possess the capacity to restrict element uptake under intense pollution, as they exhibit a decrease in element concentration, possibly reflecting an active elemental exclusion mechanism. Among the annual macroalgae, green (*Cladophora*) accumulated the greatest amounts of elements, followed by brown (*Codium*) and red (*Ceramium*) [35].

The most studied pollutants are heavy metals, including cadmium, considered a chronic source of contamination. Seaweeds can chelate non-essential metals using phytochelatins, a mechanism that could result in high levels of reactive oxygen species (ROS) and reduced cellular antioxidant capacity, as well as diminished enzyme activity due to competition with essential metals. Oxidative stress triggers structural changes in amino acids, sugars, lipids, fatty acids and other compounds, as algae have primary metabolites. The exposure of *Gracilaria caudata* to cadmium (Cd^{2+} from $CdSO_4 \cdot 8H_2O$) at IC_{50} (3 mg/mL) determined the variation in 20 metabolites, mostly structurally related to glyoxylate, but also ascorbate, floridoside and proline. Cd^{2+} exposure also caused the impairment of five metabolic pathways, which led to amino acid accumulation, as well as carbon biotransformation intermediate compounds and antioxidants' responses to cadmium [36].

Chlorine dioxide (ClO_2) water treatment in power plants and desalination plants is practiced to control biomass and biofouling. *Ulva reticulata* and *Hypnea musciformis* were exposed to ClO_2 to assess the risk associated with this water decontamination method on different types of macroalgae. It was concluded that the levels of photosynthetic pigments chlorophyll a and carotenoids increased during the first two days of exposure and decreased afterwards. The same variation was observed for polyphenols. The increase might be a response to the oxidative stress induced by ClO_2, which also determined an alteration in the fatty acids' profile [37].

Another category of water pollutants is the UV organic filters in sunscreens such as oxybenzone, which was tested on the red macroalga *Gracilaria vermiculophylla* during a twenty-day exposure. The 0.1 mM concentration significantly lowered the pigment (chlorophyll a and carotenoids) concentration and the rate of photosynthesis. A 100-times lower oxybenzone concentration (0.001 mM) determined only a pigment decrease without another physiological response [38].

A current aquatic pollutant is bisphenol A, largely spread across the oceans and seas. When *Ulva rigida* (green) was exposed for 24–48 h to 40–100 mg/L bisphenol A, chloroplasts were entirely discolored. In addition, 5 mg/L bisphenol determined a growth increase by 21%, while a lower concentration of 0.1 mg/L almost doubled the algae culture within 30 days, with the stimulating effect being dose-dependent. Chlorophyll a and b levels changed within the first hours of BPA exposure and declined under BPA treatment at both high (100 mg/L) and low (0.01 mg/L) concentrations [39].

In conclusion, environmental factors—such as habitat complexity, seasonality, ocean acidification, UV radiation, and pollution—exert a significant and often species-specific influence on the chemical composition and toxicity of macroalgae. These changes not only affect their ecological interactions but also have practical implications for their safety and efficacy in human applications. Higher toxicity levels in reef-associated species, seasonal fluctuations in bioactive compounds, and alterations due to pH or pollutants emphasize the need for careful selection, monitoring, and standardization of algal biomass intended for use in topical formulations for skin health. Understanding these environmental impacts is essential to ensure the consistent quality and safety of algal-derived products. For practical purposes, we summarized these key environmental influences in Figure 3.

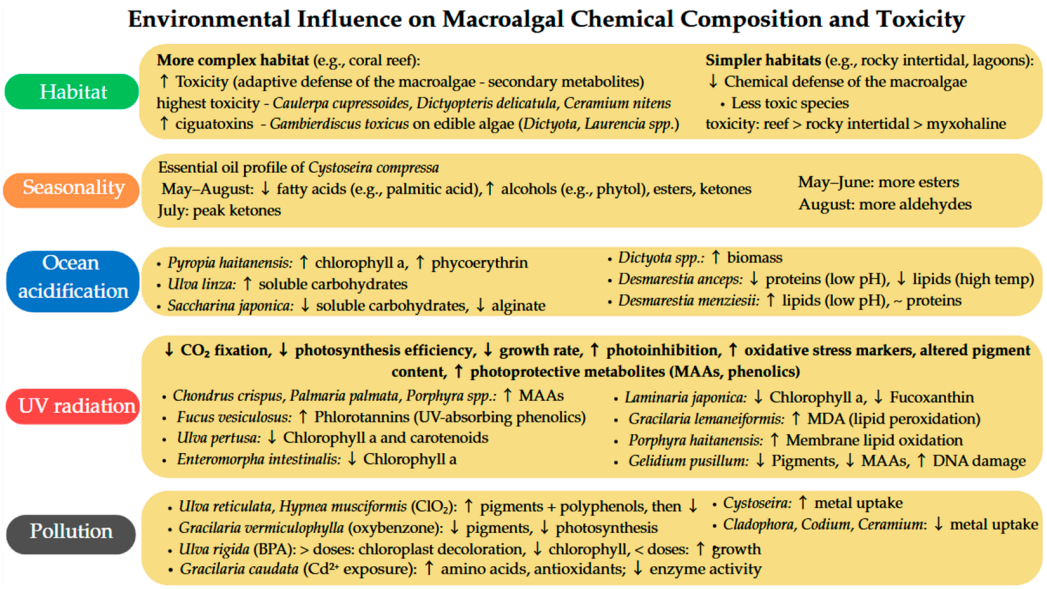


Figure 3. Summarization of environmental influences on macroalgal chemical composition and toxicity.

Environmental factors, including geographically dependent habitat complexity, seasonal variation, ocean acidification, UV radiation and pollution, have a significant and often species-specific influence on the chemical composition and toxicity of macroalgae. These changes not only affect their ecological roles but also have direct implications for their use in food, pharmaceutical and cosmetic applications. Metabolite profile variability, which includes shifts in phlorotannin levels, qualitative and quantitative differences in MAAs, lipids or polysaccharides content, can lead to inconsistent bioactivity across batches. Consequently, this may create both safety and efficacy issues, derived, for example, from fluctuant concentrations of toxic or allergenic compounds or variations in antioxidant, photoprotective or nutritional properties. Such inconsistencies pose challenges for the reproducibility of the bioactive content.

Significant variation depending on the harvest season and location was described for the protein, carbohydrate, fatty acid and mineral profiles of certain *Laminaria* species (*digitata*, *hyperborea*) or *Ascophyllum nodosum* [40]. The impact of the season on sulfated polysaccharides content and antioxidant activity was highlighted for the red algae genera *Codium* and *Osmundea* [41]. From the perspective of extraction methods, different solvents, temperatures or processing conditions can alter both the quantity and quality of the recovered metabolites. The regulatory procedure of the European Commission or FDA requires evidence for batch consistency, validated analytical methods and well-characterized toxicological profiles for considering algal ingredients for consumer use approval [42,43].

To ensure bioactive content reproducibility and consumer safety of algae and the derived products or extracts, strategies for standardized harvesting and for cultivation under controlled conditions, validated extraction methods and harmonized protocols are needed.

5. Regulatory and Safety Considerations of Key Compounds

The successful translation of macroalgal metabolites into cosmetic applications depends not only on their bioactivity, but also on their regulatory status and safety profile. There are two classes of compounds that are of particular interest considering their biological effects, but also their limited regulatory approval, phlorotannins and MAAs.

Phlorotannins, a particular group of polyphenols from brown algae, have exhibited potent antioxidant, anti-inflammatory and photoprotective properties [44]. Preclinical studies consistently reported favorable safety profiles, with low acute toxicity and no evidence of mutagenicity at cosmetic-relevant concentrations [42,45,46]. However, most available evidence is derived from in vitro assays or animal models, with very limited human safety data [42,47]. Importantly, phlorotannins are not yet specifically listed in the EU CosIng database, and no monographs exist under FDA or SCCS evaluations. This regulatory gap limits their routine use in European cosmetics. Moreover, the EU Cosmetics Regulation prohibits animal testing, while the REACH framework may still require animal data for complex toxicity endpoint, leading to conflicting requirements and regulatory uncertainty [42]. Although advances in alternative testing methods, such as reconstructed human epidermis assays, are promising, validation for marine extracts remains deficient [46]. Overall, phlorotannins are regarded as promising natural cosmetic ingredients, but comprehensive safety documentations and harmonized regulation and guidance are required for extended market insertion [45,47].

MAAs such as shinorine and porphyra-334 function as natural UV-absorbing compounds and have been studied as eco-friendly sunscreen filters. Toxicological assessment reports suggest excellent dermal tolerability, no genotoxicity and strong photostability [48,49]. Although some Asian regulatory authorities, such as the one in Japan, have allowed limited use of MMAs in cosmetic formulations, they are still not included in the EU list of permitted UV filters according to Regulation (EC) No. 1223/2009, nor are they FDA-approved sunscreen ingredients [49,50]. Thus, as observed for phlorotannins, validation of non-animal methods is needed, along with further human safety data, which together would permit the harmonization between the different international regulations regarding the use of MAAs in sunscreen cosmetic products.

Although a detailed discussion of toxicological evaluations, considering NOAEL values or irritation and sensitization assays, lies beyond the scope of this review, such studies are mandatory for supporting future regulatory approval of macroalgae-derived ingredients, including for cosmetic use purposes. Comprehensive reviews dedicated to toxicological milestones would enhance the quality of the present formulation and regulation-oriented perspective of the current study.

6. Extraction Methods of Bioactive Compounds from Macroalgae

Extraction is a crucial step in obtaining bioactive compounds from algae. After algae are collected, the biomass undergoes several processes depending on the desired compounds to be extracted. The specific process used depends on the targeted bioactive molecule. Typically, the process begins with a pre-treatment of the algal biomass such as drying the biomass either naturally or in industrial ovens at temperatures below 40 °C to prevent the degradation of sensitive bioactive compounds like proteins, vitamins, or enzymes. Alternatively, lyophilization, a vacuum-based low-temperature drying method, may be used. The dried or lyophilized biomass is then ground to a precise particle size, either for direct usage in cosmetics or to extract active components. However, to enhance cosmetic products with specific active molecules, various extraction methods are used. Extraction methods are categorized as classical or modern based on their innovation level. Classical extraction methods include percolation, maceration, Soxhlet extraction, and both solid–liquid and liquid–liquid extractions. Modern techniques, developed for greater purity and sustainability, include microwave-assisted, ultrasound-assisted, enzyme-assisted methods, and advanced processes like supercritical fluid extraction and pressurized liquid extraction. These modern approaches align with “green chemistry” principles, aiming

to minimize energy use, solvent reliance, and environmental impact while enhancing efficiency [14,51].

6.1. Classical Extraction Methods

6.1.1. Maceration

Maceration is a classic method of extraction performed on macroalgae. This technique involves soaking ground dried or fresh algal material in commonly used solvents such as methanol, ethanol or water, usually at room temperature or slightly higher temperatures, for 24–72 h. This is a gentle process that allows the solvent to penetrate the cells and dissolve active compounds: polyphenols, flavonoids, pigments and other secondary metabolites. Antioxidants and pigments can be extracted from various macroalgae. The yield and activity of the extracts depend on solvent choice, extraction time and algal species [52,53].

6.1.2. Percolation

Percolation is an extraction method where a solvent is continuously passed through a column of macroalgal material, allowing for efficient extraction of bioactive compounds and larger extract volumes compared to static maceration. Its effectiveness is influenced by solvent choice and extraction conditions. Baliano et al. have utilized this technique to create bioactive methanolic algae extracts of *Padina gymnospora* for wound-healing applications [54].

6.1.3. Soxhlet Extraction

Soxhlet extraction is considered a continuous solvent extraction method that selectively extracts targeted compounds from solid ones at room pressure and boiling temperature. Compared to maceration and percolation, this process uses less solvent and takes less time.

This method has multiple advantages over conventional approaches. It is faster than maceration and percolation, does not need filtration of the extract, allows for the processing of multiple samples at once and enables solvent recycling. However, there might be an increased risk of thermal degradation due to the extraction conditions: higher temperatures and long extraction time. Bhuyar et al. used this method to study the antibacterial and antioxidant properties of the red seaweed *Kappaphycus alvarezii*. The results showed that the hot water extract had a total phenolic content of 19.10 $\pm$ 0.81 mg GAE/g DW, while the ethanolic Soxhlet extract had a slightly higher content of 20.25 $\pm$ 0.03 mg GAE/g DW [55,56].

6.1.4. Hot-Water Extraction

The most reliable and effective method for extracting bioactive compounds from algae, especially polysaccharides, is hot-water extraction. Since water is a harmless and nontoxic solvent that readily permeates plant tissue, hot-water extraction is the most common technique for extracting polysaccharides [57]. This technique can generate extracts that have substantial biological activity, such as antioxidant, immunomodulatory, and hypolipidemic effects, even if the yields may differ based on extraction parameters, including duration, temperature, and algae-to-water ratio. Hot-water extraction is still an excellent choice for food, medicinal, and cosmetic applications based on marine polysaccharides because of its convenience of application, low cost, and ability to maintain the integrity of sensitive compounds [58].

6.2. Modern Extraction Methods

6.2.1. Microwave-Assisted Extraction

Microwave-assisted extraction (MAE) is an advanced technique increasingly used to recover valuable bioactive compounds from macroalgae, offering significant advantages over conventional methods. By rapidly heating the solvent and algal biomass with microwave energy, MAE breaks down cell walls and promotes the release of compounds such sodium alginate, phenolics, phlorotannins, polysaccharides, and carotenoids [59–62]. In comparison to hours-long conventional extractions, studies have demonstrated that MAE can produce higher yields and a higher total phenolic content in significantly less time (e.g., 15 min at 110 °C) while simultaneously enhancing the extracts antioxidant and enzyme-inhibiting properties [59–61,63]. All things considered, MAE is a fast, efficient, and environmentally friendly method to extract important bioactives from macroalgae, offering distinct advantages over conventional extraction techniques in terms of yield, quality, and environmental impact [64].

6.2.2. Ultrasound-Assisted Extraction

Using ultrasonic waves to break down cell walls and promote the release of essential compounds like phenolics, polysaccharides, pigments, and proteins, ultrasound-assisted extraction (UAE) is a modern, effective method to extract bioactive components from macroalgae. Compared to traditional techniques, UAE has been demonstrated to significantly enhance the antioxidant activity and yields of active ingredients such as tannins, phenols, phlorotannins, flavonoids, and fucoxanthin [65–69]. Phycobiliproteins and amino acids can also be extracted with UAE, and extraction efficiency can be increased by combining it with other techniques like homogenization or maceration [66,70]. Because of the high quality and bioactivity of the extracts, the method is considered environmentally friendly, requiring less energy and solvents, and it is suitable for use in food, cosmetics, and nutraceuticals. Overall, UAE provides a fast, scalable, and sustainable method for optimizing the recovery of compounds from macroalgae [66,67,71,72].

6.2.3. Enzymatic-Assisted Extraction

Enzymatic-assisted extraction (EAE) is an innovative and gentle method for isolating valuable bioactive compounds from macroalgae, using specific enzymes to break down cell walls and release target molecules such as polysaccharides and proteins. Compared to conventional chemical extraction techniques, EAE has been effectively used to extract ulvan from green macroalgae and high-molecular-weight fucoidans from brown macroalgae, often yielding larger and more native-like molecules [73,74]. Process variables including pH, temperature, and extraction time are crucial for optimizing yield and purity. The selection of enzymes, such as cellulases, alginate lyases, and proteases, can be tailored to the macroalgal species and the desired compound [73–76]. EAE is also useful for protein extraction, especially when combined with other methods like ultrasound or pulsed electric fields. This improves the extracts' antioxidant activity and gives higher yields [76–78]. EAE offers a sustainable, efficient, and selective approach for obtaining high-quality bioactives from macroalgae, supporting their use in diverse biotechnological and industrial fields [78,79].

6.2.4. Pressurized Liquid Extraction

Pressurized liquid extraction (PLE) is a green technology that uses high temperatures and pressures to efficiently extract bioactive compounds from macroalgae, such as fatty acids, polyphenols, carotenoids, and phycobiliproteins. By modifying the polarity and extraction temperature of different solvents, such as ethanol, water, acetone, and ethyl

acetate, PLE enables the selective extraction of specific compounds. For instance, ethanol-water mixtures are useful for optimizing polyphenol and flavonoid content, producing extracts with strong antioxidant and antimicrobial activity, while PLE with ethyl acetate at high temperatures can selectively extract long-chain fatty acids including oleic, arachidonic, and eicosapentaenoic acids [75,80,81]. The yield and quality of extracted compounds are significantly impacted by the macroalgae's drying technique—oven or freeze-drying—and the precise PLE parameters such as temperature, pressure, and solvent ratio; under ideal circumstances, some studies have found that the extraction yield can increase by up to six times for carotenoids and tocopherols [81]. Although PLE is an adaptable, fast, and eco-friendly extraction method, its efficacy is dependent on the specific parameter optimization for each macroalgal species and its desired bioactive [82,83].

6.2.5. Supercritical Fluid Extraction

Supercritical fluid extraction (SFE), most commonly using supercritical CO_2, is a green and efficient method for extracting high-value bioactive compounds from macroalgae, including fatty acids, phenolics, flavonoids and pigments such as carotenoids and chlorophylls. SFE operates at high pressures and moderate temperatures, allowing for selective extraction without the use of toxic organic solvents, preserving the integrity and bioactivity of sensitive compounds [84–86]. Strong antioxidant, anti-inflammatory, and antibacterial properties have been shown by SFE extracts from macroalgae, making them useful for use in food, cosmetics, nutraceuticals, and even as plant biostimulants in agriculture. Furthermore, SFE produces stable extracts with minimal batch-to-batch variation, which is crucial for industrial applications, and is considered environmentally safe and sustainable. Although SFE is quite effective for many bioactives, depending on the macroalgal species and compound polarity, other techniques, including UAE, may be more effective for extracting some polyphenols [84–88].

Thus, the extraction method plays a crucial role in determining the quality, stability, and bioactivity of algal-derived compounds intended for cosmetic applications. These methods are summarized in Figure 2. While classical techniques such as maceration, percolation, Soxhlet extraction and hot water extraction remain relevant due to their simplicity, modern approaches like microwave-assisted, ultrasound-assisted, enzymatic, pressurized liquid, and supercritical fluid extraction offer significant advantages. These advanced methods can align with the principles of green extraction. Ultimately, selecting the most suitable extraction method depends on the specific bioactive target, desired purity, and intended end use, with a growing emphasis on sustainability and regulatory compliance.

7. Quantitative Analysis of Bioactive Compounds in Macroalgae

Because algae contain a wide variety of antioxidants, pigments, polysaccharides, and other active compounds, they are becoming increasingly acknowledged as important sources of bioactive ingredients for cosmetic and pharmaceutical purposes. A variety of analytical and bioassay techniques have been developed to extract, identify, and assess the activity of chemicals originating from algae that are essential to skin health and cosmetic efficacy to maximize these advantages. The most used methods for the identification and quantification of algal compounds are chromatography, spectroscopy, colorimetry, and spectrophotometry.

Alcohols, esters, amines, and acids are among the various functional groups that can be verified to be present in algal extracts using Fourier-transform infrared (FTIR) spectroscopy [89,90]. The structural identification of the main polyphenols and phlorotannins can be performed by nuclear magnetic resonance (NMR) spectroscopy. Total phenolic content is typically determined using colorimetric assays like the Folin–Ciocâlteu test,

whilst phlorotannins are determined using the 2,4-dimethoxybenzaldehyde assay [90]. Spectrophotometric techniques are also used to determine the protein content and estimate pigment [89].

Certain types of algae compounds are more suitable for specific analytical techniques, and the use of these techniques is closely related to both regulatory quality control and functional validation. To confirm the identity and purity of bioactive polysaccharides used as thickeners or moisturizers in cosmetics, polysaccharides are frequently analyzed using FTIR and NMR spectroscopy. These methods offer structural information on glycosidic linkages while methylation–GC-MS enables detailed linkage profiling. Polyphenols and phlorotannins are commonly quantified through HPLC or UHPLC coupled with MS or HRMS, as these methods effectively differentiate structurally similar oligomers and facilitate the correlation with antioxidant and anti-inflammatory bioactivities pertinent to skin protection. MAAs and pigments including carotenoids and chlorophylls are successfully analyzed using HPLC-DAD or LC-MS/MS, with spectrophotometry allowing for rapid bulk quantification for quality control purposes. This analysis of pigments directly substantiates claims regarding UV protection and photostability. The most effective method for analyzing fatty acids, sterols, and volatile metabolites is GC-MS, which guarantees precise quantification and the identification of potentially harmful or unstable substances. These customized methods not only guarantee precise characterization but also satisfy legal requirements for ingredient safety and standardization (such as ISO 16128), which call for confirmed analytical fingerprints to prove the reliability and consistency of cosmetic raw materials.

7.1. Liquid Chromatography

High-performance liquid chromatography (HPLC), ultra-high-performance liquid chromatography (UHPLC), and liquid chromatography–mass spectrometry (LC-MS) are widely used for analyzing polyphenols, pigments, phlorotannins, amino acids, and toxins in algae [91–96]. UHPLC with diode-array detection (DAD) and tandem mass spectrometry (MS/MS) allows for simultaneous quantification of multiple amino acids and related compounds [92,93]. Hydrophilic interaction liquid chromatography (HILIC) is effective for separating polar compounds like phlorotannins [94].

Hartman et al. developed an HILIC method for the analysis of five MAAs. The HILIC Poroshell 120 column demonstrated the best separation efficiency and peak morphologies in less than 20 min. The MAAs were eluted in the following order: asterina-330, shinorine, palythine, mycosporine-serinol, and porphyra-334. The mobile phase was water/acetonitrile with ammonium acetate at pH 6.6, which was essential to preserve selectivity. The analysis was performed on different algae species, such as *Porphyra* sp., *Porphyra* ssp., *Palmaria palmata*, *Lichina pygmaea*, *Catenella repens*, *Catenella nipae* (strain 2818), *Catenella nipae* (strain 4006), and *Catenella caespitosa* [97].

In a more recent study, a UHPLC method with a diode array detector, DAD, was developed for the determination of 11 MAAs in various algal species, such as *Gracilaria chilensis*, *Pyropia plicata*, *Porphyra columbina*, *Chondrus crispus*, and *Jania rubens*. This technique used a Phenomenex Luna Omega C18 column (1.6 µm particle size) and separated all target substances completely in less than 8 min. The mobile phase consisted of water with 0.25% formic acid and 20 mM ammonium formate (phase A) and acetonitrile (phase B) [92].

MAAs were also separated and identified by high-performance countercurrent chromatography (HPCCC) from two red macroalgae species: *Pyropia columbina* and *Gelidium corneum*. The separation was performed using a 134 mL HPCCC column with PTFE tubing and a biphasic solvent system composed of ethanol, acetonitrile, saturated ammonium sulfate solution, and water (1:0.5:1:1 $v/v/v/v$). This technique effectively separated

highly polar chemicals with a mobile phase flow rate of 3 mL/min and a rotational speed of 1600 rpm. Among all MAAs, shinorine, porphyra-334, palythine, asterina-330, and mycosporine-serinol were successfully isolated [98].

Proteins from three different species of macroalgae, *Saccharina latissima*, *Codium* spp., and *Mastocarpus stellatus*, were extracted using aqueous and alkaline-soluble protein extraction followed by enzymatic hydrolysis with alcalase. Reversed-phase HPLC coupled with electrospray ionization quadrupole time-of-flight mass spectrometry (HPLC-ESI-QTOF/MS) was used to separate and identify 37 different peptides. A porous-shell fused-core Ascentis Express C18 column (150 × 2.1 mm, 2.7 µm particle size) and a corresponding guard column were used for the peptide separation process. A gradient elution program designed for effective peptide separation was used to create the mobile phase, which was composed of water with 0.5% formic acid (A) and methanol with 0.5% formic acid (B). A QTOF mass spectrometer equipped with Agilent Jet Stream technology was used to perform the mass spectrometry analysis in positive electrospray ionization (ESI) mode [99].

One study performed by Steevensz et al. evaluates phlorotannins in five species of brown macroalgae, including *Saccharina longicruris*, *Ascophyllum nodosum*, *Fucus vesiculosus*, *Fucus spiralis*, and *Pelvetia canaliculata*, applying a rapid and efficient ultra-high-performance liquid chromatography coupled with high-resolution mass spectrometry (UHPLC-HRMS) method using HILIC. The procedure revealed different phlorotannin profiles among species according to degrees of polymerization and allowed for the identification of a wide range of phlorotannins, including high-molecular-weight molecules up to 6000 Da [94].

Isoflavone compounds were identified and quantified in sea algae samples (*Sargassum muticum*, *Sargassum vulgare*, *Hypnea spinella*, *Porphyra* sp., *Undaria pinnatifida*, *Chondrus crispus* and *Halopytis incurvus*) using a new hyphenated technique. Samples were sonicated and extracted with supercritical CO_2 modified by MeOH/H_2O. Separation was carried out on a Zorbax SB-CN column using a 0.2% acetic acid–acetonitrile gradient. Detection was performed by Agilent 6460 Triple Quadrupole LC/MS in negative ESI mode [95].

A more recent study, conducted by Sardari et al. employed ultra-high-performance liquid chromatography coupled with high-resolution tandem mass spectrometry (UHPLC-HRMS/MS) to identify and characterize phlorotannins in two brown algae species: *Saccharina latissima* and *Ascophyllum nodosum*. Four phlorotannin species were identified in *A. nodosum* and one in *S. latissima* by UHPLC-HRMS, which after purification by solid phase extraction (SPE), produced purer, more concentrated fractions [100].

Yum et al. developed an analytical method for simultaneous quantification of five fatty acids in macroalgae, including myristic acid, palmitic acid, cis-palmitvaccenic acid, stearic acid, and oleic acid. The method employs SPE for sample purification and derivatization with trimethylaminoethyl (TMAE) to enhance ionization efficiency for liquid chromatography–tandem mass spectrometry (LC–MS/MS) analysis. Chromatographic separation was achieved using a CAPCELL PAK C18 MGII S3 column. The mobile phase consisted of distilled water and acetonitrile containing 5 mM ammonium acetate. The derivatized fatty acids were detected within 13.5 min using electrospray ionization in positive mode and multiple-reaction monitoring [101].

Liquid chromatography is a fundamental method for examining a variety of substances found in algae, such as MAAs, phlorotannins, amino acids, and proteins. This is essential for quality control and research on algae-based products due to its speed, sensitivity, and versatility. Quantification of these molecules also provides a direct basis for functional validation. For example, amino acids and peptides have well-established functions in hydration and barrier repair, phlorotannins exhibit antioxidant and anti-inflammatory

properties pertinent to skin health, and MAAs are known to be UV-absorbing substances used in photoprotection. Therefore, the LC-based methods allow for structural correlations between algal constituents and their cosmetic bioactivities, in addition to ensuring accurate metabolite profiling.

7.2. Gas Chromatography

Gas chromatography, especially when coupled with mass spectrometry, is widely used to rapidly identify and profile fatty acids, esters, alcohols, carbohydrates, phytosterols, and volatile organic compounds in cosmetic macroalgae, supporting their evaluation and development as effective cosmetic ingredients.

Gu et al. used one-dimensional gas chromatography–mass spectrometry (GC–MS) and comprehensive two-dimensional gas chromatography (GC×GC) with flame ionization detection to analyze fatty acid methyl esters (FAMEs) [102]. Although these compounds were isolated from the marine benthic diatoms *Cylindrotheca closterium* and *Seminavis robusta*, the method may have applications for the assay of fatty acids extracted from macroalgae. Several columns, such as HP-5MS, DB-WAX, HP-88, and two ionic liquid stationary phases (SLB-IL 82 and SLB-IL 100) were tested. The best separation performance and lowest column bleeding were observed with the ionic liquid columns, particularly SLB-IL 82. The mobile phase consisted of helium (GC–MS) or hydrogen (GC×GC) as carrier gases, with programmed oven temperature gradients. For high-resolution profiling, GC×GC used flow modulation, whereas MS mode used electron ionization (EI). These techniques allowed for detailed characterization of the fatty acid profiles of both algae species, particularly those that contain uncommon and polyunsaturated fatty acids [102].

Shobier et al. analyzed the chemical composition and antifungal activity of extracts from six Mediterranean macroalgae: *Ulva lactuca*, *Ulva fasciata*, *Enteromorpha compressa*, *Pterocladia capillacea*, *Hypnea musciformis*, and *Padina pavonica*. The analysis was conducted using GC/MS on a Hewlett-Packard HP-5890 Series II system equipped with a capillary column (30 m × 0.25 mm, 0.25 µm) fused with phenyl polysilphenylene siloxane. The mobile phase consisted of helium as the carrier gas at 1.0 mL/min. The mass spectrometer operated in EI mode. Important bioactive substances that contribute to the extracts' antifungal properties have been found [103].

Glycosidic linkages in unfractionated polysaccharides from five brown seaweed species, including *Macrocystis tenuifolia*, *Fucus vesiculosus*, *Alaria marginata*, *Saccharina latissima*, and *Himanthalia elongata*, were examined in a study using an improved methylation-GC-MS approach. After undergoing a three-step methylation process in heated DMSO, alcohol-insoluble residues were converted to partially methylated alditol acetates. GC was used for separation, and electron ionization mass spectrometry (EI-MS) was used for identification. The weak methanolysis-sodium borodeuteride pretreatment step made it possible to identify and quantify the uronic acid linkages in alginates. This technique allowed for detailed linkage profiling of unfractionated polysaccharides and enabled a comparison of polysaccharide composition across different seaweed species, tissues, harvest years [104].

Palaniyappa et al. developed a GC/MS method to analyze the bioactive compounds from the green seaweed *Caulerpa racemosa*. For the separation, a Shimadzu QP2020 instrument was used, which was equipped with an integrated mass spectrometer (operated in EI mode) and an SH-Rxi-5Sil-MS capillary column (30 m length, 0.25 mm internal diameter, 0.25 µm film thickness). The mobile phase consisted of helium. This technique permitted the identification of numerous bioactive metabolites such 3-hexadecene, phthalic acid, and 3,7,11,15-tetramethyl-2-hexadecen-1-ol, highlighting the chemical

richness of marine algae and their potential antioxidant, antibacterial, and therapeutic applications [105].

GC-based techniques are particularly essential for the analysis of volatile and low-molecular-weight metabolites, including fatty acids, sterols, and secondary alcohols, many of which contribute to antioxidant activity, antimicrobial protection, and the maintenance of the skin lipid barrier. Accordingly, GC serves not only as a robust tool for chemical profiling but also as a way to support the functional significance of algae extracts in cosmetic compositions.

These studies suggest that liquid and gas chromatographic methods are essential for accurately identifying, quantifying, and monitoring a wide range of active compounds such as amino acids, proteins, carbohydrates, isoflavones, phlorotannins, ensuring product safety, efficacy, and compliance with regulatory standards.

To conclude, the growing interest in algae as sustainable and multifunctional sources of bioactive compounds has driven the development of advanced analytical techniques for their characterization. Liquid and gas chromatography, coupled with spectrophotometric, colorimetric, and spectroscopic methods, play a pivotal role in the identification and quantification of key metabolites such as polysaccharides, amino acids, proteins, pigments, fatty acids, and phlorotannins.

Crucially, these analytical techniques offer not only accurate chemical profiling, but also a solid basis for functional validation of bioactive compounds: accurate measurement of MAAs confirms their well-established photoprotective qualities, phlorotannin characterization supports their anti-inflammatory and antioxidant potential, and fatty acids and peptide analysis supports their contributions to skin barrier integrity and antimicrobial effectiveness.

By integrating chemical composition data with functional assays, the specific metabolites responsible for cosmetic activity can be rigorously identified. Beyond bioactivity validation, these techniques are integral to compliance with cosmetic regulatory frameworks. For example, ISO 16128 emphasizes the need for reproducibility, ingredient traceability, and natural origin verification. All of these necessitate established procedures for accurate identification and quantification. While FTIR and NMR spectroscopic fingerprints are increasingly being used to validate polysaccharide-rich extracts, chromatographic and mass spectrometric methods are essential for assuring batch-to-batch consistency of phlorotannins and pigments.

Nonetheless, challenges persist, including limited availability of reference standards for certain algal metabolites, seasonal and geographical variations in compound abundance, and the imperative for stringent inter-laboratory validation to meet regulatory requirements. Addressing these constraints is essential to ensure that algal extracts reliably demonstrate bioactivity while fulfilling the rigorous safety, efficacy, and quality standards necessary for cosmetic commercialization.

8. Evaluation of Biological Activities of Algae Through in Vitro and in Vivo Studies

The beneficial impact of marine algal extracts on skin health is obtained through mechanisms such as the inhibition of melanin synthesis, mitigation of oxidative stress, anti-inflammatory effects, protection against UV and anti-aging properties. Data about the activity and beneficial effects of the macroalgal-derived ingredients on acquired from in vitro, in vivo and human studies are summarized in Tables 4 and 5.

8.1. Prevention of Age-Related Skin Changes

Marine algae are considered valuable components in anti-aging formulations due to their wide spectrum of demonstrated benefits. For example, *F. vesiculosus* extract has

been shown to enhance skin firmness and elasticity by increasing integrin expression in dermal fibroblasts. In a clinical study involving the application of a gel containing 1% of *F. vesiculosus* extract, a significant improvement in skin elasticity was determined after a five-week treatment period [106]. In other research, the role of fucoidan-rich macroalgal extracts was assessed in dermocosmetic applications. In vitro assays demonstrated that fucoidans can significantly inhibit enzymes implicated in cutaneous aging and protein glycation. These compounds have been associated with skin-calming effects, photoprotection, and wrinkle depth reduction. Fucoidans obtained from *Ascophyllum nodosum* exhibit multiple mechanisms of action relevant to skin rejuvenation, including suppression of leukocyte elastase activity (thereby preserving elastic fiber integrity), stimulation of dermal fibroblast proliferation, enhancement of collagen synthesis, and important antioxidant activity demonstrated through DPPH and TEAC assay [13,107].

In another clinical study, extracts from *Ulva lactuca* and *Lola implexa* were incorporated into creams and serums and further applied by volunteers aged over 50 for a seven-day trial. The results indicated that serum preparations produced a superior hydration response immediately after application compared to creams. Moreover, the serum containing 10% active extract induced the most important firming effect in single-use testing. The two formulations were effective in increasing skin moisture retention and improving firmness, showing their potential in reducing visible signs of aging.

To date, numerous algae-based skincare products are currently available on the market. Among them, extracts from *Chlamydocapsa* sp. are incorporated into hydrogels and creams designed to improve the signs of cutaneous aging, to enhance the skin's protective barrier, and to decrease transepidermal water loss (TEWL). *F. vesiculosus* extracts are included in facial treatments for their abilities to diminish dark under-eye circles and promote collagen synthesis, thereby enhancing skin elasticity. These bioactive compounds reflect the applicability of marine ingredients in modern skincare products [108,109].

F. vesiculosus, *Laminaria flexicaulis*, and *Ascophyllum nodosum* are the most used marine macroalgae in commercial anti-aging cosmetic formulations, owing to their increased number of bioactive compounds with skin-regenerative properties [110].

8.1.1. Inhibition of Collagenase and Elastase and Implications for the Prevention of Skin Aging

MMPs, particularly collagenases, are enzymes responsible for degrading the structural matrix of the skin by targeting collagen; these changes lead to skin laxity and reduced firmness. Elastase is another proteolytic enzyme that degrades elastin, further leading to the formation of wrinkles. Therefore, the active compounds that inhibit collagenases and elastase activity are considered important and effective ingredients in anti-aging skincare products. One major factor for extrinsic skin aging is represented by prolonged UV exposure that promotes the generation of reactive oxygen species (ROS) and initiates the mitogen-activated protein kinase (MAPK) signaling cascades. This activation leads to the phosphorylation of the transcription factor activator protein-1 (AP-1) and to an increase in MMP expression. Marine polysaccharides have shown significant capacity to inhibit collagenase and elastase activity. For example, polysaccharides extracted from the brown alga *Hizikia fusiforme* demonstrated inhibitory effects on collagenase and elastase activities in cultured human dermal fibroblasts. These extracts preserved the collagen biosynthesis and downregulated MMP expression. Similarly, methanolic extracts of *Corallina pilulifera*, which are high in phenolic compounds, significantly reduced the expression of MMP-2 and MMP-9 in UV-stimulated dermal fibroblasts in a dose-dependent relationship. Additionally, phlorotannins from *Ecklonia cava*, *E. stolonifera* and *Eisenia bicyclis* have been shown to exert important MMP-1 suppression. In particular, *E. cava* phlorotannins inhibited MMP-2 and MMP-9 expression. Among these

phlorotannins, compounds such as eckol, dieckol, dioxinodehydroeckol, and bieckol were identified as principal inhibitors of MMPs in human fibroblasts. Furthermore, it was observed that peptide extracts from *Poryphyra yezonensis* added to human fibroblast increased the production of elastin and collaged and decreased the expression of MMP protein [111,112].

8.1.2. Hyaluronidase Inhibition Activity

Another enzyme involved in the process of aging is hyaluronidase, responsible for the degradation of hyaluronic acid. Among the algal compounds, many phlorotannin derivatives, such as fucophloroethol, fucodiphloroethol, fucotriphloroethol, 7-phloroeckol, phlorofucofuroeckol, and bieckol/dieckol, extracted from *Cystoseira nodicaulis*, have shown important hyaluronidase inhibitory activity. Additionally, other phlorotannins, like dieckol, eckol, bieckol, and phlorofucofuroeckol, obtained from *Eisenia bicyclis* and *Ecklonia kurome*, have exhibited significant hyaluronidase inhibition; of these compounds, bieckol demonstrated the most pronounced effect [111,113].

8.2. Antioxidant Activity

To date, numerous algal species have demonstrated significant antioxidant properties, which are important for reducing oxidative stress and protecting against cellular damage. Fucoidan isolated from *Sargassum tenerrimum* has demonstrated important antioxidant activity, effectively neutralizing DPPH and superoxide radicals. In another study, fucoidan extracted from *Costaria costata* exhibited anti-aging effects in human foreskin fibroblasts by inhibiting UVB-induced MMP-1 expression and enhancing the production of type 1 pro-collagen. Porphyran, a polysaccharide derived from *Porphyra haitanensis*, has shown significant antioxidant efficacy in vitro and in vivo. In a murine model of aging using Kumming mice, administration of porphyran led to a reduction in malondialdehyde (MDA) concentrations, an indicator of lipid peroxidation and oxidative stress. Additionally, an increased total antioxidant capacity (TAOC) and enhanced activity of critical antioxidant enzymes, including superoxide dismutase (SOD) and glutathione peroxidase (GSH-Px), were observed [113].

8.3. Anti-Melanogenic Activity

Since skin exposure to UV radiation stimulates melanin production in melanocytes, the application of cosmetics containing tyrosinase inhibitors represents a common approach to reduce skin hyperpigmentation. Tyrosinase is considered a key enzyme in the process of melanin synthesis, which determines the pigmentation of skin and hair color. In this regard, a study conducted by Cha and colleagues [114] investigated 43 species of marine algae to evaluate their efficacy to inhibit tyrosinase activity. The objective of the study was to evaluate the potential of marine algae as skin-whitening agents by assessing their influence on melanogenesis. Experimental models included murine melanocyte cultures and zebrafish embryos, and the study evaluated tyrosinase activity and melanin content analysis. Several species exhibited significant antimelanogenic effects, namely, *Endarachne binghamiae*, *Sargassum siliquastrum*, *Ecklonia cava*, and *Ishige okamurae Yendo*. Among these, *S. siliquastrum* and *E. cava* were particularly effective in reducing melanin levels in melanocytes, while all tested extracts induced an important inhibition of pigmentation in zebrafish larvae, an effect likely mediated through the suppression of tyrosinase activity. Other studies investigated the anti-melanogenic activity of algae-derived fucoidan. It was shown that fucoidan reduced the melanin ratio in murine melanocytes by activating the ERK pathway, leading to downregulation of melanogenesis-related proteins such as MITF and TYR. Fucoxanthin isolated from *L. japonica* has been investigated for its effects on UVB-irradiated guinea pigs and mice. The compound demonstrated effective inhibition of tyrosinase activity and

melanin production under UVB exposure. Furthermore, brown algae extracts from *Sargassum polysytum* and *Padina tenuis* have been shown to significantly decrease melanin content in human epidermal melanocyte cultures. In an in vitro study, Park and collaborators evaluated the effects of *Pyropia yezoensis* on melanogenesis across multiple human cell lines, including melanocytes, dermal fibroblasts, and keratinocytes. The findings demonstrated that the extract possessed strong tyrosinase inhibitory activity and enhanced collagen synthesis by suppressing the expression of matrix metalloproteinases MMP-2 and MMP-9. Additionally, the extract enhanced the production of procollagen enzymes, suggesting that it could be used as a multifunctional cosmetic ingredient targeting skin aging and hyperpigmentation [113,115].

8.4. Moisturizing Activity

A good level of skin hydration plays a fundamental role in the prevention of skin aging by preserving healthy skin appearance and maintaining elasticity while reinforcing the skin barrier against environmental factors. Polysaccharides derived from algae are a sustainable and readily available resource, offering a cost-efficient solution for bioactive ingredients with moisturizing properties. In this sense, studies have shown that polysaccharides extracted from *Saccharina japonica*, a brown alga, exhibited superior moisturizing properties and water retention capacity. The polysaccharides from *S. japonica* demonstrated greater water retention capacity and hydration potential than hyaluronic acid, a valuable ingredient widely used in moisturization studies. In parallel, *Chondrus crispus*, a red alga rich in both polysaccharides and essential minerals, has been well recognized for its hydrating and moisture-enhancing properties.

In the case of green algae, extracts from *Codium tomentosum* have been shown to contribute to the regulation of water distribution within the epidermis, thereby reducing TEWL, particularly in dry environmental conditions. Additionally, DNA isolated from various marine algal sources, including *Undaria pinnatifida*, *Durvillea antarctica*, *Ascophyllum nodosum*, *Cladosiphon okamuranus*, *Pediastrum duplex*, and *Polysiphonia lanosa*, has been investigated for its capacity to enhance skin moisturization. A study carried out by Sayin and colleagues [112] assessed the antimicrobial potential of alginate extracted from *Sargassum vulgare*, evaluating its efficacy as a natural preservative in cosmetic formulations. The results indicated that this alginate extract exhibited higher antimicrobial activity against *Staphylococcus aureus*, *Pseudomonas aeruginosa*, *Candida albicans*, *Aspergillus brasiliensis*, and *Escherichia coli* compared to a commercially available herbal preservative containing glyceryl caprylate and glyceryl undecylenate. Besides this application, alginate is also used in cosmetics as a delivery system for lipophilic ingredients. This strategy provides protection of the actives and allows for their controlled release. Innovative formulations have recently included alginate-based nanofiber patches infused with spirulina extract and overlaid with polycaprolactone nanofibers. In vitro evaluations using human keratinocyte cell lines confirmed the absence of cytotoxicity for all components. Furthermore, the patches significantly improved skin hydration and demonstrated enhanced adhesive performance. In conclusion, alginates have a broad range of applications in cosmetic formulations. Their ability to maintain moisture levels in both skin and hair makes them valuable components in products such as creams, emulsions, face masks, and hair gels, where they act as humectants. In addition, alginates contribute to the physical stability of emulsions by preventing phase separation, act as effective gelling agents under acidic conditions, and are widely utilized to regulate product consistency [116].

Table 4. Active ingredients from macroalgae and their skin beneficial effects.

Active Ingredients from Algae	Beneficial Effects in Skin Health	Reference
Main active ingredients from algae and their skin health benefits		
Phlorotannins, carotenoids, photolyase, mycosporine-like amino acids	UV protection	[117]
Tocopherols, polyphenols, β-carotenoids (vitamin A), other carotenoids	Skin protection (radical scavenging and immune system stimulation)	
(Sulfated) polysaccharides, glycosaminoglycans	Skin moisturizing	
Essential and nonproteinogenic amino acids, highly unsaturated fatty acids	Skin smoothing and regeneration	
Phlorotannins, phloroglucinol and its oligomers	Skin whitening	
Low-molecular-weight fucoidans	Stimulation of collagen synthesis	
Bioactive extracts from specific algae species and their in vitro/in vivo *demonstrated effects*		
Alginates (*Sargassum vulgare*)	↗ antimicrobial properties (on *Pseudomonas aeruginosa*, *Staphylococcus aureus*, *Candida albicans*, *Escherichia coli*, *Aspergillus brasiliensis* strains)	[116]
Brown algae polysaccharides (*Hizikia fusiforme*)	UVB protection (protection collagen synthesis and ↘ MMPs expression in UVB-irradiated human dermal fibroblasts	[112]
Fucoidans (*Sargassum tenerrimum*, *Laminaria japonica*, *Fucus vesiculosus*)	Antioxidant activity (superoxide radical scavenging properties)	[113]
Fucoidans (*Ascophyllum nodosum*)	Anti-aging, UV protection, wrinkle reduction, antioxidant, collagen synthesis	[13]
Fucoidan (*Laminaria cichorioides*)	Beneficial effect in atopic dermatitis (inhibits production of IgE)	[118]
Laminarin	UVB protection (↘ ROS production and ↗endogenous antioxidant levels against UVB irradiation	[119]
Phlorotannins from *Cystoseira nodicaulis*, *Cystoseira tamariscifolia*, *Cystoseira usneoides Fucus spiralis*	Hyaluronidase inhibition, antioxidant activity (superoxide radical scavenging properties, lipid peroxidation inhibition)	[120]
Polysaccharides from *Saccharina japonica*	Skin moisturizing (moisture-absorption and moisture-retention abilities)	[121]
Porphyran from *Porphyra haitanensis*	Antioxidant capacity (↗ antioxidant enzyme activity-aging mice)	[122]
Porphyran from *Pyropiaa yezoensis*	Anti-inflammatory activity in LPS-stimulated macrophages	[123]
HMW ulvans	↗ hyaluronan biosynthesis in dermal fibroblasts	[124]
Ecklonia cava, *E. kurome*, *Ishige sinicola* extracts	Anti-acne activity *(on Cutibacterium acnes)*	[125]
Fucus vesiculosus extract	↗ skin elasticity	[106]
Marine complex including *Ulva lactuca*, *Lola implexa* extracts	Skin moisturizing, skin firming and tightening	[109]
Pyropia yezoensis extract	↗ collagen synthesis, prevents its degradation (human skin fibroblasts) ↘ melanin content (inhibits tyrosinase activity)	[115]

Table 4. *Cont.*

Active Ingredients from Algae	Beneficial Effects in Skin Health	Reference
Sargassum muticum, *Osmundea pinnatifida*, *Codium tomentosum* water-based extracts	In vitro antioxidant activity (hydroxyl-radical scavenging properties)	[111]
Undaria pinnatifida extract (85% fucoidan) and *Fucus vesiculosus* co-extract, (60% fucoidan, 30% polyphenol)	Soothing, UV protection, wrinkle depth reduction; *Fucus vesiculosus* extract—antioxidant effect	[108]

TEWL—transepidermal water loss, MMPs—matrix metalloproteinases, LPS—lipopolysaccharide-stimulated, ↗—increasing; ↘—decreasing, HMW—high-molecular-weight.

Table 5. Summary of clinical studies on macroalgae-derived cosmetic formulations.

Algae Species (Type)	Formulation	Study Design (Subjects, Duration)	Outcomes	Main Cosmetic Effect	Reference
Codium tomentosun (green)	Moisturizing cream (5%)	7 days, 10–12 women	Hydration ↑ 2–3× vs. placebo; improved barrier	Hydration/ barrier support	[126]
Laminaria japonica (brown)	Cream (0–15%)	Single use, 10 women	Dose-dependent hydration; 10% ↓ TEWL	Hydration/ barrier support	[126]
Rhizoclonium hieroglyphicum (green)	Cream (0.3%)	30 subjects, 1 week	Immediate + sustained hydration; superior to glycerin	Hydration	[126]
Sargassum hornieri (brown, fucoidan)	Lotion (1%)	3 weeks, forearm study	↓ TEWL; ↑ hydration; restored barrier	Barrier function/ hydration	[127]
Fucus vesiculosus + *Ulva lactuca* (brown + green) +ectoin	Serum mist (split-face)	28 days, 33 adults	+17% hydration; pH normalized	Hydration/ wrinkle reduction	[128]
Brown algal alginate + calcium	Sheet mask	Single use	↑ hydration, pH regulation; ↓ wrinkles, ↑ smoothness; maintained microbiome diversity; ↓ *Corinebacterium*	Hydration/ microbiome/ anti-wrinkle	[129]
Fucus vesiculosus (brown)	Cream (1%)	5 weeks, 10 women	↑ elasticity, 7–8% ↓ skin thickness	Firming/ anti-aging	[126]
Undaria pinnatifida + *Fucus vesiculosus* (brown)	Gel (0.3%)	UVB test, 25 subjects	↓ UV erythema, ↓ TEWL	Photoprotection/ anti-aging	[126]
Fucus vesiculosus (brown, fucoidan/ polyphenols)	Gel (0.3%)	60 days, 30 subjects	↑ brightness, ↓ wrinkles, ↓ age spots	Brightening/ anti-aging	[126]
Porphyra umbilicalis (red, MAAs)	Cream (0.005%) vs. suncreen	4 weeks, 20 women	UVA protection; ↑ firmness, ↑ smoothness	Photoprotection/ anti-aging	[130]

Table 5. *Cont.*

Algae Species (Type)	Formulation	Study Design (Subjects, Duration)	Outcomes	Main Cosmetic Effect	Reference
Ascophyllum nodosum (brown) + herbal extract	Botanical regiment	18 weeks, 56 women; 1 year extension	Comparable to hydroquinone/ tretinoin; no rebound pigmentation	Anti-pigmentation	[126]
Laminaria digitata + *Gelidium cartilagineum* + *Pelvetia canaliculata* (brown + red)	Anti-cellulite cream	4 weeks, 90 women	↓ thigh/ waist/ hip circumference; ↑ firmness	Slimming/ firming	[126]
Fucus vesiculosus + *Furcellaria lumbricalis* (brown + red)	Anti-cellulite cream	12 weeks, 35 women	↓ cellulite grade; ↓ adipose thickness	Anti-cellulite/ firming	[126]
Laminaria digitata (brown, oligosaccharide-zinc complex)	Gel	8 weeks (acne vulgaris	↓ lesion severity; ↓ sebum; ↓ P.acnes	Anti-acne	[131]

In the studies reviewed in Table 4, some algae-derived ingredients were tested as whole extracts, while others were evaluated as isolated compounds, making a direct comparison of their efficacy challenging.

In vitro and in vivo preclinical studies provide consistent evidence for supporting the antioxidant, anti-inflammatory and skin-protective properties of macroalgal extracts and ingredients. These findings request further validation in human studies, which are compiled in Table 5.

The wide spectrum of biological effects exhibited by macroalgal extracts, mainly antioxidant, anti-inflammatory, anti-melanogenic and anti-aging activities, together with the enhanced skin moisturization effect, justifies their increasing use in topical formulations. From a practical perspective, marine macroalgae represent not only a sustainable and renewable resource, but also high-potential compounds for the development of multifunctional cosmetics intended to prevent skin aging, improve hydration and support skin health. This corresponds to the current industry trends that promote multifunctional, bio-based formulations with multiple skin benefits within a single product.

While these multifunctional benefits support the growing use of macroalgal extracts in topical products, their market adoption remains challenging. As observed in Tables 1–3, in regulatory databases such as COSING, macroalgal ingredients are classified as "skin conditioning," reflecting the broad accepted effects focused on improvements in the skin's overall condition, as outlined by Cosmetic Products Regulation (EC) No. 1223/2009 and Regulation (EU) No. 655/2013. While scientific studies report more specific effects, such as antioxidant activity, wrinkle reduction or photoprotection, these require rigorous validation through standardized assays and clinical trials to meet regulatory standards. Thus, the general classification in COSING contrasts with targeted bioactivities described in the research studied. Therefore, future research should focus on the validation of these claims through well-designed and well-conducted methodologies and their acceptance by regulatory authorities.

8.5. Skin Regeneration Activity

Another important application of marine algal extracts lies in their demonstrated effects in wound care. Table 6 highlights some of topical systems loading macroalgae-derived compounds, such as ulvan, laminarin and fucoidan, with demonstrated biological activity in skin regeneration. These compounds have pro-healing properties by modulating different phases of the wound-healing process, and by promoting wound contraction, collagen synthesis and reducing the inflammatory response. Although these compounds exhibit beneficial effects per se, their efficacy is often significantly enhanced when combined with antibacterial agents or antibiotics and incorporated into advanced delivery systems, such as hydrogels, wound patches or nanofibrous scaffolds. For example, fucoidan has been successfully incorporated into a gelatin/oxidized carboxymethyl cellulose hydrogel, resulting in accelerated re-epithelialization and reduced inflammatory response demonstrated in in vivo models [132]. Ulvan incorporated into nanofibrous patches or silver-loaded hydrogels has shown significant contributions to wound contraction, decreased inflammation at wound sites and improved vascularization, leading to an accelerated healing process [133,134]. In the case of laminarin, its combination with silver nanoparticles or 3D graphene foams promoted antibacterial activity and enhanced cell migration, thus showing the tissue regenerative potential [135].

Table 6. Topical systems loading macroalgae-derived compounds and their effects in wound healing.

Phytocompound-Based Topical Systems	Biological Activity Beneficial in Wound Healing	Reference
	Ulvan	
Nanofibrous patches (ulvan, polyethylene oxide)	In vivo study: anti-inflammatory, antioxidant effects, ↘ inflammation, restoring biophysical parameters of skin	[133]
Wet-spun fibers, 3D printed hydrogel	In vitro cell studies: higher cell viability than alginate and chitosan in biocompatibility tests	[136]
Polycaprolactone-ulvan fibrous composite mats	In vitro cell studies-NIH3T3 fibroblasts: ↗ cellular proliferation, ↗ expression α-SMA and MMP-9 genes	[137]
Ulvan/gelatin-based nanofibrous patches	In vivo study with burn wound mouse model: faster wound contraction during early stages of healing, ↘ inflammation, uniform wound closure	[138]
Chitosan-ulvan hydrogels with cellulose nanocrystals and epidermal growth factor	In vitro cytocompatibility studies, in vivo wound-healing study on mice: epithelial regeneration and collagen deposition	[139]
Ulvan-based hydrogel matrix loaded with silver nanoparticles and human umbilical cord mesenchymal stem cell lyophilized powder	In vitro antibacterial activity, cytocompatibility, ↗ cell proliferation and cell migration, In vivo study with type II diabetes mellitus mouse model, ↗ wound-healing effect	[140]
Ulvan/Silver nanoparticle hydrogel films	In vitro antimicrobial activity, In vivo study with Wistar rats with second-degree burns accelerated wound healing, modulating inflammation, ↗ re-epithelialization, ↗ vascularization	[134]
Crosslinked ulvan/Chitosan complex films	In vitro studies: biocompatibility, scratch assay—↗ HaCaT cell migration and proliferation In vivo study with Sprague Dawley rats: regeneration of dermis, collagen production	[141]

Table 6. *Cont.*

Phytocompound-Based Topical Systems	Biological Activity Beneficial in Wound Healing	Reference
	Laminarin	
Cystoseira barbata laminaran based cream	In vitro antibacterial and antioxidant activity In vivo study with Wistar rats: ↗ collagen deposition, ↗ fibroblast and vascular density	[142]
Hydrogel patch of methacrylated laminarin loaded with ciprofloxacin	In vitro antibacterial activity, biocompatibility human dermal fibroblasts	[143]
3D graphene foam/laminarin hydrogel composite scaffold	In vitro: biocompatibility ↗ cell migration	[144]
Dialdehyde-modified laminarin- silver nanoparticles	In vitro antibacterial activity and inhibition of biofilm formation Cell viability and scratch assay: ↗ migration of human HaCaT	[135]
	Fucoidan	
Gelatine/fucoidan nanogel-coated silver nanoparticles	In vitro antibacterial activity and inhibition of biofilm formation Cell viability and scratch assay: ↗cell regeneration	[145]
Fucoidan-loaded gelatin/oxidized carboxymethyl cellulose hydrogel	In vitro: cytocompatibility—RAW 264.7 macrophages, human dermal fibroblasts; protection against oxidative stress, ↘ NO production in LPS-stimulated RAW 264.7 macrophages, ↗ collagen synthesis and cell migration in HDF cells In vivo wound-healing model- mice: ↗ full-thickness wound healing	[132]
Fucoidan loaded PVA/Dextran blend electrospun nanofibers	In vivo studies-Sprague Dawley rats: ↗ wound-healing rate: ↘inflammatory response through antioxidant effects, ↗ epidermal regeneration and collagen deposition	[146]
Fucoidan-coated cotton dressing loaded with silver nanoparticles	In vitro antibacterial activity, cytotoxicity fibroblast cell line, scratch assay In vivo infected wound mouse model: inhibition of bacterial infection, tissue proliferation and collagen deposition	[147]
Fucoidan-loaded neutrophil membrane-coated nanoparticles	In vitro antibacterial activity, intracellular uptake ability of RAW264.7 cells In vivo MRSA-infected trauma mouse mode: long term antibacterial effect, accumulation in the infection site, ↗ infected wound closure	[148]
Moxifloxacin chitosan/fucoidan nanoparticle-loaded pullulan microneedle patch	In vitro antibacterial activity Ex vivo permeation study, cytotoxicity In vivo biocompatibility, BALB/c mice infectious wound model: accelerated wound healing, rapid wound closure	[149]
Fucoidan confined gold nanoparticles hydrogel	In vitro antibacterial activity, blood compatibility, cytocompatibility, anti-inflammatory assay on LPS-induced Raw 264.7 macrophage model, *S. aureus*-infected full-thickness wound-healing test: adherence to wound site, ↗ tissue regeneration, ↘ bacterial growth, ↘ inflammatory responses	[150]

↗—increasing; ↘—decreasing.

In conclusion, the current research direction has evolved from simple phytocompound isolation and development of basic formulations to the incorporation of macroalgal-derived actives into performant, functionalized wound care formulations with controlled release and high biocompatibility.

9. Formulation Strategies and Challenges

For their use in topical products, algae are typically processed as algae extracts or as powders. It is essential—as previously discussed—to ensure a high quality and safety of these products, and thus, for these to be standardized in active compounds and well characterized. An additional critical aspect is the concentration selected for incorporation into the final formulation. As algae extracts show high and wide-ranged activity, their reported content in cosmetic formulations usually does not exceed 10% by weight and the average is below 5% by weight [151]. However, at present, there are no specific regulations establishing the maximum permissible levels of algae-derived compounds in skincare and cosmetic products, which adds complexity to the regulatory framework. Moreover, the absence of strict criteria for evaluating the safety of algal production further complicates their integration into the international market [152]. Despite their great potential, several challenges arise in the formulation of algal bioactives. Many compounds—such as polyphenols, polysaccharides, and carotenoids—exhibit low chemical stability, being especially vulnerable to oxygen, light, high temperatures, enzymatic reactions, heavy metal exposure, and extended periods of storage [153–155].

An adequate delivery system allows researchers to improve the performance and stability of the ingredients of interest [156]. The choice of formulation strategy largely depends on the type of algae extract, its solubility and the concentration to be incorporated, as well as the intended characteristics of the topical product. It has been shown that emulsions and encapsulation of the algae extracts are one of the most used strategies that allow for the extension of the stability of the compounds of interest [153]. The primary strategy to protect functional ingredients and enhance their performance upon skin contact is encapsulation. Commonly employed delivery systems in cosmetics include vesicular carriers (liposomes, silicone vesicles, niosomes, transfersomes, and other systems), emulsion-based systems (microemulsions, nanoemulsions, multiple emulsions, liquid crystals, and Pickering emulsions), and particulate carriers (nano- and microparticles, porous polymeric systems, cyclodextrin complexes) [151]. These carriers can subsequently be incorporated into emulsions, suspensions, or other topical formulations. An effective delivery system not only improves the stability and bioavailability of sensitive compounds but enhances their overall performance [151]. For example, Lourenço-Lopes compared the stability of fucoxanthin as a free molecule, in an emulsion, or encapsulated, and reported that fucoxanthin encapsulation is considered one of the best approaches, followed by its emulsion [153]. Importantly, formulations must rely on safe, eco-friendly technologies and account for scalability in manufacturing [151].

To highlight their practical importance, Table 7 summarizes some commercially available topical products enriched with various algae species, indicating their product types and claimed effects, to highlight their practical applications.

According to Table 7, algae were incorporated in multiple types of cosmetic products, including creams, serums, shampoos, and solid soaps, illustrating the versatility of macroalgae extracts in skincare, although they are most commonly formulated in creams (emulsions). A wide range of algae species are used in commercially available products, from red algae (e.g., *Jania rubens*) to brown algae (e.g., *Fucus vesiculosus*, *Fucus serratus*, *Laminaria japonica*, *Laminaria digitata*, *Laminaria cloustoni*) and green algae (e.g., *Ulva lactuca*), highlighting the diversity of bioactive compounds that can be harnessed for cosmetic

purposes. The claimed effects of these products encompass moisturizing, antioxidant activity, skin barrier repair, anti-aging, UV protection, and skin regeneration, reflecting the multifunctional potential of algae-derived compounds. Notably, some products combine multiple algae species, potentially leveraging synergistic effects to enhance their benefits in skin health.

Table 7. Commercially available topical products loaded with algae (non-exhaustive list).

Algae Species	Product Type	Claimed Effects	Ref.
Jania rubens extract	Serum	Moisturizing, smoothing, antioxidant, plumping, detoxing	[157]
Undaria pinnatifida, *Ecklonia cava*, *Laminaria japonica*, *Hizikia fusiforme*, *Porphyra yezoensis*, *Laminaria digitata*, *Laminaria cloustoni*, *Enteromorpha compressa*, *Codium tomentosum*, *Codium fragile*, *Agarum cribosum*, *Ulva lactuca* extracts	Cream	Moisturizing, smoothing, skin barrier-repairing, protecting, nourishing	[158]
Ascophyllum nodosum, *Fucus vesiculosus*, *Crithmum maritimum*, *Corallina officinalis* extracts	Cream	Moisturizing, regenerating	[159]
Prasinococcus capsulatus exopolysaccharides	Cream	Protecting, hydrating, anti-aging	[160]
Fucus serratus extract	Shampoo	Moisturizing, UV-protecting, long-lasting skin protection	[161]
Laminaria japonica powder	Solid soap	Moisturizing, smoothing,	[162]
Ascophyllum nodosum, *Fucus vesiculosus* extracts	Serum	Energizing, antioxidants	[163]

Besides the examples from Table 7, a noteworthy case is also represented by the large number of skincare products based on algae extracts from the cosmetic brand Algologie® (France). Its formulations are centered around the patented Algo4® complex, which combines extracts from brown macroalgae and red microalgae (*Undaria pinnatifida*, *Porphyridium cruentum*) with coastal plants extracts, providing moisturizing, protection, and anti-aging effects. The whole product portfolio covers a wide range of applications, including moisturizing, purifying, energizing, and anti-aging effects. The product range includes lotions, creams, gel-creams, foams, serums, demonstrating the feasibility of incorporating multiple marine-derived actives into various modern cosmetic formulations [164]. Other examples are from the Thalgo® (France) skincare brand specializing in using marine ingredients and advanced technologies to create products aimed at revitalizing, moisturizing, and protecting the skin. A representative product from Thalgo®'s portfolio is Micronised Marine Algae, a powder product designed for steam baths or at-home thalassotherapy that helps to remineralize and revitalize the skin. The active ingredients include micronized marine algae powders from species such as *Fucus vesiculosus*, *Laminaria digitata*, and *Lithothamnion calcareum*. Thalgo® also includes algae in a wide range of skincare products, including creams, serums, masks, cleansing gels, all formulated with marine ingredients to address diverse skin needs [165].

This diversity illustrates the versatility of marine-derived extracts and their feasibility for incorporation into different types of topical formulations, as well as their use as powders. This overview demonstrates the practical application of algae extracts in real-world topical formulations and underscores their growing relevance in modern skincare.

10. Conclusions

This review represents a synthesis of marine macroalgae-derived compounds relevant to skin health. The novelty of this work lies in the broad discussion from taxonomic, ecological, and biochemical data to modern extraction techniques and quantitative analysis of active compounds. Marine macroalgae, brown, red, and green, represent a promising and sustainable source of structurally diverse bioactive compounds with significant potential in topical dermatological and cosmetic formulations. Their metabolites, including polysaccharides, polyphenols, peptides, lipids, pigments, and vitamins, have demonstrated multifunctional biological activities such as antioxidant, anti-inflammatory, moisturizing, photoprotective. Nevertheless, the chemical composition of macroalgae is subject to variability influenced by taxonomic differences, environmental conditions, and seasonal dynamics, posing challenges for reproducibility and standardization in product development. Recent advancements in extraction methods (e.g., ultrasound-assisted extraction, supercritical fluid extraction) and analytical techniques (HPLC, GC-MS and FTIR) have improved the efficiency and selectivity of compound isolation and quantification. In addition to the description of isolated bioactives, this review includes evidence from in vitro and in vivo studies that demonstrate the biological activities in skin applications, considering the efficacy and dermal safety, particularly in the context of wound-healing and anti-aging interventions. Moreover, this review highlighted the diversity of commercially available products loading algae, demonstrating their practical application and huge interest. It also outlined the formulation strategies employed in topical products, noting that while incorporation into emulsions remains the most common approach, encapsulation into modern delivery systems represents a key advancement for enhancing their performance. These findings prove the usefulness of integrating macroalgae-derived compounds as effective and biocompatible ingredients in modern cosmeceutical formulations. The present review aimed to provide a theoretical basis for formulators and scientists in developing safe, effective and multifunctional skin health products within the current sustainability trends.

Author Contributions: Conceptualization, C.B. and M.M. and M.-L.M.; methodology, C.B.; investigation, M.M. and E.I.D. and A.A.O.; writing—original draft preparation, M.M. and C.B. and E.I.D. and A.A.O. and D.A.S.; writing—review and editing, C.B. and E.I.D.; visualization, D.A.S.; supervision, C.B. and M.-L.M.; funding acquisition, C.B. All authors have read and agreed to the published version of the manuscript.

Funding: This research was financially supported by Iuliu Hatieganu University of Medicine and Pharmacy, Cluj-Napoca, Romania, Grant 32154/15/16.12.2024.

Data Availability Statement: Data are contained within this article.

Conflicts of Interest: The authors declare no conflicts of interest.

References

1. El-Chaghaby, G.A.; Rashad, S. An overview of algae prospects in cosmeceuticals. *J. Egypt. Women's Dermatol. Soc.* **2021**, *18*, 161–166. [CrossRef]
2. Kelman, D.; Posner, E.K.; McDermid, K.J.; Tabandera, N.K.; Wright, P.R.; Wright, A.D. Antioxidant activity of Hawaiian marine algae. *Mar. Drugs* **2012**, *10*, 403–416. [CrossRef]
3. Wang, H.D.; Chen, C.C.; Huynh, P.; Chang, J.S. Exploring the potential of using algae in cosmetics. *Bioresour. Technol.* **2015**, *184*, 355–362. [CrossRef]
4. Thiyagarasaiyar, K.; Goh, B.H.; Jeon, Y.J.; Yow, Y.Y. Algae Metabolites in Cosmeceutical: An Overview of Current Applications and Challenges. *Mar. Drugs* **2020**, *18*, 323. [CrossRef]
5. Lee, R. *Phycology*, 4th ed.; Cambridge University Press: Cambridge, UK, 2008.
6. Khan, M.; Cheng, J.; Bankole, P. *The Algae World—Classification of Algae*; IntechOpen: London, UK, 2015.

7. Łęska, B.; Messyasz, B.; Schroeder, G. Application of Algae Biomass and Algae Extracts in Cosmetic Formulations. In *Algae Biomass: Characteristics and Applications: Towards Algae-Based Products*; Chojnacka, K., Wieczorek, P.P., Schroeder, G., Michalak, I., Eds.; Springer International Publishing: Cham, Switzerland, 2018; pp. 89–101.
8. Cho, S.; Lee, D.H.; Won, C.H.; Kim, S.M.; Lee, S.; Lee, M.J.; Chung, J.H. Differential effects of low-dose and high-dose beta-carotene supplementation on the signs of photoaging and type I procollagen gene expression in human skin in vivo. *Dermatology* **2010**, *221*, 160–171. [CrossRef]
9. Commission, E. CosIng—Cosmetics Ingredients. Available online: https://ec.europa.eu/growth/tools-databases/cosing/ (accessed on 18 August 2025).
10. Gupta, A.; Singh, A.P.; Singh, V.K.; Singh, P.R.; Jaiswal, J.; Kumari, N.; Upadhye, V.; Singh, S.C.; Sinha, R.P. Natural Sun-Screening Compounds and DNA-Repair Enzymes: Photoprotection and Photoaging. *Catalysts* **2023**, *13*, 745. [CrossRef]
11. Castro, V.; Oliveira, R.; Dias, A.C.P. Microalgae and cyanobacteria as sources of bioactive compounds for cosmetic applications: A systematic review. *Algal Res.* **2023**, *76*, 103287. [CrossRef]
12. Resende, D.I.S.P. Trends in the use of marine ingredients in anti-aging cosmetics. *Algal Res.* **2021**, *55*, 102273. [CrossRef]
13. López-Hortas, L.; Flórez-Fernández, N.; Torres, M.D.; Ferreira-Anta, T.; Casas, M.P.; Balboa, E.M.; Falqué, E.; Domínguez, H. Applying Seaweed Compounds in Cosmetics, Cosmeceuticals and Nutricosmetics. *Mar. Drugs* **2021**, *19*, 552. [CrossRef] [PubMed]
14. Santos, J. Extraction and Formulation of Macroalgal Phenolic Compounds for Cosmetic Application. Master's Thesis, Technical University of Lisbon, Lisbon, Portugal, 2021.
15. Shafie, M.H.; Kamal, M.L.; Zulkiflee, F.F.; Hasan, S.; Uyup, N.H.; Abdullah, S.; Hussin, N.A.M.; Tan, Y.C.; Zafarina, Z. Application of Carrageenan extract from red seaweed (Rhodophyta) in cosmetic products: A review. *J. Indian Chem. Soc.* **2022**, *99*, 100613. [CrossRef]
16. Robinson, M.; Visscher, M.; Laruffa, A.; Wickett, R. Natural moisturizing factors (NMF) in the stratum corneum (SC). I. Effects of lipid extraction and soaking. *J. Cosmet. Sci.* **2010**, *61*, 13–22.
17. Ozanne, H.; Toumi, H.; Roubinet, B.; Landemarre, L.; Lespessailles, E.; Daniellou, R.; Cesaro, A. Laminarin Effects, a β-(1,3)-Glucan, on Skin Cell Inflammation and Oxidation. *Cosmetics* **2020**, *7*, 66. [CrossRef]
18. Wang, L.; Oh, J.Y.; Kim, Y.S.; Lee, H.G.; Lee, J.S.; Jeon, Y.J. Anti-Photoaging and Anti-Melanogenesis Effects of Fucoidan Isolated from. *Mar. Drugs* **2020**, *18*, 427. [CrossRef] [PubMed]
19. Manandhar, B.; Wagle, A.; Seong, S.H.; Paudel, P.; Kim, H.R.; Jung, H.A.; Choi, J.S. Phlorotannins with Potential Anti-tyrosinase and Antioxidant Activity Isolated from the Marine Seaweed. *Antioxidants* **2019**, *8*, 240. [CrossRef] [PubMed]
20. Cotas, J.; Leandro, A.; Monteiro, P.; Pacheco, D.; Figueirinha, A.; Gonçalves, A.M.M.; da Silva, G.J.; Pereira, L. Seaweed Phenolics: From Extraction to Applications. *Mar. Drugs* **2020**, *18*, 384. [CrossRef]
21. Thomas, N.V.; Kim, S.K. Beneficial effects of marine algal compounds in cosmeceuticals. *Mar. Drugs* **2013**, *11*, 146–164. [CrossRef]
22. Kumar, L.R.G.; Paul, P.T.; Anas, K.K.; Tejpal, C.S.; Chatterjee, N.S.; Anupama, T.K.; Mathew, S.; Ravishankar, C.N. Phlorotannins-bioactivity and extraction perspectives. *J. Appl. Phycol.* **2022**, *34*, 2173–2185. [CrossRef]
23. Ziboh, V.A.; Miller, C.C.; Cho, Y. Metabolism of polyunsaturated fatty acids by skin epidermal enzymes: Generation of antiinflammatory and antiproliferative metabolites. *Am. J. Clin. Nutr.* **2000**, *71*, 361S–366S. [CrossRef]
24. Aslam, A.; Bahadar, A.; Liaquat, R.; Saleem, M.; Waqas, A.; Zwawi, M. Algae as an attractive source for cosmetics to counter environmental stress. *Sci. Total Environ.* **2021**, *772*, 144905. [CrossRef]
25. Fabrowska, J.; Łęska, B.; Schroeder, G.; Messyasz, B.; Pikosz, M. Biomass and Extracts of Algae as Material for Cosmetics. In *Marine Algae Extracts*; Wiley: Hoboken, NJ, USA, 2015; pp. 681–706.
26. Fujimura, T.; Tsukahara, K.; Moriwaki, S.; Kitahara, T.; Sano, T.; Takema, Y. Treatment of human skin with an extract of *Fucus vesiculosus* changes its thickness and mechanical properties. *J. Cosmet. Sci.* **2002**, *53*, 1–9.
27. Alvarez-Hernández, S.; Lozano-Ramírez, C.; Rodríguez-Palacio, M. Influence of the Habitat on Marine Macroalgae Toxicity. *Annu. Res. Rev. Biol.* **2019**, *33*, 1–9. [CrossRef]
28. Cruz-Rivera, E.; Villareal, T.A. Macroalgal palatability and the flux of ciguatera toxins through marine food webs. *Harmful Algae* **2006**, *5*, 497–525. [CrossRef]
29. Dromard, C.R.; Bouchon-Navaro, Y.; Harmelin-Vivien, M.; Bouchon, C. The nutritional quality of non-calcified macroalgae in Guadeloupe (Lesser Antilles) evaluated by their biochemical composition. *Gulf Caribb. Res.* **2017**, *28*, GCFI1-GCGI6. [CrossRef]
30. Cresson, P.; Ruitton, S.; Noisette, F.; Harmelin-Vivien, M. Isotopic and biochemical composition of Western Mediterranean macroalgae. *Eur. J. Phycol.* **2023**, *59*, 21–37. [CrossRef]
31. Generalić Mekinić, I.; Čagalj, M.; Tabanelli, G.; Montanari, C.; Barbieri, F.; Skroza, D.; Šimat, V. Seasonal Changes in Essential Oil Constituents of Cystoseira compressa: First Report. *Molecules* **2021**, *26*, 6649. [CrossRef]
32. Ji, Y.; Xu, Z.; Zou, D.; Gao, K. Ecophysiological responses of marine macroalgae to climate change factors. *J. Appl. Phycol.* **2016**, *28*, 2953–2967. [CrossRef]
33. Burnham, K.A.; Nowicki, R.J.; Hall, E.R.; Pi, J.; Page, H.N. Effects of ocean acidification on the performance and interaction of fleshy macroalgae and a grazing sea urchin. *J. Exp. Mar. Biol. Ecol.* **2022**, *547*, 151662. [CrossRef]

34. Schram, J.B.; Schoenrock, K.M.; McClintock, J.B.; Amsler, C.D.; Angus, R.A. Ocean warming and acidification alter Antarctic macroalgal biochemical composition but not amphipod grazer feeding preferences. *Mar. Ecol. Prog. Ser.* **2017**, *581*, 45–56. [CrossRef]
35. Zakharikhina, L.V.; Gorbunova, T.L.; Ryndin, A.V.; Lesnikova, P.S.; Rogozhina, E.V. Chemical composition and growth responses of brown, green, and red macroalgae to pollution in the Russian black sea. *Mar. Pollut. Bull.* **2024**, *207*, 116831. [CrossRef]
36. Araujo-Motta, L.; Alves-Lima, C.; Zambotti-Vilella, L.; Colepicolo, P. Metabolome of Cadmium Stressed *Gracilaria caudata* (Rhodophyta). *Phycology* **2023**, *3*, 255–269. [CrossRef]
37. El-Sherbiny, M.M.; Satheesh, S.; Ba-Akdah, M.A. Physiological Responses of Marine Macroalgae to Chlorine Dioxide Treatment. *Thalassas* **2021**, *37*, 291–302. [CrossRef]
38. Xing, Q.; Kim, Y.W.; Kim, D.; Park, J.-S.; Yoo, H.I.; Yarish, C.; Kim, J.K. Effects of the ultraviolet filter oxybenzone on physiological responses in a red macroalga, *Gracilaria vermiculophylla*. *Aquat. Bot.* **2022**, *179*, 103514. [CrossRef]
39. Malakhova, L.; Lobko, V.; Murashova, A.; Malakhova, T.; Zheleznova, S.; Egorov, V. Morphological changes and biochemical reaction of *Ulva rigida* in response to the toxic effect of bisphenol A under experimental conditions. *Aquat. Bot.* **2023**, *184*, 103579. [CrossRef]
40. Garcia-Vaquero, M.; Rajauria, G.; Miranda, M.; Sweeney, T.; Lopez-Alonso, M.; O'Doherty, J. Seasonal Variation of the Proximate Composition, Mineral Content, Fatty Acid Profiles and Other Phytochemical Constituents of Selected Brown Macroalgae. *Mar. Drugs* **2021**, *19*, 204. [CrossRef] [PubMed]
41. Miguel, S.P.; D'Angelo, C.; Ribeiro, M.P.; Simões, R.; Coutinho, P. Chemical Composition of Macroalgae Polysaccharides from Galician and Portugal Coasts: Seasonal Variations and Biological Properties. *Mar. Drugs* **2023**, *21*, 589. [CrossRef]
42. Pistollato, F.; Madia, F.; Corvi, R.; Munn, S.; Grignard, E.; Paini, A.; Worth, A.; Bal-Price, A.; Prieto, P.; Casati, S.; et al. Current EU regulatory requirements for the assessment of chemicals and cosmetic products: Challenges and opportunities for introducing new approach methodologies. *Arch. Toxicol.* **2021**, *95*, 1867–1897. [CrossRef]
43. Wells, M.L.; Potin, P.; Craigie, J.S.; Raven, J.A.; Merchant, S.S.; Helliwell, K.E.; Smith, A.G.; Camire, M.E.; Brawley, S.H. Algae as nutritional and functional food sources: Revisiting our understanding. *J. Appl. Phycol.* **2017**, *29*, 949–982. [CrossRef]
44. Hermund, D.B.; Torsteinsen, H.; Vega, J.; Figueroa, F.L.; Jacobsen, C. Screening for New Cosmeceuticals from Brown Algae. *Mar. Drugs* **2022**, *20*, 687. [CrossRef]
45. Zheng, H.; Zhao, Y.; Guo, L. A Bioactive Substance Derived from Brown Seaweeds: Phlorotannins. *Mar. Drugs* **2022**, *20*, 742. [CrossRef]
46. Knight, J.; Rovida, C.; Kreiling, R.; Zhu, C.; Knudsen, M.; Hartung, T. Continuing Animal Tests on Cosmetic Ingredients for REACH in the EU. *ALTEX* **2021**, *38*, 653–668. [CrossRef]
47. Soleimani, S.; Yousefzadi, M.; Nezhad, S.B.M.; Pozharitskaya, O.N.; Shikov, A.N. Evaluation of fractions extracted from *Polycladia myrica*: Biological activities, UVR protective effect, and stability of cream formulation based on it. *J. Appl. Phycol.* **2022**, *34*, 1763–1777. [CrossRef]
48. Nishida, Y.; Kumagai, Y.; Michiba, S.; Yasui, H.; Kishimura, H. Efficient Extraction and Antioxidant Capacity of Mycosporine-Like Amino Acids from Red Alga Dulse *Palmaria palmata* in Japan. *Mar. Drugs* **2020**, *18*, 502. [CrossRef] [PubMed]
49. Pirotta, G. Sunscreen Regulation in the World. In *Sunscreens in Coastal Ecosystems: Occurrence, Behavior, Effect and Risk*; Tovar-Sánchez, A., Sánchez-Quiles, D., Blasco, J., Eds.; Springer International Publishing: Cham, Switzerland, 2020; pp. 15–35.
50. The European Parliament and The Council of the European Union. *Regulation (EC) No 1223/2009 of the European Parliament and of the Council of 30 November 2009 on Cosmetic Products*; The European Parliament and The Council of the European Union: Brussels, Belgium, 2009.
51. Bitwell, C.; Indra, S.S.; Luke, C.; Kakoma, M.K. A review of modern and conventional extraction techniques and their applications for extracting phytochemicals from plants. *Sci. Afr.* **2023**, *19*, e01585. [CrossRef]
52. Belyagoubi, L.; Belyagoubi-Benhammou, N.; Atik-Bekkara, F.; Abdelouahid, D.E. Influence of harvest season and different polarity solvents on biological activities, phenolic compounds and lipid-soluble pigment contents of *Spirogyra* sp. from Algeria. *Adv. Tradit. Med.* **2022**, *22*, 359–369. [CrossRef]
53. Gager, L.; Connan, S.; Molla, M.; Couteau, C.; Arbona, J.-F.; Coiffard, L.; Cérantola, S.; Stiger-Pouvreau, V. Active phlorotannins from seven brown seaweeds commercially harvested in Brittany (France) detected by 1H NMR and in vitro assays: Temporal variation and potential valorization in cosmetic applications. *J. Appl. Phycol.* **2020**, *32*, 2375–2386. [CrossRef]
54. Bhuyar, P.; Rahim, M.H.; Sundararaju, S.; Maniam, G.P.; Govindan, N. Antioxidant and antibacterial activity of red seaweed *Kappaphycus alvarezii* against pathogenic bacteria. *Glob. J. Environ. Sci. Manag.* **2020**, *6*, 47–58. [CrossRef]
55. Garcia-Vaquero, M.; Rajauria, G.; Tiwari, B. Chapter 7—Conventional extraction techniques: Solvent extraction. In *Advances in Green and Sustainable Chemistry*; Elsevier: Amsterdam, The Netherlands, 2020.
56. Wassie, T.; Niu, K.; Xie, C.; Wang, H.; Xin, W. Extraction Techniques, Biological Activities and Health Benefits of Marine Algae. *Front. Nutr.* **2021**, *8*, 747928. [CrossRef]

57. Phomkaivon, N.; Pongponpai, P.; Kosawatpat, P.; Thongdang, B.; Pan-utai, W. Extraction, Characterisation and Evaluation of Antioxidant and Probiotic Growth Potential of Water-Soluble Polysaccharides from *Ulva rigida* Macroalgae. *Foods* **2024**, *13*, 1630. [CrossRef]
58. Sosa-Hernández, J.E.; Escobedo-Avellaneda, Z.; Iqbal, H.M.N.; Welti-Chanes, J. State-of-the-Art Extraction Methodologies for Bioactive Compounds from Algal Biome to Meet Bio-Economy Challenges and Opportunities. *Molecules* **2018**, *23*, 2953. [CrossRef]
59. Yuan, Y.; Zhang, J.; Fan, J.; Clark, J.; Shen, P.; Li, Y.; Zhang, C. Microwave assisted extraction of phenolic compounds from four economic brown macroalgae species and evaluation of their antioxidant activities and inhibitory effects on α-amylase, α-glucosidase, pancreatic lipase and tyrosinase. *Food Res. Int.* **2018**, *113*, 288–297. [CrossRef]
60. Amarante, S.; Catarino, M.; Marçal, C.; Silva, A.; Ferreira, R.; Cardoso, S. Microwave-Assisted Extraction of Phlorotannins from *Fucus vesiculosus*. *Mar. Drugs* **2020**, *18*, 559. [CrossRef]
61. Lopes, A.; Correia-Sá, L.; Vieira, M.; Delerue-Matos, C.; Soares, C.; Grosso, C. Sustainable Carotenoid Extraction from Macroalgae: Optimizing Microwave-Assisted Extraction Using Response Surface Methodology. *Life* **2024**, *14*, 1573. [CrossRef]
62. Torabi, P.; Hamdami, N.; Keramat, J. Microwave-assisted extraction of sodium alginate from brown macroalgae *Nizimuddinia zanardini*, optimization and physicochemical properties. *Sep. Sci. Technol.* **2021**, *57*, 872–885. [CrossRef]
63. Garcia-Vaquero, M.; Ummat, V.; Tiwari, B.; Rajauria, G. Exploring Ultrasound, Microwave and Ultrasound–Microwave Assisted Extraction Technologies to Increase the Extraction of Bioactive Compounds and Antioxidants from Brown Macroalgae. *Mar. Drugs* **2020**, *18*, 172. [CrossRef] [PubMed]
64. Spagnuolo, D.; Genovese, G. Comparative polysaccharides extraction methods ulvans from *Ulva ohnoi* (*Chlorophyta*): Advantages of microwave-assisted techniques. *Algologia* **2025**, *35*, 73–83. [CrossRef]
65. Song, Y.; Lee, J.; Kwon, H.K.; Kim, M.; Shin, S.; Kim, S.; Son, H.; Park, C.; Yoo, H.Y. Efficient Ultrasound-Assisted Extraction of Bioactive Molecules from Brown Macroalga *Sargassum horneri*: Optimal Extraction, Antioxidant and Cytotoxicity Evaluation. *Int. J. Mol. Sci.* **2025**, *26*, 2749. [CrossRef]
66. Goksen, G. Elucidation and quantification health-promoting phenolic compounds, antioxidant properties and sugar levels of ultrasound assisted extraction, aroma compositions and amino acids profiles of macroalgae, *Laurencia papillosa*. *Ultrason. Sonochem.* **2023**, *98*, 106527. [CrossRef]
67. Garcia-Vaquero, M.; Ravindran, R.; Walsh, O.; O'Doherty, J.; Tiwari, B.; Rajauria, G. Evaluation of Ultrasound, Microwave, Ultrasound–Microwave, Hydrothermal and High Pressure Assisted Extraction Technologies for the Recovery of Phytochemicals and Antioxidants from Brown Macroalgae. *Mar. Drugs* **2021**, *19*, 309. [CrossRef]
68. Garcia-Vaquero, M.; Rajauria, G.; Tiwari, B.; Sweeney, T.; O'Doherty, J. Extraction and Yield Optimisation of Fucose, Glucans and Associated Antioxidant Activities from Laminaria digitata by Applying Response Surface Methodology to High Intensity Ultrasound-Assisted Extraction. *Mar. Drugs* **2018**, *16*, 257. [CrossRef]
69. Cikoš, A.-M.; Aladić, K.; Velić, D.; Tomas, S.; Lončarić, P.; Jerković, I. Evaluation of ultrasound-assisted extraction of fucoxanthin and total pigments from three croatian macroalgal species. *Chem. Pap.* **2022**, *77*, 1545–1559. [CrossRef]
70. Mittal, R.; Tavanandi, H.; Mantri, V.; Raghavarao, K. Ultrasound assisted methods for enhanced extraction of phycobiliproteins from marine macro-algae, *Gelidium pusillum* (*Rhodophyta*). *Ultrason. Sonochem.* **2017**, *38*, 92–103. [CrossRef]
71. Kumar, Y.; Singhal, S.; Tarafdar, A.; Pharande, A.; Ganesan, M.; Badgujar, P. Ultrasound assisted extraction of selected edible macroalgae: Effect on antioxidant activity and quantitative assessment of polyphenols by liquid chromatography with tandem mass spectrometry (LC-MS/MS). *Algal Res.-Biomass Biofuels Bioprod.* **2020**, *52*, 102114. [CrossRef]
72. Cikoš, A.M.; Jokić, S.; Šubarić, D.; Jerković, I. Overview on the Application of Modern Methods for the Extraction of Bioactive Compounds from Marine Macroalgae. *Mar. Drugs* **2018**, *16*, 348. [CrossRef] [PubMed]
73. Nguyen, T.T.; Mikkelsen, M.; Tran, V.; Trang, V.T.D.; Rhein-Knudsen, N.; Holck, J.; Rasin, A.; Cao, H.; Vân, T.; Meyer, A. Enzyme-Assisted Fucoidan Extraction from Brown Macroalgae *Fucus distichus* subsp. *evanescens* and *Saccharina latissima*. *Mar. Drugs* **2020**, *18*, 296. [CrossRef]
74. Romero, A.M.; Morales, J.J.P.; Klose, L.; Liese, A. Enzyme-Assisted Extraction of Ulvan from the Green Macroalgae Ulva fenestrata. *Molecules* **2023**, *28*, 6781. [CrossRef]
75. Quitério, E.; Grosso, C.; Ferraz, R.; Delerue-Matos, C.; Soares, C. A Critical Comparison of the Advanced Extraction Techniques Applied to Obtain Health-Promoting Compounds from Seaweeds. *Mar. Drugs* **2022**, *20*, 677. [CrossRef]
76. Yücetepe, A.; Aydar, E.F.; Dogu-Baykut, E.; Dinç, H.; Onat, İ.A.; Demircan, E.; Şensu, E.; Okudan, E.; Özçelik, B. Optimization of Protein Extraction from *Halopteris scoparia* Macroalgae by Ultrasonic-Assisted Enzymatic Extraction (UAEE): Bioactive, Chemical, and Technological Properties. *ACS Food Sci. Technol.* **2024**, *4*, 1375–1387. [CrossRef]
77. Maribu, I.; Blikra, M.; Eilertsen, K.-E.; Elvevold, K. Protein enrichment of the red macroalga *Palmaria palmata* using pulsed electric field and enzymatic processing. *J. Appl. Phycol.* **2024**, *36*, 3665–3673. [CrossRef]
78. Steinbruch, E.; Wise, J.; Levkov, K.; Chemodnov, A.; Israel, Á.; Livney, Y.; Golberg, A. Enzymatic cell wall degradation combined with pulsed electric fields increases yields of water-soluble-protein extraction from the green marine macroalga *Ulva* sp. *Innov. Food Sci. Emerg. Technol.* **2023**, *84*, 103231. [CrossRef]

79. Gordalina, M.; Pinheiro, H.; Mateus, M.; Da Fonseca, M.; Cesário, M. Macroalgae as Protein Sources—A Review on Protein Bioactivity, Extraction, Purification and Characterization. *Appl. Sci.* **2021**, *11*, 7969. [CrossRef]
80. Otero, P.; Quintana, S.; Reglero, G.; Fornari, T.; García-Risco, M. Pressurized Liquid Extraction (PLE) as an Innovative Green Technology for the Effective Enrichment of Galician Algae Extracts with High Quality Fatty Acids and Antimicrobial and Antioxidant Properties. *Mar. Drugs* **2018**, *16*, 156. [CrossRef]
81. Sáez-González, L.; Carreño-Díaz, M.; Blázquez-Abellán, G.; Santander-Ortega, M.; Martínez-García, R.; Martínez, L.; Carbajal, J.; Castro-Vázquez, L. Antioxidant Valorization of PLE Extracts from Macroalgae (*Cladophora glomerata*): In Vitro Assessment of Nanoemulsions Against Oxidative Stress. *Antioxidants* **2024**, *13*, 1370. [CrossRef] [PubMed]
82. De Sousa, A.C.S.P.; Alves, A.A.A.; Martins, J.R.P.; Feitosa, F.X.; De Sant'Ana, H.; Da Silva Júnior, I.J. Enhanced recovery of r-phycoerythrin using recombination cell-assisted pressurized fluid extraction: Yield, characterization, and antioxidant evaluation. *Sep. Purif. Technol.* **2024**, *354*, 128896. [CrossRef]
83. De Sousa, A.C.S.P.; Martins, J.R.P.; Alves, A.; Maranhão, S.S.A.; Pessoa, C.; Feitosa, F.; De Sant'Ana, H.; Da Silva, I.J. Extraction and characterization of R-phycoerythrin from wet and lyophilized macroalgae *Solieria filiformis* by pressurized water method. *Algal Res.* **2024**, *80*, 103493. [CrossRef]
84. Messyasz, B.; Michalak, I.; Łęska, B.; Schroeder, G.; Górka, B.; Korzeniowska, K.; Lipok, J.; Wieczorek, P.; Rój, E.; Wilk, R.; et al. Valuable natural products from marine and freshwater macroalgae obtained from supercritical fluid extracts. *J. Appl. Phycol.* **2017**, *30*, 591–603. [CrossRef]
85. Singh, S.; Verma, D.K.; Thakur, M.; Tripathy, S.; Patel, A.; Shah, N.; Utama, G.L.; Srivastav, P.P.; Benavente-Valdés, J.R.; Chávez-González, M.; et al. Supercritical fluid extraction (SCFE) as green extraction technology for high-value metabolites of algae, its potential trends in food and human health. *Food Res. Int.* **2021**, *150 Pt A*, 110746. [CrossRef]
86. Sarkar, S.; Gayen, K.; Bhowmick, T. Green extraction of biomolecules from algae using subcritical and supercritical fluids. *Biomass Convers. Biorefinery* **2022**, 1–23. [CrossRef]
87. Michalak, I.; Chojnacka, K.; Dmytryk, A.; Wilk, R.; Gramza, M.; Rój, E. Evaluation of Supercritical Extracts of Algae as Biostimulants of Plant Growth in Field Trials. *Front. Plant Sci.* **2016**, *7*, 1591. [CrossRef]
88. Michalak, I.; Górka, B.; Wieczorek, P.; Rój, E.; Lipok, J.; Łęska, B.; Messyasz, B.; Wilk, R.; Schroeder, G.; Dobrzyńska-Inger, A.; et al. Supercritical fluid extraction of algae enhances levels of biologically active compounds promoting plant growth. *Eur. J. Phycol.* **2016**, *51*, 243–252. [CrossRef]
89. Kalasariya, H.S.; Pereira, L.; Patel, N.B. Comprehensive Phytochemical Analysis and Bioactivity Evaluation of *Padina boergesenii*: Unveiling Its Prospects as a Promising Cosmetic Component. *Mar. Drugs* **2023**, *21*, 358. [CrossRef]
90. Sharma, G.; John, J. Identification of polyphenols using UPLC-QTOF MS/MS, in-vitro photoprotective and antiaging activities of brown macroalga *Padina tetrastromatica*. *Algal Res.* **2023**, *75*, 103255. [CrossRef]
91. Kiani, H.; Aznar, R.; Poojary, M.M.; Tiwari, B.K.; Halim, R. Chromatographic Techniques to Separate and Identify Bioactive Compounds in Microalgae. *Front. Energy Res.* **2022**, *10*, 904014. [CrossRef]
92. Zwerger, M.; Ganzera, M. Fast and Efficient Separation of Eleven Mycosporine-like Amino Acids by UHPLC-DAD and Their Quantification in Diverse Red Algae. *Mar. Drugs* **2022**, *20*, 395. [CrossRef] [PubMed]
93. Terriente-Palacios, C.; Diaz, I.; Castellari, M. A validated ultra-performance liquid chromatography with diode array detection coupled to electrospray ionization and triple quadrupole mass spectrometry method to simultaneously quantify taurine, homotaurine, hypotaurine and amino acids in macro- and microalgae. *J. Chromatogr. A* **2019**, *1589*, 83–92. [CrossRef] [PubMed]
94. Steevensz, A.; Mackinnon, S.; Hankinson, R.; Craft, C.; Connan, S.; Stengel, D.; Melanson, J. Profiling phlorotannins in brown macroalgae by liquid chromatography-high resolution mass spectrometry. *Phytochem. Anal. PCA* **2012**, *23*, 547–553. [CrossRef] [PubMed]
95. Klejdus, B.; Lojková, L.; Plaza, M.; Šnóblová, M.; Štěrbová, D. Hyphenated technique for the extraction and determination of isoflavones in algae: Ultrasound-assisted supercritical fluid extraction followed by fast chromatography with tandem mass spectrometry. *J. Chromatogr. A* **2010**, *1217*, 7956–7965. [CrossRef]
96. Lawrence, J.F.; Niedzwiadek, B.; Menard, C.; Lau, B.P.Y.; Lewis, D.; Kuper-Goodman, T.; Carbone, S.; Holmes, C. Comparison of Liquid Chromatography/Mass Spectrometry, ELISA, and Phosphatase Assay for the Determination of Microcystins in Blue-Green Algae Products. *J. AOAC Int.* **2001**, *84*, 1035–1044. [CrossRef]
97. Hartmann, A.; Becker, K.; Karsten, U.; Remias, D.; Ganzera, M. Analysis of Mycosporine-Like Amino Acids in Selected Algae and Cyanobacteria by Hydrophilic Interaction Liquid Chromatography and a Novel MAA from the Red Alga Catenella repens. *Mar. Drugs* **2015**, *13*, 6291–6305. [CrossRef]
98. Vega, J.; Bárcenas-Pérez, D.; Fuentes-Ríos, D.; López-Romero, J.M.; Hrouzek, P.; Figueroa, F.L.; Cheel, J. Isolation of Mycosporine-like Amino Acids from Red Macroalgae and a Marine Lichen by High-Performance Countercurrent Chromatography: A Strategy to Obtain Biological UV-Filters. *Mar. Drugs* **2023**, *21*, 357. [CrossRef]
99. Pérez-Míguez, R.; Plaza, M.; Castro-Puyana, M.; Marina, M.L. Separation and identification of peptides in hydrolysed protein extracts from edible macroalgae by HPLC-ESI-QTOF/MS. *Algal Res.* **2019**, *39*, 101465. [CrossRef]

100. Sardari, R.R.R.; Prothmann, J.; Gregersen, O.; Turner, C.; Nordberg Karlsson, E. Identification of Phlorotannins in the Brown Algae, *Saccharina latissima* and *Ascophyllum nodosum* by Ultra-High-Performance Liquid Chromatography Coupled to High-Resolution Tandem Mass Spectrometry. *Molecules* **2021**, *26*, 43. [CrossRef] [PubMed]
101. Yum, T.; Kim, E.-Y.; Kim, Y.; Choi, S.; Paeng, K.-J. The Development of an Extraction Method for Simultaneously Analyzing Fatty Acids in Macroalgae Using SPE with Derivatization for LC–MS/MS. *Molecules* **2024**, *29*, 430. [CrossRef] [PubMed]
102. Gu, Q.; David, F.; Lynen, F.; Vanormelingen, P.; Vyverman, W.; Rumpel, K.; Xu, G.; Sandra, P. Evaluation of ionic liquid stationary phases for one dimensional gas chromatography–mass spectrometry and comprehensive two dimensional gas chromatographic analyses of fatty acids in marine biota. *J. Chromatogr. A* **2011**, *1218*, 3056–3063. [CrossRef] [PubMed]
103. Shobier, A.H.; Abdel Ghani, S.A.; Barakat, K.M. GC/MS spectroscopic approach and antifungal potential of bioactive extracts produced by marine macroalgae. *Egypt. J. Aquat. Res.* **2016**, *42*, 289–299. [CrossRef]
104. Bajwa, B.; Xing, X.; Serin, S.C.; Hayes, M.; Terry, S.A.; Gruninger, R.J.; Abbott, D.W. Characterization of Unfractionated Polysaccharides in Brown Seaweed by Methylation-GC-MS-Based Linkage Analysis. *Mar. Drugs* **2024**, *22*, 464. [CrossRef]
105. Palaniyappan, S.; Sridhar, A.; Kari, Z.A.; Téllez-Isaías, G.; Ramasamy, T. Evaluation of Phytochemical Screening, Pigment Content, In Vitro Antioxidant, Antibacterial Potential and GC-MS Metabolite Profiling of Green Seaweed Caulerpa racemosa. *Mar. Drugs* **2023**, *21*, 278. [CrossRef]
106. Fitton, J.H.; Dell'Acqua, G.; Gardiner, V.-A.; Karpiniec, S.S.; Stringer, D.N.; Davis, E. Topical Benefits of Two Fucoidan-Rich Extracts from Marine Macroalgae. *Cosmetics* **2015**, *2*, 66–81. [CrossRef]
107. Gómez-Mascaraque, L.G.; Martínez-Sanz, M.; Martínez-López, R.; Martínez-Abad, A.; Panikuttira, B.; López-Rubio, A.; Tuohy, M.G.; Hogan, S.A.; Brodkorb, A. Characterization and gelling properties of a bioactive extract from. *Curr. Res. Food Sci.* **2021**, *4*, 354–364. [CrossRef]
108. Xhauflaire-Uhoda, E.; Fontaine, K.; Piérard, G.E. Kinetics of moisturizing and firming effects of cosmetic formulations. *Int. J. Cosmet. Sci.* **2008**, *30*, 131–138. [CrossRef]
109. Cha, S.H.; Ko, S.C.; Kim, D.; Jeon, Y.J. Screening of marine algae for potential tyrosinase inhibitor: Those inhibitors reduced tyrosinase activity and melanin synthesis in zebrafish. *J. Dermatol.* **2011**, *38*, 354–363. [CrossRef]
110. Clarys, P.; Barel, A. *Handbook of Cosmetic Science and Technology—New Trends in Antiaging Cosmetic Ingredients and Treatments*, 3rd ed.; CRC Press: Boca Raton, FL, USA, 2009.
111. Jesumani, V.; Du, H.; Aslam, M.; Pei, P.; Huang, N. Potential Use of Seaweed Bioactive Compounds in Skincare-A Review. *Mar. Drugs* **2019**, *17*, 688. [CrossRef]
112. Sayin, S.; Depci, T.; Naz, M.; Sezer, S.; Karaaslan, M.G.; Aras, A.; Uğur, S.; Çetïn, Z.; Saygili, E.I.; Ateş, B. Characterization and evaluation of the antimicrobial properties of algal alginate; a potential natural protective for cosmetics. *J. Res. Pharm.* **2022**, *26*, 198–209. [CrossRef]
113. Park, J.; Lee, H.; Choi, S.; Pandey, L.K.; Depuydt, S.; De Saeger, J.; Park, J.-T.; Han, T. Extracts of red seaweed, *Pyropia yezoensis*, inhibit melanogenesis but stimulate collagen synthesis. *J. Appl. Phycol.* **2021**, *33*, 653–662. [CrossRef]
114. Kim, J.H.; Lee, J.E.; Kim, K.H.; Kang, N.J. Beneficial Effects of Marine Algae-Derived Carbohydrates for Skin Health. *Mar. Drugs* **2018**, *16*, 459. [CrossRef] [PubMed]
115. Wang, L.; Lee, W.; Oh, J.Y.; Cui, Y.R.; Ryu, B.; Jeon, Y.J. Protective effect of sulfated polysaccharides from celluclast-assisted extract of *Hizikia fusiforme* against ultraviolet B-induced skin damage by regulating NF-κB, AP-1, and MAPKs signaling pathways in vitro in human dermal fibroblasts. *Mar. Drugs* **2018**, *16*, 239. [CrossRef] [PubMed]
116. Adamiak, K.; Sionkowska, A. State of Innovation in Alginate-Based Materials. *Mar. Drugs* **2023**, *21*, 353. [CrossRef] [PubMed]
117. Rahse, W. Proven Active Ingredients for Various Categories of Skin Creams. In *Cosmetic Creams*; Rahse, W., Ed.; Wiley: Hoboken, NJ, USA, 2019; pp. 175–230.
118. Iwamoto, K.; Hiragun, T.; Takahagi, S.; Yanase, Y.; Morioke, S.; Mihara, S.; Kameyoshi, Y.; Hide, M. Fucoidan suppresses IgE production in peripheral blood mononuclear cells from patients with atopic dermatitis. *Arch. Dermatol. Res.* **2011**, *303*, 425–431. [CrossRef] [PubMed]
119. Ahn, J.H.; Kim, D.W.; Park, C.W.; Kim, B.; Sim, H.; Kim, H.S.; Lee, T.K.; Lee, J.C.; Yang, G.E.; Her, Y.; et al. Laminarin Attenuates Ultraviolet-Induced Skin Damage by Reducing Superoxide Anion Levels and Increasing Endogenous Antioxidants in the Dorsal Skin of Mice. *Mar. Drugs* **2020**, *18*, 345. [CrossRef]
120. Ferreres, F.; Lopes, G.; Gil-Izquierdo, A.; Andrade, P.B.; Sousa, C.; Mouga, T.; Valentão, P. Phlorotannin extracts from fucales characterized by HPLC-DAD-ESI-MSn: Approaches to hyaluronidase inhibitory capacity and antioxidant properties. *Mar. Drugs* **2012**, *10*, 2766–2781. [CrossRef]
121. Wang, J.; Jin, W.; Hou, Y.; Niu, X.; Zhang, H.; Zhang, Q. Chemical composition and moisture-absorption/retention ability of polysaccharides extracted from five algae. *Int. J. Biol. Macromol.* **2013**, *57*, 26–29. [CrossRef]
122. Zhang, Q.; Li, N.; Liu, X.; Zhao, Z.; Li, Z.; Xu, Z. The structure of a sulfated galactan from *Porphyra haitanensis* and its in vivo antioxidant activity. *Carbohydr. Res.* **2004**, *339*, 105–111. [CrossRef]

123. Jiang, Z.; Hama, Y.; Yamaguchi, K.; Oda, T. Inhibitory effect of sulphated polysaccharide porphyran on nitric oxide production in lipopolysaccharide-stimulated RAW264.7 macrophages. *J. Biochem.* **2012**, *151*, 65–74. [CrossRef]
124. Adrien, A.; Bonnet, A.; Dufour, D.; Baudouin, S.; Maugard, T.; Bridiau, N. Pilot production of ulvans from *Ulva* sp. and their effects on hyaluronan and collagen production in cultured dermal fibroblasts. *Carbohydr. Polym.* **2017**, *157*, 1306–1314. [CrossRef] [PubMed]
125. Choi, J.S.; Bae, H.J.; Kim, S.J.; Choi, I.S. In vitro antibacterial and anti-inflammatory properties of seaweed extracts against acne inducing bacteria, Propionibacterium acnes. *J. Environ. Biol.* **2011**, *32*, 313–318. [PubMed]
126. Murphy, M.J.; Dow, A.A. Clinical Studies of the Safety and Efficacy of Macroalgae Extracts in Cosmeceuticals. *J. Clin. Aesthet. Dermatol.* **2021**, *14*, 37–41.
127. Kang, J.W.; Hyun, S.H.; Kim, H.M.; Park, S.Y.; Lee, J.A.; Lee, I.C.; Bae, J.S. The effects of fucoidan-rich polysaccharides extracted from *Sargassum horneri* on enhancing collagen-related skin barrier function as a potential cosmetic product. *J. Cosmet. Dermatol.* **2024**, *23*, 1365–1373. [CrossRef]
128. Janssens-Böcker, C.; Wiesweg, K.; Doberenz, C. The Tolerability and Effectiveness of Marine-Based Ingredients in Cosmetics: A Split-Face Clinical Study of a Serum Spray Containing *Fucus vesiculosus* Extract, Ulva lactuca Extract, and Ectoin. *Cosmetics* **2023**, *10*, 93. [CrossRef]
129. Janssens-Böcker, C.; Wiesweg, K.; Doberenz, C. Exploring the Therapeutic Potential of Algae-Based Sheet Masks in Skincare: A Comprehensive Study of Cosmetological Benefits and Microbiome Balanced Interactions. *J. Cosmet. Dermatol. Sci. Appl.* **2023**, *13*, 277–301. [CrossRef]
130. Schmid, D.; Schürch, C.; Zülli, F. UVA-screening compounds from red algae protect against photoageing. *Personal Care* **2024**, *1*, 29–31.
131. Capitanio, B.; Sinagra, J.L.; Weller, R.B.; Brown, C.; Berardesca, E. Randomized controlled study of a cosmetic treatment for mild acne. *Clin. Exp. Dermatol.* **2012**, *37*, 346–349. [CrossRef]
132. Jeong, J.W.; Park, D.J.; Kim, S.C.; Kang, H.W.; Lee, B.; Kim, H.W.; Kim, Y.M.; Linh, N.V.; Jung, W.K. Wound healing effect of fucoidan-loaded gelatin/oxidized carboxymethyl cellulose hydrogel. *Int. J. Biol. Macromol.* **2025**, *286*, 138254. [CrossRef] [PubMed]
133. Kikionis, S.; Koromvoki, M.; Tagka, A.; Polichronaki, E.; Stratigos, A.; Panagiotopoulos, A.; Kyritsi, A.; Karalis, V.; Vitsos, A.; Rallis, M.; et al. Ulvan-Based Nanofibrous Patches Enhance Wound Healing of Skin Trauma Resulting from Cryosurgical Treatment of Keloids. *Mar. Drugs* **2022**, *20*, 551. [CrossRef] [PubMed]
134. Sulastri, E.; Lesmana, R.; Zubair, M.S.; Abdelwahab Mohammed, A.F.; Elamin, K.M.; Wathoni, N. Ulvan/Silver nanoparticle hydrogel films for burn wound dressing. *Heliyon* **2023**, *9*, e18044. [CrossRef] [PubMed]
135. Sharma, G.; Alle, M.; Son, H.K.; Kim, J.C. Dialdehyde modification of laminarin for facile synthesis of ultrafine silver nanoparticles with excellent antibacterial and wound healing properties. *Int. J. Biol. Macromol.* **2022**, *222*, 1364–1375. [CrossRef]
136. Foroughi, J.; Ruhparwar, A.; Aloko, S.; Wang, C.H. Manufacturing Ulvan Biopolymer for Wound Dressings. *Macromol. Mater. Eng.* **2024**, *309*, 2300268. [CrossRef]
137. Hwang, P.A.; Chen, H.Y.; Chang, J.S.; Hsu, F.Y. Electrospun nanofiber composite mat based on ulvan for wound dressing applications. *Int. J. Biol. Macromol.* **2023**, *253*, 126646. [CrossRef]
138. Terezaki, A.; Kikionis, S.; Ioannou, E.; Sfiniadakis, I.; Tziveleka, L.-A.; Vitsos, A.; Roussis, V.; Rallis, M. Ulvan/gelatin-based nanofibrous patches as a promising treatment for burn wounds. *J. Drug Deliv. Sci. Technol.* **2022**, *74*, 103535. [CrossRef]
139. Mariia, K.; Arif, M.; Shi, J.; Song, F.; Chi, Z.; Liu, C. Novel chitosan-ulvan hydrogel reinforcement by cellulose nanocrystals with epidermal growth factor for enhanced wound healing: In vitro and in vivo analysis. *Int. J. Biol. Macromol.* **2021**, *183*, 435–446. [CrossRef]
140. Ren, Y.; Aierken, A.; Zhao, L.; Lin, Z.; Jiang, J.; Li, B.; Wang, J.; Hua, J.; Tu, Q. hUC-MSCs lyophilized powder loaded polysaccharide ulvan driven functional hydrogel for chronic diabetic wound healing. *Carbohydr. Polym.* **2022**, *288*, 119404. [CrossRef]
141. Don, T.M.; Ma, C.H.; Huang, Y.C. In Situ Release of Ulvan from Crosslinked Ulvan/Chitosan Complex Films and Their Evaluation as Wound Dressings. *Polymers* **2022**, *14*, 5382. [CrossRef]
142. Sellimi, S.; Maalej, H.; Rekik, D.M.; Benslima, A.; Ksouda, G.; Hamdi, M.; Sahnoun, Z.; Li, S.; Nasri, M.; Hajji, M. Antioxidant, antibacterial and in vivo wound healing properties of laminaran purified from *Cystoseira barbata* seaweed. *Int. J. Biol. Macromol.* **2018**, *119*, 633–644. [CrossRef]
143. Amaral, K.R.; Silva, A.S.; Santos, L.F.; Castanheira, E.J.; Mendes, M.C.; Costa, D.C.S.; Rodrigues, J.M.M.; Marto, J.; Mano, J.F. Biomimetic Adhesive Micropatterned Hydrogel Patches for Drug Release. *Adv. Healthc. Mater.* **2023**, *12*, e2301513. [CrossRef]
144. Feng, L.; Hao, Y.; Zhu, M.; Zhai, Y.; Yang, L.; Liu, Y.; Cheng, G. Incorporation of Laminarin-Based Hydrogel with Graphene Foam to Enhance the Toughness of Scaffold and Regulate the Stem Cell Behavior. *ACS Biomater. Sci. Eng.* **2019**, *5*, 5295–5304. [CrossRef]
145. Hao, J.; Liu, X.; Du, Y. Fabrication of gelatine/fucoidan nanogel-coated silver nanoparticles for the treatment of wound healing therapy and nursing care. *Regen. Ther.* **2025**, *29*, 282–291. [CrossRef]

146. Phulmogare, G.; Rani, S.; Lodhi, S.; Patil, U.K.; Sinha, S.; Ajazuddin; Gupta, U. Fucoidan loaded PVA/Dextran blend electrospun nanofibers for the effective wound healing. *Int. J. Pharm.* **2024**, *650*, 123722. [CrossRef] [PubMed]
147. Saravanakumar, K.; Li, Z.; Kim, Y.; Park, S.; Keon, K.; Lee, C.M.; Ahn, G.; Cho, N. Fucoidan-coated cotton dressing functionalized with biomolecules capped silver nanoparticles (LB-Ag NPs-FN-OCG) for rapid healing therapy of infected wounds. *Environ. Res.* **2024**, *246*, 118004. [CrossRef] [PubMed]
148. Li, J.; Wang, J.; Zhang, Z.; Pan, Y.; Jiang, Z.; Hu, Y.; Wang, L. Fucoidan-loaded, neutrophil membrane-coated nanoparticles facilitate MRSA-accompanied wound healing. *Mater. Des.* **2023**, *227*, 111758. [CrossRef]
149. Younas, A.; Dong, Z.; Hou, Z.; Asad, M.; Li, M.; Zhang, N. A chitosan/fucoidan nanoparticle-loaded pullulan microneedle patch for differential drug release to promote wound healing. *Carbohydr. Polym.* **2023**, *306*, 120593. [CrossRef]
150. Peng, J.; Liu, C.; Mo, M.; Huang, Y.; Lu, Y.; Xiao, M.; Zhao, X.; Ruan, Q.; Ti, H. Construction of multifunctional hydrogel containing pH-responsive gold nanozyme for bacteria-infected wound healing. *Int. J. Biol. Macromol.* **2024**, *283*, 137746. [CrossRef]
151. Hernández Muñoz, A.C.; Rodríguez Martínez, I.A.; Serafini, M.R.; Aragón, D.M. Innovative applications of marine-derived algae in cosmetics: A patent review (2010−2023). *Algal Res.* **2024**, *84*, 103806. [CrossRef]
152. Michalak, I.; Dmytryk, A.; Chojnacka, K. Algae Cosmetics. In *Encyclopedia of Marine Biotechnology*; Wiley: Hoboken, NJ, USA, 2020; pp. 65–85.
153. Lourenço-Lopes, C.; Garcia-Oliveira, P.; Carpena, M.; Fraga-Corral, M.; Jimenez-Lopez, C.; Pereira, A.G.; Prieto, M.A.; Simal-Gandara, J. Scientific Approaches on Extraction, Purification and Stability for the Commercialization of Fucoxanthin Recovered from Brown Algae. *Foods* **2020**, *9*, 1113. [CrossRef]
154. Robal, M.; Truus, K.; Volobujeva, O.; Mellikov, E.; Tuvikene, R. Thermal stability of red algal galactans: Effect of molecular structure and counterions. *Int. J. Biol. Macromol.* **2017**, *104*, 213–223. [CrossRef]
155. Jimenez-Lopez, C.; Pereira, A.G.; Lourenço-Lopes, C.; Garcia-Oliveira, P.; Cassani, L.; Fraga-Corral, M.; Prieto, M.A.; Simal-Gandara, J. Main bioactive phenolic compounds in marine algae and their mechanisms of action supporting potential health benefits. *Food Chem.* **2021**, *341*, 128262. [CrossRef]
156. Costa, R.; Santos, L. Delivery systems for cosmetics—From manufacturing to the skin of natural antioxidants. *Powder Technol.* **2017**, *322*, 402–416. [CrossRef]
157. Evoluderm. Detox Serum. Available online: https://www.evoluderm.com/en/products/serum-detox?srsltid=AfmBOor_OwLMq3KGtuZBOGg1yIdTau3bxRVpwiudgng5mZ6_yPUwcnqs (accessed on 21 August 2025).
158. heimish. Marine Care Deep Moisture Nourishing Melting Cream. Available online: https://heimish.us/products/renewal-marine-care-deep-moisture-nourishing-melting-cream-60ml-2-03fl-oz-copy (accessed on 21 August 2025).
159. Farmona. Moisturizing and Regenerating Night Bio-Cream. Available online: https://farmona.pl/en/products/moisturizing-and-regenerating-night-bio-cream/ (accessed on 21 August 2025).
160. NALA. Antipollution Face Cream—Combination Skin—Seaweed & Cucumber. Available online: https://nala.eu/products/antipollution-face-cream-combination-skin-seaweed-cucumber?_pos=4&_psq=algae&_ss=e&_v=1.0 (accessed on 21 August 2025).
161. NALA. Blonde Hair Purple Shampoo—Violet Absolute Extract, Algae Extract, Lime Extract. Available online: https://nala.eu/products/blonde-hair-purple-shampoo-violet-absolute-extract-algae-extract-lime-extract?_pos=1&_psq=algae&_ss=e&_v=1.0 (accessed on 21 August 2025).
162. NALA. Natural Soap—Seaweed. Available online: https://nala.eu/products/natural-soap-seaweed?_pos=2&_psq=algae&_ss=e&_v=1.0 (accessed on 21 August 2025).
163. evanhealy. Sea Algae Serum. Available online: https://www.evanhealy.com/products/sea-algae-serum?variant=32645363040349 (accessed on 21 August 2025).
164. Algologie. Algologie Natural Marine Based Skincare. Available online: https://www.algologie.com/gb/ (accessed on 21 August 2025).
165. Thalgo. Available online: https://www.thalgo.fr/ (accessed on 21 August 2025).

Disclaimer/Publisher's Note: The statements, opinions and data contained in all publications are solely those of the individual author(s) and contributor(s) and not of MDPI and/or the editor(s). MDPI and/or the editor(s) disclaim responsibility for any injury to people or property resulting from any ideas, methods, instructions or products referred to in the content.